Biomineralisation and biogeochemical mobility of chemical elements: phytolith dissolution and its implication in geoarchaeology

Nafsika Chrysoula Andriopoulou

A thesis submitted for the degree of

Doctor of Philosophy

MRED, Technical University of Crete

Chania, July 2020

«This research is co-financed by Greece and the European Union (European Social Fund- ESF) through the Operational Programme «Human Resources Development, Education and Lifelong Learning» in the context of the project "Strengthening Human Resources Research Potential via Doctorate Research" (MIS-5000432), implemented by the State Scholarships Foundation (IKY)»

Members of the doctoral thesis committee:

Prof. dr. George Christidis (PhD supervisor)

School of Mineral Resources Engineering, Technical University of Crete, GR

Dr. Panagiotis Karkanas (PhD co-supervisor)

Director, Wiener Laboratory for Archaeological Science, American School of Classical Studies at Athens, GR

Prof. dr. Dimitrios Panias (PhD co-supervisor)

School of Mining and Metallurgical Engineering, National Technical University of Athens, GR

Prof. dr. Konstantinos Komnitsas

School of Mineral Resources Engineering, Technical University of Crete, GR

Asst. prof. dr. Dan Cabanes

Dept. of Anthropology and Center for Human Evolutionary Studies, Rutgers, the State University of New Jersey, US

Prof. dr. Dorian Fuller

Institute of Archaeology, University College London, UK

Prof. dr. Nikolaos Nikolaidis

School of Environmental Engineering, Technical University of Crete, GR

Nafsika C. Andriopoulou

Technical University of Crete

MRED, 73100 Chania Greece

E-mail: nafsika.andriopoulou@gmail.com

https://orcid.org/0000-0002-1278-1209

Contents

Acknowledgements

I wish to express my gratitude to many wonderful people that offered their support to improve this thesis and the State Scholarships Foundation (IKY) for its financial support.

My sincere thanks go to:

Prof. dr. George Christidis (PhD supervisor)
School of Mineral Resources Engineering, Technical University of Crete, GR

Dr. Panagiotis Karkanas (PhD co-supervisor)
Director, Wiener Laboratory for Archaeological Science, American School of Classical Studies at Athens, GR

Prof. dr. Dimitrios Panias (PhD co-supervisor)
School of Mining and Metallurgical Engineering, National Technical University of Athens, GR

Prof. dr. Konstantinos Komnitsas
School of Mineral Resources Engineering, Technical University of Crete, GR

Asst. prof. dr. Dan Cabanes
Dept. of Anthropology and Center for Human Evolutionary Studies, Rutgers, the State University of New Jersey, US

Prof. dr. Dorian Fuller
Institute of Archaeology, University College London, UK

Prof. dr. Nikolaos Nikolaidis
School of Environmental Engineering, Technical University of Crete, GR

and the reviewer(s) and editor(s) of Archaeological and Anthropological Sciences

for their insightful comments and suggestions.

Dr. Panagiotis Karkanas
Director, Wiener Laboratory for Archaeological Science, American School of Classical Studies at Athens, GR

Dr. Georgia Tsartsidou
Ephoreia of palaeoanthropology-Speleology, Athens, GR

and Prof. dr. Soultana-Maria Valamoti
School of History and Archaeology, Aristotle University of Thessaloniki, GR

for entrusting me with the study of the archaeological samples.

Stela Chatzigeorgiou, MSc
Agricultural School of Mesara, Crete, GR

Georgios Doumos
Irini's garden/organic farm, Pella, GR

Dr. Evangelos Korpetis
Dept. of Cereals, Institute of Plant Breeding and Genetic Resources, Thessaloniki, GR

Dr. Kostas Koutis
Aegilops, Network for Biodiversity and Ecology in Greece, Volos, GR

Dr. Andreas Pallides
Agricultural Research Institute - Ministry of Agriculture, Rural Development and Environment, Nicosia, CY

Panagiotis Saitanoudis
Peliti, Alternative Community, Drama, GR

and Agathi Vlassi
Vioporos, Ecological farm, Corfu, GR

for generously offering the plant and soil samples.

Eleni Chamilaki
School of Mineral Resources Engineering, Technical University of Crete, GR

Dr. Panagiotis Karkanas
Director, Wiener Laboratory for Archaeological Science, American School of Classical Studies at Athens, GR

Dr. Evangelia Kiriatzi
Fitch Laboratory, British School at Athens, GR

Dr. Dimitrios Michailidis
Wiener Laboratory for Archaeological Science American School of Classical Studies at Athens, GR

Dr. Noémi Müller
Fitch Laboratory, British School at Athens, GR

Dr. Antonios Stratakis
School of Mineral Resources Engineering, Technical University of Crete, GR

Prof. dr. Nikolaos Pasadakis
School of Mineral Resources Engineering, Technical University of Crete, GR

Asst. prof. dr. Despina Pentari
School of Mineral Resources Engineering, Technical University of Crete, GR

Dr. Evangelos Petrakis
School of Mineral Resources Engineering, Technical University of Crete, GR

Pavlina Rotonto, MSc
School of Mineral Resources Engineering, Technical University of Crete, GR

Maria-Liliana Saru, MSc
School of Environmental Engineering, Technical University of Crete, GR

Dr. Stylianos Sfakiotakis
School of Mineral Resources Engineering, Technical University of Crete, GR

Dr. Konstantina Tyrovola
School of Environmental Engineering, Technical University of Crete, GR

Prof. dr. Despina Vamvuka
School of Mineral Resources Engineering, Technical University of Crete, GR

and Dr. Eftychia Repouskou
School of Mineral Resources Engineering, Technical University of Crete, GR

for making available the laboratory equipment necessary for the analyses.

Dr. Emmanouil Anadranistakis
Hellenic National Meteorological Service, GR

Dr. Ethel Allué
Catalan Institute of Human Paleoecology and Social Evolution (IPHES)

Dimitra Athenaki, MSc
Academic Affairs, School of Mineral Resources Engineering, Technical University of Crete, GR

Maria Bolieraki
Librarian, Library and Information Centre of the Technical University of Crete, GR

Prof. dr. Francesc Burjachs Casas
Catalan Institute of Human Paleoecology and Social Evolution (IPHES) and Rovira I Virgili University, SP

Panagiotis Chatzidakis
Electrical Engineer at Hellenic Petroleum (HELPE), GR

Nikolaos Kosmadakis, MA
Art director at The Design Bar, Crete, GR

Pantelis Koukousoulas
Independent Computer Software Professional, Crete, GR

Prof. dr. Ioannis Liritzis
Department of Mediterranean Studies, University of the Aegean, GR

Dr. Pagona Makri
School of Mineral Resources Engineering, Technical University of Crete, GR

Irini Marentaki
Secretariat, School of Mineral Resources Engineering, Technical University of Crete, GR

Panayiotis Michael
Department of Meteorology, Nicosia, CY

Vangelis Michelakis
Agricultural University of Athens, GR

Maria Ntaountaki
Library Director, Library and Information Centre of the Technical University of Crete, GR

Assoc. prof. dr. Panagiotis Partsinevelos
School of Mineral Resources Engineering, Technical University of Crete, GR

Prof. Emer. dr. Vasilis Perdikatsis
School of Mineral Resources Engineering, Technical University of Crete, GR

Theodoros Papathanasiou
School of Electrical and Computer Engineering, Technical University of Crete, GR

Prof. dr. Victor Paz
Archaeological Studies Program, Univesity of the Philippines, Quezon, PHL

Dr. Michael Schöbel
X-ray Center, Vienna University of Technology, AT

Olga Pantelaki, MSc
School of Mineral Resources Engineering, Technical University of Crete, GR

Dr. Anaya Sarpaki
Archaeologist-archaeobotanist, Independent scholar, Crete, GR

Dr. Linda Scott Cummings
President and CEO at PaleoResearch Institute, Colorado, US

Giorgo Skretis
Sculpture and Environmental Art, The Glasgow School of Art, UK

Varvara Terzaki-Pallikari
Penelope Gandhi Mission, The University of Mountains, Crete, GR

and Dimitris Trigkakis, MSc
School of Electrical Engineering and Computer Science, Oregon State University, US

for the inspiration or overall contribution towards my research.

My appreciation goes to:

my PhD supervisor Prof. dr. George E. Christidis for the impact he has had
since the beginning (March 2010) of my research activity at Technical University of Crete,

my PhD co-supervisor Dr. Panagiotis Karkanas for my geoarchaeological training
during the ''International Field School on Site Formation, Stratigraphy, and Geoarchaeology'',

my MSc supervisor Asst. prof. dr. Dan Cabanes for introducing me to phytolith analysis
and the world of mineral formation by organisms, or *biomineralisation*,

and Assoc. prof. dr. Panagiotis Partsinevelos for supporting my efforts
to explore the integration of microscopy and photogrammetry.

My love goes to:

my parents Andreas (†) and Mary,
my sister Freya and her husband Nikos, my niece Aiolia N.,
my grandmothers Nafsika (†) and Chrysoula (†), Periklis (†), Niki,
Sofia and her son George, my student Maria; and all my friends, especially
Andreas, Angelos, Antonia, Despina, Esra, Irini L., Irini T., Loukia, Nikoletta and Rodanthi.
Special thanks my therapist Katerina and all people that we have played together music.

This thesis is dedicated to the memory of
my Cretan grandfather Michail Litinas (†),
Home is where the heart is.

Biomineralisation and biogeochemical mobility of chemical elements: phytolith dissolution and its implication in geoarchaeology

Abstract

A growing amount of research has been done on biominerals produced in plant tissues, microscopic SiO_2-rich phytoliths included, because of the useful information they may provide on the natural and the anthropogenic environment. The relationship between nature and humanity is fundamental in archaeological interpretation. Environmental changes are associated with biogeochemical processes and with chemical element mobility in soil horizons, and the understanding of such processes is crucial for the comprehensive study of archaeological materials. Phytoliths are produced through biomineralisation processes that take place in most plant species, and they are eventually released in soils and sediments after the decomposition or/and burning of the plant material. Cereals, and especially wheat (*Triticum* spp.), produce great quantities of SiO_2-rich phytoliths and and their impact on human economies over time has been well documented.

Biogenic silicon ($bSiO_2$) is the earliest known natural bioskeleton and its unique physicochemical properties make it a suitable material for a wide range of applications in the geosciences and archaeology. Even though the biogeochemical cycle of silicon has been studied extensively, most existing studies have restricted their focus on diatoms. Despite the study of phytoliths being an internationally emerging field, scientific interest has remained limited mainly to their systematic classification and morphometry. In particular, in the context of Greece and Cyprus, it is only the last decade that their significance has been acknowledged. Despite the significant contributions having been made in this area, recent studies on SiO_2-rich phytoliths have not put enough emphasis on the investigation of phytolith stability in relation to the biogeochemical depositional

environment and on the preservation of their morphotypes, relating it to important environmental parameters such as soil pH, temperature and water availability. Furthermore, the degree in which the presence of other chemical elements affect the dissolution of biogenic silicon, and therefore affecting phytolith preservation in soils and sediments, has been scarcely covered. Preservation status is one of the most important factors for the reliable interpretation of phytolith morphotypes. In most studied cases, the mineralogical or/and chemical composition of phytoliths is affected by a variety of morphological alterations that have been caused by *in situ* taphonomic or/and laboratory processes during their lifespan.

The present doctoral thesis aims to make a contribution to the research lack outlined above and to expand this field of study. In particular, the dissolution mechanism of phytoliths is investigated in relation to variations of pH, temperature and time, by the means of long-term batch experiments. Moreover, the mobility of silicon (Si) and 7 other main and trace chemical elements (K, Mg, Al, Ca, Fe, Sr, Ba) is being studied with the use of inductively coupled plasma mass spectrometry (ICP-MS), and visualised with MATLAB software. In addition, a multi-analytical characterisation of phytoliths was performed in order to understand their microstructure and behaviour after their extraction from plants by means of two conventional methods: the dry and the wet ashing method. For the high resolution characterisation of phytoliths extracted from either the entire plant (excluding the roots) or different parts of the plant, the inflorescence and the stems-leaves; a variety of analytical techniques were employed, including powder X-Ray Diffraction (XRD), Energy Dispersive X-Ray Fluorescence spectrometry (ED-XRF), Fourier-Transform Infrared spectroscopy (FTIR), Thermogravimetric and Differential Thermogravimetric Analysis (TGA-DTGA), elemental (Carbon-Hydrogen-Nitrogen-Sulphur) analysis (CHNS), Scanning Electron Microscopy with Energy Dispersive Spectroscopy (SEM/EDS), optical microscopy and photomicrography. The quantification of morphotypes for phytoliths originating in the plants (counting at least 250 phytoliths per microscope slide and morphological

classificating according to form, texture and anatomical origin on the basis of the International Code for Phytolith Nomenclature (ICPN Working Group: Madella *et al*. 2005) was carried out both before and after dissolution, and visualised using the python programming language. Phytoliths from soils and archaeological sediments were also extracted. Furthermore, the integrated use of microscopy and photogrammetry for the three-dimensional (3D) representation of biominerals was proposed as a useful tool in geoarchaeology.

The laboratory analyses took place at the Technical University of Crete (School of Mineral Resources Engineering and School of Environmental Engineering), the American School of Classical Studies at Athens (Malcolm H. Wiener Laboratory for Archaeological Science) and the British School at Athens (Fitch Laboratory). The studied phytoliths were parts of three sample groups: (1) ''modern'' wheats (*Triticum monococcum/Triticum durum*) from five organic crops in Greece (Crete, Volos, Corfu and Pella) and one conventional crop in Cyprus (Pafos), (2) the corresponding soils for these samples, and (3) archaeological sediments from three nearby the cultivations archaeological sites in Greece (Knossos, Crete, Palea Castle Volos and Toumba Thessaloniki).

The comprehensive mineralogical and biogeochemical study contributes to the understanding of the geochemical cycle of silicon and to geoarchaeological research, through the insights gained on the post-depositional alterations that SiO_2-rich phytoliths are subjected to over time, and how this relates to the mobility of other soil elements. Furthermore, the mineralogical and chemical composition of the recovered phytoliths is controlled by the extraction method, strongly suggesting that comparison of phytoliths extracted from plants is meaningful only if the method of extraction remains the same. Physicochemical characteristics of fresh phytoliths extracted from plants provided useful information on their preservation state after laboratory processing, that may further contribute to the study of aged phytoliths. Dimensional characteristics and texture of the

majority of the phytoliths changed with rising pH and temperature, suggesting that long cells dendritic morphotypes may alter to long cells echinates or/and to long cells verrucates morphotypes. Moreover, this study provided information about phytoliths characteristics after burning. Phytoliths obtained from plants using the dry method of extraction here are therefore suitable for fire incidents with implications to archaeology. The overall physicochemical characterisation of phytoliths may further contribute to the interpretation of phytolith assemblages from paleontological, archaeological and ethnographical contexts for the diachronic study of human-plant interactions.

Keywords: biomineralisation, phytoliths, wheats, methods of extraction, biogenic silicon, dissolution, mobility of chemical elements, geochemistry, geoarchaeology, archaeobotany

Βιοορυκτοποίηση και βιογεωχημική κινητοποίηση χημικών στοιχείων: διαλυτοποίηση φυτολίθων και εφαρμογές της στη γεωαρχαιολογία

Περίληψη (abstract in Greek)

Αυξανόμενο πλήθος ερευνών έχει γίνει σε βιοορυκτά που παράγονται σε φυτικούς ιστούς, συμπεριλαμβανομένων των μικροσκοπικών φυτολίθων πλούσιων σε SiO_2, λόγω των χρήσιμων πληροφοριών που μπορούν να προσφέρουν για το φυσικό και το ανθρωπογενές περιβάλλον. Η σχέση ανάμεσα στη φύση και την ανθρωπότητα είναι θεμελιώδης στην αρχαιολογική ερμηνεία. Οι περιβαλλοντικές αλλαγές συνδέονται με τις βιογεωχημικές διεργασίες και την κινητικότητα των χημικών στοιχείων στους εδαφικούς ορίζοντες, και η κατανόηση αυτών των διαδικασιών είναι ζωτικής σημασίας για τη διεξοδική μελέτη των αρχαιολογικών υλικών. Οι φυτόλιθοι παράγονται μέσω διεργασιών βιοορυκτοποίησης που λαμβάνουν χώρα στα περισσότερα φυτικά είδη και απελευθερώνονται τελικά στα εδάφη και ιζήματα μετά την αποσύνθεση ή/και την καύση του φυτικού υλικού. Τα δημητριακά, και ιδιαίτερα το σιτάρι (*Triticum* spp.), παράγουν μεγάλες ποσότητες φυτολίθων πλούσιων σε SiO_2 και η συμβολή τους στην ανθρώπινη οικονομία κατά την πάροδο του χρόνου έχει τεκμηριωθεί καλά.

Το βιογενές πυρίτιο ($bSiO_2$) είναι το παλαιότερο γνωστό φυσικό βιοορυκτό και οι μοναδικές φυσικοχημικές του ιδιότητες, το καθιστούν κατάλληλο υλικό για ένα ευρύ φάσμα εφαρμογών στις γεωεπιστήμες και στην αρχαιολογία. Παρόλο που ο βιογεωχημικός κύκλος του πυριτίου έχει μελετηθεί εκτεταμένα, οι περισσότερες υπάρχουσες μελέτες έχουν περιορίσει την εστίαση τους στα διάτομα. Αν και η μελέτη των φυτολίθων αποτελεί διεθνώς αναδυόμενο τομέα, το επιστημονικό ενδιαφέρον παρέμεινε περιορισμένο κυρίως στη συστηματική ταξινόμηση και στη μορφομετρία τους. Ειδικότερα στο πλαίσιο της Ελλάδας και της Κύπρου, μόνο την τελευταία

δεκαετία έχει αναγνωριστεί η σημασία τους. Παρά τις σημαντικές συνεισφορές που έγιναν στον τομέα αυτό, οι πρόσφατες μελέτες φυτολίθων πλούσιων σε SiO_2 δεν έδωσαν αρκετή έμφαση στη διερεύνηση της σταθερότητας φυτόλιθων σε σχέση με το βιογεωχημικό περιβάλλον απόθεσης και στη διατήρηση των μορφοτύπων τους, συσχετίζοντας σημαντικές περιβαλλοντικές παραμέτρους, όπως το pH του εδάφους, τη θερμοκρασία και την υδατική διαθεσιμότητα. Επιπλέον, ο βαθμός στον οποίο η παρουσία άλλων χημικών στοιχείων επηρεάζει τη διαλυτοποίηση του βιογενούς πυριτίου, και ως εκ τούτου επηρεάζει τη διατήρηση των φυτολίθων στα εδάφη και τα ιζήματα έχει καλυφθεί ελάχιστα. Η κατάσταση διατήρησης τους είναι ένας από τους σημαντικότερους παράγοντες για την αξιόπιστη ερμηνεία των μορφοτύπων των φυτολίθων. Στις περισσότερες περιπτώσεις που έχουν μελετηθεί, η ορυκτολογική ή/και χημική σύνθεση των φυτολίθων επηρεάζεται από μια ποικιλία μορφολογικών μεταβολών που έχουν προκληθεί από *in situ* ταφονομικές ή/και εργαστηριακές διεργασίες κατά τη διάρκεια της ζωής τους.

Η παρούσα διδακτορική διατριβή στοχεύει να συνεισφέρει στα προαναφερόμενα ερευνητικά κενά και να επεκτείνει το γνωστικό τομέα. Συγκεκριμένα, ο μηχανισμός διαλυτοποίησης των φυτολίθων ελέγχεται σε σχέση με τις μεταβολές του pH, της θερμοκρασίας και του χρόνου, με τη βοήθεια μακροχρόνιων πειραμάτων διαλείποντος έργου. Επίσης, η κινητικότητα του πυριτίου (Si) και 7 άλλων κύριων στοιχείων και ιχνοστοιχείων (K, Mg, Al, Ca, Fe, Sr, Ba) μελετάται με φασματομετρία μάζας επαγωγικά συζευγμένου πλάσματος (ICP-MS), και απεικονίζεται με το λογισμικό MATLAB. Επιπλέον, διεξήχθη ένας πολυαναλυτικός χαρακτηρισμός φυτολίθων, προκειμένου να κατανοηθεί η μικροδομή και η συμπεριφορά τους μετά την εξαγωγή τους από τα φυτά με δύο συμβατικές μεθόδους: τη μέθοδο ξηρής και υγρής καύσης. Για τον υψηλής ανάλυσης χαρακτηρισμό φυτολίθων που εξάγονται είτε από ολόκληρο το φυτό (μη συμπεριλαμβανομένων των ριζών) ή από διάφορα μέρη του φυτού, την ταξιανθία και τα στελέχη-φύλλα; χρησιμοποιήθηκαν διάφορες αναλυτικές τεχνικές,

συμπεριλαμβανομένης της περίθλασης ακτίνων-Χ κόνεως (XRD), φασματομετρίας φθορισμού ακτίνων-Χ με ενεργειακή διασπορά (ED-XRF), φασματοσκοπίας υπερύθρου μετασχηματισμού-Fourier (FTIR), θερμοβαρυμετρικής ανάλυσης (TGA-DTGA), στοιχειακής (άνθρακα-υδρογόνου-αζώτου-θείου) ανάλυσης (CHNS), ηλεκτρονικής μικροσκοπίας σάρωσης με φασματοσκοπία ενεργειακής διασποράς (SEM/EDS), οπτικής μικροσκοπίας και φωτομικρογραφίας. Η ποσοτικοποίηση των μορφοτύπων των φυτολίθων που προέρχονται από τα φυτά (μετρώντας τουλάχιστον 250 φυτόλιθους ανά αντικιμενοφόρο πλάκα και μορφολογικά ταξινονομώντας σύμφωνα με τη φόρμα, την υφή και την ανατομική προέλευση βάσει του *Διεθνούς Κώδικα Ονοματολογίας των Φυτολίθων*) πραγματοποίηθηκε τόσο πριν όσο και μετά τη διαλυτοποίηση, και οπτικοποίηθηκε με τη χρήση της γλώσσας προγραμματισμού python. Εξήχθησαν επίσης φυτόλιθοι από τα εδάφη και τα αρχαιολογικά ιζήματα. Επιπρόσθετα, η ολοκληρωμένη χρήση μικροσκοπίας και φωτογραμμετρίας για την τρισδιάστατη (3D) αναπαράσταση των φυτολίθων προτάθηκε ως χρήσιμο εργαλείο στη γεωαρχαιολογία.

Οι εργαστηριακές αναλύσεις πραγματοποιήθηκαν στο Πολυτεχνείο Κρήτης (Σχολή Μηχανικών Ορυκτών Πόρων και Σχολή Μηχανικών Περιβάλλοντος), στην Αμερικανική Σχολή Κλασικών Σπουδών στην Αθήνα (Εργαστήριο Αρχαιολογικών Ερευνών Malcolm H. Wiener) και στη Βρετανική Σχολή Αθηνών (Εργαστήριο Fitch). Οι φυτόλιθοι που μελετήθηκαν προέρχονταν από τρεις ομάδες δειγμάτων: (1) ‘’σύγχρονοι’’ σίτοι (*Triticum monococcum/Triticum durum*) από πέντε βιολογικές καλλιέργειες στην Ελλάδα (Κρήτη, Βόλος, Κέρκυρα και Πέλλα) και μία συμβατική καλλιέργεια στην Κύπρο (Πάφος), (2) εδάφη που αντιστοιχούν με αυτά τα δείγματα, και (3) αρχαιολογικά ιζήματα από τρεις αρχαιολογικούς χώρους στην Ελλάδα (Κνωσός Κρήτη, Κάστρο Παλαιών Βόλου και Τούμπα Θεσσαλονίκης) που γειτνιάζουν με τις καλλιέργειες.

Η εκτεταμένη ορυκτολογική και βιογεωχημική μελέτη συμβάλλει στην κατανόηση του γεωχημικού κύκλου του πυριτίου και στη γεωαρχαιολογική έρευνα, μέσω των πληροφοριών που έχουν αποκτηθεί, σχετικά με τις μετα-αποθετικές μεταβολές που οι πλούσιοι σε SiO_2 φυτόλιθοι υφίστανται με την πάροδο του χρόνου, και τον τρόπο με τον οποίο αυτές σχετίζονται με την κινητικότητα άλλων στοιχείων στο εδάφος. Επιπρόσθετα, η ορυκτολογική και χημική σύνθεση των ανακτηθέντων φυτολιθών ελέγχεται με τη μέθοδο εξαγωγής, υποδεικνύοντας έντονα ότι η σύγκριση των φυτολίθων που λαμβάνονται από τα φυτά έχει νόημα μόνο εάν η μέθοδος εξαγωγής παραμένει η ίδια. Τα φυσικοχημικά χαρακτηριστικά των φρέσκων φυτολίθων που εξήχθησαν από τα φυτά παρείχαν χρήσιμες πληροφορίες σχετικά με την κατάσταση διατήρησης τους μετά από εργαστηριακή επεξεργασία, γεγονός που μπορεί να συμβάλλει περαιτέρω στη μελέτη των ηλικιωμένων φυτολίθων. Τα χαρακτηριστικά των διαστάσεων και της υφής της πλειοψηφίας των φυτολίθων αλλάξαν με την αύξηση του pH και της θερμοκρασίας, υποδεικνύοντας ότι οι επιμήκεις δενδροειδείς μορφότυποι μπορούν να τροποποιηθούν σε επιμήκεις ακανθώδεις ή/και επιμήκεις ανάγλυφους μορφότυπους. Επιπρόσθετα, η μελέτη προσέφερε πληροφορίες σχετικά με τα χαρακτηριστικά των φυτολίθων μετά από καύση. Οι φυτόλιθοι που λήφθηκαν από τα φυτά με τη χρήση της ξηρά μεθόδου εξαγωγής είναι συνεπώς κατάλληλοι για περιστατικά φωτιάς με εφαρμογές στην αρχαιολογία. Ο συνολικός φυσικοχημικός χαρακτηρισμός των φρέσκων φυτολίθων μπορεί να προσφέρει περαιτέρω στην ερμηνεία φυτολιθικών συνόλων από παλαιοντολογικά, αρχαιολογικά και εθνογραφικά πλαίσια για τη διαχρονική μελέτη των αλληλεπιδράσεων ανθρώπου-φυτού.

Λέξεις κλειδιά: βιοορυκτοποίηση, φυτόλιθοι, μέθοδοι εξαγωγής, σιτάρια, βιογενές πυρίτιο, διαλυτοποίηση, κινητικότητα χημικών στοιχείων, γεωχημεία, γεωαρχαιολογία, αρχαιοβοτανική

Every day, before our eyes,
the highest forms of life are springing
from a very elementary form.

H. Bergson

1 INTRODUCTION

1.1 Plant biomineralisation: the case of SiO_2-rich phytoliths

Since Earth's dawn, energy flow embeds life through biogeochemical cycles (Morowits 1968). Biogeochemical cycles reflect the circulation of the chemical substances through biotic and abiotic compartments of the Earth. The behaviour of one element or compound affects the behaviour of another over space and time. Schrödinger (1944) argues that the subatomic particles should be understood not as isolated entities, but as interconnected entities. By analogy, each species -flora and fauna- has its own generative potential which is bounded in the biogeochemical cycles and interacts to its biotic and abiotic environment. Biogeochemical cycles (i.e. carbon, nitrogen, oxygen, silicon, phosphorus) have fundamental implications at regional or global scales (Conley 2002; Galloway 1996; Smil 2000; Song *et al.* 2012; Struyf *et al.* 2009). Terrestrial and marine plant species strongly affect the various silicon pools and their respective contribution to silicon cycle through biosilification process. Biosilification in particular is a biomineralisation process widely encountered across plant lineages, single cell organisms through to higher plants by which silicon is incorporated into organisms in the form of SiO_2 thereby forming patterned biosilica (Arnott 1982; Currie and Perry 2007; Ehrlich *et al.* 2010; Epstein 1994, 1999; Iler 1979; Perry 2003; Sangster *et al.* 2001; Trembath-Reichert *et al.* 2015).

Biomineralisation is the natural process by which living organisms -bacteria, protists, plants or animals- form/produce minerals. Biominerals can be inspiring as some of the most interesting forms of nature (Haeckel 1904). During biomineralisation, accumulations of organic and inorganic compounds with inhomogeneous distributions of diverse shapes and sizes are formed (Ehrlich *et al.* 2010; Lowenstam 1981; Lowenstam and Weiner 1989; Weiner 2010). The most common constituents of the human body that are

composed of biominerals are the bones and teeth (Mann 2001). Biominerals frequently involve amorphous silica, calcium carbonates, and calcium oxalates and phosphates alongside specialised organic macromolecules (Arnott 1982; Lowenstam 1981; Lowenstam and Weiner 1989; Trembath-Reichert *et al*. 2015; Weiner 2010). Biomineralisation may be biologically induced or biologically controlled (also termed matrix-mediated). In biologically induced biomineralisation the organism modifies its proximal environment and creates physicochemical conditions favoring mineral precipitation. On the other hand, in biologically controlled biomineralisation the formation of minerals is controlled by the organism, and organic matrices produced by the organism are responsible for the control *(*Aizenberg *et al*. 1994; He *et al*. 2014; Lowenstam 1981; Lowenstam and Weiner 1989; Webb 1999).

Biosilification has been an important process for terrestrial plants over their >400 myr evolutionary history (Conley 2002; Ehrlich *et al*. 2010; Perry 2003; Raven and Giordano 2009; Trembath-Reichert *et al*. 2015). It may occur in a large number of aquatic species, such as diatoms (Hildebrand and Wetherbee 2003), silicoflagellates (Preisig 1994) and radiolaria (Anderson 1983). In terrestrial plants, biomineralisation mainly involves the transport and mineralisation of silicon and calcium, and in particular silica i.e. SiO_2 (Currie and Perry 2007; Dietrich *et al*. 2003; Ehrlich *et al*. 2010; Lins *et al*. 2002; Piperno 1988, 2006), calcium carbonate (Nitta *et al*. 2006; Taylor *et al*. 1993) and calcium oxalate (Coté 2009; He *et al*. 2012a, 2012b; Lersten and Horner 2011; Mazen *et al*. 2004; Pérez Cuadra and Hermann 2013) in the non-protoplasmic inclusions (phytoliths, cystoliths and idioblasts) of plant cells. Smaller amounts of other chemical elements have also been identified in several plants (Franceschi and Schueren 1986; He *et al*. 2012a, 2012b; Horner and Wagner 1980; Krejci *et al*. 2011; Pritchard *et al*. 2000).

Phytoliths (Fig. 1) are microscopic biominerals formed in plant tissues that embed a wide array of information (Meunier and Collin 2001; Mulholland and Rapp 1992; Pearsall 2015; Piperno 1988, 2006). Phytoliths are the outcome of biomineralisation processes that occur during the life of most plant species, where a variety of minerals are being polymerised (Lowenstam 1981; Lowenstam and Weiner 1989; Weiner 2010). The category of SiO_2-rich phytoliths, known also as opaline, is a research tool of great importance to the geosciences and archaeology (Albert *et al*. 2009; Alexandre *et al*. 1997b; Andriopoulou 2014; Ball *et al*. 2016; Cabanes *et al*. 2012; Esteban *et al*. 2018; Madella *et al*. 2002; Tsartsidou *et al*. 2007; Rodríguez-Cintas and Cabanes 2017), especially when used in conjunction with other proxies. Silicon is recognised as a beneficial quasi-essential mineral nutrient for many plants, having also a great importance in the history of plant sciences (Browne 1944; Sachs 1862; de Saussure 1804).

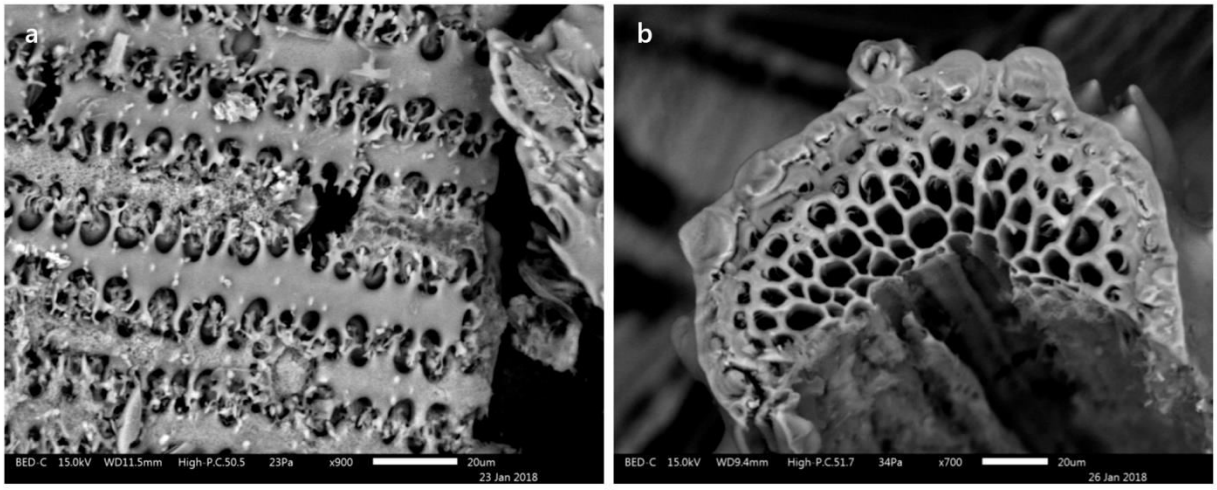

Fig. 1 SiO_2-rich phytoliths extracted from wheat through Scanning Electron Microscope (photomicrographs: Andriopoulou)

Silicon was first identified by Lavoisier in 1787, but was not isolated in an amorphous state until the work of Gay-Lussac in 1811 (Duffin 2006). Preliminary research in the chemistry of Si have been conducted, among others, by Marshall (1949), Hauser (1955),

Stöber (1956), Sosman (1965), and in phytoliths by Davy (1814), Struve (1835) and Ehrenberg (1841). Ehrenberg was the first to name these silica particles "phytolitharia" (Deflandre 1963), and therefore the term “phytolith” was introduced from the Greek φυτό+λίθος = plant+stone. The word opaline derives from opal, the Sanskrit word *upala*, meaning precious stone (Campbell 2017) or from *opalus*, the ancient Latin name for the gem (Pliny the elder 75-79, from Kostov 2008). According to Piperno (1988), at least four periods of phytolith research can be distinguished: “period of discovery and exploration by the pioneers Struve and Ehrenberg (1835-1895), “period of botanical research” (1895-1936), 3) “period of ecological research” (1955-1975), and “period of archaeological and palaeoenvironmental research” (1978-present). According to Hart (2016) there is a fifth period (2000-present), the “period of expanding applications”. The “period of expanding applications” includes, among others, studies on phytolith dissolution/preservation (Cabanes *et al*. 2011, 2015; Fraysse *et al*. 2006a, 2006b, 2009); and digital technologies like computer-based scanning software to study the phytolith morphometrics (Ball *et al*. 1999; Ball and Brotherson 1999; Evett and Cuthrell 2016; Out *et al*. 2014) and photogrammetry for refining phytolith measurable properties and identifications (Andriopoulou *et al*. 2019).

Plant growth depends on various mineral nutrient elements present in the soil. The study of the phytolith pool (biogenic SiO_2, plant-available Si, or pedogenic SiO_2) is based on the physical and chemical properties of nearly amorphous opal-A ($SiO_2 \cdot nH_2O$), the hydrated form of SiO_2. Silicon (^{14}Si) is ubiquitous on the earth surface; it is the second most abundant element in the earth’s crust after oxygen, making up approximately 25-28% of it (Duffin 2006; Wollast and Mackenzie 1983). Four stable isotopes of silicon exist in the natural environment: ^{28}Si, ^{29}Si, ^{30}Si and radioactive ^{32}Si, the first of which has the highest relative abundance on Earth (Barnes *et al*. 1975). Silicon dioxide is found in essentially in many living organisms. In humans, blood contains 1 ppm of SiO_2 (Baumann

1960, from Iler 1979), and chalcedony (a microcrystalline form of SiO_2) was also identified in the cerebral cortex and brain hippocampus (Figueroa *et al.* 2008). Silicon may also play a role in human collagen and bone health (Jugdaohsingh 2004, 2007), and the link between Si for plant growth and its implication for human health and dietary Si sources (plant-based food) should receive attention. Plants are in a continuous interaction with minerals and Si in plants is mainly derived from the weathering of silicate minerals such as quartz and feldspar in the soil (Prychid *et al.* 2003; Sommer *et al.* 2006), that constitute more than 75% of the earth's crust.

The elemental silicon is oxidised in biological systems and may be encountered as: (1) soluble monosilicic (known also as orthosilicic) acid [$Si(OH)_4$], a weakly acidic molecule (pKa 9.8) and fundamental building block used in the formation of SiO_2, or (2) its ionised form, polysilicic acid [$Si(OH)_3O_2$] (predominating at a pH>9.2), which is soluble but according to Casey *et al.* (2004) is probably immobile in plants (i.e. wheat) and (3) pure silica (SiO_2), the nearly amorphous and usually polymerised material produced from monosilic acid. Several variables affect the silica condensation from the molecular level upwards, solubility and preservation, including concentration, pH, temperature, and the presence of other ions (Iler 1979; Perry 2003).

The silicate minerals undergo biological, physical and chemical weathering and release Si into the soil solution that forms silicic acid (H_4SiO_4) (Drever 1994), which is an essential nutrient for terrestrial and aquatic plants. In natural systems, various soils contain different concentrations of Si depending on environmental and anthropogenic factors, such as the parent rock and plant cultivation (Matichenkov and Bocharnikova 2001; Meena *et al.* 2014; Sommer *et al.* 2006). The Si content can vary greatly, from ~1-45% dry weight in soils (Sommer *et al.* 2006) and it is has been reported that biogenic silicon that is dominantly composed of phytoliths may constitute an important Si-pool in

soil during plant litter decomposition (Lucas *et al.* 1993). Silicon in plants ranges from ~0.1-15% dry weight, mainly according to its available concentration in the substrate and the plant's phylogenetic variation (Epstein 1994, 1999; Hodson *et al.* 2005; Jarvis 1987; Kaltsikes and Larter 1970; Van der Vorm 1980).

Between the two major groups of Angiosperms, SiO_2 accumulation is generally greater in monocotyledonous than in dicotyledonous plants (Currie and Perry 2007; Ollendorf 1992). Phytoliths are produced only in higher monocotyledonous (i.e. only about half of the major clades within the monocotyledonous) (Prychid *et al.* 2003). The Poaceae (known also as Gramineae), Equisetaceae and Cyperaceae generally have the highest Si content (>4% dry weight) (Hodson *et al.* 2005; Piperno 2006). Plants that have higher than ~1.5% Si levels per dry biomass in their leaves are known as accumulators and plants that have levels below ~0.5% are known as non-accumulators (Marafon and Endres 2013). Silicon varies also depending on the soil type (Sommer *et al.* 2006) and plant's age (Ponzi and Pizzolongo 2003). It has been suggested that silification can be variable even within a single cell (Sørensen *et al.* 2008) and that older plants seem to contain more SiO_2 than their younger counterparts (de Saussure 1804; Henriet *et al.* 2008). The composition of nearly amorphous SiO_2, that is in general more soluble than its crystalline counterparts, transforms into a crystalline form with aging (Junius 1985; Wilding *et al.* 1977). It has been suggested that carbohydrate polymers, hemicellulose and cellulose, might influence/control ordered SiO_2 deposition in neutral pH conditions (Perry and Lu 1992). More research is still required to refine our understanding of the mineralogy and chemistry of SiO_2-rich phytoliths, including other chemical elements occluded in the phytolith body (so-called PhytOK), as well as the dynamic relationship between the SiO_2 deposits and their biogeochemical environment.

1.2 Phytolith formation and function in higher plants

Plants absorb Si from the soil solution in various amounts as monosilicic acid [$Si(OH)_4$] through their roots (Marschner 1995). After the uptake through the root system, Si in the form of silicic acid is deposited as amorphous silica within specific plant compartments (Fig. 2). Silicon uptake travels in the plant across water channels, such as aquaporines (Grégoire *et al.* 2012). Silicon is penetrating the xylem and then gets transferred to the shoots where it accumulates. Several channel-type and efflux transporters are required for the uptake, translocation, and distribution of Si inside the plant (Ma and Yamaji 2006). Sangster *et al.* (2001) studied the distribution of silicon during wheat plant growth and they found that the majority of the silicon provided should be in a solid state in the aerial parts in a relatively short time, after approximately 8-10 days.

Silicic acid is carried upwards to the aerial target organs through xylem, a water-conducting tissue which is part of the plant's transpiration stream (Piperno 1988, 2006), as a result of two main mechanisms (Liang *et al.* 2006; Mitani and Ma 2005). These mechanisms are the active transportation of $Si(OH)_4$ by metabolic processes (Ma and Yamaji 2008), and the passive non-selective flow along with other elements through the permeable plant membranes (Epstein 1999). Both active and passive uptake mechanisms may coexist within the same plant (Liang *et al.* 2007). Wheat is considered as an active transporter of silicon (Casey *et al.* 2004; Rains *et al.* 2006).

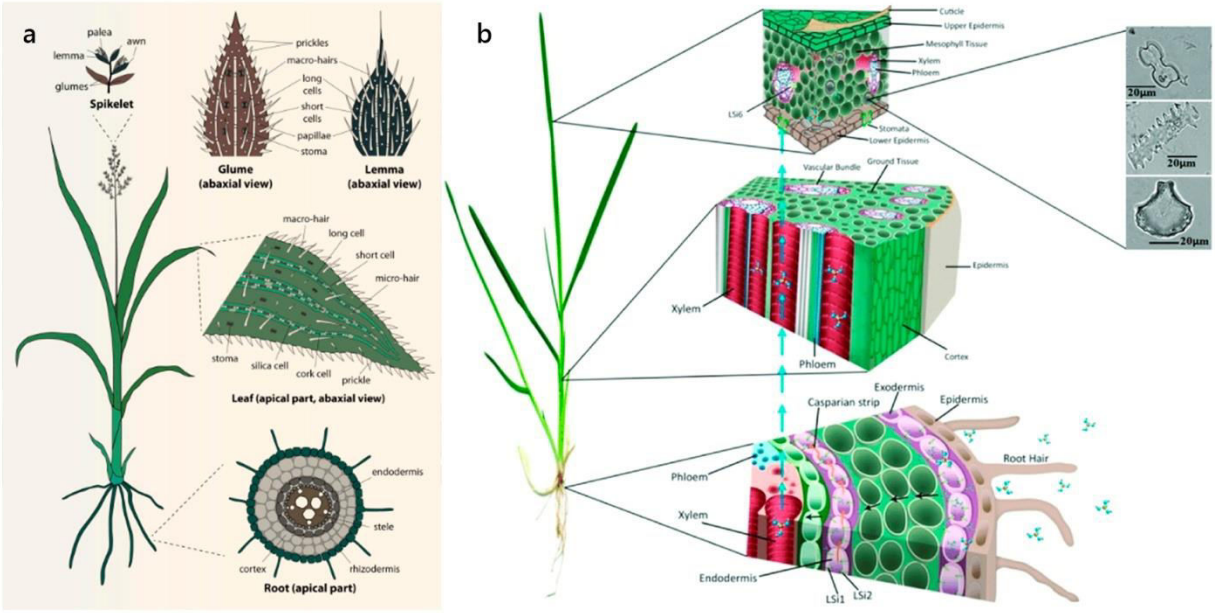

Fig. 2 (a) silica deposition in the root cross section, the leaf epidermis and the inflorescence of wheat. White colour represents silicified cells (source: Santosh *et al*. 2017); and **(b)** example of phytolith formation within *Oryza sativa* (rice) (source: Rashid *et al*. 2019)

The concentration of monosilicic acid ranges from approximately 0.1 to 0.6 mM in soil solutions (Epstein 1999). According to Curry and Perry (2007) there has been no evidence of the occurrence of biosilicification reactions in soil. Casey *et al.* (2004) suggested that in wheat sap the forms of silicon present were mono- and disilicic acids, with a ratio of 7:1; but this part of Si is minimal compared to the solid form. Thence, the monomer $Si(OH)_4$ which saturates at ~1.67 mM, condenses to form a polymer that has the composition $(SiO_2)_n$ in plant tissues (Currie and Perry 2007; Ma and Yamaji 2006). The SiO_2-rich phytoliths may vary colourless or light brown to opaque in colour (Jones and Beavers 1963; Parr 2006; Prat 1931, from Prychid *et al.* 2003), with a refractive index ~1.430-1.458 (Jones and Milne 1963) and are hydrated with ~2-15 wt.% water (Bartoli and Wildnig 1980; Piperno 2006). The silica is then deposited *in situ* within the growing plant, forming microscopic mineralised replicas of the cells. In that manner these discrete silica particles, phytoliths, may partly or wholly reproduce vegetal cellular morphologies, known as

morphotypes (ICPN Working Group: Madella *et al.* 2005; International Committee for Phytolith Taxonomy: Neumann *et al.* 2019).

Phytoliths range not only in form but also is size and deposition location (Piperno 1988, 2006). In particular, among plant taxa microscopic phytoliths occur in a variety of sizes, commonly 10-30 µm in diameter and up to 200 µm in length (Pironon *et al.* 2001). Silica can be deposited in various cellular locations, such as within or between cells or as part of the cell wall alongside polysaccharides like cellulose (Blackman 1969; Prychid *et al.* 2003). In monocotyledons, the phytoliths are primarily observed in the epidermis, common for most grasses and sedges (Prychid *et al.* 2003). Mehra and Sharma (1965) reported that sedge (Cyperaceae) phytoliths are only located over the veins. However phytoliths may also be located in the leaves of sedges and in the pericarp of nutlets (sedge 'cones') (Fuller, personal communication 2020; Weisskopf 2010). By comparison, phytoliths in other plants are almost exclusively observed in the sheath cells or vascular bundles, as in the case of palms (Arecaceaea) and bananas (Musaceae) (Prychid *et al.* 2003). In dicotyledons, arboreal or herbaceous, phytoliths are usually in the ray or axial parenchyma cells (Metcalfe and Chalk 1983). Silica usually remains in the same place once deposited (Raven 1983) and laid down in the aerial structures, both vegetative and reproductive (Piperno 2006). However it can rarely be found also in subterranean organs, i.e. the roots and sometimes in the rhizome, usually in very low concentrations (Sangster and Hodson 1992).

Silicon can be beneficial for many crops including wheat under stressful conditions (Bélanger *et al.* 2003; Eneji *et al.* 2008; Ma 2004; Yeo *et al.* 1999). For example, it has been suggested that silicon enhances wheat resistance to freezing stress (Liang *et al.* 2008) and oxidative damage under drought stress (Gong *et al.* 2005). Under salinity stress, wheat treated with silicon showed a decrease in sodium (Na) and chlorine (Cl) uptake

(Bybordy 2014; Saqib *et al*. 2008; Tuna *et al*. 2008) and an increase in macronutrients uptake, such as nitrogen (N), potassium (K) and calcium (Ca) (Mali and Aery 2008; Tuna *et al*. 2008). Biomineralisation in the plant kingdom may act as an agent for mechanical support, protection/defense, photosynthesis optimisation, detoxification, among others, and these functions may depend on the localisation, abundance, morphology, size and composition of the biominerals (Lowenstam and Weiner 1989; Pierantoni *et al*. 2018; Strömberg *et al*. 2016; Wainwright *et al*. 1976). There have been proposed several hypotheses about the functions of SiO_2-rich phytoliths in plants. Silicon as a quasi-essential element has an important role in plant life. By their deposition in inter- and intracellular spaces throughout the plant, phytoliths may give structural, physiological and protective benefits to plants (Epstein 1999; He *et al*. 2014; Liang *et al*. 2007; Piperno 1988, 2006).

Phytoliths may provide mechanical support to the plant and elasticity in the cells (Hossain *et al*. 2002), and may reduce transpiration rates and prevent the collapse of cell walls when water is moving through the plant and evaporates from its aerial parts (Gong *et al*. 2003; Raven 1983). Due to their high impermeability, phytoliths may play a protective role against the consumption of plant mass by herbivorous animals (McNaughton and Tarrants 1983), insects (Massey *et al*. 2006; de Souza *et al*. 2014) and pathogens (Chain *et al*. 2009). Recent studies have shown that phytoliths alongside other non-protoplasmic inclusions may promote photosynthesis. Indeed, due to their structure phytoliths may interfere with the interception and dispersal of sunlight to the chloroplasts, thereby enabling the plants to use the incoming light flux efficiently (He *et al*. 2014; Gal *et al*. 2012; Kuo-Huang *et al*. 2007; Pierantoni *et al*. 2017, 2018).

Soil contamination with heavy metals is widespread and it is suggested that phytoliths may also reduce the toxic effects of metals absorbed by the plant via ion-exchange processes. Zhang *et al*. (2017) suggested the following main mechanisms of silicon role in plant detoxification: adsorption, complexation/co-precipitation of toxic metal ions with silicon, immobilisation of toxic metal ions in growth media, uptake processes, and compartmentation of metal ions within plants. It has been reported that in wheat silicon (Si) may be responsible for the alleviation of cadmium (Cd) (Hussain *et al*. 2015; Rizwan *et al*. 2012), chromium (Cr) (Durgesh *et al*. 2015) and aluminium (Al) (Cocker *et al*. 1998) toxicity. Other authors however, have supported that Si is not effective in decreasing Al toxicity in wheat (Hodson and Evans 1995). Taken together the aforementioned previous work it is evident that SiO_2-rich phytoliths have a major bearing on plant life and thus for the ecosystem.

1.3 The importance of phytoliths for geosciences and archaeology

Botanical evidence in the archaeological record is subdivided into three main categories: (a) macroremains, (b) microremains and (c) chemical evidence (Ford 1979). Phytoliths (microbotanical remains) are of great importance to the geosciences and archaeology and the applications of the study of phytoliths in conjunction with other archaeobotanical remains are wide (Allué *et al*. 2017; Meunier and Collin 2001; Mulholland and Rapp 1992; Pearsall 2015; Piperno 1988, 2006; Strömberg *et al*. 2018). Phytolith morphotypes reproduce partly or wholly cellular morphologies and their morphological characteristics may lend themselves for the identification of plants up to the species level (ICPN Working Group: Madella *et al*. 2005; International Committee for Phytolith Taxonomy: Neumann *et al*. 2019; Parr and Sullivan 2005; Rudall *et al*. 2014).

It is important that the morphotypes are morphologically, mineralogically and chemically unaltered at the highest possible level to obtain robust information for the plant identification and be interpreted reliably. The different tissues in the plant organs have cells that often present distinct morphologies. When these cells are silicified they produce phytoliths that are characteristic of the various parts (Ball *et al.* 1999; Tsartsidou *et al.* 2007). Hence, certain phytolith morphotypes relate to specific parts of the plant (e.g. inflorescence, leaves, stem) that may correlate for example with specific past human activity (e.g. gathering, harvesting, irrigation, cooking, foddering) (Esteban *et al.* 2018; Hart and Matson 2009; Harvey and Fuller 2005; Rosen 1999; Rosen and Weiner 2004). An International Code for Phytolith Nomenclature that involves descriptions of the shape, texture and anatomical origin (i.e. histological location) of phytoliths has been developed (ICPN Working Group: Madella *et al.* 2005). Recently, an updated International Code for Phytolith Nomenclature has been developed by the International Committee for Phytolith Taxonomy: Neumann *et al.* (2019). Dentritic long cells, hair and papillae, for example, are linked to inflorescence, stomata and mesophyll are linked to to leaves and psilate long cells to leaves or stems.

The study of the relationship between humans and their environment, especially vegetation, is pivotal in archaeological (or historical) interpretation (Ingold 2000; Manetas 2018; Pearsall 2015; Renfrew and Bahn 2019). Phytolith study in archaeological sites may provide useful information about agro-pastoral practices and the use of space, water and fire, and further may shed light on the relationship between past humans and the plant environment, terrestrial or aquatic (mostly the former) and consequent impacts on modern human cognition (Albert *et al.* 2009; Alexandre *et al.* 1997b; Ball *et al.* 2016; Barboni *et al.* 1999; Braadbaart *et al.* 2019; Cabanes *et al.* 2009, 2012; Esteban *et al.* 2018;

Friesem *et al*. 2014; Madella *et al*. 2009; Petö *et al*. 2015; Rosen 2005; Rovner 1971; Shahack-Gross *et al*. 2014; Tsartsidou *et al*. 2007; Wroth *et al*. 2019).

Apart from soils and sediments, phytoliths have often been identified on several artefacts, such as tools (Dominguez-Rodrigo *et al*. 2001; García-Granero *et al*. 2017), pottery (Liu *et al*. 2020; Petö and Vrydaghs 2016; Thompson *et al*. 1995; Yao *et al*. 2012), baskets and mats (Rosen 2005; Wendrich and Ryan 2010), and rarely on textiles (Zhang 2016) and paper (Li 2018), all providing information on human activity. The understanding of human activity is fundamental to archaeology (Renfrew and Bahn 2019). Hodder (2012) proposed that ''*entities (isolated substances) and objects (things presented to the mind) can only be known through their property of being things (that unite people and other things into homogenous mixtures)*''. Phytoliths may be also detected in human teeth (Cummings and Magennis 1997; Gügel *et al*. 2001; Lalueza Fox *et al*. 1994*;* Reinhard and Danielson 2005), animal teeth (Acuña-Mesén and García-Díaz 1998; Cionchon *et al*. 1990; Winklera *et al*. 2019) and the digestive system or faeces (Chapuis 1980; Chevalier *et al*. 2001) providing information, among others, on the (palaeo)diet, (palaeo)pathology and (palaeo)environment.

The last decade there has been growing interest in the identification of cereals or cereal preparations (Fuller and Gonzalez Carretero 2018; Hayden *et al*. 2016; Liu *et al*. 2020; Valamoti 2011), and especially wheat (often when its chaff has been processed) in the archaeological contexts using, among others, phytolith analysis (Albert *et al*. 2008; Andriopoulou 2014; Ball *et al*. 1999; Berlin *et al*. 2003; Cabanes *et al*. 2012; dal Corso *et al*. 2018). Cereals (e.g. wheat, barley, oat, rye, corn, rice, sorghum, millet) are of high significance to the economy for their adaptability to different environmental conditions, and of the approximately 10,000 grass species in the Poaceae family, about 50 are

cultivated as cereals, of these fewer than 12 can be considered major crops (Murphy 2007).

Wheat, a monocotyledonous grass, absorbs quite a large amount of Si, approximately 50-150 kg Si ha^{-1} (Snyder *et al.* 2006) and its phytolith production can be about 20 times greater than in the wood/bark of dicotyledons (Albert and Weiner 2001). Wheat is a significant food source for humans, an important animal feed, and it is a rich source of secondary products that has played a central role in human economies from the pre-agricultural phase to the first agricultural societies and up to the present (Jones *et al.* 1998; Nesbitt and Samuel 1996; Valamoti 2009; Zohary *et al.* 2012). People have used wheat and its derivatives for a very long time for food, to make beverages, for medicine, as food for animals or straw for bedding and for other uses such as a structural material, fuel, temper for pottery and for industrial purposes (Valamoti 2009, and references therein). Furthermore wheat is not only used in everyday life settings but also in feasts and rituals (Megas 2001; Miligou-Markantoni 2006). Wheat remains in archaeological sites in Greece are an important source of information (Megaloudi 2006; Sarpaki 1995; Valamoti 2003, 2009) and archaeological records very often contain phytolith assemblages.

Archaeobotanical assemblages suggest that *Triticum turgidum* L. subsp. *dicoccon* (Schrank) Thell. [emmer, tetraploid (2n=28 chromosomes), hulled (i.e. the glumes tightly enclose the grains) wheat] is especially prominent in Neolithic and Bronze Age, and especially throughout the Near East. The noun ''dicoccon'' in Greek when forming adjectives may become ''dicoccum'' in Latin (Morrison 1998, from Goncharov *et al.* 2009). Emmer wheat was one of the first cereals domesticated in the Old World, cultivated from approximately 9700 BCE in the Levant (Fuller *et al.* 2012), and subsequently in South-

Western Asia, Northern Africa and Europe with the spread of Neolithic agriculture (Fuller and Lucas 2014). *Triticum monococcum* L. subsp. *monococcum* [einkorn, diploid (2n=14 chromosomes), hulled wheat] is also sometimes present in prehistoric Greece (Colledge and Conolly 2007; Evans 1964; Halstead 1994; Jones 1986; Kroll 1981, 2003; Megaloudi 2006; Renfrew 2003; Sarpaki 1995; Valamoti 2003) and Cyprus (Colledge and Conolly 2007; Falconer and Fall 2013; Hansen 1994).

Triticum monococcum L. subsp. *monococcum* with normally single-grained spikelets is the domesticated variety of its wild progenitor, *Triticum monococcum* L. subsp. *aegilopoides* (Link) Thell [wild einkorn, diploid (2n=14 chromosomes), hulled wheat], which started being widely cultivated by humans at approximately 7500 BCE, during the Pre-Pottery Neolithic A (PPNA) or B (PPNB) periods (Zohary *et al.* 2012). Cultivated einkorn remains have been found in sites of the Fertile Cresent and the Eastern Mediterranean, such as Abu Hureyra in Syria (de Moulins 2000), Jericho in Palestine (Hopf 1983), Franchthi Cave in Greece (Kroll 1981) and Cap Andreas-Kastros in Cyprus (Van Zeist 1981). *Triticum turgidum* L. subsp. *durum* (Desf.) Husn. [tetraploid (2n=28 chromosomes), hard, naked (i.e. free-threshing) wheat), is also present but rare and becomes apparent in the Mediterranean only later, during the Bronze Age (Evans 1964; Valamoti 2009). In modern-day Greece, the cultivation of *Triticum monococcum* is more limited compared to *Triticum durum*, mostly used in pasta production and *Triticum aestivum* L. subsp. *aestivum* [hexaploid (2n=42 chromosomes), soft, naked bread wheat], mostly used in bakery and milling (Rubel 2011; Valamoti 2009). Detailed taxonomic classification of wheats is provided, among others, by Goncharov *et al.* (2009). Additional ''lost''/extinct archaeological wheat species have been reported (Fuller *et al.* 2012; Köhler-Schneider 2003).

Agricultural origins is a topic of continuing interest among geoscientists and archaeologists, and phytolith analysis is a useful tool for the distinction between some domesticated and wild plants (Ball *et al.* 2016; Pearshall *et al.* 2015). For example, double-peaked glume cell phytoliths from the husks are unique to the genus *Oryza* and may separate domesticated rice from the wild rice species (Gu *et al.* 2013; Lu *et al.* 2002; Zhao *et al.* 1998). Furthermore, it has been suggested that within the genus *Triticum* the inflorescence papilla phytoliths increased in size and pit number as ploidy level of wheat increased (Tubb *et al.* 1993, from Hodson 2016). Ploidy levels of domesticated wheat species range from diploid (2n=14) to hexaploid (2n=42) (Dvorak 2001; Matsuoka 2011). The analysis of well preserved phytoliths may also facilitate the distinction between closely related grasses, such as wheats and barleys (Andriopoulou 2014; Ball *et al.* 1999).

Phytoliths have also ecological and geochemical significance and they are used for understanding silicon cycling (Conley 2002; Struyf *et al.* 2009), potassium cycling (Nguyen *et al.* 2015) and for carbon sequestration (Parr and Sullivan 2005). Palaeoenvironmental reconstruction is based on geomorphological, sedimentary and biological indicators (Lowe and Walker 2007, from Karkanas 2010b). Evidence for the flora of an area comes mainly from the biological indicators that include phytoliths, pollen, seeds, calcified root systems, leaf impressions in sediment, and carbonised, waterlogged or desiccated plant remains (Pearsall 2015; Piperno 1988, 2006). Phytolith analysis has often been employed sometimes alongside palynology for the study of the palaeoclimate and palaeovegetation (Barboni *et al.* 1999; Calegari *et al.* 2015; Rovner 1971; Scott 2002) and for the distinguishing of various photosynthetic pathways in plants within a particular region (McInerney *et al.* 2011; Twiss 1986). Quaternary records provide an opportunity to examine the nature of the vegetation in relation to climate change. Palynology provides strong indicators of regional climatic and environmental conditions

(Burjachs 1994; Sánchez Goñi *et al.* 2017), whereas phytoliths are strong indicators of local conditions (Piperno 2006; Traoré 2015).

The applications of the study of phytoliths are therefore wide for the understanding of the choices made by humans from prehistoric times to the present day. From the aforementioned it becomes apparent that phytoliths are a suitable tool for geoarchaeology and for investigating paleontological, archaeological and ethnographical contexts. Phytoliths may also provide complementary information to various scientific disciplines. They are important biosignatures not only for the research of the past but also, in combination with palynological analysis, for soil discrimination in forensic science investigation (Marumo and Yanai 1986). Furthermore, plant silica has been tested for use in high performance concrete (Chandrasekhar *et al.* 2002) and as a filler in epoxy resin for electronic devices (Suwanprateeb and Hatthapanit 2002). Plant silica has been also studied for medical purposes, such as for pharmacological applications (Umemoto *et al.* 1973), and for health problems in animals (Forman and Sauer 1962) and in humans (O'Neill *et al.* 1986). Finally, phytoliths have the potential for use in bio-inspired nanotechnologies (Neethirajan *et al.* 2009) that may contribute to the development of new materials for optical, biomedical and other innovative applications.

Despite SiO_2-rich phytoliths being an emerging research field, the interest has remained limited to their classification and morphometry, and not enough emphasis has been given on understanding phytolith composition and stability in relation to the biogeochemical environment or/and laboratory processes. It is important to evaluate the state of preservation of a fossil assemblage of phytoliths before interpreting its archaeological significance. This doctoral thesis aims to contribute to this relatively lack of empirical study and to expand this field.

In particular, a multi-analytical characterisation of studied phytoliths was performed in order to understand their microstructure, mineralogy, chemistry after their extraction from plants, soils and archaeological sediments. Physicochemical characteristics of fresh phytoliths extracted from wheats provided useful information on the their preservation state after laboratory processing (Andriopoulou and Christidis 2020). Factors like temperature and water availability may alter phytolith behaviour and under alkaline pH conditions they can partially or totally dissolve (Bartoli and Wilding 1980; Cabanes *et al.* 2011, 2015; Fraysse *et al.* 2006a, 2006b, 2009; Loucaides *et al.* 2010; Nguyen *et al.* 2014; Prentice and Webb 2016). Here, the dissolution mechanism and kinetics of SiO_2-rich phytoliths is later investigated in relation to variations of pH, temperature and time. Additionally, the integrated use of microscopy and photogrammetry for the 3D representation of phytoliths and other biominerals was proposed as a useful tool in geoarchaeology (Andriopoulou *et al.* 2019).

2 RESEARCH QUESTIONS

Lavoisier (1743-1794) considered nature a vast chemical laboratory in which all kinds of composition and decomposition are taking place (Fonash and Marcel 2018). Within this framework, SiO_2 is usually chemically more stable and less prone to biological degradation than other biominerals, rendering SiO_2-rich phytoliths relatively resistant to pre- and postdepositional processes in soils and sediments. In most studied cases, the concentrations of phytoliths in soils are relatively lower than the concentrations of phytoliths in archaeological sites (Albert *et al.* 2001; Cabanes *et al.* 2012; Tsartsidou *et al.* 2008). For a better understanding of the responses of biogenic SiO_2 pools to anthropogenic impact, it is crucial to obtain knowledge on phytolith physicochemical characteristics.

Phytoliths are accumulated in soil horizons alongside other remains (Piperno 1988, 2006; Weiner 2010) through the succession of taphonomic processes: necrolysis, biostratinomy and diagenesis (Madella and Lancelotti 2012). Plants are also known to recycle phytoliths deposited in the soils where they grow (Alexandre *et al.* 1997a; Cabanes *et al.* 2012). Generally, phytoliths are considered to have minimal dispersion after deposition, forming a record of the vegetation that has been deposited *in situ* (Piperno 2006). This, however, depends on the soil characteristics, e.g. in cases of vertical transport in sand-formed soils (Fishkis *et al.* 2010) or secondary parameters, e.g. biological activity (Hart 2003). It has been suggested, for example, that earthworms might increase the amount of water-extractable Si in the soil, thus contributing to Si-availability for plants (Georgiadis *et al.* 2019). In an early study, Kutuzova (1968) showed that during the first stages of biogenic SiO_2 decomposition, the plant tissue becomes an arena for microbial activity growth, mainly for bacteria and fungi. The study of the impact of bacteria or/and fungi on phytolith dissolution still remains very limited (Alfredsson *et*

al. 2016; Kutuzova 1968; Fraysse *et al*. 2010; Struyf *et al*. 2007), and might be worth investigating further.

The highest phytolith concentrations are usually found in the topsoils of undisturbed soils (Sommer *et al*. 2006) and decrease with depth (Cabanes and Shahack-Gross 2015). Phytoliths are released to the topsoil after the degradation or burning of the plants or dung, and subsequently they may gradually be transferred to deeper horizons or evacuated by hydrographical or/and aerial pathways (Piperno 1988, 2006). For example, it has been reported that wildfires may cause a re-distribution of phytoliths in an area, with the resulting ashes containing a mix of both local and non-local phytolith assemblages (Fredlund and Tieszen 1994). In any case, the distribution of phytoliths in the soils and sediments is related to the ratio of phytolith input (e.g. plant degradation) to output (e.g. dissolution processes) in a system (Alexandre *et al*. 1997a, 1997b).

When phytoliths are deposited in certain biogeochemical environments they may rarely be preserved over extremely long periods of time, including millions of years (Bamford *et al*. 2006; Prasad *et al*. 2005). Due to the relative durability of the biomineral, the replicated silicate forms may endure the plant's life and its decay, even in the cases where the plant is digested and discharged by animals (i.e. dung/coprolites) (Cabanes *et al*. 2009; Miller 1984; Karkanas 2006; Shahack-Gross *et al*. 2005; Smith *et al*. 2019), or/and in cases of (controlled) fire (Albert and Cabanes 2008; Esteban *et al*. 2018; Friesem *et al*. 2014; Karkanas *et al*. 2002; Rowlett 2000; Out 2009). According to Albert and Cabanes (2008) the remaining burnt residues of the combustion depend on the use of naturally-dried or fresh fuel. Rowlett (2000) studied a series of red campfire-sized patches in Kenya dating back ca. 1.6 million years, and the results from the multi-analysis of the spikey-looking spherical phytolith concentrations suggest that, among others, palm wood was used as fuel for the putative fires.

In order to obtain robust information regarding plant identification and to interpret phytoligh assemblages reliably, it is important that phytolith morphotypes remain morphologically, mineralogically and chemically unaltered at the highest possible level. Alterations in phytolith morphology may occur at temperatures as low as 600ºC (Runge and Runge 1997); however phytoliths from some species retain their diagnostic morphologies even up to 1000ºC (Wu *et al.* 2012). In a recent experiment investigating the alterations occurring in wheat phytoliths under exposure to temperatures between 550ºC and 1050ºC (unpublished personal data), it was found that certain morphotypes (e.g. rondels) usually preserve their morphological characteristics up to 900ºC, whereas when heated beyond 1050ºC they get vitrified. These observations are more pronounced when the phytoliths originate in the inflorescence, than the stem-leaves of the plant.

Even though phytoliths, compared with other archaeobotanical remains, remain relatively stable for a long time under the impact of taphonomic processes in most cases (Bamford *et al.* 2006; Prasad *et al.* 2005), their stability is frequently affected by the geochemical parameters of their burial environment (Bartoli and Wilding 1980; Cabanes *et al.* 2011; Cabanes and Shahack-Gross 2015; Karkanas 2010a; Loucaides *et al.* 2008). The composition of phytoliths is evidently affected by a variety of alterations caused by *in situ* taphonomic (Albert *et al.* 2006; Madella and Lancelotti 2012) or/and laboratory processes (Andriopoulou and Christidis 2020; Jenkins 2009). However, the preservation status is one of the most important factors for the reliable interpretation of archeological assemblages (Goldberg and Macphail 2006; Karkanas 2010a, 2010b; Schiffer 1987) including phytoliths. Parameters that affect the stability of phytoliths may include, among others, the morphology, chemistry and mineralogy of the primary material, the reaction time, soil pH, temperature, exposure to fire, humidity, the solid/liquid ratio, ventilation, pressure, certain mechanical forces, bioturbation, the activity of the plant's roots and various microorganisms/insects/fungi, and other secondary conditions that may affect

phytoliths to a great extent. Therefore it is recognized that the context where phytoliths are found has an impact on their preservation.

The various phytolith morphotypes do not have the same resistance to depositional and post-depositional processes and this should be taken into consideration in order to avoid interpretation errors of phytolith assemblages. Cabanes *et al.* (2011) suggested that individual phytolith morphotypes from wheat demonstrate various levels of stability under alkaline conditions and that the presence of relatively unstable morphotypes (e.g. hairs, papillae and long cells with decorated margins) is the best indicator of a well-preserved assemblage. According to previous results, ''modern'' inflorescence phytoliths are less stable than those from the stem-leaves, the ca. 3000 year old fossil phytolith assemblage is more stable than the modern assemblage, and burnt phytoliths are less stable than unburnt ones. Colouration and refractive index are two helpful parameters towards determining if a phytolith assemblage has been subjected to burning. Burnt phytoliths usually have a dull opaque finish (Parr 2006), and when an assemblage contains a large fraction of individual phytoliths with a refractive index higher than 1.440 it is indicative of exposure to burning (Elbaum 2003).

Taphonomic processes (e.g. dissolution and transport) may have an impact on the successive disarticulation/fragmentation, weathering or/and the potential destruction of SiO_2-rich phytoliths. Dissolution of biominerals remains only partially understood up to this day and it has become one of the most contemporary prominent and promising topics for interdisciplinary research. Fraysse *et al.* (2009) suggest that datasets on phytolith dissolution and reactivity in soil solutions should be introduced into conventional computer codes that describe the weathering process, such as PROFILE (Sverdrup and Warfvinge 1993) and WITCH (Godderis *et al.* 2006). This would be beneficial towards the understanding and prediction of dissolution processes in soil

systems. To obtain a better understanding of the large amount of chemical reactions and processes taking place in aquatic solutions, the study of the physicochemical properties of the material subjected to dissolution is necessary.

Previous studies on the terrestrial biogeochemical cycle of silicon show that phytoliths may undergo total or partial dissolution, especially in alkaline environment (Cabanes *et al.* 2011; Cabanes and Shahack-Gross 2015; Fraysse *et al.* 2006a, 2006b, 2009; Loucaides *et al.* 2008, 2010; Nguyen *et al.* 2014; Prentice and Webb 2016), and transport in the burial environment (Hart 2003; Hart and Humphreys 1997; Denis 2017; Farmer *et al.* 2005; Fishkis *et al.* 2010). The dissolution of Si-O-Si linkages includes hydrolysis in an excess of water, release of monosilicic/orthosilicic acid (Si-O bonds) according to this reaction $SiO_2+2H_2O \leftrightarrow Si(OH)_4$ (break of Si-O bonds occurs) and formation of Si-OH (silanol) groups (Dove and Crerar 1990; Iler 1979). When siloxane bonds that surround the surface silicon are broken, the latter is removed from the surface in the form of a silicic acid molecule, $Si(OH)_4$. Increasing pH usually leads to the deprotonation of surface silanol groups, further supporting the breaking of the bridging siloxane bonds (Dove and Elston 1992). Base promoted dissolution of biosiliceous material takes place when the solution pH exceeds the point of zero surface charge (pH_{zpc}) of the solid, which for biogenic SiO_2 is in the range of 1.2-4 (Dixit and Van Cappellen 2002).

Dissolution depends, among others, on a variety of factors, such as pH, temperature, time, ionic strength, the nature of the original material of study and that of the solvents being used. The SiO_2 solubility increases with pH increase, and especially when pH>9 (Iler 1979). Alkali cations (e.g. $\equiv SiONa^0$) adsorbed on the SiO_2 surface may often promote the dissolution kinetics of silica (Dove and Elston 1992). Additionally, apart from pH, temperature (Van Capellen and Qiu 1997a) and time (Dove and Elston 1992) are crucial factor for the evolution of SiO_2 surface reactivity.

Physicochemical properties of plant SiO_2-rich microstructures affect their dissolution kinetics. Fraysse *et al.* (2006b) suggested that surface areas of *Nastus borbonicus* (bamboo) phytoliths indicated large differences during dissolution. Bamboo belongs to Bambusoideae that is a subfamily of the Poaceae family (Soreng *et al.* 2015). Dissolution is a significant factor affecting the progressive alteration of the physicochemical characteristics of SiO_2-rich phytoliths, having a strong impact on the preservation and surface quality of their morphotypes, and therefore it should be taken into consideration for reliable geoarchaeological interpretations. In general, scientific interest has remained limited to the systematic classification and morphometry of phytoliths, and the various methods of determining the preservation status of phytolith assemblages mainly rely on visual examination that focuses on the presence or absence of morphotypes which are weathered and display pitted surfaces or/and irregular decoration (Fredlund and Tieszen 1994; Piperno 2006). Phytoliths of certain plant species tend to be either more soluble than others or showed similar solubilities. For example phytoliths from beeches (Fagaceaee) and horsetails (Equisetaceae) are less resistant to dissolution than phytoliths from pines, or some plants (larch tree and elm, horsetail, fern, and grasses) dissolution rates are similar (Bartoli and Wilding 1980; Fraysse *et al.* 2009). Previous studies have shown that the solubility of SiO_2-rich phytoliths is similar to that of inorganic amorphous silica, and that their dissolution rates are between those of quartz and vitreous silica, exhibiting similar pH dependence (Fraysse *et al.* 2006a, 2006b, 2009).

Environmental heterogeneity may play a significant role in silicon accumulation. The biogeochemical cycle of silicon is dynamic and connects many terrestrial, lacustrine and marine environments (Alexandre *et al.* 1997a; Mackenzie and Garrels 1966; Tréguer *et al.* 1995) in the long (Berner 2003) and in the short (Puppe *et al.* 2017) term. Plants, especially cereals, play a major role in silicon cycling in terrestrial ecosystems (Guntzer *et al.* 2012), and phytoliths exert a strong influence on the Si-cycle in superficial continental

environments (Piperno 1988, 2006). In temperate ecosystems, an average of ~60% of the biogeochemical cycle of silicon is controlled by phytoliths (Gérard *et al.* 2008). Plants are known to be an important source of silicon that is 10^2 to 10^4 times more soluble than silicon from the weathering of silicate minerals (Fraysse *et al.* 2010). Enhanced chemical weathering provides pools of elements to the soils and sediments. The weathering of silicate minerals such as feldspars, amphiboles, and pyroxenes, mainly through hydrolysis, leads to the formation of phyllosilicates (secondary aluminosilicates) and the release of dissolved silicon (H_4SiO_4) (Currie and Perry 2007), which is an essential nutrient for numerous terrestrial and aquatic organisms (Guntzer *et al.* 2012). It has been suggested that the silicon flux from land to ocean contributes to more than ca. 80% of the dissolved silicon input to the oceans (Tréguer *et al.* 1995). Furthermore, a major fraction of dissolved silicon enriching the rivers may originate not only from the weathering of silicate rocks, but also from the dissolution of phytoliths and freshwater diatoms (Derry *et al.* 2005).

Diatom frustules and phytoliths are both composed of hydrated amorphous SiO_2 and according to Van Cappellen *et al.* (2002) there is a difference in the dissolution rates and surface properties of fresh versus sedimentary diatoms, probably due to differences in specific surface area, possible aluminium content, temperature, and degree of undersaturation. Other studies suggested that the solubility of aquatic biogenic silica is highly dependent on temperature, within the ranges of ~800-1,000 mM Si at 3°C and ~1,500-1,700 mM Si at 23°C (Lawson *et al.* 1978; Kamatani 1982). The biogenic pool is mainly composed of phytogenic/plant-derived (e.g. phytoliths) and protistic/protophytic (e.g. diatoms) silica (Puppe *et al.* 2017; Sommer *et al.* 2006), but there are also minor components of zoogenic (e.g. sponge spicula) (Maldonado *et al.* 2011), protistic/protozoic (e.g. testate amoebae) (Aoki *et al.* 2007) and microbial (e.g. bacteria) origin (Sommer *et al.* 2006). An integrated approach about the dynamics of biogenic

silicon accumulation is pivotal for the deeper understanding of the biogeochemical cycling of silicon. Even though the biogeochemical cycle of silicon has been studied extensively, the majority of existing studies has restricted its focus the sinlge-cell photosynthetic microalgae class of diatoms (Moschen *et al.* 2005; Van Cappellen *et al.* 2002).

Biomineralisation, dissolution, and preservation processes are dependent on a variety of biological, physical and chemical parameters. Despite the significant contributions on phytolith analysis, the majority of the recent studies on SiO_2-rich phytoliths have not put enough emphasis on the investigation of phytolith stability (especially wheat-derived) in relation to the biogeochemical depositional environment and on the preservation of their morphotypes, while maintaining at the same time a focus on the influence of important environmental parameters such as water availability, temperature and soil pH. As pH increases, the deprotonation of silanol groups ($>Si\text{-}OH^0 \leftrightarrow Si\text{-}O^- + H^-$) takes place, facilitating the breaking of bridging siloxane bonds ($>Si\text{-}O\text{-}Si<$) (Dove and Elston 1992). Loucaides *et al.* (2008) studied the dissolution rates of phytoliths, diatoms, biosiliceous lake sediments and synthetic silica for a pH typical of seawater (pH 8.1) and a pH typical of a river water (pH 6.3), and proposed that the average dissolution rates double as pH increases.

''At the fundamental level reactions between solids and liquids involve a coupled sequence of mass transport, adsorption/desorption phenomena, heterogeneous reaction, chemical transformations of intermediates, etc., whose identification, separation and kinetic quantification are all necessary if the mechanism of the process is to be fully understood and described'' (Compton *et al.* 1993, from Dorozhkin 2012). The degree in which the presence of other chemical elements affects the dissolution of phytoliths, subsequently affecting their preservation in soils and sediments, has been scarcely covered. According

to previous studies, the dissolution rates of SiO_2 are enhanced by the presence of alkali salts, probably because the alkali cations enhance the nucleophilic properties of water and therefore increase the frequency of hydrolysis attacks at the surface of SiO_2 (Dove and Elston 1992). For example, aluminium and iron oxides in soils usually interact with SiO_2 and produce colloidal complexes that are not taken up by biological systems and hence may reduce the availability of soluble silica (Exley and Birchall 1992).

Apart from the impact of pre- and postdepositional processes, including excavation sampling, the different laboratory processes of extraction from plants, soils, sediments and artefacts/ecofacts (e.g. pottery/dental calculus) may also cause morphological, structural and compositional alterations of the phytolith morphotypes, introducing various biases for the interpretation of the phytolith record. Reference collections of phytoliths extracted from ''modern'' plants are a valuable tool for the study of phytoliths from archaeological sites (Pearsall 2015; Tsartsidou 2007). The most widely and well established methods of phytolith extraction from modern plant material are the dry ashing (or the use of spodograms, spodos<σπόδος in Greek<ash) and the wet ashing (known also as acid digestion) methods (Bowdery 1989; Corbineau *et al.* 2013; Piperno 1988; Rovner 1971, 1972). Both extraction methods may alter the resulting material in a different manner (Jones and Milne 1963; Pearsall 2015; Piperno 1988). Paracelsus (1493-1541), used extensively the dry ashing of plants for alchemical uses and for the preparation of spagyrics (Junius 1985). Other, less common methods of phytolith extraction are microwave digestion (Parr *et al.* 2001) and acetolysis (da Costa *et al.* 2016).

The dry ashing method involves heating at ca. 550°C for 4-6 h to oxidise the organic material, followed by the chemical treatment of the resulting ashes with hydrochloric acid for the removal of carbonates and hydrogen peroxide for the removal of residual organic matter (Bowdery 1989; Parr *et al.* 2001). In wet ashing, the phytoliths are oxidised with

sulphuric acid (H_2SO_4) and hydrogen peroxide (H_2O_2) (Geis 1973; Kelly 1990), or more commonly with nitric acid (HNO_3) and potassium chlorate ($KClO_3$) (Bowdery 1989; Rovner 1971, 1972). Even though the evaluation of the impact of extraction methods on the state of phytoliths (after the completion of laboratory processes) is of high importance for the assessment of the representative nature of the resulting phytoliths with respect to the original phytolith input, only a few studies have focused on this issue (Jones and Milne 1963; Jenkins 2009; Kameník *et al.* 2013; Nguyen *et al.* 2014; Parr *et al.* 2001; Sun *et al.* 2012; Wang *et al.* 2014).

Besides the existing bibliography on the composition of phytoliths (Anala and Nambisan 2015; Bartoli and Wilding 1980; Buján 2013; Carnelli *et al.* 2002; Hart 2001; Hodson *et al.* 2008; Javed *et al.* 2010; Jones and Beavers 1963; Lanning *et al.* 1961; Morikawa and Saigusa 2004; Puppe and Leue 2018; Shillito *et al.* 2009; Wu *et al.* 2014; Wüst and Bustin 2003), to the extent of our knowledge, only few studies focus on the impact of laboratory extraction processes on phytolith composition (Kameník *et al.* 2013; Nguyen *et al.* 2014; Watling *et al.* 2011; Wilding and Drees 1974). In order to understand phytolith characteristics with the least possible bias, a suitable method of extraction that produces the most phytoliths and that is the least aggressive on the resulting material should be carefully selected.

Wilding and Drees (1974), for example, analysed opals from soils and plants with a combination of the dry and the wet method, as well as low-temperature ashing at oxidising atmosphere. The main crystalline phases identified were α-quartz and cristobalite associated with an amorphous opaline phase in soil and leaf isolates, and their occurrence was attributed to synthesis within tissues as a function of plant metabolism and subsequent deposition in the soil. In an early study on plant opals from soils, Jones and Beavers (1963) studied, among others, their chemical composition, XRD

patterns, infrared spectra and differential analysis curves. Kameník *et al*. (2013) analysed *Hordeum vulgare* (barley) phytoliths extracted with the dry and wet methods, followed by calcination (at 600°C for 50 min), using neutron activation analysis and concluded that the sole use of the wet method was inefficient in the removal of organic matter. Moreover, in ashed *Oryza sativa* (rice) samples (at 400°C for 6 h), the soluble Si was up to 46% of total Si content of the ashes, indicating that the burning of the straw may produce SiO_2-rich ashes for an appropriate Si supply of crops in short term (Nguyen *et al*. 2014). Wu *et al*. (2014) observed a negative relationship between the flux element composition in phytoliths and the temperatures at which rice phytoliths from different parts of the plant deform. After the use of the wet method, the occluded carbon of *Bambusa vulgaris* (common bamboo) phytoliths indicated the presence of cellulose, lignin and carboxylic acids in addition to amine nitrogen and ammonia (Watling *et al*. 2011). Calcination of (*Triticum* spp.) wheat husks (up to 500°C for 1h) and subsequent treatment with potassium permanganate ($KMnO_4$) solution enhanced the formation of amorphous SiO_2 in the oxidising environment, without formation of other mineral phases (Javed *et al*. 2010). More recently, variations in the transmission FTIR and DRIFT spectra were reported between biogenic silicon structures such as fresh phytoliths extracted from plants (Poaceae and Equisetaceae) using the dry method (at 450°C for 12 h) and aged phytoliths from soils (Puppe and Leue 2018). The fresh phytoliths showed organic impurities that might be assigned to occluded organic matter, while aged phytoliths showed additional impurities of mineral origin. Tran *et al*. (2019) examined the possible encapsulation of Cu in phytoliths extracted from *Axonopus compressus* (carpet-grass) using the dry method (at 600°C for 2 h).

Despite the significance of the aforementioned studies, the understanding of how the various extraction methods of wheat phytoliths influence their mineralogical composition remains very limited. Thus, a comparative study of the main phytolith extraction methods

on ''modern'' plants and how these affect the subsequent phytolith assemblage is very important. The present study aims to make a contribution to the research lack outlined above, expanding this field of study. It examines the preservation biases of phytoliths and at the same time expands the field of knowledge, towards a better understanding of wheat phytolith mineralogical, chemical and morphological characteristics.

Several vascular plants are known to produce silicates (Currie and Perry 2007; Dietrich *et al*. 2003; Lins *et al*. 2002; Piperno 2006), calcium carbonates (Nitta *et al*. 2006; Taylor *et al*. 1993) and calcium oxalates (Coté 2009; He *et al*. 2012a, 2012b; Lersten and Horner 2011; Mazen *et al*. 2004; Pérez Cuadra and Hermann 2013). Smaller amounts of calcium phosphate (Horner and Wagner 1980), calcium sulphate (He *et al*. 2012a; Pritchard *et al*. 2000), barium sulphate (He *et al*. 2012b; Krejci *et al*. 2011), strontium sulphate (He *et al*. 2012b), strontium oxalate (Franceschi and Schueren 1986) and magnesium oxalate (He *et al*. 2012b) have also been reported in several plants. In addition, plant biominerals may contain several impurities, such as aluminium (Hodson and Sangster 1993), iron (Rodríguez *et al*. 2005), potassium (Sangster *et al*. 2009), manganese, zinc, cadmium (Sarret *et al*. 2007), copper and titanium (Clarke 2003). Through the insights gained on the post-depositional alterations that SiO_2-rich phytoliths undergo over time, the comprehensive mineralogical and geochemical study contributes to the understanding of the biogeochemical cycle of silicon, its relationship with the mobility of other soil elements, and to geoarchaeological research. This study also sheds light on the impact of the standard conventional methods of phytolith extraction from ''modern'' plants on phytolith composition and morphology.

The analyses were carried out either on entire plant excluding roots, or independently on the lower and upper parts of the plants (stem-leaves and inflorescence respectively). Despite the wide range of available bibliography on topics such as the variations in the

concentrations of several nutrients during the life cycle of wheat (Karlen and Whitney 1980), the seasonal and environmental patterns of accumulation and redistribution of mineral nutrients in wheat (Batten *et al.* 1986; Hocking 1994; Masoni *et al.* 2007; Wardlaw and Willenbrink 2000) and the partitioning of particular elements among the various wheat organs (Gregory *et al.* 1979; Kutman *et al.* 2011, 2012; Maillard *et al.* 2015), limited information is available on the distribution of chemical elements in different parts of the plant (Folk and Hoops 1982; Milton and Davidson 1946).

The integration of mineralogical and chemical analysis, coupled with the study of the morphological characteristics of wheat phytoliths, may prove a very useful tool in research on phytolith dissolution. In order to better understand the reactivity of SiO_2-rich phytoliths in soil solutions, we determined their solubility (Si, K, Mg, Al, Ca, Fe, Sr, Ba) and *k* rate constants of silicon. Moreover, the understanding of the 3D characteristics of the reactive surface of their morphotypes is important for the understanding of their preservation in the archaeological record. The aforementioned objectives are achieved through four main directions: (1) the extraction and multi-analytical characterisation of SiO_2-rich phytoliths from plants. Test samples were analysed with two different methods of extraction (dry and wet method), (2) the study of the dissolution mechanism plant phytoliths in relation to variations of pH, temperature and time. This was supplemented by the quantification of phytolith morphotypes extracted from plants before and after dissolution, (3) the extraction and characterisation of phytoliths from soils and archaeological sediments, and (4) the study of the surface morphology through the 3D representation of biominerals of not only plant but also animal origin. In particular:

(1a) The extraction and multi-analytical characterisation of SiO_2-rich phytoliths from different plant parts of two different wheat species that were grown during the same period under the similar environmental conditions in Greece and Cyprus. Despite the

study of phytoliths being an internationally emerging field, in Greece and Cyprus it is only during the last decade that their significance has been acknowledged. The mineralogical, chemical and morphological characterisation of the samples was performed using X-Ray Diffraction (XRD), Fourier Transform Infrared (FTIR) Spectroscopy, Thermogravimetric and Differential Thermogravimetric Analysis (TGA-DTGA), X-Ray Fluorescence (XRF), elemental (Carbon-Hydrogen-Nitrogen-Sulphur) analysis (CHNS), Scanning Electron Microscopy coupled with Energy Dispersive Spetrometry (SEM/EDS), optical microscopy and photomicrography. The analyses were carried out independently on stems-leaves and inflorescence and part of the analyses were carried out for the entire plant, excluding roots. These analytical techniques have been used previously in the study of the mineralogical or/and chemical composition of phytoliths or/and plant ashes/charchoal (Allué 2009; Anala and Nambisan 2015; Andriopoulou 2014; Buján 2013; Fraysse *et al.* 2006b; Ghaly and Ergudenler 1991; Jakes and Mitchell 1996; Liodakis *et al.* 2005; Misra *et al.* 1993; Pironon *et al.* 2001; Puppe and Leue 2018; Prajapati *et al.* 2014; Shillito *et al.* 2009; Trinh *et al.* 2017; Vamvuka and Kakaras 2011; Wu *et al.* 2014). In our previous study, phytoliths found in modern wheat and barley, modern soils and experimental sediments were also analysed in terms of mineralogy, phytolith content and morphotypes (Andriopoulou 2014).

(1b) In addition, a multi-analytical characterisation of phytoliths for some samples was performed to understand their microstructure and behaviour after their extraction from plants by means of two conventional methods: the dry and the wet ashing method (Andriopoulou and Christidis 2020).

(2a) The study of the dissolution mechanism of SiO_2-rich phytoliths extracted from the entire plant excuding roots, in relation to variations of pH (5, 7, 8.5), temperature (5, 20, 40 °C) and time (1-75 days), by means of long-term batch experiments. Additionally,

the mobility of Si and 7 other main and trace chemical elements (K, Mg, Al, Ca, Fe, Sr, Ba) was determined by inductively coupled plasma mass spectrometry (ICP-MS), a method previously used for the study of phytoliths, among others, by Fraysse *et al.* (2006). The solubility data for K, Si, Mg, Ca, Sr, Ba (element concentration versus time, at defined pH and temperature), were visualised with MATLAB software. Subsequently, the first-order kinetic constants *k* for the dominant dissolved element (Si) were found from log-linear plots. The log-linear plots, where C_0 is the initial Si concentration and $C_{(eq)}$ is the equilibrium Si solubility, were created using excel®.

(2b) Furthermore, the quantification of morphotypes for phytoliths originating in the plants (counting at least 250 phytoliths per microscope slide and with morphological classification according to form, texture and anatomical origin on the basis of the International Code for Phytolith Nomenclature (ICPN Working Group: Madella *et al.* 2005) was carried out both before and after dissolution. The results the quantification of phytoliths were visualised using the python programming language.

(3a) Moreover, the phytoliths extracted from soils were morphologically characterised using optical microscopy. Mineralogical and chemical characterisation of the soils in which the plants were grown in Greece (Crete, Volos, Corfu and Pella) and Cyprus (Pafos) using X-ray diffraction (XRD) and X-ray fluorescence (XRF). The understanding of the mineralogy/chemistry of the soils in which the collected plants were grown may contribute to topics related to agriculture, such as plant nutrition or/and fertilisation.

(3b) Mineralogical and chemical characterisation of archaeological sediments (including artefacts) from three nearby archaeological sites in Greece (Knossos, Crete, Palea Castle Volos and Toumba Thessaloniki) using X-ray diffraction (XRD) and X-ray fluorescence (XRF) was performed. Furthermore, the phytoliths extracted from sediments

were morphologically characterised using optical microscopy. The understanding of potential phytoliths recovered from archaeological sediments/artefacts may shed light in issues related to past human activity, such as where it took place, by identifying hearths, or what kind of technological means were used, e.g. type of plant fuel. In addition, the pH of soil and sediment samples was determined.

(4a) The study of the surface morphology and potential weathering through the 3D representation and visualisation of wheat phytoliths. Taking into account the importance of the surface properties for dissolution, in the present study the integration of microscopy and photogrammetry for the non-destructive imaging and 3D representation of the surface of microscopic biominerals was proposed (Andriopoulou *et al.* 2019). The overall 3D morphology reconstruction was based on digital photogrammetry principles. Overlapping images were collected from two separate sources, a Scanning Electron Microscope (SEM) and a pocket size electronic microscope.

(4b) The 3D method described above was implemented using samples primarily of plant origin; however samples of animal origin (rodent teeth), having a more complex surface relief than the former, were also studied. Towards this end, the first findings of a metric-oriented approach through microscope camera calibration and novel geometric distance unit set-ups towards a robust measurement methodology are provided in the present study.

3 MATERIALS AND METHODS

3.1 Materials

The following three groups of samples were studied: (a) ''modern'' plants, (b) ''modern'' soils and (c) archaeological sediments.

3.1.1 Plants (*Triticum monococcum* and *Triticum turgidum*)

The present research focuses on the study of wheat phytoliths in *Triticum monococcum* L. subsp. *monococcum* and *Triticum turgidum* L. subsp. *durum* (Desf.) Husn. The classification of the *Triticum* L. genus is as follows: phylum: Angiospermatophyta, class: Monocotyledoneae, order: Poales, family: Poaceae (Gramineae), subfamily: Pooideae, tribus: Triticeae, subtribus: Triticinae, genus: Triticum. In total, six mature wheat samples were studied. The selected plants where of the same age, sown between November and December and harvested between June and July in five regions in different condition of growth. The wheats were cultivated in Greece and Cyprus. All plants were healthy, however the Corfu sample was previously slightly affected by the insect pest *Sitophilus granarius* (wheat weevil) during storage. Furthermore, all plants apart from the Cyprus sample were cultivated without fetilisers or phytoprotection.

The varieties studied were *Triticum monococcum* and *Triticum durum* wheat, known locally by the names of the traditional varieties Kaploutzas and Limnos/Kyperounda respectively. Macroscopically, *Triticum monococcum* has awns, a narrow spike and fragile tiller that form the small seed, covered by a husk. Dorofeev *et al.* (1979) provide detailed morphological description of einkorn wheat. One of its botanical varieties is *vulgare* (Percival 1921), of which Kaploutzas is a branch, a variety grown primarily in Northern Greece (Karamanos 2008). *Triticum durum* has awns, a dense spike, a strong tiller and huskless seeds. *Limnos* is the oldest botanical variety of hard wheat found in Greece, with

its seeds first produced locally in 1932. It was created by selection of the Akbasak type, *leucurum* variety (Karamanos 2008). Kyperounda variety is mainly grown in Cyprus and one characteristic is that has brown awns, while Limnos has yellowish.

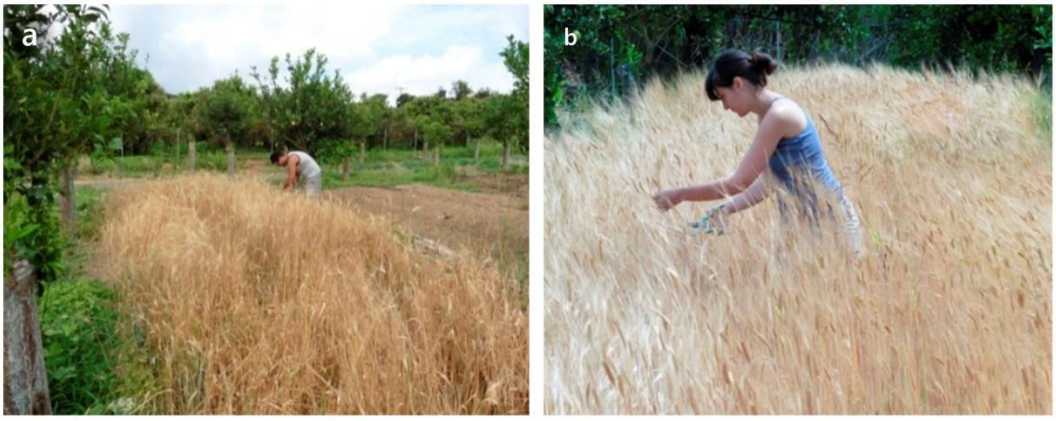

Fig. 3 Harvesting two plots. In order to better understand the life cycle of wheat, and changes in the phytolith assemblage that are related to the particular stage in the life cycle of the plant, we cultivated: **(a)** *Triticum durum;* and **(b)** *Triticum monococcum* in an experimental field at Chania, Crete (photos: Michelakis and Andriopoulou). Soil samples for future phytolith analyses were taken from the plots at different depths, before (2015) and after (2016) the cultivation period. Control samples were also taken. Next soil sampling is planned during 2021 with a further aim to study phytolith preservation over time

According to the criterion of anatomical origin, the analysed phytoliths came both from the entire and from the differentiated in upper and lower plant, giving stems-leaves and inflorescences respectively. Different parts of plants may reflect human activities, including seasonal activities such as harvesting (Fig. 3). The root system, when available, was separated from the rest of the plant material and stored, to prevent soil contamination. The initial intention was that three categories of sample are obtained for stems, leaves and inflorescences respectively. However, the quantity of leaves in the provided material was insufficient for all the laboratory analyses and the detailed characterisation of the material. Multi-analytical characterisation on phytoliths was

performed in order to understand their microstructure and behaviour after their extraction from plants by means of two methods: the dry and the wet ashing method. The phytoliths were chemically and mineralogically characterised for the plant as an entire and in parts, according to its anatomical origin (stems/leaves and inflorescences). Phytoliths extracted from the entire plants using only dry method were used in the dissolution experiments.

Phytoliths were extracted from the following plant samples: (1) *Triticum monococcum* stem-leaves at Pella (dry method), (2) *Triticum monococcum* stem-leaves at Pella (wet method), (3) *Triticum monococcum* inflorescence at Pella (dry method), (4) *Triticum monococcum* inflorescence at Pella (wet method), (5) *Triticum durum* stem-leaves at Pella (dry method), (6) *Triticum durum* stem-leaves at Pella (wet method), (7) *Triticum durum* inflorescence at Pella (dry method), (8) *Triticum durum* inflorescence at Pella (wet method), (9) *Triticum durum* stem-leaves at Cyprus (dry method), (10) *Triticum durum* inflorescence at Cyprus (dry method), (11) *Triticum durum* inflorescence at Crete (dry method), (12) *Triticum durum* stem-leaves at Crete (dry method), (13) *Triticum monococcum* inflorescence at Volos (dry method), (14) *Triticum monococcum* stem-leaves at Volos (dry method), (15) *Triticum durum* stem-leaves at Cyprus (dry method), (16) *Triticum durum* inflorescence at Cyprus (dry method). These samples were analysed using optical microscopy, XRD, FTIR, ED-XRF, CHNS, TGA-DTGA and SEM-EDS. The multi-analytical characterisation of plant samples was repeated once.

The specimens include apart from wheat phytoliths also teeth of rodent species. The teeth were used only for the formulation of the 3D models. The teeth were a (*Microtus* sp.) molar (Fig. 61) and a (*Rattus* sp.) molar (Fig. 62).

3.1.2 Soils and areas of study in Greece and Cyprus

Five soil samples were studied, four from different areas across Greece and the fifth from a cultivation in Cyprus. Samples were at depths of 0-20 cm (depending on actual soil depth). Generally, after plant litter degradation the phytoliths are released in the upper soil horizons (Meunier *et al.* 1999). The sampling regions (Fig. 4) for the plants and the respective soils are the following: (a) Messara, Crete (GPS: 35° 02' 8.40" N, 24° 50' 27.59" E), (b) Ano Lechonia, Volos (GPS: 39° 21' 39.71" N, 22° 56' 32.93" E), (c) Aridaia, Pella (GPS: 40° 58' 23.02" N, 22° 03' 23.00" E), (d) Vragkaniotika, Corfu (GPS: 39° 37' 14.48" N, 19° 55' 11.10" E), and (e) Pafos, Cyprus (GPS: 34° 46' 36.44" N, 32° 25' 28.24" E). The selection of these regions was based on the diverse climatic conditions of the Eastern Mediterranean, and in particular on the average annual rainfall (mm) and on the average for the coldest and hottest month during the cultivation period according to Hellenic National Meteorological Service and Department of Meteorology, Nicosia, Cyprus. *Triticum monococcum* plants were grown in Volos and Pella and *Triticum durum* plants were grown in Cyprus, Corfu and Pella.

The samples containing both plant and soil material were generously offered by the Agricultural School of Messara at Crete, by the Network for Biodiversity and Ecology in Agriculture, Aegilops at Volos, by the Irini's garden-organic farm at Pella, Vioporos, Ecological farm at Corfu and by the Agricultural Research Institute (Ministry of Agriculture, Rural Development and Environment, Cyprus). The cultivations in Greece were organic without any phytoprotection and fertilisers. By contrast the Cyprus field was with various wild plants the previous year, and fertilisers along with phytoprotection products were used subsequently.

3.1.4 Sediments and archaeological sites in Greece

Six archaeological sediment samples were studied, originating from the three following sites in Greece (Fig. 4): (1) Knossos, Crete; (2) Castle of Palea, Volos, and (3) Toumba, Thessaloniki. The samples from Knossos and Castle Palea were supplied by Dr. Tsartsidou (Ephoreia of palaeoanthropology-Speleology, Athens). The samples from Toumba were supplied by Prof. dr. Valamoti (School of History and Archaeology, Aristotle University of Thessaloniki). The selection of these archaeological sites was made on the basis of their vicinity to the aforementioned cultivation sites and the suggested or confirmed presence of micro- or macro-archaeobotanical wheat residues occurring from previous studies or from the neighbouring layers. According to the summary tables for the presence of wheat cereals in Bronze Age Greece by Valamoti (2009, p. 200-201), the archaeobotanical studies suggest the presence *Triticum monococcum* and rarely *Triticum durum* alongside a variety of other plants (i.e. barley, grape), during the (Late) Bronze Age in the selected sites: Knossos, Crete and Toumba, Thessaloniki. In Castle of Palea, Volos there are remains of *Triticum dicoccum*, but the presence of *Triticum monococcum* or/and *Triticum durum* has yet to be confirmed.

The studied archaeological samples were: (1) *KN5* (47.46 g derived from a layer of a Minoan room), (2) *KN10* (15.02 g derived from the inner part of a vessel at the Minoan room), (3) *TB2008* (6.98 g derived from a kiln), (4) *TB2013* (24.44 g derived from a grinding tool), (5) *ΚΑΣ25* (14.44 g derived from thin layer overlying a yellowish Mycenaean floor), and (6) *ΚΑΣ27* (10.07 g derived from a pebbled Mycenaean floor, older than the previous one).

Fig. 4 Map of the areas of study with total annual precipitation (mm) and average annual temperature (^{o}C) for the year 2014. Cultivations: **(a)** Messara, Crete, **(b)** Ano Lechonia, Volos **(c)** Aridaia, Pella, **(d)** Vragkaniotika, Corfu and **(e)** Pafos, Cyprus. Archaeological sites: **(a)** Knossos, Crete, **(b)** Castle of Palea, Volos; and **(c)** Toumba, Thessaloniki

[This map is made in html/css/javascript using the library leaflet (https://leafletjs.com/), the background is in GeoJSON by at https://www.naturalearthdata.com/, the icons are from https://www.flaticon.com/authors/smashicons CC-BY licensed and the color scales are from http://colorbrewer2.org/ based on the research work of Brewer (2016)]

The archaeological site of Knossos, located at Kephala hill of Çelebi, approximately 5 km southeast of the city of Heraklion in the island of Crete, is known as the core of the Minoan civilisation, that flourished between 2000-1350 BC. Knossos was discovered by Kalokairinos (1843-1907) in 1878 (Aposkitou 1979; Kopaka 2015). Evans with Hogarth, Mackenzie and Fyfe, systematically proceeded with the excavations for about thirty years, gradually revealing a substantial part of the city, the cemetery and the labyrinthine palace complex covering an area of 20,000 m^2, and a wide range of artefacts and

frescoes (Evans 1901, 1903, 1964; Mackenzie 1903; Warren 2000). The palace of Knossos is associated with the mythology of the Labyrinth-Minotaur and of Daedalus and Icarus. The surveys continue up to the present under the supervision of the British School at Athens and the 23rd Ephorate of Prehistoric and Classical Antiquities (Bennet 2013; Christakis 2018; Efstratiou *et al*. 2004; Karetsou 2004).

The beginnings of habitation in Knossos date back to the Neolithic period (6700-3200 BC), and the habitation continues uninterrupted until the Prepalatial period (3000-1900 BC). The first palace was destroyed at ~1700 BC, probably as a result of an earthquake. During the Neopalatial period a second castle was built upon the ruins of the former, becoming the centre of social, economic, political and religious activity until 1350-1380 BC, when it was destroyed in a fire. Mycenaeans settled in Knossos at around 1450 BC, as evidenced by the findings of a Linear B script archive, and therefore the region was inhabited again, lasting between the late Mycenaean period and the Roman times (Castelden 2001; Palmer 1961). In the present study, the two samples from Knossos excavation are from a Minoan room, third section; west prolongation; group sixty-four, third layer and the inner part of a vessel found at the Minoan room Π1/Χ2 (in Greek), group sixty-one 61 (A1636). The original inventory numbers and documented information of the samples are: *KN5* and *KN10* respectively. The initial weight of the samples was 47.46 g and 15.02 g accordingly.

The site of Toumba (Northern Greece), also known as Toumba of Kalamaria, is located in Ano Toumba, Thessaloniki, about 2 km away from the coastline of the Thermaic gulf. At the hillside of the Mount Choriatis complex, the site has the formation of a tell, and the fills that have accumulated over the centuries in that location have resulted in the gradual formation of the "toumba" and the "trapeza" characteristic features. The "toumba" has an approximate height of 20 m, its base surface area measures ~13,000 m^2 and its peak ~7,000 m^2 (Kostakis and Andreou 1987). The "trapeza" (resembling an

encircled area extending mainly to the west and north of the "toumba") has a maximum height of approximately 10 m and a total surface area of ~30,000 m^2 (Rey 1921). Toumba was initially considered to be a tomb.

The first excavation attempt in Toumba was done in 1899 by Makridi Bey and the first known reference is by Körte (Körte 1899, from Kiriatzi 2000). From 1984 onwards, a systematic academic excavation has been carried out at the site by the School of History and Archaeology of the Aristotle University of Thessaloniki, with the permission of the Ministry of Culture and Sports and the Supervision of the Thessaloniki Ephorate of Antiquities. Chourmouziadis and Kostakis were previous directors of the excavation which is currently directed by Andreou. The archaeological record of ceramics showed evidence of long-term habitation on the tell, dating from the prehistoric times to the Hellenistic period, when increased habitation activity was noted. The stratigraphy is continuous from the end of the 3rd millennium-beginning of the 2nd millennium (Middle Bronze Age) to the end of the 4th century BC-beginning of the 3rd century BC (Andreou *et al*. 1990; Andreou and Kostakis 1996), an event associated with the founding of Thessaloniki in 316/315 BC and the resettlement of the population in the new city (Soueref 1996, from Kiriatzi 2000).

On the basis of excavation data, the long period of settlement on the tell is divided in at least 14 phases, corresponding to the stratigraphic substrates which are primarily originating in prehistoric times (Middle Bronze Age, Late Bronze Age, Early Iron Age), but also in historic times up to the 4th century BC, while indications suggest a subsequent systematic use of the locality during the Medieval times (Kostakis and Andreou 1987; Andreou and Kostakis 1996). The original inventory numbers and documented information of the samples are: *Toumba 2008* (*TB2008* here) derived from a kiln and *Toumba 2013 (TB2013* here*)* derived from a grinding tool. The initial weight of the samples was 6.98 g and 24.44 g respectively.

The sampling at Castle of Palea, Volos (central Greece) was carried out in 2011 by the 13th Ephorate of Prehistoric and Classical Antiquities of the Ministry of Culture and Sports (Skafida *et al*. 2015). The site is on the artificial hill of Agioi Theodoroi, a hill of ~11.50 m height, covering an area of ~12.000 m^2. The hill was formed through continuous habitation since prehistoric times (Batziou-Efstathiou 2003; Deilaki 1974; Skafida 2012a; Stamatopoulou 2011), and the remnants of a Bronze Age settlement (3000 - 1100 BC) are evident today (Theocharis 1957, 1961). It is believed that this site was an ancient Mycynaean Iolkos (Tsountas 1900), a city that has been mentioned, among other written sources, in Homer's Iliad (B 712) (Adrymi-Sismani 2007). After the initial excavation by Tsountas and the 1955 earthquakes in the region, systematic excavations were carried out there under the auspices of the Archaeological Society at Athens (Theocharis 1957; 1961). Subsequent studies of Linear B tablets (Skafida *et al*. 2012) and other archaeological findings (Asderaki-Tzoumerkioti *et al*. 2018; Rehren *et. al*. 2015), further support the hypothesis that the settlement once was the historical nucleus of the city of Volos, an administrative and commercial hub for the region.

The two samples from Castle of Palea are from the excavation section "Trench III" located at the western slope of the hill, found in a part of a two-storied building with a big courtyard. This building was considered by Theocharis to be a Late-Hellenic IIIB period (1300-1200 BC) palace (Skafida *et al*. 2015; Theocharis 1957). The original inventory numbers and documented information of the samples are: *ΚΑΣ25* (in Greek) that is a thin layer overlying the yellowish Mycenaean floor and *ΚΑΣ27* (in Greek) that is from a pebbled Mycenaean floor, older than the previous one. The initial weight of the samples was 14.44 g and 10.07 g respectively.

3.2 Methods

3.2.1 Extraction of phytoliths from plant material

The phytoliths were extracted from dried mature plants using a slightly modified version of the dry ashing method (Parr *et al.* 2001). The entire plants excluding roots and including leaves, stems and inflorescences were manually cut, stored in bakers and washed twice in deionised water using the sonicator bath for ca. 15 min, to remove impurities attached to the plant surface. The washed plant material was dried overnight in an oven (WTC Binder) at 120°C and weighted.

The dried parts of the plant material were transferred to crucibles and burned in a muffle furnace (Nabertherm) at 550°C for 4h. The resulting ashes were transferred to 50-mL falcon tubes. Ten (10) mililitre of 10% hydrochloric acid (HCl) was added to the tubes to dissolve the carbonate minerals, with extra HCl being added when necessary, until bubbling ceased. The samples were then vortexed (Vibracell) for a few seconds and centrifuged at 3500 rpm for ca. 5 min. The supernatant was discarded and 10 mL of deionised H_2O was added to the tubes, which were centrifuged under the same conditions as before. Washing with H_2O was repeated twice and the samples were dried overnight at 80°C.

Subsequently, the samples were transferred to watch glasses and 30 mL of 33% hydrogen peroxide (H_2O_2) was added, to eliminate the remaining organic material. The watch glasses were heated on a hotplate at 80°C to accelerate oxidation. Further H_2O_2 was gradually added until no charcoal/organic remains were macroscopically observed. The remaining peroxide was eliminated by centrifugation at 3500 rpm for ca. 5 min followed by washing with deionised H_2O. The samples were dried overnight at 80°C, softly scratched off from the watch glasses with a spatula and weighted. The remaining

fraction after the elimination of carbonates and organic material is named Acid Insoluble Fraction (AIF) and is composed mainly of phytoliths.

In addition, phytoliths were extracted from several dried mature plants using a slightly modified version of the wet ashing method (Rovner *et al.* 1971, 1972). More specifically, the plant material was rinsed with deionised H_2O, dried overnight at 120°C, transferred into test tubes and oxidised using 10 mL of concentrated nitric acid (HNO_3) and a pinch of potassium chlorate ($KClO_3$). The material was then heated on a hotplate at 80°C and regularly stirred until its colour changed from the initial light brown to yellowish, and finally transferred to test tubes. The samples were then vortexed for a few secods and centrifuged at 3500 rpm for ca. 5 min. The supernatant was discarded and 10 mL of deionised H_2O was added to the tubes, centrifuged at 3500 rpm for ca. 5 min and decanted. The last washing step was repeated twice. The samples were left overnight to dry at 80°C. The remaining fraction (AIF) was mainly composed of phytoliths. The weight of the material was recorded before and after the phytolith extraction by each method as the AIF.

3.2.2 Optical microscopy and extracted phytoliths

Approximately 0.5-0.9 mg of the AIF (phytoliths) extracted from each method, was transferred to a microscope slide with a Pasteur pipette. 4 drops of mounting medium (Entellan, Merck Millipore) were then added and mixed with the sample to evenly distribute the phytoliths over the slide. A 24 mm x 24 mm cover-slip was placed over each suspension. The phytoliths were studied using a Zeiss Axioscop 40 polarised light microscope (x 2.5, x 5, x 10, x 20, and x 50) with an attached digital camera for photomicrographs using the LAS software (The Leica Application Suite) at the Fitch Laboratory of the British School at Athens.

Three different microscope slides were prepared from each sample and the phytoliths were identified and counted. At least 250 individual phytoliths were studied in each slide before and after dissolution experiments, according to the standard literature (Meunier and Collin 2001; Mulholland and Rapp 1992; Piperno 1988, 2006; Twiss *et al.* 1969). The identification of about 50 single phytoliths with consistent morphology gives an error margin of 40% in the interpretation of the results, whereas identification of about 200 single phytoliths decreases the error margin to 24%, and identification of 265 single phytoliths to 12% (Albert and Weiner 2001). A review of quantification methods in phytolith analysis is provided by Strömberg (2009).

For each sample, the average percentage of each identified morphotype was calculated. Individual phytoliths within silica skeletons (phytoliths in anatomical connection) were identified separately to morphotype groups (ICPN Working Group: Madella *et al.* 2005) and added to the general count. Main morphotypes groups are: (a) inflorescence phytoliths e.g. dentritic long cells, papillae, (b) stem and leaves phytoliths e.g. bulliform cells, psilate long cells, and (c) non-assignable phytoliths, which means that may appear both in the inflorescence and the stem-leaves, e.g. wavy long cells, rondel short cells, etc. Then non-assignable morphotypes remained in the non-assignable count whereas characteristic morphotypes from inflorescence and stem-leaves were added to their respective counts.

The quantification of phytoliths extracted from plant samples (Corfu, Crete, Cyprus, Pella I, Pella II, Volos) was carried out both before and after the dissolution experiments [75 days at (a) pH=7, T=20ºC, (b) pH=7, T=40ºC, (c) pH=8.5, T=20ºC and (d) pH=8.5 T=40ºC]. The results presented below were visualised using the python programming language. More specifically, the matplotlib python library was used, due to provision of

matlab-like functionality for plotting results (see chapter 4.2 *Quantification of plant phytolith morphotypes before and after dissolution*).

3.2.3 Extraction of phytoliths from soils/sediments

''Modern'' soils and archaeological sediments obtained from the experimental fields and archaeological sites were subjected to the rapid phytolith extraction method (Katz *et al*. 2010). Briefly, a weighted quantity (around 30 mg) of each air-dried, homogenized sample was placed in a 0.5 mL conical plastic Eppendorf centrifuge tube, to which 50 µl of equivolume solution of 6N HCl was added with an adjustable pipette, to dissolve carbonate minerals, and 450 µl of 2.4 g/mL SPT [$Na_6(H_2W_{12}O_{40})$ H_2O] were subsequently added. The tube was vortexed for a few sec, sonicated for ca. 15 min, vortexed again for a few sec and centrifuged for ca. 5 min at 5000 rpm using the Eppendorf Minispin centrifuge of the School of Environmental Engineering, TUC.

The supernatant where the phytoliths were in suspension was finally transferred to a new tube with an adjustable pipette. It was vortexed once again and an aliquot of 50 µl of it was placed on a microscope slide and covered with a 24 mm x 24 mm cover-slip. Phytoliths were counted and identified at x 2.5, x 5, x 10, x 20, and x 50 magnifications using an optical microscope. At least 200 individual soil phytoliths were identified for each slide with the same method used for the ''modern'' plant material. Few (less than 50) individual sediment phytoliths were also identified.

Furthermore, the pH of the soil and sediment samples was measured (3 repetitions) with a pH meter (WTW/inoLab®) at 25°C. The measurement is performed by placing the electrode of the pH meter in a sample:deionised water mixture (for active acidity) in ratio 1:2,5. Before measuring, the pH meter was calibrated using standard buffer solutions at pH 4, pH 7 and pH 10.

3.2.4 Powder X-ray Diffraction (XRD)

The mineralogy of the all samples was examined by powder X-ray diffraction (XRD) at the Laboratory of Applied Mineralogy of the School of Mineral Resources Engineering, Technical University of Crete, with a Bruker D8 Advance diffractometer equipped with a LynxEye silicon strip detector, using Ni-filtered Cu-Ka radiation (40 kV, 40 mA), 0.298° divergence and anti-scatter slits, and a step size of 0.019 °2θ, with counting time 1 sec per strip step (total time 63.5 sec per step). Data were evaluated with the EVA® software provided by Bruker. The mineralogical composition of the samples was determined on random powders prepared after grinding with an agate pestle and mortar and mounting by side loading on Al-holders to avoid preferred orientation.

3.2.5 Fourier Transform Infrared spectroscopy (FTIR)

Infrared (IR) spectra of the AIF samples were obtained using a Perkin Elmer 1000 Fourier Transform Infrared (FTIR) spectrometer in the range 400-4000cm^{-1} at the Hydrocarbons Chemistry and Technology Laboratory of the School of Mineral Resources Engineering, Technical University of Crete. Each spectrum was the average of 20 scans collected at 4 cm^{-1} resolution. One and a half (1.5) milligrams of the samples was diluted in 150 mg potassium bromide (KBr) and pressed in 13mm KBr discs, which were subsequently dried at ~150°C overnight. The collected FTIR spectra were evaluated with the Spectrum® software.

3.2.6 Scanning Electron Microscopy with Energy Dispersive Spectroscopy (SEM/EDS)

Carbon coated and uncoated AIF samples were examined with a JEOL, JSM-IT300LV Scanning Electron Microscope, equipped with an Oxford Aztec STD X-act Energy Dispersive X-Ray Microanalytical system at the Malcolm H. Wiener Laboratory for Archaeological Science of the American School of Classical Studies, Athens Greece. Investigation was performed with an acceleration voltage of 15 kV at 10-11.8 mm working distance. The carbon coated samples, were studied in high vacuum conditions, and the uncoated ones in a low vacuum. Some samples were also examined with a JEOL, JSM-5400 Scanning Electron Microscope at the School of Mineral Resources Engineering, Technical University of Crete.

3.2.7 Energy Dispersive X-ray Fluorescence spectrometry (ED-XRF) and elemental analysis for organic carbon, hydrogen, nitrogen and sulphur (CHNS)

The chemical composition of all samples was determined by energy dispersive X-ray fluorescence spectrometry with a Bruker AXS S2 Ranger XRF spectrometer at the Laboratory of Inorganic and Organic Geochemistry and Organic Petrography of the School of Mineral Resources Engineering, Technical University of Crete using fusion beads. Two (2) grams of the ground AIF sample previously dried at 100°C for 2 h was incinerated in the muffle furnace at 1050°C for 2h to determine the loss on ignition (LOI). Subsequently, ca. 1.5 g of ignited sample was weighted and mixed with flux consisting of 50% lithium tetraborate ($Li_2B_4O_7$) and 50% lithium metaborate powder ($LiBO_2$) in a 1:5 sample: flux ratio. The powder was homogenised, placed in a platinum crucible, 3-4 drops of lithium chloride solution (LiCl) were then added, and heated at 1050°C for ca. 20 min. The glass bead was then cooled in a platinum plate for ca. 3 min and stored in a

desiccator for XRF analysis. A Pd tube was used, the voltage was 5-50 kV depending on the element (F-Ca=8 kV and Ca-Sr=40 kV) and the maximum current was 2000 μA.

The organic C, H, N, and S content of the samples were determined with an Organic Elemental Analyser Flash 2000 of Thermo Scientific at the Laboratory of Hydrocarbons Chemistry and Technology of the School of Mineral Resources Engineering, Technical University of Crete. Data acquisition was performed by the Eager Xperience software, provided by Thermo Scientific. Ca. 10 mg of each dried sample (AIF) and ca. 10 mg of catalyst vanadium pentoxide (V_2O_5) were mixed and put in a tin container. The mixture was combusted resulting in an exothermic reaction triggered by the highly oxidised environment at a temperature of 900°C. The reactor was connected to the analytical column CC, on its turn connected to a channel of the thermal conductivity detector TCD. Temperature rises to ca. 1800°C instantly causing the sample combustion. The nitrogen oxides and SO_3, possibly formed, were reduced to elemental nitrogen and sulphur dioxide, and the oxygen excess was retained. The gas mixture (N_2, CO_2, H_2O and SO_2) flew into the chromatographic column where elemental separation occurred. The eluted gases are sent to the thermal conductivity detector TCD that generates electrical signals, which, properly processed by the Eager Xperience software, provide the percentages of C, H, N, and S contained in the sample.

3.2.8 Thermogravimetric-Differential Thermogravimetric Analysis (TGA-DTGA)

Differential Thermal and Thermogravimetric Analyses (DTA-TG) was carried out on the AIF samples using a Perkin Elmer TGA-6 thermogravimetric analyser at the Laboratory of Solid Fuels Beneficiation and Technology of the School of Mineral Resources Engineering, Technical University of Crete. Approximately 20-25 mg of the samples was

heated at atmospheric pressure in the temperature range 40-900°C with a heating rate of 10°C/min in an N_2 atmosphere.

3.2.9 Batch experiments and inductively coupled plasma mass spectrometry (ICP-MS): solubility and dissolution kinetics of plant phytoliths

SiO_2-rich phytolith dissolution study and gradual measurements of the concentration of dissolved Si and 7 other chemical elements (K, Mg, Al, Ca, Fe, Sr, Ba) were performed through batch experiments (closed system) and the use of inductively coupled plasma mass spectrometry (ICP-MS). Dissolution experiment was set up to mimic natural reactivity of biogenic silicon after burning. Fire is a process of significant impact on ecosystems, and its results are in many cases evident in the archaeological record (Albert and Cabanes 2008; Parr 2006; Rowlett 2000; Wroth *et al.* 2019). Phytoliths obtained from wheats using the dry method of extraction are therefore suitable for fire incidents.

Processes controlling the kinetics of silica-water interactions in weathering environments originate at the interface between solid and solution. Experiments were conducted by adding 0.15 g of phytoliths in 45 ml of deionised H_2O in 50 ml tubes that have been previously overnight treated with 10% hydrochloric acid (HCl) to remove possible contamination. The reaction progress was monitored by measuring the concentration of 8 dissolved chemical elements as a function of time. The samples (with replicates) were allowed to react for 1 to 75 days and individual experiments were set up for each time interval. The samples reacted at pH 5, 7 and 8.5 and temperature 5, 20 and 40°C either in a fridge (Beko) for the 5°C or in a thermostated water-bath (Memmert) for 20 and 40°C experiments. The suspensions (at 5 and 40˚ C) were periodically stirred (manually). The experiments at 20 ˚C were carried out under continuous agitation in a shaking table (Edmund Büchler KS-10).

During experimental runs the precision of the measurements was approximately ±0.01-0.02 for pH and ±1°C for temperature, that produce negligible uncertainties. Adjusting the pH of a solution, with the addition of the acid or base, consequently alters the ionic speciation and electrolyte concentration of the solution. Acidic conditions were achieved by the gradual addition of 1N hydrochloric acid ($HCl + H_2O \rightarrow H_3O^+ + Cl^-$) while neutral or alkaline conditions were achived by the gradual addition of 2N NaOH ($NaOH + H_2O \rightarrow OH^- + Na^+$). Reacting solutions (HCl and NaOH) pH ranging from 2 to 12. The pH of the phytolith solutions was measured using a a glass electrode (Mettler Toledo) calibrated with buffers (National Institute of Standards and Technology) at 25°C, and the temperature was measured with laboratoty thermometers (ISOLAB).

The batch experiments were conducted at the School of Mineral Resources Engineering, Technical University of Crete and the ICP-MS analyses (ICP-MS 7500cx coupled spectrometer equipped with Autosampler Series 3000, both by Agilent Technologies) were carried out at the School of Environmental Engineering, Technical University of Crete. The conditions of operation of the spectrometer were the following: RF power = 1500 W, Plasma gas flow = 0.82 L/min, Auxiliary gas flow = 0.26 L/min, Sampling/Skimmer cone = Ni, Nebulizer type = MicroMist, S/C temperature = 2^o C, Replicates = 3, Collision gas = He, Collision gas flow = 4.5 ml/min, Reaction gas = H_2, Reaction gas flow = 3.5 ml/min, Solution uptake = 160 μL/min, Integration time = 0.30 sec per mass. The data obtained from ICP-MS were converted to concentrations using an external calibration curve [at least 5 concentration levels, with a correlation coefficient (r) of 0.99] using standard purity compounds (Merck). The detection limits were derived from the calibration curves with appropriate mathematical calculations (Chemstation Software by Agilent). The results were considered satisfactory when the relative standard deviation (RSD%) was within acceptable limits (RSD% <10%).

For the visualisation of the data obtained from ICP-MS, we used a numerical computing environment, MATLAB (v2017a), due to its low learning curve and plethora of data visualisation features. This environment provides robust functionality both for 2D and 3D plotting through its proprietary programming language, with access to graphical interfaces for further plot customisation. To plot our data, we began by exporting them from excel® sheets to "comma separated values" (CSV) files. Subsequently, the data were uploaded into the MATLAB environment, and they were separated into groups of relevant information to obtain the appropriate plots/graphs.

3.2.10 Three-dimensional representation of biominerals and micro-photogrammetry

The overall three-dimensional (3D) morphology reconstruction was based on digital photogrammetry principles. Overlapping images were collected from a Scanning Electron Microscope (SEM). The 3D project took place at the Malcolm H. Wiener Laboratory for Archaeological Science of the American School of Classical Studies at Athens and the SenseLab research group of the School of Mineral Resources Engineering, Technical University of Crete. The samples were examined with a JEOLJSM-IT300LV Scanning Electron Microscope, equipped with an Oxford Aztec STD X-act Energy Dispersive X-Ray Microanalytical system at the ASCSA. Investigation was performed with an acceleration voltage of 15 kV at 10-11.8 mm working distance. The 3D reconstruction processing was undertaken by a specialised photogrammetric software, providing sets of overlapping SEM images. In order to establish a concise coordinate system on the resulting models, a set of distances upon the samples were measured during the SEM image acquisition.

4 RESULTS AND DISCUSSION

4.1 Weight of the Acid Insoluble Fraction (AIF)

The stem-leaves and inflorescences using the dry method of extraction showed different weight percentage of AIF (Fig. 5). In the dry method that was used for all plant samples (Cyprus, Crete, Volos, Pella I, Pella II and Corfu) the weight percentage of AIF relative to initial wheat weight ranges from ca. 1.2 to 3.5% for stem-leaves, the and from ca. 12.7 to 16.9% for the inflorescence. In general, the inflorescences produce clearly more AIF that is composed mainly of phytoliths, than the stem-leaves regardless of the wheat species (i.e. genetics) and area of study (i.e. environment).

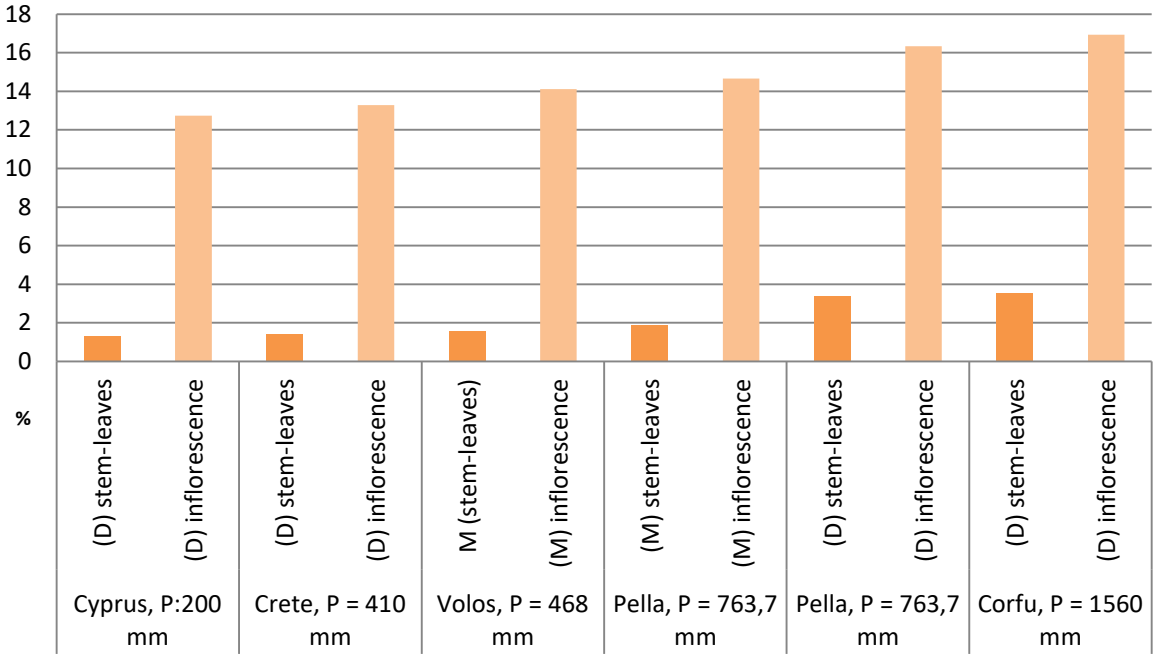

Fig. 5 Weight percentages of the AIF relative to the original plant material (inflorescence or stem-leaves) using dry method for all plant samples (M): *Triticum monococcum* or (D): *Triticum durum*

Previous studies demonstrated that phytolith analysis can be used as a method to identify past water availability (Jenkins 2001, 2016; Katz *et al.* 2013; Madella *et al.* 2009; Rosen and Weiner 1994; Weisskopf *et al.* 2015). Both plants seem to accumulate relatively higher concentrations of AIF as precipitation of the area of study increases (Fig. 5). This is in accordance with Rosen and Weiner (1994), who showed that emmer wheat grown with irrigation in semi-arid plots produced phytoliths with greater number of silicified cell per phytolith than emmer wheat that was dry-farmed in Israel. Jenkins (2001) has also shown that phytolith content in wheat is increased when irrigation and rainfall are increased in Jordan. A previous study supports that phytolith concentration in *Avena sterilis* (oat) tends to be positively correlated with water availability in Israel (Katz *et al.* 2013).

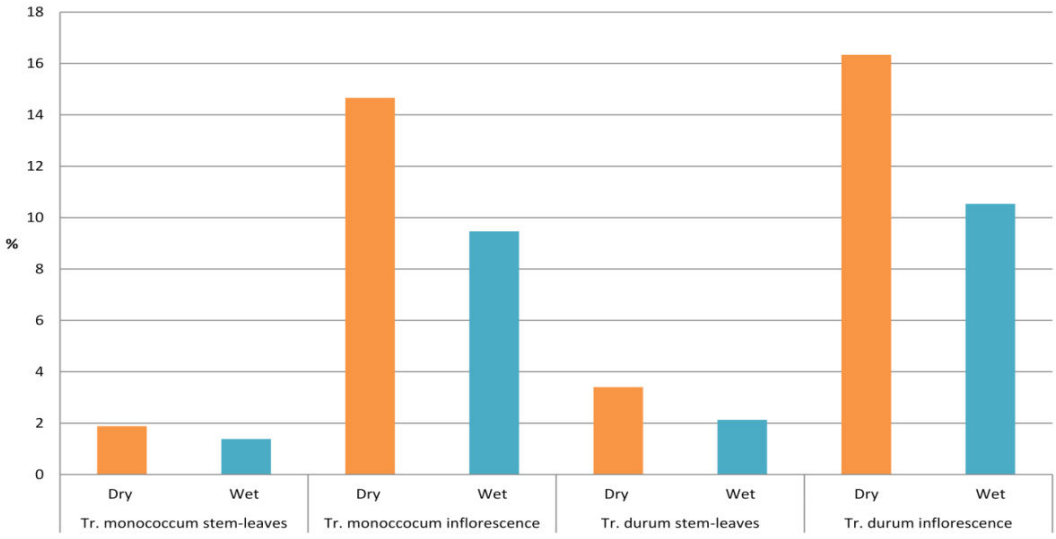

Fig. 6 Weight percentages of the AIF relative to the original plant material (inflorescence or stem-leaves) using dry or wet method for Pella samples (*Triticum monococcum* or *Triticum durum*)

The dry and wet methods for plant samples from Pella yielded different weight percentages of AIF (Fig. 6). In the dry method, the weight percentage of AIF relative to initial wheat weight ranges from ca. 14.6 to 16.3% of the initial weight for the

inflorescences and from ca. 1.8 to 3.4% of the initial weight for the stems-leaves. In the wet method that was used only for Pella samples, the weight percentage of AIF relative to the initial wheat weight is lower compared with the dry method, ranging from ca. 9.4 to 10.5% for the inflorescences and from ca. 1.3 to 2.1% for the stems-leaves. In general, the dry method produces more AIF, which is composed mainly of phytoliths, than wet method regardless of the wheat species and anatomical origin of the phytoliths (inflorescence or stem-leaves) in accordance with Jenkins (2009). Heat treatment removed the majority of the volatile matter, increasing the mineral matter content. For both methods, the inflorescences and stems-leaves of *Triticum durum* accumulated relatively higher concentrations of AIF than their counterparts of *Triticum monococum*.

4.2 Quantification of plant phytolith morphotypes before and after dissolution

The quantification of phytoliths extracted from plant samples (Corfu, Crete, Cyprus, Pella I, Pella II, Volos) was carried out both before and after the dissolution experiments (75 days). At least 250 individual plant phytoliths were identified in each microscopic slide. Three different slides were prepared from each sample. For each sample, the average percentage of each identified morphotype was calculated. The dissolution experiments (used for the quantification of phytoliths) where made with following variables: (a) pH=7, T=20ºC, (b) pH=7, T=40ºC, (c) pH=8.5, T=20ºC and (d) pH=8.5 T=40ºC.

The results presented below were visualised using the python programming language (Figs. 9-12, Figs. 64-111 of appendix 1). A python program was developed to automatically extract the data that was previously gathered into excel® sheets, and plot: (a) the absolute values of average percentages of present phytolith morphotypes; and (b) the relative difference between average percentages of present phytolith morphotypes, before and after the dissolution (experiments under different pH and temperature).

Fig. 7 present characteristics morphotypes of phytoliths previously extacted from wheat and barley (Andriopoulou 2014). A future challenge remains the classification of morphotypes by automatic image analysis.

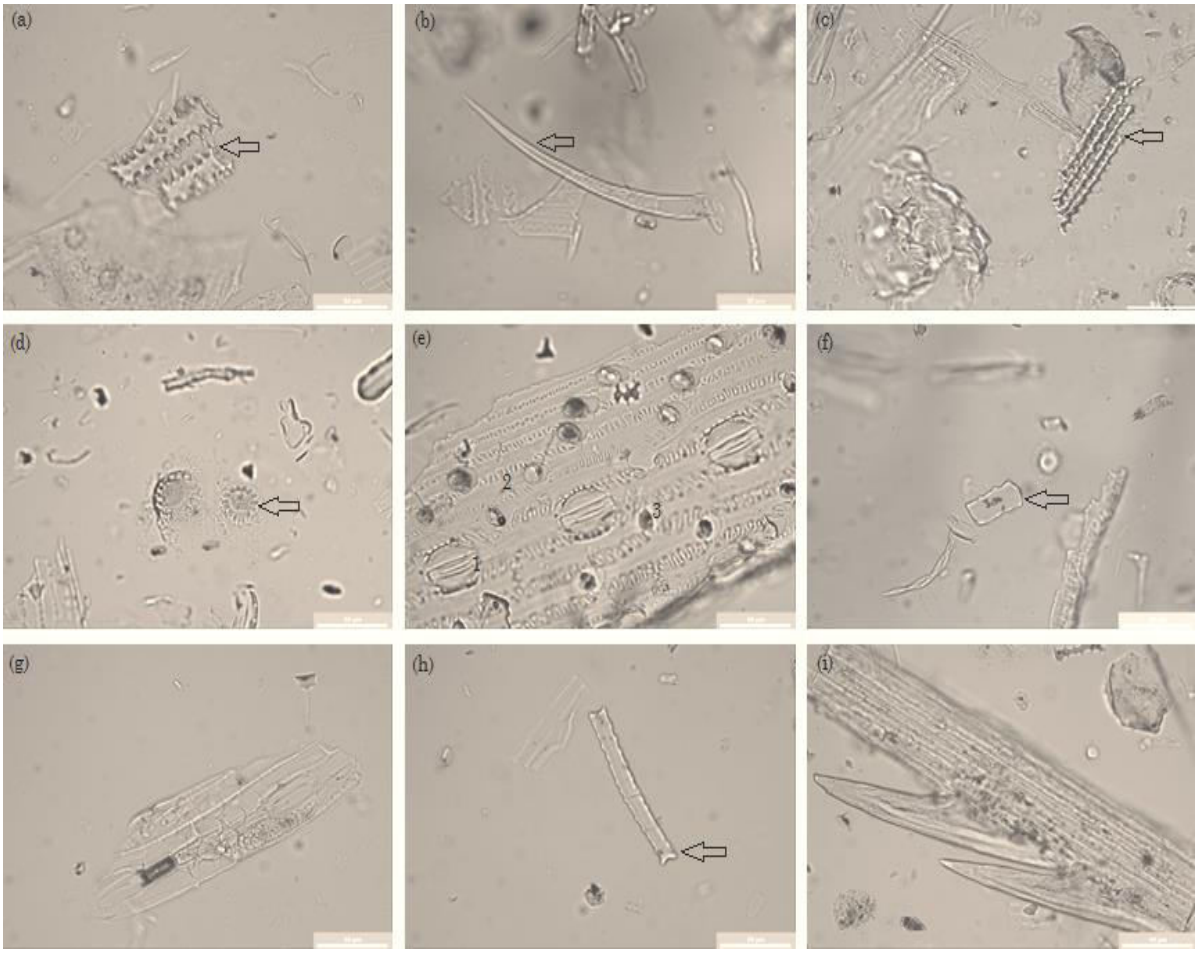

Fig. 7 Photomicrographs of phytolith morphotypes in wheat and barley: **(a)** two dentritic long cells in anatomical connection from *Triticum aestivum*; **(b)** hair from *Triticum spelta*; **(c)** four echinate long cells in anatomical connection from *Hordeum vulgare*; **(d)** two papillae *Triticum dicoccum*; numerous pits can be seen around the periphery of each papillae; **(e)** anatomically connected phytoliths from *Triticum durum* leaves; 1. stomata, 2, wavy long cell, 3, rondel short cell *Triticum aestivum* **(f)** crenate long cell from *Triticum spelta*; **(h)** parallelepiped elongate rugulate from *Triticum aestivum;* and **(g)** mesophyl from *Triticum dicoccum*; i) two prickles from *Hordeum vulgare* (photomicrographs: Andriopoulou 2014)

Table 1 Main phytolith morphotypes present in the studied plant samples and their abbreviations

Phytolith morphotypes	Abbreviations
Bulliform cell cuneiform rugulate	(Bc c r)
Cylindroid rugulate	(C r)
Epidermal appendage-Hair monocotyledon	(EA Hm)
Epidermal appendage-Pricke rugulate	(EA P)
Long cell dentritic	(LC d)
Long cells echinate	(LC e)
Long cell verrucate	(LC v)
Long cell wavy	(LC w)
Long cell wavy rugulate	(Lc wav r)
Papillae	(Pa)
Parallelepiped elongate psilate	(P El p)
Parallelepiped elongate rugulate	(P El r)
Short cells rondel	(ShC R)
Rondel rugulate	(ShC R)
Stomata	(St)
Weathered	-
Melted	-
Fragmented	-

The phytoliths were classified morphologically according to their form, texture and possible anatomical origin. The phytolith morphotypes were identified based on the International Code for Phytolith Nomenclature (ICPN Working Group: Madella *et al*. 2005) and further standard literature (Meunier and Collin 2001; Mulholland and Rapp 1992; Piperno 1988, 2006; Twiss *et al*. 1969). The following main morphotypes were identified (Table 1): (Bc c r) Bulliform cell cuneiform rugulate, (C r) Cylindroid rugulate, (EA Hm) Epidermal appendage-Hair monocotyledon, (EA P) Epidermal appendage-Pricke rugulate, (LC d) Long cell dentritic, (LC e) Long cells echinate, (LC v) Long cell verrucate, (LC w) Long cell wavy, (Lc wav r) Long cell wavy rugulate, Long cell wavy from leaves, Long cell wavy from inflorescence, (Pa) Papillae, (P El p) Parallelepiped elongate psilate, (P El r) Parallelepiped elongate rugulate, (ShC R) Short cells rondel, (ShC R) Rondel rugulate, Rondel from leaves, Rondel from inflorescence, (St) Stomata, Weathered,

Melted and Fragmented. Rarely, (Bcp) Bulliform cell parallelipedal, (C p) Cylindroid psilate, (C sn), Cylindroid sinuous, (P El m) Parallelepiped elongate mesophyl, (ShC T) Short cell trapeziform, (Crnt) Crenate and (Crnt long) Crenate long were also identified.

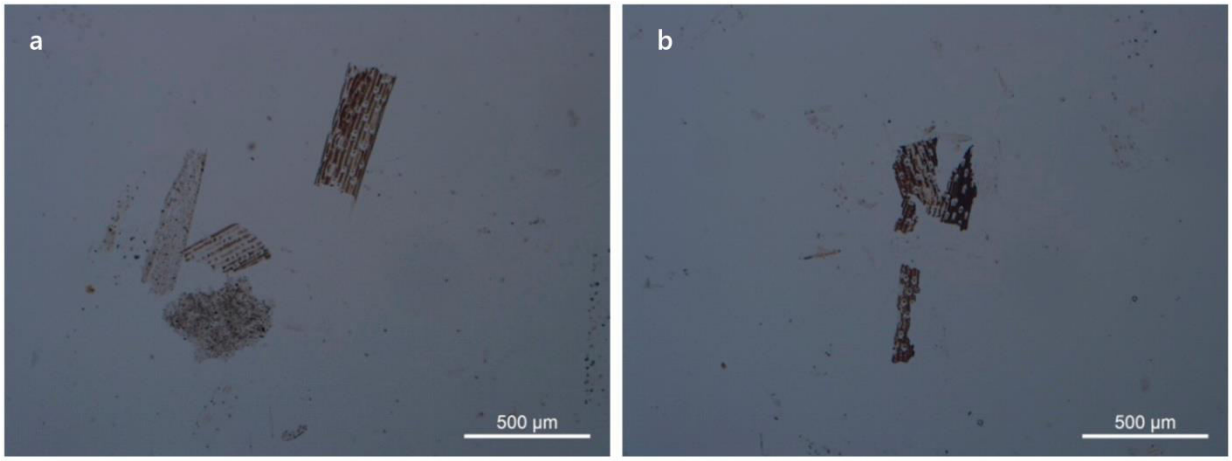

Fig. 8 Wheat phytoliths: muticellular structures **(a)** before dissolution; **(b)** after dissolution. The chemical/mechanical alterations of the phytoliths after the dissolution experiments are evident (photomicrographs: Andriopoulou)

Previous studies have shown that certain morhotypes show different stability (Albert *et al.* 2006; Cabanes *et al.* 2011). The stability may originate from chemical, mechanical or mixed factors (Fig. 8). Cabanes *et al.* (2011) showed that different phytolith morphotypes from *Triticum aestivum* (wheat) have different stabilities under alkaline conditions and at constant temperature. They assessed how differential dissolution may affect the interpretation of the microarchaeobotanical record. Based on our results, the absolute values of average percentages of some phytolith morphotypes remained relatively constant, despite the change in pH and temperature. In particular, relatively stable morphotypes are short cell rondels (Fig. 7 e-3), located within multi-cell structures with spherical/elliptical geometries. The stability of the rondels is in agreement with Cabanes *et al.* (2011). An additional observation was the high stability of the stomata. A stoma (Fig. 7 e-1) is an intercellular space (aperture) limited by two specialised cells called guard cells (Esau 1965), together with the subsidiary cells bordering the guard cells

and functionally connected. This stability, and thus mechanical resistance, may be related to their function on the leaves, which serve the plants' evapotranspiration. Water in the transpiration stream is distributed throughout the leaves in the vascular bundles, and the the main pathway of water loss through the leaves is via the stomata (Bange 1953).

Dimensional characteristics and texture of the majority of the phytoliths (apart from the short cells rondels and stomata) change with pH and temperature. In the present study, as the pH and temperature rise, the decorated morphotypes (long cells dentritic, long cells echinate and long cells verrucate) that are related to the inflorescence, showed variations. For example, at pH=7 with rising temperature, the presence of dentritic morphotypes decreased by 50% and at pH=8.5 with rising temperature they decrease by 75%. Dentritic morphotypes (i.e. decorations in the form of needle-like protrusions from the main body that are further subdivided) appear to decrease and echinate morphotypes (i.e. decorations in the form of pointed spines) to increase considerably with rising pH and temperature. It is suggested that dendritics may alter to echinates or/and to verrucates (i.e. decorations as wide as, or wider than 1μm). This observation should be taken into account when studying phytoliths from archaeological sediments, because it indicates that some morphotypes might have been absent from the archaeological record, not because they did not deposited, but because they did not preserve their initial morphological characteristics over time. This has important implication for the use of some phytolith ratio indices that are used in some identification approaches or crop-processing studies (Andriopoulou 2014; Ball *et al.* 1996; Ball and Brotherson 1992; Madella *et al.* 2009; Out *et al.* 2014). As a consequence, if there is an alteration of dendritics to echinates or/and verrucates, then we cannot rely on their ratio indices, unless it is confirmed that there is not alteration at all.

Furthermore, apart from the gradual change of the dimensional characteristics of morphotypes, the texture of most of morphotypes (especially parallelepiped elongated and long cells waved) tended to change from psilate/smooth to rugulate/rugose. In some cases some pits, probably due to chemical alteration, were observed on the outer surface of the morphotypes. Microcracks and fractures were also observed due to mechanical alteration, mainly at the edges of the large morphotypes. Moreover, sometimes (e.g. strongly alkaline sample from Crete) the tip of the hairs/trichomes (epidermal appendages that result from outgrowth of the plant epidermis) was absent. Hairs (Fig. 7 b) are elongated outgrowing, with a relatively wide base, an elongated shaft and a narrow end (tip). After dissolution, the amount of fragmented morphotypes is no longer assigned to specific morphotypes. Moreover, the weathered morphotypes with irregular shapes and pitted surfaces, increased as expected. Weathered morhotypes showed strong chemical or sometimes mechanical weathering, and frequently cavities were observed on the surfaces of elongate phytoliths. To understand further morphotypes changes associated with dissolution we also studied their surfaces by SEM [see chapter 4.6, *Scanning Electron Microscopy with Energy Dispersive Spectroscopy (SEM/EDS*)].

The abundance of melted mophotypes that showed signs of burning, deformation or/and shrinkage did not change significantly. However, their boundaries were less stable. Accordingly to Cabanes *et al.* (2011) burnt phytoliths are more soluble than their unburnt counterparts. Finally, the majority of the morphotypes from *Triticum monococcum* were less stable than their counterparts from *Triticum durum* regardless the increase of the pH and temperature during dissolution process. The samples originating from the inflorescence of *Triticum monococcum* contain abundant amorphous matter (i.e. phytoliths) regardless of extraction method (see XRD traces below). Here, the structure and composition of the glumes may have an impact on the results. *Triticum monococcum*

is a non-shattering hulled wheat, which means that the glumes tightly enclose the grains, opposite to *Triticum durum*, which is a free-threshing naked wheat. Generally, the amorphous phases have a higher dissolution rate than their associated, more thermodynamically stable, crystalline polymorphs (Jones and Segnit 1971). As a result the anatomical origin of phytoliths may be correlated with phytolith stability and preservation in the archaeological record.

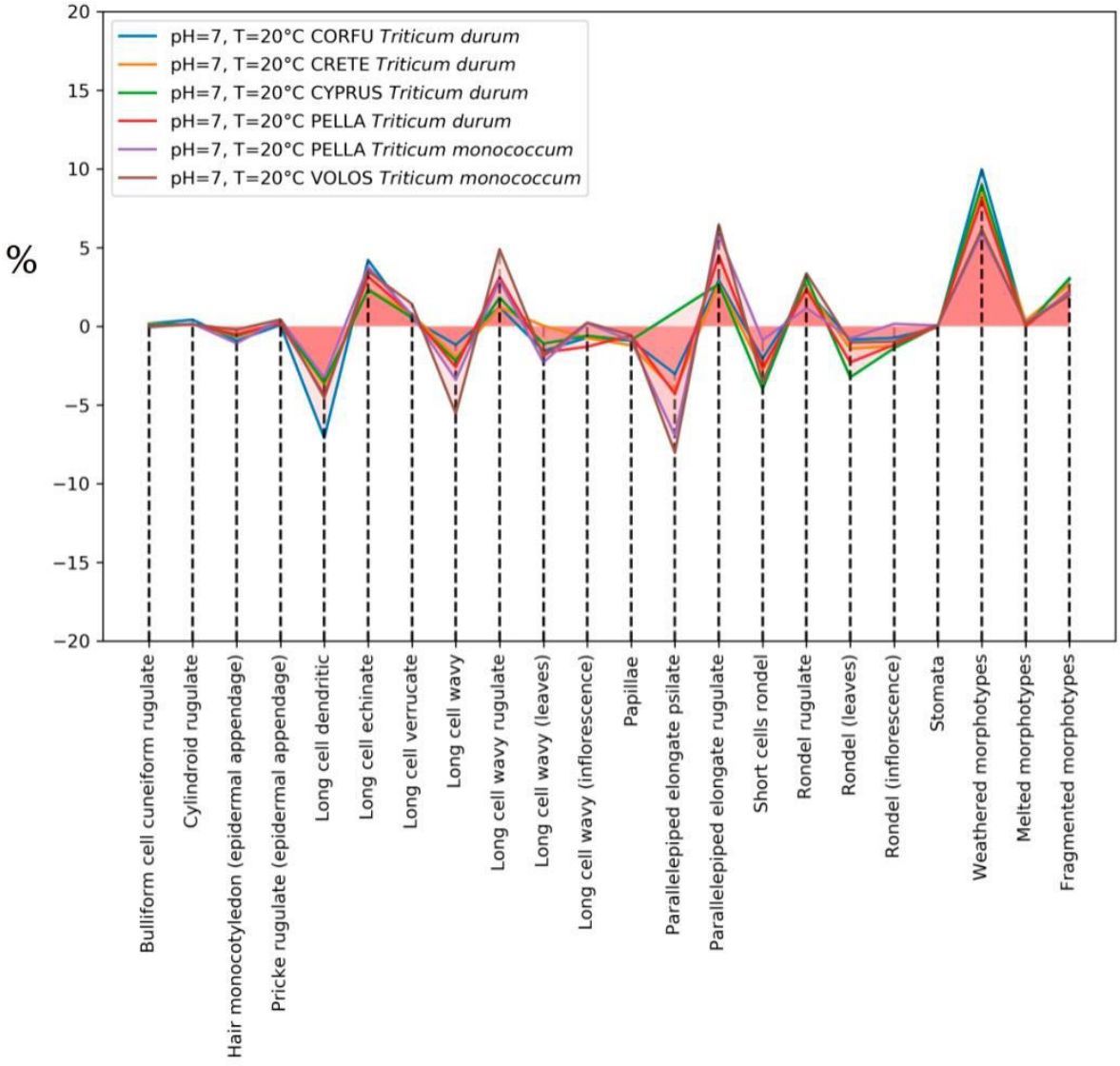

Fig. 9 The relative difference between average percentages of phytolith morphotypes (all samples), before and after the dissolution experiments (pH=7, T=20˚C)

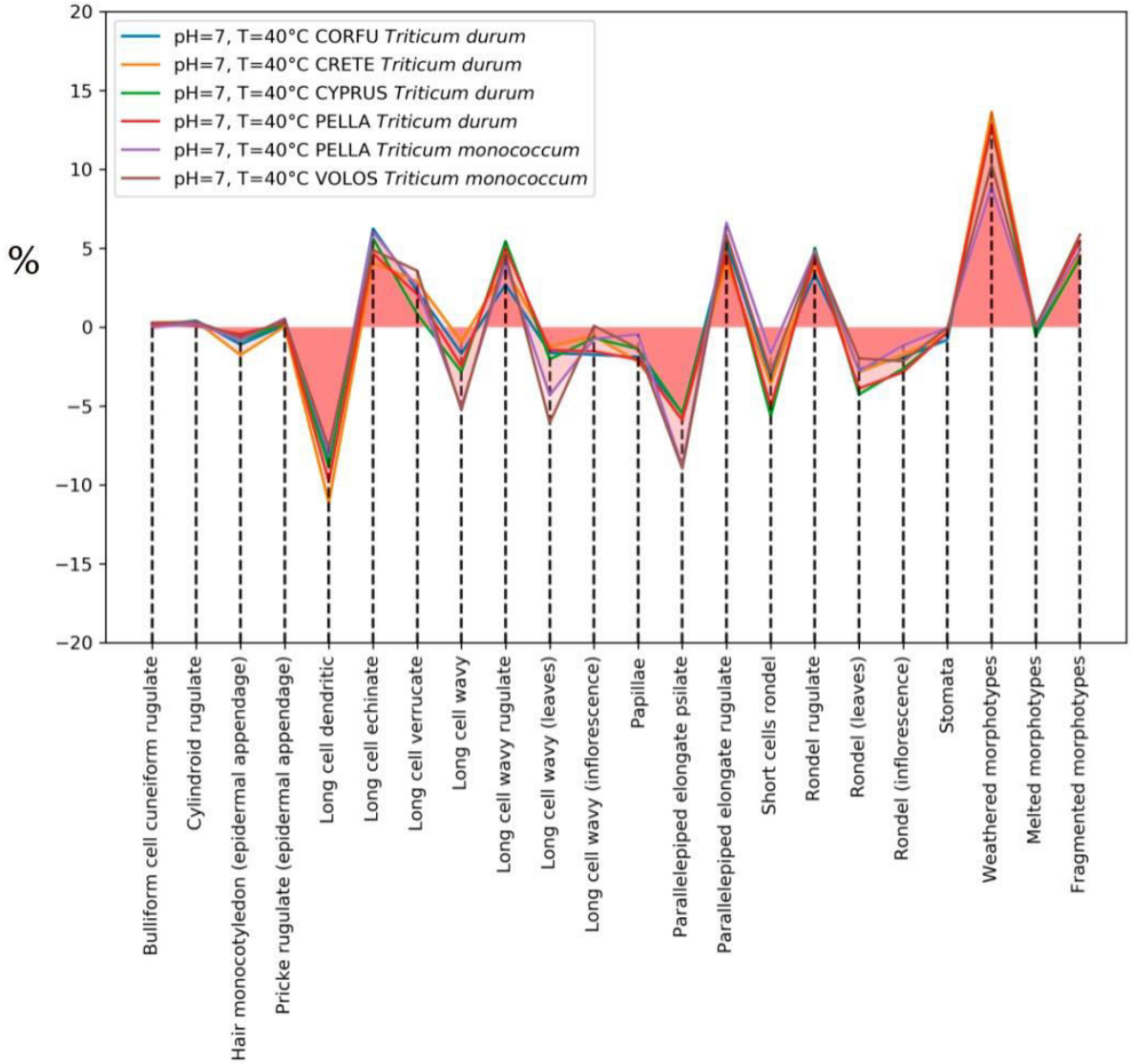

Fig. 10 The relative difference between average percentages of phytolith morphotypes (all samples), before and after the dissolution experiments (pH=7, T=40˚C)

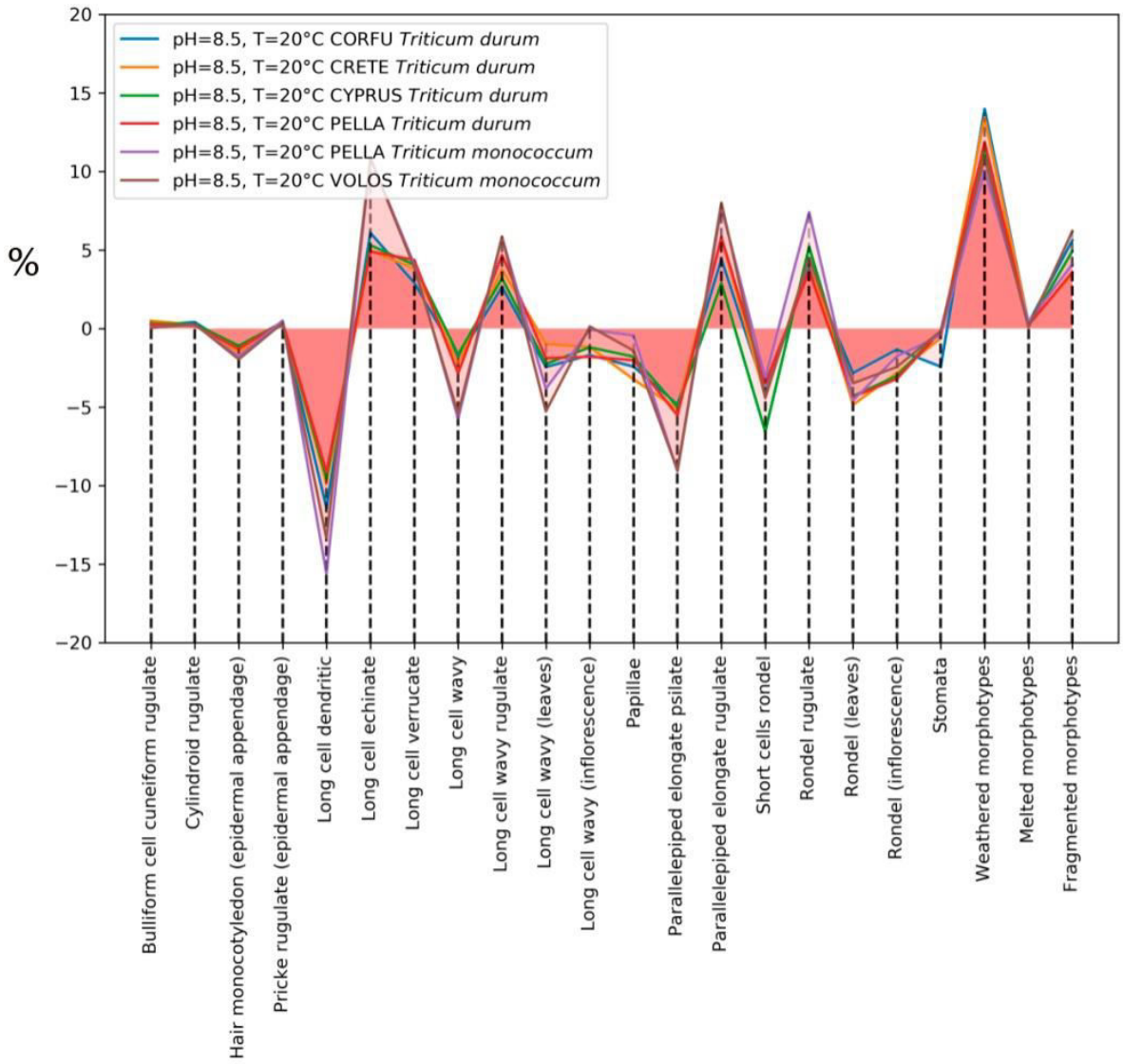

Fig. 11 The relative difference between average percentages of phytolith morphotypes (all samples), before and after the dissolution experiments (pH=8.5, T=20˚C)

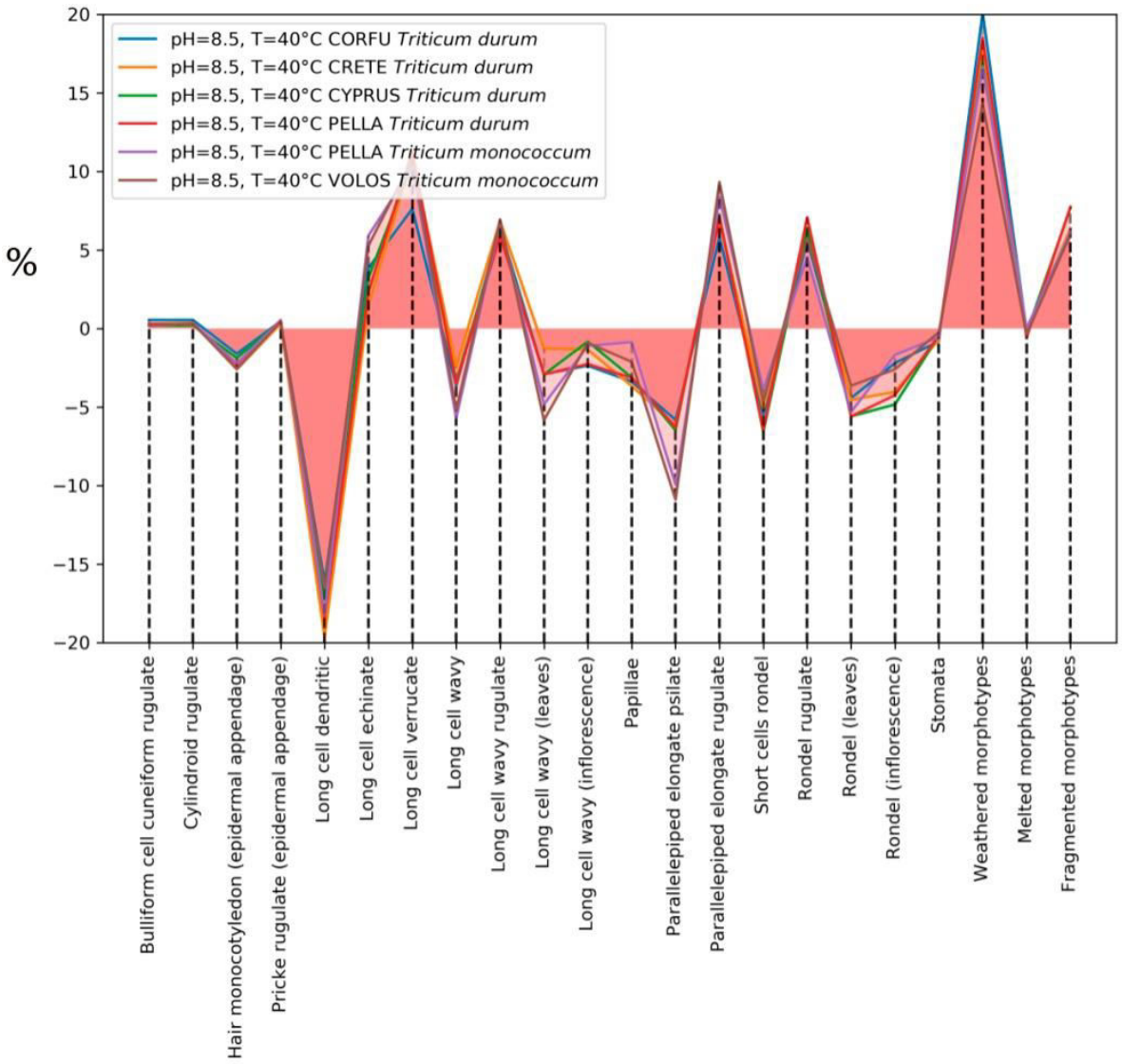

Fig. 12 The relative difference between average percentages of phytolith morphotypes (all samples), before and after the dissolution experiments (pH=8.5, T=40˚C)

4.3 Phytoliths from soils and sediments: archaeological case studies

The study of phytoliths from cultivated soils (Cyprus, Crete, Volos, Pella I, Pella II, Corfu) and archaeological sediments (Knossos, Toumba Thessaloniki, Castle Palea) provided the opportunity to investigate the impact of taphonomic processes on phytolith morhotypes. The studied soils, sediments and their pH values are presented in Table 2. All samples are characterised as alkaline (according to NRCS slightly alkaline is 7.4-7.8, moderate alkaline is 7.9-8.4, strongly alkaline is 8.5-9.0 and very strongly alkaline is above 9.0). The pH of the soils at 25°C is 7.45 (Cyprus, *Triticum durum*), 7.93 (Crete, *Triticum durum*), 7.41 (Volos, *Triticum monococcum*), 7.50 (Pella, *Triticum monococcum*), 7.58 (Pella, *Triticum durum*) and 7.62 (Corfu *Triticum durum*). The pH of the sediments at 25°C is 8.69 (*KN5* and *KN10*), 8.44 (*ΚΑΣ25*), 8.12 (*ΚΑΣ27*), 9.32 (*TB2008*) and 9.13 (*TB2013*).

Table 2 Average pH of soils and archaeological sediments (3 repetitions) at room temperature (25°C)

Soil and sediment samples	**pH**
CYPRUS (*Tr. durum*)_soil	7.45
CRETE (*Tr. durum*)_soil	7.93
VOLOS (*Tr. monococcum*)_soil	7.41
PELLA I (*Tr. monococcum*)_soil	7.50
PELLA II (*Tr. durum*)_soil	7.58
CORFU (*Tr. durum*)_soil	7.62
KNOSSOS (*KN5*)_sediment	8.69
KNOSSOS (*KN10*)_sediment	8.44
TOUMBA (*TB2008*)_sediment	9.32
TOUMBA (*TB2013*)_sediment	9.13
CASTLE PALEA (*ΚΑΣ25*)_sediment	8.44
CASTLE PALEA (*ΚΑΣ27*)_sediment	8.12

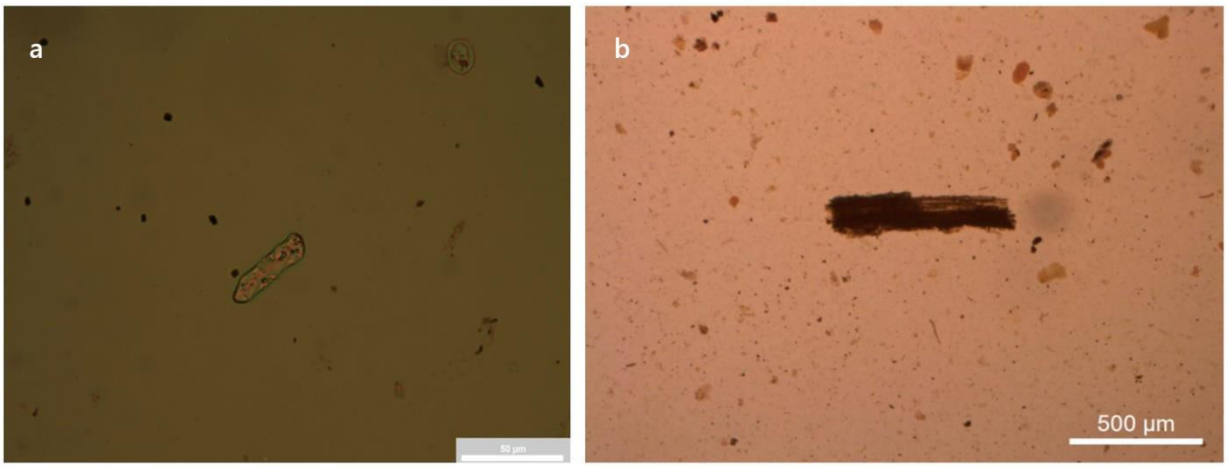

Fig. 13 Photomicrographs: **(a)** transparent wheat phytolith extracted from archaeological sediment; and **(b)** opaque phytolith extracted from ''modern'' soil. Opaqueness results from organic matter occluded within the phytolith. Organic matter degrades very fast in terms of the archaeological timescale (photomicrographs: Andriopoulou)

Previous studies suggested that phytoliths may undergo dissolution, especially in alkaline pH (Cabanes *et al.* 2011; Cabanes and Shahack-Gross 2015; Fraysse *et al.* 2006a, 2006b, 2009; Loucaides *et al.* 2008, 2010; Nguyen *et al.* 2014; Prentice and Webb 2016). Fraysse *et al.* (2006b) showed that phytoliths specific surface area decreases by 30% after 1 month reaction corresponding to dissolution of 30% of initial mass, and this may be related to the preferential dissolution of fine particles adhering to phytolith surface or microstructure heterogeneities.

Information on physicochemical surface properties of phytoliths are pivotal for understanding dissolution processes. In the present study, phytoliths from more alkaline contexts exhibited more intense alterations of their dimensional characteristics than phytoliths from less alkaline contexts. This is in accordance with Cabanes and Shahack-Gross (2015), who suggested that phytolith geometry is an important factor for phytolith dissolution and corresponding preservation. The dissolution rate of phytoliths is related to the surface area of the interface between the biogenic SiO_2 and the solvent (e.g. H_2O)

and the morphological characteristics of phytoliths may affect its geometric surface area and its specific surface area (i.e. ratio between the surface area and mass of the phytolith).

Previous microscopic observations of phytoliths have been used to understand formation processes in deposits, such as caves (Karkanas 2006) and middens (Shillito *et al*. 2008). In the present study, observations of the phytoliths using optical microscopy suggested that the depositional environment (i.e. soil or sediment) is closely related with phytolith physicochemical characteristics, such as opaqueness (Fig. 13). In particular, transparent phytoliths were extracted from archaeological sediments, while opaque phytoliths were extracted from ''modern'' soils. Opaqueness results from small amounts of organic matter occluded within the phytolith during the process of silification. Transparent SiO_2-rich bodies originate from an opaque silica gel stage and that granular inclusions within them are the remains of the nucleus and cytoplasmic contents (Prat 1931, from Prychid *et al*. 2003), and darker forms reflect higher quantities of occluded organic carbon pigmentation (Jones and Beavers 1963; Rovner 1971; Wilding and Dress 1974). Organic matter affects a wide range of biological, chemical and physical properties that control soil productivity and resistance to degradation (Dick and Gregorich 2004). Organic matter generally degrades very fast in terms of the archaeological timescale and the pH will decrease if organic matter degrades and releases organic acids (Weiner 2010). It has been suggested that occluded organic matter in phytoliths usually strength their surface against dissolution because organic matrix may act as a protective shield against hydrolysis of Si–O–Si bonds of the SiO_2 network (Nguyen *et al*. 2014; Parr and Sullivan 2005; Van Cappellen *et al*. 2002).

A total of 6 samples from the soils from the regions where plants grow were analysed. Table 3 lists the percentages of the main phytolith morphotypes found in the soil samples. Discussion for the quantification of phytoliths extracted from the plant samples is given in chapter 4.2. The decorated morphotypes (e.g. long cells dentritic, long cells echinate and long cells verrucate) that are related to the inflorescence, showed variations. The differences in the percentages of decorated long cells in the soils are clarified. In particular, dendritics range from ca. 5.1 to 17.8%, echinates range from ca. 4.4 to 9.4% and verrucates range from ca. 5.5 to 10.2%.

The most abundant morphotypes in all samples are weathered and fragmented phytoliths, as well as parallelepiped elongated long cells rugulated and long cells wavy rugulated. The percentages of weathered and fragmented phytoliths show a variation and range from ca. 9.6 to 19.8% and ca. 14.2 to 24.7%, respectively. Here, weathering and fragmentation of phytoliths tends to be positively correlated with the rise of pH and water availability of the area of study. The sample from Crete has the higher pH (pH=7.93, strongly alkaline) between soil samples and the percentages of weathered and fragmented are 17.8% and 21.7%, respectively. The sample from Corfu is related with the higher precipitation (P=1560 mm, condition of high water availability) between soil samples and the percentages of weathered and fragmented are 19.8% and 24.7%, respectively. The reaction of cations, such as K^{+}, Mg^{2+}, Ca^{2+}, and Fe^{2+} from dissolving oxides and in consequence with phytoliths, may also have an effect on their solubility (Nguyen *et al.* 2014), and thus on their preservation state. According to Cabanes *et al.* (2012, 2015) additional factors for the different phytolith preservation may be the burial depth, the rate of sediment accumulation, the effects of plant overgrowth and root activity on phytoliths, and the geometric surface to bulk ratio of individual phytoliths.

Table 3 Average percentages of the most abundant phytolith morphotypes (>1%) present in each soil sample. Triplicate samples were analysed and the standard deviations are shown

Morphotype /Soil sample	**Cyprus** *Triticum durum* **pH 7.45 P:200 mm**	**Crete** *Triticum durum* **pH 7.93 P:410 mm**	**Volos** *Triticum monococcum* **pH 7.41 P:468 mm**	**Pella** *Triticum monococcum* **pH 7.5 P:763.7 mm**	**Pella** *Triticum durum* **pH 7.58 P:763,7 mm**	**Corfu** *Triticum durum* **pH 7.62 P:1560 mm**
Bulliform cell cuneiform rugulate	1.1± 0.4	0.8± 0.3	0.5± 1.2	0.6 ± 1.2	1.2± 2.1	1.9± 0.9
Crenate	0.5 ±1.3	0.0	0.2 ± 0.1	0.1 ± 0.3	0.2 ± 0.4	0.4 ± 0.2
Crenate long	0.3 ± 0.4	0.9 ± 1.2	0.4 ± 0.5	0.3± 0.3	0.7 ± 1.2	0.4 ± 1.9
Cylindroid rugulate	1.2± 1.9	0.8± 3.1	0.2 ± 2.1	1.4± 0.9	1.3± 1.8	2.0± 0.3
Epidermal appendage. Hair monocotyledon	0.1± 0.3	0.2± 0.4	0.5 ± 1.6	0.3 ± 0.2	0.1± 0.6	0.3 ± 0.8
Epidermal appendage. **P**rickerugulate	0.3 ± 0.1	0.1 ± 0.9	0.3 ± 1.1	0.2 ±0.8	1.4 ± 0.7	0.2 ±0.8
Long cell dentritic	17.8± 1.1	5.1± 0.6	10.7± 1.3	9.2± 1.2	12.1± 0.9	8.3± 2.1
Long cells echinate	7.8± 0.2	4.9 ± 1.6	6.8 ± 1.8	9.4± 0.8	9.2± 0.3	4.4± 1.7
Long cell verrucate	5.5± 0.2	9.1± 0.1	10.2 ± 1.0	8.2± 1.9	8.8± 0.9	9.2± 0.7
Long cell wavy	5.4± 0.2	6.2 ± 0.7	3.4 ±0.9	5.0± 1.6	6.2± 1.6	3.3± 0.4
Long cell wavy rugulate	8.3± 0.4	9.3 ± 0.2	13.4±0.4	11.1 ± 0.9	8.3± 0.5	9.0± 0.2
Papillae	0.2± 0.1	0.1± 0.7	0.4± 0.8	1.2± 0.2	1.3± 0.2	0.4± 0.2
Parallelepiped elongate psilate	7.3± 1.6	2.6± 1.1	3.1±0.2	5.2± 3.2	3.1± 1.5	2.2± 0.5
Parallelepiped elongate rugulate	11.2± 0.2	9.2± 0.8	9.8±0.7	13.1± 0.2	9.2±1.9	7.2± 1.8
Short cells rondel	2.2± 0.3	1.8 ± 1.8	1.9± 0.2	1.9± 0.1	3.8± 0.3	2.1± 0.8
Rondel rugulate	0.8 ± 0.7	0.9 ±0.2	1.9 ± 0.5	0.9± 0.1	0.8± 1.3	0.6 ± 1.6
Stomata	4.3 ± 0.6	6.3 ± 0.3	5.4 ± 0.2	4.4 ± 1.6	3.2 ± 1.3	3.1± 1.3
Weathered	9.6 ± 1.5	17.8 ± 0.2	10.3 ± 0.8	11.9 ± 0.7	11.4 ± 0.8	19.8 ± 0.8
Melted	1.0± 0.4	2.2 ± 0.1	1.8 ± 0.7	1.4 ± 0.2	0.9 ± 0.3	0.5 ± 0.8
Fragmented	15.1 ± 0.8	21.7 ± 1.4	18.8 ± 0.4	14.2 ± 0.7	16.8 ± 0.5	24.7 ± 0.4

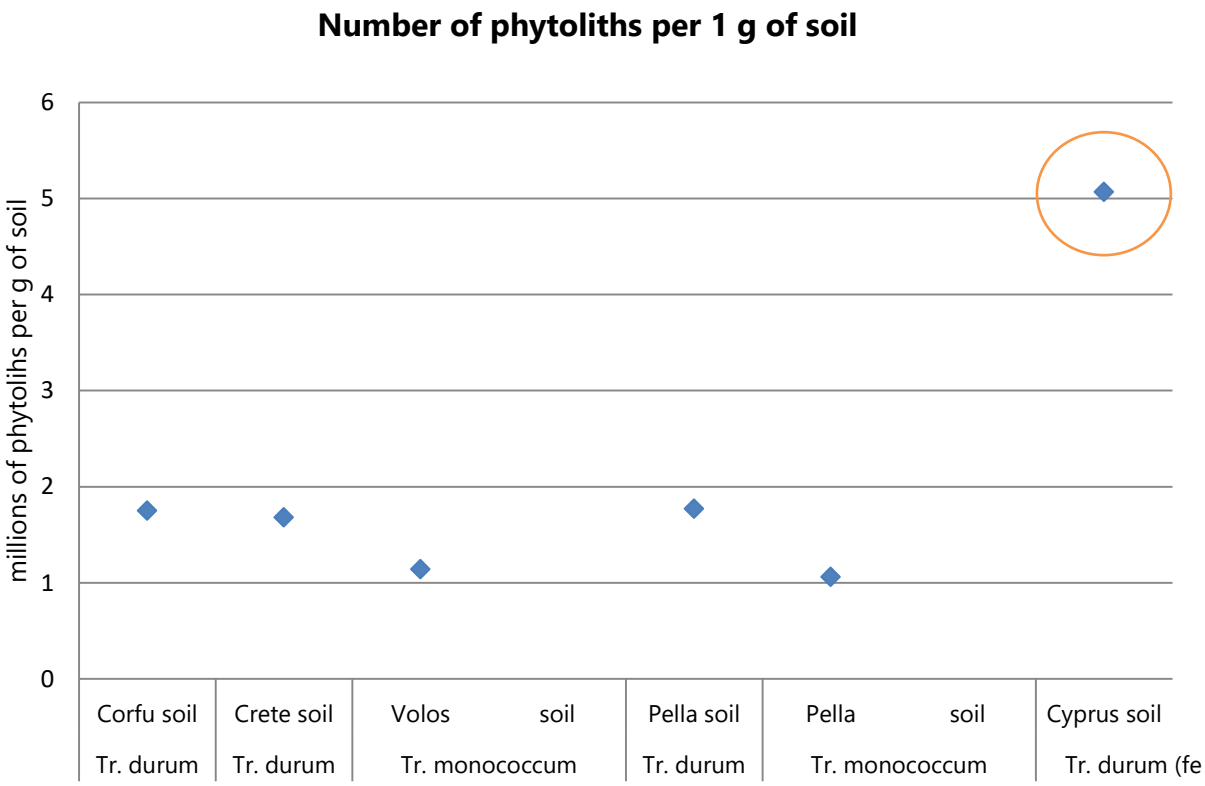

Fig. 14 Concentrations of phytoliths in the studied soils

Figure 14 shows the concentrations of phytoliths in 1 g of soil. The concentrations of phytoliths range from approximately 1 million phytoliths to approximately 5 million phytoliths. Phytolith concentration in the sample from Cyprus appears significantly higher than in the remaining samples, probably because fertilisers and phytoprotection products were used in the Cyprus field, opposite to the organic cultivations in Greece. The main fertiliser used in the Cyprus soil was the NPK 20/20/0 in a dosage of 30 kg per 1000 m^2. The first number in fertilisers signifies the percentage content of nitrogen (N), the second of phosphorus (P) and the third of potassium (K). A 34.5/0/0 top dressing was used in a dosage of 12 kg per 1000 m^2. The following herbicides were used for phytoprotection: Atlantis by Bayer while in cultivation and Goal Goal®2XL by Dow

AgroSciences LLC along with Control Mega during the fallowing period. Atlantis is a combination of twosulfonylurea herbicides with foliar and some root activity, Goal Goal® 2XL is used for postemergence and preemergence residual weed control with the main following ingredients: oxyfluorfen 2-chloro-1-(3-ethoxy-4-nitrophenoxy), 4-(trifluoromethyl) benzene, and Control Mega is a dense solution of the isopropylamine salt glyphosate and other additives. The presence of the aforementioned chemical products may explain the surplus of phytoliths in Cyprus soil sample. According to previous studies, natural fertiliser (e.g. ruminant dung) shows high concentrations of phytoliths (Shahack-Gross and Finkelstein 2008) and therefore its use may potentially increase the concentration of phytoliths in soils. Samples from Cyprus field where fertiliser was added, showed higher number of phytoliths than samples from the remaining fields. The fact that fertiliser addition probably affects the phytolith content in the soil may prove useful for the identification of fertilisers in the archaeological record and therefore for the detection of human agricultural past activity.

In archaeobotanical studies of wheat and barley, weeds play a significant role in determining crop-processing stages (Harvey and Fuller 2005, and references therein). In the present study, phytolith assemblages from the ''modern'' soils do not correspond to the phytolith assemblages produced by ''modern'' plants. The differences in phytoliths concentration may be, among others (preservation, harvesting etc.), the outcome of phytolith deposition in the soils from other plants (i.e. dicotyledonous weeds) that were already present in the areas. Phytolith assemblages are formed by monocotyledonous (i.e. wheats *Triticum monococcum* and *Triticum durum*) and dicotyledonous plants. According to our results, the percentage of monocotyledonous morphotypes is soil samples ranges from 30.35 to 51.43%. In particular it is: 51.43% in Cyprus, 40.32% in Crete, 36.02% in Volos, 34.98% in Pella I, 30.35% in Pella II, and 36.11% in the Corfu sample. In contrast, dicotyledonous morphotypes are less abundant, with percentages

ranging from 1.92 to 10.23%, with silicified polyhedral epidermal cells with rugulate surfaces being the most common type. In particular dicotyledonous morphotypes are: 3.21% in Cyprus, 4.63% in Crete, 10.23% in Volos, 1.92% in Pella I, 2.34% in Pella II and 9.6% in Corfu.

In Crete, the field was cultivated mainly with *Solanum lycopersicum* (tomato) and remained uncultivated in the following twelve years, during which period *Andropogon diastachyos* (bluestem grass), *Chrysanthemum coronarium* (garland chrysanthemum), *Malva sylvestris* (mallow) and *Sonchus oleraceus* (sow thistle) were the main plants of the field (Chatzigeorgiou, personal communication 2017). In Volos, *Avena barbata* (slender wild oat), *Hordum murinum* (wall barley), *Lamium album* (white nettle), *Lolium rigidum* (annual ryegrass), *Pisum sativum* (pea), *Plantago lanceolate* (ribwort plantain), *Sinapis arvensis* (charlock mustard), *Sonchus oleraceus* (sow thistle), *Taraxacum officinalis* (dandelion) represent the main plants of the field before the cultivation of wheats (Koutis, personal communication 2017). In Corfu, the field was uncultivated for two years and mainly contained *Cichorium intybus* (chicory), *Foeniculum vulgare* (fennel), *Sinapis arvensis* (charlock mustard) (Vlassi, personal communication 2017). In Pella, the field had wheats (*Triticum monococcum*, *Triticum durum* and *Triticum spelta*) and *Arctium lappa* (greater burdock) (Doumos, personal communication 2017). Finally, in Cyprus, the field was one year cultivated with *Triticum durum* and one year uncultivated alternately, with some wild plants grown in the area, which however were not identified (Pallides, personal communication 2017).

The fact that phytolith assemblages in soils do not correspond to phytolith assemblages in plants may also be related to the harvest process. Because of the harvesting the inflorescence, stem and leaves of the wheats have been removed from the fields. This diminishes the chances for cultivated plants growing in a field to leave a

complete, strong phytolith imprint in the soil. The identification of plant remains not only in ''modern'' soils, but also in archaeological sediments (across sites and between sites) through phytolith analysis is important in understanding human activity patterns such as wheat processing stages (Fig. 15). Tsartsidou *et al.* (2008) studied the use of plants and several human activities in an agropastoral village in Greece (Sarakini) and developed a method of quantifying the differences in the phytolith assemblages when compared to regional control samples (i.e. areas with no activity in the same area). One year later, Tsartsidou *et al.* (2009) used this method to study the phytolith assemblages in a prehistoric site (Makri) that is in the same region as their aforementioned study. They suggested that wheat and barley were cultivated for human and animal use in the area during the Neolithic period.

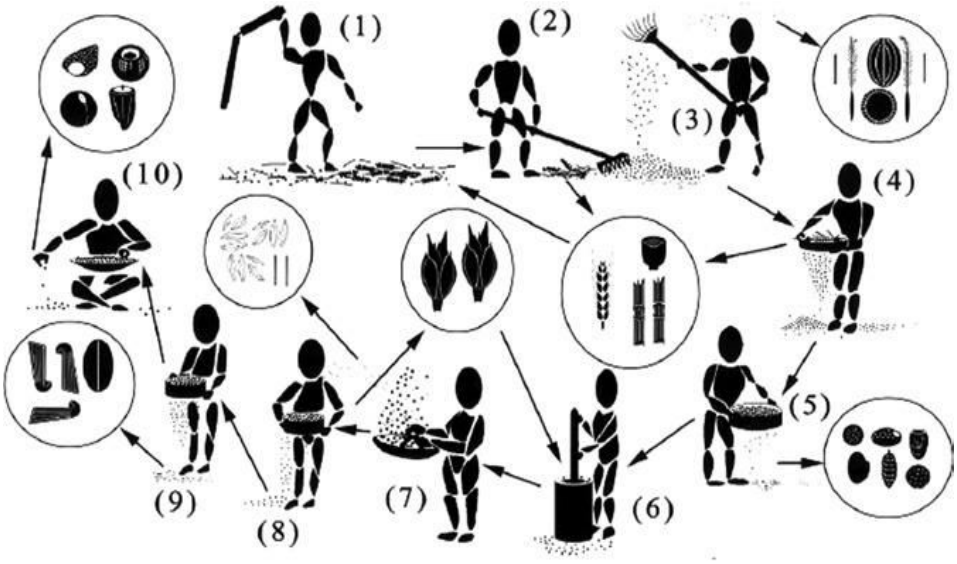

Fig. 15 Hulled wheat (wheat with persistently enclosing hulls like *Triticum monoccocum*) processing stages: **(1)** threshing, **(2)** raking, **(3)** first winnowing - light weed seeds and some awns are removed, **(4)** coarse sieving - weed seed heads, unbroken ears, straw fragments are removed and unbroken ears are rethreshed, **(5)** first fine sieving - small weed seeds and awns are removed, **(6)** pounding, **(7)** second winnowing paleas, lemmas and some awns are removed, **(8)** sieving with medium-coarse sieve - spikelet forks and unbroken spikelets - repounded, **(9)** second fine sieving - glume bases, awns, remaining small weed seeds, tail grain and awns removed; and **(10)** hand sorting - removal of grain-sized weeds by hand (source: Stevens 2003, in Zapata *et al.* 2004)

Archaeological sites vary throughout place and time and as a result phytolith studies are oriented towards a broad range of contexts. Phytoliths can be found in bulk soils/sediments samples, as well as sometimes in artefacts, such as pottery (Liu *et al.* 2020; Petö and Vrydaghs 2016; Thompson *et al.* 1995; Yao *et al.* 2012) and features, such as ash layers (Albert and Cabanes 2008; Albert and Weiner 2001; Canti 2003). Artefact plant residues are either primary (i.e. those associated with original artifact) use or secondary (i.e. those associated with post-depositional processing). In the present study, the archaeological samples were collected from different environments so that they may represent diverse human cultural practices. The extraction involved separation of phytoliths from the sample matrix, so that the obtained residue could be mounted on a slide for observation under the optical microscope.

The archaeological samples originated from an activity area (an indoor living space), an artefact (the interior of a ceramic vessel), a combustion residue (ashes next to the kiln), a food processing tool (a grinding stone) and construction materials (plaster floors of a building). Previous studies have suggested or confirmed the presence of micro- or macro-wheat residues in the studied archaeological sites in Greece: Knossos (Efstratiou *et al.* 2004; Evans 1903, 1964; Jones 1984; Livarda 2008; Sarpaki 2009), Toumba (Kotsachristou 2009; Valamoti 2009) and Castle of Palea (Jones 1982; Tsartsidou, personal communication 2017). However, in the present study, the available archaeological samples did not contain the minimum number of phytoliths (>50) needed for a reliable interpretation of the plant component (Albert and Weiner 2001), suggesting that post-depositional processes impact the presence of phytoliths. There is also a possibility that the rapid extraction method (Katz *et al.* 2010) used here might have not been able to seperate all phytoliths from the archaeological sediments, suggesting that more methods of phytoliths extraction from soils and sediments should be developed. Furthermore, the

low amount of phytoliths may also be related with human use of plants that poorly produce phytoliths (e.g. woody species) (Tsartsidou *et al.* 2007).

During the early excavations in Knossos, a variety of archaeobotanical samples were collected (Evans 1903, 1964), including grains and spikelets of wheat (*Triticum monococcum*, *Triticum dicoccum* and *Triticum aestivum*). These samples were initially studied by Helbaek, but the results remained unpublished (Helbaek 1968, from Sarpaki 2009). Macro-remains of wheat at the settlement are reported by Efstratiou *et al.* (2004) and Sarpaki (2009, 2012). In addition, Jones (1984) and Livarda (2008) mention the presence of free-threshing wheat alongside other cereals and pulses at the positions of the Unexplored Mansion and the Little Palace in Knossos respectively. Micro-remains of wheat, namely phytolith assemblages from the Neolithic deposits of Knossos were studied by Madella (2013).

In the present study, two samples from Knossos (*KN5* and *KN10*) were analysed by optical microscopy. Sample *KN5* originated from a general anthropic layer (a layer of a Minoan room); by contrast sample *KN10* originated from a specific structure (the inner part of a ceramic vessel at the Minoan room). Although phytoliths from grasses are almost absent in *KN5* sample, few phytoliths from dicotyledons were recovered suggesting an input of noncrop plants. It is possible that either the use of the Minoan room might have affected the preservation of phytoliths due to possible frequent trampling, or a period of abandonment of the Minoan room might have affected the phytolith input, mainly with the input of dicotyledons plants. Regarding the *KN10* sample, only scarce phytoliths from grasses, probably cereals were recovered from the inner part of the ceramic vessel. Hypothetically, the vessel was used for the storage or transport of food or/and fodder.

It would be interesting to analyse an extra sample from the outer part and compare the results apart from sample *KN10*, but no sample was available. For better understanding the use/function of the vessel, archaeological control samples should be compared to assess phytolith contamination. In general, the collection of control samples from different geogenic layers is important in order to establish whether the potential phytoliths in archaeological layers represent anthropogenic input. Supplementary analysis of organic residues may also be helpful. Below the main processes affecting the organic residues in archaeological ceramics are presented (Fig. 16).

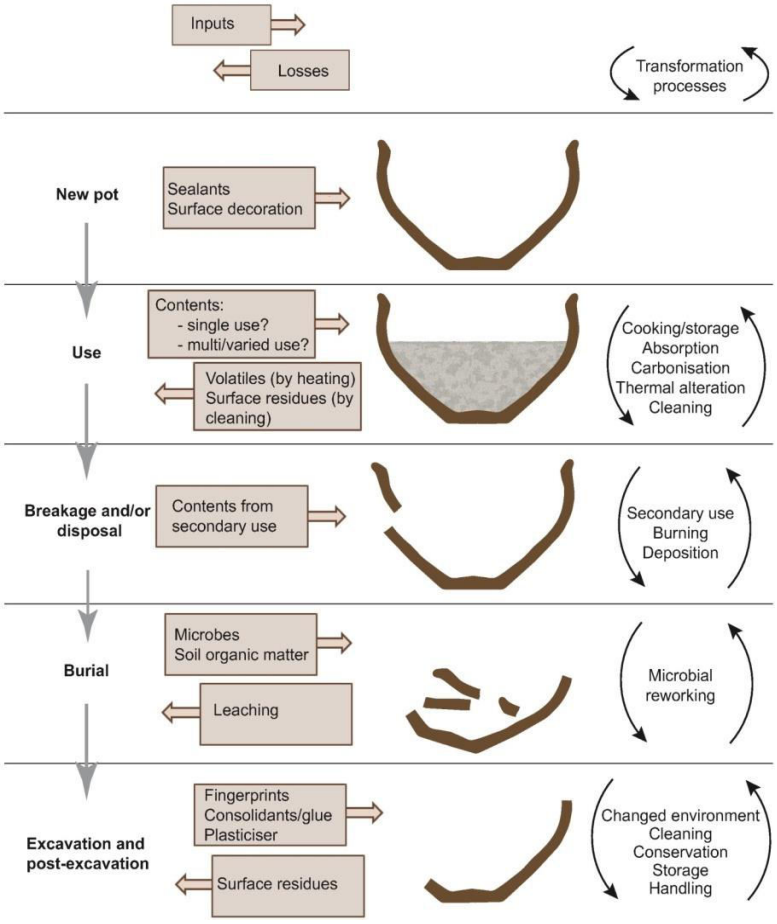

Fig. 16 Main processes affecting organic residues in archaeological ceramics [source: adapted from Historic England (2017) after Stacey (2009), in Roffet-Salque *et al.* (2017)]

Nitsch *et al*. (2017) have identified a range of crop species [einkorn, emmer, ''new type'' glume wheat, hulled (likely 2- and 6-row) barley, spelt, free-threshing wheat, lentil, bitter vetch, Celtic bean, grass pea and millet] at Toumba. Previous work on wheats at Toumba shows that the *Triticum monococcum* is represented mainly by glume bases and *Triticum durum* is represented mainly by grains and less by rachis internodes, with more intense presence of *Triticum monococcum* than *Triticum durum* (Kotsachristou 2009; Valamoti 2009). In the present study, two samples from Toumba (*TB2008* and *TB2013*) were analysed by optical microscopy. The sample *TB2008* was derived from a kiln and appear to contain morphologies akin to phytoliths, which were hardly detectable probably due to melting (Fig. 17 a). The morphologies can not serve as a diagnostic marker for the characterisation of specific taxa; however few polyhedral phytoliths, which seem to belong to Anacardiaceae family, most probably *Pistacia* spp. (mastic tree) were also recovered. The phytolith analysis shows that most probably mastic tree had been used as a fuel in the kiln. A controlled fire is mainly composed of the products of the fuel combustion, usually wood and leaves. Previous studies had also focused on the study of fire residues from plants where plants have been used as fuel (Albert *et al*. 2000; Esteban *et al*. 2018; Rowlett 2000).

In any case, due to the low production of phytoliths by ligneous tissues only large accumulations of wood ash are detectable through phytolith analysis. The sample *TB2013* derived from a grinding tool. The traditional process of manual cereal grinding has been object of several archaeological and ethnological studies (Alonso 2019, and references therein). Previous archaeo- or ethnobotanical studies on grinding and pouding tools suggest the presence of wheat on the artefacts (Ertug-Yaras 2002, García-Granero *et al*. 2017; Peña-Chocarro *et al*. 2009; Radomski and Neumann 2011). In the present study, thirty-three (33) phytoliths probably from wheat (*Triticum* spp.) or barley (*Hordeum* spp.) inflorescence were recovered from sample *TB2013* (Fig. 17 b).

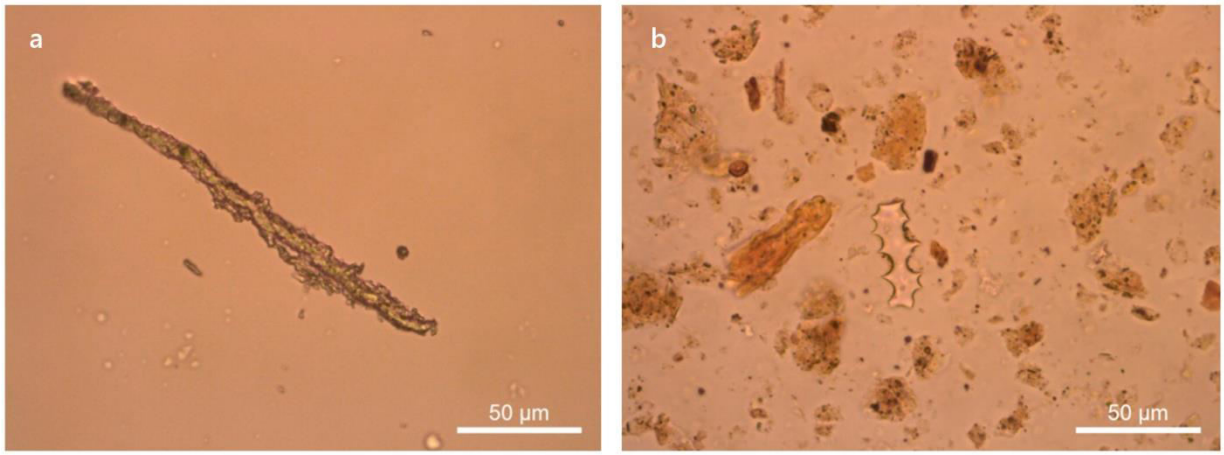

Fig. 17 Photomicrographs: **(a)** unidentified morphotype with surface alterations, probably due to melting. The phytolith is extracted from *TB2008* sample; and **(b)** transparent decorated phytolith in the centre of the photomicrograph. The phytolith is extracted from *TB2013* sample and probably comes from wheat (*Triticum* spp.) or barley (*Hordeum* spp.) inflorescence (photomicrographs: Andriopoulou)

According to previous studies in Castle of Palea, Volos wheat grains, in particular of the *Triticum dicoccum* variety are present, but the presence of *Triticum monococcum* or/and *Triticum durum* has yet to be confirmed. Jones (1982) reported few quantities of reported grains of free-threshing wheat in the area. The presence of wheat in the Castle of Palea is further supported by a previous analysis of phytolith assemblages collected from the ground (of the neighbouring layers), with findings of wheat husk phytoliths (Tsartsidou, personal communication 2017). The research of Tsartsidou has contributed not only to the understanding of the use of wheat and other plants such as barley, reed and rush on the site, but also to the understanding of the different uses of different spaces in the building. In conjunction with manure findings in the vicinity, the same study suggests agricultural and livestock activities (Skafida *et al.* 2015).

In the present study, two samples from Castle Palea (*KAΣ25* and *KAΣ27*) were analysed by optical microscopy. The *KAΣ25* sample was taken from a thin layer overlaying a yellowish Mycenaean floor and the *KAΣ27* sample was taken from a pebbled Mycenaean floor, older than the previous one. Analysis underlined the absence of phytoliths in both samples. Water evaporation caused precipitation of gypsum ($CaSO_4 \cdot 2H_2O$) detected in Castle Palea samples (see XRD traces below), which may break up sediments mechanically and potentially may affect the preservation of microbotanical remains. A similar process could be observed before on floors in buildings at Çatalhöyük (Turkey), where trampling may mix and disaggregate plaster fragments and botanical remains (Matthews 2010).

Alkaline conditions generally occur in sediments that contain calcite, as calcite buffers the pH of the water in the sediment to around 8.2 (Lippmann 1973; Weiner, 2010). The pH of the studied archaeological sediments at 25°C is ranges between 8.12 and 9.32. According to mineralogical analysis (see XRD traces below) the sediments samples contain calcite ($CaCO_3$). The solubility of phytoliths increases with increasing pH, thus phytoliths may be absent from some samples because they dissolved totally. Friesem (2016) proposed that *''the biggest challenge archaeologists face is to distinguish between evidence of absence (i.e. people did not act in a certain way, which left no traces whatsoever) and absence of evidence (i.e. activity remains were deposited on the floor but post-depositional processes erased any traces)''*.

4.4 Powder X-ray Diffraction (XRD)

4.4.1 Mineralogical analysis of plant samples

The results of the XRD analysis for the plant samples are summarised in Table 4, the results for stem-leaves in Table 5 and 7 for inflorescence in Table 6 and 8.

Table 4 Mineral phases present in the samples and their abbreviations and chemical formulae

Mineral phases	Abbreviations	Chemical formulae
Ammonium carbonate hydrate	Ammch	$(NH_4)_2CO_3{\cdot}H_2O$
Anhydrite	Anh	$CaSO_4$
Aphthitalite	Aph	$(K,Na)_3Na(SO_4)_2$
Arcanite	Arc	K_2SO_4
Barbosalite	Brb	$Fe^{2+}Fe_3{}^{+2}(PO_4)_2(OH)_2$
Bassanite	Bss	$CaSO_4{\cdot}1/2H_2O$
Baylissite	Bls	$K_2Mg(CO_3)_2{\cdot}4H_2O$
Brucite	Brc	$Mg(OH)_2$
Calcite	Cal	$CaCO_3$
Celestite (or Celestine)	Cls	$SrSO_4$
Chlorocalcite	Chlc	$KCaCl_3$
Illite/Muscovite	Ill/Ms	$(K,H_3O)(Al, Mg, Fe)_2(Si, Al)_4O_{10}[(OH)_2\ (H_2O)]$ / $KAl_2(AlSi_3O_{10})(F,OH)_2$
Monetite	DCPA	$CaHPO_4$
Monohydrocalcite	Mnhc	$CaCO_3{\cdot}H_2O$
Mundrabillaite	Md	$(NH_4)_2Ca(PO_3OH)_2{\cdot}H_2O$
Schertelite	Scher	$(NH_4)_2Mg(PO_3OH)_2{\cdot}4H_2O$
Strontianite	Str	$SrCO_3$
Struvite	St	$(NH_4)Mg(PO_4){\cdot}6H_2O$

The phases identified after the mineralogical analysis of all plant samples using dry extraction method (Cyprus, Crete, Volos, Pella I, Pella II, Corfu), and wet extraction method (Pella I, Pella II), are anhydrite, aphthitalite, arcanite, barbosalite, bassanite, baylissite, brucite, calcite, celestite, chlorocalcite, monetite, monohydrocalcite, mundrabillaite, schertelite, strontianite, illite/muscovite; and probably ammonium carbonate hydrate and struvite. The minerals that are identified in XRD derive from the process of the plant material (during acid treatment or/and burning of the residual inorganic wheat material) and they do not directly relate to phytoliths. In addition, the hump (bell-shaped increase of the background) at 10-30°2θ indicates the presence of amorphous matter, most probably opal ($SiO_2 \cdot nH_2O$). The amorphous matter, as it is observed in XRD traces, is the result of the phytolith presence.

This study is at odds with previous work, because organic minerals typically reported in plant biominerals (e.g. or/and whewellite weddellite) (Garvie 2003; Monje and Baran 2000) were not present in the samples. Previous work on directly isolated cactus biominerals without any laboratory pre-treatment reported the presence of weddellite and α-quartz (Monje and Baran 2000), whereas cacti slices dried at 60°C followed by dissolution of the organic matter in diluted sodium hypochlorite (NaOCl) consisted of weddelite, calcite and some Mg- and Ca-bearing minerals (Garvie 2003). When the plants are calcined, the calcium oxalate crystals [whewellite, $CaC_2O_4 \cdot H_2O$ and weddellite $Ca(C_2O_4) \cdot 2H_2O$] are converted into calcium carbonate when the temperature reaches ca. 430-510°C (Frost and Weier 2004). Also, CaOx usually turns into POCC [Pseudomorphose d'Oxalate de Calcium en Calcite (in French)<Pseudomorphosis of Calcium Oxalate to Calcite or calcium carbonate pseudomorph] (Brochier and Thinon 2003).

Calcium is an important element for plants and through its formation of ionic bonds with pectins it becomes a main component of cell walls (McAinsh and Pittman 2008). For example, hairs/trichomes of *Lesquerella ovalifolia* (roundleaf bladderpod) contain abundant calcium carbonate in the form of calcite, accompanied with a small amount of opal (Lanning 1961). Calcium carbonate crystals are usually formed inside cystoliths (Setoguchi *et al*. 1989), and calcite in mature leaves is enclosed in a siliceous sheath (Bauer *et al*. 2011). Ca-bearing minerals, in particular chlorocalcite and monohydrocalcite, were detected in all plant parts for both species and using both extraction methods, whereas calcite was observed only in plants treated with the wet method. In the stem-leaves from Crete sample and the inflorescence of Corfu sample, chlorocalcite was not detected. Furthermore, in the stem-leaves from Corfu sample and the inflorescence of Volos sample, monohydrocalcite was not detected.

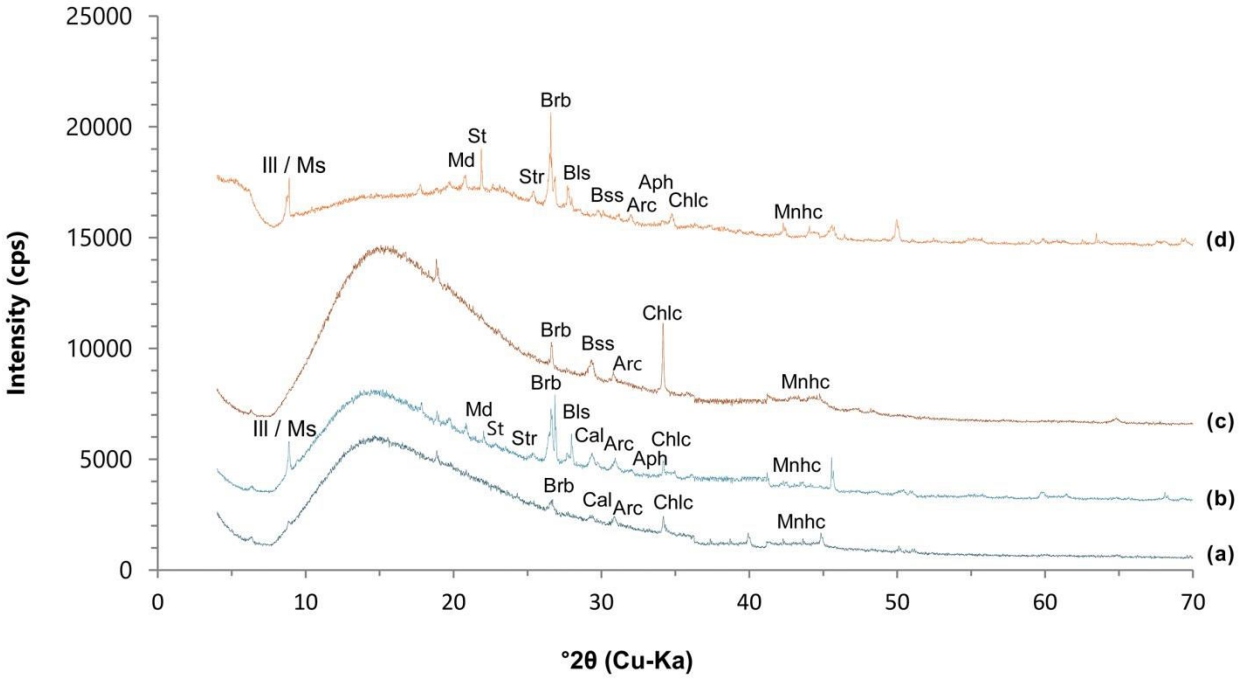

Fig. 18 XRD traces for *Triticum durum* and *Triticum monococcum* stem-leaves from Pella using dry and wet method: **(a)** *Triticum monococcum* stem-leaves (wet method), **(b)** *Triticum durum* stem-leaves (wet method), **(c)** *Triticum monococcum* stem-leaves (dry method); and **(d)** *Triticum durum* stem-leaves (dry method). The hump in the range 10-30 °2θ is related with the presence of amorphous matter (i.e. phytoliths). The following mineral phases are present in these samples: Arcanite (Arc), Barbosalite (Brb), Bassanite (Bss), Baylissite (Bls), Calcite (Cal), Chlorocalcite (Chlc), Illite/Muscovite (Ill / Ms) Monohydrocalcite (Mnhc), Mundrabillaite (Md), Strontianite (Str) and probably Struvite (St)

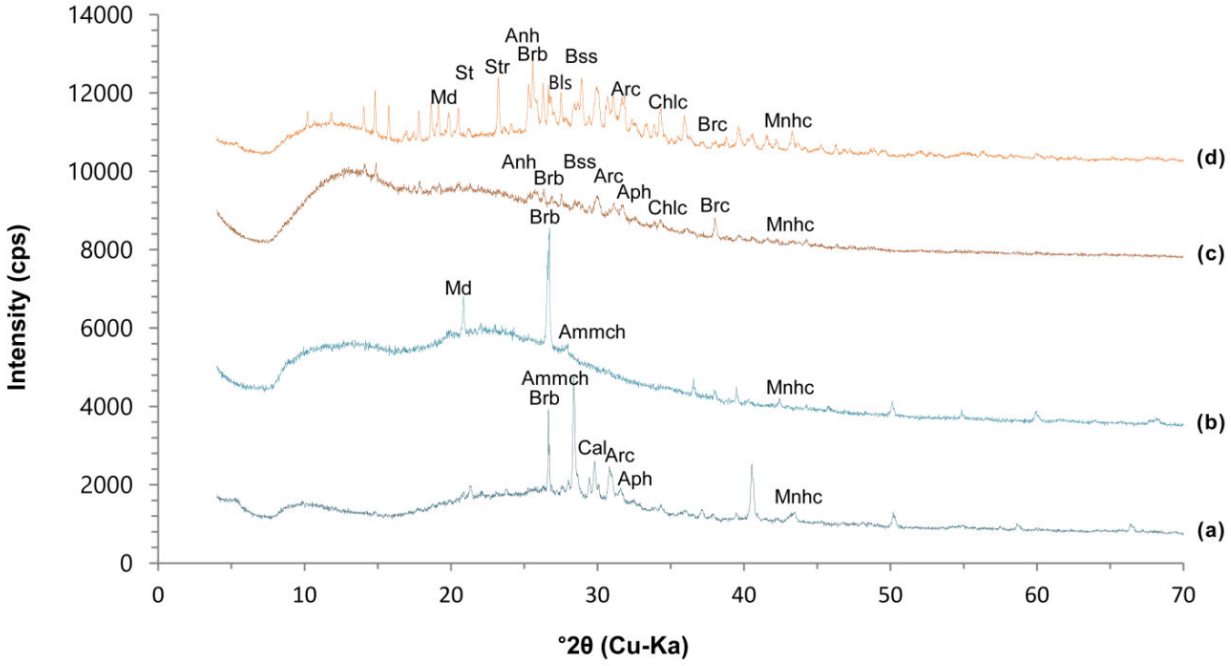

Fig. 19 XRD traces for *Triticum durum* and *Triticum monococcum* inflorescence from Pella using dry and wet method: **(a)** *Triticum monococcum* inflorescence (wet method), **(b)** *Triticum durum* inflorescence (wet method), **(c)** *Triticum monococcum* inflorescence (dry method); and **(d)** *Triticum durum* inflorescence (dry method). The hump in the range 10-30 °2θ is related with the presence of amorphous matter (i.e. phytoliths). The following mineral phases are present in these samples: Anhydrite (Anh), Aphthitalite (Aph), Arcanite (Arc), Barbosalite (Brb), Bassanite (Bss), Baylissite (Bls), Brucite (Brc), Calcite (Cal), Chlorocalcite (Chlc), Monohydrocalcite (Mnhc), Mundrabillaite (Md), Strontianite (Str), and probably Ammonium carbonate hydrate (Ammc) and Struvite (St)

Table 5 Mineralogical composition of the *Triticum durum* and *Triticum monococcum* stem-leaves from Pella (I and II) using dry or wet method

Mineral phases	*Tr. durum* stem-leaves **PELLA II (dry method)**	*Tr. monococcum* stem-leaves **PELLA I (dry method)**	*Tr. durum* stem-leaves **PELLA II (wet method)**	*Tr. monococcum* stem-leaves **PELLA I (wet method)**
Arcanite K_2SO_4	X	X	X	X
Aphthitalite $(K,Na)_3Na(SO_4)_2$	X		X	
Barbosalite $Fe^{2+}Fe_3^{+2}(PO_4)_2(OH)_2$	X	X	X	X
Bassanite $CaSO_4 \cdot 1/2H_2O$	X	X		
Baylissite $K_2Mg(CO_3)_2 \cdot 4H_2O$	X		X	
Calcite $CaCO_3$			X	X
Chlorocalcite $KCaCl_3$	X	X	X	
Illite/Muscovite $(K,H_3O)(Al, Mg, Fe)_2(Si, Al)_4O_{10}[(OH)_2 (H_2O)]$ / $KAl_2(AlSi_3O_{10})(F,OH)_2$	X		X	
Monohydrocalcite $CaCO_3 \cdot H_2O$	X	X	X	X
Mundrabillaite $(NH_4)_2Ca(PO_3OH)_2 \cdot H_2O$	X		X	
Strontianite $SrCO_3$	X		X	
Struvite $(NH_4)Mg(PO_4) \cdot 6H_2O$	X		X	

Each laboratory method has a different impact on the mineralogy of phytoliths and their surrounding matrix, which is of high importance for their preservation and therefore for their accurate interpretation. Overall, a greater variety of minerals were detected when the samples were processed with the dry method compared with the wet method, which might indicate the presence of neoformed mineral phases (secondary mineral

formation), due to the exposure of the samples to relatively high temperatures during the dry method of phytolith extraction.

Table 6 Mineralogical composition of the *Triticum durum* and *Triticum monococcum* inflorescence from Pella (I and II) using dry or wet method

Mineral phases	*Tr. durum* Inflorescence **PELLA II (dry method)**	*Tr. monococcum* inflorescence **PELLA I (dry method)**	*Tr. durum* Inflorescence **PELLA II (wet method)**	*Tr. monococcum* Inflorescence **PELLA I (wet method)**
Ammonium carbonate hydrate $(NH_4)_2CO_3 \cdot H_2O$			X	X
Anhydrite $CaSO_4$	X	X		
Aphthitalite $(K,Na)_3Na(SO_4)_2$		X		X
Arcanite K_2SO_4	X	X		X
Barbosalite $Fe^{2+}Fe_3^{+2}(PO_4)_2(OH)_2$	X	X	X	X
Bassanite $CaSO_4 \cdot 1/2H_2O$	X	X		
Baylissite $K_2Mg(CO_3)_2 \cdot 4H_2O$	X			
Brucite $Mg(OH)_2$	X	X		
Calcite $CaCO_3$				X
Chlorocalcite $KCaCl_3$	X	X		
Monohydrocalcite $CaCO_3 \cdot H_2O$	X	X	X	X
Mundrabillaite $(NH_4)_2Ca(PO_3OH)_2 \cdot H_2O$	X		X	
Strontianite $SrCO_3$	X			
Struvite $(NH_4)Mg(PO_4) \cdot 6H_2O$	X			

Bassanite was detected in the stem-leaves and inflorescences of both plant species only after processing with the dry method, and anhydrite was only detected in the inflorescences with the use of the dry method. Bassanite and anhydrite are metastable phases in the system $CaSO_4$ - H_2O (Murat and Foucalt 1977). Anhydrite might have formed during calcination of the samples by reaction between calcium and sulphur present in the plant, and bassanite is the product of partial rehydration of anhydrite upon exposure to the atmosphere. Gypsum, which is the stable hydrated phase in the system $CaSO_4$ - H_2O was not identified in any plant sample.

The lack of diffraction maxima attributed to SiO_2 polymorphs is at odds with the abundance of SiO_2 in the samples (see Tables 13-15) and the absence of quartz (Monje and Baran 2000; Wilding and Drees 1974) is related with the presence of amorphous phases. The presence of amorphous phases (i.e. phytoliths) is indicated by the hump in the range 10-30°2θ (Figs. 18-23). Quartz was identified in all soils (Table 10) and all archaeological sediments (Table 12), however quartz was not identified in the plant samples (Tables 5-8) using either dry or wet method of phytolith extraction.

Characteristic XRD traces of both wheat species from Pella (I and II) samples using dry and wet extraction method are presented in Fig. 18 (stem-leaves) and Fig. 19 (inflorescence). Charcteristic XRD traces for both wheat species, stem-leaves and inflorescence from all samples (Cyprus, Crete, Volos, Pella I, Pella II, Corfu) using only dry extraction method are presented in Fig. 20 (*Triticum durum* stem-leaves), Fig. 21 (*Triticum monococcum* stem-leaves), Fig. 22 (*Triticum durum* inflorescence), and Fig. 23 (*Triticum monococcum* inflorescence).

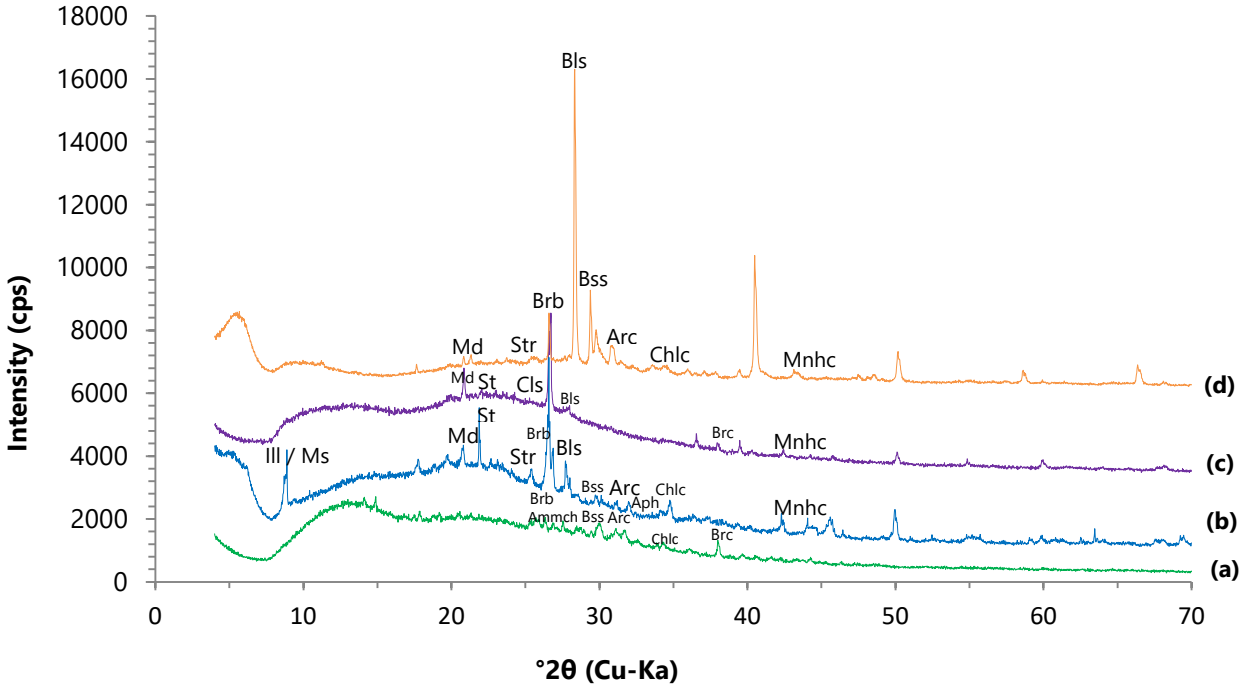

Fig. 19 XRD traces for *Triticum durum* stem-leaves from: **(a)** Corfu, **(b)** Pella II, **(c)** Crete; and **(d)** Cyprus using dry method. The hump in the range 10-30 °2θ is related with the presence of amorphous matter (i.e. phytoliths). The following mineral phases are present in these samples: Arcanite (Arc), Aphthitalite (Aph), Barbosalite (Brb), Bassanite (Bss), Baylissite (Bls), Brucite (Brc), Chlorocalcite (Chlc), Celestite (Cls), Monohydrocalcite (Mnhc), Illite/Muscovite (Ill / Ms), Mundrabillaite (Md), Strontianite (Str), and probably Ammonium carbonate hydrate (Ammc) and Struvite (St)

Even if great care was taken to extract pure phytoliths, the presence of illite/muscovite in the stem-leaves of *Triticum durum* from Pella suggests that clay was not thoroughly eliminated with either method. It is yet to be determined whether the clay mineral is incorporated in phytoliths while the plant grows or if it is a surface (or airborne) contaminant due to the contact of phytoliths with soil. Plants absorb Al along with Si, which might co-precipitate in their tissues (Hodson and Sangster 1993).

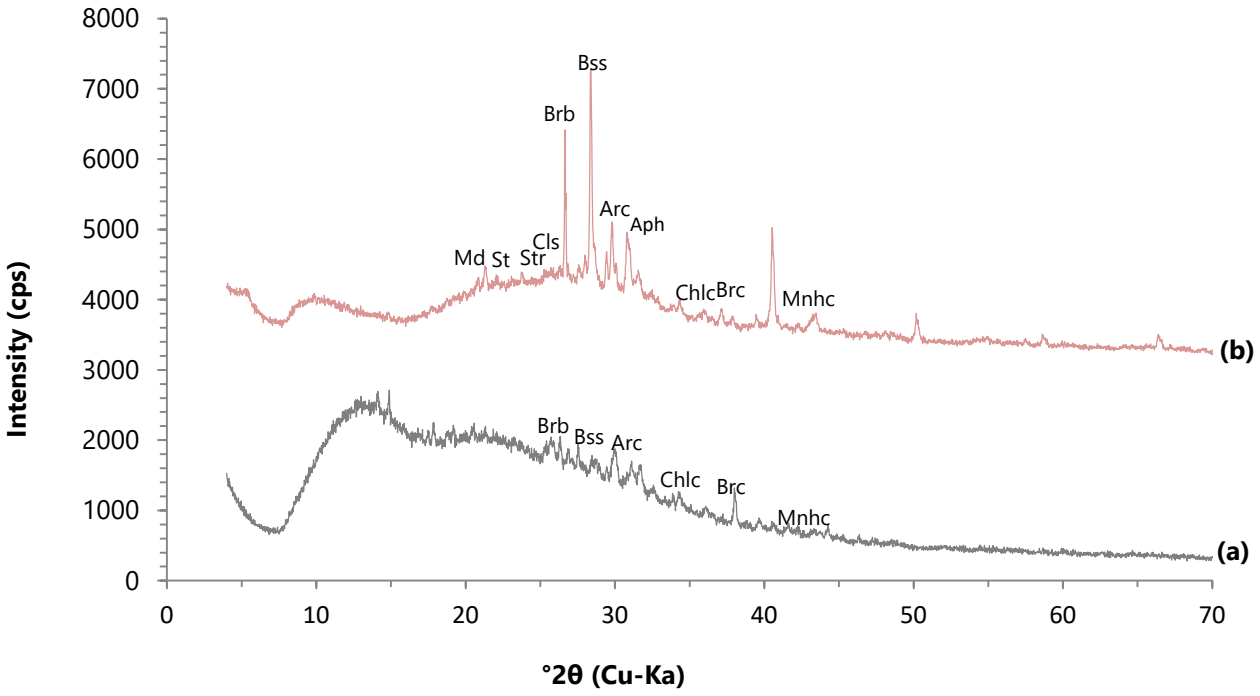

Fig. 20 XRD traces for *Triticum monococcum* inflorescence from: **(a)** Pella I; and **(b)** Volos using dry method. The hump in the range 10-30 °2θ is related with the presence of amorphous matter (i.e. phytoliths). The following mineral phases are present in these samples: Arcanite (Arc), Aphthitalite (Aph), Barbosalite (Brb), Bassanite (Bss), Brucite (Brc), Chlorocalcite (Chlc), Celestite (Cls), Monohydrocalcite (Mnhc), Mundrabillaite (Md), Strontianite (Str), and probably Struvite (St)

Plant-specific variations in the mineralogy of the stem-leaves and the inflorescence were also observed, regardless of extraction method. The fact that a greater number of mineralogical phases were identified for *Triticum durum* than for *Triticum monococcum* might be attributed to genetic, soil-related or/and anthropogenic factors (e.g. the use of fertilisers). Calcium phosphate (monetite) and magnesium phosphate (schertelite) was probably identified only in the N-P-K fertilised *Triticum durum* sample from Cyprus.

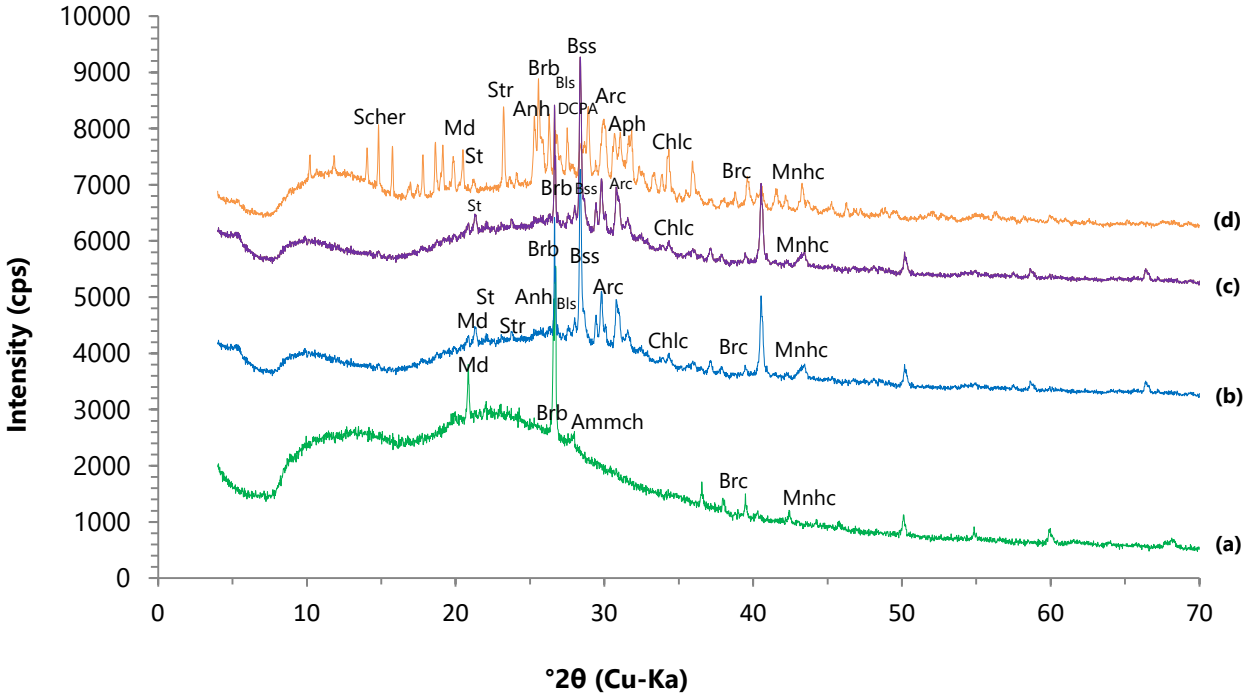

Fig. 21 XRD traces for *Triticum durum* inflorescence from: **(a)** Corfu, **(b)** Pella II, **(c)** Crete; and **(d)** Cyprus using dry method. The hump in the range 10-30 °2θ is related with the presence of amorphous matter (i.e. phytoliths). The following mineral phases are present in these samples: Anhydrite (Anh), Arcanite (Arc), Aphthitalite (Aph), Barbosalite (Brb), Bassanite (Bss), Baylissite (Bls), Brucite (Brc), Chlorocalcite (Chlc), Monetite (DCPA), Monohydrocalcite (Mnhc), Mundrabillaite (Md), Schertelite (Scher), Strontianite (Str), and probably Ammonium carbonate hydrate (Ammc) and Struvite (St)

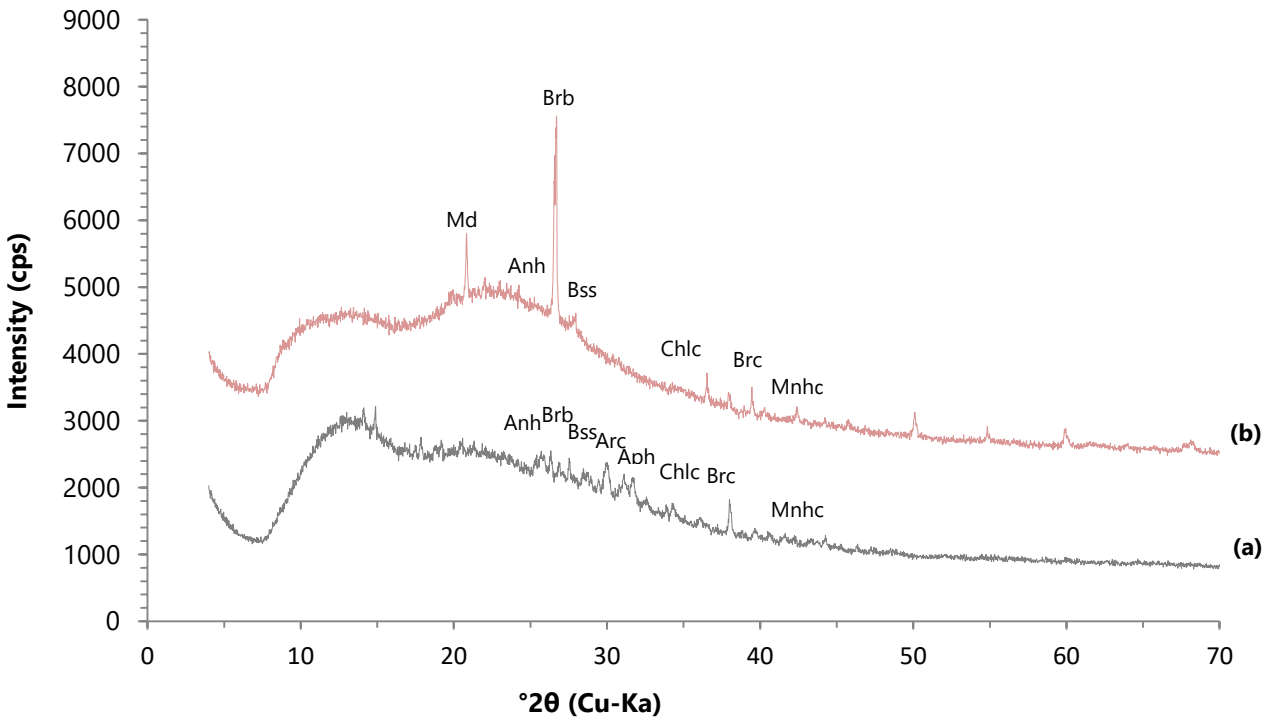

Fig. 22 XRD traces for *Triticum monococcum* inflorescence from **(a)** Pella I; and **(b)** Volos using dry method. The hump in the range 10-30 °2θ is related with the presence of amorphous matter (i.e. phytoliths). The following mineral phases are present in these samples: Anhydrite (Anh), Arcanite (Arc), Aphthitalite (Aph), Barbosalite (Brb), Bassanite (Bss), Brucite (Br), Chlorocalcite (Chlc), Monohydrocalcite (Mnhc) and Mundrabillaite (Md)

Table 7 Mineralogical composition of the *Triticum durum* or *Triticum monococcum* stem-leaves from Cyprus, Crete, Volos, Pella I, Pella II and Corfu using dry method

Mineral phases	*Tr. durum* stem-leaves **CYPRUS** (dry m.)	*Tr. durum* stem-leaves **CRETE** (dry m.)	*Tr. durum* stem-leaves **PELLA II** (dry m.)	*Tr. durum* stem-leaves **CORFU** (dry m.)	*Tr. monococcum* stem-leaves **VOLOS** (dry m.)	*Tr. monococcum* stem-leaves **PELLA I** (dry m.)
Ammonium carbonate hydrate $(NH_4)_2CO_3 \cdot H_2O$				X		
Anhydrite $CaSO_4$					X	X
Arcanite K_2SO_4	X		X	X		X
Aphthitalite $(K,Na)_3Na(SO_4)_2$						X
Barbosalite $Fe^{2+}Fe_3^{+2}(PO_4)_2(OH)_2$	X		X	X	X	X
Bassanite $CaSO_4 \cdot 1/2H_2O$	X		X		X	X
Baylissite $K_2Mg(CO_3)_2 \cdot 4H_2O$	X	X	X			
Brucite $Mg(OH)_2$		X		X	X	X
Chlorocalcite $KCaCl_3$	X		X	X	X	X
Celestite $SrSO_4$		X				
Illite/Muscovite $(K,H_3O)(Al, Mg, Fe)_2(Si, Al)_4O_{10}[(OH)_2,H_2O)$ / $KAl_2(AlSi_3O_{10})(F,OH)_2$			X			
Monohydrocalcite $CaCO_3 \cdot H_2O$	X	X	X		X	X
Mundrabillaite $(NH_4)_2Ca(PO_3OH)_2 \cdot H_2O$	X	X	X		X	
Strontianite $SrCO_3$	X		X			
Struvite $(NH_4)Mg(PO_4) \cdot 6H_2O$		X	X			

Table 8 Mineralogical composition of the *Triticum durum* or *Triticum monococcum* inflorescence from Cyprus, Crete, Volos, Pella I, Pella II and Corfu using dry method

Mineral phases	*Tr. durum* inflorescence **CYPRUS** (dry m.)	*Tr. durum* inflorescence **CRETE** (dry m.)	*Tr. durum* inflorescence **PELLA II** (dry m.)	*Tr. durum* inflorescence **CORFU** (dry m.)	*Tr. monococcum* inflorescence **VOLOS** (dry m.)	*Tr. monococcum* inflorescence **PELLA I** (dry m.)
Ammonium carbonate hydrate $(NH_4)_2CO_3 \cdot H_2O$				X		
Anhydrite $CaSO_4$	X					
Arcanite K_2SO_4	X	X	X		X	X
Aphthitalite $(K,Na)_3Na(SO_4)_2$	X		X		X	
Barbosalite $Fe^{2+}Fe_3^{+2}(PO_4)_2(OH)_2$	X	X	X	X	X	X
Bassanite $CaSO_4 \cdot 1/2H_2O$	X	X	X		X	X
Baylissite $K_2Mg(CO_3)_2 \cdot 4H_2O$	X	X	X			
Brucite $Mg(OH)_2$	X		X	X	X	X
Celestite $SrSO_4$					X	
Chlorocalcite $KCaCl_3$	X	X	X		X	X
Monetite $CaHPO_4$	X					
Monohydrocalcite $CaCO_3 \cdot H_2O$	X	X	X	X	X	X
Mundrabillaite $(NH_4)_2Ca(PO_3OH)_2 \cdot H_2O$	X		X	X	X	
Schertelite $(NH_4)_2Mg(PO_3OH)_2 \cdot 4H_2O$	X					
Strontianite $SrCO_3$	X		X		X	
Struvite $(NH_4)Mg(PO_4) \cdot 6H_2O$	X	X	X		X	

4.4.2 Mineralogical analysis of soil samples

Soil is the dynamic link between the biosphere and lithosphere, and refers to the products of *in-situ* weathering and biological processes that take place at the surface of the earth (Goldberg and Macphail 2006). The results of the XRD analysis for the soil samples [Cyprus, Crete, Volos, Corfu and Pella (I and II)] are summarised in Tables 9 and 10. The phases identified are albite, anatase, ankerite, calcite, chlorite, dolomite, hornblende, kaolinite, K-feldspar (orthoclase), illite/muscovite, paragonite, serpentine, smectite, talc and quartz (Fig. 23).

Table 9 Mineral phases present in the soils and their abbreviations and chemical formulae

Mineral phases	Abbreviations	Chemical formulae
Albite	Ab	$NaAlSi_3O_8$
Anatase	Ant	TiO_2
Ankerite	Ank	$Ca(Fe^{2+}, Mg,Mn^{2+})(CO_3)_2$
Calcite	Cal	$CaCO_3$
Chlorite	Chl	$(Mg, Fe)_3(Si, Al)_4O_{10}(OH)_2$
Dolomite	Dol	$CaMg(CO_3)_2$
Hornblende	Hbl	$Ca_2(Mg, Fe, Al)_5(Al, Si)_8O_{22}(OH)_2$
Ilite/Muscovite	Ill / Ms	$(K,H_3O)(Al, Mg, Fe)_2(Si, Al)_4O_{10}[(OH)_2, H_2O)$ / $KAl_2(AlSi_3O_{10})(F,OH)_2$
Kaolinite	Kln	$Al_2Si_2O_5(OH)_4$
K-feldspar (orthoclase)	Kfs	$KAlSi_3O_8$
Paragonite	Pg	$NaAl_2(Si_3Al)O_{10}(OH)_2$
Quartz	Qtz	SiO_2
Serpentine	Srp	$D_3[Si_2O_5](OH)_4$ (D = Mg, Fe, Ni, Mn, Al, Zn)
Smectite	Sme	$A_{0.3}D_{2-3}[T_4O_{10}]Z_2 \cdot nH_2O$
Talc	Tlc	$Mg_3Si_4O_{10}(OH)_2$

The phases identified at soil sample from Cyprus are albite, ankerite, calcite, kaolinite, illite/muscovite, serpentine, smectite and quartz. The phases determined at soil sample from Crete are albite, anatase, calcite, chlorite, K-feldspar (orthoclase), illite/muscovite, paragonite, serpentine, talc, quartz and probably smectite. The soil sample from Volos consists of albite, calcite, chlorite, hornblende, kaolinite, K-feldspar (orthoclase), illite/muscovite, serpentine, talc, quartz and probably anatase. The phases identified at soil samples from Pella (I and II) are albite, anatase, calcite, dolomite, hornblende, K-feldspar (orthoclase), illite/muscovite, smectite, talc and quartz. Finally, sample from Corfu consists of albite, anatase, calcite, K-feldspar (orthoclase), illite/muscovite, smectite, quartz and some kaolinite.

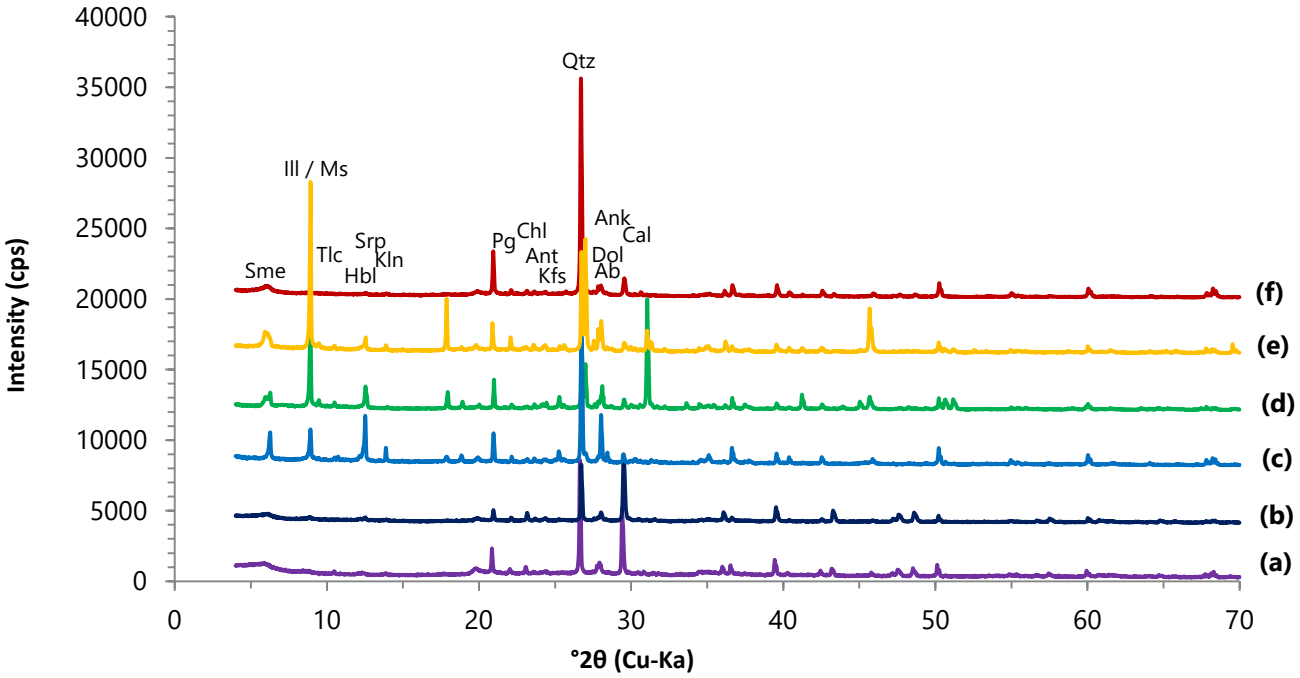

Fig. 23 XRD traces for soils: **(a)** Cyprus: Albite (Ab), Ankerite (Ank), Calcite (Cal), Kaolinite (Kln), Illite/Muscovite (Ill / Ms), Serpentine (Srp), Smectite (Sme) and Quartz (Qtz), **(b)** Crete: Albite (Ab), Anatase (Ant), Calcite (Cal), Chlorite (Chl), K-feldspar (orthoclase) (Kfs), Illite/Muscovite (Ill / Ms), Paragonite (Pg), Serpentine (Srp), Smectite (Sme), Talc (Tlc), and Quartz (Qtz), **(c)** Volos: Albite (Ab), Anatase (Ant), Calcite (Cal), Chlorite (Chl), Hornblende (Hbl), Kaolinite (Kln), K-feldspar (orthoclase) (Kfs), Illite/Muscovite (Ill / Ms), Serpentine (Srp), Talc (Tlc) and Quartz (Qtz), **(d)** Pella I: Albite (Ab), Anatase (Ant), Calcite (Cal), Dolomite (Dol), Hornblende (Hbl), K-feldspar (orthoclase) (Kfs), Illite/Muscovite, (Ill / Ms), Smectite (Sme), Talc (Tlc) and Quartz (Qtz), **(e)** Pella II: Albite (Ab), Anatase (Ant), Calcite (Cal), Dolomite (Dol), Hornblende (Hbl), K-feldspar (orthoclase) (Kfs), Illite/Muscovite (Ill / Ms), Smectite (Sme), Talc (Tlc) and Quartz (Qtz); and **(f)** Corfu: Albite (Ab), Anatase (Ant), Calcite (Cal), Kaolinite (Kln), K-feldspar (orthoclase) (Kfs), Illite/Muscovite (Ill / Ms), Smectite (Sme) and Quartz (Qtz)

Table 10 Mineralogical composition of the soils

Mineral phases	Cyprus	Crete	Volos	Pella I	Pella II	Corfu
Albite $NaAlSi_3O_8$	X	X	X	X	X	X
Anatase TiO_2		X	X	X	X	X
Ankerite $Ca(Fe^{2+},Mg,Mn^{2+})(CO_3)_2$	X					
Calcite $CaCO_3$	X	X	X	X	X	X
Chlorite $(Mg, Fe)_3(Si, Al)_4O_{10}(OH)_2$		X				
Dolomite $CaMg(CO_3)_2$				X	X	
Hornblende $Ca_2(Mg,Fe,Al)_5(Al,Si)_8O_{22}(OH)_2$			X	X	X	
Illite/Muscovite $(K,H_3O)(Al, Mg, Fe)_2(Si, Al)_4O_{10}[(OH)_2,H_2O)$ / $KAl_2(AlSi_3O_{10})(F,OH)_2$	X	X	X	X	X	X
Kaolinite $Al_2Si_2O_5(OH)_4$	X		X			X
K-feldspar (orthoclase) $KAlSi_3O_8$		X	X	X	X	X
Paragonite $NaAl_2(Si_3Al)O_{10}(OH)2$		X				
Quartz SiO_2	X	X	X	X	X	X
Serpentine $(Mg, Fe, Ni, Mn, Zn)_{2-3}(Si, Al,Fe)_2O_5(OH)_4$	X	X	X			
Smectite $A_{0.3}D_{2-3}[T_4O_{10}]Z_2 \cdot nH_2O$	X	X		X	X	X
Talc $Mg_3Si_4O_{10}(OH)_2$		X	X	X	X	

4.4.3 Mineralogical analysis of sediment samples

Minerals in archaeological sites can be formed in different ways. Geogenic minerals are derived from the weathering of igneous or metamorphic rocks. Authigenic minerals are those that form *in-situ* in the sediments as a result of changing chemical environments. Biogenic minerals are produced by organisms. Anthropogenic minerals are the products of human activities (Weiner 2010). The results of XRD analysis of the sediment samples are summarised in Tables 11 and 12. The phases identified are albite, anatase, calcite, chlorite, dolomite, gypsum, halite, hematite, hornblende, illite/muscovite, K-feldspar, pyrite, quartz, smectite and talc (Fig. 24)

Table 11 Mineral phases present in the sediments and their abbreviations and chemical formulae

Mineral phases	Abbreviations	Chemical formulae
Albite	Ab	$NaAlSi_3O_8$
Anatase	Ant	TiO_2
Calcite	Cal	$CaCO_3$
Chlorite	Chl	$(Mg, Fe)_3(Si, Al)_4O_{10}(OH)_2$
Dolomite	Dol	$CaMg(CO_3)_2$
Gypsum	Gyp	$CaSO42H_2O$
Halite	Hl	$NaCl$
Hematite	Hem	Fe_2O_3
Hornblende	Hbl	$Ca_2(Mg, Fe, Al)_5(Al, Si)_8O_{22}(OH)_2$
Illite / Muscovite	Ill / Ms	$(K,H_3O)(Al, Mg, Fe)_2(Si, Al)_4O_{10}[(OH)_2, H_2O)$ / $KAl_2(AlSi_3O_{10})(F,OH)_2$
K-feldspar (orthoclase)	Kfs	$KAlSi_3O_8$
Pyrite	Py	FeS_2
Smectite	Sme	$A_{0.3}D_{2-3}[T_4O_{10}]Z_2 \cdot nH_2O$
Quartz	Qtz	SiO_2
Talc	Tlc	$Mg_3Si_4O_{10}(OH)_2$

The main constituents of the studied archaeological samples are quartz, calcite and clays. Quartz is the most stable form of silicon dioxide, and thus is the most common mineral in the archaeological context (Iler 1979; Weiner 2010). Calcite is the most stable member of the calcium carbonate group of minerals. When sediments are composed of a carbonate mineral (e.g. calcite, dolomite) the pH often will be maintained at ~8.2 due to the buffering effect of the carbonate-bicarbonate system (Lippmann 1973). Usually, under such conditions, the calcite component of plant ash is stable, but the SiO_2-rich phytoliths are not (Cabanes *et al.* 2011; Weiner 2010). Furthermore, clay minerals are major components of soils and therefore of most sediments in archaeological sites (Rosen 1986; Weiner 2010). The most common form of clay minerals in the studied samples is illite/muscovite and some smectite.

The phases identified at *KN5* sample taken from a layer of a Minoan room are albite, calcite, illite/muscovite and quartz. The phases determined at *KN10* sample collected from the inner part of a ceramic vessel) are albite, calcite, illite/muscovite, quartz and smectite. The *KAΣ25* sample from a thin layer overlaying a yellowish Mycenaean floor consists of albite, anatase, calcite, chlorite, dolomite, gypsum, halite, hematite, hornblende, illite/muscovite, smectite and quartz. The phases identified at *KAΣ27* sample collected from a pebbled Mycenaean floor, older than the previous one, are albite, anatase, calcite, chlorite, dolomite, gypsum, halite, hematite, hornblende and quartz. The *TB2008* sample that was taken from a kiln are albite, anatase, calcite, chlorite, hornblende, K-feldspar, pyrite, quartz, and talc. Finally, *TB2013* sample collected from a grinding stone consists of albite, anatase, calcite, chlorite, illite/muscovite, K-feldspar and quartz.

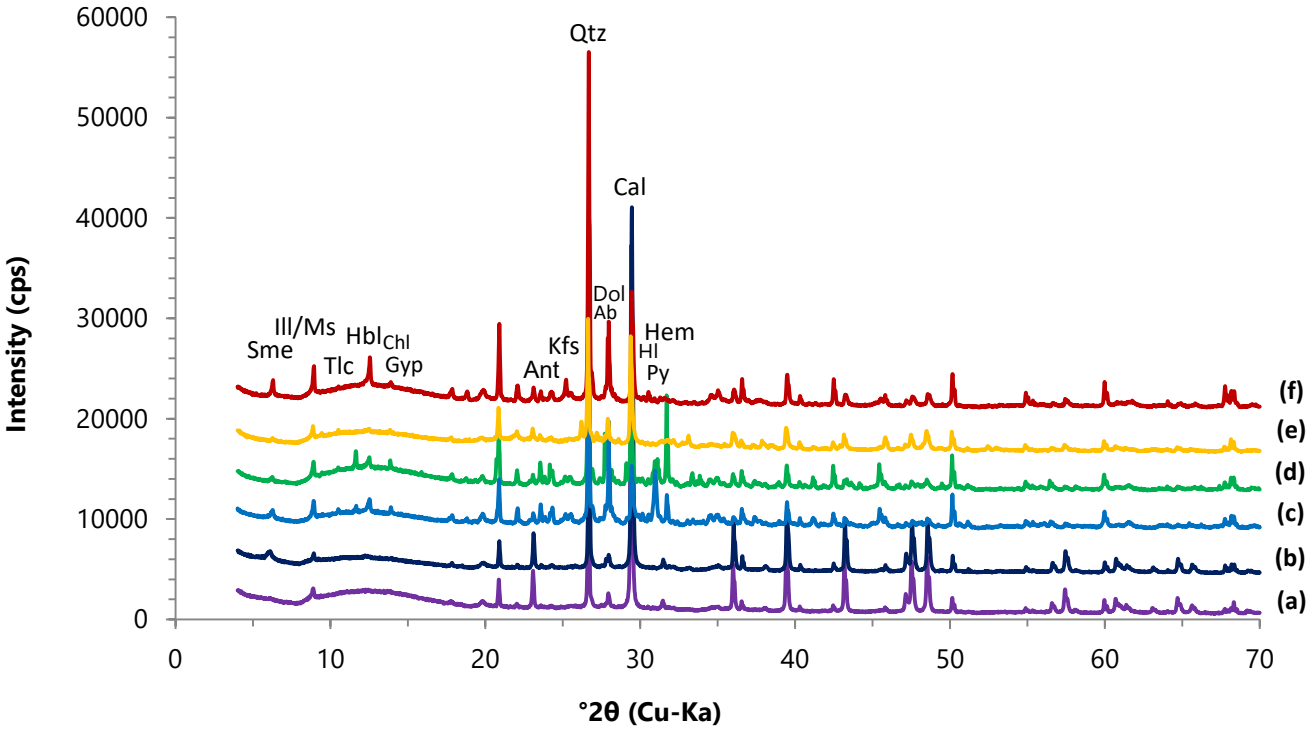

Fig. 24 XRD traces for archaeological sediments: **(a)** *KN5*: Albite (Ab), Calcite (Cal), Illite/Muscovite (Ill / Ms), Quartz (Qtz), **(b)** *KN10:* Albite (Ab), Calcite (Cal), Illite/Muscovite (Ill / Ms), Quartz (Qtz), Smectite (Sme), **(c)** *ΚΑΣ25*: Albite (Ab), Anatase (Ant), Calcite (Cal), Chlorite (Chl), Dolomite (Dol), Gypsum (Gyp), Halite (Hl), Hematite (Hem), Hornblende (Hbl), Illite/Muscovite (Ill / Ms), Quartz (Qtz), Smectite (Sme), **(d)** *ΚΑΣ27:* Albite (Ab), Anatase (Ant), Calcite (Cal), Chlorite (Chl), Dolomite (Dol), Gypsum (Gyp), Halite (Hl), Hematite (Hem), Hornblende (Hbl), Quartz (Qtz), **(e)** *TB2008*: Albite (Ab), Anatase (Ant), Calcite (Cal), Chlorite (Chl), Hornblende (Hbl), K-feldspar (Kfs), Pyrite (Py), Quartz (Qtz), Talc (Tlc); and **(f)** *TB2013*: Albite (Ab), Anatase (Ant), Calcite (Cal), Chlorite (Chl), Illite/Muscovite (Ill / Ms), K-feldspar (Kfs), Quartz (Qtz)

Table 12 Mineralogical composition of the archaeological sediments

Mineral phases	Knossos 5	Knossos 10	Palea 25	Palea 27	Toumba 2008	Toumba 2013
Albite $NaAlSi_3O_8$	x	x	x	x	x	x
Anatase TiO_2			x	x	x	x
Calcite $CaCO_3$	x	x	x	x	x	x
Chlorite $(Mg, Fe)_3(Si, Al)_4O_{10}(OH)_2$			x	x	x	x
Dolomite $CaMg(CO_3)_2$			x	x		
Gypsum $CaSO_4 \cdot 2H_2O$			x	x		
Halite NaCl			x	x		
Hematite Fe_2O_3			x	x		
Hornblende $Ca_2(Mg,Fe,Al)_5(Al,Si)_8O_{22}(OH)_2$			x	x	x	
Illite/Muscovite $(K,H_3O)(Al, Mg, Fe)_2(Si, Al)_4O_{10}[(OH)_2,H_2O)$ / $KAl_2(AlSi_3O_{10})(F,OH)_2$	x	x	x			x
K-feldspar (orthoclase) $KAlSi_3O_8$					x	x
Pyrite FeS_2					x	
Smectite $A_{0.3}D_{2-3}[T_4O_{10}]Z_2 \cdot nH_2O$		x	x			
Quartz SiO_2	x	x	x	x	x	x
Talc $Mg_3Si_4O_{10}(OH)_2$					x	

4.5 Fourier Transform Infrared spectroscopy (FTIR)

FTIR spectroscopy is the study of the interaction of infrared radiation with matter. When irradiated, functional groups in phytoliths vibrate or rotate in specific mode, which corresponds to the absorption of a particular frequency. The FTIR spectra of the plant samples (*Triticum durum* or *Triticum monococcum* from Cyprus, Crete, Volos and Corfu) using dry method are presented in Fig. 25 (stem-leaves) and Fig. 26 (inflorescence).

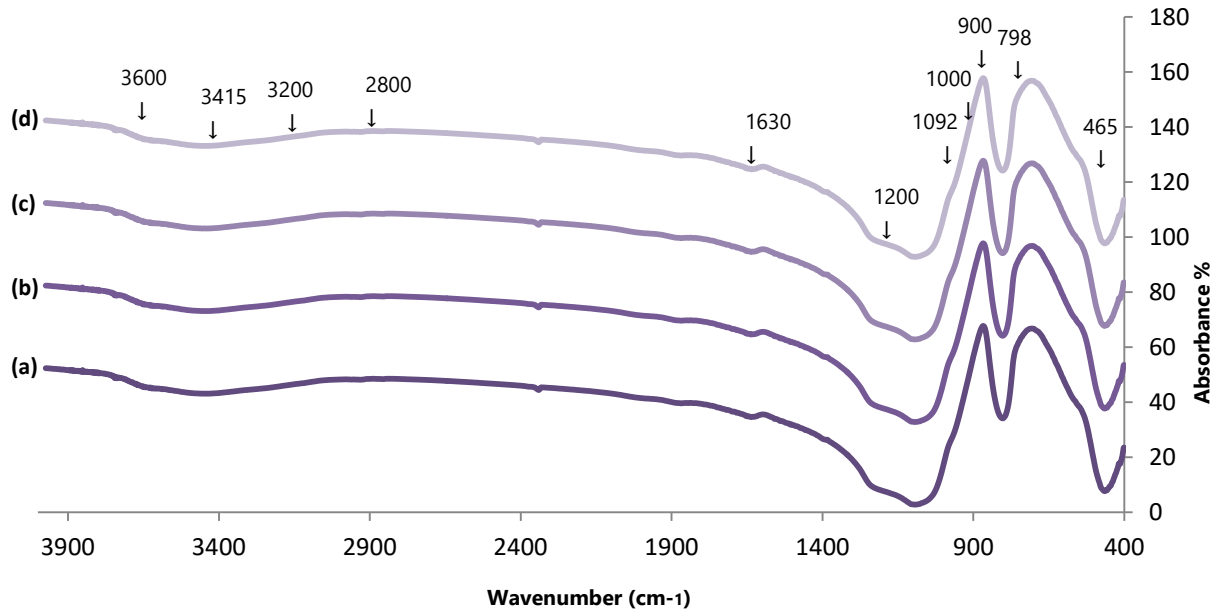

Fig. 25 FTIR spectra for *Triticum durum* or *Triticum monococcum* stem-leaves using dry method: **(a)** *Triticum durum* Cyprus, **(b)** *Triticum durum* Crete, **(c)** *Triticum monococcum* Volos; and **(d)** *Triticum durum* Corfu. Main bands at: ~465 cm^{-1}, 798 cm^{-1} and 1092 cm^{-1} (SiO_2 species), ~900-1000 cm^{-1} (Si-OH bending), ~1000-1200 cm^{-1} (Si-O stretching overlap with the SO_4 and PO_4 stretching) ~1630 cm^{-1} and ~3415 cm^{-1} (adsorbed water), (~3200-3600 cm^{-1}) (adsorbed water and hydrous sulphates and phosphates), ~2,800-3600 cm^{-1} (hydroxyl molecules)

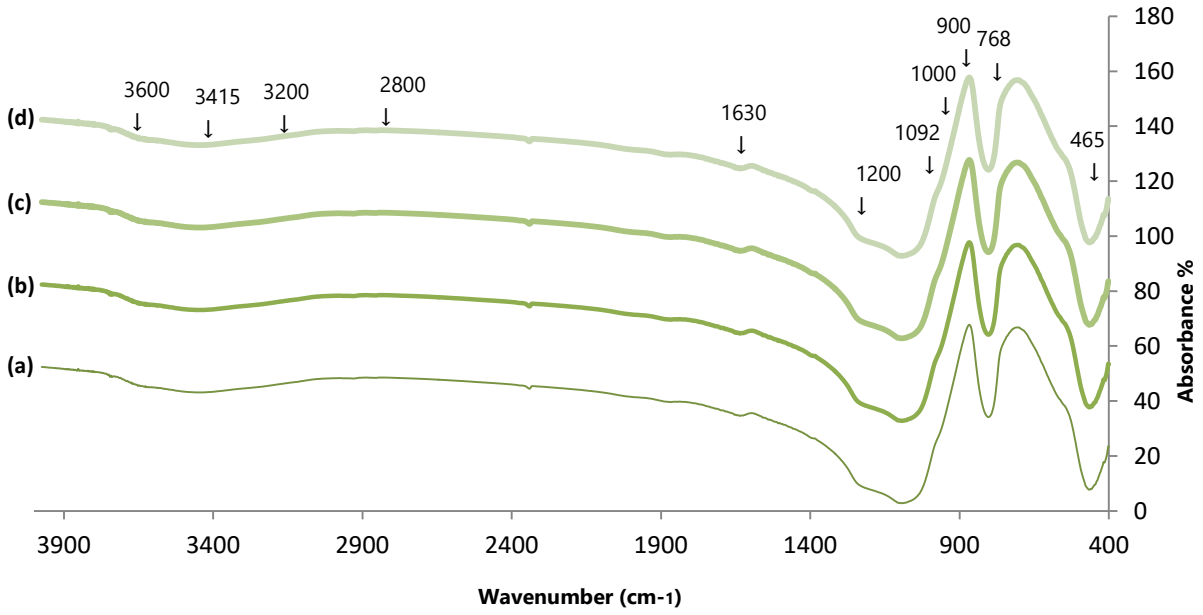

Fig. 26 FTIR spectra for *Triticum durum* or *Triticum monococcum* inflorescence using dry method: **(a)** *Triticum durum* Cyprus, **(b)** *Triticum durum* Crete, **(c)** *Triticum monococcum* Volos; and **(d)** *Triticum durum* Corfu. Main bands at: ~465 cm^{-1}, ~798 cm^{-1} and ~1092 cm^{-1} (SiO_2 species), ~900-1000 cm^{-1} (Si-OH bending), ~1000-1200 cm^{-1} (Si-O stretching overlap with the SO_4 and PO_4 stretching) ~1630 cm^{-1} and ~3415 cm^{-1} (adsorbed water), (~3200-3600 cm^{-1}) (adsorbed water and hydrous sulphates and phosphates), ~2,800-3600 cm^{-1} (hydroxyl molecules)

The spectra display absorption bands at ~465 cm^{-1}, ~798 cm^{-1} and ~1092 cm^{-1} that are related with SiO_2 species (Si-O bending, Si-O-Si stretching and Si-O stretching vibration respectively) (Chester and Elderfield 1968; Chukanov and Chervonnyi 2014). The appearance of a single band at ~798 cm^{-1} indicates that the SiO_2 is nearly amorphous (Gendron-Badou *et al.* 2003). The OH region showed bands of medium intensity (free and bound O-H groups) corresponding to Si-OH bending vibration between ~900 and 1000 cm^{-1} (Chukanov and Chervonnyi 2014). The Si-O asymmetric stretching bands between ~1000 and 1200 cm^{-1} overlap with the SO_4 symmetric stretching bands (Myreni 2000; Ross 1974a) and the PO_4 symmetric stretching band (Ross 1974b).

The OH-stretching region (~3200-3600 cm^{-1}) receives contribution from adsorbed water and from hydrous sulphates and phosphates (Adler and Kerr 1965; Ross 1974a, 1974b). Typical sulphates detected in plant samples are anhydrite, aphthitalite and arcanite, and phosphates are barbosalite, mundrabillaite, probably struvite; and rarely monetite and schertelite (Table 4). Moreover, hydroxyl molecules embedded in the molecular structure of biogenic silicon may appear at ~2,800-3600 cm^{-1} region (Moenke 1974). The stretching and bending bands of adsorbed water at ~1630 cm^{-1} and ~3415 cm^{-1} are quite evident (H-O-H bending vibration: ~1630 cm^{-1} and H-O-H stretching vibration: ~3200-3450 cm^{-1}) (Cheng *et al.* 2013; Gendron-Badou *et al.* 2003). This may offer supplementary information for phytolith porosity. The SiO_2-rich phytolith total water content is ~2-15 wt.% water (Bartoli and Wilding 1980; Piperno 2006). Most of the water present in the structures is molecular water (H_2O_{mol}). This relatively high amount of water content in phytoliths, compared with other silica polymorphs, may be attributed to their porous nature.

In general, the water content present in primary silicates (e.g. quartz) changes during heating (or diagenesis), with physically absorbed molecular water loss at relatively low temperatures (~150ºC) (Iler 1979). In our study, the bands of adsorbed water at ~1630 cm^{-1} and ~3415 cm^{-1} appeared, even after overnight drying (~150°C) of the phytolith samples. Previous studies have focused in the determination of the water contents in non- and micro-crystalline silica structures and how the related mineral properties change during diagenesis (Awadh and Yaseen 2019; Jones and Segnit 1971; Flörke *et al.* 1982; Graetsch *et al.* 1985; Langer and Flörke 1974). According to these studies, total water content decreases with increasing crystal order of the microstructures [non-crystalline opal-A → microcrystalline opal-C and opal-CT→ (micro)crystalline quartz]. In particular, the total water content is: ~0.5-2.5% wt. (for quartz), ~1-3% wt. (for opal-C), ~3-10% wt. (for opal-CT) and ~10-12% wt. (for opal-A), and the relative ratio of water

species H_2O_{SiOH}/H_2O_{mol} is:~0% (for quartz), ~0.02% (for opal-C and opal-CT) and ~0.1-0.7% (for opal-A).

The FTIR spectra of the plant samples from *Triticum durum* and *Triticum monococcum* from Pella using dry or wet extraction method are presented in Fig. 27 (stem-leaves) and Fig. 28 (inflorescence).

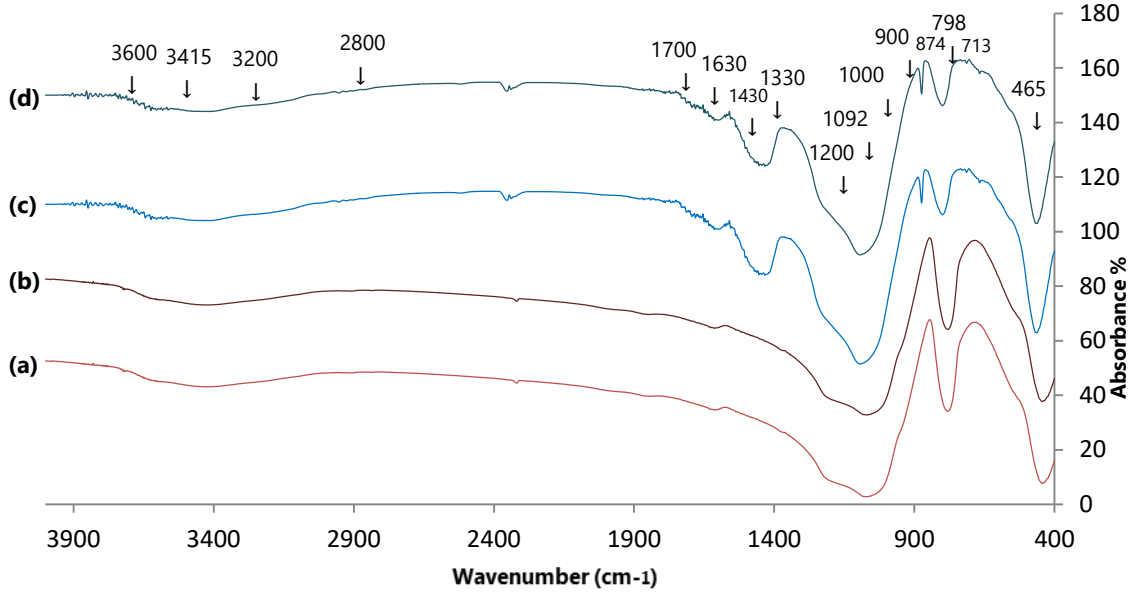

Fig. 27 FTIR spectra for *Triticum durum* and *Triticum monococcum* stem-leaves from Pella using dry and wet method: **(a)** *Triticum durum* stem-leaves (dry method), **(b)** *Triticum monococcum* stem-leaves (dry method), **(c)** *Triticum durum* stem-leaves (wet method); and **(d)** *Triticum monococcum* stem-leaves (wet method). Main bands at: ~465 cm^{-1}, ~798 cm^{-1} and ~1092 cm^{-1} (SiO_2 species), ~900-1000 cm^{-1} (Si-OH bending), ~1000-1200 cm^{-1} (Si-O stretching overlap with the SO_4 and PO_4 stretching) ~1630 cm^{-1} and ~3415 cm^{-1} (adsorbed water), (~3200-3600 cm^{-1}) (adsorbed water and hydrous sulphates and phosphates), ~2,800-3600 cm^{-1} (hydroxyl molecules), ~1430 cm^{-1} (carbonate asymmetric stretching band), ~713 cm^{-1} and ~874 cm^{-1} (plane bending vibrations of the CO_3^{2-} ion in carbonate minerals), ~1330-1700 cm^{-1} (organic matter)

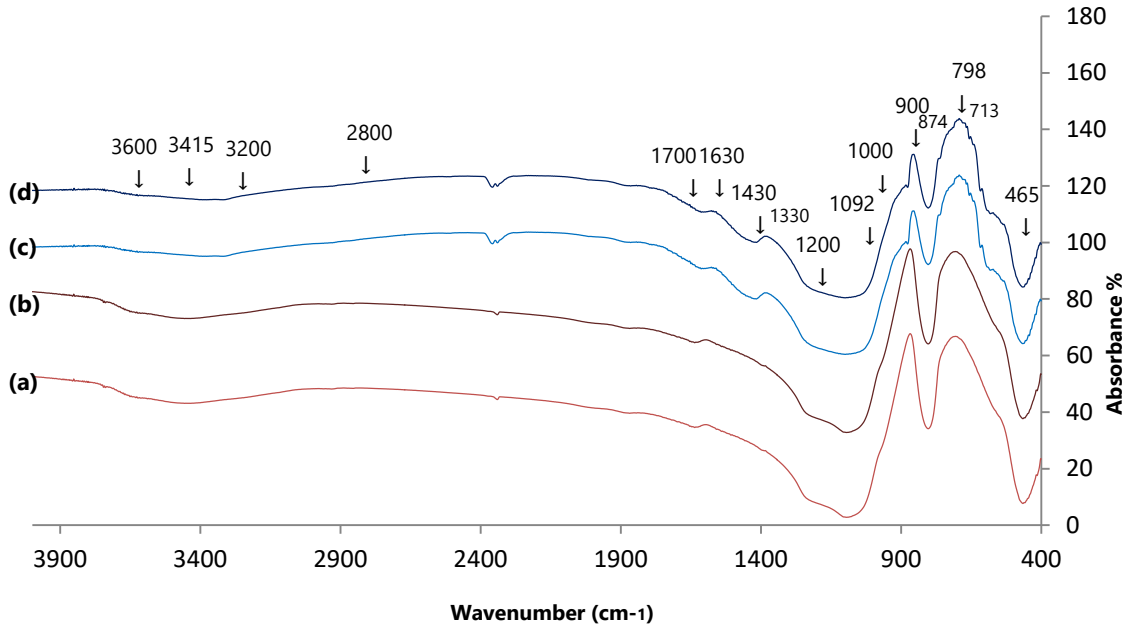

Fig. 28 FTIR spectra for *Triticum durum* and *Triticum monococcum* inflorescence from Pella using dry and wet method: **(a)** *Triticum durum* inflorescence (dry method), **(b)** *Triticum monococcum* inflorescence (dry method), **(c)** *Triticum durum* inflorescence (wet method); and **(d)** *Triticum monococcum* inflorescence (wet method). Main bands at: ~465 cm^{-1}, ~798 cm^{-1} and ~1092 cm^{-1} (SiO_2 species), ~900-1000 cm^{-1} (Si-OH bending), ~1000-1200 cm^{-1} (Si-O stretching overlap with the SO_4 and PO_4 stretching) ~1630 cm^{-1} and ~3415 cm^{-1} (adsorbed water), (~3200-3600 cm^{-1}) (adsorbed water and hydrous sulphates and phosphates), ~2,800-3600 cm^{-1} (hydroxyl molecules), ~1430 cm^{-1} (carbonate asymmetric stretching band), ~713 cm^{-1} and ~874 cm^{-1} (plane bending vibrations of the CO_3^{2-} ion in carbonate minerals), ~1330-1700 cm^{-1} (organic matter)

The use of HCl and H_2O_2 in the dry method seems to have eliminated the majority of the carbonates and organic matter respectively. However, the carbonate asymmetric stretching band is noticed at ~1430 cm^{-1} for both species and plants parts after the application of wet method. The sharp bands at ~713 cm^{-1} and 874 cm^{-1} are attributed to the out-of-plane and in-plane bending vibrations respectively of the CO_3^{2-} ion in carbonate minerals, such as calcite (Adler and Kerr 1962; White 1971). Furthermore, the bands between ~1330-1700 cm^{-1} suggest that some organic matter remains to phytoliths (Gendron-Badou *et al.* 2003; Puppe and Leue 2018). Observation of the phytoliths under

the optical microscope confirmed the presence of organic matter in the cavities and in the silica structure itself.

4.6 Scanning Electron Microscopy with Energy Dispersive Spectroscopy (SEM/EDS)

The different concentrations of Si in solution during dissolution, described in chapter 4.9 (*Solubility and dissolution kinetics of phytoliths: batch experiments and archaeological implications*) are related to the apparent solubilities of the several phytoliths morphotypes. The morphology of the SiO_2-rich phytoliths before and after the dissolution observed by miscroscopy varied considerably in form and size between wheat organs (inflorescences and stems-leaves) (see chapter 4.2).

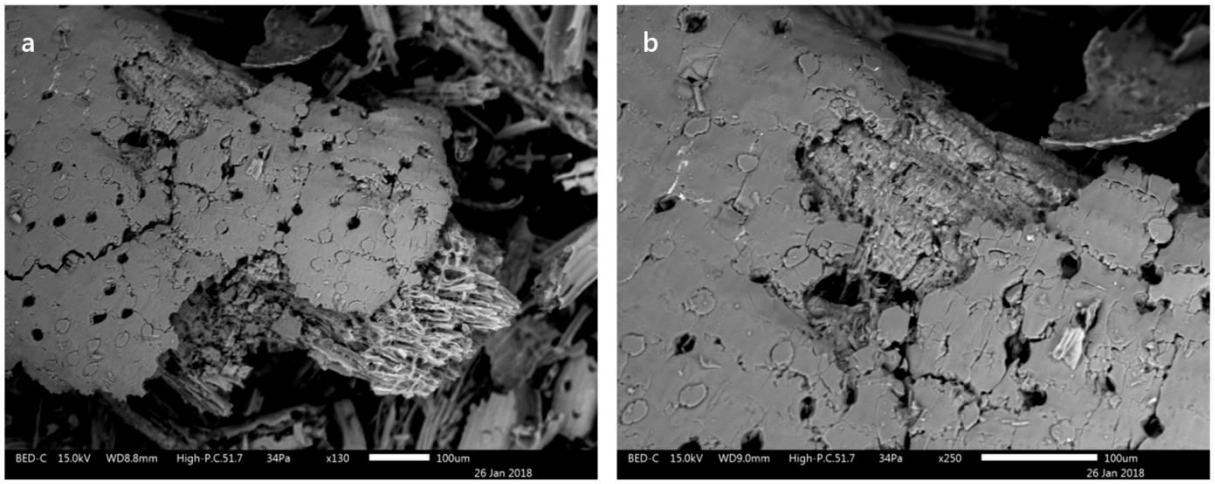

Fig. 29 SEM photomicrographs of the phytoliths: **(a, b)** phytolith assemblage with evident mechanical and chemical alterations after dissolution (75 days). Phytoliths were extracted from *Triticum durum* Corfu using the dry method (photomicrographs: Andriopoulou)

Several phytoliths morphotypes have been identified according to the International Code for Phytolith Nomenclature that involves descriptions of the shape, texture and anatomical origin (i.e. histological location) of phytoliths (ICPN Working Group: Madella *et al.* 2005). Dentritic long cells, hair and papillae, for example, are linked to inflorescence, stomata and mesophyll to leaves, psilate long cells to leaves or stems. Characteristic SEM

photomicrographs with alterated phytolith aggregations (after dissolution) are presented above (Fig. 29 a, b).

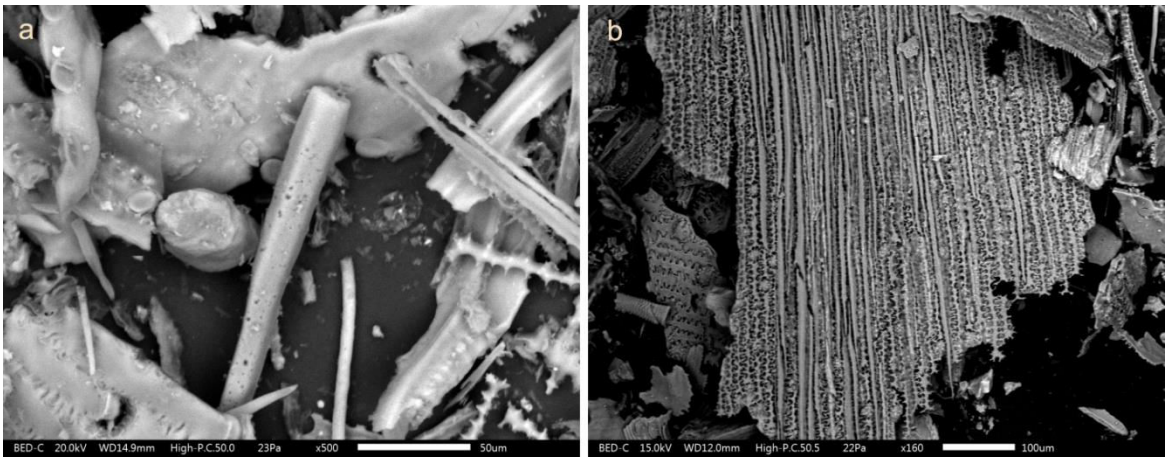

Fig. 30 SEM photomicrographs of the phytoliths: **(a)** phytolith assemblage from *Triticum durum* from Pella using the wet method. The parallelepipedal elongate cell presented in the center has rugulate and pitted surface; and **(b)** dentritic and echinate long cells in anatomical connection from *Triticum durum* inflorescence from Pella using the dry method. Heating depending the conditions may enhance the cohesion of phytoliths (photomicrographs: Andriopoulou)

In the present study, observation of the phytoliths under the optical microscope showed that the wet ashing produced more phytoliths overshadowed by the presence of organic matter than the dry ashing, and that the dry method provided cleaner and more transparent phytoliths than the wet method (Fig. 31 b), in accordance with Parr *et al.* (2001). Previous work has shown that the wet ashing although effective (Rovner *et al.* 1971), has some disadvantages related to oxidation. The main limitations of wet ashing are the differential digestion rates of organic matter (Jenkins 2009; Kameník *et al*. 2013; Parr *et al.* 2001; Pearsall 2015; Theunissen 1994) and the apparent loss of phytolith residue (Pearsall 2015).

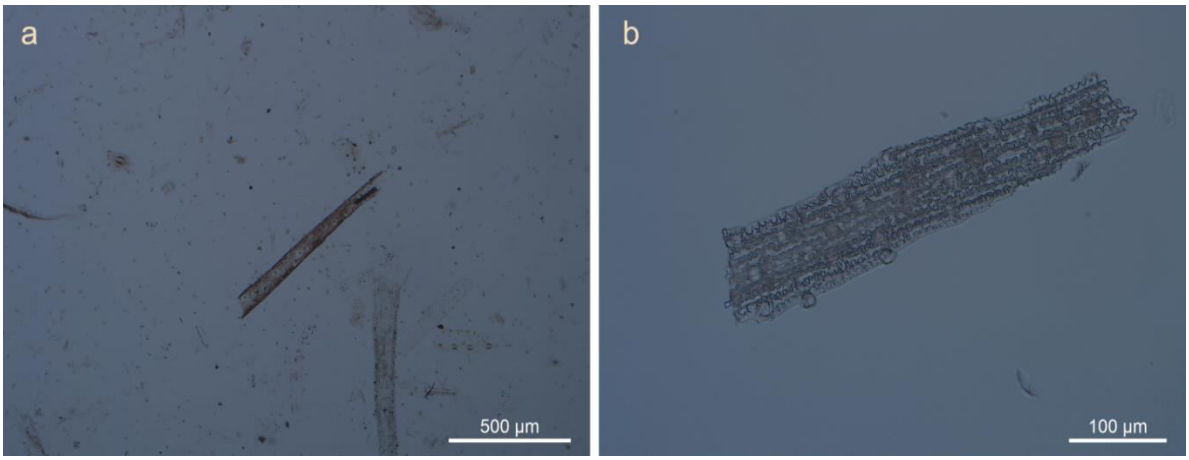

Fig. 31 Photomicrographs of phytoliths from the optical microscope: **(a)** parallelepipedal elongate cell from *Triticum durum* using the wet ashing method. The phytolith presented in the centre is opaque and overshadowed with organic matter; and **(b)** dentritic and echinate long cells in anatomical connection from *Triticum durum* inflorescence using the dry ashing method. The phytoliths are more clear and transparent to light (photomicrographs: Andriopoulou)

Phytoliths contain occluded carbon (Jones and Beavers 1963; Hodson 2016; Hodson *et al*. 2008; Wilding and Dress 1974). The dry method is more efficient in removing charcoalified tissues, while simultaneously retaining the phytolith morphology (Wang *et al*. 2014). In the present study, despite the overall levels of detected carbon being relatively higher for the wet method than the dry method, the organic matter had not been homogenously digested from the different phytolith parts, which makes the task of identifying their morphotypes more complex (Fig. 31 a). Also some phytoliths morphotypes may be more resistant than other. For example, depending on the laboratory extraction methods, rondel morphotypes that are more spheroidal, seem to be preserved better than elongates, and elongate morphotypes more than decorated long cells such dentritics that are more delicate.

Furthermore, there were not significant differences in size in specific phytolith morphotypes from the same organ between the two methods. However, these differences were significant before and after the dissolution process. Dry ashing may alter the size, curvature and refractive index of phytoliths (Elbaum 2003; Jones and Milne 1963; Pearsall 2015). The surface area of the phytoliths has been reported to be smaller in the dry ashed samples than in those from the acid extraction (Jones and Milne 1963). Dry ashing at 500-600°C also causes shrinkage of phytoliths (Pearsall 2015). However, the differences in patterns of dimension and curvature of specific phytoliths morphotypes both extracted with dry and wet ashing are not statistically significant (Parr *et al*. 2001). If the firing temperature does not exceed 500-550°C for a limited time, there will usually be no detectable evidence of strong morphological impact on the phytoliths, rendering the dry ashing a reliable method for phytoliths morphotypes better preservation (Parr *et al*. 2001; Wu *et al*. 2014).

Despite the advances in existing morphometric phytolith analysis (Ball *et al*. 1999, 2016; Portillo and Albert 2011), this technique is time consuming, each analysis requires a minimum number of phytoliths measured and each measurement has to be performed individually. For rapid and reliable calculation of the surface area of phytoliths an integrated approach based on microscopy and photogrammetry, was proposed recently for the non-destructive imaging and 3D representation of the surface, where relative or absolute metrics may be estimated (Andriopoulou *et al*. 2019). Especially, the combination of specific surface area (SSA, which is equal to the ratio between the 3D surface area and mass of the phytoliths) and elemental composition may influence phytolith stability and thus preservation during taphonomic (e.g. dissolution) or/and laboratory processes (e.g. extraction methods).

Regarding the chemical composition of the phytoliths, the samples are mainly composed of SiO_2. Carbon, Mg, Al, P, S, K, Ca, Fe and rarely Sr, Cl and Cu were also detected. The elemental analysis (SEM/EDS spectra) that was conducted on clean phytolith surfaces confirms the mineralogical analysis results previously presented. The chemical composition can be used to infer the mineral identity. This is not always unequivocal but may provide useful information. The composition varied depending on the analysed particle or zone (cell wall and cell centre) of the phytoliths morphotypes. Characteristic spectra/EDS analysis of phytoliths from *Triticum monococcum* leaf cell wall and cell centre using both methods are provided in Fig. 32. Slicon and sometimes Ca were observed along the entire cell wall whereas K and P tend to accumulate in the outer layer of the wall.

Sometimes Sr was also present in phytoliths from both wheat species and both anatomical parts. Characteristic spectrum/EDS analysis of phytoliths from *Triticum durum* from Crete are provided in Fig. 33. Strontium in the samples may be either belongs to the phytolith itself or it may be related with the presence of strontianite ($SrCO_3$) or/and celestite ($SrSO_4$) in the plant samples (see XRD traces above). This is in accordance with previous studies that have shown that Sr was incorporated into minerals formed in various other plants (Franceschi and Schueren 1986; He *et al*. 2012a, 2012b; Raven and Giordano 2009). Strontium and and Cl were detected in some phytoliths, but it was not possible to discern any pattern in their distribution. A previous study has shown tha Cl preferentially accumulated in the sheaths relative to the blades of the *Triticum aestivum* (wheat) leaves (Boursier *et al*. 1987). Chlorine in the present samples may be either belongs to the phytolith itself or it may be related with the presence of chlorocalcite ($KCaCl_3$) in the plant samples (see XRD traces above).

(a)

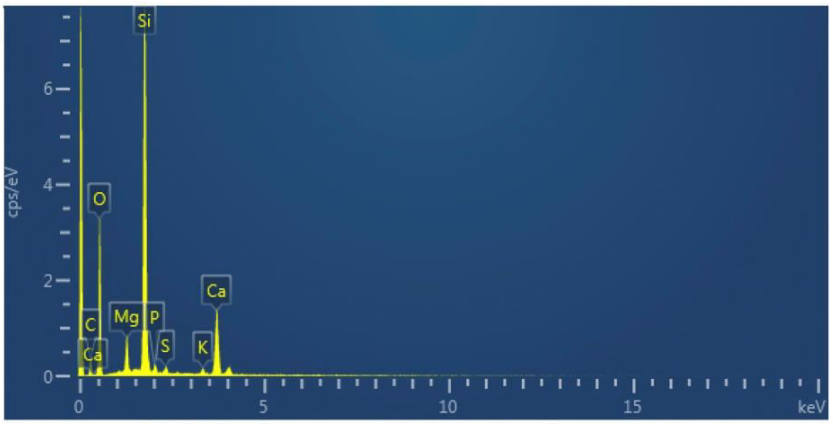
Si
O
C
Ca
Mg
P
S
K
Ca
cps/eV
0
2
4
6
0
5
10
15
keV

(b)

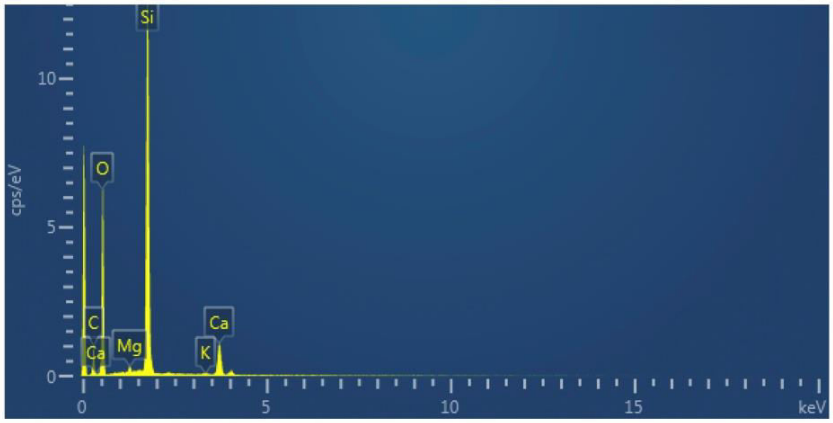
Si
O
C
Ca
Mg
K
Ca
cps/eV
0
5
10
0
5
10
15
keV

(c)

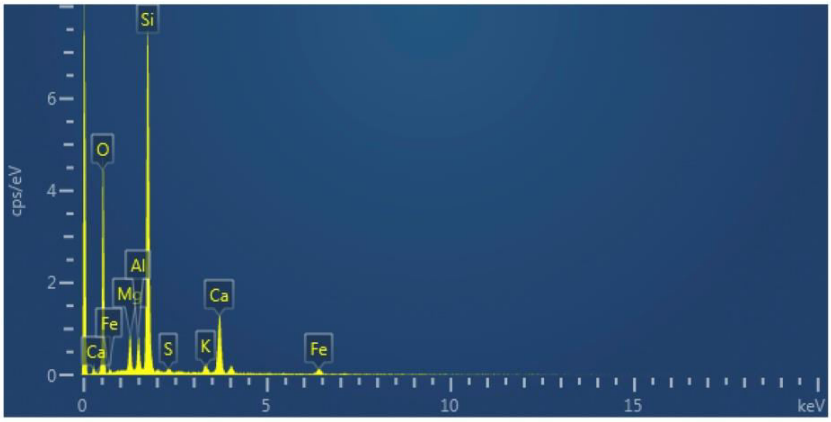
Si
O
Al
Mg
Fe
Ca
Ca
S
K
Fe
cps/eV
0
2
4
6
0
5
10
15
keV

(d)

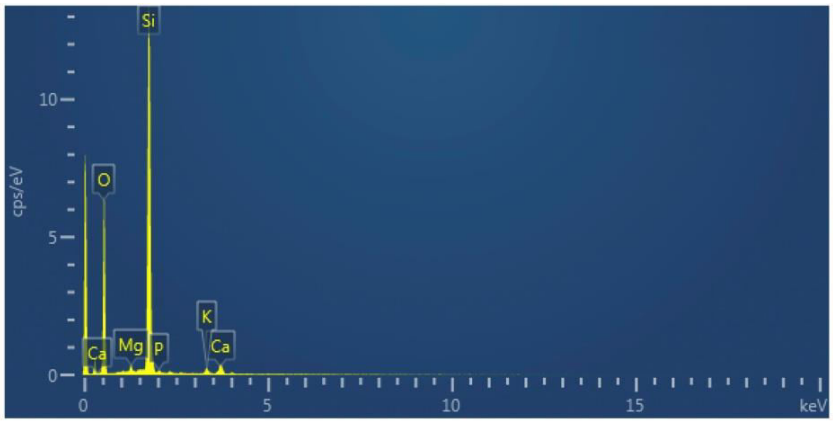
Si
O
K
Ca
Mg
P
Ca
cps/eV
0
5
10
0
5
10
15
keV

Fig. 32 Characteristic EDS spectra of phytolith from: **(a)** *Triticum monococcum* leaf (cell wall) from Pella using dry method. Oxygen (O), silicon (Si), carbon (C), magnesium (Mg), phosphorus (P), sulphur (S), potassium (K), and calcium (Ca) are present. **(b)** *Triticum monococcum* leaf (cell wall) from Pella using wet method. Presence of oxygen (O), silicon (Si), carbon (C), magnesium (Mg), potassium (K), and calcium (Ca), **(c)** *Triticum monococcum* leaf (cell centre) from Pella using dry method. Presence of oxygen (O), silicon (Si), magnesium (Mg), aluminium (Al), phosphorus (P), potassium (K), calcium (Ca), and iron (Fe); and **(d)** *Triticum monococcum* leaf (cell centre) from Pella using wet method. Presence of oxygen (O), silicon (Si), magnesium (Mg), phosphorus (P), potassium (K), and calcium (Ca)

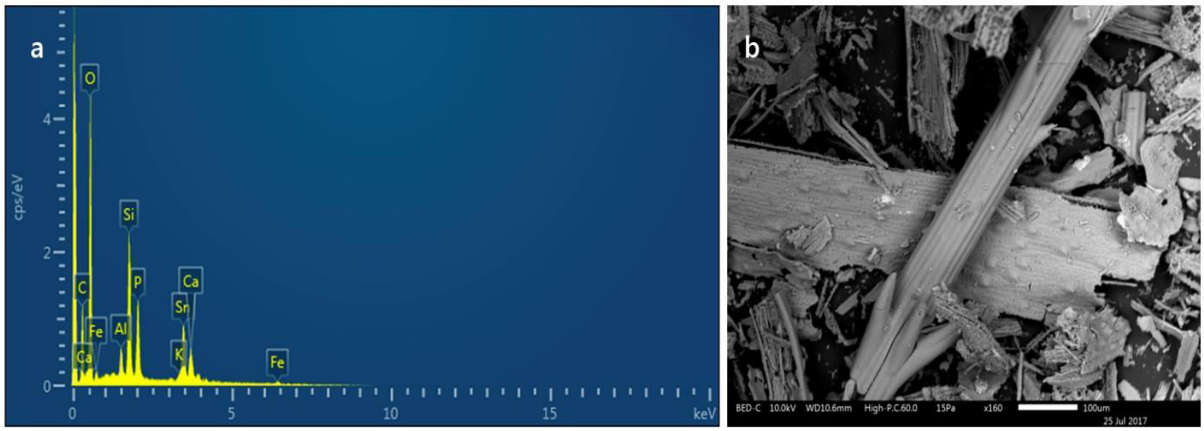

Fig. 33 SEM photomicrograph that presents a phytolith assemblage (*Triticum durum*, Crete, dry method) and its EDS spectrum. Among other chemical elements, strontium (Sr) was observed in phytoliths from either inflorescence or stem/leaves (photomicrograph: Andriopoulou)

Even if Cu has low mobility in neutral soils, sometimes (especially in alkaline soils) bioavailable Cu is translocated from plant roots to other tissues (Delplace *et al.* 2020; Garnett and Graham 2005; Morikawa and Saigusa 2004; Piper 1939; Tran *et al.* 2019). Piper (1939) showed that heavy metals including Cu were retained in plant SiO_2 using dry extraction method, in amounts which represented a relatively large proportion of the total. Copper may be remobilised within all plant organs, such as in the case of *Triticum aestivum* (wheat) studied by Garnett and Graham (2005). Tran *et al.* (2019) showed the

encapsulation of Cu in phytoliths from *Axonopus compressus* (carpet-grass) in an orange growing area in Vietnam, where Cu-rich fungicides have been excessively applied. Delplace *et al.* (2020) studied phytoliths from reeds (*Arundo donax* and *Phragmites australis*) grown in a mining area in Spain, and also showed the encapsulation of some heavy metals, including Cu, in phytoliths. Furthermore, the mean contents of Cu was found statistically ($LSD_{0.05}$) the same in young and old dry-ashed leaves (ca. 500˚C for 6h) from *Vaccinum corymbosus* (blueberry) (Morikawa and Saigusa 2004). Despite the importance of these studies, the localisation of Cu within phytolith structure was not fully understood.

Hodson and Sangster (2002) detected Cu (as well as Mn, Fe and Zn) in the endodermal, epidermal and transfusion tissues (the layer of tracheids and parenchyma surrounding the vascular bundles) in the needles of *Pinus strobes* (white pine). Pyatt (1999) detected 21 chemical elements, including Cu, in the needles and stems of *Pinus nigra* (Corsican pine) from uncontaminated and contaminated areas in Cyprus. In our study, Cu was detected in the narrow end (tip) of the hairs (trichomes) of SiO_2-rich phytoliths extracted from *Triticum durum* inflorescence that was grown in the N-P-K fertilised soil of Cyprus (Fig. 34). Copper concentration in plant tissues may vary depending on several environmental and antropogenic factors such as nitrogen supply; plants grown under high nitrogen supply usually require significantly more Cu (Marschner 1995). In any case the presence of Cu in our Cyprus sample might not necessarily reflect the use of fertilisers, but may be related to the ophiolitic rocks of the Troodos Complex and the soils linked with these rocks (Friedrich *et al.* 1984; Gass 1980). Cyprus, one of the most important sources of copper in the Eastern Mediterranean, is famous for the copper mines (Cyprus-type Cu-sulphide deposits, e.g. Moore and Vine 1971; Sawkins 1990) and the metal trade with the Aegean, Sardinia, Egypt and Near East since the Bronze Age (Gale and Stos-Gale 1982; Gale 1991).

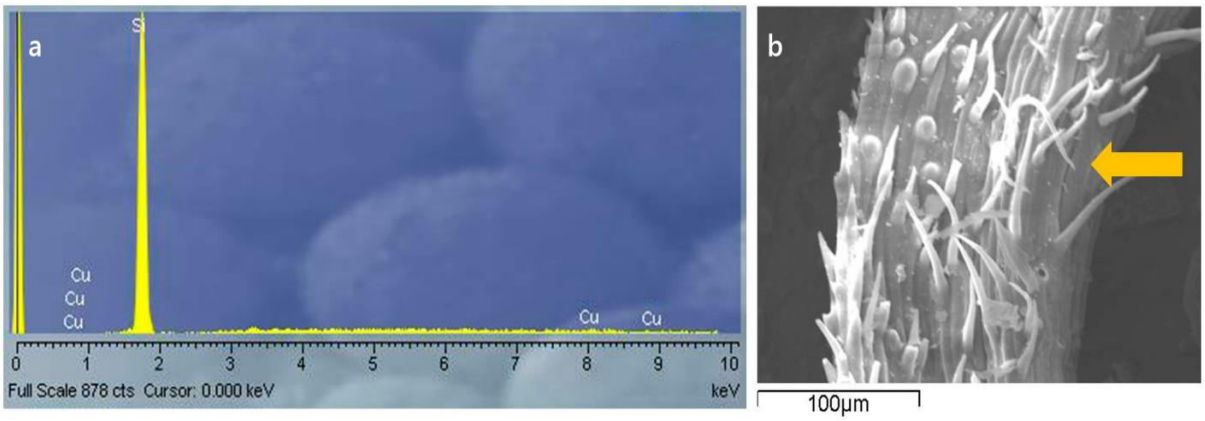

Fig. 34 EDS spectrum of phytoliths from *Triticum durum* inflorescence from Cyprus using dry method and SEM photomicrograph that presents elongates epidermal appendages (hairs) in the cell wall. Copper (Cu) was detected in the narrow end (orange arrow) of the SiO_2-rich hairs (photomicrograph: Andriopoulou)

In the present study, silicon was detected in the entire trichome (tip, shaft and base). According to Sowers and Thurston (1979), Si is detected in trichomes tips of *Urtica pilulifera* (Roman nettle) enhancing their mechanical stability. The specific localisation of chemical elements in plant hairs may indicate a genetic control of their encapsulation, and probably a functional component. Taking into account that hairs play a role in the defensive mechanism of several plants (de Souza *et al.* 2014; Strömberg *et al.* 2016) and that trace amount is required for some metabolic processes in plants (Epstein and Bloom 2005), an hypothesis may be that Cu in the hairs may provide additional hardness or/and stiffness to structure. The detailed localisation of Cu in the present wheat phytoliths invites further studies on its systematic distribution across the family.

4.7 Energy Dispersive X-ray Fluorescence (ED-XRF) and CHNS analysis

The major and trace element composition of wheat phytoliths from the inflorescences and stems-leaves extracted with only the dry method (samples: Cyprus, Crete, Volos, and Corfu), obtained by the XRF and CHNS analysis is listed in Table 13. The chemical composition of phytoliths extracted both with the dry and wet method (samples: Pella I and Pella II) is provided in Table 14.

Silicon dioxide is more abundant in phytoliths obtained with the dry method than with the wet method and in inflorescence rather than stem-leaves (Tables 14 and 16). The loss of ignition (LOI) was considerably higher in stems-leaves than inflorescences of both species and for both methods of phytolith extraction. The concentration of the remaining chemical elements, with some exceptions such as S, follows a similar trend to that of Si, being more abundant at the inflorescence and lower at the stem-leaves.

The majority of the elements, apart from Si (e.g. Ti, Al, Fe, Mn, Mg, Ca, Na, C) range between 0.1 and 5.8% of total phytolith mass in previous works (Bartoli and Wilding 1980; Jones and Milne 1963). In the present study, the inflorescence of *Triticum monococcum* is generally more enriched in elements than the stem-leaves, except for S, which shows the opposite trend, with generally higher concentrations occurring at the stem-leaves compared with the inflorescence. In addition, S is less abundant in phytoliths collected by the wet than their counterparts collected by the dry method. Sulphur participates in photosynthetic and respiratory electron transport through iron-sulphur clusters (Epstein and Bloom 2005).

Table 13 Chemical composition of phytoliths [inflorescences (I), stems-leaves (S-L)] using dry extraction method for *Triticum monococcum* (M) or *Triticum durum* (D) for plant samples from Cyprus, Crete, Volos, and Corfu

Weight%	Cyprus S-L (D) Dry	Cyprus I (D) Dry	Crete S-L (D) Dry	Crete I(D) Dry	Volos S-L (M) Dry	Volos I(M) Dry	Corfu S-L (D) Dry	Corfu I(D) Dry
SiO_2	26.08	67.36	28.61	75.62	21.05	75.02	24.01	59.18
TiO_2	0.01	0.01	0.01	0.05	0.00	0.02	0.00	0.21
Al_2O_3	0.21	0.20	0.31	1.14	0.12	0.51	0.02	5.51
Fe_2O_3	0.10	0.10	0.12	0.45	0.04	0.26	0.03	1.96
MnO_2	0.01	0.03	0.01	0.04	0.01	0.02	0.01	0.03
MgO	0.03	1.83	0.09	0.26	0.34	0.22	0.54	1.45
CaO	0.33	1.06	0.32	2.66	0.28	1.43	0.28	1.87
Na_2O	0.00	0.17	0.01	0.00	0.00	0.00	0.13	0.92
K_2O	0.50	4.12	0.26	1.36	0.74	1.99	0.63	1.58
P_2O_5	0.13	6.46	0.24	0.57	1.34	0.75	1.95	0.58
SO_3	0.76	0.73	0.92	0.75	0.90	1.09	0.71	0.43
LOI	70.67	17.67	68.10	16.00	74.40	18.53	70.59	25.04
Total	98.83	99.74	99.00	98.90	99.22	99.84	98.90	98.76

Similar results were obtained from *Triticum durum*, with higher concentrations of chemical elements at the inflorescence than at the stem-leaves, with minor exceptions in Mg and P. The higher concentration of P and K were observed in the inflorescence of the N-P-K fertilised sample from Cyprus (Table 14). Moreover, the phytoliths obtained with the dry method from *Triticum durum* are richer in SiO_2 compared with *Triticum monococcum,* which may be attributed to genetic factors, considering that the plants were grown during the same period and under the same climatic conditions. Additionally, the phytoliths separated by the dry method have higher SiO_2 concentrations at the inflorescences than at the stems-leaves, irrespective of plant variety.

Table 14 Chemical composition of phytoliths [inflorescences (I), stems-leaves (S-L)] using dry and wet extraction method for *Triticum monococcum* (M) or *Triticum durum* (D) for plant sample from Pella I and Pella II

Weight%	Pella_I S-L (M) Dry	Pella_I S-L (M) Wet	Pella_I I (M) Dry	Pella_I I (M) Wet	Pella_II S-L (D) Dry	Pella_II S-L (D) Wet	Pella_II I(D) Dry	Pella_II I(D) Wet
SiO_2	18.11	20.34	76.38	75.01	28.78	27.89	78.69	76.97
TiO_2	0.01	0.01	0.04	0.03	0.00	0.01	0.03	0.03
Al_2O_3	0.29	0.36	0.92	0.94	0.00	0.02	0.79	0.83
Fe_2O_3	0.12	0.06	0.37	0.19	0.03	0.01	0.32	0.21
MnO_2	0.01	0.01	0.02	0.01	0.01	0.01	0.02	0.01
MgO	0.20	0.05	0.44	0.14	0.39	0.11	0.27	0.09
CaO	0.43	1.88	1.77	5.02	0.32	1.23	0.89	3.28
Na_2O	0.00	0.00	0.00	0.00	0.00	0.00	0.77	0.11
K_2O	0.11	0.21	0.50	0.74	1.08	1.46	0.70	0.98
P_2O_5	0.07	0.15	0.41	0.56	1.93	0.33	0.69	0.29
SO_3	1.05	1.52	1.05	1.24	0.67	0.98	0.62	0.85
LOI	78.12	74.19	16.45	15.68	64.98	66.86	14.98	15.98
Total	98.52	98.78	98.35	99.56	98.19	98.91	98.77	99.63

The co-deposition of SiO_2 with certain metals may promote toxin neutralisation in several plants such as wheat, where Si may be responsible for the alleviation of Cd (Hussain *et al*. 2015; Rizwan *et al*. 2012), Cr (Tripathi *et al*. 2015) and Al (Cocker *et al*. 1998) toxicity, although the role of Si in decreasing aluminium toxicity in wheat has been questioned (Hodson and Evans 1995). In the present study, all samples had low Al concentration with the exception of *Triticum durum* (Corfu) inflorescence. Carnelli *et al*. 2002 studied aluminium in tissues of 20 species (Poaceae/Gramineae, Cyperaceae, Ericaceae and Coniferae), and suggested that woody species produced much higher proportion of phytoliths containing aluminium than herbaceous species.

Phytoliths occlude small amounts of organic compounds, first evidenced by the production of C and N during dry ashing (Jones and Beavers 1963, from Alexandre *et al.* 2015). Nitrogen is a major constituent of organic compounds and NanoSIMS analysis reported a nitrogen/carbon (N/C) ratio of 0.27 for wheat phytoliths of *Triticum durum* associated with the presence of amino acids (Alexandre *et al.* 2015). Yet, the CHNS analyses indicated that the phytoliths are free of N (LOI included), in accordance with previous report on nitrogen concentrations in phytoliths (Jones and Beavers 1963). In the present study mature plants were used. The low concentration of N in phytoliths, seems to depend on the organ that the phytoliths are extracted (Hodson *et al.* 2008) of to the time of cultivation, being lower at the end of the cultivation period than at the beginning (Sinclair *et al.* 2000). A previous study by Hodson *et al.* (2008) reported between 0.01% and 0.06% N in wheat, depending on the organ that the phytoliths were extracted from.

In the present study, carbon was present in the cavities and in the silica structure itself, in accordance with Alexandre *et al.* 2015. Here, C (LOI included) ranges between 5.6 and 5.8% of total phytolith mass in inflorescences and between 0.1 and 2.9% of total phytolith mass in stem-leaves for both methods of extraction. A previous study by Hodson (2016) showed that the results vary depending on the methodology employed from approximately 0.1% to 6.0% carbon. Furthermore, H (LOI included) ranges between 2.86 and 4.56% of total phytolith mass in inflorescences and between 0.58 and 1.24% of total phytolith mass in stem-leaves for both extraction methods.

Table 15 presents the chemical composition of the phytoliths extracted from the entire plants, excluding the roots, using the dry method (samples: Cyprus, Crete, Volos, Pella I, Pella II and Corfu). All samples are rich in SiO_2. The detailed chemical compositions of the materials extracted are presented below.

Table 15 Chemical composition of phytoliths extracted from the entire plant, excluding the roots, using dry extraction method for *Triticum monococcum* (M) or *Triticum durum* (D) for plant samples from Cyprus, Crete, Volos, Pella I, Pella II and Corfu

Weight%	Cyprus Entire (D) Dry	Crete Entire (D) Dry	Volos Entire (M) Dry	Pella_I Entire (M) Dry	Pella_II Entire (D) Dry	Corfu Entire (D) Dry
SiO_2	36.48	40.29	39.37	33.63	40.21	34.93
TiO_2	0.01	0.02	0.04	0.02	0.01	0.21
Al_2O_3	0.21	0.51	0.23	0.44	0.18	1.42
Fe_2O_3	0.08	0.22	0.11	0.19	0.11	0.46
MnO_2	0.03	0.03	0.01	0.01	0.01	0.02
MgO	0.31	0.35	0.29	0.28	0.3	0.34
CaO	0.51	0.94	0.47	0.59	0.54	0.7
Na_2O	0.12	0.01	0.00	0.00	0.67	0.33
K_2O	1.47	0.6	0.98	0.29	0.42	0.94
P_2O_5	1.92	0.39	0.92	0.17	1.59	1.49
SO_3	0.77	0.66	0.99	1.04	0.62	0.65
LOI	57.51	55.18	56.23	63.08	54.37	58.07
Total	99.42	99.2	99.64	99.74	99.03	99.56

Both environmental and genetic factors affect the physicochemical conditions related to the biological regulation of chemical element deposition within the plant (Piperno 2006). Thus the elemental composition of phytoliths, for example from calcined Ericaceae and phytoliths from fresh Poaceae and Apiaceae is influenced both by species and soil characteristics (Buján 2013; Hart 2001). In addition phytoliths from calcined *Vaccinum corymbosus* (blueberry) were dominated by Si and this was more pronounced in leaves compared with other parts of the plant, suggesting that genetic factors might also get involved in the overall chemical composition of phytoliths (Morikawa and Saigusa 2004). It is reported that organic environment such as proteins (i.e. biological macromolecules) may play a significant role in biosilification processes (Elbaum *et al.* 2007; Harrison 1996). Testing these factors in our phytoliths is beyond the objectives of the present study.

Although there is little available information on the composition of different parts for this plant species (cf. Canti 2003), it is considered that the variation may be systematic based on previous chemical analysis studies on wheat (Folk and Hoops 1982; Hodson *et al.* 2008; Milton and Davidson 1946). A better understanding of the distribution of nutrients across the plant may not only provide useful knowledge to the fields of geoarchaeology and archaeobotany, but it may also be a significant contribution to issues on plant nutrition and physiology. For example, Si is primary associated with the cell wall and Ca serves an important function as a growth factor. Magnesium, Mn, and Fe are integral constituents of enzymes or other essential entities of the metabolism. Potassium, Mg, Na, Mn and Ca serve to activate or control the activity of the enzymes. Phosporus is essential in energy acquisition and utilisation, and in the genome (Epstein and Bloom 2005). Likewise, the differences in chemical composition may have an impact on human/animal diet and health, on baking or pasting properties, and on issues regarding the presence of precious, heavy or toxic metals in the soil-plant system.

The elemental composition of the soils are summarised in Table 16. All samples are rich in SiO_2 (average > 50% in total). The soils with lower concentration of CaO are from Volos and Corfu sample (3.59-3.79%), while Cretan sample has the higher concentration of CaO (21.21%). The MgO concentration in soils ranges between 0.84-2.34%, with the exception of Pella soils (8.92-9.27%). The Al_2O_3 concentration ranges between 6.37-10.52%, Fe_2O_3 between 2.36-5.98%, while TiO_2, Na_2O, K_2O and P_2O_3 have a lower percentage (0.06-3.88%). Three groups of soils with similar chemical characteristics are observed: (a) Crete, Pella I and Pella II, (b) Cyprus, (c) Volos and Corfu.

Table 16 Chemical composition of the soils, where the plants were grown

Weight%	Cyprus	Crete	Volos	Pella_I	Pella_II	Corfu
SiO_2	50.42	37.74	75.39	38.58	43.33	73.30
TiO_2	0.49	0.47	0.41	0.40	0.49	0.37
Al_2O_3	9.86	6.81	6.37	9.79	10.52	6.37
Fe_2O_3	5.98	4.08	2.63	3.87	4.35	2.58
MnO_2	0.13	0.08	0.07	0.08	0.09	0.06
MgO	2.34	2.12	0.84	8.92	9.27	0.86
CaO	12.18	21.21	3.79	12.30	13.73	3.59
Na_2O	2.41	1.23	1.99	2.67	3.88	0.82
K_2O	1.12	0.72	1.23	2.22	2.35	1.33
P_2O_5	0.34	0.78	0.11	0.25	0.63	0.10
LOI	14.36	23.72	6.36	20.88	10.38	8.99
Total	99.63	98.99	99.20	99.96	99.02	98.37

In most cases, accumulation of SiO_2-rich phytoliths occurs in soils when their turnover rate is greater than losses by Si dissolution (Meunier 1999). In the present study, the concentration of Si of the soils affects the concentration of SiO_2-rich phytoliths extracted from inflorescences and stem-leaves to some degree (Fig. 35), confirming that geochemical characteristics of soils, by constraining or promoting Si dissolution, play an important role in Si accumulation by wheats.

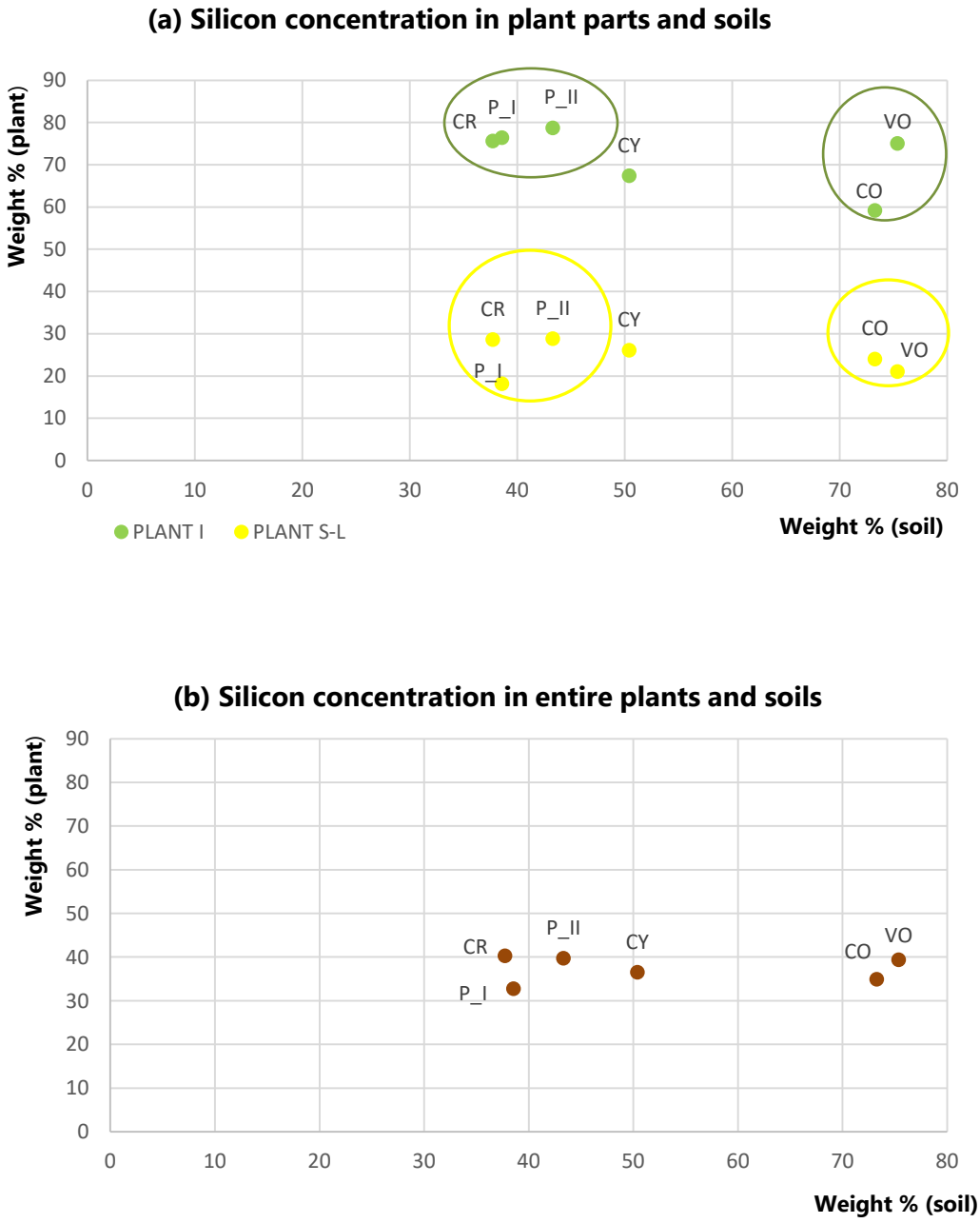

Fig. 35 The following groups of soils with similar chemical characteristics are observed: a. Crete, Pella I and Pella II, b. Volos and Corfu and c. Cyprus. **(a)** correlation of the concentration of Si in plant inflorescence (green dots: PLANT I) or in plant stem-leaves (yellow dots: PLANT S-L) and the concentration of Si in the soils, where the plants were grown (CY: Cyprus, CR: Crete, VO: Volos, P_1: Pella I, P_2: Pella II, CO: Corfu); and **(b)** correlation of the concentration of Si in entire plants (excluding roots) (brown dots) and the concentration of Si in the soils, where the plants were grown (CY: Cyprus, CR: Crete, VO: Volos, P_1: Pella I, P_2: Pella II, CO: Corfu)

The elemental concentration of wheat phytoliths extracted from inflorescence, stem-leaves and soils, from Cyprus, Crete, Volos, Pella I, Pella II and Corfu are presented in Figs. 37-42. Note that the vertical axis of the six diagrams below is expressed in logarithmic scale. During wheat growth, elements may be re-translocated through plant system (from roots to stem, stem to leaves and leaves to grains in inflorescence), and some particles might be occluded within phytolith structure when Si precipitates (Fig. 36).

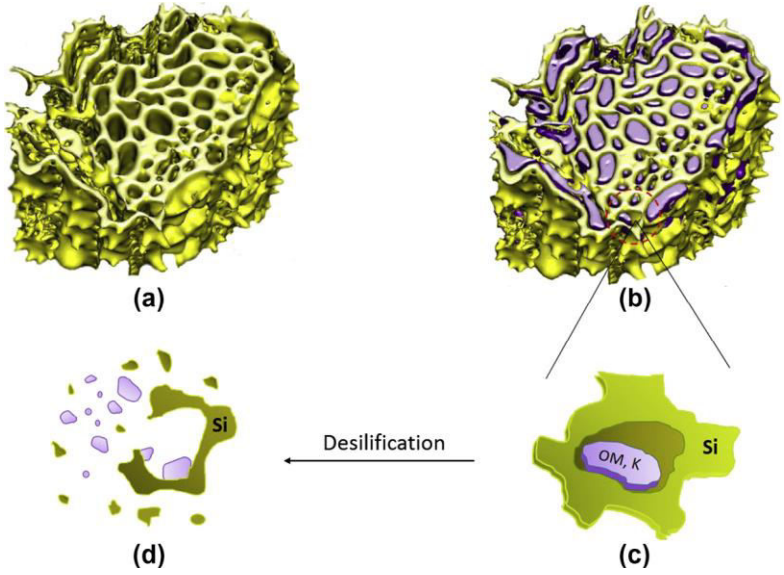

Fig. 36 (a) Principal arrangement of SiO_2-rich phytolith structures (green colour), **(b)** SiO_2-rich phytolith structures fulfilled by occluded particles such as potassium (purple colour), **(c)** and **(d)** plant cell during desilification process (source: Nguyen 2015)

Plant growth largely depends on the combination and concentration of mineral nuntrients available in the soil (Marschner 1995). According to the results obtained from XRF analysis of phytoliths from plants and soils, for both wheat species, there is a relationship between the soil composition and the plant parts (stem-leaves or inflorescence) (Fig. 36-41). The concentration of some chemical elements in inflorescence, such as the plant macronutrients P (which is a key element for metabolic pathways) and K (which has a key role at osmosis and ion transport into cells) are quite

higher than their concentration in soils. While Si tends to be immobilised by precipitation that forms SiO_2-rich phytoliths (Marschner 1995; Nguyen *et al.* 2014), it is probable that P is more mobile in plant (Trihn *et al*. 2017). Mobility is closely related to the tendency of an element to be stable in water-soluble form. According to previous studies on *Oryza sativa* (rice), P-pool (Trihn *et al.* 2017) and K-pool (Nguyen *et al.* 2014) may be additional sources for crops when the straw is returned to the soils. Pottasium concentration was also high in the inflorescences suggesting that is an element which is readily taken up from the bulk soil to the root, and then transferred to the other parts of the plant. The high mobility of K was further confirmed by the dissolution experiments (see chapter 4.9). Pottasium is released faster than Si, and thus its release might affect the solubility of dissolved Si (Si free in the soil solution or adsorbed to Fe or Al oxides/hydroxides). The high mobility of K within short-diastance transport (i.e. between individual cells and between neighbor tissues), as well as within long distance translocation through the xylem and phloem has been also previously reported (Marschner 1995).

Futhermore, the concentration of P and K in inflorescence were significant higher in the fertilised plant sample from Cyprus than their concentration in soils. This corresponds to the application of fertiliser (NPK 20/20/0) in the soil. With fertilisation, the amount of P and K in the soil increases, and more P ad K in the soil becomes available to the crop. Relatively higher concentration of Al and Mg in inflorescences than soils was observed in the samples from Corfu. This may be related with the proximal environment and growing conditions (e.g. water uptake and water loss). The sample from Corfu is related with the higher precipitation (1560 mm) between samples, and this may affect the physicochemical conditions that are related to the biological regulation of chemical elements deposition within the plant.

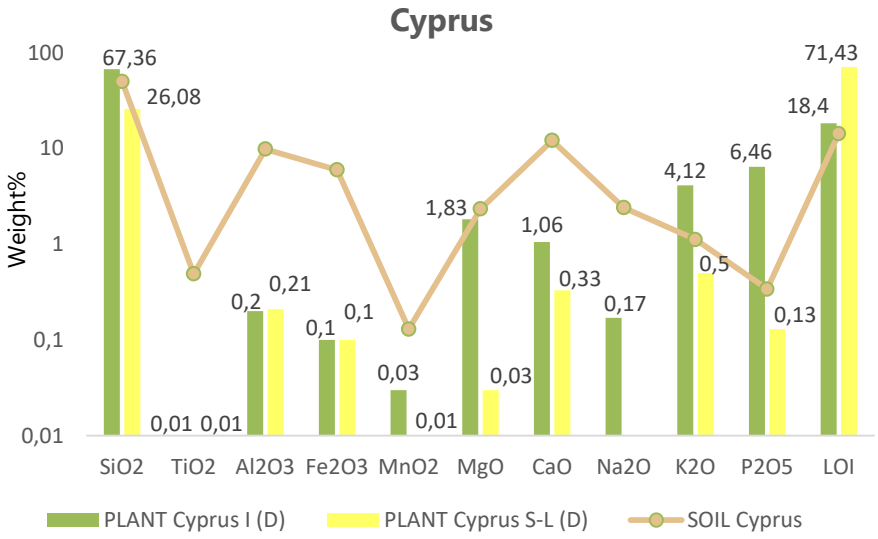

Fig. 37 The elemental concentration of phytoliths extracted from inflorescence (green columns), stem-leaves (yellow columns) and soil (brown line) from *Triticum durum* (D) Cyprus sample

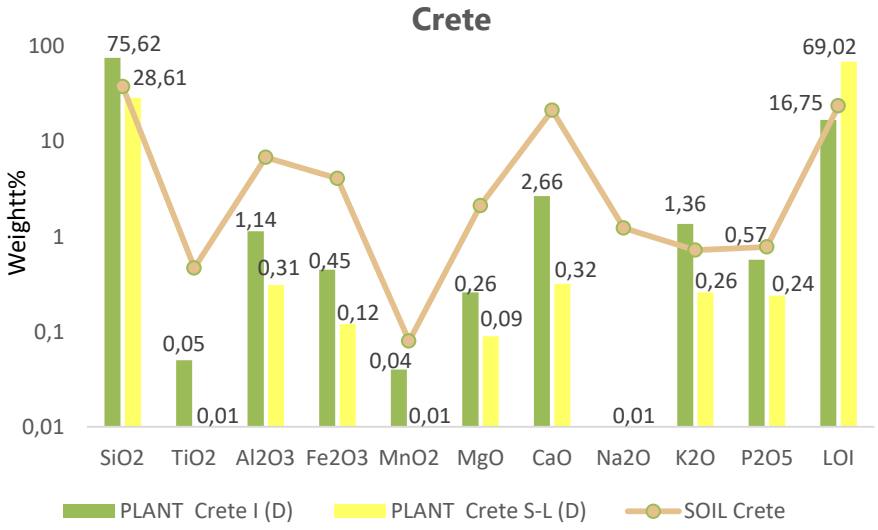

Fig. 38 The elemental concentration of phytoliths extracted from inflorescence (green columns), stem-leaves (yellow columns) and soil (brown line) from *Triticum durum* (D) Crete sample

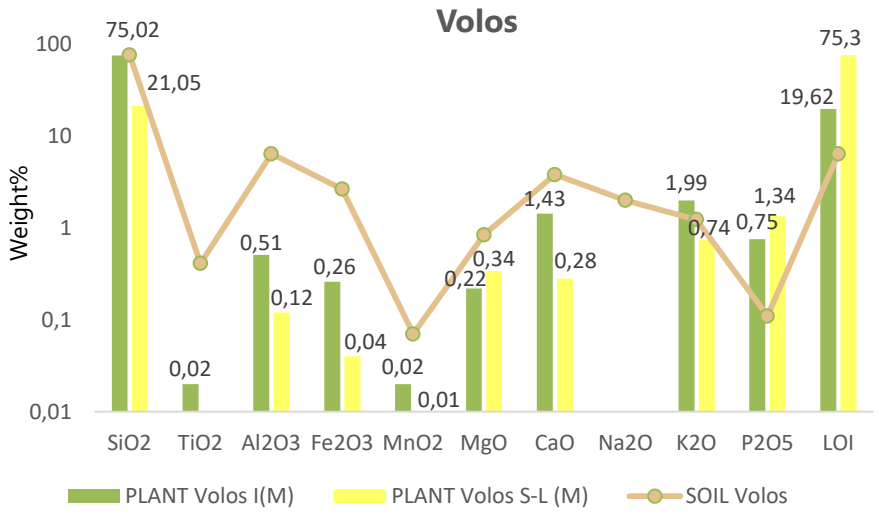

Fig. 39 The elemental concentration of phytoliths extracted from inflorescence (green columns), stem-leaves (yellow columns) and soil (brown line) from *Triticum monococcum* (M) Volos sample

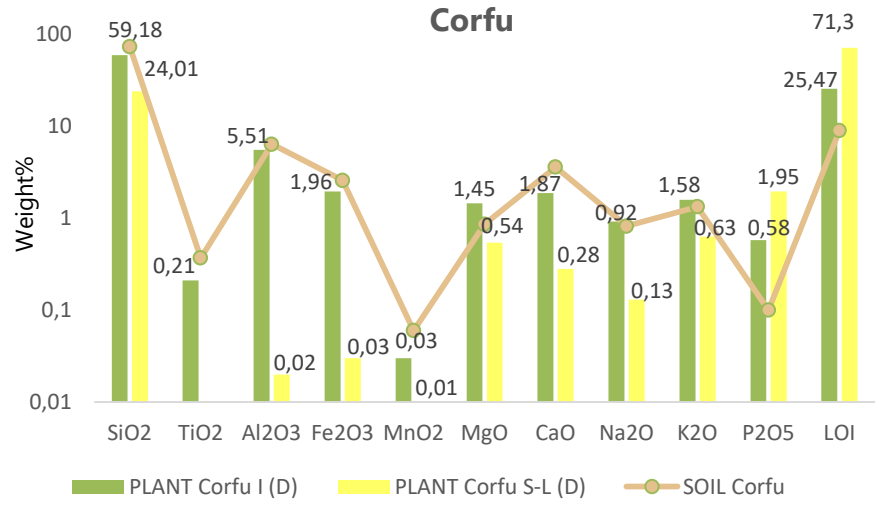

Fig. 40 The elemental concentration of phytoliths extracted from inflorescence (green columns), stem-leaves (yellow columns) and soil (brown line) from *Triticum durum* (D) Corfu sample

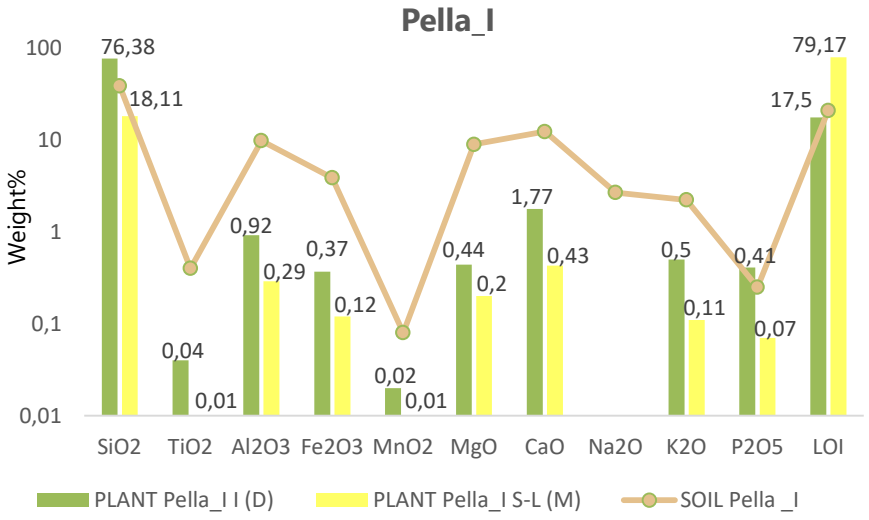

Fig. 41 The elementalconcentration of phytoliths extracted from inflorescence (green columns), stem-leaves (yellow columns) and soil (brown line) from *Triticum monococcum* (M) Pella sample

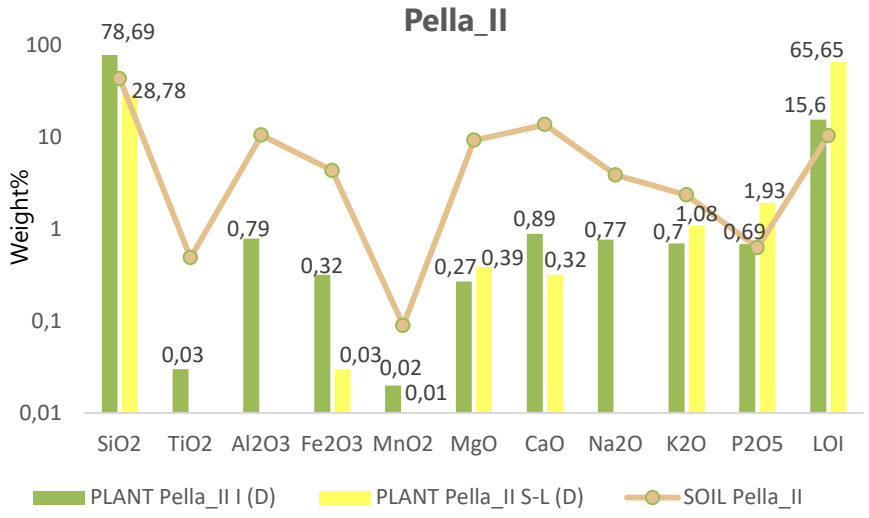

Fig. 42 The elemental concentration of phytoliths extracted from inflorescence (green columns), stem-leaves (yellow columns) and soil (brown line) from *Triticum durum* (D) Pella sample

The elemental composition of the archaeological sediments samples are summarised in Table 17. All samples are quite rich in SiO_2 (average>40% in total). The richer sediments in CaO are from Knossos (33.13-33.58%). The chemical compositional trends reflect mainly the relative abundances of silicate and carbonate minerals in the samples (see XRD traces above). In the sediments, the Al_2O_3 concentration ranges between 5.51 and 11.36%. TiO_2, Fe_2O_3, MgO, Na_2O, K_2O and P_2O_3 have a lower percentage (0.04-5.39%).

Table 17 Chemical composition of the archaeological sediments

Weight%	**Knossos 5**	**Knossos 10**	**Palea 25**	**Palea 27**	**Toumba 2008**	**Toumba 2013**
SiO_2	35.13	33.58	47.18	49.57	63.31	61.19
TiO_2	0.31	0.29	0.66	0.51	0.27	0.60
Al_2O_3	7.22	6.57	11.36	9.84	5.51	11.32
Fe_2O_3	3.25	3.36	5.39	4.41	2.48	5.28
MnO_2	0.05	0.04	0.09	0.09	0.13	0.10
MgO	1.48	1.45	3.91	3.73	1.57	2.15
CaO	40.15	43.47	10.30	14.55	18.05	8.70
Na_2O	2.65	2.55	4.66	3.86	1.92	2.27
K_2O	1.21	1.07	2.24	2.57	1.93	2.20
P_2O_5	2.60	3.03	0.34	0.99	3.12	0.94
LOI	5.50	4.38	13.28	9.62	1.55	4.95
Total	99.55	99.79	99.41	99.74	99.84	99.70

4.8 Thermogravimetric analysis-Differential Thermogravimetric Analysis (TGA-DTGA)

The DTG-TG curves of phytoliths extracted from the plants using the dry method are presented in Fig. 44 for stem-leaves and Fig. 45 for inflorescence. The curves correspond both to stem-leaves and inflorescence of: (a) Cyprus, *Triticum durum* (b) Crete, *Triticum durum*, (c) Volos, *Triticum monococcum*, (d) Pella I, *Triticum monococcum*, (e) Pella II, *Triticum durum*; and (f) Corfu, *Triticum durum*. The DTG-TG curves of phytoliths from the inflorescence and from stems-leaves after their extraction (from Pella samples) are presented in Fig. 46 for dry method and Fig. 47 for wet method. A difference is observed in the thermal curves of the two species in both the dry and the wet method, which is related to the mineralogical composition of the phytoliths. In both extraction methods, the results of thermogravimetric analysis are in accordance with the XRD traces above. Moreover, due to the different mineralogical composition a difference in the position and intensity of the thermal events is expected when comparing the inflorescences and the stems-leaves.

The SiO_2-rich phytoliths consist of hydrated minerals (see FTIR spectra above), with ~2-15 wt.% water (Bartoli and Wilding 1980; Piperno 2006). According to Bartoli and Wilding (1980) phytoliths of deciduous origin are more hydrated than coniferous analogues, and phytoliths of gramineneous (e.g. wheat) origin are generally intermediate between coniferous and deciduous forms. The total water content and concentration ratio of molecular water to silanol water (Si-OH) are characteristic for the different SiO_2 forms (Heaney 1993) and the water content in the various silica forms decreases with increasing crystal order (Awadh and Yaseen 2019). The thermogravimetric (TG) and derivative thermogravimetric (DTG) curves showed that during the drying process, the moisture content of phytoliths extracted with the wet method decreases rapidly and

mass loss is observed in the temperature range of ~30-90°C. These weight losses correspond to evaporation of physisorbed water due to dehydration. The step drying process is reported at ~150°C since between ~120 and 150°C, the curves presented a flat line for most samples as presented below.

The removal of CO_2 from carbonates and possibly SO_2 from sulphates occurs at ~650°C, broad for *Triticum monococcum* inflorescence and stem-leaves (wet method). The endothermic peak observed at ~850°C for *Triticum monococcum* stem-leaves (dry method) is attributed to the decomposition of Ca-bearing minerals. Between ~150 and 850°C a series of reactions involving decarboxylation, decarbonylation, fragmentation, and rearrangement take place. For samples using the dry method, a slight gain of mass was recorded at ~800°C corresponding probably to crystallization and secondary mineral formation. The final step of weight loss for the phytoliths was at ~950°C. The overall weight loss for wet method is higher than the weight loss for dry method. This is in accordance with the LOI results (Table 16). Furthermore, the weight loss of the *Triticum durum* (naked wheat) is higher than the weight loss of the *Triticum monococcum* (hulled wheat) with the exception of *Triticum monococcum* stem-leaves using wet method. Naked and hulled grains from wheat are shown in Fig. 43.

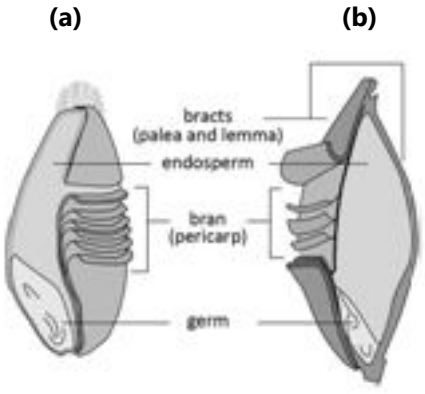

Fig. 43 Wheat grains: **(a)** naked; and **(b)** hulled (source: Alonso 2019)

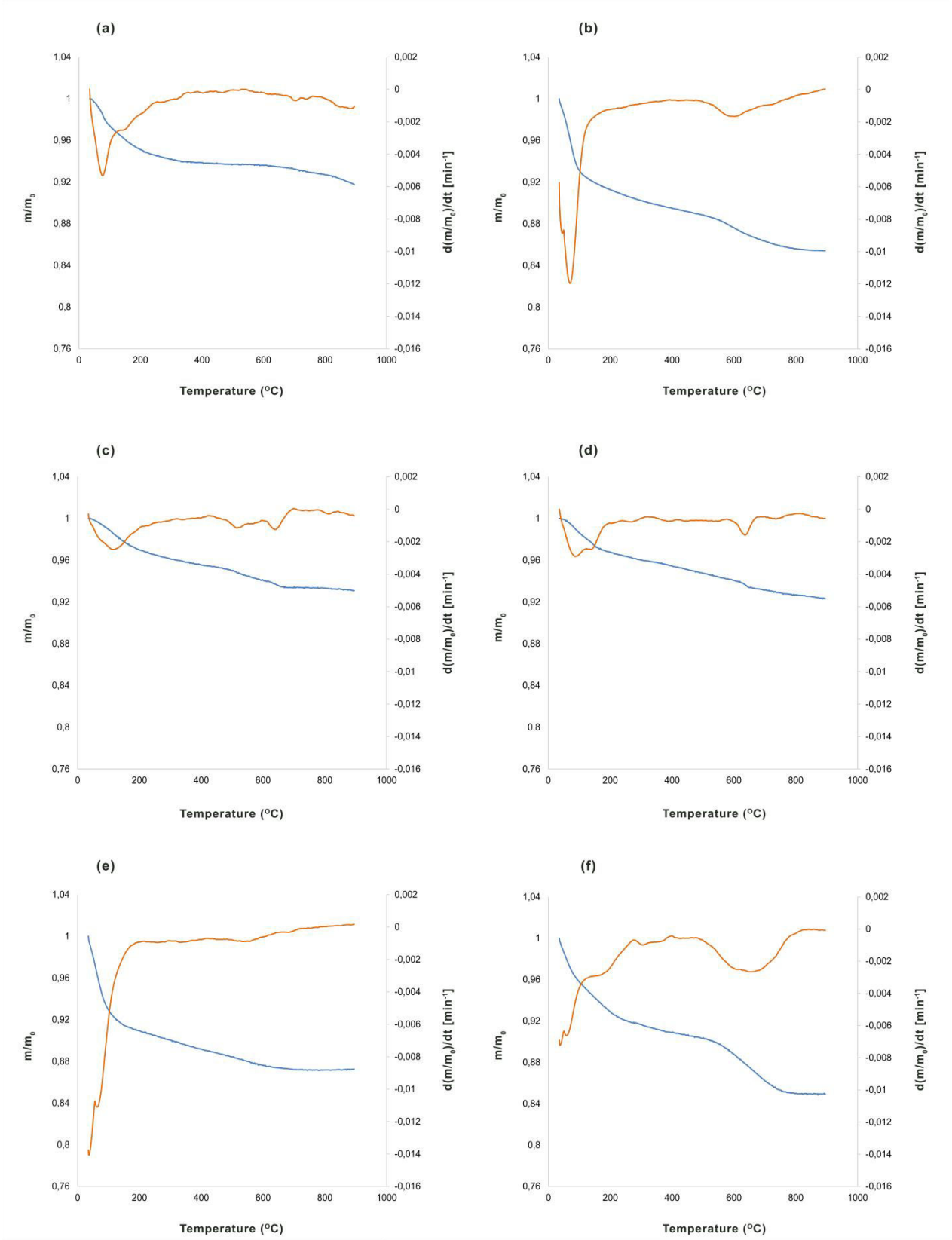

Fig. 44 DTG-TG curves for stem-leaves (dry method): **(a)** Cyprus, **(b)** Crete, **(c)** Volos, **(d)** Pella I, **(e)** Pella II, **(f)** Corfu

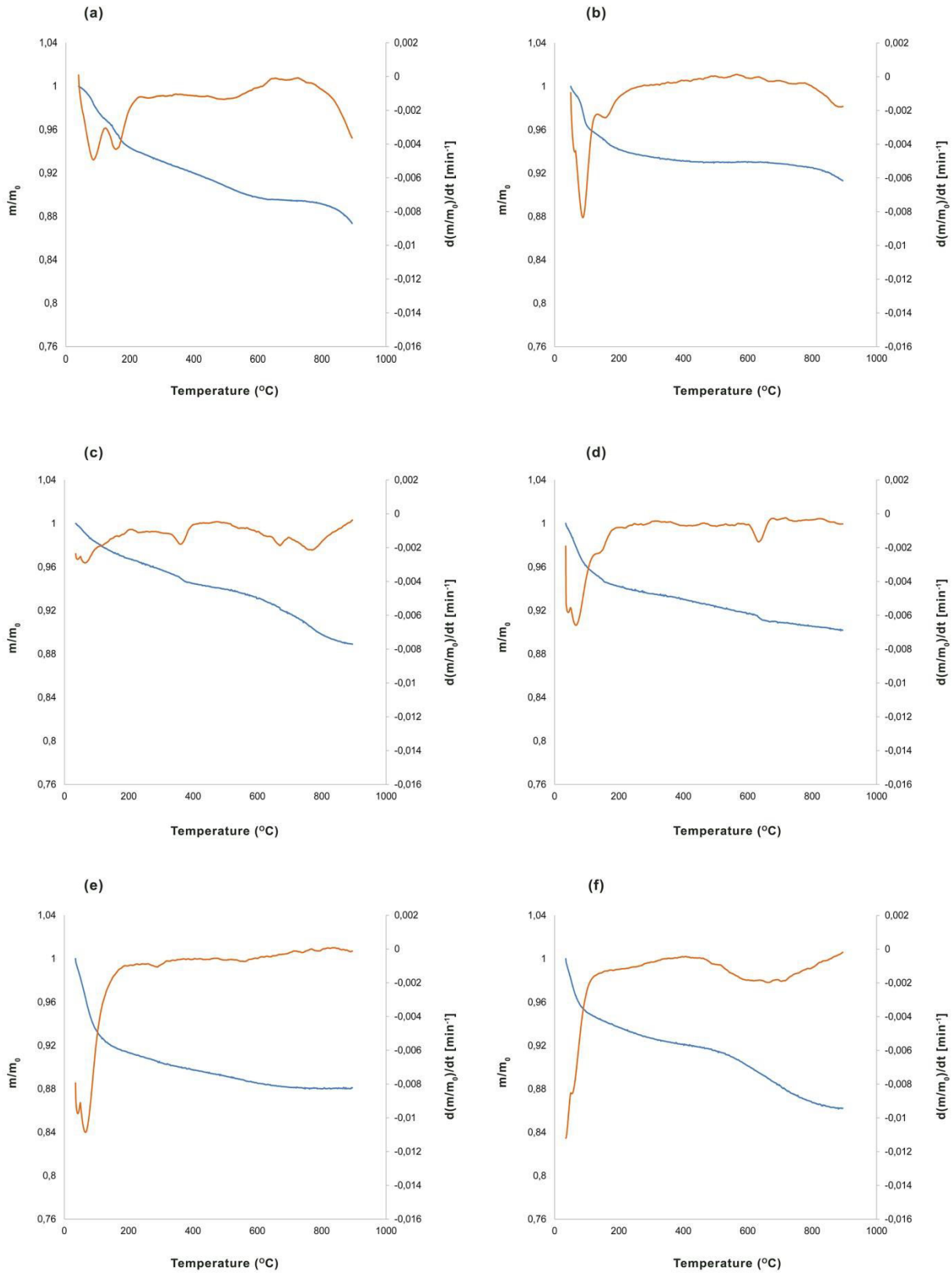

Fig. 45 DTG-TG curves for inflorescences (dry method): **(a)** Cyprus, **(b)** Crete, **(c)** Volos, **(d)** Pella I, **(e)** Pella II, **(f)** Corfu

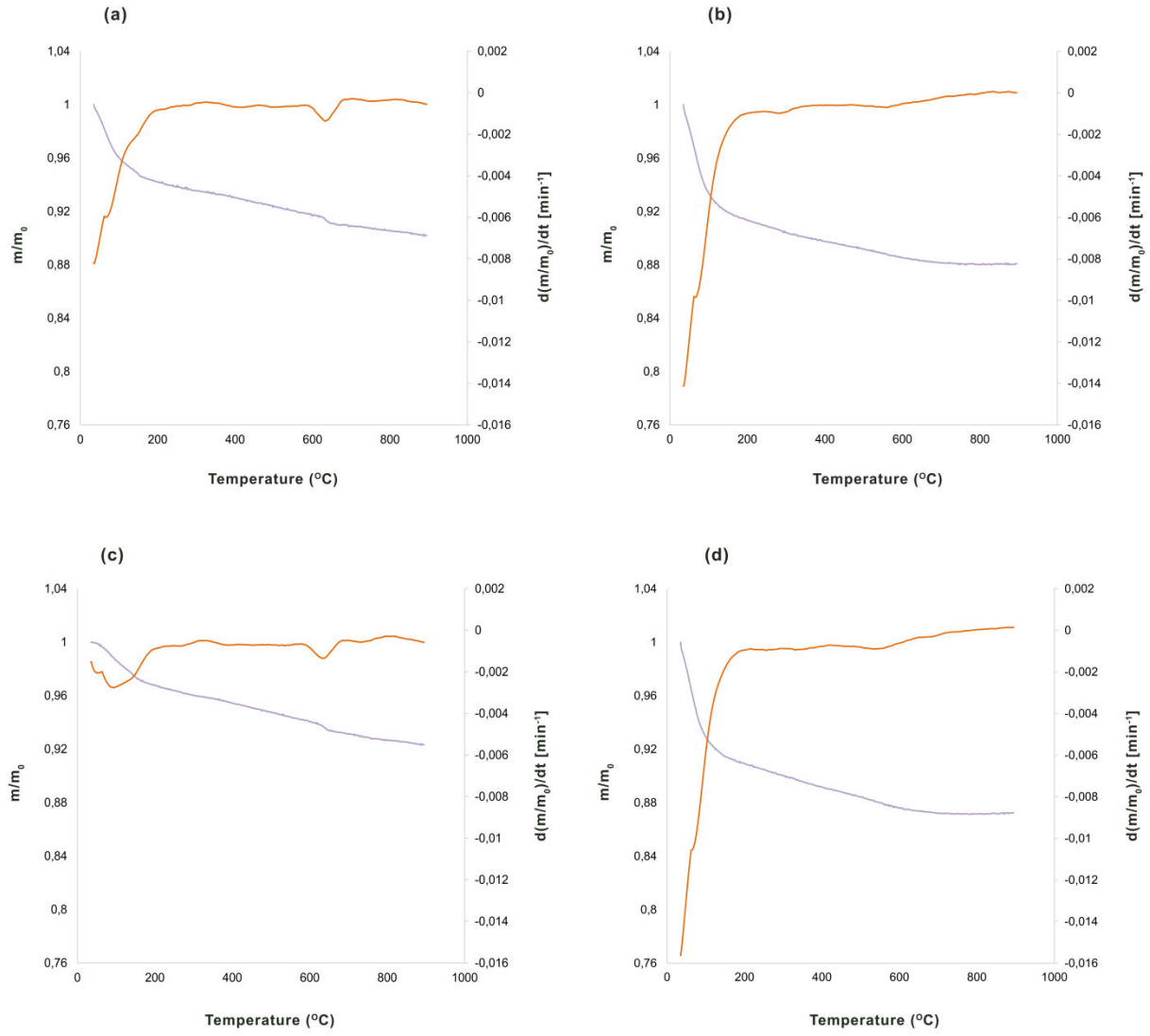

Fig. 46 DTG-TG curves for stem-leaves and inflorescence from Pella using dry method: **(a)** *Triticum monococcum* inflorescence, **(b)** *Triticum durum* inflorescence, **(c)** *Triticum monococcum* stem-leaves; and **(d)** *Triticum durum* stem-leaves

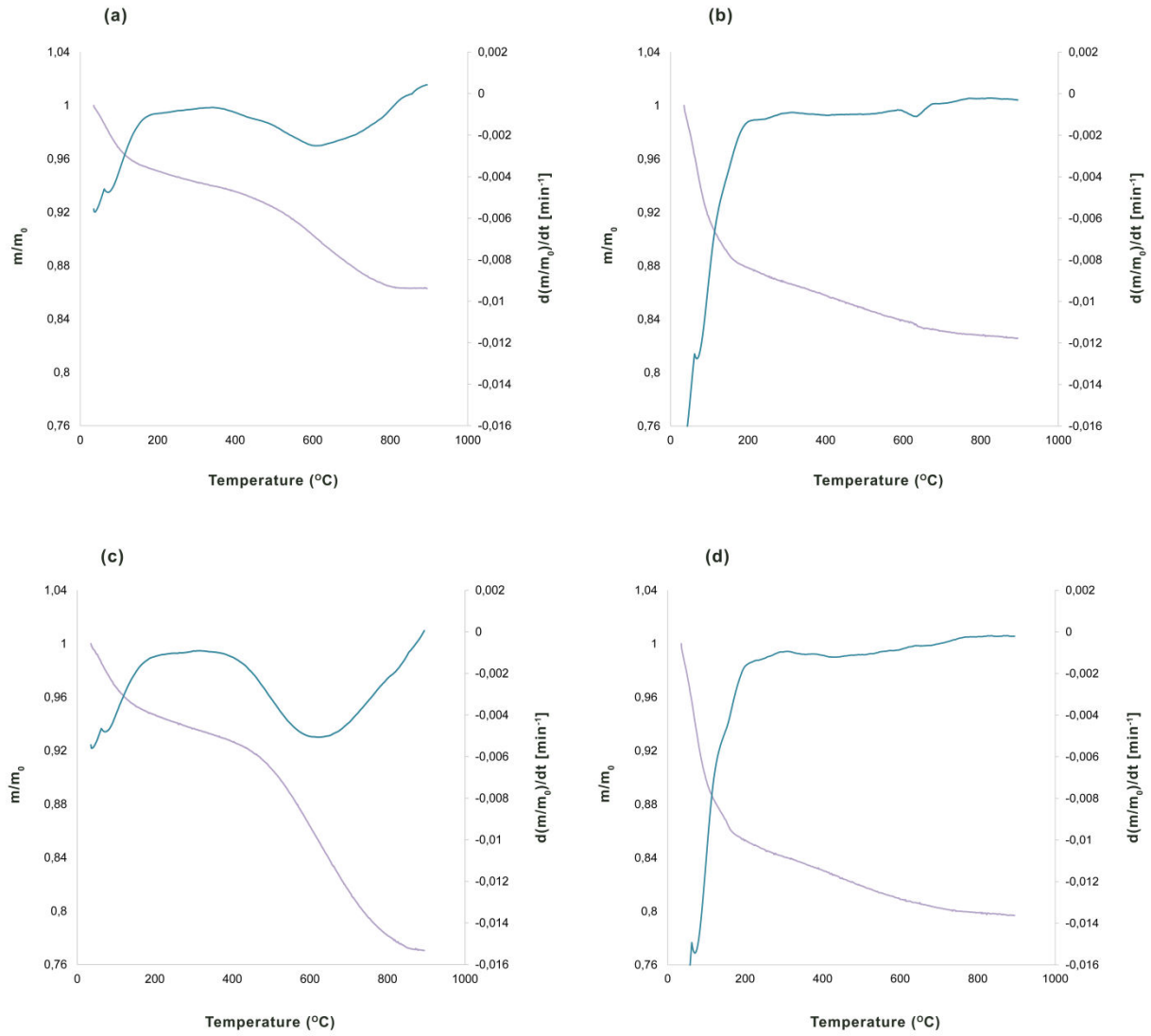

Fig. 47 DTG-TG curves for stem-leaves and inflorescence from Pella using wet method: **(a)** *Triticummonococcum* inflorescence, **(b)** *Triticum durum* inflorescence, **(c)** *Triticum monococcum* stem-leaves; and **(d)** *Triticum durum* stem-leaves

4.9 Batch experiments, solubility and dissolution kinetics of plant phytoliths: geoarchaeological implications

Dissolved biogenic SiO_2 plays a pivotal role as source of plant-available Si in soils (Conley 2002; Sommer *et al.* 2006; Struyf 2009). Phytoliths are released during plant litter, ash or dung degradation in litter horizon and are then transferred to deeper horizons or removed and transported by hydrographical (or aerial) paths (Bartoli and Wilding 1980; Meunier *et al.* 1999). Chemical components of phytoliths may be related with the availability of chemical elements (e.g. Si, K, Mg, Al, Ca, Fe, Sr, Ba) in the substrate, as well as the plant's phylogenetic variation (Epstein 1994, 1999; Hodson *et al.* 2005; Jarvis 1987; Kaltsikes and Larter 1970; Van der Vorm 1980). When phytoliths are buried in the soils after the decomposition or/and burning of the plant material, their morphology and mineralogical/chemical components undergo alterations (Albert *et al.* 2006; Madella and Lancelotti 2012).

Phytoliths at archaeological sites might undergo partial or total loss, principally depending on the environment in which the phytolith were buried (Goldberg and Macphail 2006), and studying phytolith solubility may provide insights into the driving mechanisms behind phytolith diagenesis. The effects of the various formation processes on phytoliths also depend on their physical and chemical properties before their burial in soils and sediments. Dissolution is a significant factor affecting the progressive alteration of the physicochemical characteristics of SiO_2-rich phytoliths, having a strong impact on the preservation status of phytoliths (Bartoli and Wilding 1980; Cabanes *et al.* 2011, 2015; Fraysse *et al.* 2006a, 2006b, 2009; Loucaides *et al.* 2010; Nguyen *et al.* 2014).

Phytolith chemical components may contain information about the plant and the environment in which it grew and developed over the course of time. Phytoliths are often useful material indicators of human occupation of a site, and their preservation status that is strongly related with dissolution processes, is one of the most important factors for reliable interpretation of phytoliths in a number of archaeological sub-disciplines (e.g. geoarchaeology, archaeobotany, micropaleontology, taphonomy). It is of high importance for geoscientists and archaeologists to study well-preserved primary assemblages (e.g. archaeobotanical remains) (Schiffer 1987). Among the many plants that produced phytoliths, wheat occupied a central role in human economies over the millennia (Jones *et al.* 1998; Nesbitt and Samuel 1996; Valamoti 2009; Zohary *et al.* 2012). The major objective of the present dissolution experiments was to determine the relative solubilities of fresh (not aged) wheat phytoliths (extracted from *Triticum monococcum* and *Triticum durum* using dry method), under conditions that are relevant to natural environments (e.g. pH of the majority of the soils under natural conditions range between ~3.5 and 8.5). Cabanes and Shahack-Gross (2015) using a rapid solubility assay coupled with data from other studies (Cabanes *et al.* 2011, 2012; Shahack-Gross *et al.* 2014) suggested that the lower the solubility of a given phytolith assemblage, the more it is composed of resistant phytoliths (i.e. it is less well preserved).

Dissolution of phytoliths was carried out in batch experiments, by adding 0.15 g of wheat phytoliths in 45 mL of deionised H_2O. The results presented in the Tables 21-26 (samples from Cyprus, Crete, Volos, Pella I, Pella II and Corfu) of appendix 2, originate from phytolith dissolution study by determination of the concentration of the dissolved Si and 7 other chemical elements (Al, Mg, Ca, K, Fe, Sr, Ba) with inductively coupled plasma mass spectrometry (ICP-MS). The final concentration is assumed to represent the solubility of the dissolving element that was in the solid sample. Temperature and pH affect the dissolution efficiency of SiO_2 and thus the weathering resistance of phytoliths.

The dissolution of phytoliths and aqueous concentrations of the elements were studied under controlled conditions at defined pH (5, 7, 8.5) and temperature (5, 20, 40 °C). The experiments at 20 ˚C were carried out under continuous agitation in a shaking table. The suspensions (at 5 and 40˚ C) were periodically stirred (manually), limiting the maximum possible SiO_2 solubility due to re-precipitation.

The evolution of the four studied main elements (Si, Mg, Ca, K) and the two trace elements (Sr, Ba) concentration (mg/g) at the aforementioned variables over time are presented in kinetic diagrams. Silicon, Mg, Ca and K concentrations over time are presented in the 54 diagrams (all elements together) of appendix 3a (Figs. 112-129), or in the 72 diagrams (each element separately) of appendix 3b (Figs. 130-165). Representative kinetic diagrams for the dissolution of phytoliths extracted from *Triticum durum*, Cyprus are given below (Figs. 48 and 52). Three-dimensional diagrams are also provided for the representation of Si concentration over the course of time in relation of both pH and temperature in appendix 6 (36 diagrams, Figs. 190-201). Representative 3D diagrams are given below (Figs. 49-50). Strontium and Ba concentrations over time are presented in the 54 diagrams of appendix 4 (Figs. 166-183). Representative Sr and Ba diagrams are given in Fig. 56. The error bars in all diagrams show the standard deviation for the repetition of two measurements of element concentration.

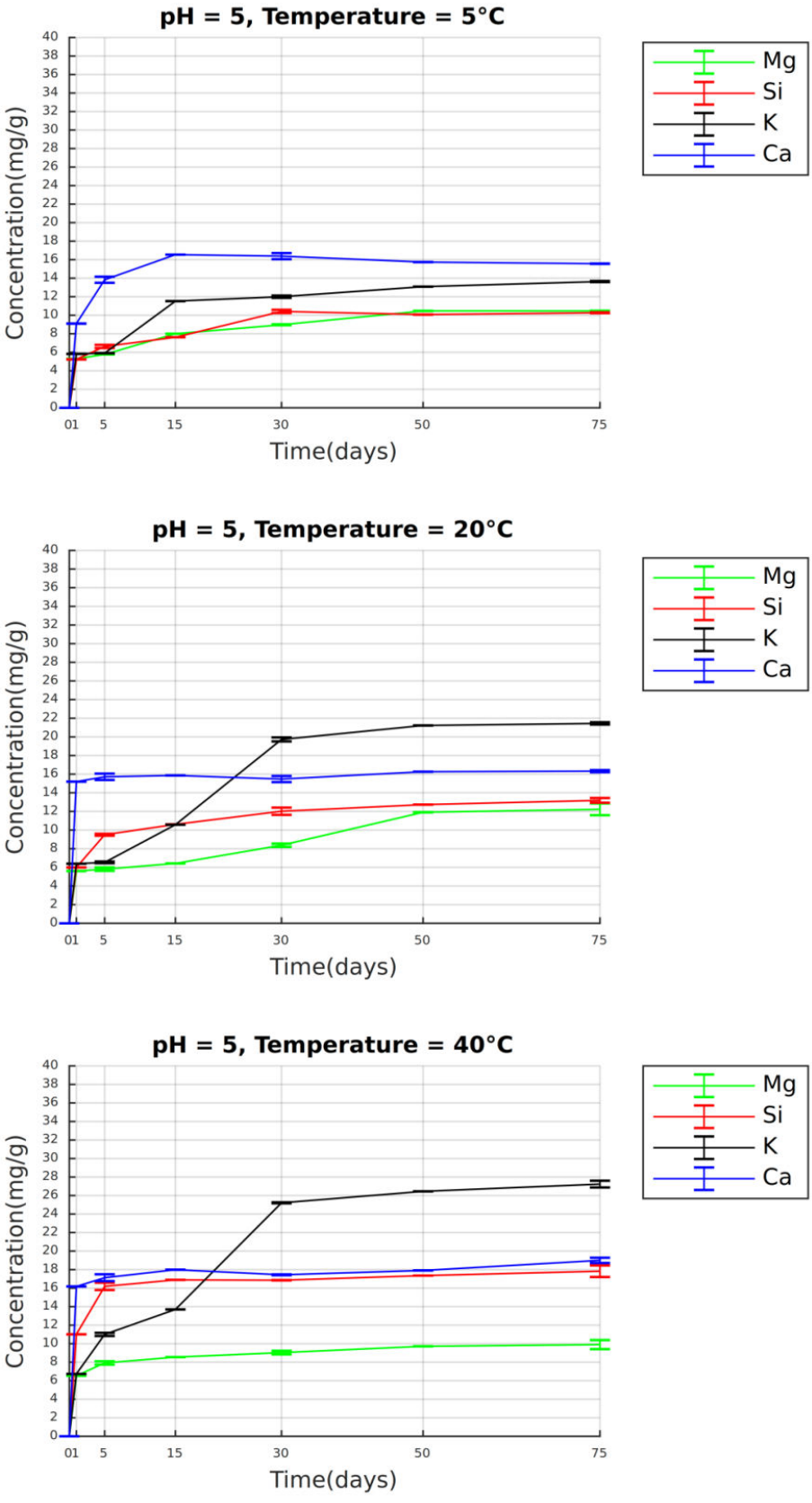

Fig. 48 Concentration (mg/g) of Mg, Si, K, Ca over the course of 75 days at pH 5 and temperature 5˚C, 20˚C, 40 ˚C (*Triticum durum,* Cyprus)

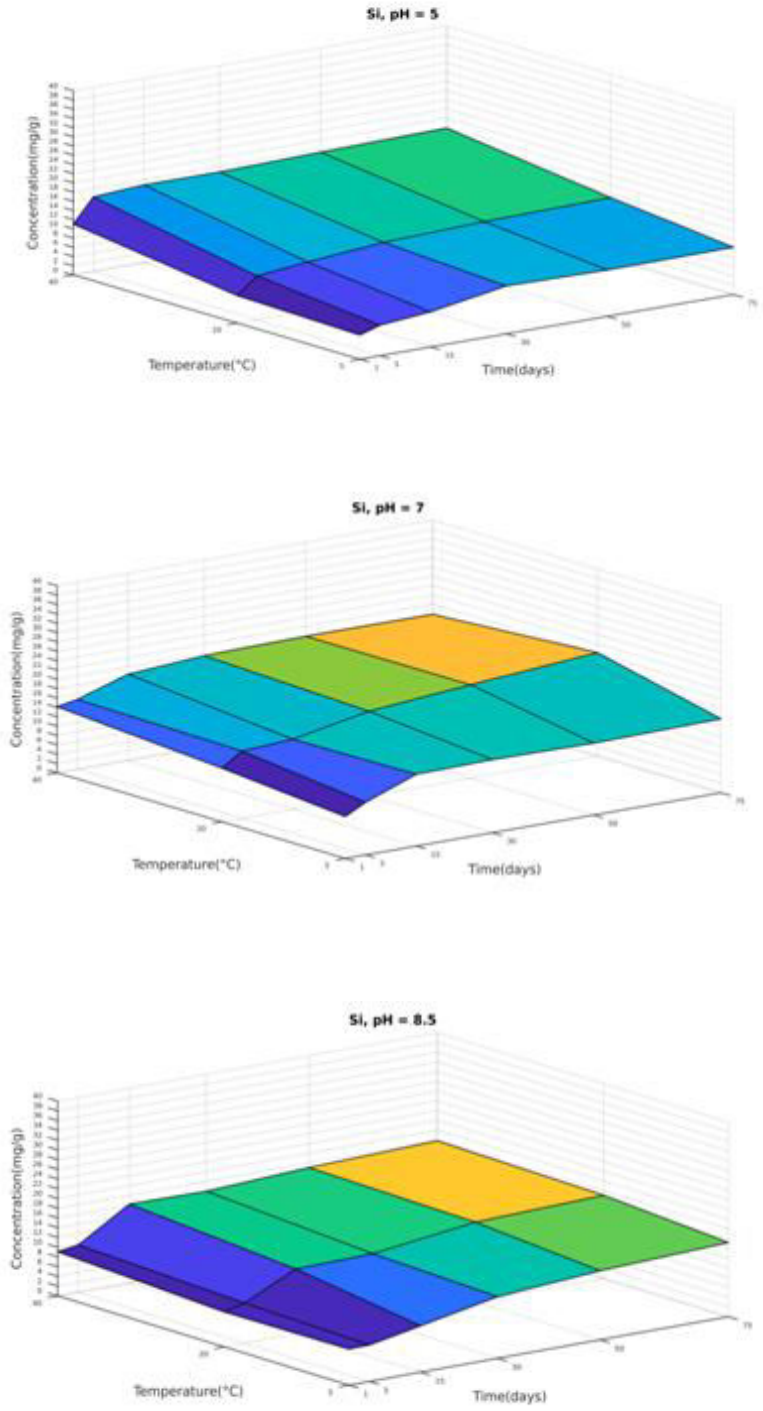

Fig. 49 Silicon concentration (mg/g) at **pH 5, 7, 8.5** and temperature 5, 20, 40˚C (*Triticum durum,* Cyprus)

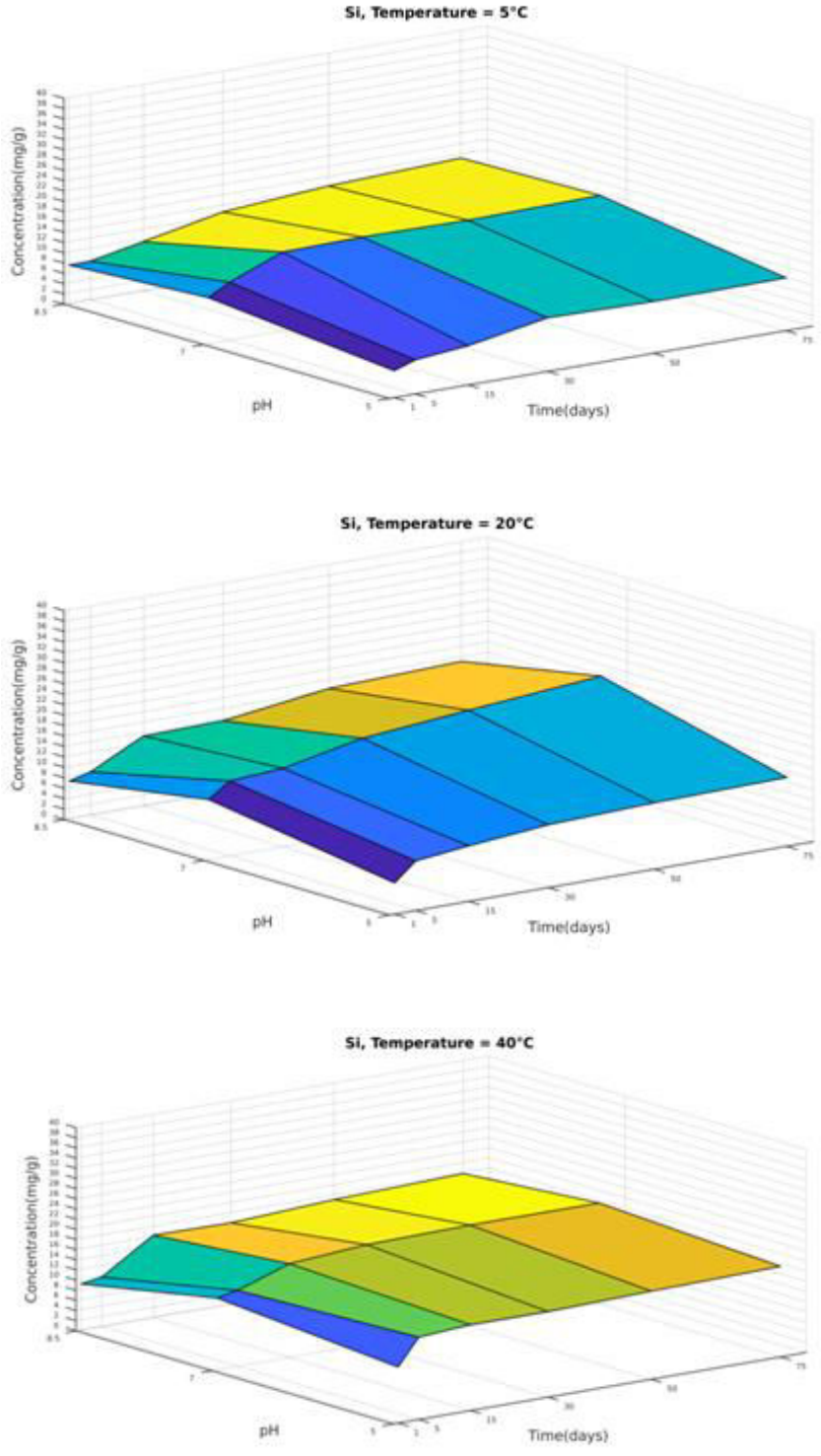

Fig. 50 Silicon concentration (mg/g) at pH 5, 7, 8.5 and **temperature 5, 20, 40˚C** (*Triticum durum,* Cyprus)

Dissolution is either: (a) congruent (stoichiometric) or (b) incongruent (non-stoichiometric). In the first case, ions of a solid might be dissolved simultaneously with the dissolution rates proportional to their molar concentrations, while in the second case ions of a solid might be dissolved or non-simultaneously with different values of the dissolution rates for each ion (Dorozhkin 2012, and references therein; Stumm 1992). According to our results, phytolith dissolution under all experimental conditions probably is incongruent suggesting that a surface layer within a biogenic SiO_2 composition different from that of the bulk may be formed.

Samples of SiO_2-rich phytoliths extracted from wheat using the dry method were suspended in the solution which initially contains no silicic acid. Silica (SiO_2) dissolution requires deprotonation of Si–OH groups and polymerisation of Si–O–Si bonds before silicic acid (H_4SiO_4) is released. Water molecules orient their electronegative oxygen towards the Si atom, leading to a transfer of electron density to the siloxane bond (>Si-O-Si<) of the SiO_2 network, thereby increasing its length and eventually breaking it (Ehrlich *et al.* 2010; Hochella and Banfield 1995; Iler 1979). Phytoliths may be considered to dissolve by the structural units and their subsequent transfer into the bulk solution. The rate of disintegration of the phytoliths structures depends on the concentration difference between the phytolith surface and the bulk solution.

The driving force for dissolution is the change of the free (or available) Gibbs energy for the transition from an undersaturated state to a state of equilibrium, that is, in the saturated solution (Gibbs 1874-1878). McClare (1971) contributed towards reformulating thermodynamics, in order that it can apply to living systems (e.g. plants), especially to energy transfer between molecules. He proposed that the energies of a system defined by some macroscopic parameter, such as temperature *T*, can be separated into two categories: (a) stored (coherent) energies that remain in a non-equilibrium state within a

characteristic time *t*, and (b) thermal (random) energies that exchange with each other and reach equilibrium (or equilibrate) at a time less than *t* (McClare 1971, from Ho 2013).

The main models developed to describe dissolution have followed two major approaches: (a) reaction-diffusion (or transport) according to the Noyes-Whitney theory which was later modified by Nerst (and Brunner) and (b) surface layer dissolution or Kossel model (Ehrlich *et al*. 2009, and references therein; Kossel 1927; Noyes and Whitney 1897). According to the reaction-diffusion model of dissolution, a transport of the chemical reagents or/and the products of chemical reactions mainly determine the overall dissolution rate, whereas the kinetically controlled surface layer model of dissolution considers chemical transformations on the surface as the main limiting factor (Dorozhkin 2012). An intermediate (both kinetically and diffusion and kinetically controlled) model has also been suggested (Nelson *et al*. 1983, from Dorozhkin 2012).

During dissolution structural ions may undergo: (a) detachment of the units from an active site (e.g. kink site) (b) surface diffusion away from the crystal steps, (c) desorption from the surface and (d) transfer of the units to the bulk solution by diffusion (Compton *et al*. 1993, from Dorozhkin 2012). A generalised concept of the dissolution is presented below (Fig. 51). All these steps are likely to be much more complicated (e.g. several chemical transformations, hydration processes of the detached and vacant site, the diffusion layer thickness *h*), and the unique qualities of each step may have an effect on the overall dissolution process. Nernst and Brunner introduced the concept of a stagnant diffusion layer (or film) across which the solute diffuses from the solid surface to bulk solution and forms a linear concentration profile. This gives the dissolution rate constant (*k*) the following meaning: $k = A\,(D/h)$, where *A* is the solid surface area, *D* is the diffusion coefficient and "*h*" is the diffusion layer thickness (Berthoud 1912).

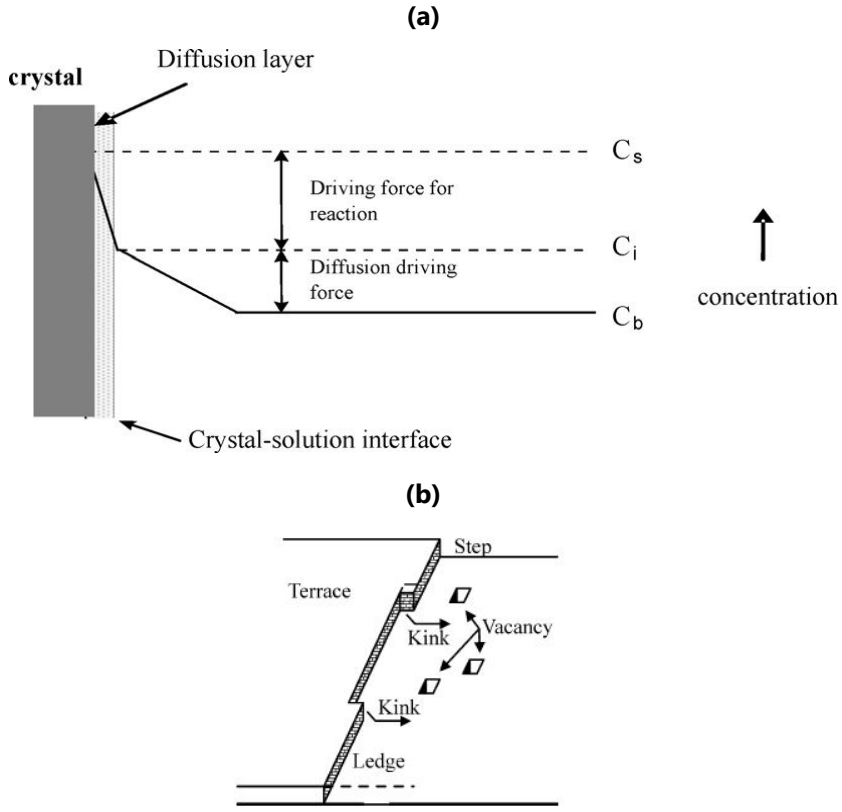

Fig. 51 Generalised concept of the dissolution: **(a)** the dissolution process according to the reaction-diffusion theory, where Cs is the solute concentration on the surface; Ci is the solute concentration on the interface; and Cb is the solute concentration in bulk; and **(b)** surface of a crystal according to surface layer dissolution model. Types of crystal imperfections/dislocations (e.g. steps, kinks, terraces, ledges, vacancies) are shown (sources: Dorozhkin 2012; Ehrlich *et al.* 2009)

Hixson and Crowell (1931) further addressed the dynamic nature of surface area during the dissolution, suggesting that the surface area of a dissolving particle changes as mass is removed, allowing the modeling of dissolving particles over longer time periods. Dissolution may emerge not only from the interplay between mass removal by diffusion (e.g. weathered morphotypes), at the exposed surface of the phytolith but also from the physical fragmentation (e.g. fragmented morphotypes) of the original phytolith. The concentration of silicic acid in the solution was then (i.e. after the transfer of the units

to the bulk solution) monitored until the concentration of dissolved Si no longer changes over the course of time. The critical process that controls the dissolution kinetics is the hydrolysis of bridging Si-O-Si bonds at the solid-solution interface.

The final dissolved Si concentration is then assumed to represent the solubility of the dissolving silicon of solid phytoliths under the specific experimental conditions. When precipitation of a chemical element just equals dissolution, the solution is in equilibrium with the solid and is said to be saturated with the element. A solution that precipitates a chemical element is supersaturated, and a solution that dissolves a chemical element is undersaturated (Stumm 1992). In other words, dissolution is triggered by undersaturation, while precipitation is triggered by supersaturation. During the course of the experiments, the Si concentration in solution and thus the degree of undersaturation are gradually changing.

In particular, the saturation state changes most rapidly at the onset of the present batch experiments, when the degree of undersaturation and the rate of dissolution are highest (see an example, Fig. 52). This initial rapid dissolution may suggest the progressive alteration and loss of a reactive surface layer (which may act as an energy barrier) or/and different levels of phytolith porosity. Previous studies of amorphous SiO_2 dissolution have also observed an initial, rapid loss of material (Fraysse *et al.* 2006a, 2006b; Prentice and Webb 2016; Van Cappellen *et al.* 2002). However, a quantitative comparison of dissolution rates among several studies is not easy because of variable conditions between laboratory experiments (e.g. batch or flow-through reactors, dry or wet method of phytolith extraction).

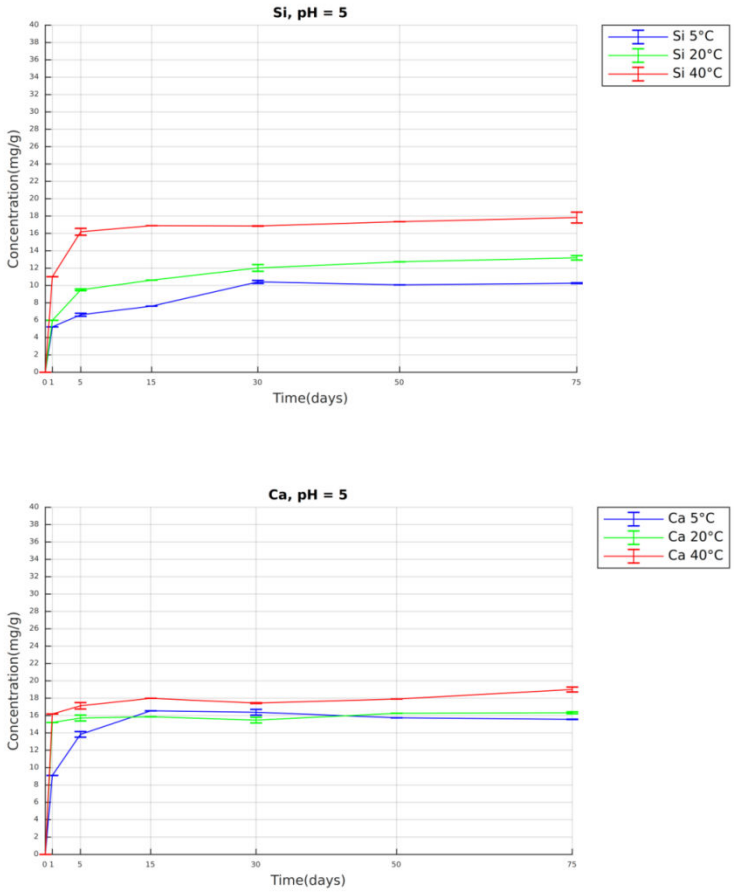

Fig. 52 Concentration (mg/g) of Si (above) and Ca (below) over the course of 75 days at pH 5 and temperature 5 ˚C, 20˚C, 40 ˚C (*Triticum durum*, Cyprus)

The general equation for the rate of dissolution of SiO_2 in aqueous solutions is fairly well established and may be written as a function of the concentration of three surface species, a protonated, a neutral, and a deprotonated surface species (>SiOH2$^+$, >SiOH, and >SiO$^-$). The equation is: $R_{diss} = k_{H+}\{>SiOH_2^+\}^m + k_{H2O}\{>SiOH\} + k_{OH-}\{>SiO^-\}^p$, where m and p stand for reaction orders and k_{H+} , k_{H2O} and k_{OH-} refer to rate constants (Ehrlich et al. 2010; Iler 1979). Assuming the order of the protonation reaction is unity (n =1), the aforementioned equitation can be also used to fit phytolith rate data in the studied pH and temperature range. Solid SiO_2 dissolves in water by the following generalised

reaction: $SiO_{2\ (s)} + 2\ H_2O = H_4SiO_{4\ (aq)}$ and the equilibrium constant for this reaction is: $K = a_{H4SiO4} / a_{SiO2}\ a^2_{H2O}$. The order of reaction that better describes the experimental results is regarded as order of the reaction. In the present study, an assumption of the order of the reaction of silicon, of the dominant element in phytoliths, was made based on the experimental results using equations which describe the reaction order each time until the equilibrium state. The following orders of reaction were tested: (a) 1/2, (b) 1st, (c) 3/2, and (d) 2nd.

The first-order reaction model describes the experimental results satisfactorily compared to other models (1/2, 3/2, and second order), and its correlation coefficient R^2 is closer to value one than other orders. Most of the previous studies have also reported that the dissolution rate of biogenic SiO_2 is controlled by first-order kinetics, in inverse linear dependence with the saturation degree of the solution (Lawson *et al.* 1978). In the first-order reactions, the experimental points (using the differential method) plot on a straight line in the semi-logaritmic plot ln C/C_o versus time, when C is the concentration of dissolved silicon at each time until the approach of equilibrium state, while C_o is the original silicon concentration in SiO_2-rich phytoliths measured with Energy Dispersive X-ray Fluorescence analysis. The semi-logaritmic plots of ln C/C_o versus time yielded in the majority of the cases two straight lines, which correspond to a two-stage reaction, namely an initial period of rapid Si leaching, followed by a period of slow Si leaching. The progressive approach of equilibrium state ($u_1 = u_2$) in the suspensions depended both on pH and temperature values. The ln C/C_o versus time (days) data for leaching of Si, at pH 5, 7, 8.5 and temperature 5, 20, 40 °C values for the all samples (Cyprus, Crete, Volos, Pella I, Pella II and Corfu) are presented in appendix 5 (Figs. 184-189). Representative diagrams are given as example in Figs. 54-55.

The first-order kinetic constants *k* for Si were found from log-linear plots of Si concentration versus time [$C = C_0 \times e^{kt} \leftrightarrow \ln C = kt + \ln C_0$]. The reaction rate (*k)* (d^{-1}) for silicon obtained from the slopes of the straight lines of curves for Si leaching were evaluated. Dissolution rate constants (d^{-1}) described either from a single stage (*k*) or from two stages (*k*1 and *k*2) are listed in tables 18-20. The correlation coefficient R^2 range between 0.749 and 1. The first stage may be related with an initial loss of a reactive surface layer and this stage probably is both surface and diffusion controlled. On the other hand, the second stage may be related with a re-precipitation of Si as the system approached saturation and this stage is probably diffusion controlled. Reaction rates are changing with increasing temperature. Usually an increase of the temperature (from 5 to 20˚C) increased the Si concentration in the solution.

Nevertheless in many cases (from 20 to 40˚C, and especially in alkaline pH) the Si concentration was reduced probably due to precipitation. Thermodynamic principles predict that Si dissolution rates generally increase with increasing driving force (Gibbs 1874-1878; Iler 1979), however the experimental results showed that this dependence is complex. The exact mechanism responsible for the Si re-precipitation here is not fully understood. Several interrelated factors, apart from the experimental conditions, may affect the reaction rates and thus precipitation (e.g. the existence of heterogonous ‘‘leaching’’ sites of phytoliths structures). Furthermore, reaction products may change the physicochemical properties of phytoliths leading to the possible formation of neoformed solid phases, or sodium ions from the reacting solution NaOH (for achieving alkaline conditions in the solution) may also act as network modifying agent of silanol groups.

Dissolved silicon seems to originate from phytolith surfaces and the SiO_2-rich matrix of the apoplast in the plant tissues. The behaviour of Si in the course of dissolution often indicated two main dissolution regimes: rapid initial element release during the first two weeks and especially within the first five days, followed by a slower element release (Figs. 48 and 52). Previous phytolith dissolution experiment by Cabanes *et al.* 2011 showed that the silicon concentrations reached a steady state after one or two weeks. According to Ehrlich *et al.* (2010) two regimes of Si release suggesting the presence of two pools of SiO_2 in plant tissues: (a) a "concentrated" pool of phytoliths (aggregates of phytoliths) and (b) individual molecules (H_4SiO_4) or small polymers dispersed in the organic matrix. In the present study, the quantification of these two different pools cannot be done, because the used dry ashing method of phytoliths extraction, with subsequent rinse of H_2O_2 eliminated the organic matrix.

The organic matrix is thought to play an important role in controlling crystal growth during the formation of minerals by organisms (Lowenstam 1981; Lowenstam and Weiner 1989; Weiner 1984), including epitaxial growth theory (Irving 1981). Elbaum *et al.* (2007) measurements of the $\delta^{13}C$ composition of ''modern'' *Triticum aestivum* (wheat) phytoliths suggested the presence of sugars or/and proteins in the water-soluble fraction, and lipids in the insoluble fraction (Elbaum *et al.* 2007). With respect to the role of the organic matter, serving as template in (bio)mineralisation processes, less aggressive methods of phytoliths extraction from plants should be developed. Furthermore, studying phytolith dissolution directly in plant tissues may offer more accurate estimates of the concentration of dissolved chemical elements.

Table 18 Silicon reaction rates (d^{-1}) obtained from one stage (*k*) and silicon reaction rates (d^{-1}) obtained from two stages (*k*1 and *k*2) of dissolved phytoliths (*Triticum durum* Cyprus, *Triticum durum* Crete, *Triticum monococcum* Volos, *Triticum monococcum* Pella I, *Triticum durum* Pella II, *Triticum durum* Corfu samples) at pH 5, 7, 8.5 and temperature 5 ˚C, 20˚C, 40 ˚C

Si REACTION RATES (d^{-1})		**pH 5 T=5˚C**	**pH 5 T=20˚C**	**pH 5 T=40˚C**	**pH 7 T=5˚C**	**pH 7 T=20˚C**	**pH 7 T=40˚C**	**pH 8.5 T=5˚C**	**pH 8.5 T=20˚C**	**pH 8.5 T=40˚C**
CYPRUS										
Tr. durum **(R^2=0.970-1)**										
	k_1	0.059	0.115	0.096	0.037	0.056	0.019	0.019	0.045	0.043
	k_2	0.018	0.011	0.004	0.001	0.004	-	-	-	-
CRETE										
Tr. durum **(R^2= 0.876 -1)**										
	k_1	0.024	0.020	0.014	0.036	0.018	0.074	0.041	0.035	0.042
	k_2	0.015	-	-	0.011	-	0.002	0.003	-	-
VOLOS										
Tr. monococcum **(R^2=0.749 - 1)**										
	k_1	0.109	0.006	0.027	0.019	0.012	0.012	0.013	0.011	0.008
	k_2	0.015	-	0.013	-	-	-		-	-
PELLA I										
Tr. monococcum **(R^2=0.979 -1)**										
	k_1	0.044	0.114	0.106	0.051	0.126	0.021	0.048	0.060	0.044
	k_2	-	0.006	0.005	-	0.002	-	-	-	-
PELLA II										
Tr. durum **(R^2= 0.887 -1)**										
	k_1	0.048	0.126	0.065	0.044	0.108	0.067	0.058	0.025	0.048
	k_2	-	0.002	0.011	-	0.005	0.001	-	0.076	-
CORFU										
Tr. durum **(R^2=0.797 - 1)**										
	k_1	0.108	0.110	0.025	0.140	0.075	0.010	0.018	0.010	0.013
	k_2	0.014	0.005	-	0.005	0.003	-	-	-	-

The various factors of climate (e.g. water availability, temperature and their duration) are related with plant evapotranspiration and photosynthesis, and may have discriminating influence on the growth and density of plant cells; and subsequently on the formation of phytoliths. Thomson (1917) in his pioneer book on growth and form wrote: *''A large part of the phenomenon of growth, both in animals and still more conspicuously in plants, is associated with turgor, that is to say, is dependent on osmotic conditions; in other words, the velocity of growth depends in great measure on the amount of water taken up into the living cells, as well as on the actual amount of chemical metabolism performed by them* (p. 125). *In a large number of physical phenomena, and in a very marked degree in all chemical reactions, it is found that rate of action is affected, and for the most part accelerated, by rise of temperature* (p. 109). *It has been often remarked that our common European trees, such for instance as the elm or the cherry, tend to have larger leaves the further north we go; but in this case the phenomenon is to be ascribed rather to the longer hours of daylight than to any difference of temperature''* (p. 123).

Based on the dissolution results of phytoliths extracted from plants grown in areas with different water regime and temperature (see map, Fig. 4), it was suggested that *k* rate constants may be used as potential proxies to study the relationship water availability and SiO_2-rich phytoliths. Furthermore, both plants seem to accumulate relatively higher concentrations of phytoliths as precipitation of the area of study increases (Fig. 5). Our results are supported by previous studies that have shown that phytolith (from Poaceae species, including wheat) concentration tends to be positively correlated with water availability (Jenkins 2001, 2016; Katz *et al.* 2013; Madella *et al.* 2009; Rosen and Weiner 1994; Weisskopf *et al.* 2015).

For example, Madella *et al.* (2009) used ratios of *fixed* (i.e. passive cells or genetically predisposed to produce SiO_2 bodies, such as rondels) and *sensitive* phytoliths (i.e. active cells or phytoliths that are formed only when there is sufficient uptake of water, such as epidermal elongates) from the wheat and barley leaves; and showed that there is some variability in phytolith production according to the water regime under which the cereal grew and sensitive forms shown to be directly influenced by the water regime. This invites further studies on the pattern of precipitation-temperature-phytolith relations across various wheat species and other Mediterranean plants. However, the correlation of phytoliths with water availability cannot be generally accepted (i.e. for all plants and all geographic contexts) because a wide range of environmental and probably genetic factors may have an impact. Testing genetic factors is beyond the objectives of this study and further research needs to be carried out in order to confirm it.

Bartoli and Wilding (1980) suggested that an important factor in controlling the Si dissolution of phytoliths is occluded water content. They showed that younger phytoliths are more hydrated (~8-11% wt. water) and susceptible to dissolution than older forms (~2-3% wt. water). Therefore it can be assumed that the Si leaching from phytoliths may be most prominent in wet than dry soils or/and sediments. In any case, in the present study *k1* rate constants were generally higher for areas with higher precipitation than those with lower precipitation (mm) at least for four samples (Crete, Volos, Pella I, Pella II) out of six samples (Cyprus, Crete, Volos, Pella I, Pella II, Corfu). This phenomenon appears to be independent of the wheat species (*Triticum durum* and *Triticum monococcum*) (Fig. 53 a). At 20˚C (temperature at which constant agitation conditions were achieved), the samples from the areas with lower precipitation exhibited lower rate constants (e.g. Crete: k = 0.020 or 2 x 10^{-2} d^{-1}), regardless of pH, in relation to the samples from the areas with higher precipitation (e.g. Pella II: $k1$ = 0.126 or 2 x 10^{-2} d^{-1} and k_2 = 0.002 or 0.2 x 10^{-2} d^{-1}) (Figs. 54-55).

(a)

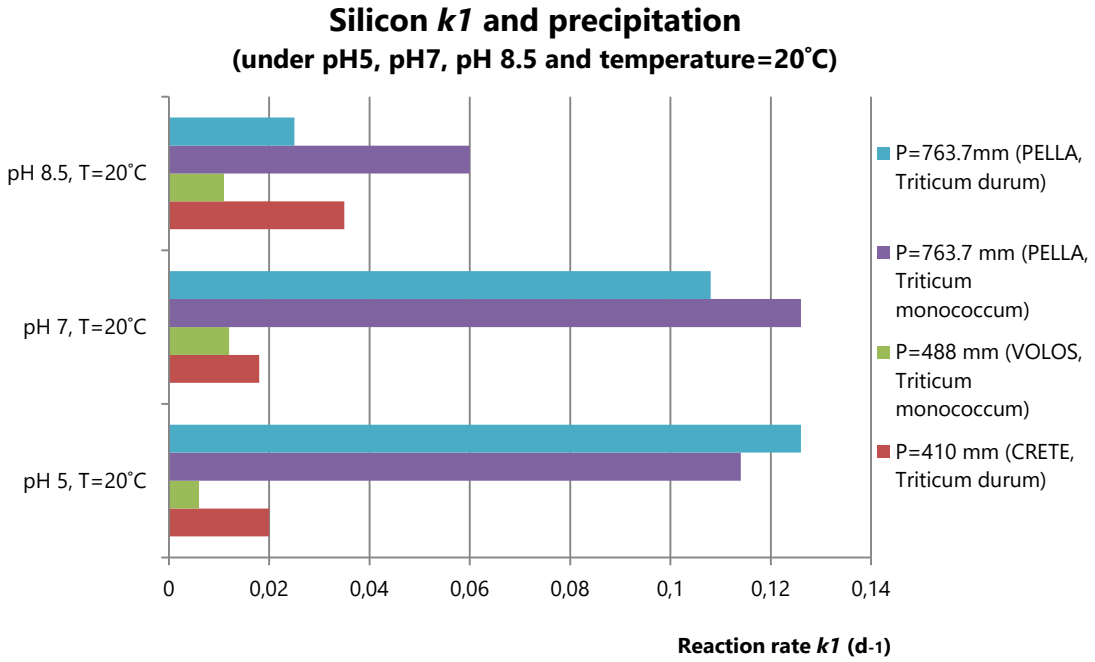

Fig. 53 (a) Silicon reaction rates *k1* (d^{-1}) of dissolved phytoliths from *Triticum monococcum* and *Triticum durum* (under pH 5, pH 7, pH 8.5, and temperature=20˚C) and precipitation of area of study (Crete, Volos, Pella)

According to Bartoli and Wilding (1980) a close positively relationship exists between the surface area and dissolution of phytoliths of coniferous, deciduous and gramineous origin under two different physiographic regions in France (a. region: mean annual rainfall ranges from 1200 to 1400 mm and mean annual temperature from 8 to 9˚C, b. region: mean annual rainfall is 750 mm and mean annual temperature is 10˚C). Phytolith with lower water contents could be expected to have lower surface areas and lower dissolution rates (Wilding *et al.* 1977). Taking into account the aforementioned points, the rate of mass removal from a dissolving phytolith should be proportional to the exposed surface area. Phytoliths extracted from plant grew in areas with higher precipitation may have greater surface area, than phytoliths extracted from plant grew in areas with lower precipitation. In that case, phytoliths with larger surface areas may be

dissolved faster than their counterparts with smaller surface area, at certain pH, temperature and time of the reaction.

The sample from Corfu is not taken into account in the comparisons of Figs. 53-55, mainly because it has delivered to us, with relatively different (i.e. lower) high of the stem and some broken awns in the inflorescence. This is related with its damage/decomposition during storage by the insect pest *Sitophilus granarius* (wheat weevil) and subsequently damage/friction after storage by the cultivators in order to naturally remove the pests (i.e. disinfestations without the use of chemical products) (Vlassi, personal communication 2015). *Triticum durum* is frequently affected by insect (and mite) pests (Pasquale and Throne 2012). Therefore it might be expected that the ratio of stem-leaves and inflorescence is relatively different from the other samples; and therefore this may have an impact on the Si reaction rate of dissolution of the entire plant. Recently, Jouquet *et al.* (2020) showed that *Odontotermes obesus* (termites), through their feeding and building activities, impact Si distribution in soils. The study of the impact of insects on the decomposition of SiO_2-rich phytoliths from plants or soils remains very limited and might be worth investigating further.

In addition, the sample from Corfu has the highest precipitation between the samples, and thus it was expected that the silicon reaction rates will be the highest between the samples. However, Pella samples (763.7 mm, T=14.22˚C) usually exhibited higher reaction rates than Corfu samples (1560 mm, T=18.61˚C), and this may be related to the responses of plants (e.g. changes of cell volume and density) to temperature. Apart from water availability, temperature and related evapotranspiration may also affect phytolith concentration (Katz *et al.* 2013; Rosen and Weiner 1994). Increasing mean annual temperature of the area incorporates both potential negative (due to lower available water in the plants) and positive (due to higher plant evapotranspiration) effects on the

growth and density of plant cells and subsequently on the phytolith physicochemical characteristics and dissolution rates. Photosynthesis and the ability of phytoliths to interfere with sunlight (He *et al.* 2014; Gal *et al.* 2012; Kuo-Huang *et al.* 2007; Pierantoni *et al.* 2017, 2018) may also have an impact on phytolith characteristics (e.g. surface-area-to-volume ratio) and possible order-disorder transition of their structure upon temperature increase.

(b)

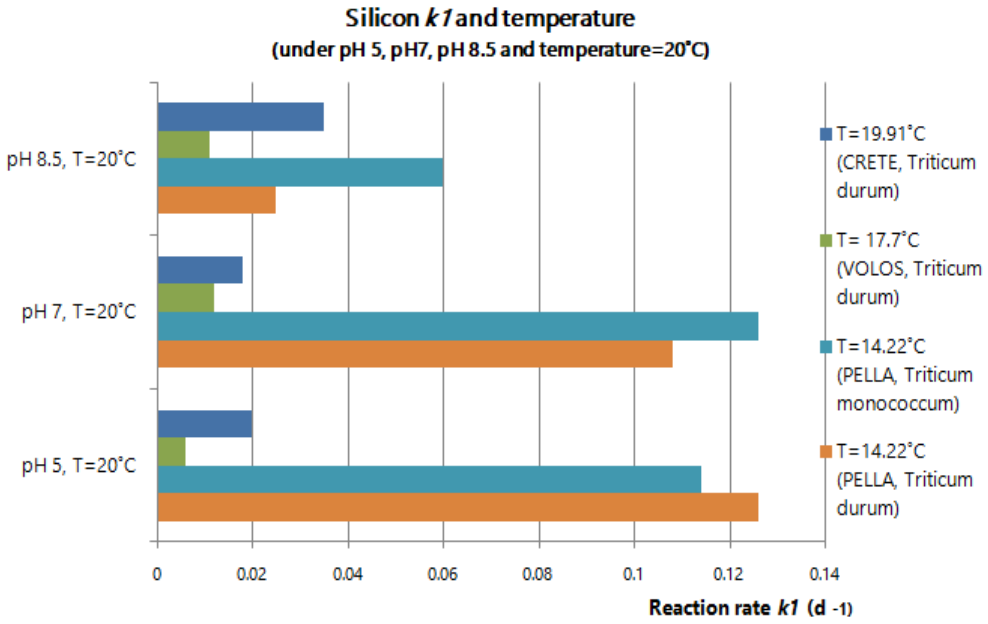

Fig. 53 (b) Silicon reaction rates *k1* (d^{-1}) of dissolved phytoliths from *Triticum monococcum* and *Triticum durum* (under pH 5, pH 7, pH 8.5, and temperature=20°C) and temperature of area of study (Crete, Volos, Pella)

Regarding the sample from Cyprus, it is not also taken into account in the comparisons of Figs. 53-55, because it has relatively different mineralogy from the other samples and was derived from a conventional cultivation (in contrast to the others in which no phytoprotection or N-P-K fertilisers were used).

Table 19 Silicon reaction rates (d^{-1}) obtained from one stage (*k*) and silicon reaction rates (d^{-1}) obtained from two stages (*k*1 and *k*2) of dissolved phytoliths (Cyprus, Crete, Volos, Pella I, Pella II, Corfu samples) in relation with the total annual precipitation (mm) for the year 2014. The experiments at 20 ˚C that were carried out under continuous agitation in a shaking table are presented in colour blue

SILICON REACTION RATES (d^{-1}) AND AREA PRECIPITATION	P=200 mm	P=410 mm	P=488 mm	P=763.7 mm	P=763.7mm	P=1560 mm
	CYPRUS *Triticum durum*	**CRETE** *Triticum durum*	**VOLOS** *Triticum monococcum*	**PELLA I** *Triticum monococcum*	**PELLA II** *Triticum durum*	**CORFU** *Triticum durum*
k_1	0.059	0.024	0.109	0.044	0.048	0.108
k_2	0.018	0.015	0.015	-	-	0.014
k_1	0.115	0.020	0.006	0.114	0.126	0.110
k_2	0.011	-	-	0.006	0.002	0.005
k_1	0.096	0.014	0.027	0.106	0.065	0.025
k_2	0.004	-	0.013	0.005	0.011	-
k_1	0.037	0.036	0.019	0.051	0.044	0.140
k_2	0.001	0.011	-	-	-	0.005
k_1	0.056	0.018	0.012	0.126	0.108	0.075
k_2	0.004	-	-	0.002	0.005	0.003
k_1	0.019	0.074	0.012	0.021	0.067	0.010
k_2	-	0.002	-	-	0.001	-
k_1	0.019	0.041	0.013	0.048	0.058	0.018
k_2	-	0.003	-	-	-	-
k_1	0.045	0.035	0.011	0.060	0.025	0.010
k_2	-	-	-	-	0.076	-
k_1	0.043	0.042	0.008	0.044	0.048	0.013
k_2	-	-	-	-	-	-

Table 20 Silicon reaction rates (d^{-1}) obtained from one stage (*k*) and silicon reaction rates (d^{-1}) obtained from two stages (*k*1 and *k*2) of dissolved phytoliths (Cyprus, Crete, Volos, Pella I, Pella II, Corfu samples) in relation with the average annual temperature (^{o}C) for the year 2014. The experiments at 20 ˚C that were carried out under continuous agitation in a shaking table are presented in colour blue

SILICON REACTION RATES (d^{-1}) AND AREA TEMPERATURE	T=20.24°C	T=19.91°C	T=18.61°C	T= 17.7°C	T=14.22°C	T=14.22°C
	CYPRUS *Triticum durum*	**CRETE** *Triticum durum*	**CORFU** *Triticum durum*	**VOLOS** *Triticum monococcum*	**PELLA I** *Triticum monococcum*	**PELLA II** *Triticum durum*
k_1	0.059	0.024	0.108	0.109	0.044	0.048
k_2	0.018	0.015	0.014	0.015	-	-
k_1	0.115	0.020	0.110	0.006	0.114	0.126
k_2	0.011	-	0.005	-	0.006	0.002
k_1	0.096	0.014	0.025	0.027	0.106	0.065
k_2	0.004	-	-	0.013	0.005	0.011
k_1	0.037	0.036	0.140	0.019	0.051	0.044
k_2	0.001	0.011	0.005	-	-	-
k_1	0.056	0.018	0.075	0.012	0.126	0.108
k_2	0.004	-	0.003	-	0.002	0.005
k_1	0.019	0.074	0.010	0.012	0.021	0.067
k_2	-	0.002	-	-	-	0.001
k_1	0.019	0.041	0.018	0.013	0.048	0.058
k_2	-	0.003	-	-	-	-
k_1	0.045	0.035	0.010	0.011	0.060	0.025
k_2	-	-	-	-	-	0.076
k_1	0.043	0.042	0.013	0.008	0.044	0.048
k_2	-	-	-	-	-	-

(a) *Triticum durum*

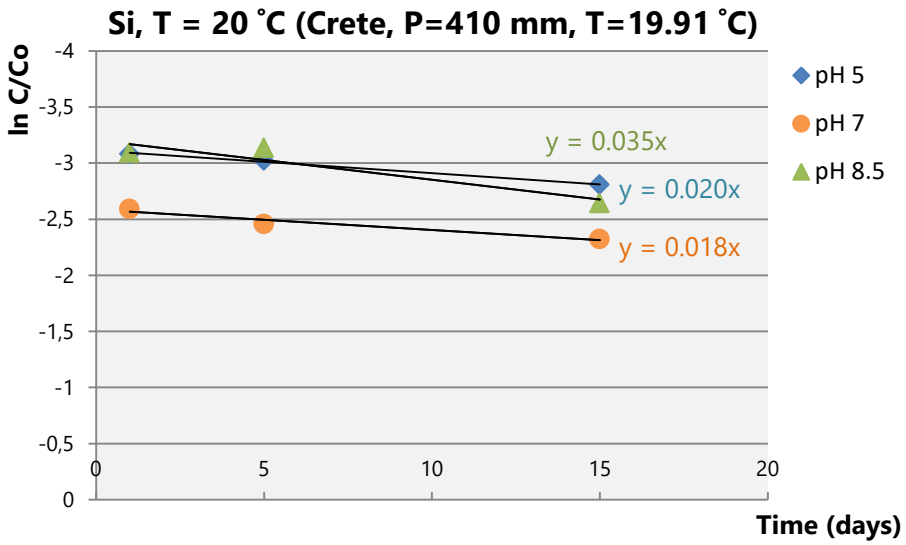

(b) *Triticum durum*

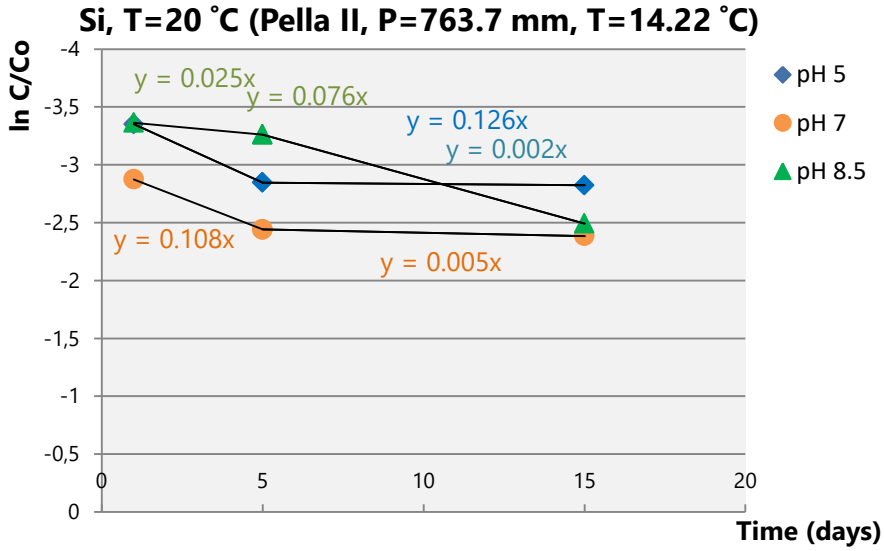

Fig. 54 The ln C/C_o versus time (days) curves for leaching of Si at pH 5, 7, 8.5 values and temperature 20 °C for the samples: **(a)** *Triticum durum* from Crete (P = 410 mm, T = 19.91 ˚C); and **(b)** *Triticum durum* from Pella II (P = 763.7 mm, T = 14.22 ˚C)

(a) *Triticum monococcum*

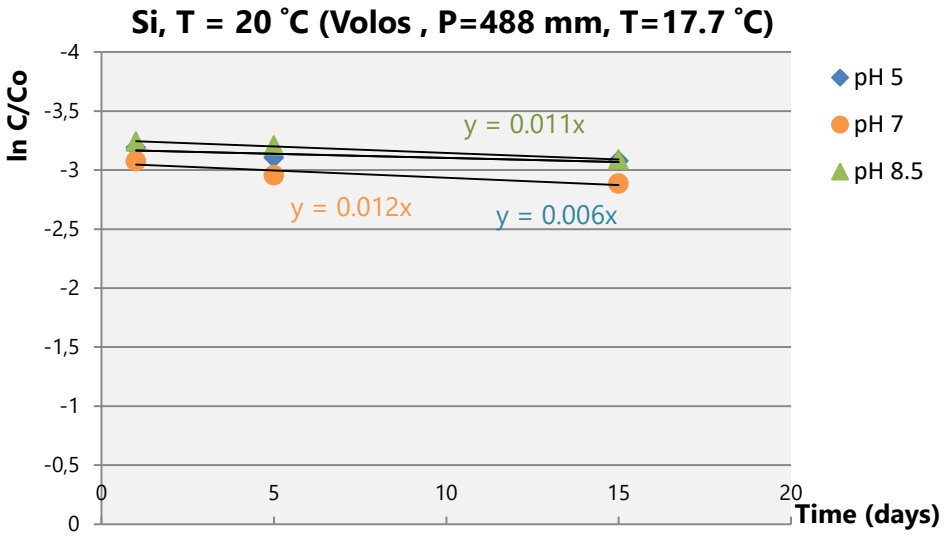

(b) *Triticum monococcum*

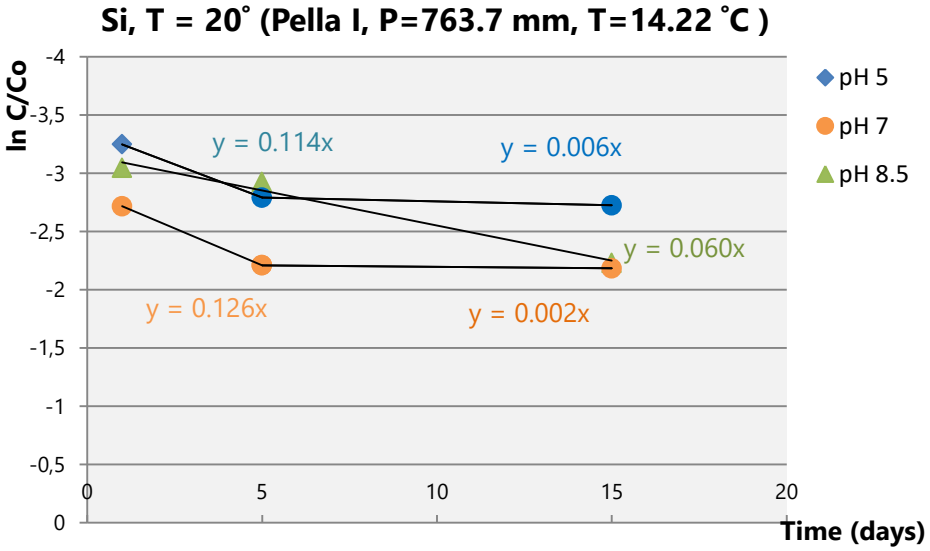

Fig. 55 The ln C/C_o versus time (days) curves for leaching of Si at pH 5, 7, 8.5 values and temperature 20 °C for the samples: **(a)** *Triticum monococcum* from Volos (P = 488 mm, T = 17.7 ˚C); and **(b)** *Triticum monococcum* from Pella I (P = 763.7 mm, T = 14.22 ˚C)

In our experiments, apart for dissolved Si, the concentration of dissolved Mg, K, Ca, Al, Fe, Sr and Ba in the solution varied exponentially with time at all pH values and temperatures used. The increased solubility is a driving force that may also change the secondary mineral phases and as a result the sensitivity of phytoliths morphotypes to the extent of reaction. The higher the concentration of the elements in the solution, the more soluble the phytoliths will be. The results indicate that Si (SiO_2-network former) and Mg, K, Ca (SiO_2-network modifiers) are mobile (appendices 3a and 3b), Fe is moderately mobile and Al is essentially immobile. Strontium and Ba showed similar behaviour (appendix 4). Between the studied main elements, K is most soluble and Si is less soluble ($K^+ > Mg^{2+} > Ca^{2+} > Si^+$). Detailed concentrations (mg/g) of all studied elements are presented in appendix 2.

Mineralogical analyses of plant samples confirmed the presence of a silicate phase, probably opal ($SiO_2 \cdot nH_2O$) (see XRD traces above). Silicon concentration in solution ranges between 22.11 - 5.23 mg/g (sample from Cyprus), 23.21 - 5.52 mg/g (sample from Crete), 15.39 - 5.14 mg/g (sample from Volos), 22.25 - 5.81 mg/g (sample I from Pella), 20.43 - 5.30 mg/g (sample II from Pella), 17.91 - 5.82 mg/g (sample from Corfu). The maximum value of silicon (wt. %) that was dissolved from the initial solid for each sample was: ~13 % (Cyprus), ~12.3% (Crete), ~8.4 % (Volos), ~14.2% (Pella I), ~10.9% (Pella II) and ~11% (Corfu). The highest Si concentrations [and the maximum values of Si (wt. %) that were dissolved from the initial solid] between the samples was from Pella I.

Representative Mg-bearing mineral phases in the plant samples were baylissite [$K_2Mg(CO_3)_2 \cdot 4H_2O$], brucite [$Mg(OH)_2$] and probably struvite [$(NH_4)Mg(PO_4) \cdot 6H_2O$] (Table 4). Magnesium concentration ranges between 12.69 - 3.05 mg/g (sample from Cyprus), 15.10 - 1.81 mg/g (sample from Crete), 13.58 - 4.19 mg/g (sample from Volos), 8.48 - 0.62 mg/g (sample I from Pella), 10.05 - 0.60 mg/g (sample II from Pella), 16.93 - 4.58

mg/g (sample from Corfu). The maximum value of magnesium (wt. %) that was dissolved from the initial solid for each sample was: ~67.9 % (Cyprus), ~71.6 % (Crete), ~77.7% (Volos), ~50.3% (Pella I), ~55.6% (Pella II) and ~78.4% (Corfu). The highest Mg concentration [and the maximum value of Mg (wt. %) that was dissolved from the initial solid] between the samples was from Corfu.

Representative K-bearing mineral phases in the plants samples were aphthitalite [$(K,Na)_3Na(SO_4)_2$], arcanite [K_2SO_4] and baylissite [$K_2Mg(CO_3)_2{\cdot}4H_2O$] (Table 4). Potassium concentration ranges between 32.97 - 5.82 mg/g (sample from Cyprus), 22.39 - 3.09 mg/g (sample from Crete), 36.50 - 5.17 mg/g (sample from Volos), 11.78 - 2.18 mg/g (sample I from Pella), 14.07 - 2.30 mg/g (sample II from Pella), 38.74 - 4.65 mg/g (sample from Corfu). The maximum value of potassium (wt. %) that was dissolved from the initial solid for each sample was: ~54.1% (Cyprus), ~90.7% (Crete), ~89.8% (Volos), ~97.9% (Pella I), ~80.8% (Pella II) and ~99.3% (Corfu). The highest K concentration [and the maximum value of K (wt. %) that was dissolved from the initial solid] between the samples was from Corfu.

Representative Ca-bearing mineral phases in the plant samples were anhydrite [$CaSO_4$,] bassanite [$CaSO_4{\cdot}1/2H_2O$], chlorocalcite [$KCaCl_3$] and monohydrocalcite [$CaCO_3{\cdot}H_2O$] (Table 4). Calcium concentration ranges between 20.44 - 4.45 mg/g (sample from Cyprus), 30.18 - 17.92 mg/g (sample from Crete), 13.52 - 4.02 mg/g (sample from Volos), 18.84 - 3.53 mg/g (sample I from Pella), 19.77 - 3.70 mg/g (sample II from Pella), 18.84 - 8.58 mg/g (sample from Corfu). The highest Ca concentration between the samples was from Crete. The maximum value of calcium (wt. %) that was dissolved from the initial solid for each sample was: ~56.1% (Cyprus), ~45% (Crete), ~40.3% (Volos), ~44.7% (Pella I), ~51.3% (Pella II) and ~37.7% (Corfu). The highest Ca concentrations [or

the maximum values of Ca (wt. %) that were dissolved from the initial solid] between the samples was from Cyprus.

Iron concentration ranges between 0.0010 - 0.0002 mg/g for the sample from Cyprus, 0.0074 - 0.0018 mg/g for the sample from Crete, 0.0076 - 0.0023 mg/g for the sample from Volos, 0.0072 - 0.0002 mg/g for the sample I from Pella, 0.0073 - 0.0009 mg/g for the sample II from Pella, 0.0022 - 0.0003 mg/g for the sample from Corfu. The maximum value of iron (wt. %) that was dissolved from the initial solid for each sample was: ~0.35% (Cyprus), ~1% (Crete), ~2% (Volos), ~1.1% (Pella I), ~1.9 % (Pella II) and ~0.1% (Corfu). The highest Fe concentrations [and the maximum values of Fe (wt. %) that were dissolved from the initial solid] between the samples was from Volos and Pella (II).

Note that iron concentrations were below detection limit of 0.0003 μg/L (for ICP-MS measurements), at temperature 40˚C and all pH values for samples from Cyprus and Corfu. Oxidation or reduction generally changes the species of ions involved in reactions of (re)mobilisation (Stumm 1992). Garnett and Graham (2005) showed that the iron content in *Triticum aestivum* (wheat), depends on both the amount of nutrient taken up by the plant post-anthesis and the amount that is remobilised from vegetative organs as they senesce. Our results showed that depending to the conditions of the aqueous medium; Fe^{3+} seems to be essentially immobile and probably was precipitated in the form of hydroxides. In contrast, in alkaline conditions Fe^{2+} usually tends to be relatively mobile in aqueous environments.

Iron oxides are effective absorbents for many anionic species under acidic and neutral pH conditions, but no under alkaline conditions. A previous study in *Oryza sativa* (rice) suggested that Si may increase the oxidising capacity of roots, which converts ferrous iron (Fe^{2+}) into ferric iron (Fe^{3+}) thereby limiting iron toxicity in the plant (Ma and

Takahashi 2002). Iron minerals commonly present in soils are goethite [γ-FeO(OH)], hematite, (Fe_2O_3), lepidocrocite [γ-FeO(OH)], magnetite ($FeO.Fe_2O_3$) and wüstite (FeO) (Cornell and Schwertmann 2001). Here, the Fe-bearing mineral phase that was detected in the studied plant samples was only barbosalite [$Fe^{2+}Fe_3^{+2}(PO_4)_2(OH)_2$] (see Table 4).

Aluminium concentrations were below detection limit of 0.005 µg/L (for ICP-MS measurements), possibly due to precipitation. Aluminium solubility is limited in strong acid condition, increases in strong alkaline conditions, and creates non-dissolved hydroxides [such as $Al(OH)_3$] in intermediate conditions (Kochian 1995). With respect to the Al content and the degree of its influence on solubility of biogenic SiO_2 structures, the results of most previous studies are contradictory (Bartoli and Wilding 1980; Fraysse *et al*. 2009; Nguyen et *al*. 2014; Van Cappellen *et al*. 2002). It has been suggested that Al may stabilise biogenic SiO_2 during dissolution. According to Van Cappelen (2002) the Al incorporation has significant effects on the solubility of diatoms, whether both during biomineralisation and after death of the organism. Phytoliths extracted from different parts of the plant may contain different chemical elements, such as Al, which may affect their stability (Bartoli and Wilding 1980; Nguyen *et al*. 2014). On the other hand, Fraysse *et al*. (2000) did not observe a correlation between Al content and the solubility of phytoliths.

Loucaides *et al*. (2010) proposed that silanol groups participating in (de)protonation reactions are not restricted to the external surface (outer region) of biogenic SiO_2 particles, but may be located beneath the external (inner region) surface. Thus, the (de)protonation reactions of the internal silanol groups may be much less sensitive to changes in ionic strength than those involving silanols in direct contact with the outside solution. Based on Loucaides *et al*. (2010) suggestion, it can be further assumed that

aged SiO_2-rich phytoliths from archaeological sediments may have lower proportions of internal sites, due to their progressive elimination and with time.

In a previous study, Loucaides *et al.* (2008) compared dissolution rates of a number of biogenic silica samples, including phytoliths extracted from horsetail (*Equisetum arvense*) and observed the catalysing effect of alkali salts (NaCl, KCl, $MgCl_2$ and $CaCl_2$) on SiO_2 dissolution. They also showed that the dissolution rates of a number of biogenic SiO_2 samples were on average 5 times higher in seawater than in freshwater. Nguyen *et al.* (2014) studied the dissolution process of phytoliths extracted from *Oryza sativa* (rice) and suggested that the effect of cations on depressing Si release decreased in the order: Al^{3+}> K^+> Na^+> Mg^{2+} > Ca^{2+}. In the present study K^+, Mg^{2+} and Ca^{2+} are also released faster than Si^+, and their release might affect the solubility of silicon. Loucaides *et al.* (2008) also proposed that organic matrix, interbedded with SiO_2-rich phytoliths may act as a protective barrier against hydrolysis of silicon, and probably reduction of organic phases during heating.

Because of the endothermic nature of the dissolution reaction, temperature has also a positive effect on the solubility of phytoliths. Dissolution experiments by Unzué-Belmonte *et al.* (2016) showed that the solubility of biogenic Si in the organic soil material (burnt at 350 °C and 550 °C, until constant weight was obtained) from *Picea abies* (spruce), *Fagus sylvatica* (beech) and *Sphagnum sp*. (peat) increased after burning. Dissolution experiments by Nguyen *et al.* (2014) showed that in ashed phytoliths from *Oryza sativa* (rice), soluble Si was found to be up to 46% of total Si content in ashes. In contrast, fresh rice samples treated only by 15% H_2O_2 were more resistant against dissolution. Our recent study on physicochemical characteristics of *Triticum durum* and *Triticum monococcum* (wheat) phytoliths, suggested that comparison of phytoliths extracted from plants is meaningful only if the method of extraction remains the same

(Andriopoulou and Christidis 2020). This should be taken into account when comparing different studies of phytolith dissolution.

In the present study, in the Cyprus sample at low pH 5 and at a low temperature of 5 ˚C, Ca dissolves more rapidly and tends to reach a steady state at approximately 15 days. In contrast, other chemical elements (Mg, Si, K) tend to dissolve with different rates. With increasing the temperature in the solution to 20˚C and 40 ˚C, a gradual increase in K concentration is observed, which at the maximum temperature appears to reach a steady state after 30 days. In addition, an increase of the pH to 7, causes greater Si-dissolution compared to pH 5, which occurs in two steps as, was mentioned previously. The first dissolution step is fast and takes place in 5 days, while the second one is virtually complete in 15 days. Then and especially after 30 days, the dissolution of Si remains constant. Moreover, K displays higher dissolved concentration than Mg, Si and Ca at steady state. The maximum K concentration is observed at pH 8.5 and temperature 40 ˚C, and becomes virtually constant after 50 days. By contrast, the concentration of Mg in the solution decreases with increasing pH and temperature. Generally, the concentration of the studied chemical elements show more pronounced changes over the first 15 days; however K stabilises more slowly at 50 days. The diagrams (Figs. 112-114, appendix 3a and and Figs. 130-135, appendix 3b) show details of the sample Cyprus and its changes in the concentration of the four elements over the course of 75 days at different pH (5, 7, 8.5) and at different temperature (5 ˚C, 20˚C, 40 ˚C).

The Volos sample displays similar behaviour as the Cyprus sample. The concentration of dissolved K was higher and reaches a steady state mainly after 50 days. An increase of pH to 8.5 results in a decrease in the K concentration in the solution. The diagrams (Figs. 118-120, appendix 3a and Figs. 142-147, appendix 3b) show details of the sample Volos

and its changes in the concentration of the four elements over time at different pH and temperature.

For the Cretan sample at all pH and at all temperatures, Ca shows the highest concentration and Mg the lowest concentration during dissolution of the phytoliths. Calcium seems to dissolve faster compared to the remaining elements. In the same sample, Si dissolves relatively fast as indicated by its pH and temperature values. In particular, a fast dissolution of Si is observed during the first 5 days, which tends to stabilise after 15 days. However, at peak pH (8.5) in the Cretan sample, Si behaves similar to K and the observed decrease in solution concentration may be due to re-precipitation. A solid phase may precipitate as soon as the concentration of the chemical elements exceeds its solubility. The diagrams (Figs. 115-117, appendix 3a and Figs. 136-141 appendix 3b) show details of the sample from Crete and its changes in concentration of the four elements over time at different pH and temperature values.

In the Pella I sample, Ca tends to dissolve more readily at low pH (5) and generally faster than K, Mg and Si, whereas as pH value increases to 7 and 8.5 at all temperatures silicon exhibits the highest concentration relative to the remaining chemical elements. The dissolution of Si attains a steady state between 15-30 days. In the Pella II sample, the behaviour of the elements appears to be similar to the Pella I. The Mg shows a low concentration at the highest pH (8.5). The diagrams (Figs. 121-123, appendix 3a and Figs. 148-153, appendix 3b) and (Fig 124-126, appendix 3a and Figs. 154-159, appendix 3b) show the Pella I and Pella II sample in detail, with changes in the concentration of Mg, Si, K, Ca over time at different pH and temperature, respectively.

For the Corfu sample, at low pH 5 Ca seems to dissolve relatively faster than the remaining elements. At higher pH and temperatures Si and Ca tend to have similar behaviour, whereas Mg has the lowest concentration in solution compared to the remaining elements. The diagrams (Figs. 127-129, appendix 3a and Figs. 160-165, appendix 3b) show details of the Corfu sample, and its changes in concentration of the studied elements over time at different pH and temperature values.

Strontium oxalate, and strontium and barium sulfate have been observed, less commonly in phylogenetic and quantitative terms, in plant species, although not in wheat species (Franceschi and Schueren 1986; He *et al*. 2012b; Krejci *et al*. 2011; Raven and Giordano 2009). For example, Franceschi and Schueren (1986) have showed that Sr was incorporated into the raphides (needle-shaped calcium oxalate crystals) of the freshwater plant *Lemna minor* (common duckweed). Furthermore, according to He *et al*. (2012a), Sr alongside Ba, Mg, and Ca were precipitated as oxalate and sulfate in various tissues, in phyllodes of *Acacia robeorum* (Robe's wattle) and sometimes in branchlets and roots.

Strontium and Ba are not essential nutrients to higher plants (Marschner 1995). These two trace elements are known to show strong correlation because they follow similar geochemical pathways (Middleton and Price 1996). According to the ICP-MC results for all studied phytoliths samples, Sr and Ba display very similar behaviour (Fig. 57) with a very rapid initial element release mainly during the five days (Fig. 56 and Figs. 166-183, appendix 4). Strontium was present in the some EDS specta (Fig. 33), and strontianite $SrCO_3$ or/and celestite ($SrSO_4$) were/was identified in the XRD traces above (Table 4). Barium may exist naturally mainly in the form of barite ($BaSO_4$). In the present study, minerals with Ba were not identified during the physicochemical characterisation of phytoliths; however Ba alongside Sr, was dissolved during batch experiments. This

suggests that Ba participated in the crystal lattice of the strontium carbonate or/and sulfate mineral, replacing Sr. The concentration of Ba (mg/g) seems to increase as the water availability increases (see Corfu sample, Fig. 57).

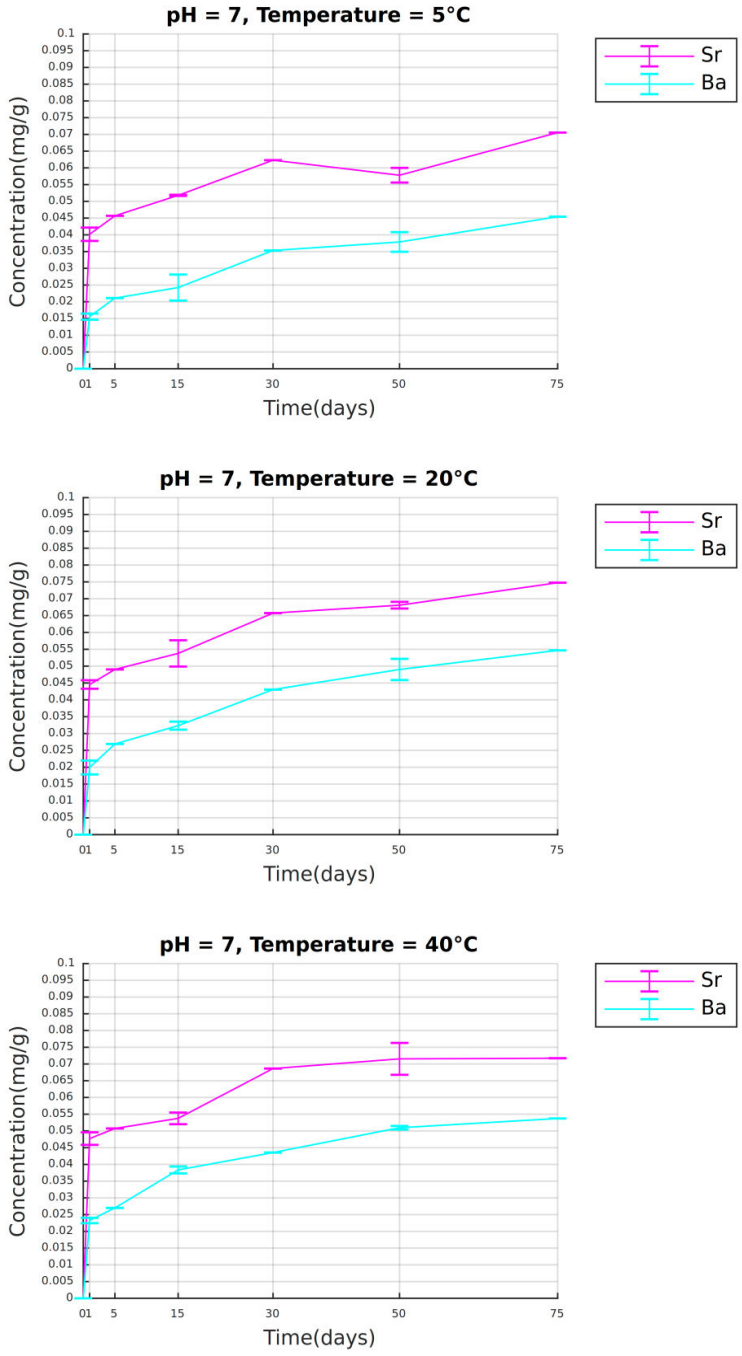

Fig. 56 Concentration (mg/g) of Sr and Ba over the course of 75 days at pH 7 and temperature 5 ˚C, 20˚C, 40 ˚C (*Triticum durum,* Corfu)

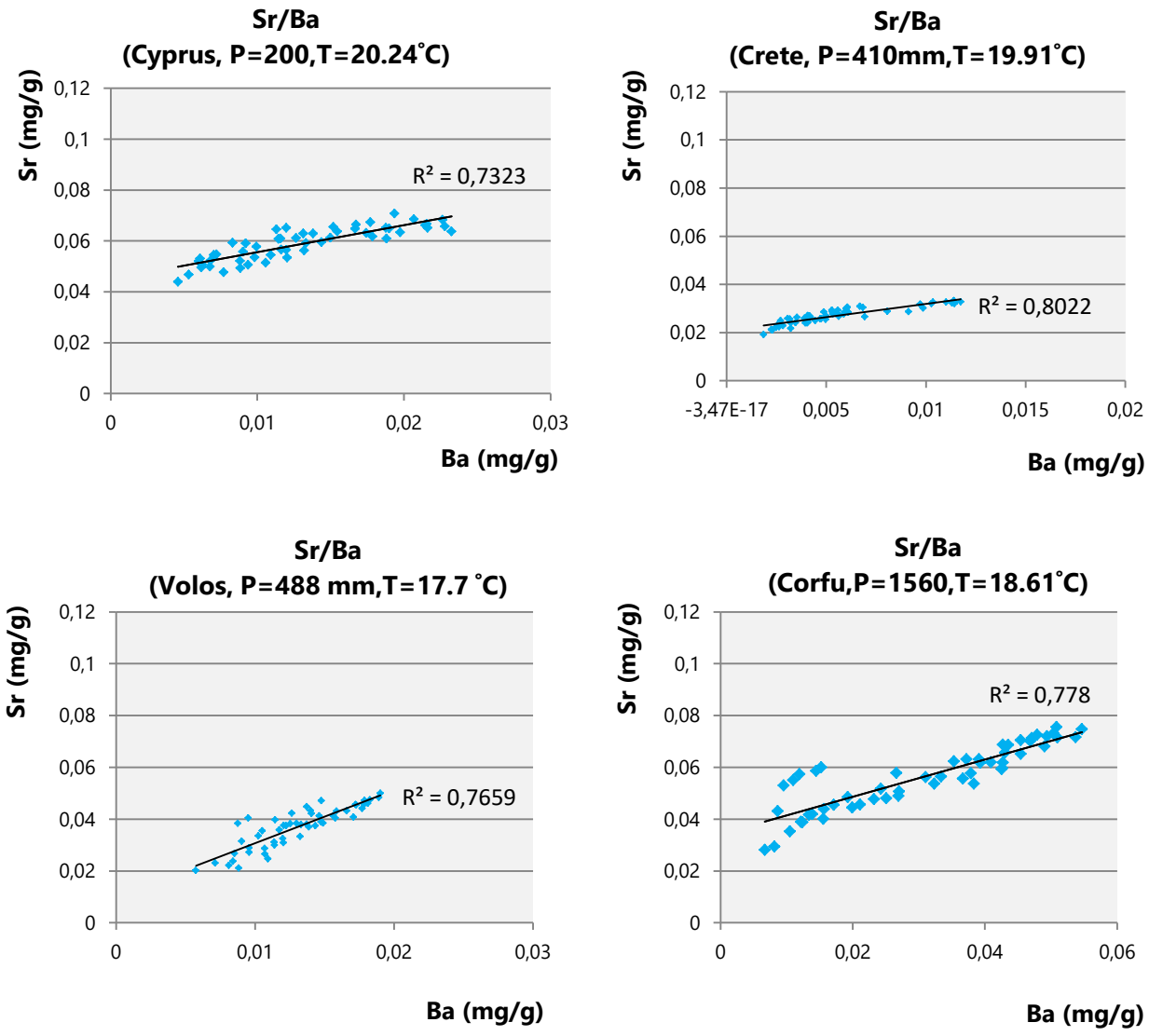

Fig. 57 Diagrams showing the variation of Sr versus Ba concentration (mg/g) during dissolution experiments. Strontium and barium display very similar behaviour. For all samples (apart from Pella samples) the two elements exhibit relatively good linear trends and coefficient of determination R^2 ranges between 0.802 and 0.732

In the present study, the concentration of dissolved Sr is generally higher than that of Ba (see examples, Figs. 56-57). Strontium concentration ranges between 0.07 - 0.04 mg/g for the sample from Cyprus, 0.03 - 0.02 mg/g for the sample from Crete, 0.05 - 0.02 mg/g

for the sample from Volos, 0.07 - 0.03 mg/g for the sample I from Pella, 0.10 - 0.03 mg/g for the sample II from Pella, and 0.08 - 0.03 mg/g for the sample from Corfu. Barium concentration ranges between 0.02 - 0.005 mg/g for the sample from Cyprus, 0.01 - 0.002 mg/g for the sample from Crete, 0.02 - 0.006 mg/g for the sample from Volos, 0.10 - 0.013 mg/g for the sample I from Pella, 0.02 - 0.003 mg/g for the sample II from Pella, and 0.05 - 0.007 mg/g for the sample from Corfu.

The chemical reactivities of the silicate minerals in H_2O may be dependent on the topography of the mineral surface, and this surface area obtained is called a geometric surface area (Hochella and Banfield 1995). Surface dissolution is affected by several factors (Fig. 58 e) and may be begin from one center (Fig. 58 a) from which originates the units detachment leading to step disintegration or it is also possible that detachment takes place simultaneously from multiple centers (Fig. 58 b and c) that may be developed in one (Fig. 58 b) or more steps (Fig. 58 c) on the surface. Alternatively, it has been suggested that the structural units' detachment takes place along spirals originating from an active site on the surface following an Archimedean spiral (Fig. 58 d)

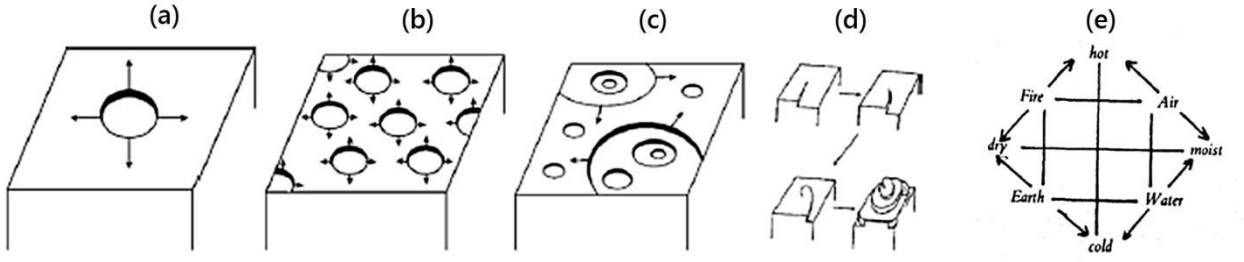

Fig. 58 Surface dissolution models: **(a)** mononuclear dissolution, **(b)** polynuclear dissolution, **(c)** polynuclear dissolution in multiples steps; birth and spread, (**d)** spiral dissolution (sources: Dorozhkin 2012; Ehrlich *et al.* 2009); and **(e)** interrelated factors that may affect dissolution process (source: Junius 1985)

In the present study, differences in the dissolution data between the samples under similar experimental conditions, may further demonstrate dependence on the siliceous material and its surface properties. The dissolution rate of phytoliths is probably proportional to the surface area of the interface between the SiO_2 and the solvent. The shape, form, volume, weight, texture and morphology of a phytolith define its specific surface area (SSA), which is equal to the ratio between the surface area and mass of the phytolith (m^2/g) or volume (m^2/m^3). According to previous studies, the specific surface area of phytoliths range between 30 and 300 m^2/g (Bartoli and Wilding 1980; Fraysse *et al.* 2006b). Fraysse *et al.* (2006b) characterised the surface properties and determined the solubility and dissolution rates of *Nastus borbonicus* (bamboo) phytoliths extracted from plants and soils. The specific surface areas (SSA) of ''soil,'' ''heated'' and ''fresh'' bamboo phytoliths were 5.2±0.1, 6.5±0.1, and 159.5±0.1 m^2/g, respectively, as determined by N_2 multipoint adsorption using the Brunauer-Emmet-Teller (BET) method. It has been also showed that the solubility of SiO_2-rich phytoliths is slightly lower than that of amorphous silica, but 17 times higher than the solubility of quartz (Fraysse *et al.* 2006b; Iler 1979; Dove and Elston 1992; Rimstidt and Barnes 1980). Take into account the importance of the surface properties for dissolution, a novel study of the surface morphology through the 3D representation of phytolith morphotypes (Andriopoulou *et al.* 2019) is developed in chapter 4.10 *(Integrated use of microscopy and photogrammetry for the 3D representation of biominerals)*.

Biogenic SiO_2 has absence of long-range order in its structure, and due to its relatively low thermodynamic stability, its dissolution kinetics in H_2O is orders of magnitude faster than those of silicate minerals, such as quartz (Alexandre *et al.* 1997a; Iler 1979; Loucaides *et al.* 2008). The reactivity of diatom frustules (Van Cappellen and Qiu 1997b) is higher compared to plant phytoliths (Fraysse *et al.* 2006b) in neutral solutions, but comparable or slightly higher than those for vitreous silica (Iler 1979; Wirth

and Gieskes 1979). More studies would be necessary to quantify the evolution of 3D reactive geometric surface area, as well as specific surface area, of phytolith morphotypes and other biogenic silicon structures during dissolution processes. Even though a substantial body of work (Fraysse *et al.* 2006b; Greenwood *et al.* 2001; Kamatani *et al.* 1980; Kamatani 1982; Kutuzova 1968; Loucaides *et al.* 2008; Prentice and Webb 2016; Van Cappellen *et al.* 2002; Van Cappellen and Qiu 1997b) is dedicated to the dissolution kinetics of biogenic SiO_2, the majority of existing studies either has restricted its focus on diatoms or they do not always take into account the 3D properties of the structures. The aforementioned parameters (e.g. time, pH, temperature, 3D phytolith surface) may affect the fate of biogenic SiO_2, and thus the progressive aging of phytoliths from biomineralisation to burial (e.g. in archaeological sites).

The experimental results of the phytolith dissolution showed that potassium, magnesium and calcium are released faster than silicon and their release might affect the solubility of silicon, and consequently the formation of minerals is soils and sediments. This may provide a basis for deeper understanding the conditions in archaeological (or paleontological, or historical) contexts under which phytoliths may be preserved. Albert *et al.* 2000 have shown that phytoliths recovered from a hearth composed by calcite were less preserved than phytoliths from hearths composed of carbonated hydroxyapatite [$Ca_{10}(PO_4,CO_3)_6(OH)_2$] and montgomeryite [$Ca_4MgAl_4(PO_4)_6(OH)_4 \cdot 12H_2O$]. The hearths were from a cave (in Israel), a context where degrading bat guano resulted in acidic solutions that infiltrated into the sediments. Therefore it may be expected that buried phytoliths in association with primary calcite ($CaCO_3$) will be relatively less well preserved, because fact that calcite usually buffers the sediment at pH ~8.2 or even higher (Karkanas *et al.* 2000, 2010a; Lippmann 1973). Calcite may be further be transformed to hydroxyapatite [$Ca_5(PO_4)_3(OH)$], and usually under lower pH (~6-7) hydroxyapatite may

be later transformed to other phosphates, such as montgomeryite (Karkanas *et al.* 2000, 2010a; Weiner 2010).

The phytoliths used in the dissolution experiments were extracted by the plants using the dry method (at 550°C for 4h). Therefore these results may offer supplementary information for plant ashes and heated/burnt phytolith (that are less stable than unburnt ones) assemblages from fire-related contexts. Temperatures in natural fires may range between ~200 and 700°C (Unzué-Belmonte *et al.* 2016, and reference therein). Ash is frequently a major component of either open-air sites (especially arid) or cave and rock-shelters that often are occupied by humans (i.e. domestic and ritual use of plants by humans) and their leaching capacity is relatively limited (Albert *et al.* 2001; Cabanes *et al.* 2009; Esteban *et al.* 2018; Friesem *et al.* 2014; Karkanas *et al.* 2002, 2006; Madella 2002; Rodríguez-Cintas and Cabanes 2017; Rowlett 2000; Schiegl *et al.* 1996). Ashes deposited in open-air sites, compared with ashes from caves environments, may be dispersed due their exposure to forces (i.e. water, wind) which result in complete or partial removal of the originally deposited remains (Goldberg and Macphail 2006). The ash fraction is composed of carbonates and silicates (the latter contain apart from Si; K, Ca, Mg, Al, Fe and P) and phytoliths occur regularly in plant ashes, although strictly speaking they are not ash but plant tissue remain (Canti 2003, and references therein). Fresh ash depending on the temperature of burning has a pH of 9-13.5 (Etiegni and Campbell 1991). Under specific conditions, calcitic ash, as mentioned above, may convert into more insoluble phosphate minerals (e.g. carbonated hydroxyapatite or dahllite; carbonated fluorapatite or francolite) (Karkanas *et al.* 2002; Weiner 2010). In any case, the dissolution of ash is an important factor in assessing volume changes of the sediment (Schiegl *et al.* 1996, from Karkanas *et al.* 2000).

Data on controlled fire use may prove useful for understanding, among others, human subsistence strategies (e.g. warmth, cooking), pyrotechnologies, mortuary practices, fuel and landscape management. Phytoliths are sometimes found in hearths and their surrounding matrix as a result of the combustion of plant material (Albert and Cabanes 2008; Albert and Weiner 2001; Braadbaart *et al.* 2019; Karkanas *et al.* 2002) or burnt dung/coprolites (Cabanes *et al.* 2009; Karkanas 2006; Miller 1984; Smith *et al.* 2019) Due to phytolith durability at relatively high temperatures, they may be a useful tool for the identification of the presence of fire (Parr 2006; Wroth *et al.* 2019), and the identification of the fuel (e.g. wood, grass) in various archaeological contexts (Albert *et al.* 2000; Esteban *et al.* 2018; Miller 1984; Out 2009; Rowlett 2000).

The experimental results may also have implications for the use of phytoliths as possible indicators of water availability, as well as the selection of the most appropriate phytolith samples used in geoachaeology and palaeoecology. It was further considered to what extent the dissolution obscure the interpretation of the original features from the three archaeological sites Knossos, Toumba, Castle Palea (see chapter 4.3, *Phytoliths from soils and sediments: archaeological case studies*). The available archaeological samples did not contain the minimum number of phytoliths (>50) needed for a reliable interpretation of the plant component (Albert and Weiner 2001). This may demonstrate that post-depositional processes (e.g. dissolution) impact phytolith presence (and size). It is important that the phytoliths morphotypes are unaltered at the highest possible level to obtain robust information for the plant identification (and consequently the understanding of the choices made by humans in the past) and be interpreted reliably. Further experiments on fresh phytoliths (i.e. either phytoliths extracted from ''modern'' plants or *in situ* study of phytoliths integrated in the plant tissues), alongside reference collections of ''modern'' plant phytoliths, are necessary to better understand the impacts of these processes at phytolith preservation.

Dissolution experiments were set up to mimic natural reactivity of biogenic silicon (after burning). However, the complete physical picture that explains behaviour of biogenic silicon during dissolution is not possible. Not only terrestrial, but also marine plant species strongly affect the various silicon pools through biosilification process. Opal, probably the dominant phase in SiO_2-rich phytoliths (see XRD traces above) exhibits significant spatial and temporal variability. A phenomenon, commonly referred to as the ''opal paradox", describes that high rates of opal accumulation are observed in the Southern Ocean, despite relatively low biosiliceous (and carbon) production in the region. In comparison, high biogenic Si productivity in the Northern Atlantic is accompanied by almost no opal preservation in the sediments (Nelson *et al.* 1995, from Pondaven *et al.* 2000). In any case, biogenic silicon solubility is an important parameter for elucidating the preservation of biogenic siliceous structures in the archaeological (and palaeoenvironmental) records, especially when used in conjunction with other proxies.

Further studies may include the understanding of the depth and pressure dependence of aged phytolith dissolution in sediments, and the correlation between the precipitation of authigenic clays (i.e. clays that form *in situ* within the sediments) and the dissolution of SiO_2-rich phytoliths, in the near surface horizons. Van Capellen and Qui (1995b) suggested that the dissolution kinetics of biogenic SiO_2 in sediments does not follow the linear rate law that forms the basis of nearly all early diagenetic models of SiO_2, instead they demonstrated a substantial decrease of the SiO_2 surface reactivity with increasing sediment depth. Chemical interactions involve the transfer of elements between clay minerals (e.g. illite/muscovite), and the infilling and replacement of the phytolith structures by clay remains a possibility. Terrestrial plant-derived Si, and other elements incorporated in phytolith structure, may act as a substrate for mineral formation and affect its different physicochemical properties in surface conditions. The presence of illite/muscovite in our plant sample (see XRD traces above) remains

uncertain, and suggests either that clay is a contaminant due to the contact of phytoliths with soil or it had been incorporated during the plant growth in phytolith structure.

Finally, understanding silicon solubility of SiO_2-rich phytoliths (i.e. desilification process) it not only important for the study of the past, but has also the potential for the use of phytoliths in bio-inspired nanotechnologies; and applications toward human (and animal) health current issues (e.g. beneficial role of Si in collagen and bones, toxic role of Si in lungs/silicosis, relation of Si with stones of the body/pathological biomineralisation). In any case, the extent of phytolith alterations needs to be assessed before phytolith study in various scientific disciplines.

4.10 Integrated use of microscopy and photogrammetry for the 3D representation of biominerals

Even though earth-related 3D surface reconstruction is widely used in geomorphology (Collin and Chisholm 1991; Lane *et al.* 1993; Westoby *et al.* 2012), its use in geoarchaeology (Siart *et al.* 2018) and especially for the microscopic record has been limited. A new insight in the optimisation of the three-dimensional (3D) reconstruction is provided through commonly used digital photogrammetry tools to enrich archaeological, especially microscopic, records. The integrated use of microscopy and photogrammetry for the 3D representation of biominerals (phytoliths, teeth) was proposed (Andriopoulou *et al.* 2019) (Fig. 59-62). Throughout related work, similar experiments merely provide visualisation of 3D specimen models. The photogrammetric reconstruction of the 3D models is limited due to the imaging environment including illumination parameters, while measurable models are unavailable due to the absence of a coordinate system.

Our approach is an advance over existing work with a similar approach to ours, which merely provides visualisations of 3D specimen models. The photogrammetric reconstruction of the 3D models is influenced by parameters of the imaging environment such as illumination and non-rigid camera-lens geometry. Thus, the underlying challenges of such an attempt are to build a geometrically reliable 3D model and subsequently to provide quantitative structures with which relative or absolute metrics can be estimated, keeping into consideration the limitations set by the lack of strict scaling or of a precise coordinate reference system.

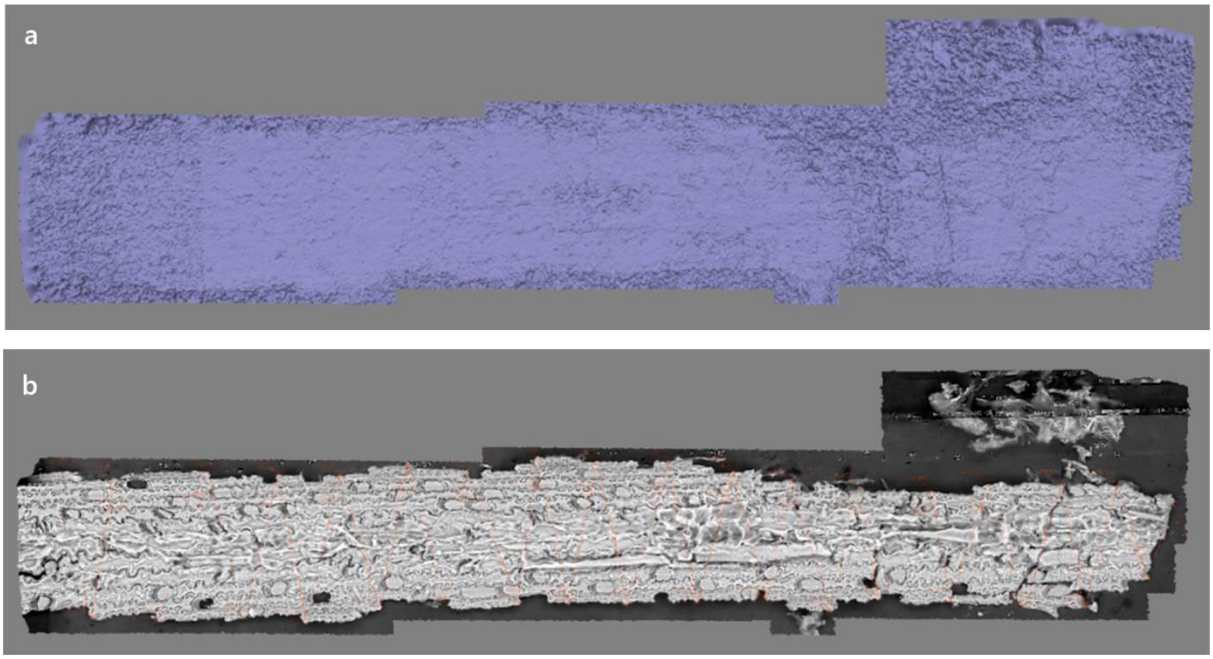

Fig. 59 Phytolith I, dentritic phytolith aggregation from wheat (*Triticum monococcum*) inflorescence: **(a)** digital surface model; and **(b)** orhthophotograph. Detection of fissures

Towards this end, the first findings of a metric-oriented approach are provided, through geometric distance unit set-ups towards a robust measurement methodology that allows distance, area and volume measurements. Part of the samples that were documented and studied are presented. Below a series of resulting photogrammetric products are presented, including three dimensional visualisation and orthorectified images (Wolf *et al.* 2014).

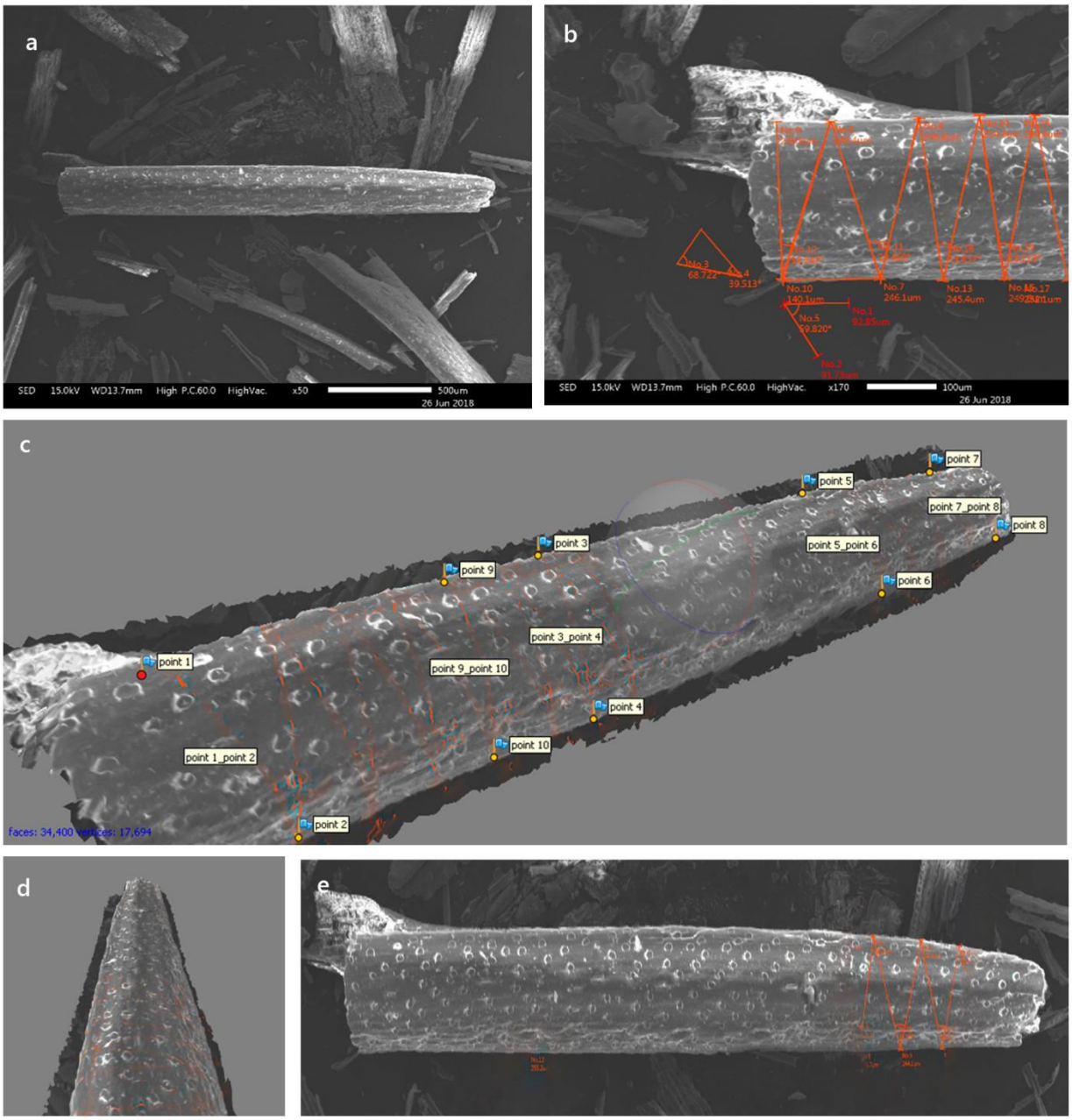

Fig. 60 Phytolith II: **a)** initial image, **(b)** control point distance measures, **(c)** control point insertion for scale estimation, **(d)** three-dimensional (3D) model; and **(e)** orthophoto generation

Often the morphology of the phytoliths may alter due to mechanical forces, (eg. translocations, water seeping, bioturbation, trampling, sampling, laboratory processes/extraction methods) or/and biogeochemical parameters (e.g. soil pH, temperature, water availability, pedogenesis, microbial and plant root activity). Previous studies have pointed out the importance of the active surface area for the stability of a phytolith (Bartoli and Wilding 1980; Cabanes and Shahack-Gross 2015; Osterrieth *et al*. 2009). Understanding the 3D characteristics of phytoliths may prove useful for the understanding of their chemically active surface area and their volume and shed light on the mechanism that leads to differential stability of phytoliths during dissolution process.

For a deeper understanding of the 3D characteristics of the phytoliths, we have also studied biominerals of animal origin, in particular *Microtus* sp. and *Rattus* sp. (rodents) teeth, which have particular texture, relief and size. Furthermore, teeth allowed an easier separation from the stub surface than phytoliths that usually are more flattened. In the next few figures additional three dimensional products are presented. The study of micromammals, often identified by their preserved teeth, may provide important information pertinent to both the palaeoecology and relative dating of archaeological or paleontological sites (Sala and Masini 2007; Reitz and Wing 2008, and references therein). Furhermore, sometimes phytoliths can be detected in animal teeth (Acuña-Mesén and García-Díaz 1998; Cionchon *et al*. 1990; Winklera *et al*. 2019) or in human teeth (Cummings and Magennis 1997; Gügel *et al*. 2001; Lalueza Fox *et al*. 1994*;* Reinhard and Danielson 2005) providing a wide range of information (e.g. palaeodiet, palaeopathology, palaeoenvironment).

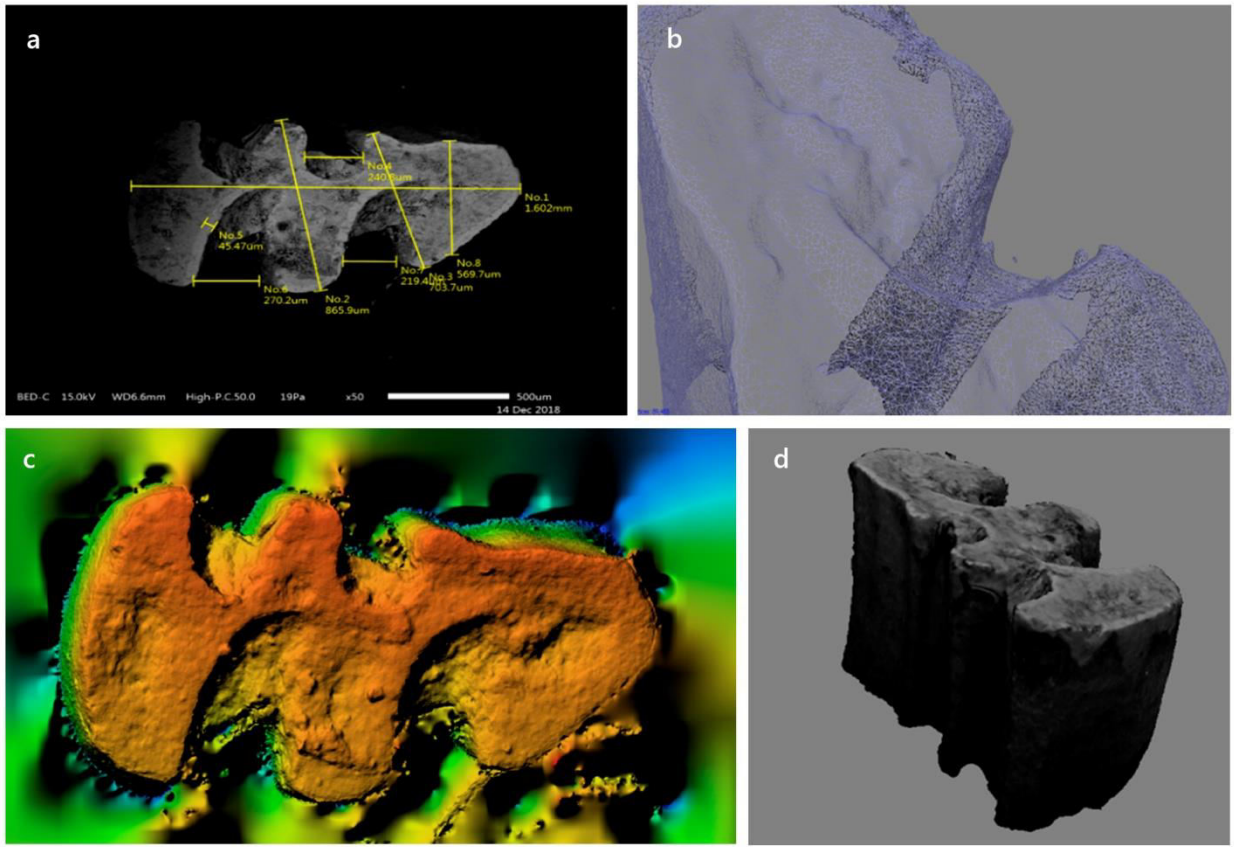

Fig. 61 Tooth I, molar from rodent (*Microtus* sp.): **(a)** measuring scaling distances, **(b)** digital surface model detail; and **(c, d)** three-dimensional morphological representations

The error of the process was estimated by comparing already measured distances through SEM and their equivalent upon the 3D model. It is noted, to avoid bias implications that this comparison did not include any distances that were used to establish the model itself. In most of the reconstructed cases the error remains quite low, in the range of 2% of the corresponding distances.

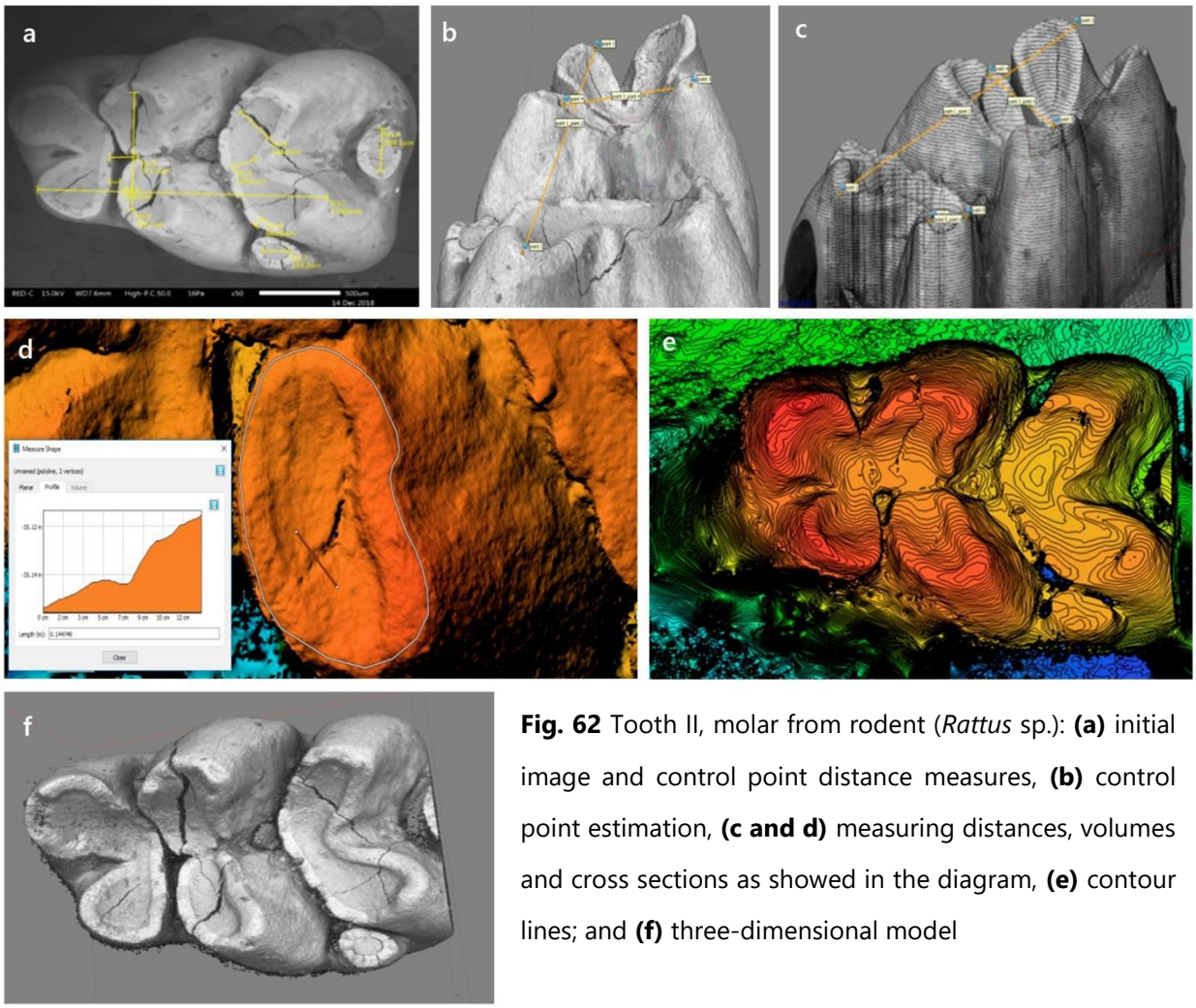

Fig. 62 Tooth II, molar from rodent (*Rattus* sp.): **(a)** initial image and control point distance measures, **(b)** control point estimation, **(c and d)** measuring distances, volumes and cross sections as showed in the diagram, **(e)** contour lines; and **(f)** three-dimensional model

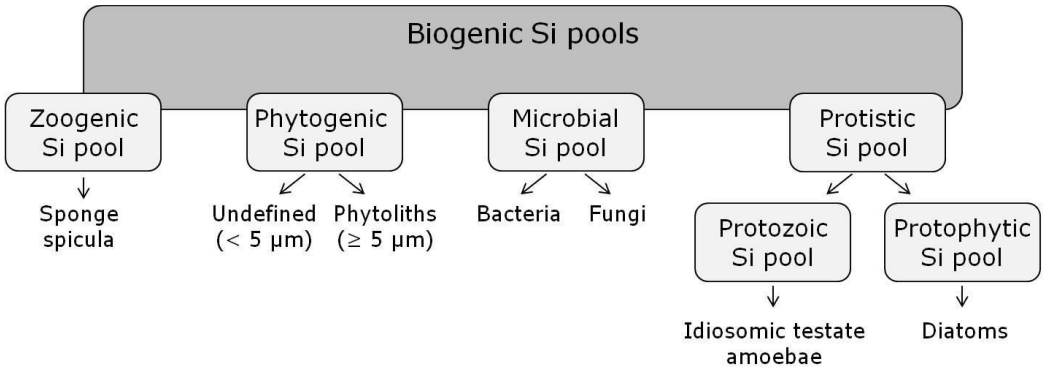

Fig. 63 Biogenic silicon pools (zoogenic, phytogenic, microbial, protistic) (source: Puppe *et al.* 2015)

The parameters of form, dimension, texture, colour and composition of the biominerals are essential for their study in all their multiple facets (i.e. taxonomy, distribution, morphometry, quantification, characterisation, preservation). A future integrated 3D reconstruction of several biogenic pools is pivotal for the deeper understanding of the biogeochemical cycling of silicon. Applications may include the study of other biogenic mineralised materials with archaeological significance, such as mollusks (Andriopoulou and Partsinevelos 2019). Our aspiration is that the application of the combined study of geometric and geochemical data presented here becomes useful for the study of other microscopic biogenic silicon pools (Fig. 63) during dissolution, introducing new insights in biomineralisation.

5 CONCLUSIONS

One of the most important factors for the reliable study of phytoliths is their preservation status. Phytolith preservation extends from the scale of their microscopic image, proceeds to the scale of the unit cell of their mineral phases and reaches the molecular structure and chemical composition. Phytoliths are likely to be subjected to a variety of morphological alterations or changes to their mineralogical or chemical composition in their life-span, caused either by *in situ* taphonomic processes, or by the methods of extraction. The overall integration of XRD, FTIR, SEM/EDS, ED-XRF, CHNS, TGA-DTGA, and optical microscopy has been employed successfully to characterise fresh wheat phytoliths. The phytoliths were extracted from *Triticum monococcum* and *Triticcum durum* (stem-leaves and inflorescence) from five organic crops in Greece and one conventional crop in Cyprus, using dry and wet method. The data obtained may further find useful implications in archaeological phytolith assemblages, and for a better understanding of the responses of biogenic SiO_2 pools to anthropogenic impact, it is crucial to obtain knowledge on phytoliths initial physicochemical characteristics.

The mineralogical and chemical composition of the recovered phytoliths is controlled by the extraction method, strongly suggesting that comparison of phytoliths extracted from plants is meaningful only if the method of extraction remains the same. The dry method produces more AIF that is mainly composed of phytoliths, than wet method regardless of the wheat species and anatomical origin of the phytoliths (stem-leaves or inflorescence). Heat treatment removed the majority of the volatile matter, increasing the mineral matter content. The dry method provided a wider range of mineralogical phases than the wet method, which might indicate the presence of neoformed mineral phases (secondary mineral formation), due to the exposure of the samples to relatively high temperatures during the dry method of phytolith extraction. The phases identified after

the mineralogical analysis of all plant samples using both methods are anhydrite, aphthitalite, arcanite, barbosalite, bassanite, baylissite, brucite, calcite, celestite, chlorocalcite, monetite, monohydrocalcite, mundrabillaite, schertelite, strontianite, illite/muscovite; and probably ammonium carbonate hydrate and struvite. The minerals that are identified in XRD derive from the process of the plant material (during acid treatment or/and burning of the residual inorganic wheat material) and they do not directly relate to phytoliths. The presence of illite/muscovite remains uncertain, and suggests either that clay is a contaminant due to the contact of phytoliths with soil or it had been incorporated during the plant growth in phytolith structure. In addition, the hump at 10-30°2θ indicates the presence of amorphous matter, most probably opal ($SiO_2 \cdot nH_2O$). The amorphous matter, as it is observed in XRD traces, is the result of the phytolith presence. Quartz was identified in all soils and all archaeological sediments, however quartz was not identified in the plant samples using either dry or wet method of phytolith extraction.

In both extraction methods, the results of thermogravimetric analysis are in accordance with the XRD traces. For both methods, the inflorescences and stems-leaves of *Triticum durum* accumulated relatively higher concentrations of phytoliths than their counterparts of *Triticum monococcum* that is possibly related to genetic and environmental parameters. The DTG-TG curves also showed that the weight loss of the *Triticum durum* is usually higher than the weight loss of the *Triticum monococcum*. The use of HCl and H_2O_2 in the dry method seems to have eliminated the majority of the carbonates and organic matter respectively. However, using FTIR analysis the carbonate asymmetric stretching band was noticed for both species and plants parts after application of the wet method, and the bands between ~1700-1330 cm^{-1} suggest that some organic matter remains to phytoliths. The overall surface of the phytoliths extracted with the dry method is sharper and their boundary shows less alterations than phytoliths

extracted with the wet method. This implies that dry method is probably better than wet method of phytolith extraction. For both methods the inflorescences produce clearly more AIF that is composed mainly of phytoliths, than the stem-leaves regardless of the wheat species and area of study.

Plant-specific variations in the mineralogy of the stem-leaves and the inflorescence were observed, regardless of the extraction method. SiO_2 is more abundant in phytoliths obtained with the dry method than with the wet method and in inflorescence rather than stem-leaves that showed high loss of ignition (LOI). Regarding the chemical composition of the phytoliths, the samples are mainly composed of SiO_2. Carbon, Mg, Al, P, S, K, Ca, Fe and rarely Sr, Cl and Cu were also detected on clean phytolith surfaces. The loss of ignition (LOI) was considerably higher in stems-leaves than inflorescences of both species and for both methods. The elemental analysis (XRF and SEM/EDS spectra) confirms the mineralogical analysis results (XRD traces). The chemical composition can be used to infer the mineral identity. This is not always unequivocal but may provide useful information. The composition varied depending on the analysed particle or zone of the phytolith morphotypes. Silicon and sometimes Ca were observed along the entire cell wall whereas K and P tend to accumulate in the outer layer of the wall. Despite the importance of previous studies, the localisation of Cu within phytolith structure was not fully understood. In the present study, Cu was detected in the narrow end (tip) of the hairs (trichomes) of SiO_2-rich phytoliths extracted from *Triticum durum* inflorescence from Cyprus. The presence of Cu in this sample might either reflect the use of fertilisers, or may be related to the ophiolitic rocks of the Troodos Complex and the soils linked with these rocks. The detailed localisation of Cu in wheat phytoliths invites further studies on its systematic distribution across the family.

Apart from laboratory processes, diagenesis may have an impact on the successive disarticulation, weathering or/and the potential destruction of phytoliths. The quantification of morphotypes for phytoliths originating in the plants on the basis of the International Code for Phytolith Nomenclature (ICPN Working Group: Madella *et al*. 2005) was carried out both before and after dissolution. Phytoliths from the corresponding soils for these samples, and archaeological sediments from three nearby the cultivations (cultivation adjacent to archaeological site), archaeological sites in Greece were also extracted. All samples are characterised as alkaline. The concentrations of plant phytoliths range from approximately 1 million phytoliths to approximately 5 million phytoliths. Phytolith concentration in the sample from the N-P-K fertilised sample from Cyprus appears significantly higher than in the remaining samples. The fact that fertiliser addition probably affects the phytolith content in the soil may prove useful for the identification of fertilisers in the archaeological record and therefore for the detection of human agricultural past activity. Phytolith assemblages from the ''modern'' soils do not correspond to the phytolith assemblages produced by ''modern'' plants. The differences in phytoliths concentration may be, among others (preservation, harvesting etc.), the outcome of phytolith deposition in the soils from other plants (i.e. dicotyledonous weeds) that were already present in the area.

The present work involved dissolution experiments of the phytoliths at different pH and temperature. Based on the dissolution experimental results, the absolute values of average percentages of some phytolith morphotypes extracted from plants before and after dissolution experiments remained relatively constant (e.g. short cell rondels) despite the change in pH and temperature. An additional observation was the high stability of the stomata. This stability, and thus mechanical resistance, may be related to their function on the leaves, which serve the plants' evapotranspiration (i.e. the main pathway of water loss through the leaves is via the stomata). Dimensional characteristics and

texture of the majority of the phytoliths (apart from the short cells rondels and stomata) change with pH and temperature. Dentritic morphotypes appear to decrease and echinate morphotypes to increase considerably with rising pH and temperature. It is suggested that dendritics may alter to echinates or/and to verrucates. This observation should be taken into account when studying phytoliths from archaeological sediments, because it indicates that some morphotypes might have been absent from the archaeological record, not because they did not deposited, but because they did not preserve their initial morphological characteristics over time. This has important implication for the use of some phytolith ratio indices that are used in some identification approaches and crop-processing studies. As a consequence, if there is an alteration of dendritics to echinates or/and verrucates, then we cannot rely on their ratio indices, unless it is confirmed that there is not alteration at all.

Furthermore, apart from the gradual change of the dimensional characteristics of morphotypes, the texture of most of morphotypes (especially parallelepiped elongated and long cells waved) tended to change from psilate/smooth to rugulate/rugose. In some cases some pits, probably due to chemical alteration, were observed on the outer surface of the morphotypes. Microcracks and fractures were also observed due to mechanical alteration, mainly at the edges of the large morphotypes. Moreover, the weathered morphotypes with irregular shapes and pitted surfaces, increased as expected. The abundance of melted mophotypes that showed signs of burning, deformation or/and shrinkage did not change significantly. However, their boundaries were less stable. The majority of the morphotypes from *Triticum monococcum* were less stable than their counterparts from *Triticum durum*.

The mineral phases identified in the soil samples are albite, anatase, ankerite, calcite, chlorite, clinochlore, dolomite, hornblende, kaolinite, K-feldspar (orthoclase), illite/muscovite, paragonite, serpentine, smectite, talc and quartz. According to the results obtained from XRF analysis of phytoliths from plants and soils, for both wheat species, there is a relationship between the soil composition and the plant parts (stem-leaves or inflorescence). Three groups of soils with similar chemical characteristics are observed: (a) Crete, Pella I and Pella II, (b) Cyprus, (c) Volos and Corfu. According to the results obtained from XRF analysis of plant and soil samples, for both wheat species, there is a relationship between the soil composition and the plant parts. The concentration of some chemical elements in inflorescence, such as the plant macronutrients P and K are quite higher than their concentration in soils. The most abundant morphotypes in all soil samples are weathered and fragmented phytoliths, as well as parallelepiped elongated long cells rugulated and long cells wavy rugulated.

The archaeological samples originated from an activity area (an indoor living space), an artefact (the interior of a ceramic vessel), a combustion residue (ashes next to the kiln), a food processing tool (a grinding stone) and construction materials (plaster floors of a building). The chemical compositional trends reflect mainly the relative abundances of silicate and carbonate minerals in the samples. The mineral phases identified are albite, anatase, calcite, chlorite, dolomite, gypsum, halite, hematite, hornblende, illite/muscovite, K-feldspar, pyrite, quartz, smectite and talc. The available archaeological samples did not contain the minimum number of phytoliths (>50) needed for a reliable interpretation of the plant component (Albert and Weiner 2001), suggesting that post-depositional processes impact the presence of phytoliths. Furthermore, the low amount of phytoliths may be also be related with human use of plants that poorly produce phytoliths (e.g. woody species). There is also a possibility that the rapid extraction method (Katz *et al.* 2010) used here might have not been able to seperate all phytoliths

from the archaeological sediments, suggesting that more methods of phytoliths extraction from soils and sediments should be developed. With respect to the role of the organic matter, serving as template in (bio)mineralisation processes, less aggressive methods of phytoliths extraction from plants should be developed. Furthermore, studying phytolith dissolution directly in plant tissues may offer more accurate estimates of the concentration of dissolved chemical elements.

Few phytoliths from dicotyledons were recovered in Knossos sample (*KN5*) suggesting an input of noncrop plants. It is possible that either the use of the Minoan room might have affected the preservation of phytoliths due to possible frequent trampling, or a period of abandonment of the Minoan room might have affected the phytolith input, mainly with the input of dicotyledons plants. Moreover, scarce phytoliths from grasses in Knossos sample (*KN10*) probably cereals were recovered from the inner part of the ceramic vessel. Hypothetically, the vessel was used for the storage or transport of food or/and fodder. The Toumba sample (*TB2008*) derived from a kiln appear to contain morphologies akin to phytoliths, which were hardly detectable probably due to melting. The morphologies can not serve as a diagnostic marker for the characterisation of specific taxa; however few polyhedral phytoliths, which seem to belong to Anacardiaceae family, most probably *Pistacia* spp. (mastic tree) were also recovered. The phytolith analysis shows that most probably mastic tree had been used as a fuel in the kiln. Moreover, thirty-three (33) phytoliths probably from wheat (*Triticum* spp.) or barley (*Hordeum* spp.) inflorescence were recovered from Toumba sample (*TB2013*) derived from a grinding tool. Analysis underlined the absence of phytoliths in both samples from Castle Palea (*ΚΑΣ25* and *ΚΑΣ27)*. Water evaporation caused precipitation of gypsum detected in these samples which may break up sediments mechanically and potentially may affect the preservation of microbotanical remains. Phytoliths at archaeological sites might undergo partial or total loss, principally

depending on the environment in which the phytolith were buried and studying phytolith solubility may provide insights into the driving mechanisms behind phytolith diagenesis.

The comprehensive mineralogical and biogeochemical study contributes to the understanding of the geochemical cycle of silicon and to geoarchaeological research, through the insights gained on the post-depositional alterations that SiO_2-rich phytoliths are subjected to over time, and how this relates to the mobility of other soil elements. The dissolution mechanism of fresh (not aged) phytoliths extracted from the entire plant using dry method is investigated in relation to variations of pH, temperature and time, by the means of long-term batch experiments (closed system), under conditions that are relevant to natural environments (e.g. stagnant/standing water conditions). Moreover, the mobility 8 chemical elements (Si, Al, Mg, Ca, K, Fe, Sr, Ba) was studied with the use of inductively coupled plasma mass spectrometry (ICP-MS) and visualised with MATLAB software. The evolution of the four studied main elements (Si, Mg, Ca, K) and the two trace elements (Sr, Ba) concentration (mg/g) at the aforementioned variables over time are presented in kinetic diagrams. The rate of disintegration of the phytoliths structures depends on the concentration difference between the phytolith surface and the bulk solution. Dissolved silicon seems to originate from phytolith surfaces and the SiO_2-rich matrix of the apoplast in the plant tissues.

The results indicate that Si (SiO_2-network former) and Mg, K, Ca (SiO_2-network modifiers) are mobile, Fe is moderately mobile and Al is essentially immobile. Also, K^+, Mg^{2+} and Ca^{2+} are released faster than Si^+, and their release might affect the solubility of silicon, and consequently the formation of minerals is soils and sediments. Between the studied main elements, K is most soluble and Si is less soluble ($K^+ > Mg^{2+} > Ca^{2+} > Si^+$). The highest Si concentrations [and the maximum values of Si (wt. %) that were dissolved from the initial solid] between the samples was from *Triticum monococcum* Pella I

sample. Depending to the conditions of the aqueous medium; Fe^{3+} seems to be essentially immobile and probably precipitated in the form of hydroxides. In contrast, in alkaline conditions Fe^{2+}usually tends to be relatively mobile in aqueous environments. Aluminium concentrations were below detection limit possibly due to precipitation. Strontium and Ba display very similar behaviour with a very rapid initial element release mainly during the five days. Strontium-bearing minerals were present in the XRD traces (alongside Sr in the EDS spectra), but Ba-bearing minerals were not identified; however Ba alongside Sr, was dissolved during batch experiments. This suggests that Ba participated in the crystal lattice of the strontium carbonate or/and sulfate mineral, replacing Sr.

Dissolution is either: (a) congruent (stoichiometric) or (b) incongruent (non-stoichiometric), and based to our results, phytolith dissolution under all experimental conditions probably is incongruent suggesting that a surface layer within a biogenic SiO_2 composition different from that of the bulk may be formed. The saturation state changes most rapidly at the onset of the present batch experiments, when the degree of undersaturation and the rate of dissolution are highest. The behaviour of Si in the course of dissolution often indicated two main dissolution regimes: rapid initial element release during the first two weeks and especially within the first five days, followed by a slower element release. This initial rapid dissolution may further suggest the progressive alteration and loss of a reactive surface layer (which may act as an energy barrier) or/and different levels of phytolith porosity.

The first-order reaction model describes the experimental results satisfactorily compared to other models (1/2, 3/2, and second order). The experimental points (using the differential method) plot on either one straight line or two strainght lines in the semi-logaritmic plot ln C/C_o versus time, and subsequently the dissolution reaction was

described either from a single stage (*k*) or from two stages (*k*1 and *k*2). The first stage may be related with an initial loss of a reactive surface layer and this stage probably is both surface and diffusion controlled. On the other hand, the second stage may be related with a re-precipitation of Si as the system approached saturation and this stage is probably diffusion controlled. Temperature and pH affect the dissolution efficiency of SiO_2 and thus the weathering resistance of phytoliths. In many cases (from 20 to 40˚C, and especially in alkaline pH) the Si concentration was reduced probably due to precipitation. The exact mechanism responsible for the Si re-precipitation here is not fully understood. Several interrelated factors, apart from the experimental conditions, may affect the reaction rates and thus precipitation. Based on the dissolution results of phytoliths extracted from plants grown in areas with different water regime and temperature, it was suggested that *k* rate constants may be used as potential proxies to study the relationship between water availability and SiO_2-rich phytoliths. Furthermore, both plants seem to accumulate relatively higher concentrations of phytoliths as precipitation of the area of study increases (here, the sample from Corfu affected by the insect pest *Sitophilus granarius* and the N-P-K fertilised sample from Cyprus are not taken into account).

Differences in the dissolution data between the samples under similar experimental conditions, may further demonstrate dependence on the siliceous material and its surface properties. Reactive surface of SiO_2-rich phytoliths, alongside time, pH and temperature, may affect the fate of biogenic SiO_2, and thus the progressive aging of phytoliths from biomineralisation to burial (i.e. an increase of pH, temperature and time decreases preservation of phytolith morphotypes). A quantifiable 3D model using micro-photogrammetry was provided that may offer measurable properties including distances, areas and volumes and shed light to questions related to the surface alterations of

(microscopic) biominerals due to mechanical forces or/and biogeochemical parameters (e.g. dissolution). The error was in the range of 2% of the corresponding distances.

Phytoliths are often found in hearths and their surrounding matrix as a result of the combustion of plant material or dung. The studied phytoliths were extracted from plants using the dry method (at 550°C for 4h), and therefore are suitable for fire incidents with implications in geosciences and archaeology, especially when used in conjunction with other proxies. The overall physicochemical characterisation of fresh phytoliths from plants may further contribute to the interpretation of aged phytoliths from archaeological (or paleontological or historical) contexts for the diachronic study of human-plant interactions, as well as to the development of new methodologies and tools for phytolith analyses. Curie (1867-1934) considered that a scientist in his laboratory is not a mere technician, he is also a child confronting natural phenomena that impress him as though they were fairy tales. Our research continues, as many questions remain unanswered while many more emerged.

Appendix - part 1

(Phytolith morphotypes before and after dissolution)

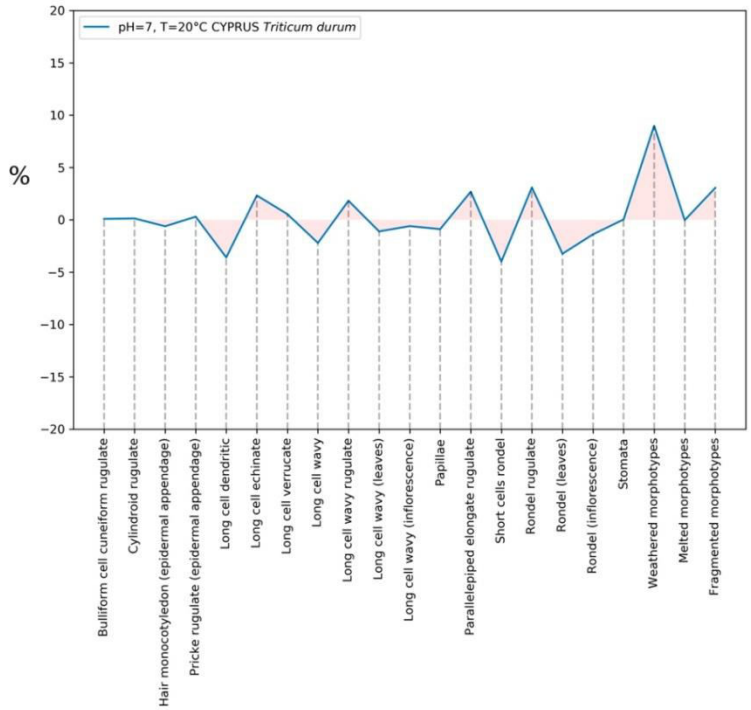

Fig. 64 The relative difference between the presence of phytolith morphotypes (Cyprus, *Triticum durum*) before and after the dissolution experiments (pH=7, T=20˚C)

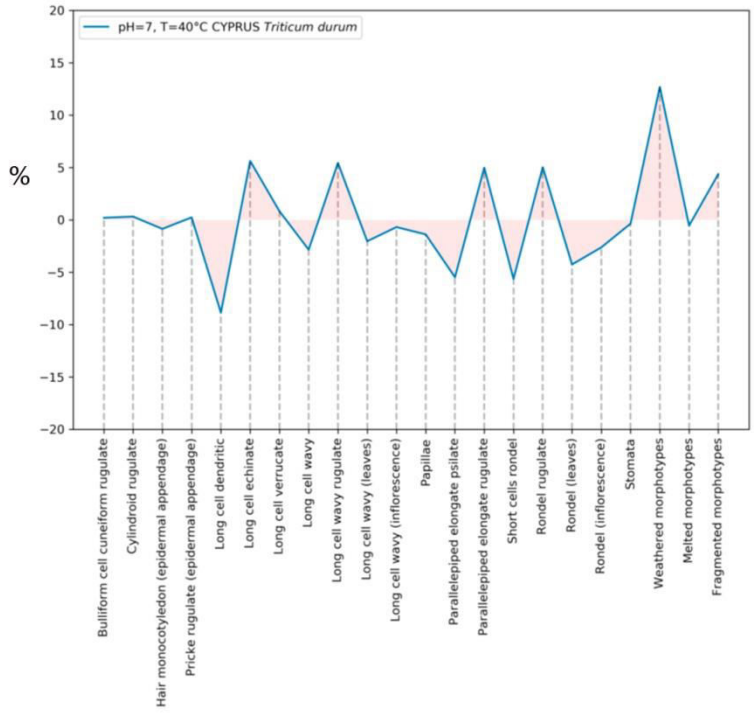

Fig. 65 The relative difference between the presence of phytolith morphotypes (Cyprus, *Triticum durum*) before and after the dissolution experiments (pH=7, T=40˚)

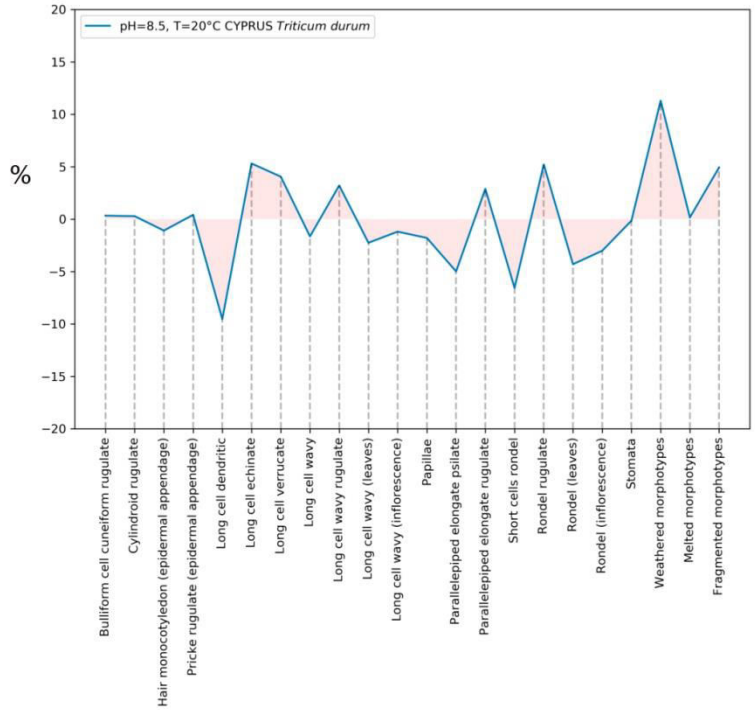

Fig. 66 The relative difference between the presence of phytolith morphotypes (Cyprus, *Triticum durum*) before and after the dissolution experiments (pH=8.5, T=20˚C)

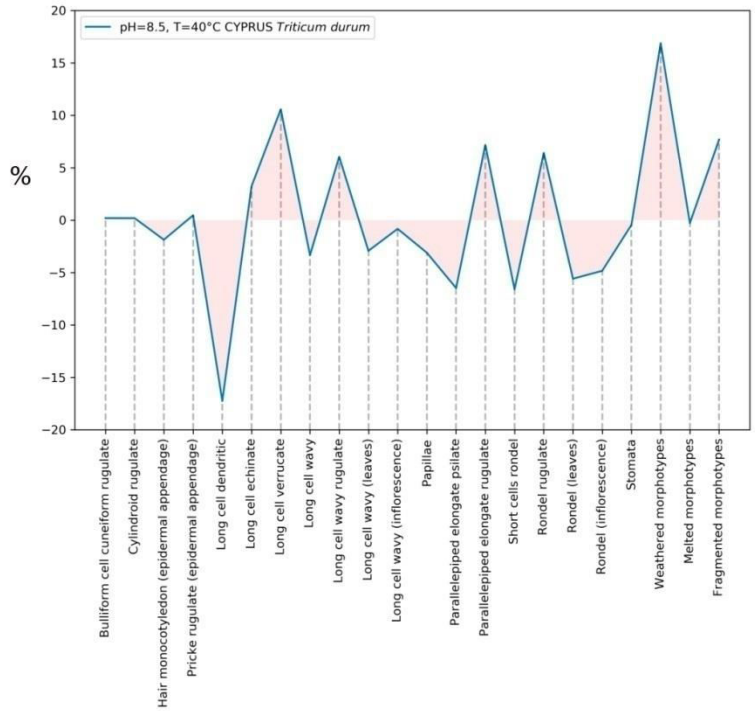

Fig. 67 The relative difference between the presence of phytolith morphotypes (Cyprus, *Triticum durum*) before and after the dissolution experiments (pH=8.5, T=40˚C)

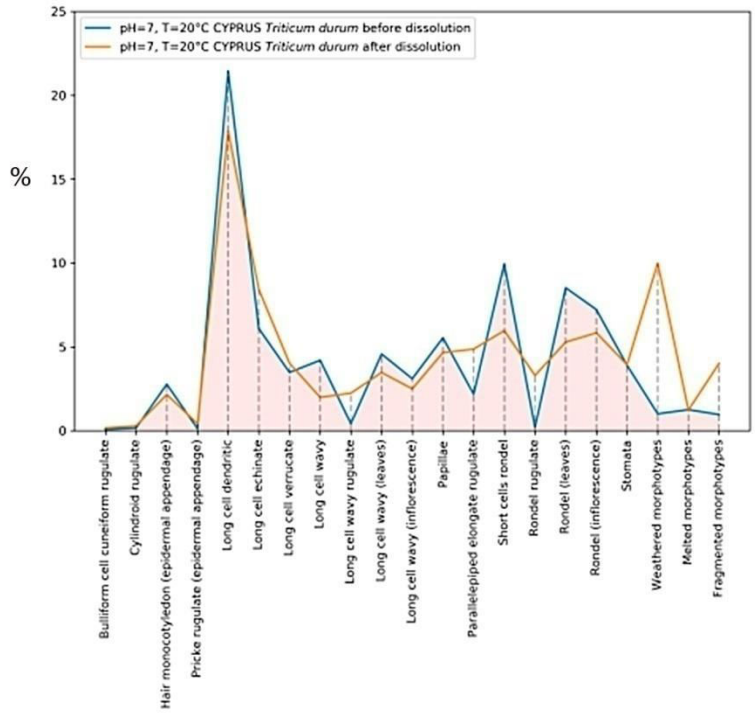

Fig. 68 The absolute value for the presence of phytolith morphotypes (Cyprus, *Triticum durum*). Blue line represents data before dissolution and orange line after dissolution (pH=7 and T=20˚C)

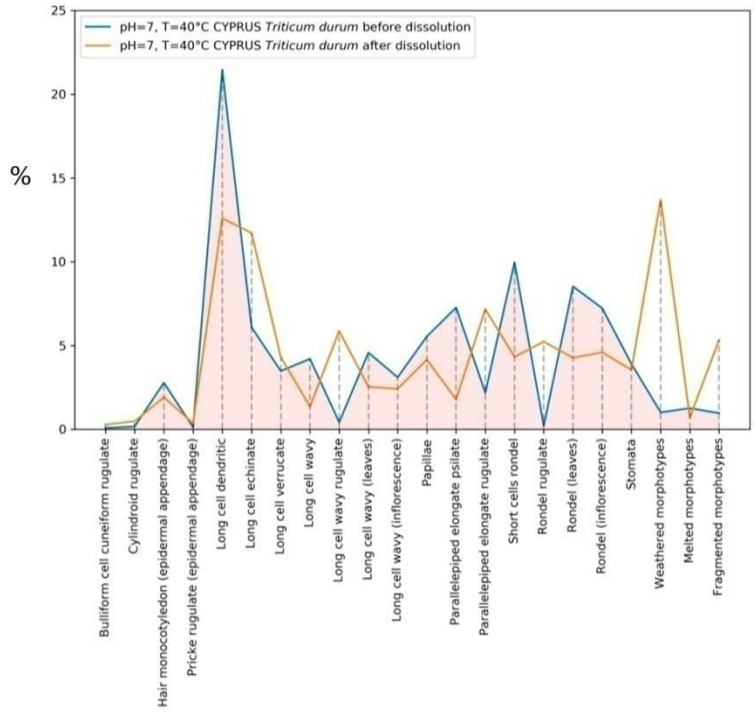

Fig. 69 The absolute value for the presence of phytolith morphotypes (Cyprus, *Triticum durum*). Blue line represents data before dissolution and orange line after dissolution (pH=7 and T=40˚C)

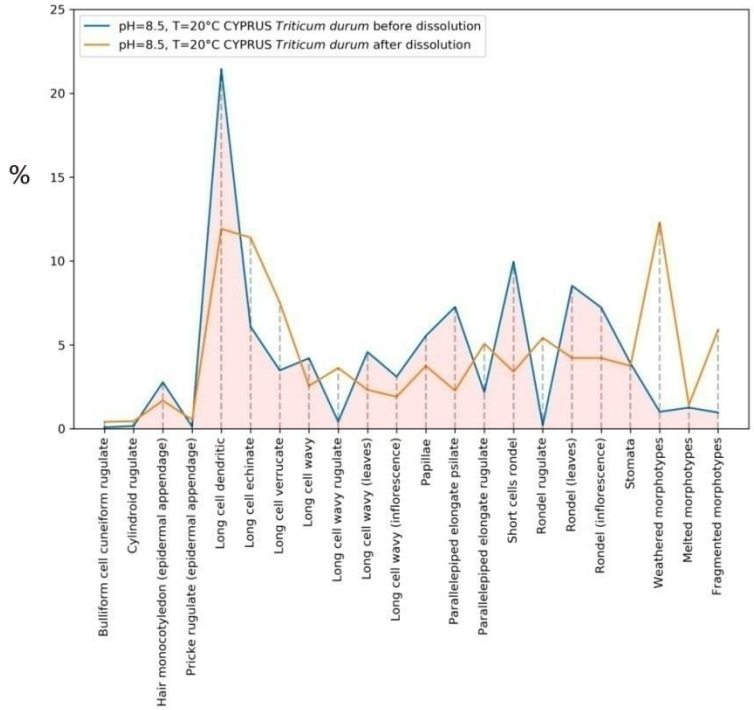

Fig. 70 The absolute value for the presence of phytolith morphotypes (Cyprus, *Triticum durum*). Blue line represents data before dissolution and orange line after dissolution (pH=8.5 and T=20˚C)

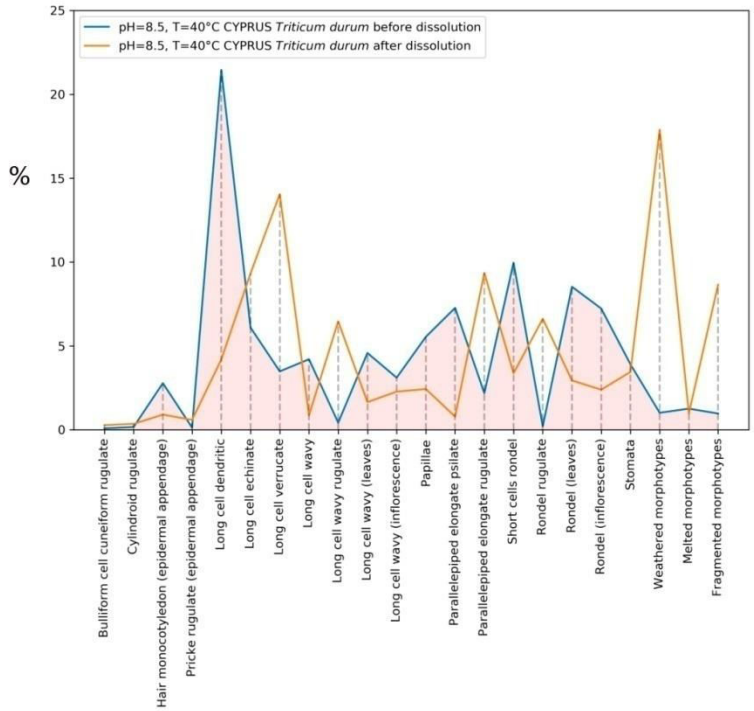

Fig. 71 The absolute value for the presence of phytolith morphotypes (Cyprus, *Triticum durum*). Blue line represents data before dissolution and orange line after dissolution (pH=8.5 and T=40˚C)

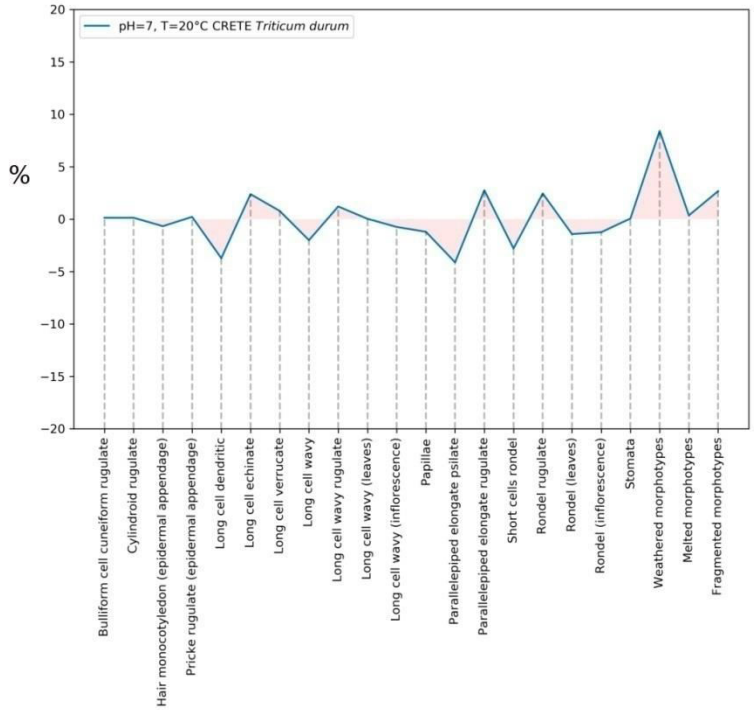

Fig. 72 The relative difference between the presence of phytolith morphotypes (Crete, *Triticum durum*) before and after the dissolution experiments (pH=7, T=20˚C)

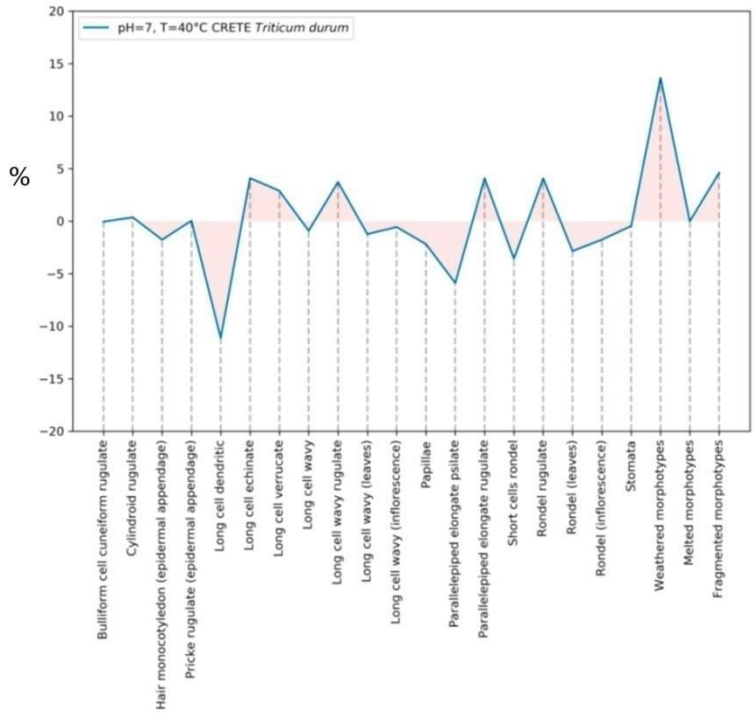

Fig. 73 The relative difference between the presence of phytolith morphotypes (Crete, *Triticum durum*) before and after the dissolution experiments (pH=7, T=40˚C)

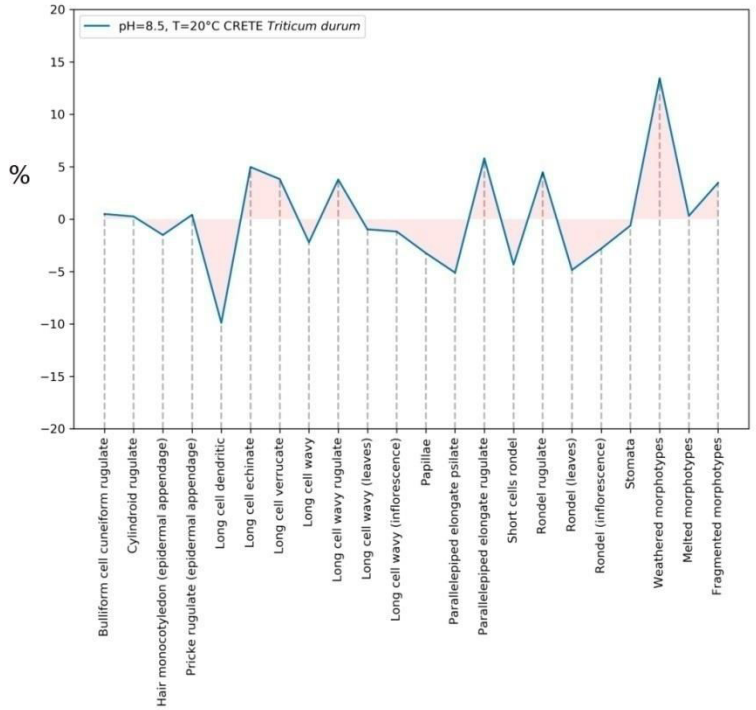

Fig. 74 The relative difference between the presence of phytolith morphotypes (Crete, *Triticum durum*) before and after the dissolution experiments (pH=8.5, T=20˚C)

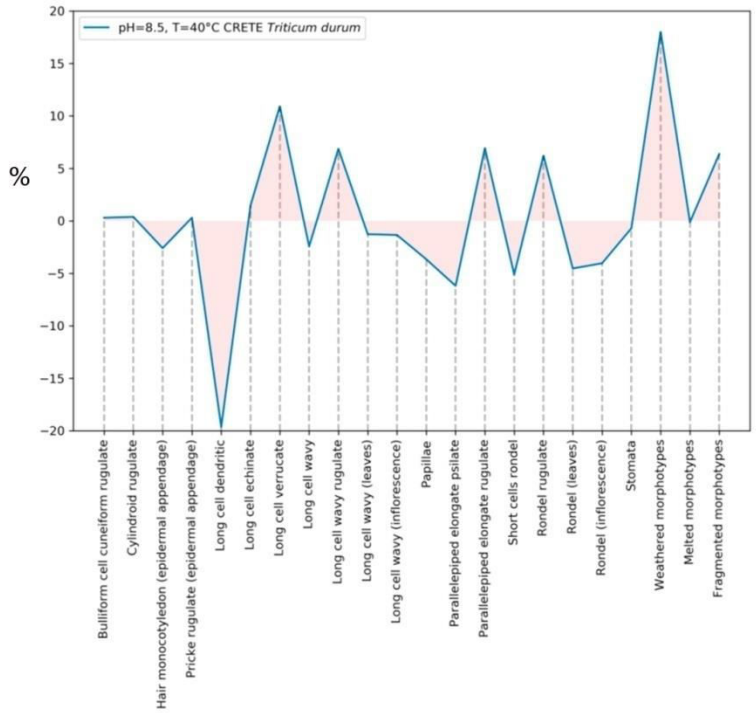

Fig. 75 The relative difference between the presence of phytolith morphotypes (Crete, *Triticum durum*) before and after the dissolution experiments (pH=8.5, T=40˚C)

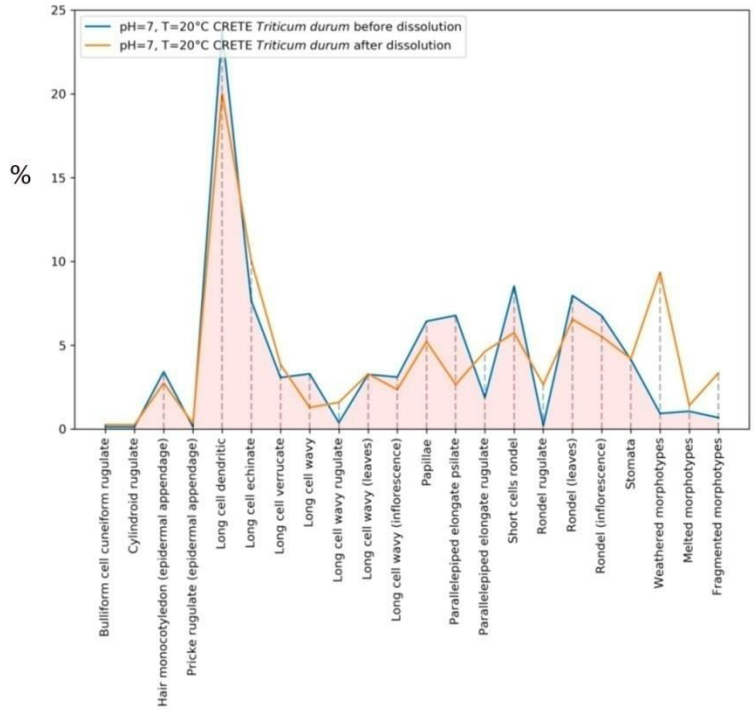

Fig. 76 The absolute value for the presence of phytolith morphotypes (Crete, *Triticum durum*). Blue line represents data before dissolution and orange line after dissolution (pH=7 and T=20˚C)

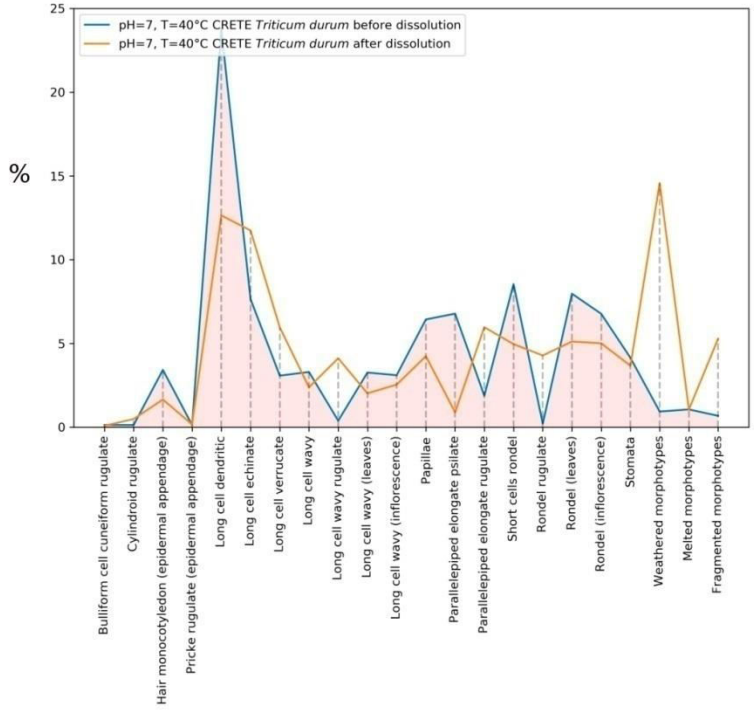

Fig. 77 The absolute value for the presence of phytolith morphotypes (Crete, *Triticum durum*). Blue line represents data before dissolution and orange line after dissolution (pH=7 and T=40˚C)

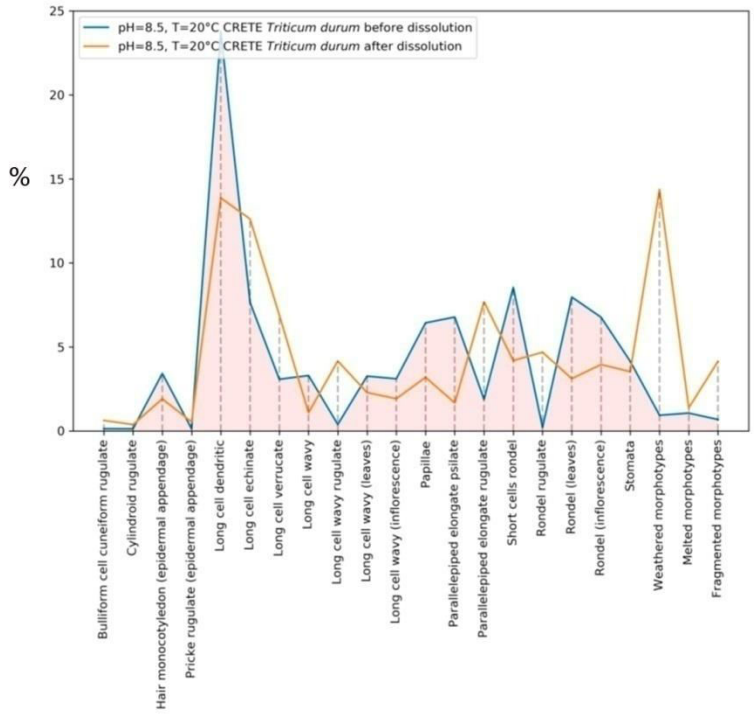

Fig. 78 The absolute value for the presence of phytolith morphotypes (Crete, *Triticum durum*). Blue line represents data before dissolution and orange line after dissolution (pH=8.5 and T=20˚C)

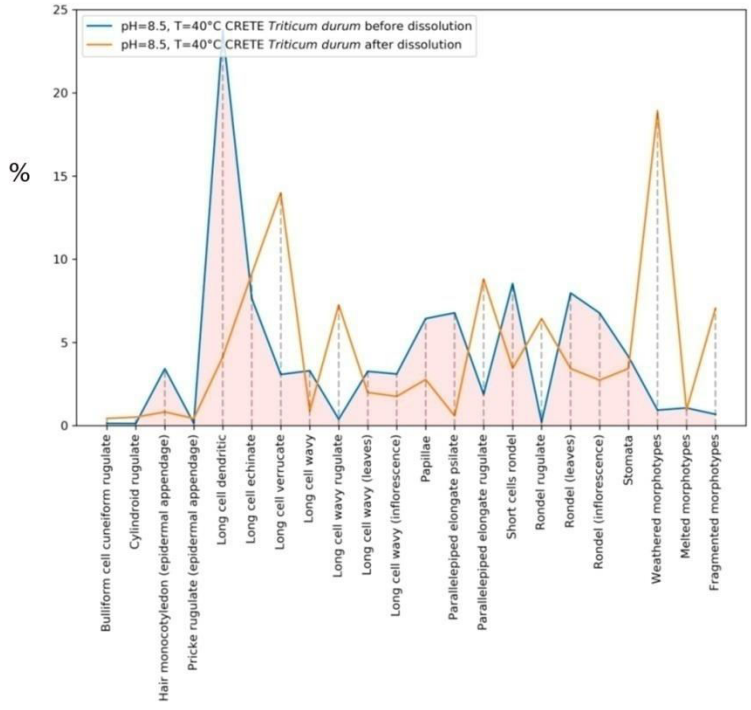

Fig. 79 The absolute value for the presence of phytolith morphotypes (Crete, *Triticum durum*). Blue line represents data before dissolution and orange line after dissolution (pH=8.5 and T=40˚C)

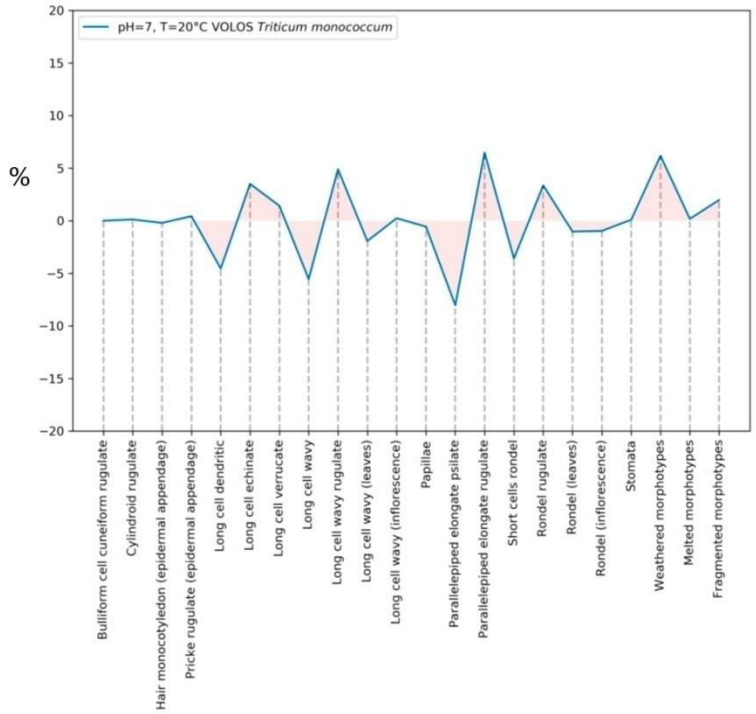

Fig. 80 The relative difference between the presence of phytolith morphotypes (Volos, *Triticum monococcum*) before and after the dissolution (pH=7, T=20˚C)

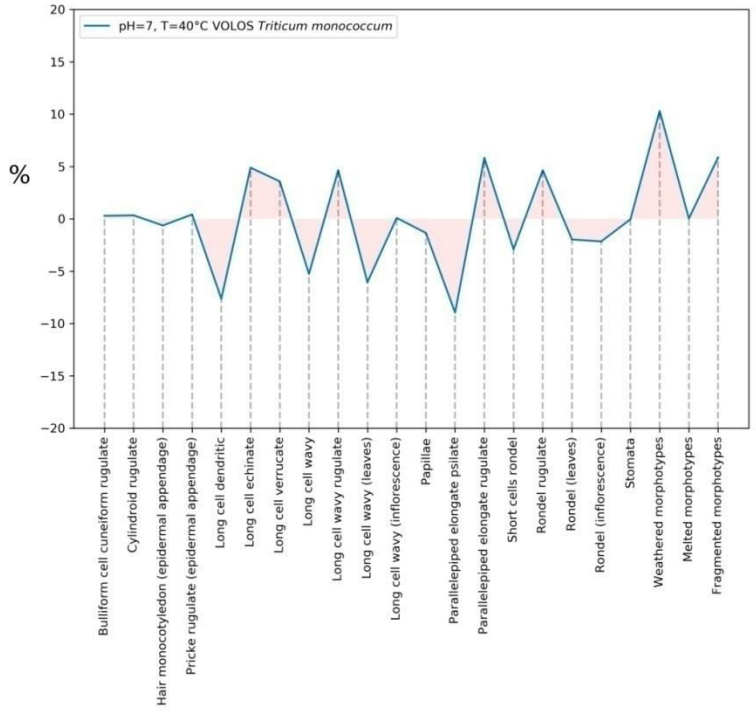

Fig. 81 The relative difference between the presence of phytolith morphotypes (Volos, *Triticum monococcum*) before and after the dissolution (pH=7 and T=40˚C)

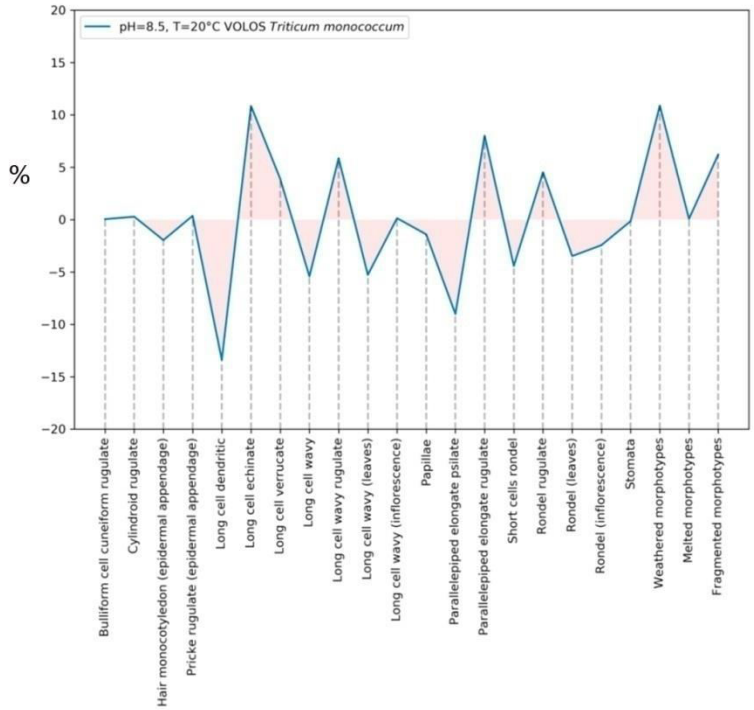

Fig. 82 The relative difference between the presence of phytolith morphotypes (Volos, *Triticum monococcum*) before and after the dissolution (pH=8.5, T=20˚C)

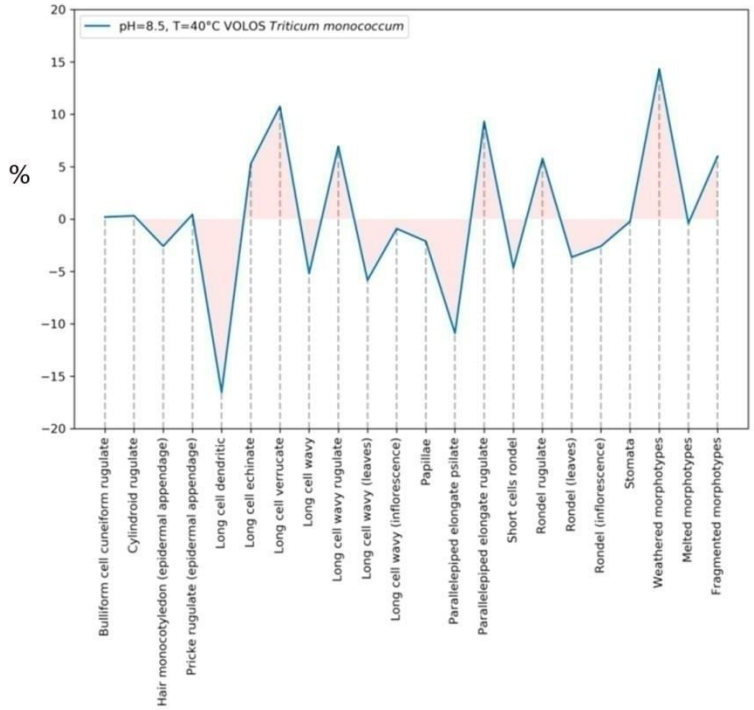

Fig. 83 The relative difference between the presence of phytolith morphotypes (Volos, *Triticum monococcum*) before and after the dissolution (pH=8.5 and T=40˚C)

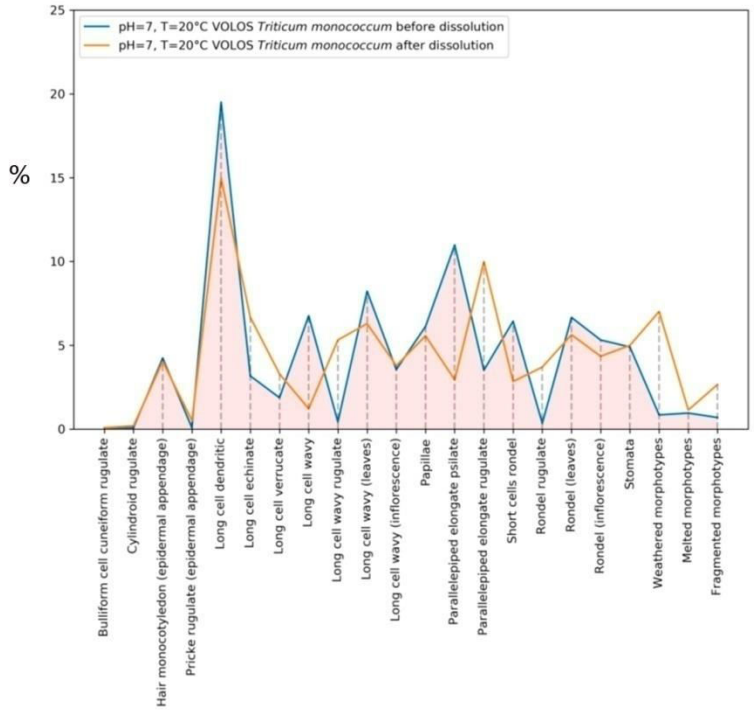

Fig. 84 The absolute value for the presence of phytolith morphotypes (Volos, *Triticum durum*). Blue line represents data before dissolution and orange line after dissolution (pH=7 and T=20˚C)

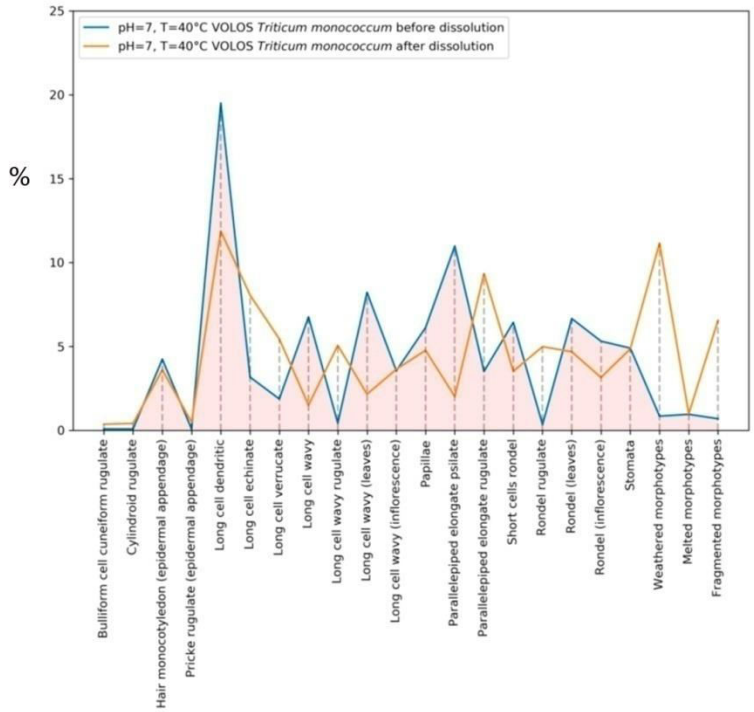

Fig. 85 The absolute value for the presence of phytolith morphotypes (Volos, *Triticum durum*). Blue line represents data before dissolution and orange line after dissolution (pH=7 and T=40˚C)

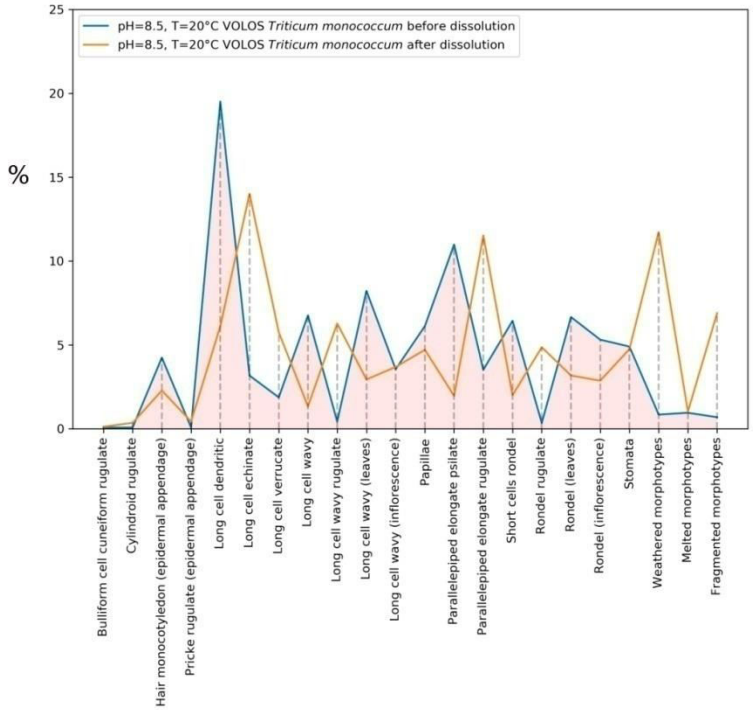

Fig. 86 The absolute value for the presence of phytolith morphotypes (Volos, *Triticum durum*). Blue line represents data before dissolution and orange line after dissolution (pH=8.5 and T=20˚C)

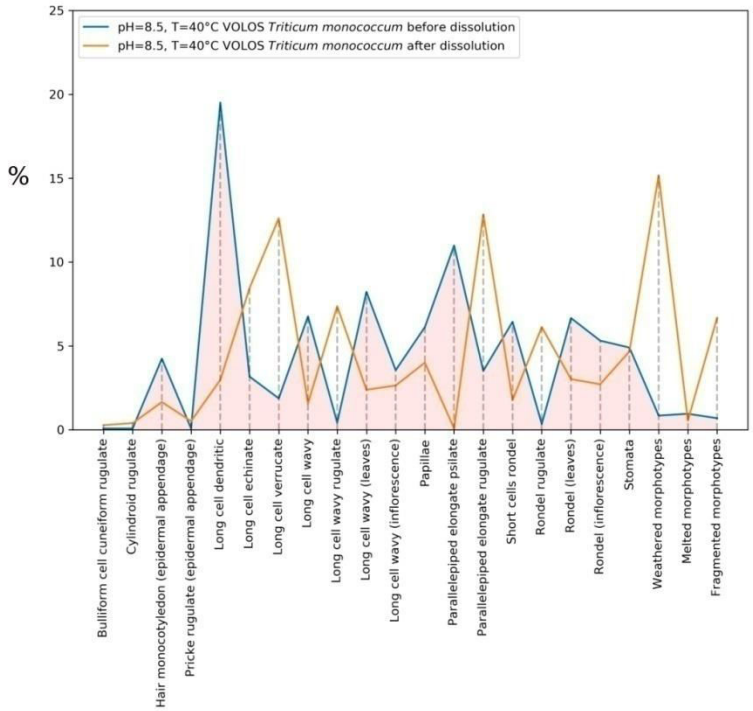

Fig. 87 The absolute value for the presence of phytolith morphotypes (Volos, *Triticum durum*). Blue line represents data before dissolution and orange line after dissolution (pH=8.5 and T=40˚C)

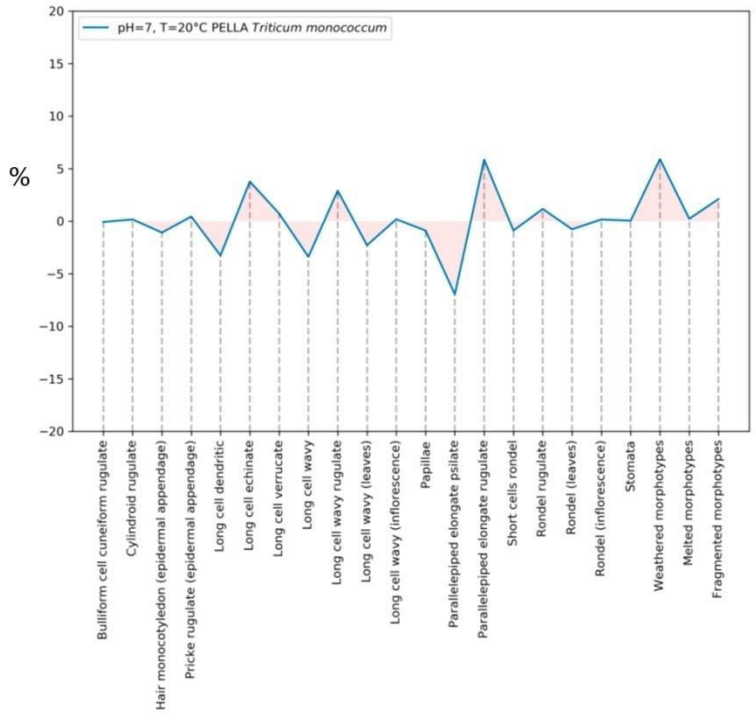

Fig. 88 The relative difference between the presence of phytolith morphotypes (Pella I, *Triticum monococcum*) before and after the dissolution (pH=7 and T=20˚C)

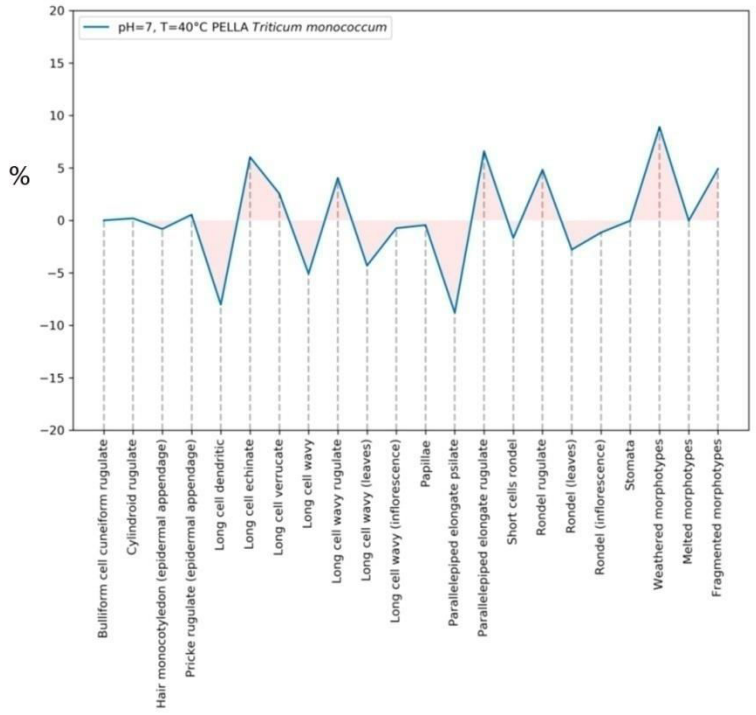

Fig. 89 The relative difference between the presence of phytolith morphotypes (Pella I, *Triticum monococcum*) before and after the dissolution (pH=7 and T=40˚C)

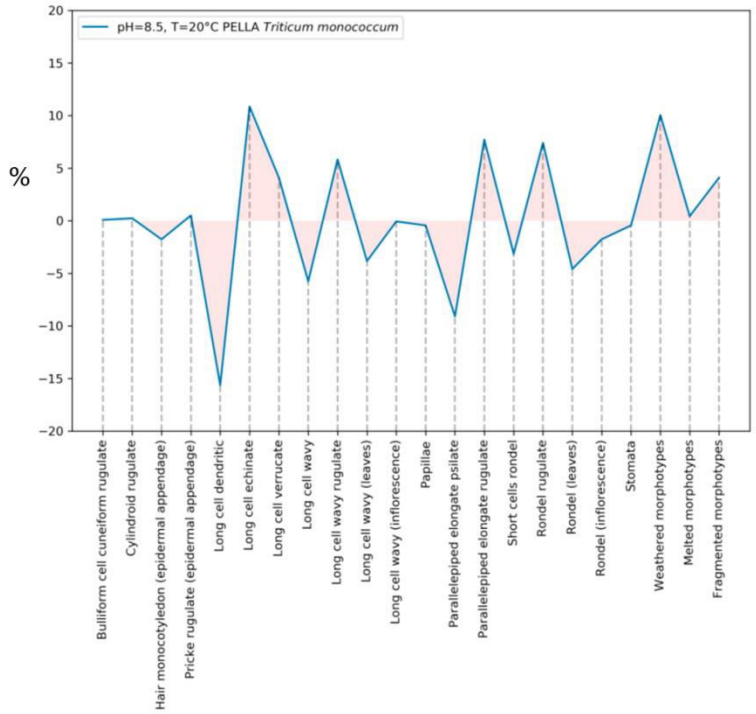

Fig. 90 The relative difference between the presence of phytolith morphotypes (Pella I, *Triticum monococcum*) before and after the dissolution (pH=8.5 and T=20˚C)

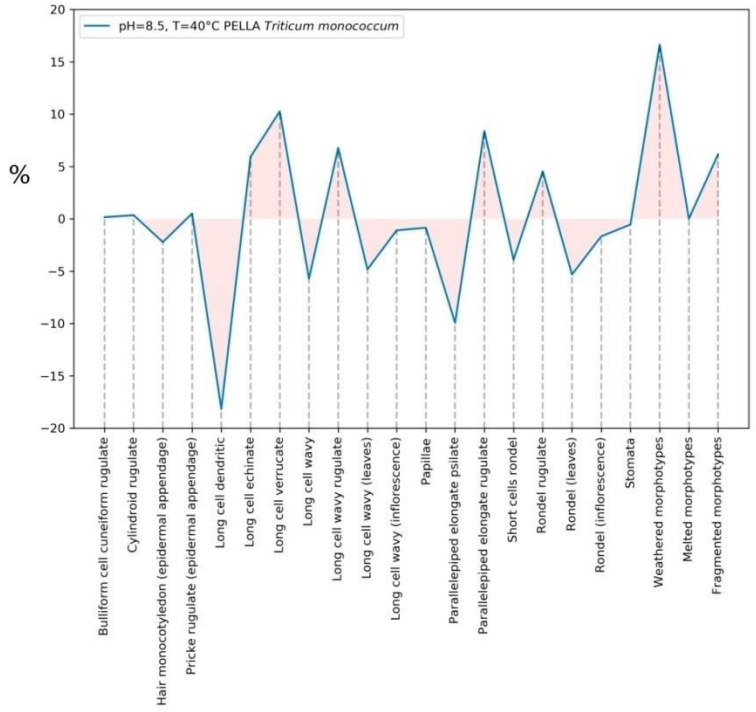

Fig. 91 The relative difference between the presence of phytolith morphotypes (Pella I, *Triticum monococcum*) before and after the dissolution (pH=8.5 and T=40˚C)

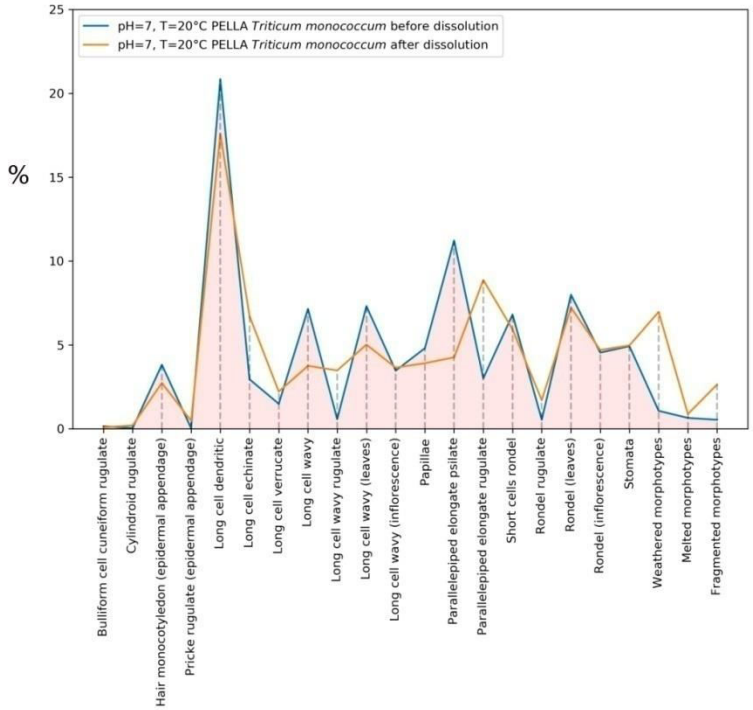

Fig. 92 The absolute value for the presence of phytolith morphotypes (Pella I, *Triticum monococcum*). Blue line represents data before dissolution and orange line after dissolution (pH=7 and T=20˚C)

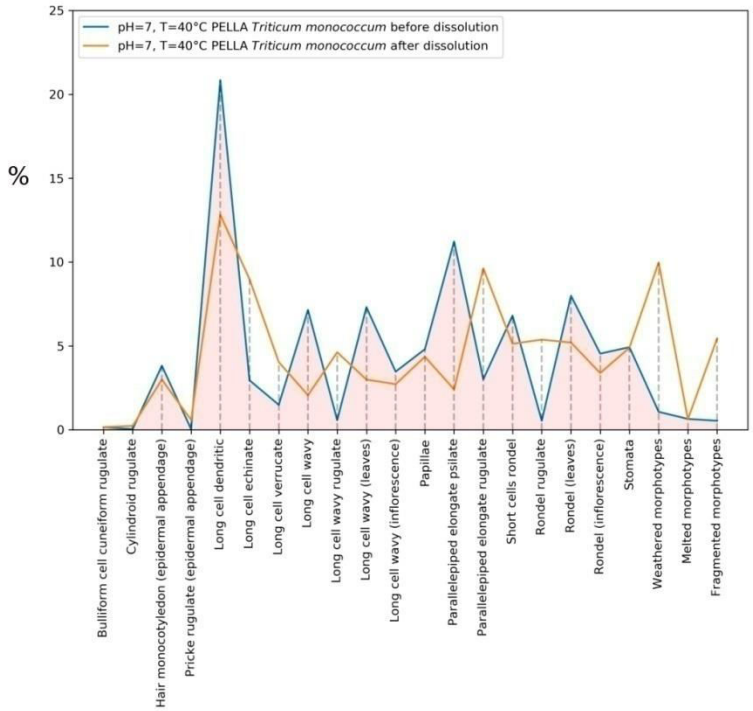

Fig. 93 The absolute value for the presence of phytolith morphotypes (Pella I, *Triticum monococcum*). Blue line represents data before dissolution and orange line after dissolution (pH=7 and T=40˚C)

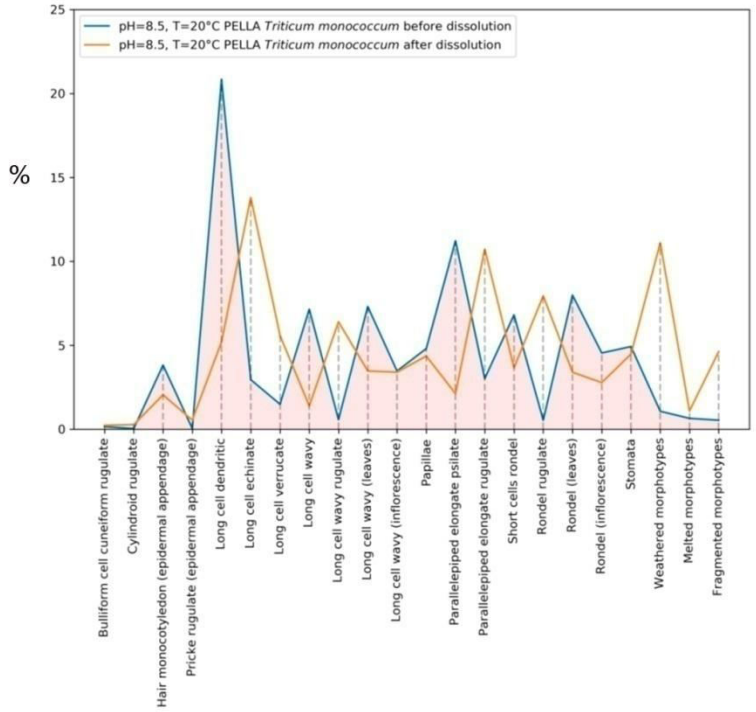

Fig. 94 The absolute value for the presence of phytolith morphotypes (Pella I, *Triticum monococcum*). Blue line represents data before dissolution and orange line after dissolution (pH=8.5 and T=20˚C)

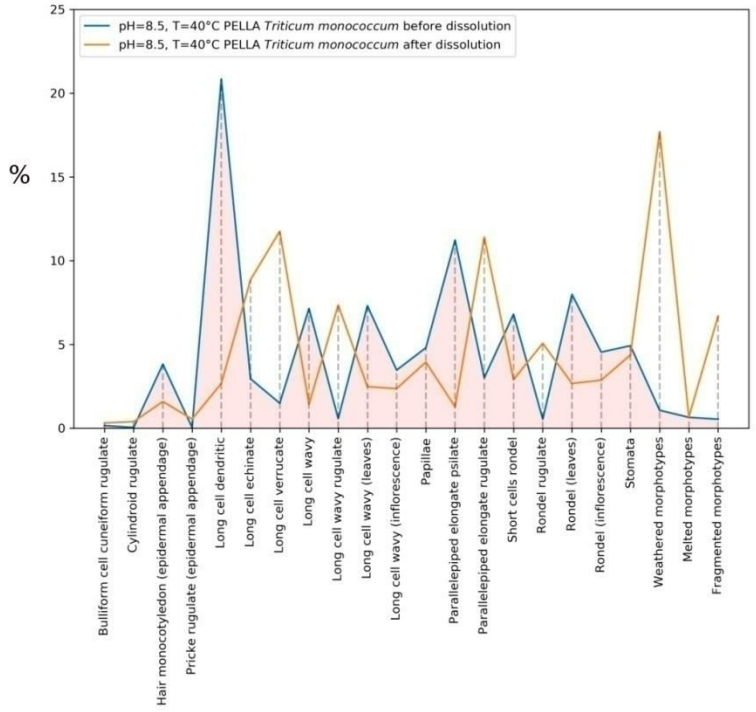

Fig. 95 The absolute value for the presence of phytolith morphotypes (Pella I, *Triticum monococcum*). Blue line represents data before dissolution and orange line after dissolution (pH=8.5 and T=40˚C)

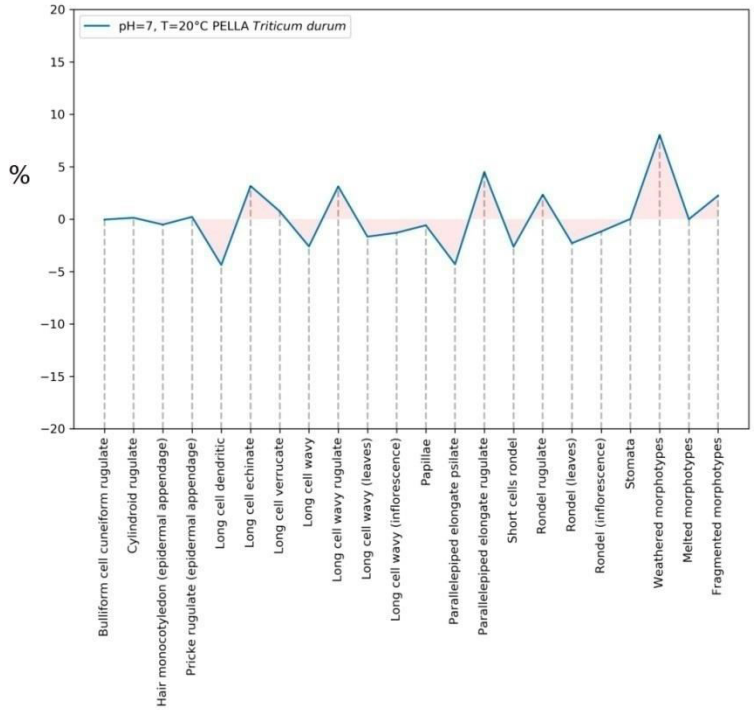

Fig. 96 The relative difference between the presence of phytolith morphotypes (Pella II, *Triticum durum*) before and after the dissolution (pH=7 and T=20˚C)

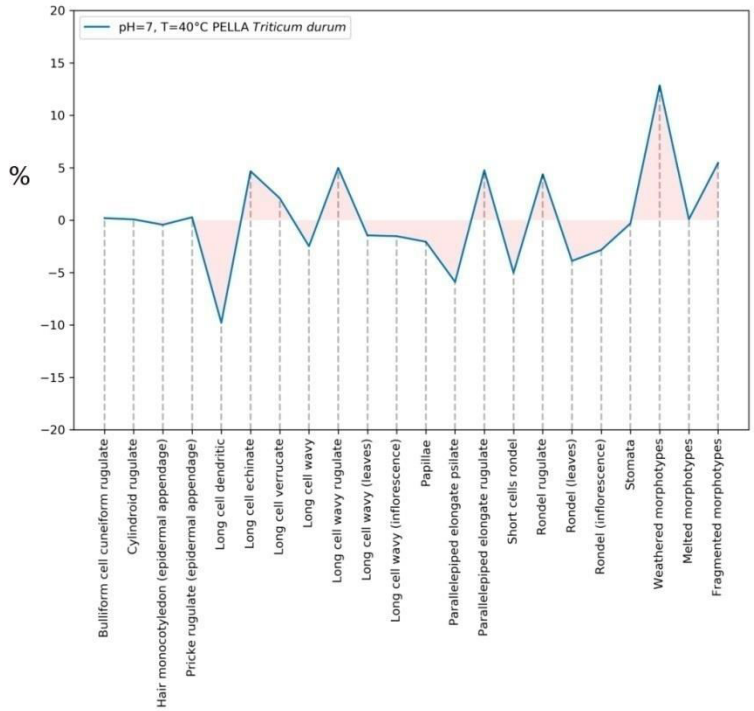

Fig. 97 The relative difference between the presence of phytolith morphotypes (Pella II, *Triticum durum*) before and after the dissolution (pH=7 and T=40˚C)

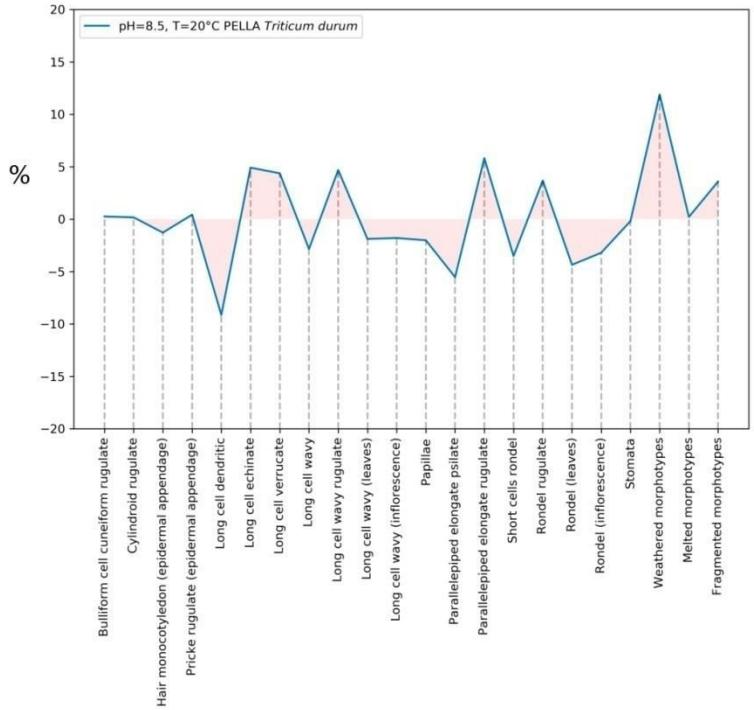

Fig. 98 The relative difference between the presence of phytolith morphotypes (Pella II, *Triticum durum*) before and after the dissolution (pH=8.5 and T=20˚C)

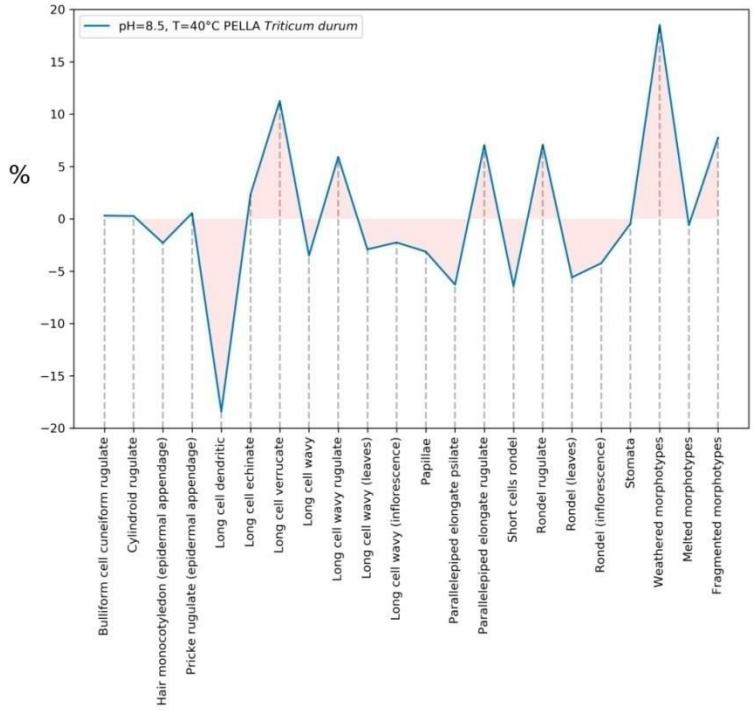

Fig. 99 The relative difference between the presence of phytolith morphotypes (Pella II, *Triticum durum*) before and after the dissolution (pH=8.5 and T=40˚C)

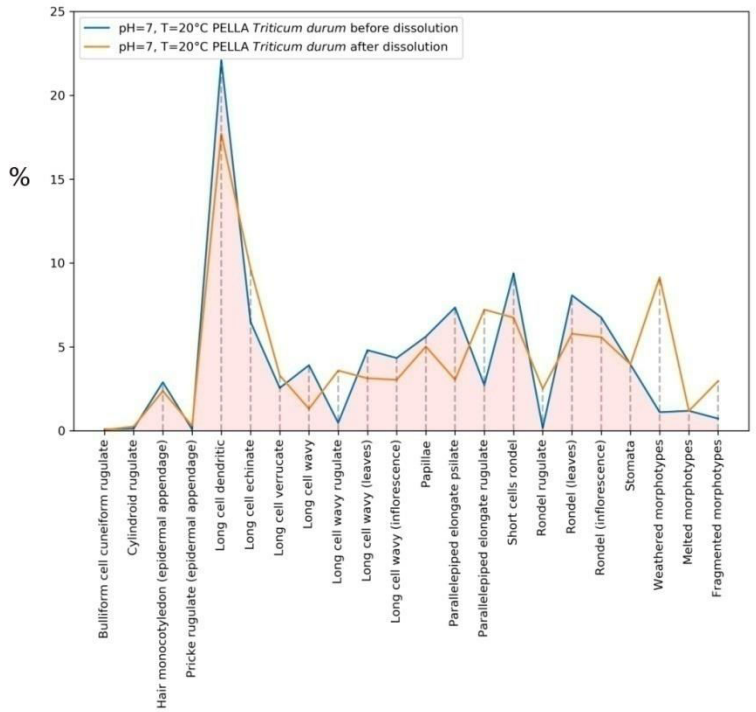

Fig. 100 The absolute value for the presence of phytolith morphotypes (Pella II, *Triticum durum*). Blue line represents data before dissolution and orange line after dissolution (pH=7 and T=20˚C)

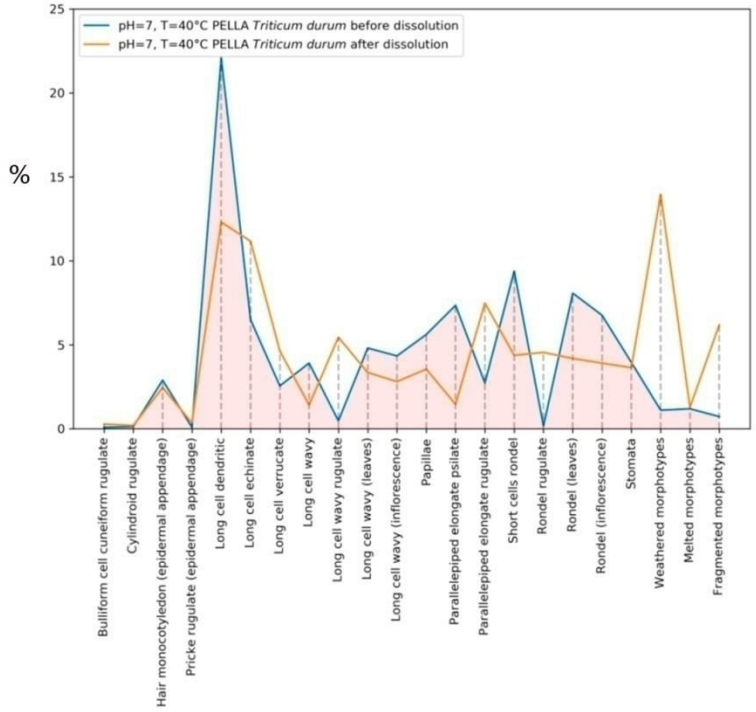

Fig. 101 The absolute value for the presence of phytolith morphotypes (Pella II, *Triticum durum).* Blue line represents data before dissolution and orange line after dissolution (pH=7 and T=40˚C)

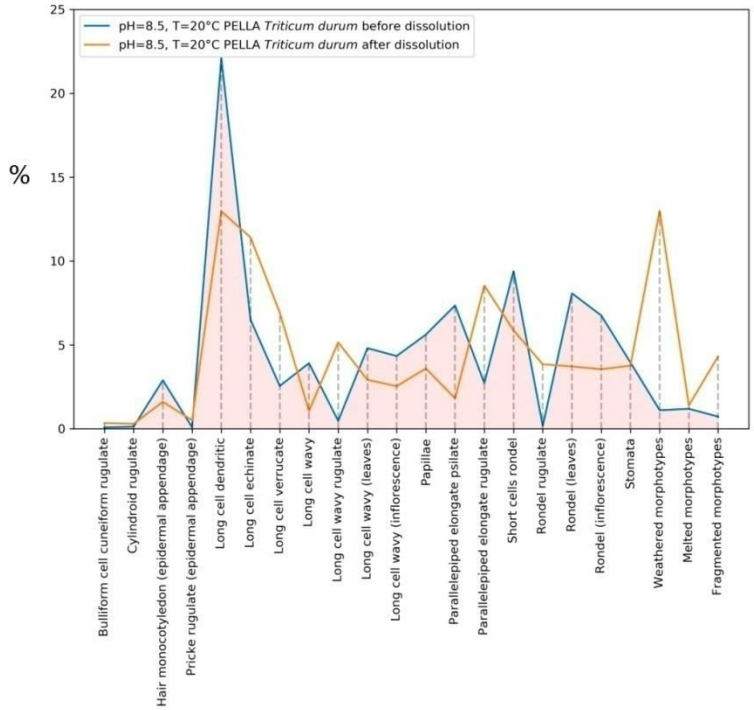

Fig. 102 The absolute value for the presence of phytolith morphotypes (Pella II, *Triticum durum*). Blue line represents data before dissolution and orange line after dissolution (pH=8.5 and T=20˚C)

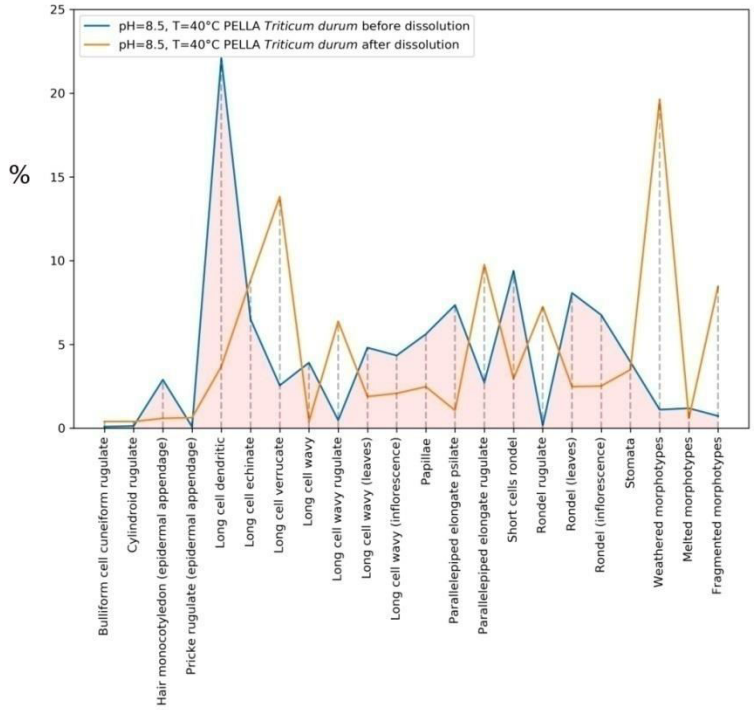

Fig. 103 The absolute value for the presence of phytolith morphotypes (Pella II, *Triticum durum*). Blue line represents data before dissolution and orange line after dissolution (pH=8.5 and T=40˚C)

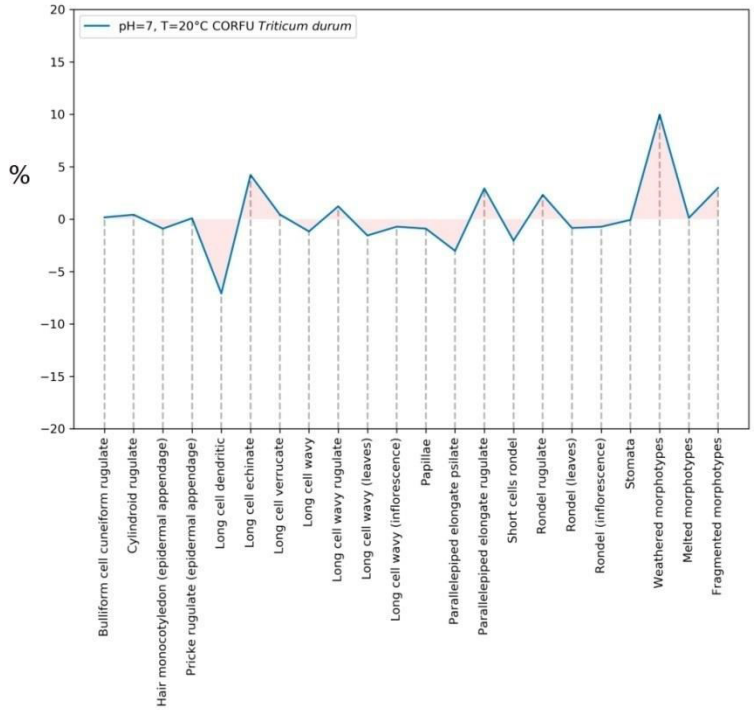

Fig. 104 The relative difference between the presence of phytolith morphotypes (Corfu, *Triticum durum*) before and after the dissolution (pH=7 and T=20˚C)

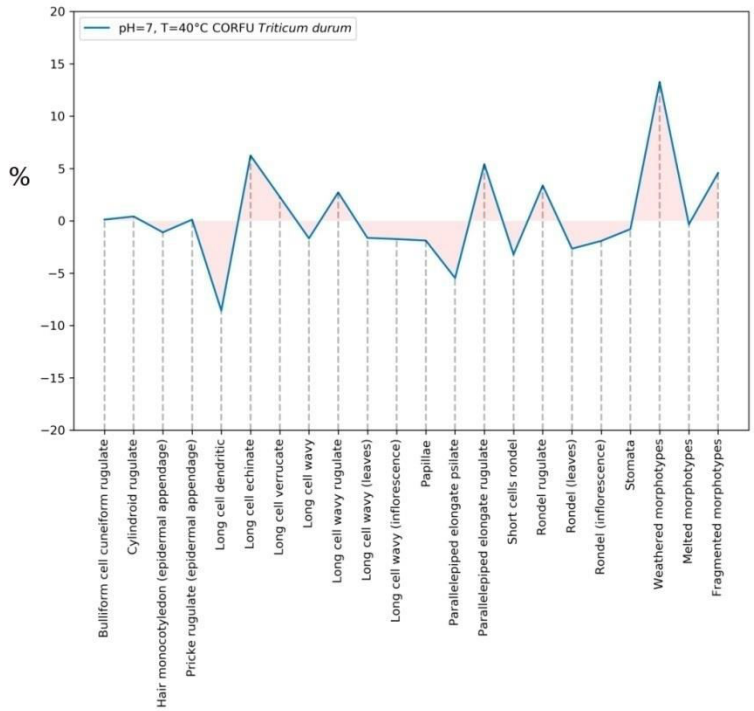

Fig. 105 The relative difference between the presence of phytolith morphotypes (Corfu, *Triticum durum*) before and after the dissolution (pH=7 and T=40˚C)

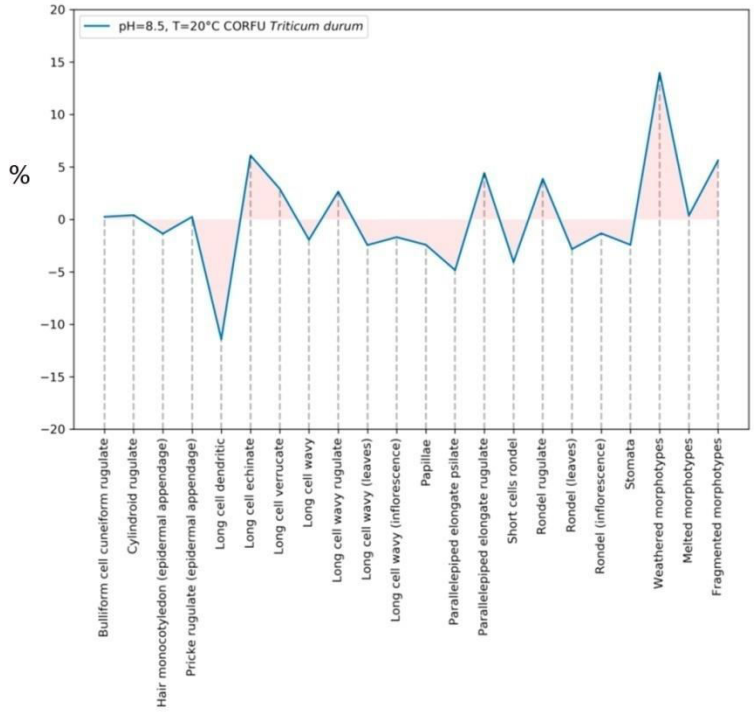

Fig. 106 The relative difference between the presence of phytolith morphotypes (Corfu, *Triticum durum*) before and after the dissolution (pH=8.5 and T=20˚C)

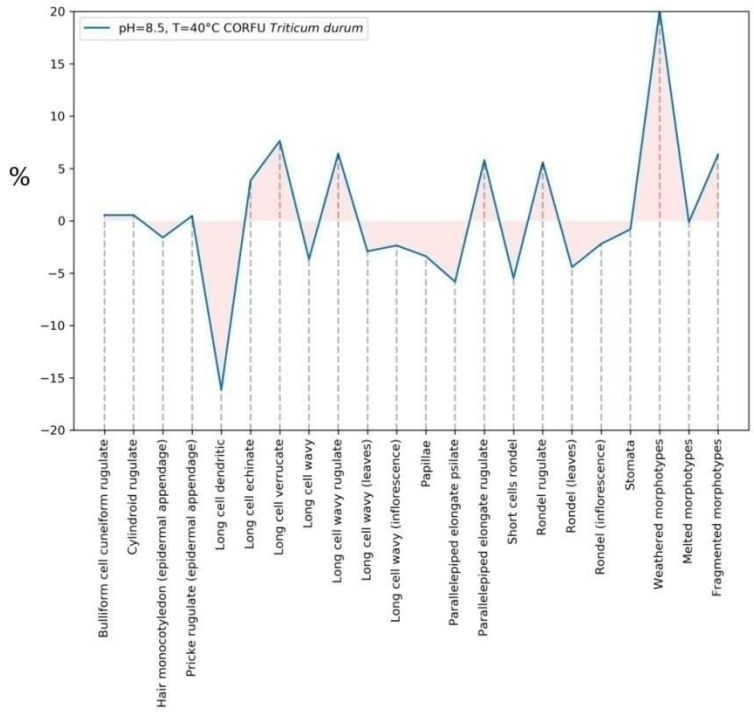

Fig. 107 The relative difference between the presence of phytolith morphotypes (Corfu, *Triticum durum*) before and after the dissolution (pH=8.5 and T=40˚C)

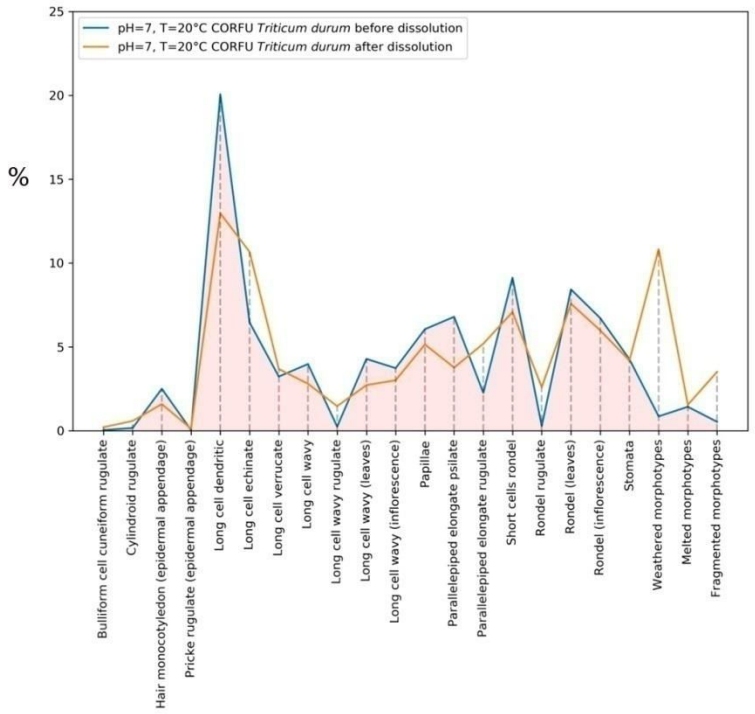

Fig. 108 The absolute value for the presence of phytolith morphotypes (Corfu, *Triticum durum*). Blue line represents data before dissolution and orange line after dissolution (pH=7 and T=20˚C)

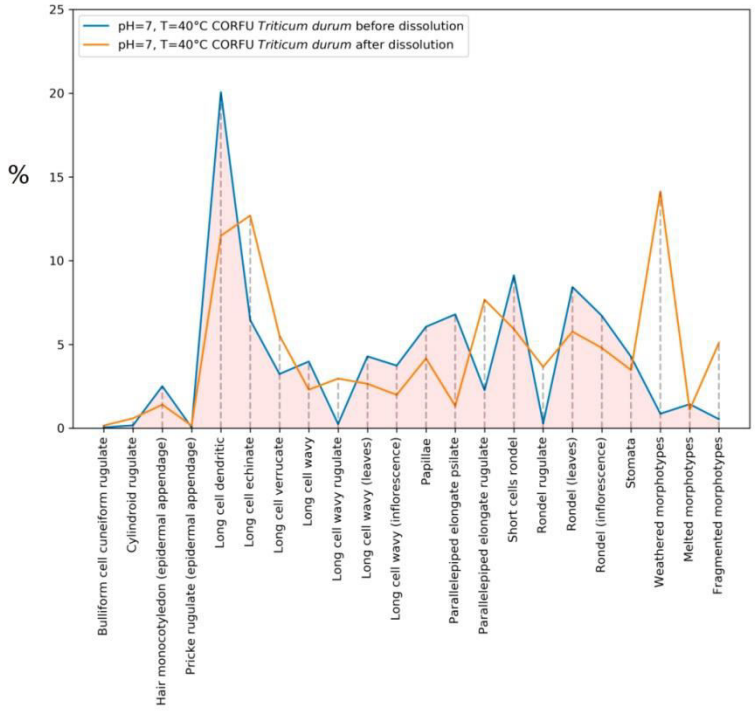

Fig. 109 The absolute value for the presence of phytolith morphotypes (Corfu, *Triticum durum*). Blue line represents data before dissolution and orange line after dissolution (pH=7 and T=40˚C)

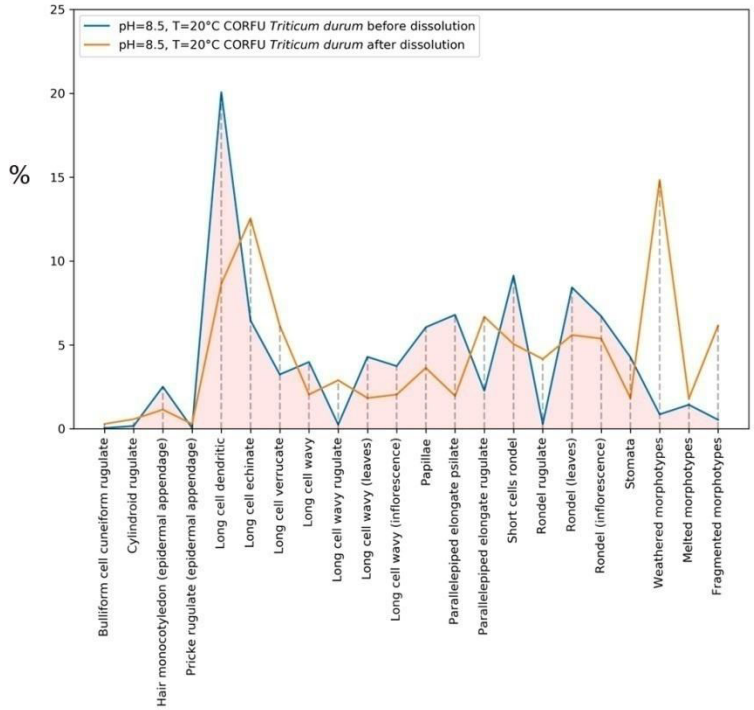

Fig. 110 The absolute value for the presence of phytolith morphotypes (Corfu, *Triticum durum*). Blue line represents data before dissolution and orange line after dissolution (pH=8.5 and T=20˚C)

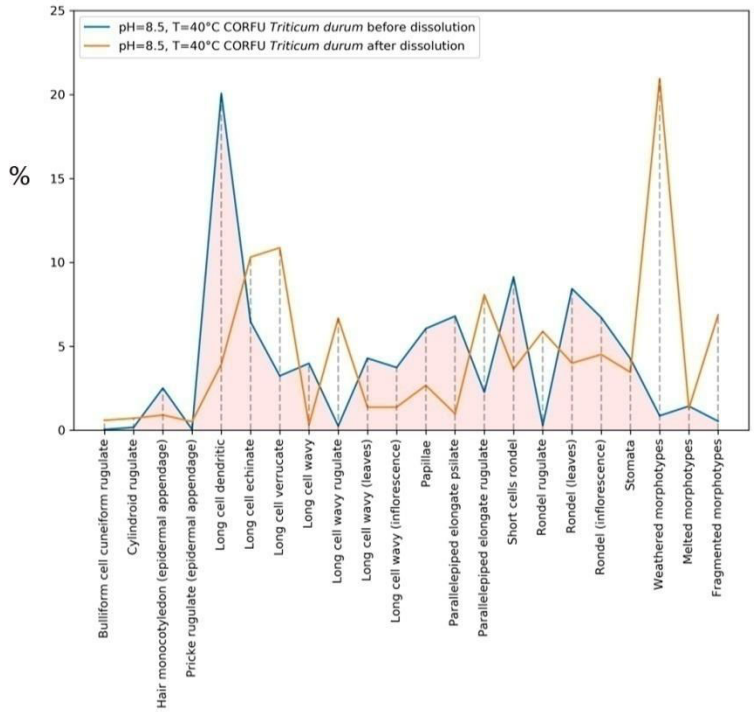

Fig. 111 The absolute value for the presence of phytolith morphotypes (Corfu, *Triticum durum*). Blue line represents data before dissolution and orange line after dissolution (pH=8.5 and T=40˚C)

Appendix – part 2

(Phytolith dissolution – Concentration of elements)

* Tables 21-26 show the concentration (mg/g) of the studied elements (Mg, Al, Si, K, Ca, Fe, Sr, Ba) from phytoliths over the course of 75 days. The standard deviation for the repetition of two measurements of the concentration is given. Dissolution was carried out in batch experiments at pH (5, 7, 8.5) and temperature (5, 20, 40 ˚C); by adding 0.15 g of phytoliths that were extracted from entire wheat (excluding roots) in 45 mL of H_2O. Code 1-5-5-1 is for sample 1, pH 5, temperature 5, day 1 etc.

1. CYPRUS

Sample	Mg	Al	Si	K	Ca	Fe	Sr	Ba
	(mg/g)	(mg/g)	(mg/g)	(mg/g)	(mg/g)	(mg/g)	(mg/g)	(mg/g)
1-5-5-1	5.2945	<DL	5.2304	5.8220	9.0971	0.0002	0.0439	0.0046
	5.7789	<DL	6.5046	5.9133	13.6005	0.0002	0.0474	0.0048
	5.7612	<DL	6.7487	5.8926	14.0646	0.0003	0.0460	0.0058
1-5-5-5	5.7701	<DL	6.6266	5.9029	13.8325	0.0002	0.0467	0.0053
	0.0126	<DL	0.1726	0.0146	0.3281	0.00005	0.0010	0.0007
1-5-5-15	8.0020	<DL	7.6208	11.5219	16.5424	0.0005	0.0508	0.0062
	9.0023	<DL	10.5347	12.0864	16.6139	0.0006	0.0506	0.0065
	8.9350	<DL	10.2890	11.9130	16.1465	0.0005	0.0492	0.0070
1-5-5-30	8.9687	<DL	10.4118	11.9997	16.3802	0.0005	0.0499	0.0068
	0.0476	<DL	0.1737	0.1227	0.3305	0.0001	0.0009	0.0003
1-5-5-50	10.4658	<DL	10.0717	13.0861	15.7404	0.0005	0.0493	0.0088
	10.4499	<DL	10.2366	13.5962	15.5791	0.0004	0.0530	0.0097
	10.4757	<DL	10.2956	13.6815	15.5521	0.0008	0.0482	0.0090
1-5-5-75	10.4628	<DL	10.2661	13.6388	15.5656	0.0006	0.0506	0.0094
	0.0183	<DL	0.0417	0.0603	0.0191	0.0003	0.0034	0.0005

Sample	Mg	Al	Si	K	Ca	Fe	Sr	Ba
	(mg/g)	(mg/g)	(mg/g)	(mg/g)	(mg/g)	(mg/g)	(mg/g)	(mg/g)
1-5-20-1	5.6062	<DL	5.9879	6.3927	15.1986	0.0002	0.0531	0.0061
	5.6794	<DL	9.5724	6.5999	15.4751	0.0006	0.0533	0.0068
	5.9384	<DL	9.4282	6.4675	15.9554	0.0005	0.0561	0.0076
1-5-20-5	5.8089	<DL	9.5003	6.5337	15.7152	0.0006	0.0547	0.0072
	0.1832	<DL	0.1020	0.0936	0.3396	0.0001	0.0020	0.0005
1-5-20-15	6.4198	<DL	10.6145	10.5775	15.8590	0.0003	0.0593	0.0083
	8.4959	<DL	12.2956	19.8762	15.7056	0.0004	0.0557	0.0087
	8.2508	<DL	11.7477	19.5743	15.2436	0.0006	0.0557	0.0094
1-5-20-30	8.3734	<DL	12.0216	19.7252	15.4746	0.0005	0.0557	0.0090
	0.1733	<DL	0.3874	0.2135	0.3267	0.0001	0.0000	0.0005
1-5-20-50	11.9082	<DL	12.7284	21.2216	16.2609	0.0005	0.0608	0.0114
	11.7819	<DL	13.0128	21.3562	16.2408	0.0006	0.0628	0.0138
	12.6727	<DL	13.3696	21.5300	16.4006	0.0007	0.0630	0.0138
1-5-20-75	12.2273	<DL	13.1912	21.4431	16.3207	0.0006	0.0629	0.0138
	0.6299	<DL	0.2523	0.1229	0.1130	0.0001	0.0002	0.0001

Sample	Mg	Al	Si	K	Ca	Fe	Sr	Ba
	(mg/g)	(mg/g)	(mg/g)	(mg/g)	(mg/g)	(mg/g)	(mg/g)	(mg/g)
1-5-40-1	6.5351	<DL	11.0120	6.7311	16.1804	<DL	0.0590	0.0092
	8.0430	<DL	16.4680	11.1219	17.3860	<DL	0.0567	0.0098
	7.7896	<DL	15.9121	10.8818	16.8643	<DL	0.0587	0.0101
1-5-40-5	7.9163	<DL	16.1901	11.0019	17.1251	<DL	0.0577	0.0099
	0.1792	<DL	0.3931	0.1698	0.3689	<DL	0.0013	0.0002
1-5-40-15	8.5471	<DL	16.8896	13.6977	17.9883	<DL	0.0612	0.0126
	8.8981	<DL	16.8381	25.1745	17.4702	<DL	0.0632	0.0129
	9.1731	<DL	16.8660	25.2529	17.4055	<DL	0.0627	0.0133
1-5-40-30	9.0356	<DL	16.8520	25.2137	17.4379	<DL	0.0629	0.0131
	0.1945	<DL	0.0198	0.0554	0.0457	<DL	0.0003	0.0003
1-5-40-50	9.7199	<DL	17.3516	26.4510	17.9064	<DL	0.0654	0.0152
	9.5542	<DL	17.3842	26.9778	18.7994	<DL	0.0643	0.0162
	10.2448	<DL	18.2681	27.4952	19.2003	<DL	0.0652	0.0171
1-5-40-75	9.8995	<DL	17.8261	27.2365	18.9999	<DL	0.0648	0.0167
	0.4883	<DL	0.6250	0.3659	0.2835	<DL	0.0007	0.0006

Sample	Mg (mg/g)	Al (mg/g)	Si (mg/g)	K (mg/g)	Ca (mg/g)	Fe (mg/g)	Sr (mg/g)	Ba (mg/g)
1-7-5-1	6.1311	<DL	8.9499	6.9738	9.7222	0.0008	0.0520	0.0060
	7.8074	<DL	11.1016	8.4518	11.0104	0.0007	0.0462	0.0066
	7.9494	<DL	11.3887	8.6278	11.0967	0.0007	0.0528	0.0057
1-7-5-5	7.8784	<DL	11.2452	8.5398	11.0535	0.0007	0.0495	0.0062
	0.1004	<DL	0.2030	0.1245	0.0610	0.00002	0.0046	0.0006
1-7-5-15	9.5913	<DL	15.3472	11.2393	14.1756	0.0008	0.0545	0.0070
	10.1764	<DL	15.0831	10.9603	14.7129	0.0008	0.0513	0.0071
	10.6178	<DL	16.1796	11.9046	15.3924	0.0002	0.0530	0.0106
1-7-5-30	10.3971	<DL	15.6313	11.4324	15.0527	0.0005	0.0521	0.0088
	0.3121	<DL	0.7754	0.6677	0.4805	0.0004	0.0012	0.0025
1-7-5-50	10.0446	<DL	15.3778	14.6393	15.2105	0.0006	0.0514	0.0106
	10.3462	<DL	16.9878	15.2386	16.0864	0.0005	0.0533	0.0117
	11.4455	<DL	14.6183	15.5362	16.7558	0.0007	0.0557	0.0101
1-7-5-75	10.8958	<DL	15.8030	15.3874	16.4211	0.0006	0.0545	0.0109
	0.7774	<DL	1.6755	0.2104	0.4733	0.0002	0.0017	0.0011

Sample	Mg (mg/g)	Al (mg/g)	Si (mg/g)	K (mg/g)	Ca (mg/g)	Fe (mg/g)	Sr (mg/g)	Ba (mg/g)
1-7-20-1	7.8402	<DL	11.4733	6.9781	11.1112	0.0005	0.0564	0.0120
	8.6147	<DL	14.2617	8.3175	11.3133	0.0008	0.0567	0.0131
	8.6880	<DL	14.4688	7.9944	11.4012	0.0006	0.0559	0.0133
1-7-20-5	8.6514	<DL	14.3652	8.1560	11.3573	0.0007	0.0563	0.0132
	0.0518	<DL	0.1465	0.2285	0.0621	0.0002	0.0006	0.0002
1-7-20-15	8.6424	<DL	15.0000	11.0235	16.4570	0.0007	0.0534	0.0120
	11.7394	<DL	17.9981	15.4762	17.2135	0.0004	0.0639	0.0169
	11.3782	<DL	18.2541	15.1152	16.6230	0.0007	0.0623	0.0179
1-7-20-30	11.5588	<DL	18.1261	15.2957	16.9183	0.0005	0.0631	0.0174
	0.2554	<DL	0.1810	0.2552	0.4175	0.0002	0.0011	0.0007
1-7-20-50	12.2555	<DL	18.9846	23.6182	20.1331	0.0009	0.0652	0.0188
	11.4842	<DL	19.7720	22.4375	19.7896	0.0009	0.0622	0.0186
	13.1263	<DL	24.4481	23.9272	20.6666	0.0009	0.0597	0.0190
1-7-20-75	12.3052	<DL	22.1101	23.1824	20.2281	0.0009	0.0609	0.0188
	1.1611	<DL	3.3065	1.0534	0.6201	0.00003	0.0018	0.0003

Sample	Mg (mg/g)	Al (mg/g)	Si (mg/g)	K (mg/g)	Ca (mg/g)	Fe (mg/g)	Sr (mg/g)	Ba (mg/g)
1-7-40-1	8.1020	<DL	14.1375	8.3602	12.2017	<DL	0.0592	0.0133
	8.7636	<DL	14.6107	8.4740	13.4413	<DL	0.0607	0.0149
	8.3225	<DL	15.2526	8.5490	13.7953	<DL	0.0619	0.0151
1-7-40-5	8.5431	<DL	14.9316	8.5115	13.6183	<DL	0.0613	0.0150
	0.3119	<DL	0.4539	0.0530	0.2504	<DL	0.0008	0.0002
1-7-40-15	9.2486	<DL	18.4329	10.8543	15.8638	<DL	0.0649	0.0190
	9.1675	<DL	19.0994	19.8393	16.6582	<DL	0.0641	0.0188
	9.5730	<DL	19.9761	20.8597	17.5191	<DL	0.0627	0.0207
1-7-40-30	9.3702	<DL	19.5377	20.3495	17.0887	<DL	0.0634	0.0198
	0.2867	<DL	0.6199	0.7216	0.6088	<DL	0.0011	0.0014
1-7-40-50	11.2839	<DL	19.8872	26.5056	17.4057	<DL	0.0666	0.0216
	12.6162	<DL	19.3891	29.2859	20.2756	<DL	0.0666	0.0224
	12.7568	<DL	20.2783	29.4866	20.6097	<DL	0.0649	0.0232
1-7-40-75	12.6865	<DL	19.8337	29.3862	20.4426	<DL	0.0658	0.0228
	0.0994	<DL	0.6287	0.1419	0.2363	<DL	0.0012	0.0006

Sample	Mg (mg/g)	Al (mg/g)	Si (mg/g)	K (mg/g)	Ca (mg/g)	Fe (mg/g)	Sr (mg/g)	Ba (mg/g)
1-8.5-5-1	6.5659	<DL	7.4163	7.6874	4.4523	0.0004	0.0523	0.0068
	7.7882	<DL	7.4211	8.7179	5.1602	0.0005	0.0488	0.0074
	7.8989	<DL	7.5176	9.3064	5.5026	0.0007	0.0467	0.0080
1-8.5-5-5	7.8435	<DL	7.4693	9.0122	5.3314	0.0006	0.0477	0.0077
	0.0783	<DL	0.0683	0.4161	0.2421	0.0001	0.0015	0.0004
1-8.5-5-15	8.6029	<DL	9.5167	10.0851	7.0352	0.0005	0.0535	0.0098
	8.6043	<DL	12.6050	12.2259	9.6136	0.0008	0.0600	0.0116
	8.2631	<DL	12.6984	11.9132	9.8186	0.0006	0.0617	0.0110
1-8.5-5-30	8.4337	<DL	12.6517	12.0695	9.7161	0.0007	0.0609	0.0113
	0.2413	<DL	0.0660	0.2211	0.1449	0.0001	0.0012	0.0004
1-8.5-5-50	8.7342	<DL	14.1829	15.5731	11.0127	0.0005	0.0646	0.0116
	10.6302	<DL	14.9905	16.5499	11.4580	0.0008	0.0486	0.0114
	11.3110	<DL	15.4555	17.1033	12.2089	0.0008	0.0645	0.0117
1-8.5-5-75	10.9706	<DL	15.2230	16.8266	11.8334	0.0008	0.0566	0.0116
	0.4814	<DL	0.3289	0.3913	0.5310	0.00003	0.0113	0.0002

Sample	Mg (mg/g)	Al (mg/g)	Si (mg/g)	K (mg/g)	Ca (mg/g)	Fe (mg/g)	Sr (mg/g)	Ba (mg/g)
1-8.5-20-1	6.8687	<DL	7.1849	7.3512	4.8559	0.0008	0.0652	0.0120
	7.1750	<DL	8.0759	9.4594	5.2123	0.0009	0.0616	0.0146
	7.2751	<DL	8.3918	9.4760	5.2329	0.0005	0.0660	0.0163
1-8.5-20-5	7.2250	<DL	8.2339	9.4677	5.2226	0.0007	0.0638	0.0154
	0.0708	<DL	0.2234	0.0117	0.0146	0.0002	0.0031	0.0012
1-8.5-20-15	7.8419	<DL	13.3506	11.7628	10.8879	0.0010	0.0673	0.0177
	10.4116	<DL	13.5283	12.3717	10.4758	0.0009	0.0609	0.0182
	10.6689	<DL	13.7508	13.1875	11.3651	0.0008	0.0626	0.0175
1-8.5-20-30	10.5402	<DL	13.6396	12.7796	10.9204	0.0008	0.0618	0.0179
	0.1819	<DL	0.1573	0.5768	0.6289	0.00004	0.0012	0.0004
1-8.5-20-50	12.1601	<DL	16.2960	19.7306	11.9189	0.0008	0.0707	0.0194
	11.6026	<DL	16.5384	23.3654	11.6045	0.0009	0.0666	0.0204
	13.0020	<DL	17.6375	24.2073	12.5795	0.0008	0.0635	0.0228
1-8.5-20-75	12.3023	<DL	17.0879	23.7863	12.0920	0.0009	0.0651	0.0216
	0.9895	<DL	0.7771	0.5953	0.6895	0.00002	0.0022	0.0017

Sample	Mg (mg/g)	Al (mg/g)	Si (mg/g)	K (mg/g)	Ca (mg/g)	Fe (mg/g)	Sr (mg/g)	Ba (mg/g)
1-8.5-40-1	3.0453	<DL	9.0657	8.4640	5.7191	<DL	0.0595	0.0144
	3.1650	<DL	9.5634	9.9107	6.1880	<DL	0.0676	0.0166
	3.2322	<DL	9.8615	10.0594	6.2335	<DL	0.0653	0.0169
1-8.5-40-5	3.1986	<DL	9.7125	9.9850	6.2107	<DL	0.0664	0.0167
	0.0475	<DL	0.2108	0.1051	0.0322	<DL	0.0016	0.0002
1-8.5-40-15	3.3421	<DL	16.2085	14.8224	9.8486	<DL	0.0686	0.0207
	3.5321	<DL	16.1385	23.6877	10.1102	<DL	0.0692	0.0215
	3.5785	<DL	15.8384	24.7181	10.5040	<DL	0.0632	0.0214
1-8.5-40-30	3.5553	<DL	15.9885	24.2029	10.3071	<DL	0.0662	0.0214
	0.0328	<DL	0.2123	0.7286	0.2785	<DL	0.0043	0.0001
1-8.5-40-50	4.1443	<DL	17.0538	32.9152	11.0104	<DL	0.0683	0.0226
	4.0445	<DL	17.4685	33.4002	10.8163	<DL	0.0689	0.0233
	4.6468	<DL	18.1045	32.5498	10.8815	<DL	0.0585	0.0232
1-8.5-40-75	4.3456	<DL	17.7865	32.9750	10.8489	<DL	0.0637	0.0232
	0.4259	<DL	0.4497	0.6013	0.0461	<DL	0.0074	0.0001

2. CRETE

Sample	Mg (mg/g)	Al (mg/g)	Si (mg/g)	K (mg/g)	Ca (mg/g)	Fe (mg/g)	Sr (mg/g)	Ba (mg/g)
	1.8924	<DL	5.6367	1.9944	20.5330	0.0032	0.0182	0.0017
	1.7352	<DL	5.4013	1.9981	19.9550	0.0034	0.0202	0.0020
2-5-5-1	1.8138	<DL	5.5190	1.9963	20.2440	0.0033	0.0192	0.0019
	0.1111	<DL	0.1665	0.0026	0.4087	0.0001	0.0014	0.0002
2-5-5-5	2.2364	<DL	6.0547	3.1421	20.4664	0.0037	0.0211	0.0023
	2.5426	<DL	7.8524	8.5035	22.2911	0.0041	0.0221	0.0025
	2.6791	<DL	7.6608	7.5690	21.8619	0.0033	0.0221	0.0024
2-5-5-15	2.6109	<DL	7.7566	8.0362	22.0765	0.0037	0.0221	0.0025
	0.0966	<DL	0.1355	0.6609	0.3035	0.0005	0.000002	0.0001
2-5-5-30	3.6031	<DL	9.7581	9.5263	23.2260	0.0044	0.0239	0.0032
	4.0287	<DL	9.9900	9.4715	22.5795	0.0041	0.0234	0.0036
	4.1390	<DL	10.2470	9.6879	23.7690	0.0045	0.0247	0.0044
2-5-5-50	4.0839	<DL	10.1185	9.5797	23.1742	0.0043	0.0240	0.0040
	0.0780	<DL	0.1817	0.1531	0.8411	0.0003	0.0009	0.0006
2-5-5-75	4.4244	<DL	10.3892	10.4498	23.7414	0.0043	0.0250	0.0044

Sample	Mg (mg/g)	Al (mg/g)	Si (mg/g)	K (mg/g)	Ca (mg/g)	Fe (mg/g)	Sr (mg/g)	Ba (mg/g)
	2.2815	<DL	8.6553	3.1268	21.3187	0.0033	0.0208	0.0023
	2.4691	<DL	8.5799	2.9915	22.1084	0.0034	0.0217	0.0022
2-5-20-1	2.3753	<DL	8.6176	3.0591	21.7136	0.0033	0.0212	0.0023
	0.1327	<DL	0.0533	0.0957	0.5584	0.0001	0.0007	0.00001
2-5-20-5	3.8185	<DL	9.1543	5.3711	22.9227	0.0038	0.0229	0.0026
	4.8906	<DL	11.3585	13.6848	27.0456	0.0031	0.0249	0.0027
	5.1173	<DL	11.3704	13.4513	26.6040	0.0032	0.0250	0.0028
2-5-20-15	5.0040	<DL	11.3645	13.5680	26.8248	0.0032	0.0250	0.0027
	0.1603	<DL	0.0084	0.1651	0.3123	0.0001	0.0001	0.00004
2-5-20-30	5.6379	<DL	11.0444	14.3898	27.8037	0.0027	0.0259	0.0031
	5.4528	<DL	11.7407	14.5585	26.7216	0.0025	0.0264	0.0033
	5.3488	<DL	11.8559	14.5725	27.1752	0.0026	0.0262	0.0038
2-5-20-50	5.4008	<DL	11.7983	14.5655	26.9484	0.0026	0.0263	0.0035
	0.0735	<DL	0.0814	0.0099	0.3207	0.0001	0.0001	0.0003
2-5-20-75	5.8893	<DL	13.4551	16.5302	29.5749	0.0026	0.0293	0.0053

Sample	Mg (mg/g)	Al (mg/g)	Si (mg/g)	K (mg/g)	Ca (mg/g)	Fe (mg/g)	Sr (mg/g)	Ba (mg/g)
	2.4141	<DL	13.0262	4.7241	24.0374	0.0025	0.0229	0.0030
	2.4951	<DL	12.9643	4.8228	23.8965	0.0023	0.0230	0.0027
2-5-40-1	2.4546	<DL	12.9952	4.7734	23.9670	0.0024	0.0229	0.0028
	0.0573	<DL	0.0438	0.0698	0.0996	0.0001	0.0001	0.0002
2-5-40-5	4.0367	<DL	13.6543	6.2586	25.2124	0.0026	0.0256	0.0032
	5.0528	<DL	16.0761	20.3109	26.2742	0.0024	0.0271	0.0038
	4.7293	<DL	15.5930	19.9967	25.8643	0.0025	0.0248	0.0040
2-5-40-15	4.8910	<DL	15.8346	20.1538	26.0693	0.0025	0.0259	0.0039
	0.2287	<DL	0.3416	0.2222	0.2898	0.0001	0.0017	0.0002
2-5-40-30	6.6690	<DL	16.7248	21.0745	29.1686	0.0020	0.0285	0.0049
	13.5908	<DL	17.7700	21.6919	29.2333	0.0020	0.0288	0.0056
	14.0585	<DL	16.9863	21.7721	28.8714	0.0017	0.0297	0.0056
2-5-40-50	13.8247	<DL	17.3782	21.7320	29.0524	0.0019	0.0292	0.0056
	0.3307	<DL	0.5542	0.0567	0.2559	0.0018	0.0007	0.00002
2-5-40-75	15.0995	<DL	17.4301	22.5877	29.4415	0.0018	0.0301	0.0060

Sample	Mg (mg/g)	Al (mg/g)	Si (mg/g)	K (mg/g)	Ca (mg/g)	Fe (mg/g)	Sr (mg/g)	Ba (mg/g)
	3.1860	<DL	8.5839	3.8100	21.7214	0.0029	0.0220	0.0029
	3.3644	<DL	8.2906	3.6309	21.4487	0.0035	0.0228	0.0024
2-7-5-1	3.2752	<DL	8.4372	3.7204	21.5851	0.0032	0.0224	0.0026
	0.1261	<DL	0.2074	0.1266	0.1928	0.0004	0.0005	0.0003
2-7-5-5	4.7036	<DL	8.9630	4.2802	23.6730	0.0037	0.0217	0.0032
	5.3459	<DL	13.6911	10.7609	24.2142	0.0041	0.0238	0.0038
	5.1299	<DL	13.8242	10.2265	24.5466	0.0038	0.0241	0.0041
2-7-5-15	5.2379	<DL	13.7576	10.4937	24.3804	0.0039	0.0239	0.0040
	0.1527	<DL	0.0941	0.3778	0.2351	0.0002	0.0002	0.0002
2-7-5-30	6.1347	<DL	16.2495	10.6452	25.1233	0.0044	0.0257	0.0047
	6.2870	<DL	16.6319	11.8675	24.9007	0.0044	0.0260	0.0051
	6.1054	<DL	16.9419	12.6020	25.3900	0.0043	0.0253	0.0044
2-7-5-50	6.1962	<DL	16.7869	12.2347	25.1454	0.0043	0.0257	0.0047
	0.1284	<DL	0.2192	0.5194	0.3460	0.0043	0.0005	0.0005
2-7-5-75	8.0186	<DL	17.3755	13.0520	25.8811	0.0043	0.0278	0.0056

Sample	Mg (mg/g)	Al (mg/g)	Si (mg/g)	K (mg/g)	Ca (mg/g)	Fe (mg/g)	Sr (mg/g)	Ba (mg/g)
	3.3751	<DL	13.6728	4.5223	23.1386	0.0031	0.0232	0.0037
	3.8451	<DL	14.4946	4.8862	24.3259	0.0035	0.0251	0.0033
2-7-20-1	3.6101	<DL	14.0837	4.7043	23.7322	0.0033	0.0241	0.0035
	0.3323	<DL	0.5811	0.2573	0.8396	0.0003	0.0013	0.0003
2-7-20-5	5.6228	<DL	16.1089	5.3625	24.5303	0.0041	0.0270	0.0042
	5.9765	<DL	18.2044	11.6891	24.4982	0.0041	0.0264	0.0043
	6.3809	<DL	18.6518	12.3662	25.2309	0.0040	0.0278	0.0039
2-7-20-15	6.1787	<DL	18.4281	12.0277	24.8646	0.0041	0.0271	0.0041
	0.2859	<DL	0.3164	0.4787	0.5181	0.0001	0.0010	0.0003
2-7-20-30	6.8179	<DL	20.5442	13.9610	28.5205	0.0052	0.0285	0.0053
	7.1297	<DL	20.7333	14.3676	29.3296	0.0053	0.0292	0.0059
	6.6581	<DL	19.5405	13.5723	27.7721	0.0052	0.0278	0.0063
2-7-20-50	6.8939	<DL	20.1369	13.9700	28.5509	0.0053	0.0285	0.0061
	0.3335	<DL	0.8434	0.5623	1.1014	0.0001	0.0010	0.0003
2-7-20-75	7.1488	<DL	21.0770	14.5532	29.5299	0.0053	0.0286	0.0091

Sample	Mg (mg/g)	Al (mg/g)	Si (mg/g)	K (mg/g)	Ca (mg/g)	Fe (mg/g)	Sr (mg/g)	Ba (mg/g)
	4.3923	<DL	15.1655	4.9277	26.4007	0.0032	0.0240	0.0044
	4.5990	<DL	15.3090	4.6113	26.5672	0.0030	0.0248	0.0038
2-7-40-1	4.4957	<DL	15.2372	4.7695	26.4839	0.0031	0.0244	0.0041
	0.1462	<DL	0.1014	0.2237	0.1177	0.0002	0.0006	0.0004
2-7-40-5	4.9871	<DL	20.5185	5.3266	26.5971	0.0031	0.0269	0.0050
	7.8047	<DL	21.1807	10.7879	30.1236	0.0034	0.0277	0.0051
	7.6173	<DL	20.9477	10.3268	28.6957	0.0038	0.0276	0.0055
2-7-40-15	7.7110	<DL	21.0642	10.5573	29.4096	0.0036	0.0277	0.0053
	0.1325	<DL	0.1647	0.3260	1.0097	0.0003	0.0001	0.0003
2-7-40-30	7.8728	<DL	21.6626	11.2076	29.5344	0.0037	0.0286	0.0061
	8.6113	<DL	21.8025	12.2236	30.0217	0.0041	0.0301	0.0067
	8.8333	<DL	21.7982	12.3754	29.3959	0.0038	0.0307	0.0070
2-7-40-50	8.7223	<DL	21.8004	12.2995	29.7088	0.0039	0.0304	0.0068
	0.1570	<DL	0.0031	0.1073	0.4425	0.0002	0.0004	0.0003
2-7-40-75	9.4687	<DL	23.2149	16.3871	30.1817	0.0041	0.0315	0.0098

Sample	Mg (mg/g)	Al (mg/g)	Si (mg/g)	K (mg/g)	Ca (mg/g)	Fe (mg/g)	Sr (mg/g)	Ba (mg/g)
	3.6086	<DL	7.5272	4.0608	22.2006	0.0037	0.0254	0.0055
	3.6398	<DL	7.4320	3.7002	21.6926	0.0031	0.0256	0.0045
2-8.5-5-1	3.6242	<DL	7.4796	3.8805	21.9466	0.0034	0.0255	0.0050
	0.0220	<DL	0.0673	0.2550	0.3592	0.0005	0.0001	0.0007
2-8.5-5-5	4.2007	<DL	7.3179	3.6318	22.1205	0.0050	0.0265	0.0042
	4.9996	<DL	12.5550	12.5053	25.1252	0.0059	0.0282	0.0065
	4.9378	<DL	12.9075	12.2200	25.4574	0.0062	0.0290	0.0053
2-8.5-5-15	4.9687	<DL	12.7312	12.3626	25.2913	0.0060	0.0286	0.0059
	0.0437	<DL	0.2493	0.2017	0.2349	0.0002	0.0006	0.0009
2-8.5-5-30	5.5005	<DL	12.1612	12.4691	25.8706	0.0063	0.0306	0.0061
	8.3951	<DL	12.2549	12.7232	26.4327	0.0065	0.0310	0.0062
	8.1290	<DL	12.6410	12.8429	26.1613	0.0069	0.0307	0.0072
2-8.5-5-50	8.2620	<DL	12.4480	12.7831	26.2970	0.0003	0.0309	0.0067
	0.1881	<DL	0.2731	0.0847	0.1919	0.0067	0.0002	0.0007
2-8.5-5-75	8.2476	<DL	15.6582	13.2646	27.7556	0.0074	0.0320	0.0103

Sample	Mg (mg/g)	Al (mg/g)	Si (mg/g)	K (mg/g)	Ca (mg/g)	Fe (mg/g)	Sr (mg/g)	Ba (mg/g)
	4.1141	<DL	8.3278	5.2784	24.1569	0.0058	0.0271	0.0053
	4.1888	<DL	8.7434	5.3528	23.7368	0.0053	0.0262	0.0059
2-8.5-20-1	4.1515	<DL	8.5356	5.3156	23.9469	0.0055	0.0267	0.0056
	0.0528	<DL	0.2939	0.0526	0.2970	0.0003	0.0006	0.0005
2-8.5-20-5	4.5309	<DL	8.1804	5.4243	24.0706	0.0036	0.0277	0.0059
	5.6562	<DL	13.2892	13.8861	24.3399	0.0047	0.0281	0.0072
	5.5772	<DL	13.4565	14.0726	25.4003	0.0055	0.0295	0.0090
2-8.5-20-15	5.6167	<DL	13.3729	13.9794	24.8701	0.0051	0.0288	0.0081
	0.0559	<DL	0.1184	0.1319	0.7498	0.0006	0.0010	0.0013
2-8.5-20-30	7.5564	<DL	13.3679	14.8314	28.8467	0.0056	0.0318	0.0097
	7.9071	<DL	14.1656	15.1752	29.6067	0.0055	0.0325	0.0108
	8.0464	<DL	13.7417	14.9656	28.9371	0.0047	0.0327	0.0112
2-8.5-20-50	7.9767	<DL	13.9536	15.0704	29.2719	0.0051	0.0326	0.0110
	0.0984	<DL	0.2997	0.1483	0.4735	0.0006	0.0002	0.0003
2-8.5-20-75	8.2444	<DL	17.2229	15.2840	29.1012	0.0051	0.0333	0.0114

Sample	Mg (mg/g)	Al (mg/g)	Si (mg/g)	K (mg/g)	Ca (mg/g)	Fe (mg/g)	Sr (mg/g)	Ba (mg/g)
	3.3863	<DL	9.0711	5.8101	17.1967	0.0021	0.0256	0.0064
	3.2039	<DL	9.6764	5.7717	18.6361	0.0027	0.0276	0.0075
2-8.5-40-1	3.2951	<DL	9.3738	5.7909	17.9164	0.0024	0.0266	0.0069
	0.1290	<DL	0.4280	0.0271	1.0178	0.0005	0.0014	0.0008
2-8.5-40-5	3.2630	<DL	9.0355	6.7000	19.7247	0.0031	0.0302	0.0099
	3.8885	<DL	16.5680	16.7302	20.6538	0.0038	0.0331	0.0101
	3.4990	<DL	15.7652	16.8878	20.2282	0.0033	0.0323	0.0106
2-8.5-40-15	3.6938	<DL	16.1666	16.8090	20.4410	0.0036	0.0327	0.0104
	0.2755	<DL	0.5677	0.1114	0.3009	0.0003	0.0005	0.0004
2-8.5-40-30	2.6127	<DL	15.8944	17.1219	26.4500	0.0030	0.0323	0.0113
	3.1199	<DL	15.8408	16.8120	27.4132	0.0036	0.0320	0.0115
	3.6335	<DL	15.1171	16.6898	27.0740	0.0032	0.0322	0.0113
2-8.5-40-50	3.3767	<DL	15.4789	16.7509	27.2436	0.0034	0.0321	0.0114
	0.3632	<DL	0.5118	0.0864	0.2399	0.0003	0.0001	0.0002
2-8.5-40-75	3.7765	<DL	17.1677	16.7209	29.3429	0.0034	0.0327	0.0117

3. VOLOS

Sample	Mg (mg/g)	Al (mg/g)	Si (mg/g)	K (mg/g)	Ca (mg/g)	Fe (mg/g)	Sr (mg/g)	Ba (mg/g)
	4.2260	<DL	4.9599	5.4218	4.5137	0.0025	0.0198	0.0058
	4.1581	<DL	5.3234	4.9102	3.5175	0.0021	0.0209	0.0056
3-5-5-1	4.1921	<DL	5.1416	5.1660	4.0156	0.0023	0.0203	0.0057
	0.0480	<DL	0.2570	0.3618	0.7044	0.0002	0.0008	0.0001
3-5-5-5	4.2140	<DL	7.9697	5.8452	6.1286	0.0031	0.0232	0.0071
	4.7586	<DL	8.1748	7.3473	6.4390	0.0030	0.0237	0.0086
	4.9788	<DL	8.6334	8.1469	6.9598	0.0029	0.0298	0.0085
3-5-5-15	4.8687	<DL	8.4041	7.7471	6.6994	0.0029	0.0268	0.0085
	0.1557	<DL	0.3243	0.5654	0.3682	0.0001	0.0044	0.0001
3-5-5-30	5.4010	<DL	11.5700	12.5699	7.4609	0.0033	0.0316	0.0090
	5.7875	<DL	12.0068	15.0457	7.7676	0.0037	0.0382	0.0089
	6.2323	<DL	12.0001	16.3421	8.3950	0.0041	0.0386	0.0086
3-5-5-50	6.0099	<DL	12.0034	15.6939	8.0813	0.0039	0.0384	0.0087
	0.3146	<DL	0.0048	0.9167	0.4436	0.0003	0.0003	0.0003
3-5-5-75	6.1364	<DL	12.3160	19.9295	8.6310	0.0044	0.0405	0.0095

Sample	Mg (mg/g)	Al (mg/g)	Si (mg/g)	K (mg/g)	Ca (mg/g)	Fe (mg/g)	Sr (mg/g)	Ba (mg/g)
	5.4265	<DL	7.4515	9.9676	5.4312	0.0033	0.0215	0.0088
	5.0777	<DL	7.7270	8.9516	4.5309	0.0034	0.0208	0.0088
3-5-20-1	5.2521	<DL	7.5892	9.4596	4.9810	0.0033	0.0212	0.0088
	0.2466	<DL	0.1948	0.7184	0.6366	0.0001	0.0005	0.00001
3-5-20-5	5.1447	<DL	8.2418	9.4960	7.8311	0.0036	0.0290	0.0096
	5.5538	<DL	8.7855	17.5635	9.5208	0.0040	0.0301	0.0113
	5.7206	<DL	8.1558	18.2781	9.8944	0.0038	0.0323	0.0114
3-5-20-15	5.6372	<DL	8.4706	17.9208	9.7076	0.0039	0.0312	0.0114
	0.1179	<DL	0.4453	0.5053	0.2641	0.0002	0.0015	0.0001
3-5-20-30	5.9426	<DL	8.8090	19.5011	10.1946	0.0042	0.0398	0.0115
	6.3420	<DL	9.4682	26.1393	10.6539	0.0037	0.0414	0.0122
	6.6198	<DL	9.6941	27.4406	10.5240	0.0032	0.0431	0.0130
3-5-20-50	6.4809	<DL	9.5811	26.7900	10.5889	0.0034	0.0423	0.0126
	0.1964	<DL	0.1597	0.9202	0.0918	0.0003	0.0012	0.0006
3-5-20-75	6.7877	<DL	12.1741	27.8076	10.8529	0.0043	0.0448	0.0137

Sample	Mg (mg/g)	Al (mg/g)	Si (mg/g)	K (mg/g)	Ca (mg/g)	Fe (mg/g)	Sr (mg/g)	Ba (mg/g)
	5.5506	<DL	6.9824	7.6655	6.0356	0.0038	0.0239	0.0115
	5.8100	<DL	6.3927	7.7980	5.3564	0.0040	0.0255	0.0103
3-5-40-1	5.6803	<DL	6.6876	7.7317	5.6960	0.0039	0.0247	0.0109
	0.1834	<DL	0.4169	0.0937	0.4803	0.0002	0.0011	0.0008
3-5-40-5	7.0677	<DL	7.3389	15.0212	9.6405	0.0035	0.0376	0.0121
	7.3431	<DL	9.6663	21.0636	9.9878	0.0044	0.0431	0.0140
	7.1673	<DL	9.7833	20.6168	10.6569	0.0035	0.0436	0.0140
3-5-40-15	7.2552	<DL	9.7248	20.8402	10.3224	0.0039	0.0433	0.0140
	0.1243	<DL	0.0827	0.3159	0.4732	0.0007	0.0004	0.0001
3-5-40-30	7.5504	<DL	11.8972	23.0124	11.4418	0.0037	0.0472	0.0148
	7.8335	<DL	12.4187	26.5294	11.9619	0.0043	0.0475	0.0177
	7.3762	<DL	12.5962	25.2412	12.2967	0.0040	0.0470	0.0181
3-5-40-50	7.6048	<DL	12.5075	25.8853	12.1293	0.0042	0.0473	0.0179
	0.3234	<DL	0.1255	0.9108	0.2367	0.0002	0.0004	0.0003
3-5-40-75	7.7902	<DL	14.2373	28.6101	13.2932	0.0046	0.0501	0.0190

Sample	Mg (mg/g)	Al (mg/g)	Si (mg/g)	K (mg/g)	Ca (mg/g)	Fe (mg/g)	Sr (mg/g)	Ba (mg/g)
	5.7461	<DL	6.6649	7.1018	5.4578	0.0031	0.0215	0.0078
	6.0750	<DL	6.7743	7.5797	5.8205	0.0040	0.0229	0.0084
3-7-5-1	5.9105	<DL	6.7196	7.3408	5.6391	0.0036	0.0222	0.0081
	0.2325	<DL	0.0773	0.3379	0.2564	0.0006	0.0010	0.0005
3-7-5-5	6.1138	<DL	7.5212	7.8911	6.4561	0.0044	0.0238	0.0084
	7.6912	<DL	9.2486	8.6214	7.3603	0.0047	0.0358	0.0100
	6.9502	<DL	9.8754	8.6769	7.7723	0.0050	0.0354	0.0110
3-7-5-15	7.3207	<DL	9.5620	8.6491	7.5663	0.0048	0.0356	0.0105
	0.5239	<DL	0.4432	0.0393	0.2914	0.0002	0.0003	0.0007
3-7-5-30	7.8353	<DL	11.8214	13.7945	9.7928	0.0046	0.0375	0.0122
	8.0811	<DL	12.8632	14.8137	10.4919	0.0049	0.0382	0.0136
	7.9015	<DL	12.0019	13.4984	10.5432	0.0045	0.0378	0.0130
3-7-5-50	7.9913	<DL	12.4325	14.1560	10.5176	0.0047	0.0380	0.0133
	0.1270	<DL	0.6090	0.9300	0.0363	0.0046	0.0003	0.0004
3-7-5-75	8.9521	<DL	13.1413	19.8412	12.0256	0.0046	0.0413	0.0146

Sample	Mg (mg/g)	Al (mg/g)	Si (mg/g)	K (mg/g)	Ca (mg/g)	Fe (mg/g)	Sr (mg/g)	Ba (mg/g)
	6.4077	<DL	8.2954	10.3127	6.4580	0.0037	0.0262	0.0093
	5.9513	<DL	8.6926	11.1335	7.1715	0.0044	0.0284	0.0098
3-7-20-1	6.1795	<DL	8.4940	10.7231	6.8148	0.0040	0.0273	0.0096
	0.3227	<DL	0.2809	0.5804	0.5046	0.0005	0.0015	0.0003
3-7-20-5	8.4629	<DL	9.5743	12.0086	8.4628	0.0047	0.0326	0.0120
	8.5713	<DL	9.7979	16.5001	8.7605	0.0048	0.0320	0.0128
	8.5782	<DL	10.7420	17.5208	9.7757	0.0051	0.0348	0.0137
3-7-20-15	8.5747	<DL	10.2699	17.0105	9.2681	0.0049	0.0334	0.0133
	0.0049	<DL	0.6676	0.7218	0.7179	0.0002	0.0020	0.0006
3-7-20-30	9.6705	<DL	13.1186	21.0649	10.4971	0.0053	0.0386	0.0149
	10.1015	<DL	14.7010	24.1818	11.2464	0.0049	0.0407	0.0152
	10.5060	<DL	14.5087	26.0099	11.0269	0.0052	0.0404	0.0163
3-7-20-50	10.3037	<DL	14.6049	25.0958	11.1366	0.0051	0.0405	0.0158
	0.2861	<DL	0.1360	1.2927	0.1552	0.0051	0.0003	0.0008
3-7-20-75	10.4090	<DL	14.2770	27.8159	12.4536	0.0051	0.0409	0.0171

Sample	Mg (mg/g)	Al (mg/g)	Si (mg/g)	K (mg/g)	Ca (mg/g)	Fe (mg/g)	Sr (mg/g)	Ba (mg/g)
	7.7978	<DL	12.1695	11.3236	7.6917	0.0044	0.0294	0.0103
	7.3652	<DL	11.4280	11.5626	8.4300	0.0048	0.0281	0.0110
3-7-40-1	7.5815	<DL	11.7987	11.4431	8.0608	0.0046	0.0288	0.0107
	0.3059	<DL	0.5243	0.1690	0.5220	0.0003	0.0009	0.0005
3-7-40-5	9.5456	<DL	13.6612	13.2856	9.0652	0.0054	0.0384	0.0130
	10.2787	<DL	14.0445	21.0008	9.6436	0.0056	0.0419	0.0133
3-7-40-15	9.9816	<DL	14.6933	22.0698	9.1913	0.0050	0.0425	0.0148
	10.1301	<DL	14.3689	21.5353	9.4175	0.0053	0.0422	0.0141
	0.2101	<DL	0.4588	0.7559	0.3198	0.0004	0.0004	0.0011
3-7-40-30	10.5764	<DL	14.5475	25.8144	11.6883	0.0054	0.0432	0.0159
	11.1086	<DL	14.5589	28.6176	12.0929	0.0056	0.0431	0.0172
	11.6162	<DL	14.9942	30.1946	12.8333	0.0054	0.0453	0.0182
3-7-40-50	11.3624	<DL	14.7766	29.4061	12.4631	0.0055	0.0442	0.0177
	0.3589	<DL	0.3078	1.1151	0.5235	0.0055	0.0015	0.0007
3-7-40-75	13.3671	<DL	15.2748	36.4960	13.2006	0.0055	0.0475	0.0183

Sample	Mg (mg/g)	Al (mg/g)	Si (mg/g)	K (mg/g)	Ca (mg/g)	Fe (mg/g)	Sr (mg/g)	Ba (mg/g)
	9.2169	<DL	6.0052	5.2960	7.3459	0.0038	0.0274	0.0100
	8.8285	<DL	5.7126	5.8161	7.0738	0.0037	0.0257	0.0115
3-8.5-5-1	9.0227	<DL	5.8589	5.5561	7.2098	0.0038	0.0266	0.0107
	0.2746	<DL	0.2069	0.3677	0.1925	0.0001	0.0011	0.0010
3-8.5-5-5	8.9970	<DL	6.7856	6.8930	8.9379	0.0053	0.0300	0.0114
	10.4748	<DL	8.2267	7.1005	8.6909	0.0058	0.0373	0.0120
	10.7310	<DL	7.7497	7.6405	9.6364	0.0053	0.0393	0.0131
3-8.5-5-15	10.6029	<DL	7.9882	7.3705	9.1636	0.0056	0.0383	0.0125
	0.1811	<DL	0.3373	0.3818	0.6685	0.0004	0.0014	0.0007
3-8.5-5-30	10.8407	<DL	9.0059	9.8849	10.4544	0.0058	0.0390	0.0148
	10.7666	<DL	10.2572	10.1737	11.7495	0.0059	0.0403	0.0153
	11.0961	<DL	10.4880	10.4128	11.8495	0.0052	0.0423	0.0159
3-8.5-5-50	10.9313	<DL	10.3726	10.2933	11.7995	0.0055	0.0413	0.0156
	0.2330	<DL	0.1632	0.1691	0.0707	0.0054	0.0015	0.0004
3-8.5-5-75	11.3314	<DL	11.1899	14.5037	12.1910	0.0054	0.0455	0.0173

Sample	Mg (mg/g)	Al (mg/g)	Si (mg/g)	K (mg/g)	Ca (mg/g)	Fe (mg/g)	Sr (mg/g)	Ba (mg/g)
	7.9827	<DL	7.4047	10.0626	8.0851	0.0046	0.0326	0.0097
	9.0141	<DL	6.9997	10.5067	8.3813	0.0052	0.0347	0.0108
3-8.5-20-1	8.4984	<DL	7.2022	10.2847	8.2332	0.0049	0.0336	0.0103
	0.7293	<DL	0.2864	0.3140	0.2094	0.0005	0.0015	0.0007
3-8.5-20-5	10.1196	<DL	7.4452	11.7319	8.9399	0.0061	0.0359	0.0117
	10.7092	<DL	8.0864	12.0178	9.2529	0.0059	0.0364	0.0138
	11.2165	<DL	8.6955	13.2448	9.9474	0.0064	0.0378	0.0139
3-8.5-20-15	10.9629	<DL	8.3910	12.6313	9.6002	0.0061	0.0371	0.0139
	0.3587	<DL	0.4307	0.8676	0.4911	0.0004	0.0010	0.0001
3-8.5-20-30	12.1897	<DL	9.3847	14.5339	11.7259	0.0064	0.0375	0.0143
	12.4867	<DL	10.2009	17.9301	12.8854	0.0067	0.0443	0.0166
	12.4460	<DL	11.0459	18.8791	12.7733	0.0063	0.0471	0.0179
3-8.5-20-50	12.4663	<DL	10.6234	18.4046	12.8293	0.0065	0.0457	0.0172
	0.0288	<DL	0.5975	0.6711	0.0792	0.0064	0.0020	0.0009
3-8.5-20-75	12.8482	<DL	11.0605	21.5775	12.7641	0.0064	0.0459	0.0178

Sample	Mg (mg/g)	Al (mg/g)	Si (mg/g)	K (mg/g)	Ca (mg/g)	Fe (mg/g)	Sr (mg/g)	Ba (mg/g)
	10.7422	<DL	11.3472	12.6819	9.5793	0.0059	0.0312	0.0119
	10.0076	<DL	11.3974	11.7098	8.6853	0.0059	0.0308	0.0122
3-8.5-40-1	10.3749	<DL	11.3723	12.1959	9.1323	0.0059	0.0310	0.0120
	0.5195	<DL	0.0355	0.6873	0.6321	0.00004	0.0003	0.0001
3-8.5-40-5	10.7369	<DL	11.3683	14.2542	10.6103	0.0062	0.0381	0.0137
	12.4908	<DL	12.1225	15.4296	11.4003	0.0061	0.0425	0.0164
	12.5630	<DL	13.1997	15.7433	11.9472	0.0063	0.0441	0.0168
3-8.5-40-15	12.5269	<DL	12.6611	15.5864	11.6737	0.0062	0.0433	0.0166
	0.0511	<DL	0.7617	0.2218	0.3867	0.0002	0.0012	0.0003
3-8.5-40-30	12.7404	<DL	14.4918	19.3529	12.9321	0.0068	0.0464	0.0180
	12.6178	<DL	14.4955	22.5675	12.7856	0.0069	0.0456	0.0176
	13.0843	<DL	15.1076	23.4816	13.0117	0.0078	0.0467	0.0186
3-8.5-40-50	12.8510	<DL	14.8016	23.0245	12.8987	0.0073	0.0461	0.0181
	0.3299	<DL	0.4328	0.6463	0.1599	0.0076	0.0008	0.0007
3-8.5-40-75	13.5782	<DL	15.3866	25.5153	13.5188	0.0076	0.0485	0.0189

4. PELLA I

Sample	Mg (mg/g)	Al (mg/g)	Si (mg/g)	K (mg/g)	Ca (mg/g)	Fe (mg/g)	Sr (mg/g)	Ba (mg/g)
4-5-5-1	2.9625	<DL	5.8092	2.3254	9.0912	0.0021	0.0311	0.0206
	5.5342	<DL	6.5650	2.9841	13.7268	0.0025	0.0370	0.0222
	5.3278	<DL	6.5796	2.8548	13.7123	0.0025	0.0405	0.0206
4-5-5-5	5.4310	<DL	6.5723	2.9194	13.7195	0.0025	0.0388	0.0214
	0.1459	<DL	0.0103	0.0914	0.0103	0.0000	0.0025	0.0011
4-5-5-15	8.0500	<DL	10.6665	6.1530	16.6417	0.0038	0.0438	0.0269
	8.0653	<DL	10.4858	6.0622	16.5368	0.0033	0.0439	0.0336
	7.9481	<DL	10.5362	6.1913	16.5345	0.0030	0.0438	0.0328
4-5-5-30	8.0067	<DL	10.5110	6.1267	16.5357	0.0031	0.0438	0.0332
	0.0829	<DL	0.0357	0.0913	0.0016	0.0002	0.0001	0.0006
4-5-5-50	7.9225	<DL	10.4997	6.4706	16.4094	0.0031	0.0439	0.0354
	7.8956	<DL	10.6654	6.6857	16.2317	0.0030	0.0426	0.0343
	7.6595	<DL	10.3216	6.6093	15.5914	0.0029	0.0423	0.0335
4-5-5-75	7.7776	<DL	10.4935	6.6475	15.9116	0.0029	0.0425	0.0339
	0.1670	<DL	0.2431	0.0540	0.4527	0.0001	0.0002	0.0006

Sample	Mg (mg/g)	Al (mg/g)	Si (mg/g)	K (mg/g)	Ca (mg/g)	Fe (mg/g)	Sr (mg/g)	Ba (mg/g)
4-5-20-1	3.3207	<DL	6.1034	2.6263	12.4997	0.0026	0.0480	0.0127
	5.9212	<DL	9.9800	3.5875	13.1401	0.0029	0.0516	0.0134
	5.8614	<DL	9.3060	3.2923	12.8321	0.0033	0.0533	0.0137
4-5-20-5	5.8913	<DL	9.6430	3.4399	12.9861	0.0031	0.0524	0.0135
	0.0423	<DL	0.4766	0.2087	0.2177	0.0003	0.0012	0.0002
4-5-20-15	6.2339	<DL	10.3071	4.4797	15.3998	0.0047	0.0643	0.0127
	8.6594	<DL	15.4186	5.8263	16.0079	0.0018	0.0510	0.0383
	8.2985	<DL	14.7077	5.8058	15.3318	0.0017	0.0480	0.0391
4-5-20-30	8.4790	<DL	15.0632	5.8160	15.6698	0.0017	0.0495	0.0387
	0.2552	<DL	0.5027	0.0146	0.4781	0.0000	0.0021	0.0006
4-5-20-50	8.2566	<DL	15.1503	7.3314	15.6411	0.0016	0.0496	0.0405
	8.0864	<DL	14.9475	7.4699	15.4955	0.0015	0.0490	0.0402
	8.3528	<DL	15.5679	7.5033	16.1190	0.0019	0.0525	0.0419
4-5-20-75	8.2196	<DL	15.2577	7.4866	15.8073	0.0017	0.0508	0.0411
	0.1884	<DL	0.4387	0.0236	0.4409	0.0003	0.0025	0.0012

Sample	Mg (mg/g)	Al (mg/g)	Si (mg/g)	K (mg/g)	Ca (mg/g)	Fe (mg/g)	Sr (mg/g)	Ba (mg/g)
4-5-40-1	4.1891	<DL	10.5502	2.7322	12.6430	0.0015	0.0569	0.0194
	5.0416	<DL	16.4570	5.1225	14.3784	0.0019	0.0600	0.0254
	4.7777	<DL	15.8593	4.8736	13.8223	0.0021	0.0631	0.0293
4-5-40-5	4.9097	<DL	16.1582	4.9981	14.1003	0.0020	0.0615	0.0274
	0.1866	<DL	0.4226	0.1760	0.3933	0.0002	0.0022	0.0028
4-5-40-15	6.7864	<DL	16.9959	6.6968	15.0850	0.0017	0.0648	0.0403
	6.5758	<DL	16.8272	7.7838	17.4590	0.0008	0.0635	0.0792
	6.4404	<DL	16.5663	7.6723	17.0963	0.0012	0.0618	0.0883
4-5-40-30	6.5081	<DL	16.6968	7.7280	17.2776	0.0010	0.0626	0.0838
	0.0958	<DL	0.1845	0.0789	0.2565	0.0003	0.0012	0.0064
4-5-40-50	6.3520	<DL	16.3822	8.0240	16.9060	0.0007	0.0612	0.0884
	6.0544	<DL	17.5578	8.6719	18.9872	0.0009	0.0690	0.1028
	6.4617	<DL	17.8960	9.2647	18.6854	0.0011	0.0654	0.0962
4-5-40-75	6.2581	<DL	17.7269	8.9683	18.8363	0.0010	0.0672	0.0995
	0.2880	<DL	0.2391	0.4191	0.2134	0.0002	0.0026	0.0047

Sample	Mg (mg/g)	Al (mg/g)	Si (mg/g)	K (mg/g)	Ca (mg/g)	Fe (mg/g)	Sr (mg/g)	Ba (mg/g)
4-7-5-1	2.8997	<DL	8.8470	2.2959	8.7484	0.0025	0.0318	0.0203
	5.0230	<DL	11.3969	5.0861	10.1064	0.0032	0.0404	0.0250
	5.1461	<DL	11.6534	5.2427	9.8606	0.0038	0.0337	0.0269
4-7-5-5	5.0845	<DL	11.5251	5.1644	9.9835	0.0035	0.0371	0.0260
	0.0871	<DL	0.1814	0.1107	0.1738	0.0005	0.0047	0.0013
4-7-5-15	6.0676	<DL	18.4228	7.7255	12.1714	0.0035	0.0468	0.0329
	6.2458	<DL	18.8949	7.9694	13.4215	0.0037	0.0500	0.0352
	6.0718	<DL	18.3668	7.8830	12.9606	0.0039	0.0463	0.0351
4-7-5-30	6.1588	<DL	18.6309	7.9262	13.1911	0.0038	0.0481	0.0352
	0.1230	<DL	0.3734	0.0611	0.3260	0.0001	0.0027	0.0001
4-7-5-50	6.8272	<DL	18.8736	8.6111	13.9512	0.0044	0.0500	0.0377
	7.0279	<DL	19.5032	8.8515	14.7429	0.0042	0.0504	0.0382
	7.2656	<DL	19.3281	8.7775	14.4125	0.0044	0.0499	0.0377
4-7-5-75	7.1467	<DL	19.4156	8.8145	14.5777	0.0043	0.0502	0.0379
	0.1681	<DL	0.1238	0.0524	0.2336	0.0001	0.0004	0.0004

Sample	Mg (mg/g)	Al (mg/g)	Si (mg/g)	K (mg/g)	Ca (mg/g)	Fe (mg/g)	Sr (mg/g)	Ba (mg/g)
4-7-20-1	3.4693	<DL	10.3879	3.1916	11.2062	0.0025	0.0466	0.0171
	5.6440	<DL	17.2627	5.3464	11.3283	0.0025	0.0526	0.0234
	5.6356	<DL	17.2042	4.9514	11.2451	0.0030	0.0526	0.0200
4-7-20-5	5.6398	<DL	17.2335	5.1489	11.2867	0.0028	0.0526	0.0217
	0.0060	<DL	0.0413	0.2793	0.0588	0.0004	0.00002	0.0024
4-7-20-15	5.5700	<DL	17.6873	9.0850	13.2573	0.0027	0.0674	0.0374
	6.5712	<DL	17.7054	8.4906	14.0057	0.0033	0.0674	0.0403
	6.7444	<DL	17.6870	8.9385	13.2530	0.0042	0.0667	0.0399
4-7-20-30	6.6578	<DL	17.6962	8.7145	13.6294	0.0037	0.0671	0.0401
	0.0128	<DL	0.0130	0.3168	0.5323	0.0007	0.0005	0.0003
4-7-20-50	7.0118	<DL	19.0601	9.1226	16.3500	0.0046	0.0671	0.0401
	7.9275	<DL	20.2100	9.4492	17.2964	0.0048	0.0647	0.0427
	7.7384	<DL	19.6517	9.6925	17.5893	0.0044	0.0578	0.0418
4-7-20-75	7.8330	<DL	19.9308	9.5708	17.4429	0.0046	0.0613	0.0423
	0.1337	<DL	0.3948	0.1720	0.2071	0.0002	0.0049	0.0007

Sample	Mg (mg/g)	Al (mg/g)	Si (mg/g)	K (mg/g)	Ca (mg/g)	Fe (mg/g)	Sr (mg/g)	Ba (mg/g)
4-7-40-1	3.7444	<DL	14.1375	3.7120	12.2017	0.0025	0.0583	0.0159
	5.8339	<DL	14.5917	5.5447	13.4238	0.0027	0.0635	0.0235
	6.1380	<DL	15.6271	5.7729	14.1340	0.0026	0.0644	0.0261
4-7-40-5	5.9860	<DL	15.1094	5.6588	13.7789	0.0026	0.0639	0.0248
	0.2150	<DL	0.7321	0.1613	0.5022	7.32E-05	0.0007	0.0018
4-7-40-15	7.4900	<DL	19.1079	6.7577	16.4447	0.0029	0.0681	0.0331
	8.0036	<DL	19.7997	9.1667	16.6690	0.0031	0.0690	0.0867
	8.5431	<DL	20.7554	9.1243	16.6083	0.0028	0.0660	0.0871
4-7-40-30	8.2733	<DL	20.2776	9.1455	16.6386	0.0030	0.0675	0.0869
	0.3814	<DL	0.6758	0.0300	0.0429	0.0002	0.0022	0.0003
4-7-40-50	8.0080	<DL	20.4828	10.1257	17.4057	0.0032	0.0693	0.0886
	8.1234	<DL	21.1539	10.4174	18.1598	0.0033	0.0718	0.0986
	7.7293	<DL	20.7825	10.0669	17.3509	0.0033	0.0684	0.0914
4-7-40-75	7.9263	<DL	20.9682	10.2422	17.7553	0.0033	0.0701	0.0950
	0.2786	<DL	0.2626	0.2479	0.5720	0.00001	0.0024	0.0051

Sample	Mg (mg/g)	Al (mg/g)	Si (mg/g)	K (mg/g)	Ca (mg/g)	Fe (mg/g)	Sr (mg/g)	Ba (mg/g)
4-8.5-5-1	2.2078	<DL	5.8845	2.1767	3.5331	0.0014	0.0343	0.0257
	3.5108	<DL	7.5272	2.9909	5.2340	0.0031	0.0398	0.0314
	3.3546	<DL	7.6597	3.3220	5.6066	0.0029	0.0416	0.0324
4-8.5-5-5	3.4327	<DL	7.5935	3.1565	5.4203	0.0030	0.0407	0.0319
	0.1104	<DL	0.0937	0.2341	0.2635	0.0001	0.0013	0.0007
4-8.5-5-15	5.0551	<DL	11.7396	6.9669	9.0081	0.0072	0.0491	0.0353
	6.0087	<DL	12.1919	8.0655	9.2985	0.0047	0.0604	0.0403
	6.0377	<DL	12.3230	7.8818	9.5283	0.0048	0.0568	0.0353
4-8.5-5-30	6.0232	<DL	12.2574	7.9737	9.4134	0.0047	0.0586	0.0378
	0.0205	<DL	0.0927	0.1299	0.1625	0.0001	0.0025	0.0036
4-8.5-5-50	6.8798	<DL	15.3482	8.3369	11.2403	0.0058	0.0611	0.0392
	6.9012	<DL	18.6131	8.5932	11.9446	0.0062	0.0671	0.0387
	7.2382	<DL	18.3230	7.7799	12.3142	0.0057	0.0658	0.0392
4-8.5-5-75	7.0697	<DL	18.4681	8.1865	12.1294	0.0060	0.0664	0.0390
	0.2383	<DL	0.2051	0.5751	0.2613	0.0004	0.0009	0.0003

Sample	Mg (mg/g)	Al (mg/g)	Si (mg/g)	K (mg/g)	Ca (mg/g)	Fe (mg/g)	Sr (mg/g)	Ba (mg/g)
4-8.5-20-1	2.3616	<DL	7.4813	2.8640	5.0563	0.0070	0.0416	0.0224
	4.7207	<DL	8.3444	3.7899	5.3856	0.0067	0.0503	0.0266
	4.7789	<DL	8.5501	3.8029	5.3316	0.0061	0.0499	0.0235
4-8.5-20-5	4.7498	<DL	8.4472	3.7964	5.3586	0.0064	0.0501	0.0251
	0.0412	<DL	0.1454	0.0092	0.0382	0.0004	0.0003	0.0022
4-8.5-20-15	4.8116	<DL	16.8910	9.1857	11.3055	0.0042	0.0608	0.0299
	4.9294	<DL	16.4627	9.5041	10.5028	0.0041	0.0614	0.0399
	4.8177	<DL	16.1136	9.8277	10.9445	0.0050	0.0493	0.0381
4-8.5-20-30	4.8736	<DL	16.2881	9.6659	10.7236	0.0045	0.0553	0.0390
	0.0790	<DL	0.2468	0.2288	0.3123	0.0007	0.0086	0.0013
4-8.5-20-50	5.1317	<DL	19.1076	11.4181	11.7840	0.0034	0.0704	0.0739
	5.1701	<DL	20.2134	11.4076	15.0787	0.0035	0.0717	0.0751
	5.6227	<DL	20.5102	12.1611	14.3583	0.0036	0.0708	0.0756
4-8.5-20-75	5.3964	<DL	20.3618	11.7844	14.7185	0.0035	0.0712	0.0754
	0.3200	<DL	0.2099	0.5328	0.5094	0.0001	0.0007	0.0004

Sample	Mg (mg/g)	Al (mg/g)	Si (mg/g)	K (mg/g)	Ca (mg/g)	Fe (mg/g)	Sr (mg/g)	Ba (mg/g)
4-8.5-40-1	0.6159	<DL	8.7610	2.6527	5.5268	0.0002	0.0505	0.0371
	1.0875	<DL	9.6271	6.9787	6.2292	0.0020	0.0691	0.0437
	1.1203	<DL	9.5711	6.8822	6.0500	0.0023	0.0690	0.0342
4-8.5-40-5	1.1039	<DL	9.5991	6.9305	6.1396	0.0021	0.0690	0.0390
	0.0232	<DL	0.0396	0.0683	0.1267	0.0002	0.0001	0.0068
4-8.5-40-15	1.2505	<DL	15.9978	8.1927	9.7205	0.0031	0.0486	0.1022
	1.2163	<DL	16.3720	8.3499	10.2564	0.0029	0.0703	0.1041
	1.4537	<DL	15.4693	8.4139	10.2592	0.0035	0.0582	0.0991
4-8.5-40-30	1.3350	<DL	15.9206	8.3819	10.2578	0.0032	0.0642	0.1016
	0.1678	<DL	0.6383	0.0453	0.0020	0.0005	0.0085	0.0035
4-8.5-40-50	1.3834	<DL	19.0296	11.1236	10.4554	0.0028	0.0682	0.1012
	1.2899	<DL	21.7505	11.3256	10.4196	0.0026	0.0700	0.1044
	1.5433	<DL	22.7584	11.7955	10.2585	0.0031	0.0721	0.0943
4-8.5-40-75	1.4166	<DL	22.2546	11.5606	10.3391	0.0029	0.0711	0.0994
	0.1791	<DL	0.7127	0.3323	0.1139	0.0004	0.0015	0.0072

5. PELLA II

Sample	Mg (mg/g)	Al (mg/g)	Si (mg/g)	K (mg/g)	Ca (mg/g)	Fe (mg/g)	Sr (mg/g)	Ba (mg/g)
5-5-5-1	4.8800	<DL	5.2988	2.3822	14.7650	0.0059	0.0578	0.0138
	5.5441	<DL	6.4055	2.7250	16.4887	0.0029	0.0629	0.0125
	5.5627	<DL	6.3412	2.6772	16.3534	0.0026	0.0626	0.0120
5-5-5-5	5.5534	<DL	6.3733	2.7011	16.4210	0.0027	0.0628	0.0122
	0.0132	<DL	0.0455	0.0338	0.0957	0.0002	0.0003	0.0004
5-5-5-15	6.2921	<DL	10.4512	4.5182	15.8628	0.0053	0.0654	0.0132
	6.6523	<DL	10.6985	4.7807	16.1455	0.0064	0.0660	0.0163
	6.4538	<DL	10.5018	4.6776	15.6556	0.0082	0.0654	0.0133
5-5-5-30	6.5531	<DL	10.6001	4.7291	15.9005	0.0073	0.0657	0.0148
	0.1403	<DL	0.1391	0.0729	0.3464	0.0012	0.0005	0.0021
5-5-5-50	6.4917	<DL	10.7601	4.6965	16.0417	0.0054	0.0672	0.0134
	8.4135	<DL	17.0263	7.1916	17.7346	0.0039	0.0795	0.0114
	8.3787	<DL	17.2488	7.3856	17.7888	0.0051	0.0787	0.0107
5-5-5-75	8.3961	<DL	17.1376	7.2886	17.7617	0.0045	0.0791	0.0110
	0.0246	<DL	0.1573	0.1372	0.0383	0.0008	0.0005	0.0005

Sample	Mg (mg/g)	Al (mg/g)	Si (mg/g)	K (mg/g)	Ca (mg/g)	Fe (mg/g)	Sr (mg/g)	Ba (mg/g)
5-5-20-1	5.2126	<DL	6.5839	2.6780	15.1305	0.0032	0.0594	0.0150
	5.8790	<DL	10.9618	3.0921	15.2777	0.0027	0.0587	0.0108
	5.7690	<DL	10.8392	2.8744	14.9001	0.0024	0.0579	0.0090
5-5-20-5	5.8240	<DL	10.9005	2.9832	15.0889	0.0025	0.0583	0.0099
	0.0778	<DL	0.0867	0.1539	0.2670	0.0002	0.0006	0.0012
5-5-20-15	6.6706	<DL	11.1661	4.8703	16.5598	0.0051	0.0701	0.0137
	8.6944	<DL	16.9013	7.8182	18.1192	0.0037	0.0800	0.0111
	8.7812	<DL	17.0962	7.9956	18.2733	0.0037	0.0808	0.0118
5-5-20-30	8.7378	<DL	16.9987	7.9069	18.1963	0.0037	0.0804	0.0115
	0.0614	<DL	0.1378	0.1254	0.1090	0.000004	0.0005	0.0005
5-5-20-50	8.8435	<DL	17.1628	8.1661	18.5845	0.0041	0.0821	0.0123
	8.8441	<DL	18.3180	9.5560	19.2568	0.0007	0.0926	0.0195
	9.4724	<DL	19.2422	10.6599	20.2835	0.0038	0.0857	0.0200
5-5-20-75	9.1583	<DL	18.7801	10.1079	19.7701	0.0022	0.0892	0.0197
	0.4443	<DL	0.6535	0.7806	0.7260	0.0022	0.0049	0.0004

Sample	Mg (mg/g)	Al (mg/g)	Si (mg/g)	K (mg/g)	Ca (mg/g)	Fe (mg/g)	Sr (mg/g)	Ba (mg/g)
5-5-40-1	5.7423	<DL	11.5107	3.4874	15.8189	0.0034	0.0636	0.0102
	6.6630	<DL	14.9321	4.1360	16.5799	0.0021	0.0661	0.0100
	6.7247	<DL	15.0337	4.0616	16.7814	0.0021	0.0659	0.0106
5-5-40-5	6.6939	<DL	14.9829	4.0988	16.6806	0.0021	0.0660	0.0103
	0.0437	<DL	0.0718	0.0526	0.1425	0.0001	0.0001	0.0004
5-5-40-15	8.2848	<DL	17.2590	9.1955	18.1832	0.0020	0.0868	0.0243
	8.4624	<DL	20.3342	10.1925	18.9848	0.0023	0.0938	0.0186
	8.2722	<DL	19.9094	9.8931	18.5825	0.0017	0.0927	0.0184
5-5-40-30	8.3673	<DL	20.1218	10.0428	18.7837	0.0020	0.0932	0.0185
	0.1345	<DL	0.3004	0.2117	0.2845	0.0004	0.0008	0.0001
5-5-40-50	8.3800	<DL	20.0112	10.0013	18.5941	0.0023	0.0928	0.0182
	8.3712	<DL	20.0970	9.8977	18.8049	0.0025	0.0938	0.0183
	9.4108	<DL	19.2985	10.5102	19.2883	0.0025	0.0969	0.0186
5-5-40-75	8.8910	<DL	19.6977	10.2040	19.0466	0.0025	0.0953	0.0185
	0.7351	<DL	0.5646	0.4331	0.3419	0.00003	0.0022	0.0002

Sample	Mg (mg/g)	Al (mg/g)	Si (mg/g)	K (mg/g)	Ca (mg/g)	Fe (mg/g)	Sr (mg/g)	Ba (mg/g)
4-7-5-1	3.5120	<DL	10.1765	2.8876	7.9702	0.0014	0.0349	0.0047
	3.6681	<DL	10.7564	3.1622	8.1345	0.0015	0.0355	0.0024
	4.2125	<DL	11.9048	3.6193	7.7286	0.0020	0.0397	0.0027
4-7-5-5	3.9403	<DL	11.3306	3.3907	7.9316	0.0018	0.0376	0.0026
	0.3849	<DL	0.8120	0.3233	0.2870	0.0004	0.0030	0.0002
4-7-5-15	6.0083	<DL	18.5211	10.3650	13.7583	0.0038	0.0661	0.0081
	5.9891	<DL	18.5498	10.3312	13.7842	0.0040	0.0663	0.0083
	5.8666	<DL	18.1556	10.0323	13.4665	0.0037	0.0644	0.0075
4-7-5-30	5.9278	<DL	18.3527	10.1817	13.6254	0.0038	0.0653	0.0079
	0.0866	<DL	0.2788	0.2114	0.2247	0.0002	0.0013	0.0006
4-7-5-50	6.0200	<DL	18.4715	10.1562	13.9445	0.0035	0.0668	0.0097
	5.8159	<DL	19.1022	9.5210	13.7398	0.0032	0.0650	0.0081
	6.4953	<DL	18.8553	9.1671	13.5684	0.0038	0.0688	0.0092
4-7-5-75	6.1556	<DL	18.9788	9.3440	13.6541	0.0035	0.0669	0.0086
	0.4804	<DL	0.1746	0.2502	0.1212	0.0005	0.0027	0.0008

Sample	Mg (mg/g)	Al (mg/g)	Si (mg/g)	K (mg/g)	Ca (mg/g)	Fe (mg/g)	Sr (mg/g)	Ba (mg/g)
4-7-20-1	3.5082	<DL	10.6022	3.5971	9.7022	0.0011	0.0440	0.0072
	3.3607	<DL	16.3346	4.6958	10.9794	0.0029	0.0493	0.0082
	3.3745	<DL	16.3563	4.6587	10.7066	0.0013	0.0491	0.0043
4-7-20-5	3.3676	<DL	16.3454	4.6773	10.8430	0.0021	0.0492	0.0063
	0.0098	<DL	0.0154	0.0263	0.1929	0.0011	0.0002	0.0028
4-7-20-15	5.0428	<DL	17.3119	11.9695	14.8861	0.0015	0.0750	0.0143
	6.9990	<DL	17.8655	12.0095	16.5488	0.0009	0.0817	0.0149
	6.9809	<DL	17.6538	11.9478	16.5202	0.0011	0.0817	0.0150
4-7-20-30	6.9900	<DL	17.7596	11.9786	16.5345	0.0010	0.0817	0.0149
	0.0128	<DL	0.1497	0.0436	0.0202	0.0002	0.0001	0.0001
4-7-20-50	7.3690	<DL	18.7797	12.2586	17.3699	0.0009	0.0855	0.0155
	7.4578	<DL	19.2341	12.1956	17.4264	0.0010	0.0864	0.0149
	8.0002	<DL	18.0953	12.7436	16.5473	0.0008	0.0835	0.0153
4-7-20-75	7.7290	<DL	18.6647	12.4696	16.9868	0.0009	0.0850	0.0151
	0.3835	<DL	0.8053	0.3875	0.6216	0.0001	0.0020	0.0002

Sample	Mg (mg/g)	Al (mg/g)	Si (mg/g)	K (mg/g)	Ca (mg/g)	Fe (mg/g)	Sr (mg/g)	Ba (mg/g)
4-7-40-1	3.5223	<DL	14.2933	4.3459	10.7521	0.0033	0.0479	0.0089
	3.7603	<DL	18.9193	5.0195	11.9971	0.0015	0.0525	0.0070
	3.7100	<DL	18.4890	4.7473	11.7447	0.0014	0.0515	0.0060
4-7-40-5	3.7351	<DL	18.7041	4.8834	11.8709	0.0015	0.0520	0.0065
	0.0356	<DL	0.3042	0.1924	0.1785	2.9E-05	0.0007	0.0007
4-7-40-15	8.4539	<DL	18.7916	7.1871	15.3277	0.0031	0.0705	0.0135
	9.4041	<DL	18.9814	7.4277	16.0239	0.0041	0.0759	0.0111
	8.7788	<DL	18.3396	9.0084	17.0926	0.0038	0.0716	0.0120
4-7-40-30	9.0914	<DL	18.6605	8.2181	16.5582	0.0039	0.0738	0.0115
	0.4421	<DL	0.4538	1.1177	0.7556	0.0002	0.0031	0.0006
4-7-40-50	9.9950	<DL	20.1964	7.6830	16.8733	0.0039	0.0805	0.0119
	10.0025	<DL	20.2946	7.6801	16.9701	0.0038	0.0805	0.0131
	10.0987	<DL	20.5740	7.7638	17.2196	0.0039	0.0819	0.0125
4-7-40-75	10.0506	<DL	20.4343	7.7219	17.0949	0.0039	0.0812	0.0128
	0.0681	<DL	0.1976	0.0592	0.1764	0.0001	0.0010	0.0004

Sample	Mg (mg/g)	Al (mg/g)	Si (mg/g)	K (mg/g)	Ca (mg/g)	Fe (mg/g)	Sr (mg/g)	Ba (mg/g)
4-8.5-5-1	2.7496	<DL	6.3438	2.3037	3.6960	0.0014	0.0385	0.0057
	4.5168	<DL	6.1038	2.4135	4.5872	0.0033	0.0479	0.0060
	4.4494	<DL	5.9097	2.3599	4.4726	0.0030	0.0466	0.0060
4-8.5-5-5	4.4831	<DL	6.0067	2.3867	4.5299	0.0031	0.0472	0.0060
	0.0477	<DL	0.1373	0.0379	0.0810	0.0002	0.0009	0.00004
4-8.5-5-15	5.2191	<DL	13.4406	8.2418	10.9557	0.0072	0.0504	0.0090
	5.4039	<DL	13.9903	9.4957	11.9774	0.0048	0.0554	0.0066
	5.5000	<DL	14.1648	9.5730	12.1458	0.0050	0.0562	0.0072
4-8.5-5-30	5.4520	<DL	14.0776	9.5343	12.0616	0.0049	0.0558	0.0069
	0.0679	<DL	0.1234	0.0547	0.1191	0.0001	0.0006	0.0005
4-8.5-5-50	5.7947	<DL	14.5359	9.7078	12.4089	0.0060	0.0582	0.0067
	6.0503	<DL	15.8480	9.3400	12.4875	0.0063	0.0592	0.0064
	6.5323	<DL	15.5338	9.8401	12.4189	0.0058	0.0575	0.0063
4-8.5-5-75	6.2913	<DL	15.6909	9.5901	12.4532	0.0060	0.0583	0.0064
	0.3409	<DL	0.2221	0.3536	0.0485	0.0003	0.0012	0.0001

Sample	Mg (mg/g)	Al (mg/g)	Si (mg/g)	K (mg/g)	Ca (mg/g)	Fe (mg/g)	Sr (mg/g)	Ba (mg/g)
4-8.5-20-1	1.9208	<DL	6.5056	2.8418	4.1638	0.0066	0.0433	0.0066
	1.7355	<DL	7.0620	3.2370	4.4880	0.0067	0.0472	0.0067
	1.7830	<DL	7.3528	3.2730	4.6718	0.0064	0.0490	0.0064
4-8.5-20-5	1.7593	<DL	7.2074	3.2550	4.5799	0.0065	0.0481	0.0065
	0.0336	<DL	0.2056	0.0255	0.1300	0.0002	0.0013	0.0002
4-8.5-20-15	1.7268	<DL	15.5477	11.8005	10.1933	0.0043	0.0508	0.0073
	1.6894	<DL	15.2637	11.3549	9.9617	0.0042	0.0492	0.0062
	1.7280	<DL	15.6403	11.5453	10.2890	0.0052	0.0514	0.0078
4-8.5-20-30	1.7087	<DL	15.4520	11.4501	10.1253	0.0047	0.0503	0.0070
	0.0273	<DL	0.2662	0.1347	0.2314	0.0007	0.0016	0.0011
4-8.5-20-50	2.0333	<DL	15.6156	12.1485	10.4208	0.0035	0.0504	0.0098
	2.0598	<DL	15.8986	12.3196	10.4735	0.0035	0.0511	0.0065
	2.1092	<DL	16.6192	13.1221	11.0554	0.0036	0.0499	0.0081
4-8.5-20-75	2.0845	<DL	16.2589	12.7208	10.7645	0.0035	0.0505	0.0073
	0.0350	<DL	0.5095	0.5675	0.4115	0.0001	0.0009	0.0011

Sample	Mg (mg/g)	Al (mg/g)	Si (mg/g)	K (mg/g)	Ca (mg/g)	Fe (mg/g)	Sr (mg/g)	Ba (mg/g)
4-8.5-40-1	0.9003	<DL	7.3457	3.6807	4.4593	0.0028	0.0488	0.0091
	1.0268	<DL	7.3028	3.6975	4.8240	0.0020	0.0546	0.0062
	1.0411	<DL	7.3764	3.7136	4.9993	0.0024	0.0555	0.0088
4-8.5-40-5	1.0340	<DL	7.3396	3.7056	4.9117	0.0022	0.0551	0.0075
	0.0101	<DL	0.0520	0.0114	0.1240	0.0003	0.0006	0.0019
4-8.5-40-15	0.6003	<DL	13.8373	13.7059	9.2675	0.0031	0.0485	0.0129
	0.7167	<DL	14.1414	13.0875	9.5125	0.0029	0.0510	0.0089
	0.7040	<DL	13.9990	12.5566	9.2538	0.0034	0.0491	0.0071
4-8.5-40-30	0.7103	<DL	14.0702	12.8221	9.3831	0.0032	0.0500	0.0080
	0.0090	<DL	0.1007	0.3754	0.1830	0.0004	0.0013	0.0013
4-8.5-40-50	0.7517	<DL	15.0118	13.3729	9.8173	0.0030	0.0521	0.0062
	0.7930	<DL	15.6281	13.8580	10.5924	0.0028	0.0559	0.0095
	0.8140	<DL	17.5305	14.2893	10.4386	0.0030	0.0504	0.0089
4-8.5-40-75	0.8035	<DL	16.5793	14.0737	10.5155	0.0029	0.0532	0.0092
	0.0148	<DL	1.3452	0.3049	0.1088	0.0002	0.0039	0.0004

6. CORFU

Sample	Mg (mg/g)	Al (mg/g)	Si (mg/g)	K (mg/g)	Ca (mg/g)	Fe (mg/g)	Sr (mg/g)	Ba (mg/g)
	4.5724	<DL	5.7717	4.4670	10.5332	0.0006	0.0289	0.0070
	4.5850	<DL	5.9904	4.8285	11.3698	0.0008	0.0275	0.0064
6-5-5-1	4.5787	<DL	5.8810	4.6478	10.9515	0.0007	0.0282	0.0067
	0.0090	<DL	0.1546	0.2556	0.5916	0.0002	0.0010	0.0004
6-5-5-5	4.6139	<DL	9.0728	5.7875	13.2976	0.0008	0.0294	0.0081
	5.2427	<DL	9.4068	7.7118	13.1044	0.0009	0.0373	0.0084
	5.1331	<DL	9.3077	7.2683	13.2510	0.0009	0.0490	0.0088
6-5-5-15	5.1879	<DL	9.3573	7.4901	13.1777	0.0009	0.0432	0.0086
	0.0775	<DL	0.0701	0.3136	0.1036	0.0000	0.0083	0.0003
6-5-5-30	5.8032	<DL	12.9716	13.2247	14.3515	0.0010	0.0530	0.0095
	6.0999	<DL	13.5451	14.8393	15.3219	0.0011	0.0546	0.0108
	6.2492	<DL	13.5673	15.5810	14.9644	0.0012	0.0557	0.0112
6-5-5-50	6.1746	<DL	13.5562	15.2101	15.1431	0.0011	0.0552	0.0110
	0.1055	<DL	0.0157	0.5245	0.2528	0.0001	0.0008	0.0003
6-5-5-75	7.3444	<DL	13.8261	19.1964	15.3494	0.0014	0.0574	0.0120

Sample	Mg (mg/g)	Al (mg/g)	Si (mg/g)	K (mg/g)	Ca (mg/g)	Fe (mg/g)	Sr (mg/g)	Ba (mg/g)
	5.4362	<DL	6.5306	8.4134	13.6398	0.0008	0.0369	0.0098
	5.5514	<DL	6.0136	8.7754	13.7420	0.0009	0.0338	0.0112
6-5-20-1	5.4938	<DL	6.2721	8.5944	13.6909	0.0008	0.0353	0.0105
	0.0815	<DL	0.3656	0.2560	0.0723	0.0001	0.0022	0.0010
6-5-20-5	5.8912	<DL	9.7701	10.4032	14.1508	0.0010	0.0390	0.0122
	6.2146	<DL	10.5930	17.3968	14.5863	0.0011	0.0395	0.0122
	5.7566	<DL	10.1056	16.6109	13.6723	0.0011	0.0384	0.0126
6-5-20-15	5.9856	<DL	10.3493	17.0039	14.1293	0.0011	0.0389	0.0124
	0.3238	<DL	0.3446	0.5557	0.6462	0.0000	0.0008	0.0002
6-5-20-30	6.7700	<DL	11.3142	19.9558	15.0632	0.0012	0.0420	0.0139
	7.6399	<DL	11.7624	25.1104	15.7359	0.0015	0.0572	0.0141
	7.7787	<DL	11.9898	25.4197	16.0511	0.0016	0.0600	0.0148
6-5-20-50	7.7093	<DL	11.8761	25.2651	15.8935	0.0015	0.0586	0.0145
	0.0981	<DL	0.1608	0.2187	0.2229	0.0001	0.0020	0.0004
6-5-20-75	8.0057	<DL	12.5697	28.2570	16.0071	0.0009	0.0338	0.0112

Sample	Mg (mg/g)	Al (mg/g)	Si (mg/g)	K (mg/g)	Ca (mg/g)	Fe (mg/g)	Sr (mg/g)	Ba (mg/g)
	6.2056	<DL	7.4329	7.1158	14.4496	<DL	0.0402	0.0122
	6.1155	<DL	6.7908	6.8214	14.1318	<DL	0.0434	0.0145
6-5-40-1	6.1606	<DL	7.1119	6.9686	14.2907	<DL	0.0418	0.0134
	0.0637	<DL	0.4540	0.2082	0.2247	<DL	0.0022	0.0016
6-5-40-5	7.5766	<DL	8.1795	13.5845	15.2534	<DL	0.0439	0.0156
	7.9879	<DL	11.1003	19.6585	15.2632	<DL	0.0447	0.0165
	7.8032	<DL	11.2191	19.9086	15.5340	<DL	0.0465	0.0178
6-5-40-15	7.8955	<DL	11.1597	19.7835	15.3986	<DL	0.0456	0.0171
	0.1306	<DL	0.0841	0.1768	0.1915	<DL	0.0013	0.0009
6-5-40-30	8.0395	<DL	15.1163	24.8989	16.4196	<DL	0.0485	0.0192
	8.2328	<DL	14.6729	26.9549	16.1061	<DL	0.0574	0.0251
	7.9694	<DL	14.3138	26.8185	15.7656	<DL	0.0584	0.0281
6-5-40-50	8.1011	<DL	14.4934	26.8867	15.9359	<DL	0.0579	0.0266
	0.1863	<DL	0.2539	0.0964	0.2408	<DL	0.0007	0.0021
6-5-40-75	8.2706	<DL	15.3054	29.0836	16.9985	<DL	0.0631	0.0391

Sample	Mg (mg/g)	Al (mg/g)	Si (mg/g)	K (mg/g)	Ca (mg/g)	Fe (mg/g)	Sr (mg/g)	Ba (mg/g)
	6.5319	<DL	7.5144	5.9439	13.2438	0.0010	0.0388	0.0162
	6.6700	<DL	7.3785	5.9926	14.0646	0.0007	0.0416	0.0149
6-7-5-1	6.6009	<DL	7.4464	5.9682	13.6542	0.0008	0.0402	0.0156
	0.0976	<DL	0.0961	0.0345	0.5804	0.0002	0.0020	0.0009
6-7-5-5	6.7398	<DL	13.0833	7.1652	16.4673	0.0011	0.0457	0.0211
	6.9085	<DL	13.0608	9.0960	15.7253	0.0012	0.0519	0.0215
	7.3503	<DL	13.8002	9.5670	16.9084	0.0013	0.0517	0.0270
6-7-5-15	7.1294	<DL	13.4305	9.3315	16.3168	0.0012	0.0518	0.0242
	0.3124	<DL	0.5229	0.3331	0.8366	0.00005	0.0002	0.0039
6-7-5-30	8.6086	<DL	14.8203	14.7476	17.8346	0.0016	0.0623	0.0353
	9.7563	<DL	16.7425	17.7130	17.4077	0.0016	0.0594	0.0399
	9.3173	<DL	15.5478	16.1708	15.6075	0.0014	0.0563	0.0358
6-7-5-50	9.5368	<DL	16.1451	16.9419	16.5076	0.0015	0.0578	0.0379
	0.3105	<DL	0.8447	1.0905	1.2730	0.0002	0.0022	0.0029
6-7-5-75	9.8948	<DL	16.3031	21.0702	16.7587	0.0017	0.0705	0.0454

Sample	Mg (mg/g)	Al (mg/g)	Si (mg/g)	K (mg/g)	Ca (mg/g)	Fe (mg/g)	Sr (mg/g)	Ba (mg/g)
	6.6802	<DL	9.5349	10.0502	16.2858	0.0011	0.0454	0.0214
	6.7198	<DL	9.4589	9.9637	15.9868	0.0010	0.0437	0.0185
6-7-20-1	6.7000	<DL	9.4969	10.0069	16.1363	0.0010	0.0446	0.0199
	0.0280	<DL	0.0538	0.0612	0.2114	0.0001	0.0013	0.0021
6-7-20-5	9.7250	<DL	12.8211	12.7336	15.3387	0.0013	0.0490	0.0269
	9.8428	<DL	13.2404	15.8032	15.6958	0.0015	0.0510	0.0315
	9.8619	<DL	13.3033	16.4221	15.3318	0.0017	0.0565	0.0332
6-7-20-15	9.8523	<DL	13.2719	16.1126	15.5138	0.0016	0.0538	0.0323
	0.0135	<DL	0.0445	0.4376	0.2574	0.0001	0.0039	0.0012
6-7-20-30	10.2293	<DL	16.1047	19.6590	15.1752	0.0019	0.0657	0.0430
	10.8950	<DL	17.3359	23.2431	15.5791	0.0020	0.0674	0.0468
	10.1297	<DL	16.9557	25.5461	15.7909	0.0021	0.0688	0.0512
6-7-20-50	10.5124	<DL	17.1458	24.3946	15.6850	0.0020	0.0681	0.0490
	0.5412	<DL	0.2688	1.6284	0.1498	0.0001	0.0010	0.0032
6-7-20-75	11.1572	<DL	16.2078	30.9073	16.8020	0.0022	0.0748	0.0547

Sample	Mg (mg/g)	Al (mg/g)	Si (mg/g)	K (mg/g)	Ca (mg/g)	Fe (mg/g)	Sr (mg/g)	Ba (mg/g)
	8.3189	<DL	14.6710	10.6249	16.7715	<DL	0.0464	0.0227
	8.2788	<DL	15.4254	11.5838	16.5773	<DL	0.0490	0.0238
6-7-40-1	8.2988	<DL	15.0482	11.1043	16.6744	<DL	0.0477	0.0232
	0.0283	<DL	0.5335	0.6781	0.1373	<DL	0.0019	0.0008
6-7-40-5	10.3683	<DL	16.9461	11.9778	16.1376	<DL	0.0507	0.0270
	10.8214	<DL	17.8759	20.2597	17.7444	<DL	0.0525	0.0376
	11.3490	<DL	17.8104	20.8069	17.9625	<DL	0.0550	0.0391
6-7-40-15	11.0852	<DL	17.8431	20.5333	17.8535	<DL	0.0538	0.0384
	0.3730	<DL	0.0464	0.3869	0.1542	<DL	0.0017	0.0010
6-7-40-30	11.7661	<DL	17.8600	27.9809	17.9883	<DL	0.0686	0.0435
	12.9822	<DL	17.6443	31.4572	17.0959	<DL	0.0682	0.0506
	14.0196	<DL	18.1852	33.4973	18.0952	<DL	0.0749	0.0513
6-7-40-50	13.5009	<DL	17.9148	32.4773	17.5956	<DL	0.0715	0.0510
	0.7335	<DL	0.3825	1.4426	0.7066	<DL	0.0048	0.0005
6-7-40-75	15.0509	<DL	17.4186	38.7404	18.8367	<DL	0.0717	0.0537

Sample	Mg (mg/g)	Al (mg/g)	Si (mg/g)	K (mg/g)	Ca (mg/g)	Fe (mg/g)	Sr (mg/g)	Ba (mg/g)
	10.0368	<DL	6.3147	4.8034	8.6938	0.0008	0.0488	0.0256
	9.7654	<DL	6.1540	4.6916	8.4590	0.0008	0.0473	0.0245
6-8.5-5-1	9.9011	<DL	6.2344	4.7475	8.5764	0.0008	0.0481	0.0251
	0.1919	<DL	0.1136	0.0790	0.1660	0.0001	0.0011	0.0008
6-8.5-5-5	11.8127	<DL	5.8187	5.3284	10.0736	0.0013	0.0632	0.0372
	11.3419	<DL	8.0597	6.1028	9.7724	0.0003	0.0570	0.0290
	11.1512	<DL	7.9449	7.1433	9.8958	0.0002	0.0554	0.0330
6-8.5-5-15	11.2466	<DL	8.0023	6.6231	9.8341	0.0003	0.0562	0.0310
	0.1349	<DL	0.0812	0.7358	0.0873	0.0001	0.0011	0.0029
6-8.5-5-30	12.6985	<DL	9.9080	8.9327	12.5561	0.0005	0.0565	0.0334
	13.3180	<DL	11.7206	10.1320	13.9582	0.0006	0.0564	0.0352
	12.7908	<DL	11.7914	10.3218	13.9755	0.0007	0.0549	0.0381
6-8.5-5-50	13.0544	<DL	11.7560	10.2269	13.9668	0.0006	0.0556	0.0367
	0.3728	<DL	0.0500	0.1343	0.0123	0.0001	0.0011	0.0020
6-8.5-5-75	14.0266	<DL	12.4707	20.1642	15.0188	0.0007	0.0593	0.0425

Sample	Mg (mg/g)	Al (mg/g)	Si (mg/g)	K (mg/g)	Ca (mg/g)	Fe (mg/g)	Sr (mg/g)	Ba (mg/g)
	9.7253	<DL	7.8853	9.4176	10.0235	0.0007	0.0615	0.0396
	9.9328	<DL	8.0629	9.6317	10.1677	0.0006	0.0621	0.0389
6-8.5-20-1	9.8290	<DL	7.9741	9.5247	10.0956	0.0007	0.0618	0.0393
	0.1468	<DL	0.1256	0.1514	0.1019	0.0001	0.0004	0.0005
6-8.5-20-5	11.1407	<DL	8.2140	9.9657	12.3640	0.0007	0.0621	0.0409
	12.1784	<DL	9.1140	10.0741	13.0997	0.0010	0.0599	0.0418
	13.0865	<DL	9.3726	11.6178	13.2674	0.0010	0.0663	0.0436
6-8.5-20-15	12.6325	<DL	9.2433	10.8460	13.1836	0.0010	0.0631	0.0427
	0.6421	<DL	0.1828	1.0915	0.1186	0.00001	0.0046	0.0013
6-8.5-20-30	13.6160	<DL	9.6770	11.7810	14.0560	0.0011	0.0688	0.0427
	14.1413	<DL	10.7128	17.8416	15.1136	0.0012	0.0709	0.0471
	15.7119	<DL	10.6094	17.1372	14.7964	0.0010	0.0716	0.0471
6-8.5-20-50	14.9266	<DL	10.6611	17.4894	14.9550	0.0011	0.0713	0.0471
	1.1106	<DL	0.0731	0.4981	0.2243	0.0001	0.0005	0.00001
6-8.5-20-75	16.0568	<DL	11.2422	20.4412	14.8959	0.0020	0.0702	0.0469

Sample	Mg (mg/g)	Al (mg/g)	Si (mg/g)	K (mg/g)	Ca (mg/g)	Fe (mg/g)	Sr (mg/g)	Ba (mg/g)
	10.6017	<DL	8.7064	11.4968	12.1716	<DL	0.0609	0.0421
	10.6930	<DL	8.8418	9.6639	12.1928	<DL	0.0585	0.0432
6-8.5-40-1	10.6473	<DL	8.7741	10.5803	12.1822	<DL	0.0597	0.0426
	0.0646	<DL	0.0958	1.2961	0.0149	<DL	0.0017	0.0008
6-8.5-40-5	11.4478	<DL	10.4103	12.7915	12.9049	<DL	0.0653	0.0454
	12.5787	<DL	11.0487	13.7670	13.7349	<DL	0.0723	0.0482
	12.8430	<DL	11.1389	13.6070	13.6396	<DL	0.0717	0.0506
6-8.5-40-15	12.7109	<DL	11.0938	13.6870	13.6872	<DL	0.0720	0.0494
	0.1869	<DL	0.0638	0.1131	0.0674	<DL	0.0004	0.0016
6-8.5-40-30	13.7291	<DL	13.4348	14.3800	13.7967	<DL	0.0726	0.0479
	13.9029	<DL	13.8682	17.8635	14.0110	<DL	0.0735	0.0504
	13.9473	<DL	13.6038	18.0335	14.1600	<DL	0.0728	0.0503
6-8.5-40-50	13.9251	<DL	13.7360	17.9485	14.0855	<DL	0.0732	0.0504
	0.0314	<DL	0.1869	0.1202	0.1053	<DL	0.0005	0.00003
6-8.5-40-75	16.9342	<DL	14.0482	24.0995	14.4494	<DL	0.0756	0.0508

Appendix - part 3a

(Concentrations of Mg, Si, K and Ca over time)

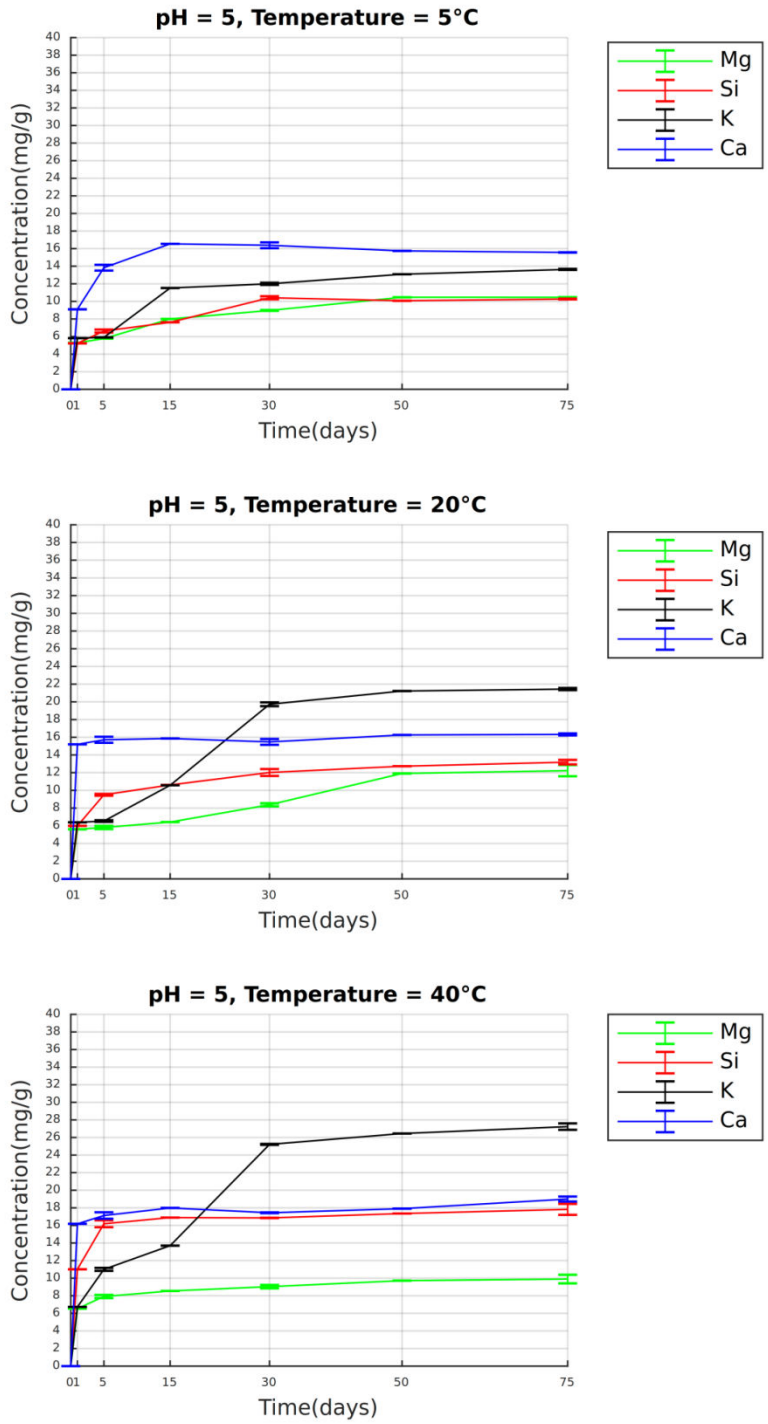

Fig. 112 Sample *Triticum durum*, Cyprus: concentration (mg/g) of Mg, Si, K, Ca over the course of 75 days at pH 5 and temperature 5 ˚C, 20˚C, 40 ˚C

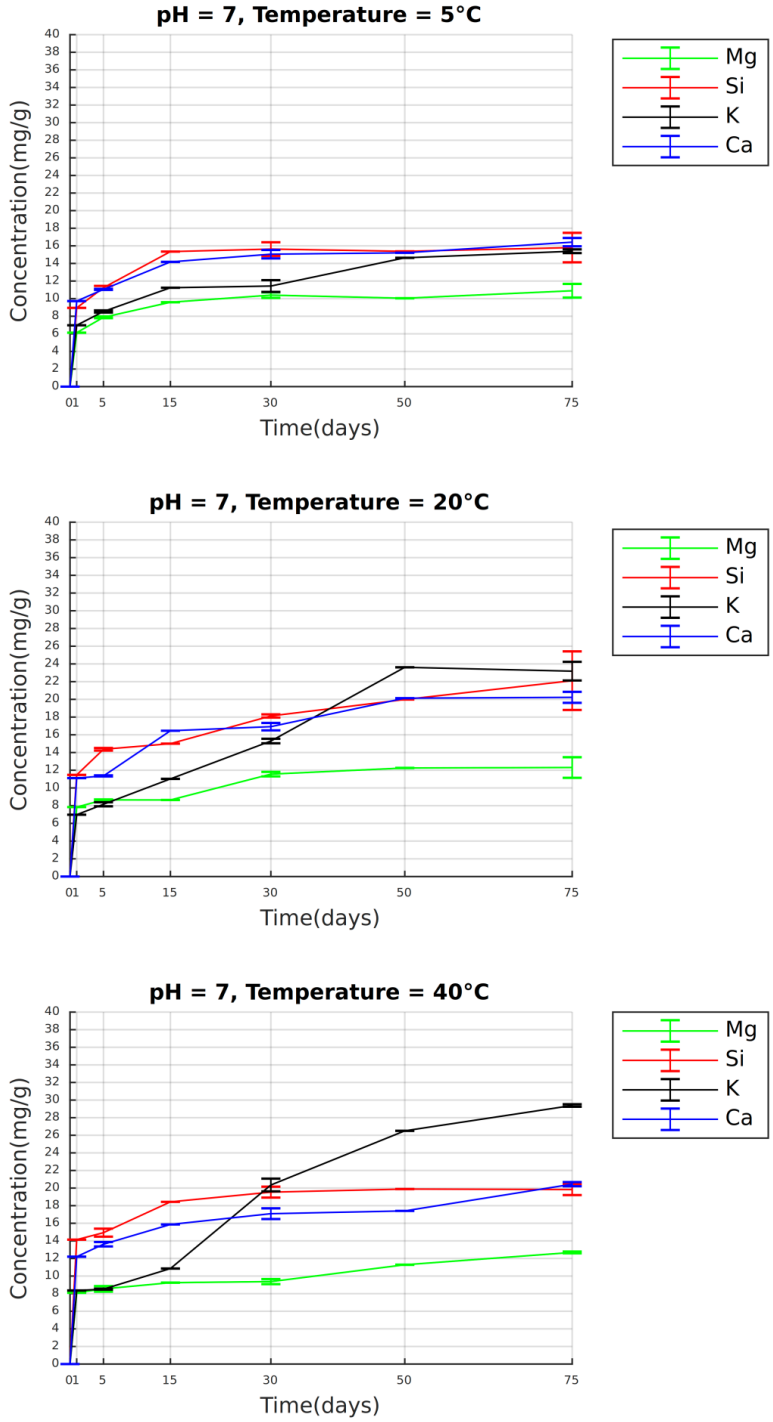

Fig. 113 Sample *Triticum durum*, Cyprus: concentration (mg/g) of Mg, Si, K, Ca over the course of 75 days at pH 7 and temperature 5 ˚C, 20˚C, 40 ˚C

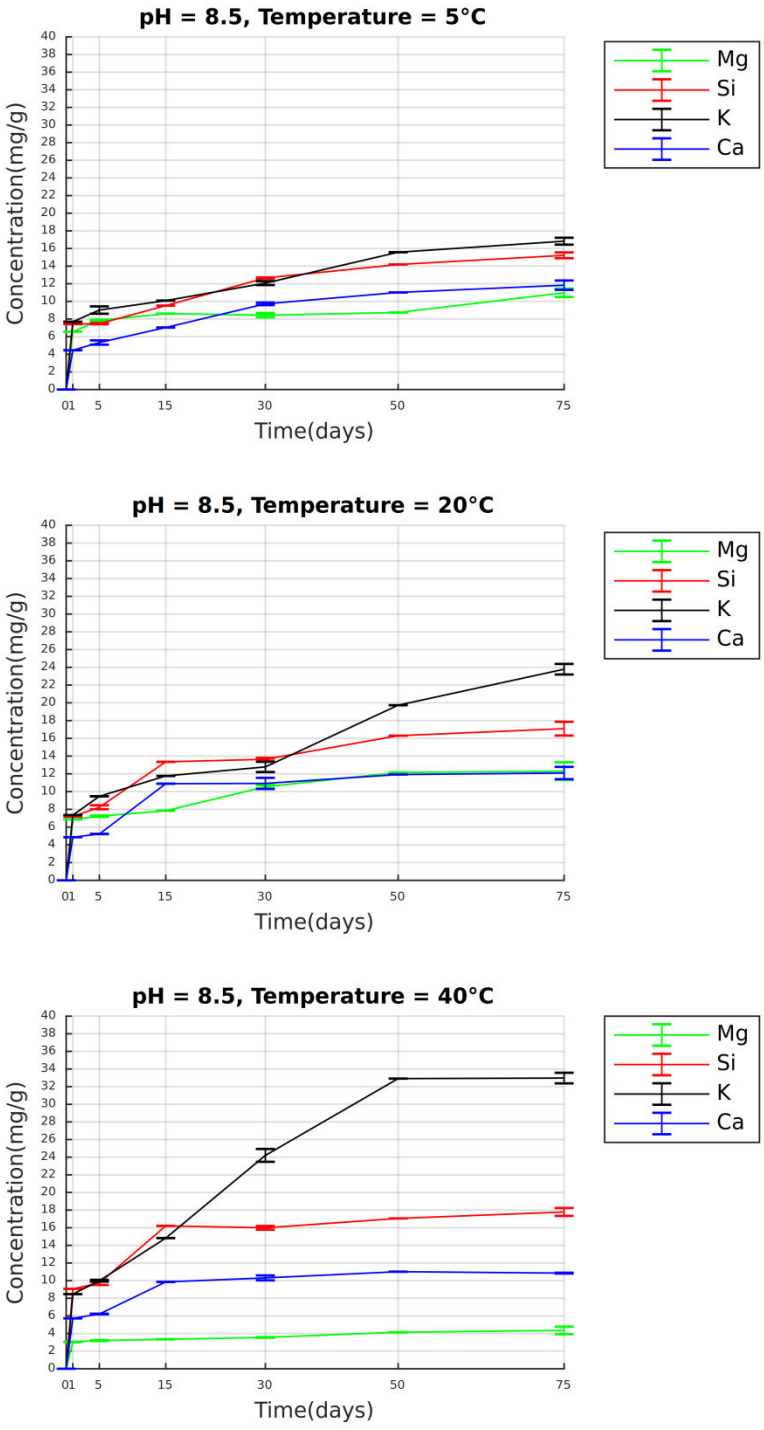

Fig. 114 Sample *Triticum durum*, Cyprus: concentration (mg/g) of Mg, Si, K, Ca over the course of 75 days at pH 8.5 and temperature 5 ˚C, 20˚C, 40 ˚C

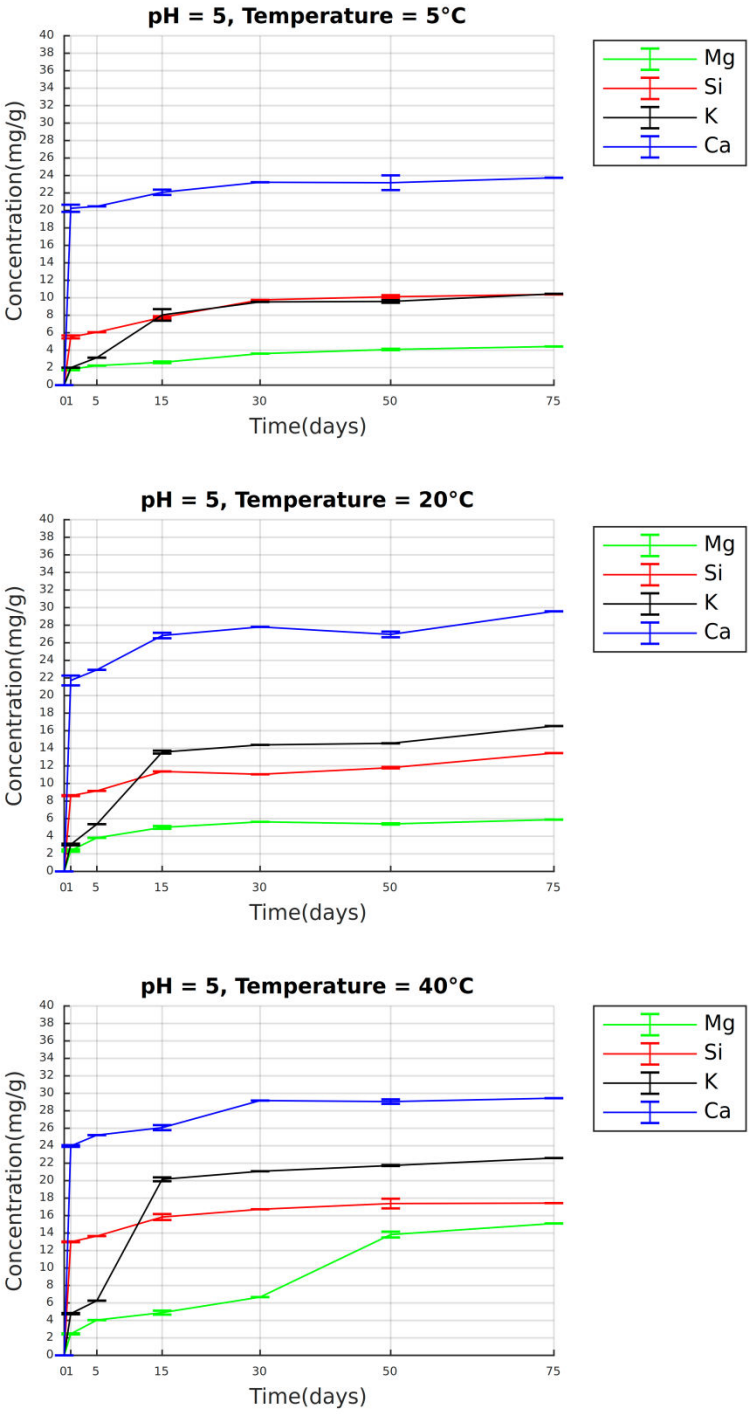

Fig. 115 Sample *Triticum durum*, Crete: concentration (mg/g) of Mg, Si, K, Ca over the course of 75 days at pH 5 and temperature 5 ˚C, 20˚C, 40 ˚C

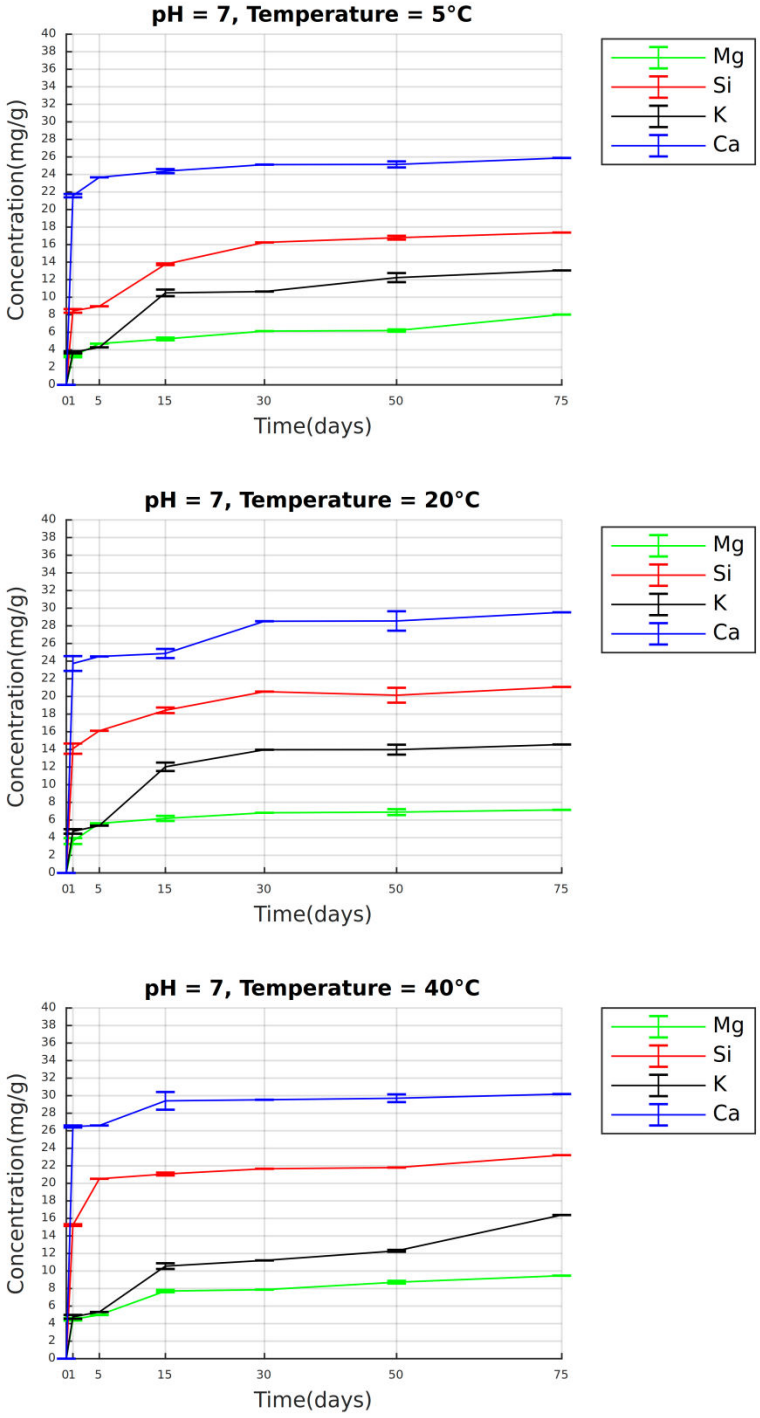

Fig. 116 Sample *Triticum durum*, Crete: concentration (mg/g) of Mg, Si, K, Ca over the course of 75 days at pH 7 and temperature 5 ˚C, 20˚C, 40 ˚C

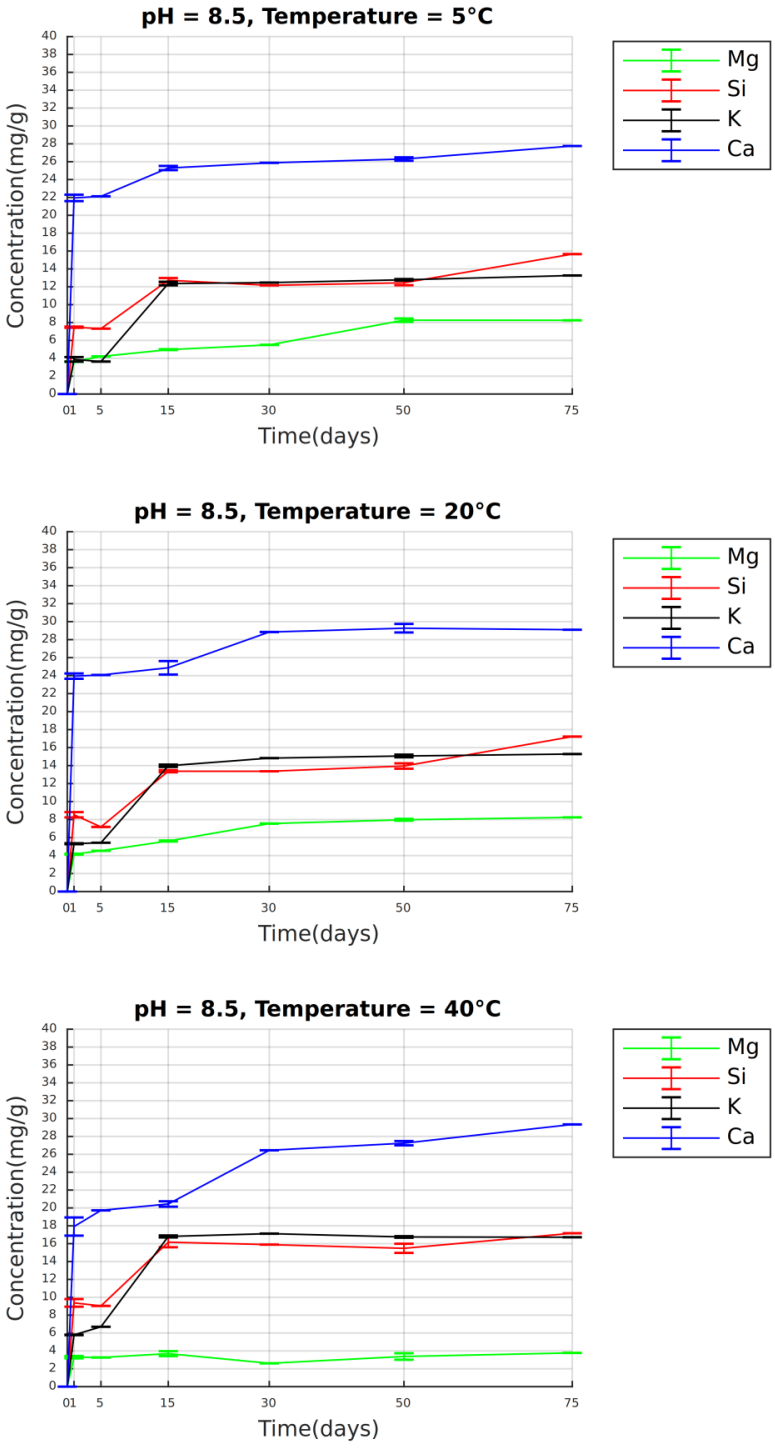

Fig. 117 Sample *Triticum durum*, Crete: concentration (mg/g) of Mg, Si, K, Ca over the course of 75 days at pH 8.5 and temperature 5 ˚C, 20˚C, 40 ˚C

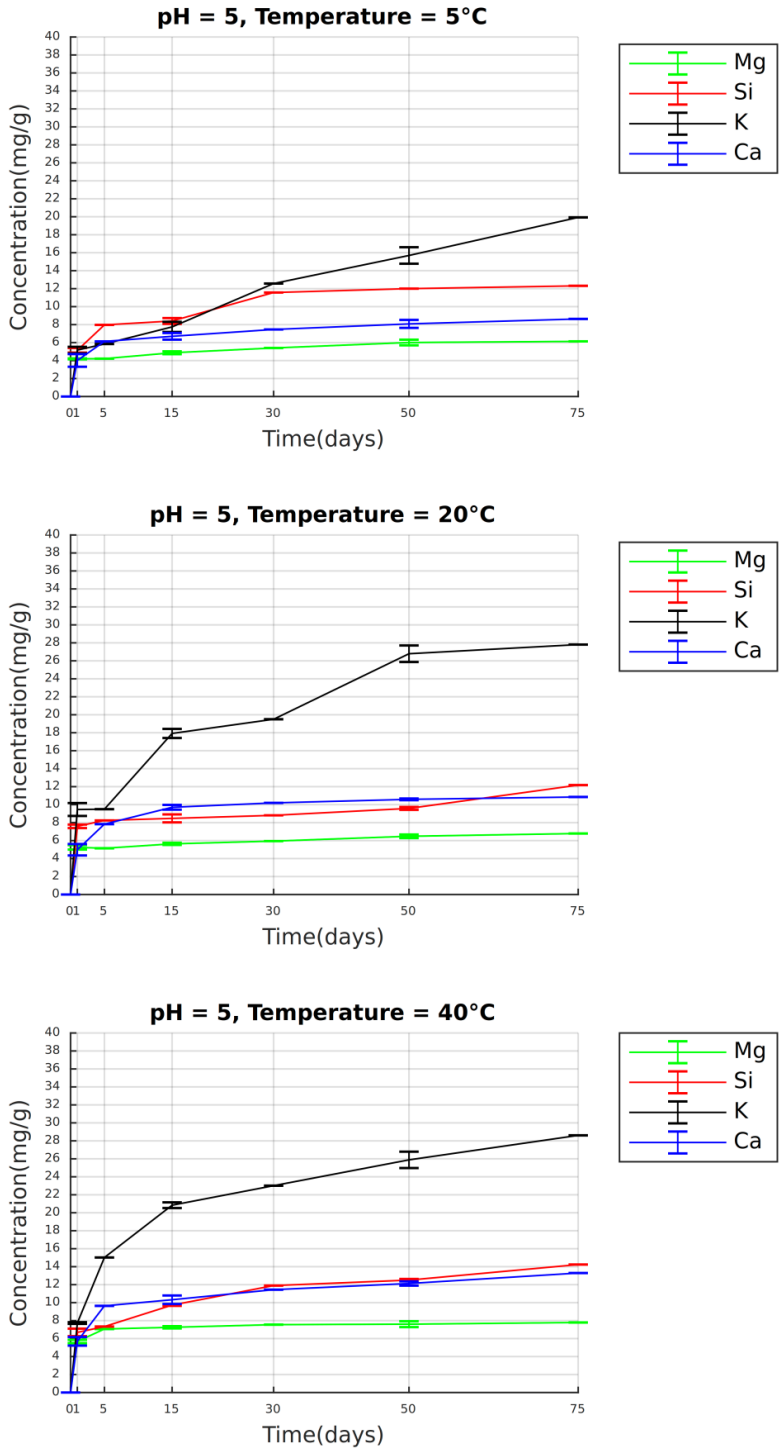

Fig. 118 Sample *Triticum monococcum*, Volos: concentration (mg/g) of Mg, Si, K, Ca over the course of 75 days at pH 5 and temperature 5 ˚C, 20˚C, 40 ˚C

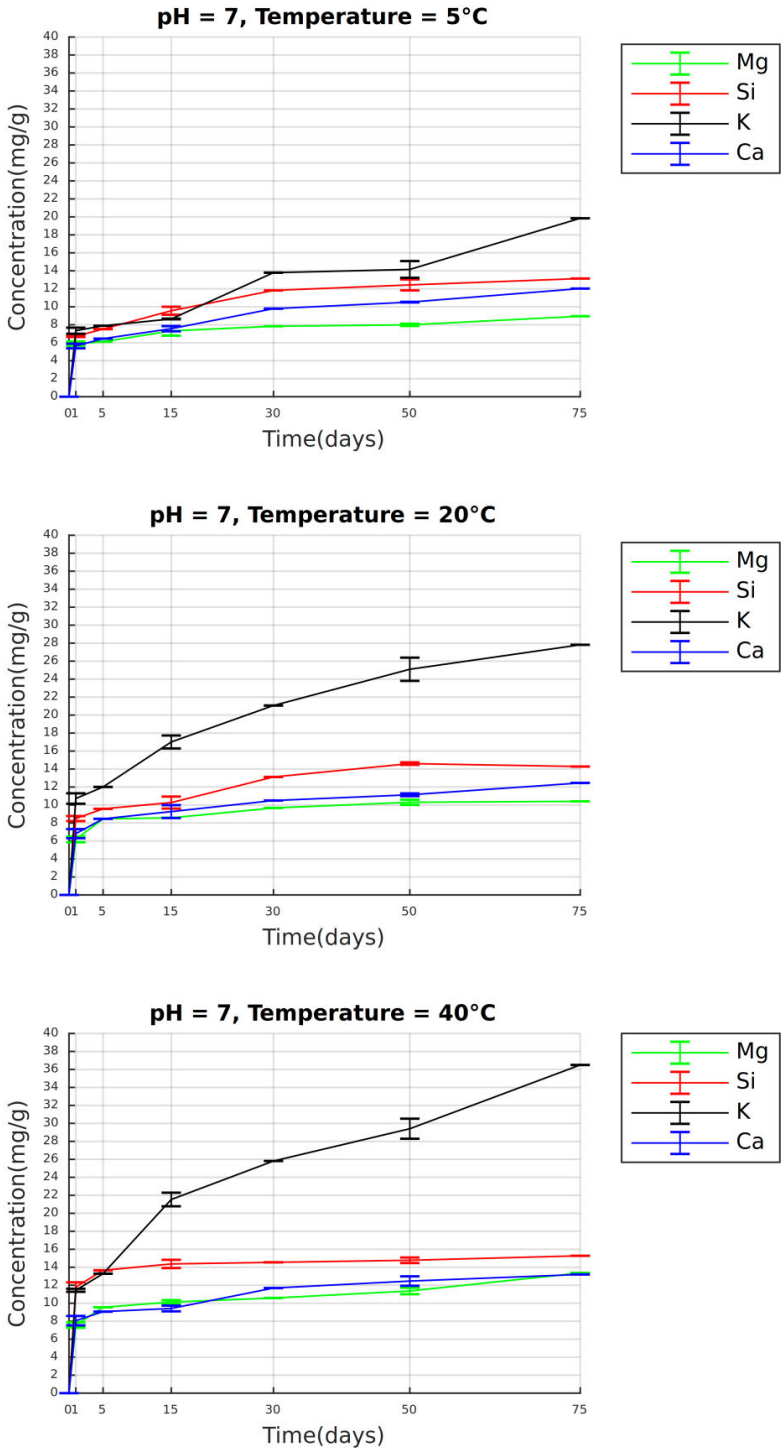

Fig. 119 Sample *Triticum monococcum*, Volos: concentration (mg/g) of Mg, Si, K, Ca over the course of 75 days at pH 7 and temperature 5 ˚C, 20˚C, 40 ˚C

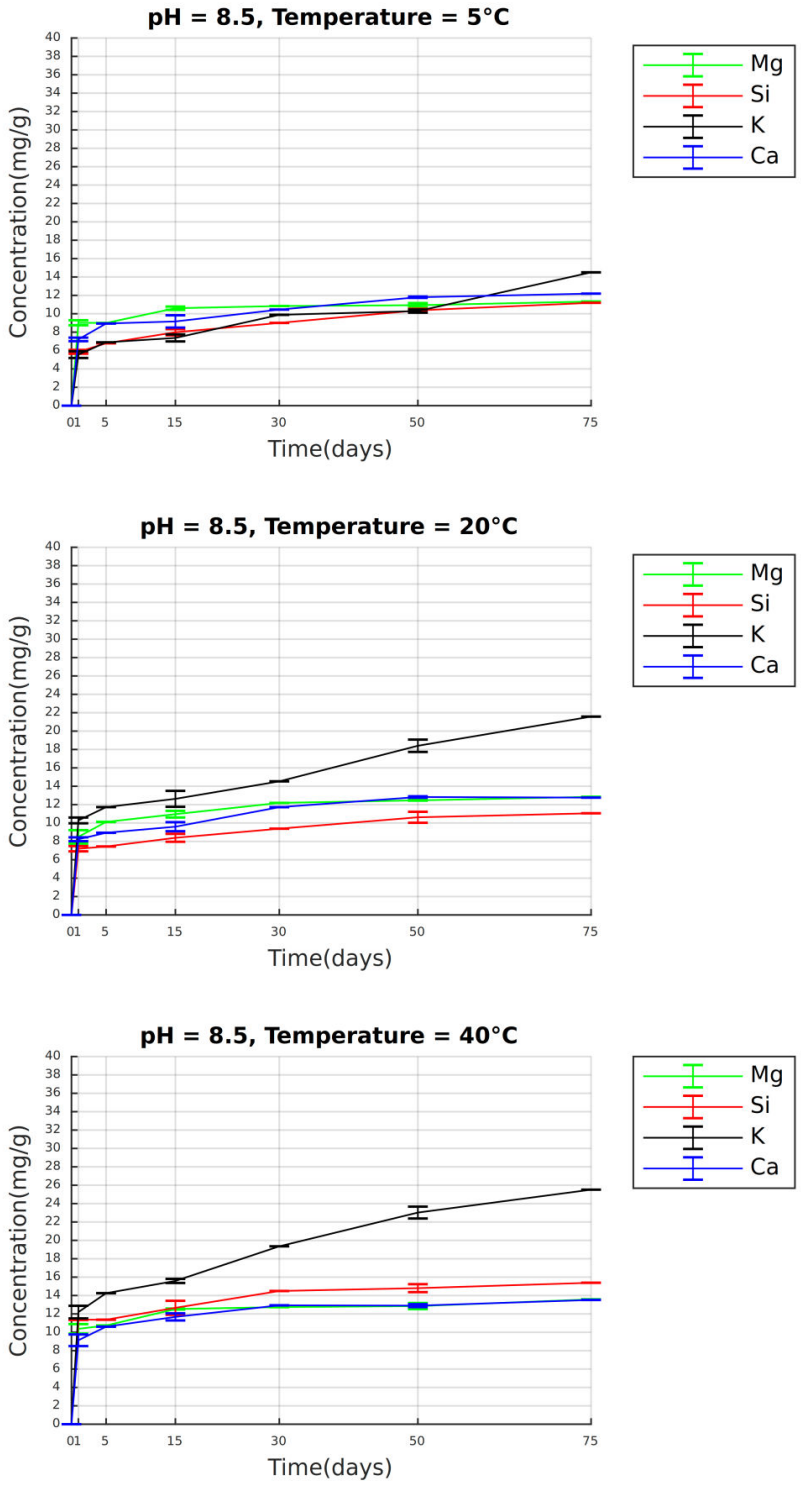

Fig. 120 Sample *Triticum monococcum*, Volos: concentration (mg/g) of Mg, Si, K, Ca over the course of 75 days at pH 8.5 and temperature 5 ˚C, 20˚C, 40 ˚C

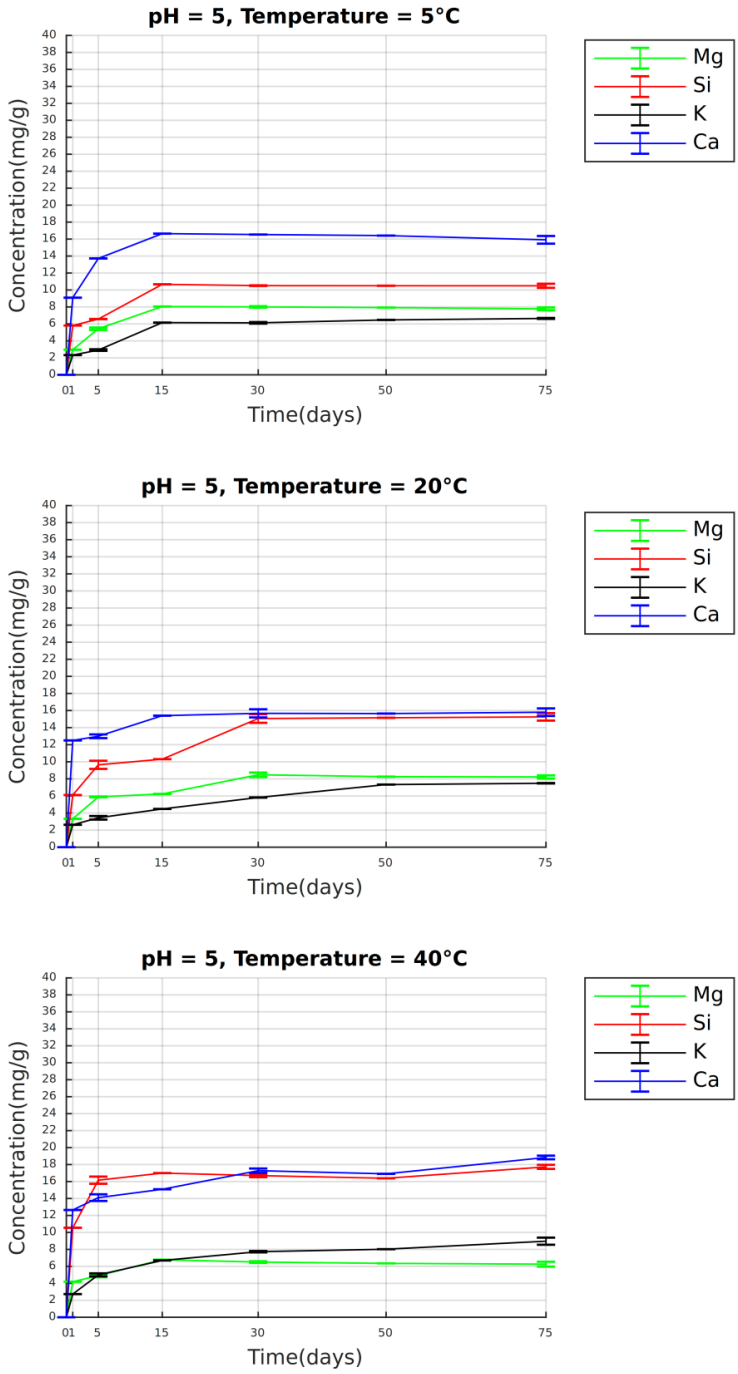

Fig. 121 Sample *Triticum monococcum,* Pella I: concentration (mg/g) of Mg, Si, K, Ca over the course of 75 days at pH 5 and temperature 5 ˚C, 20˚C, 40 ˚C

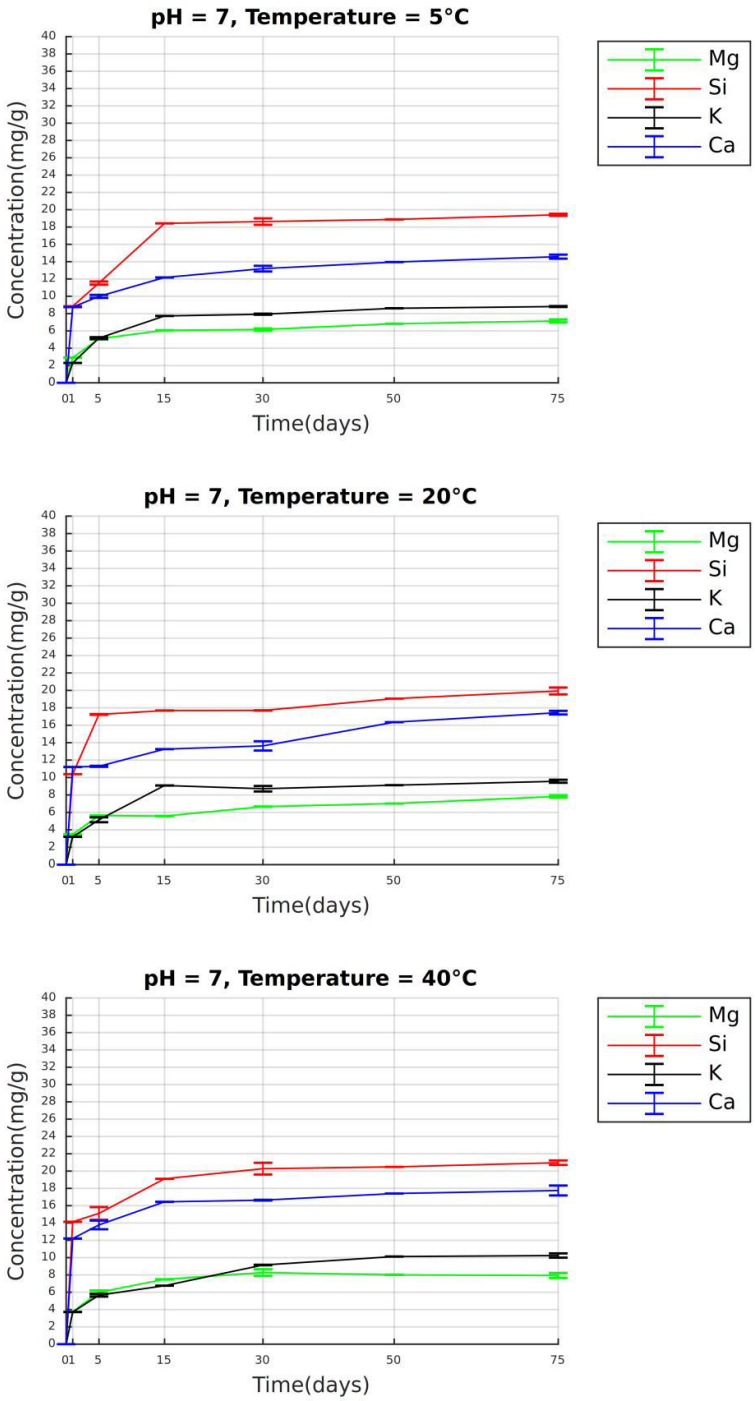

Fig. 122 Sample *Triticum monococcum,* Pella I: concentration (mg/g) of Mg, Si, K, Ca over the course of 75 days at pH 7 and temperature 5 ˚C, 20˚C, 40 ˚C

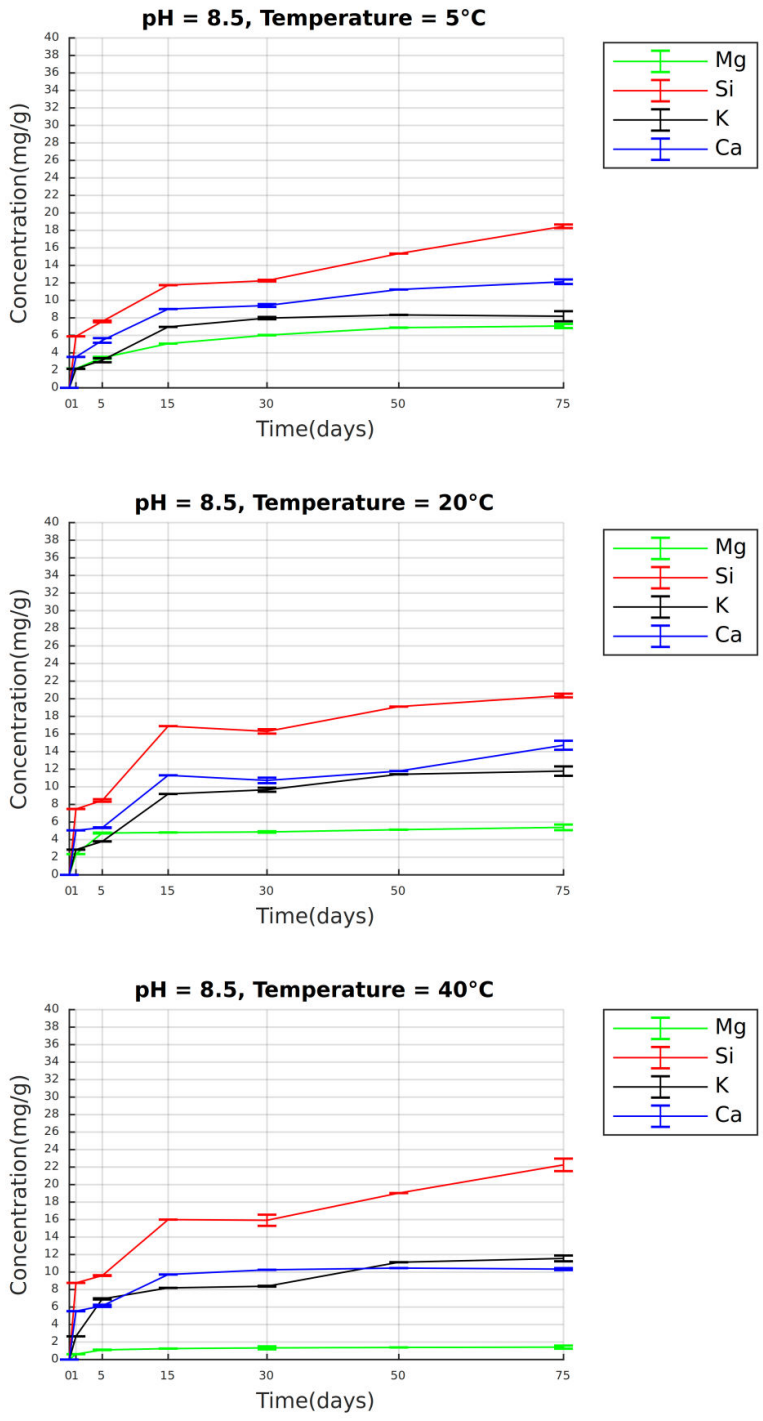

Fig. 123 Sample *Triticum monococcum,* Pella I: concentration (mg/g) of Mg, Si, K, Ca over the course of 75 days at pH 8.5 and temperature 5 ˚C, 20˚C, 40 ˚C

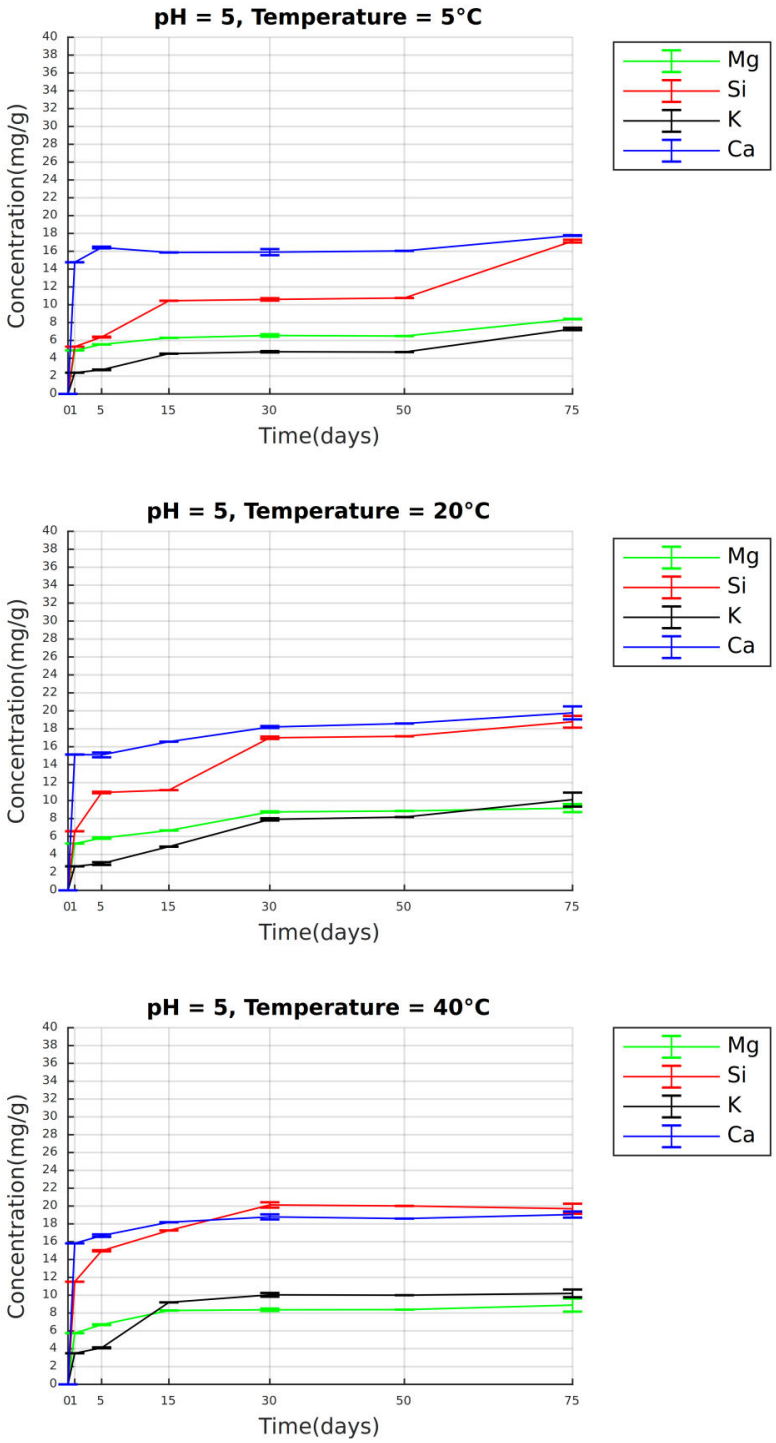

Fig. 124 Sample *Triticum monococcum,* Pella II: concentration (mg/g) of Mg, Si, K, Ca over the course of 75 days at pH 5 and temperature 5 ˚C, 20˚C, 40 ˚C

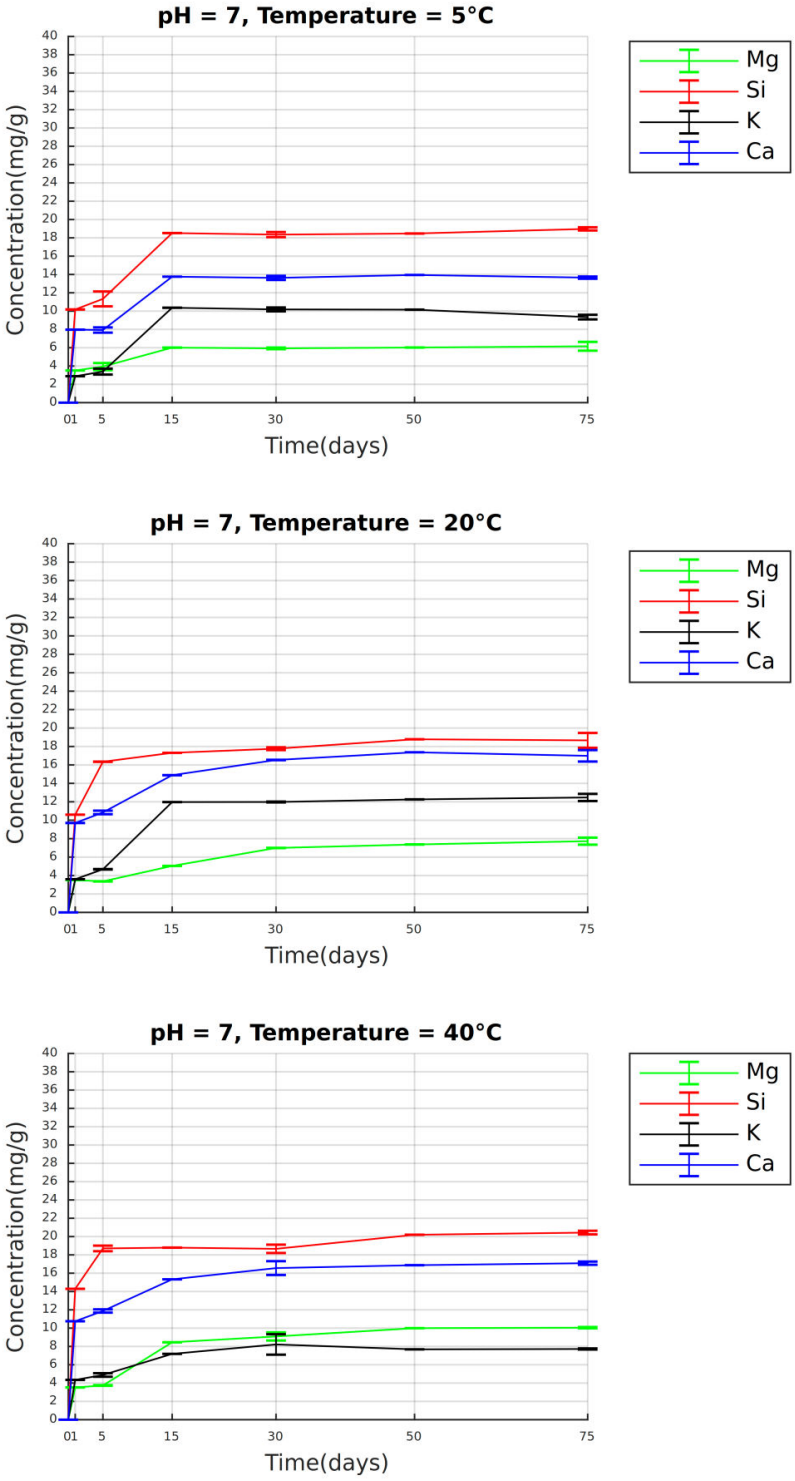

Fig. 125 Sample *Triticum durum,* Pella II: concentration (mg/g) of Mg, Si, K, Ca over the course of 75 days at pH 7 and at temperature 5 ˚C, 20˚C, 40 ˚C

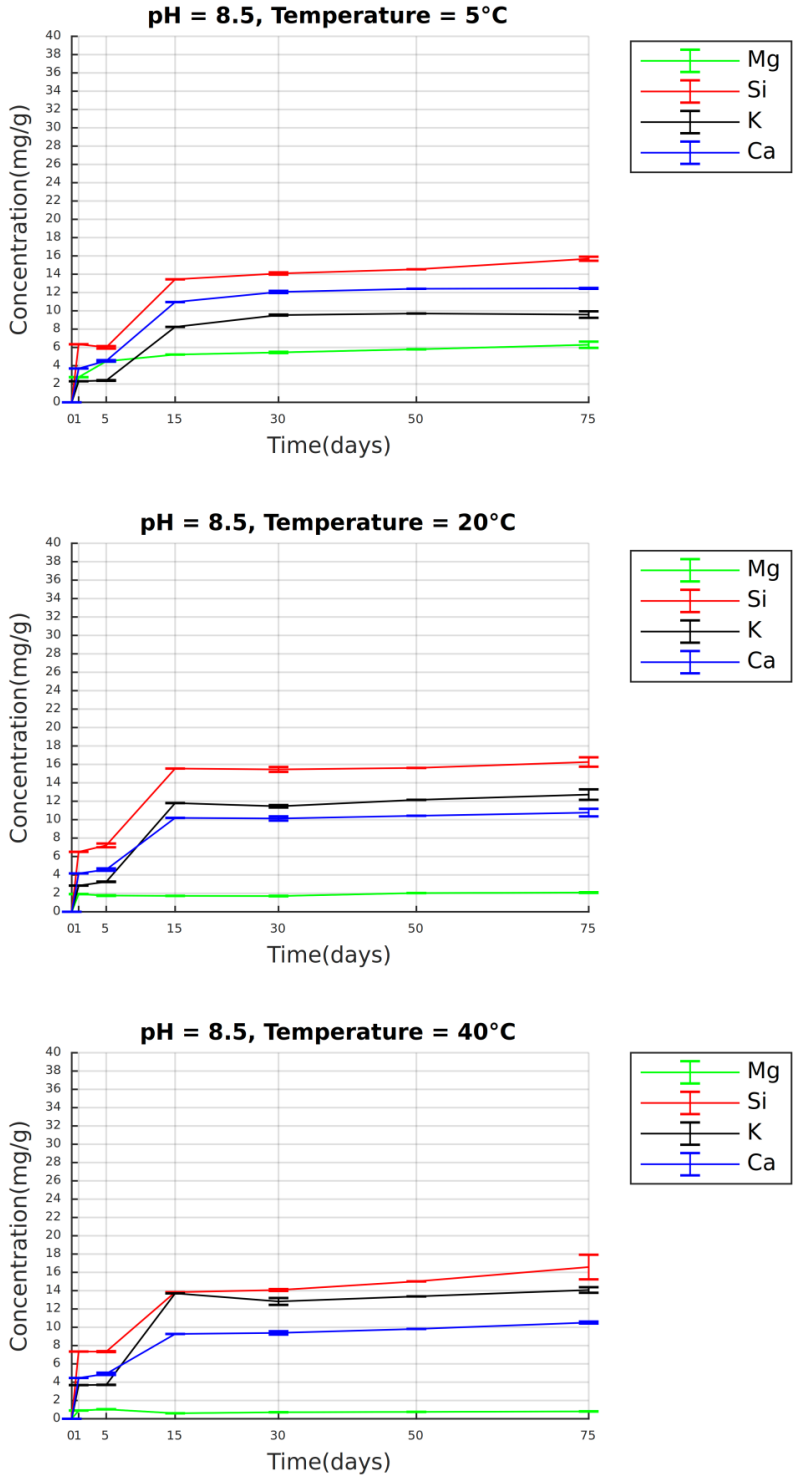

Fig. 126 Sample *Triticum durum,* Pella II: concentration (mg/g) of Mg, Si, K, Ca over the course of 75 days at pH 8.5 and temperature 5 ˚C, 20˚C, 40 ˚C

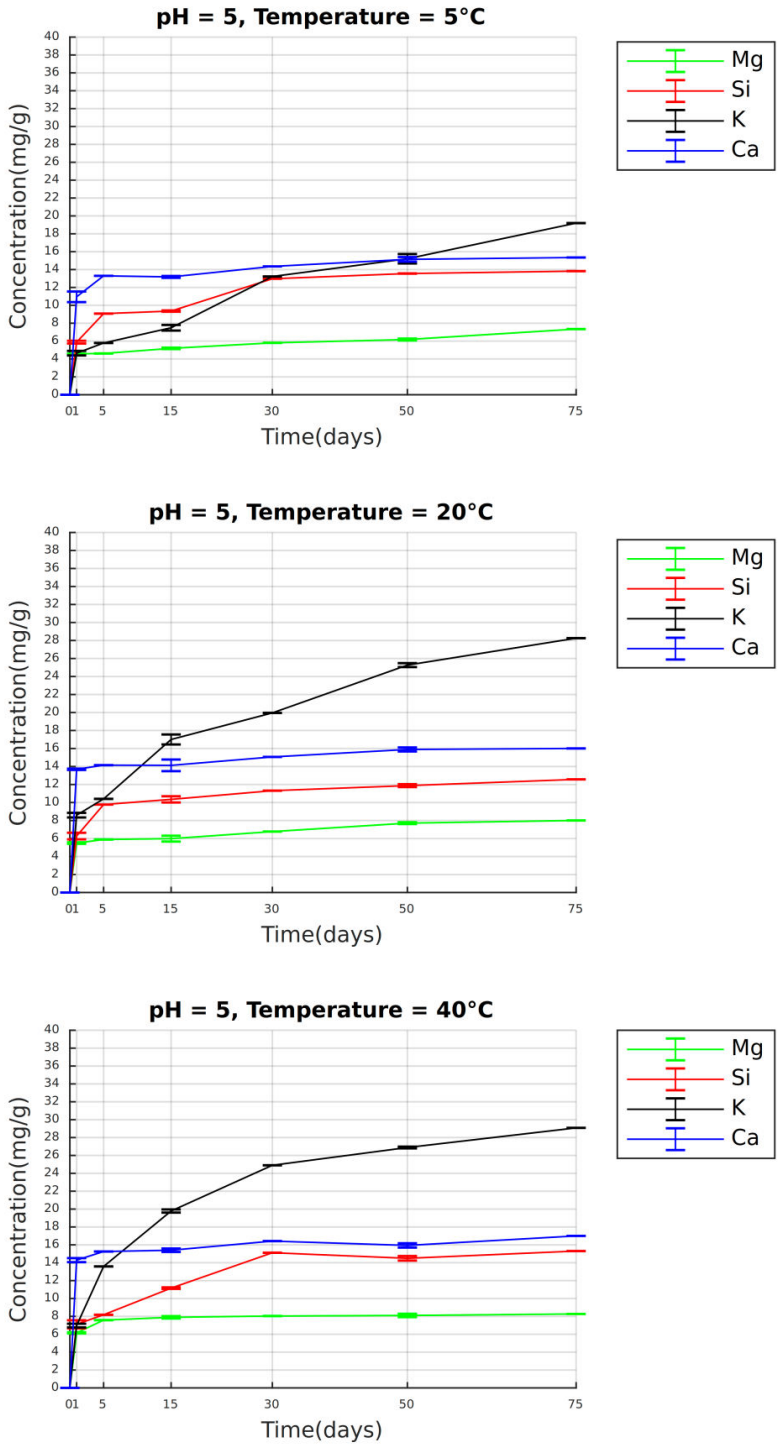

Fig. 127 Sample *Triticum durum,* Corfu: concentration (mg/g) of Mg, Si, K, Ca over the course of 75 days at pH 5 and temperature 5 ˚C, 20˚C, 40 ˚C

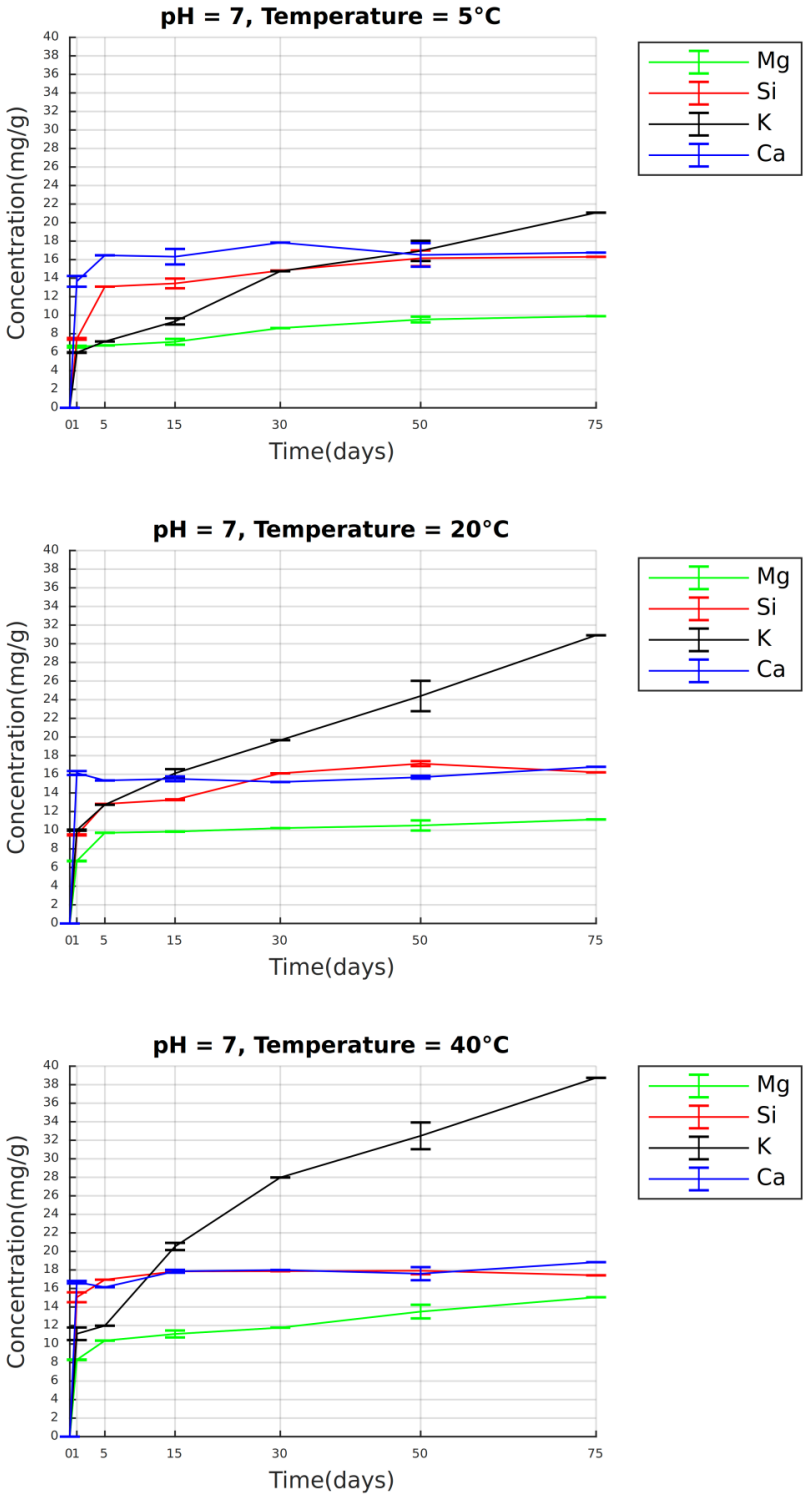

Fig. 128 Sample *Triticum durum,* Corfu: concentration (mg/g) of Mg, Si, K, Ca over the course of 75 days at pH 7 and temperature 5 ˚C, 20˚C, 40 ˚C

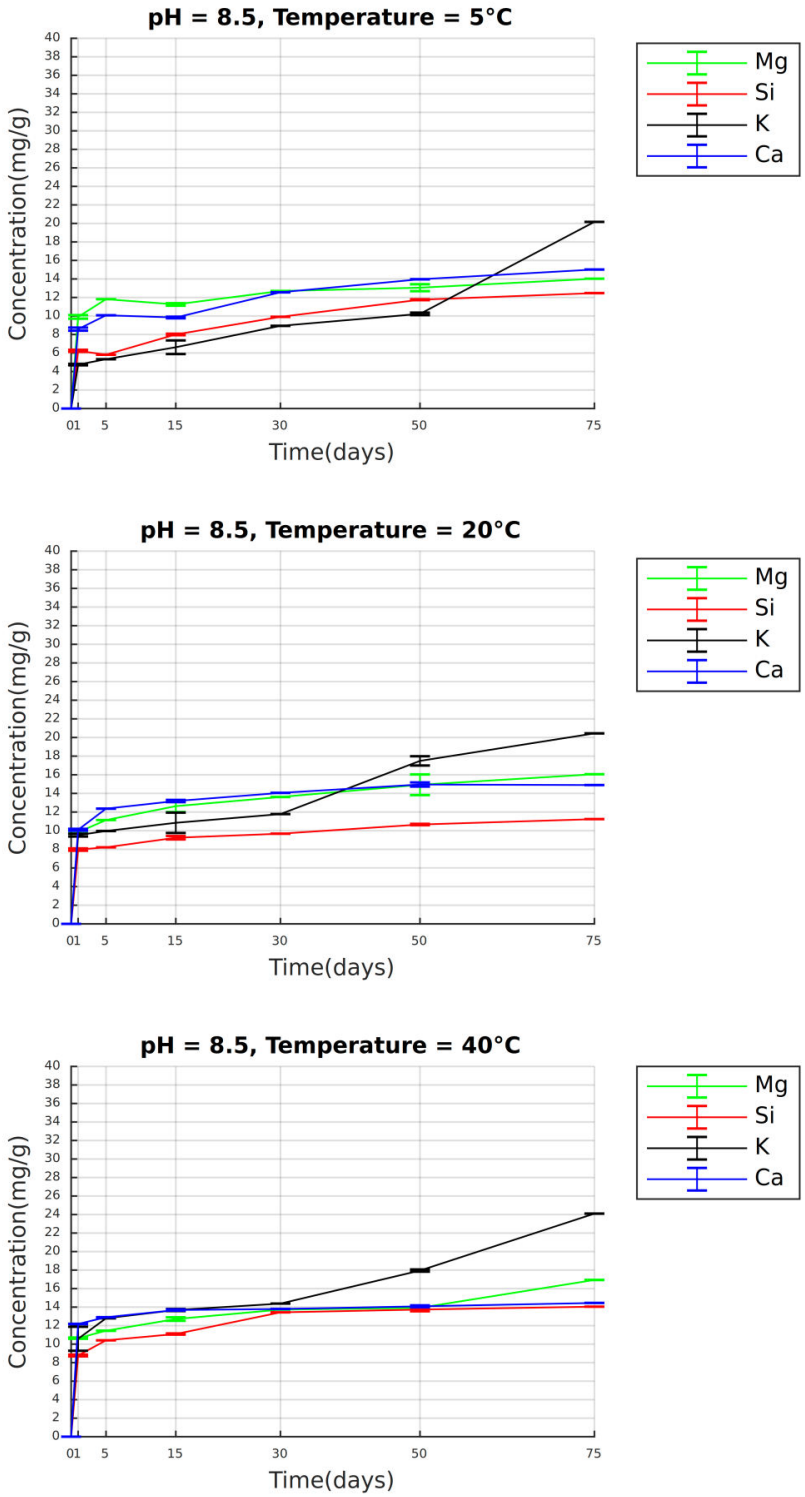

Fig. 129 Sample *Triticum durum,* Corfu: concentration (mg/g) of Mg, Si, K, Ca over the course of 75 days at pH 8.5 and temperature 5 ˚C, 20˚C, 40 ˚C

Appendix – part 3b

(Concentrations of Mg, Si, K and Ca over time)

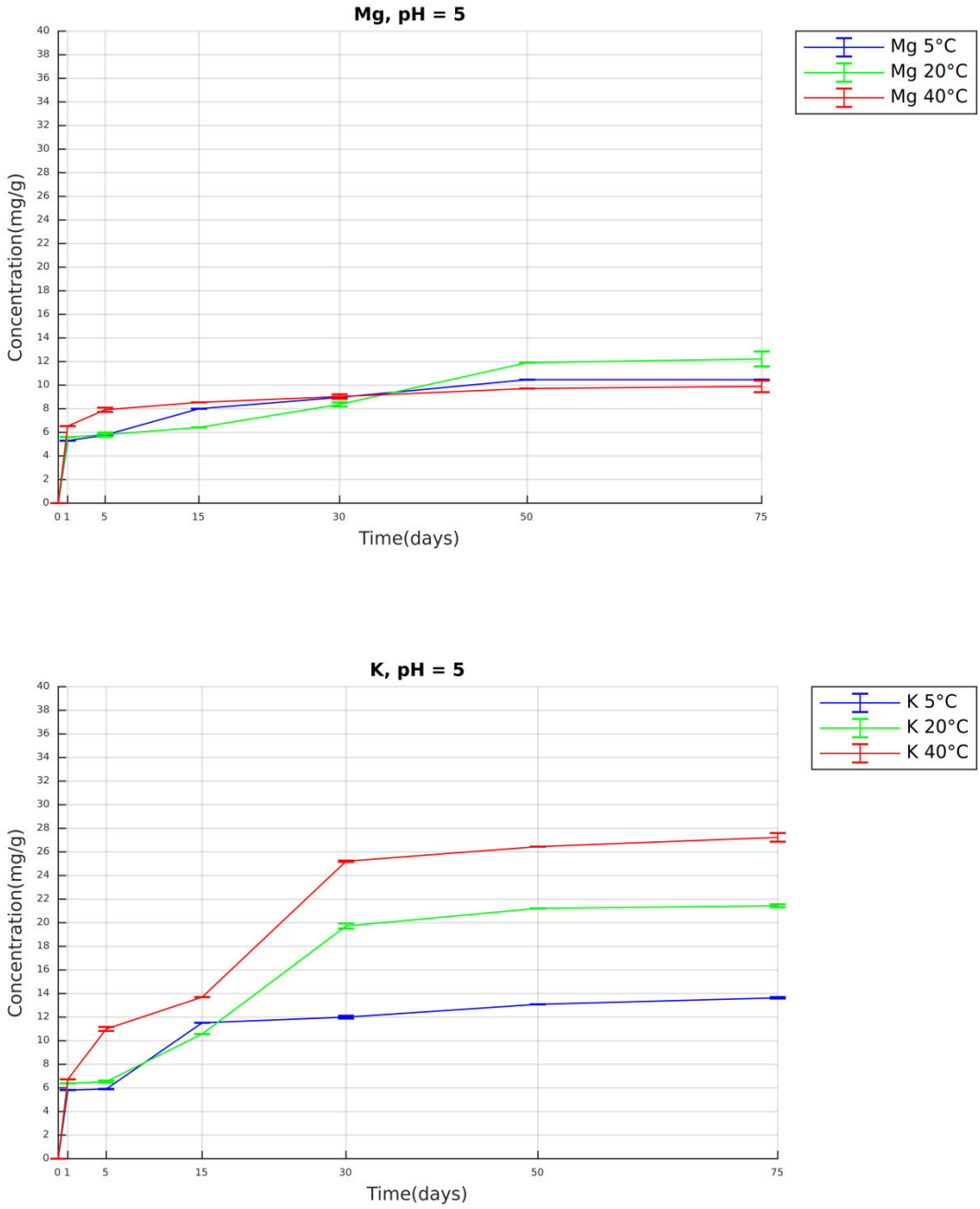

Fig. 130 Sample *Triticum durum,* Cyprus: concentration (mg/g) of Mg (above) and K (below) over the course of 75 days at pH 5 and temperature 5 ˚C, 20˚C, 40 ˚C

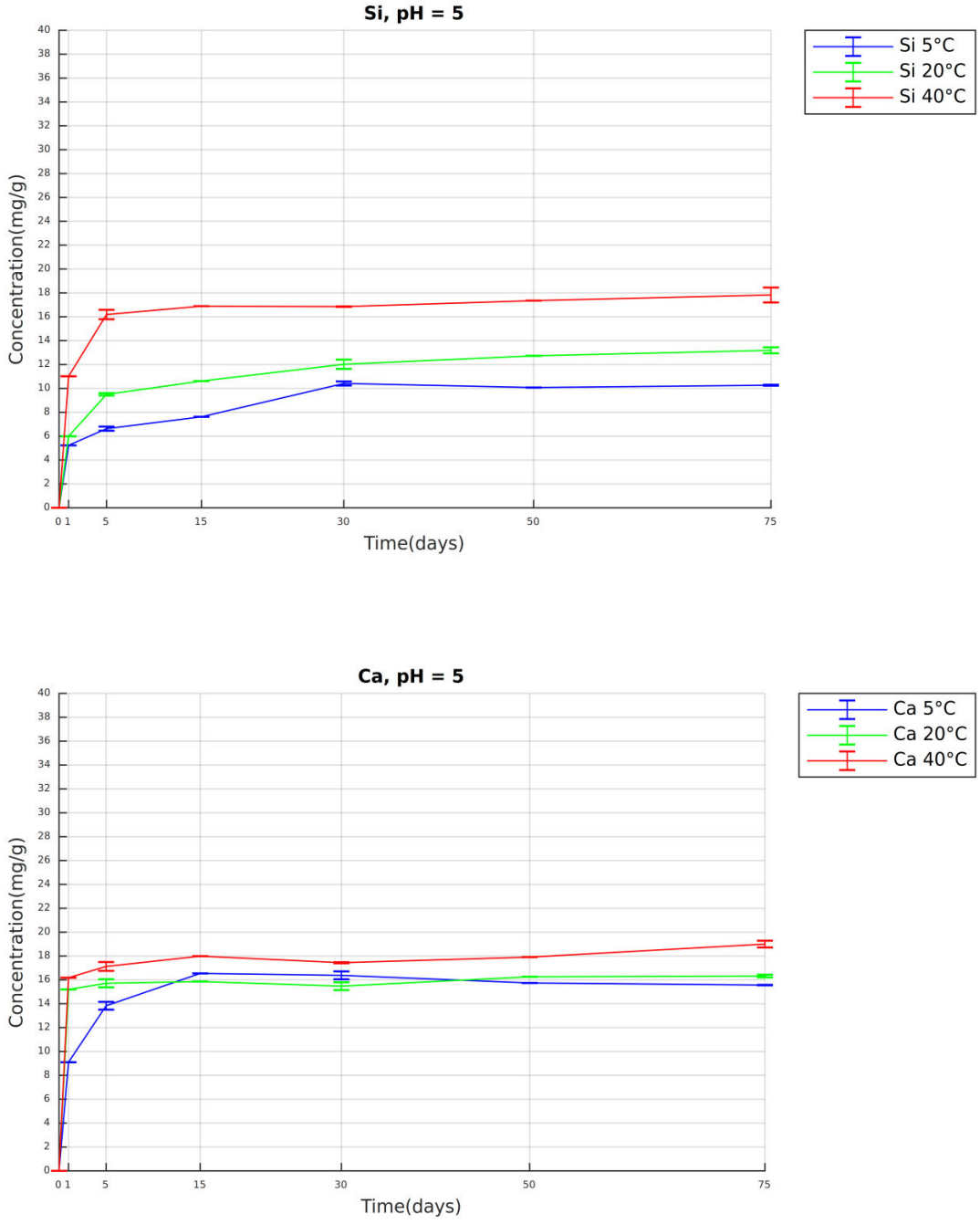

Fig. 131 Sample *Triticum durum,* Cyprus: concentration (mg/g) of Si (above) and Ca (below) over the course of 75 days at pH 5 and temperature 5 ˚C, 20˚C, 40 ˚C

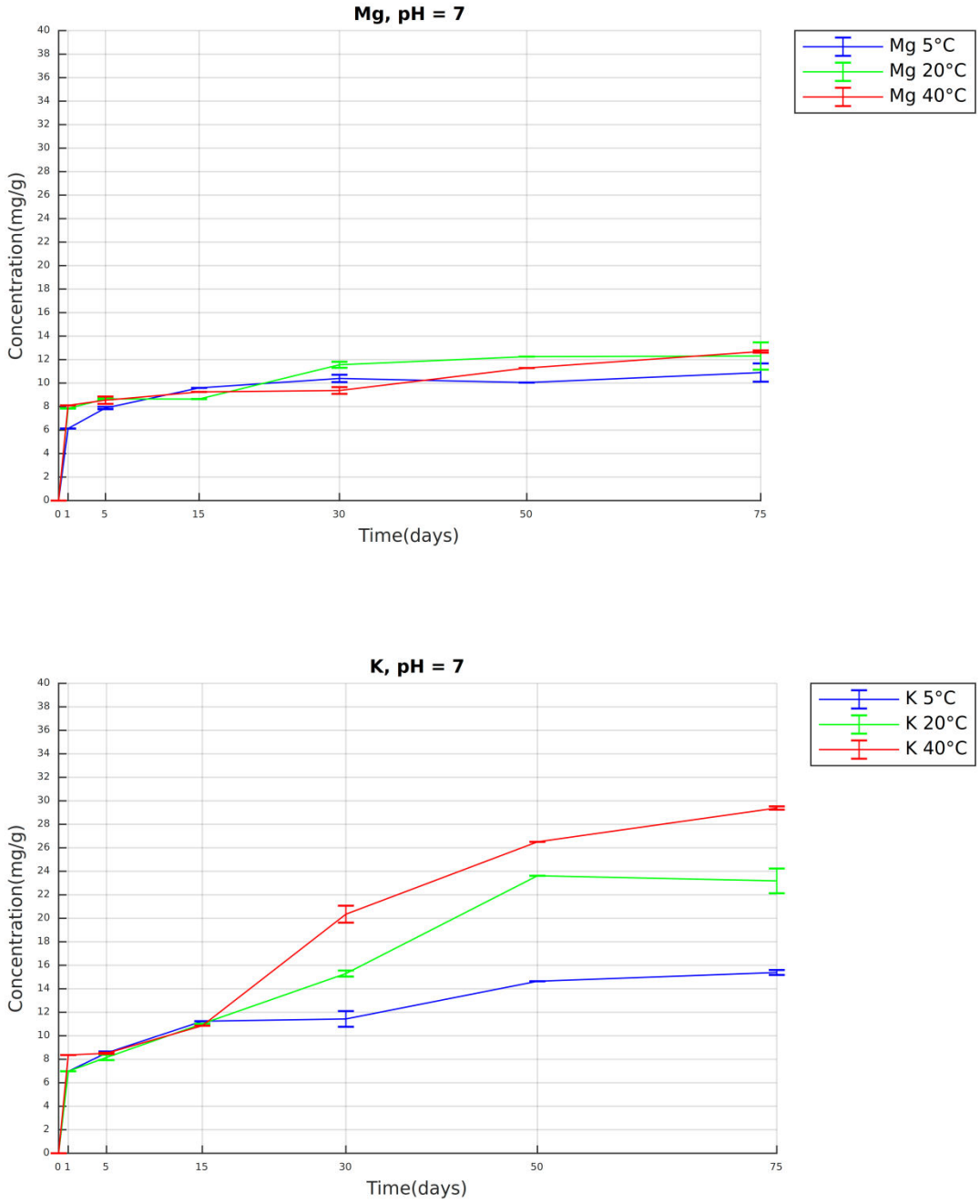

Fig. 132 Sample *Triticum durum*, Cyprus: concentration (mg/g) of Mg (above) and K (below) over the course of 75 days at pH 7 and temperature 5 ˚C, 20˚C, 40 ˚C

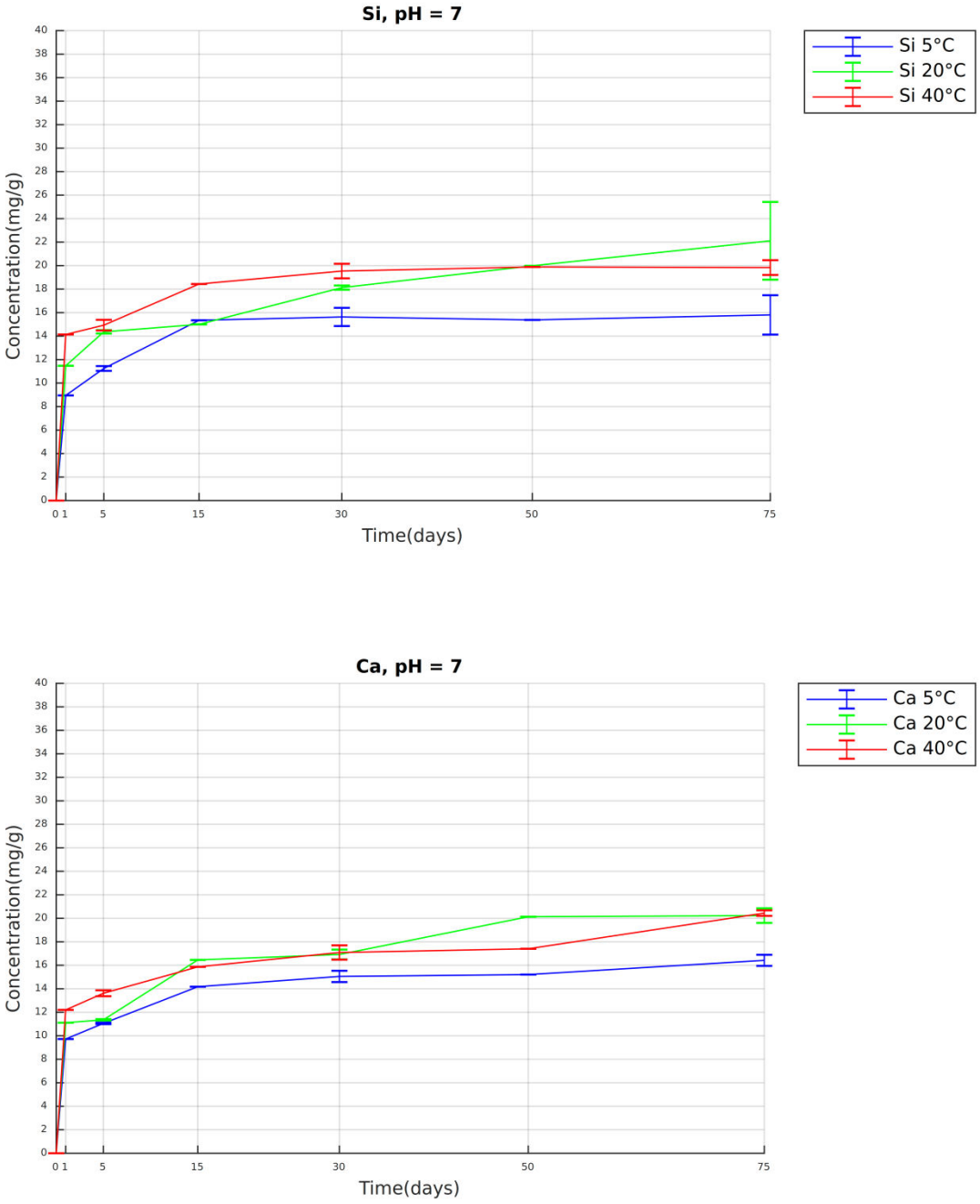

Fig. 133 Sample *Triticum durum,* Cyprus: concentration (mg/g) of Si (above) and Ca (below) over the course of 75 days at pH 7 and temperature 5 ˚C, 20˚C, 40 ˚C

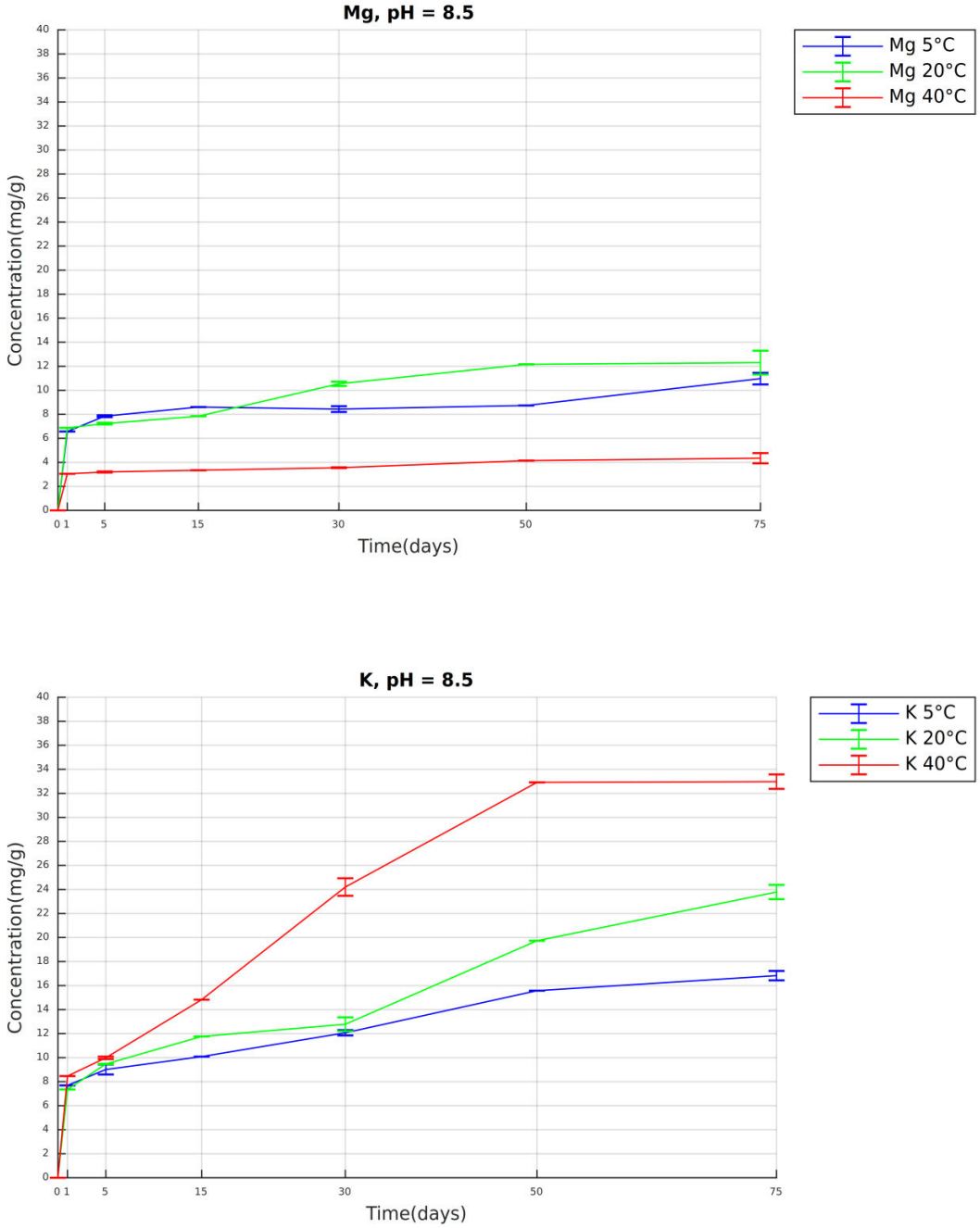

Fig. 134 Sample *Triticum durum,* Cyprus: concentration (mg/g) of Mg (above) and K (below) over the course of 75 days at pH 8.5 and temperature 5 ˚C, 20˚C, 40 ˚C

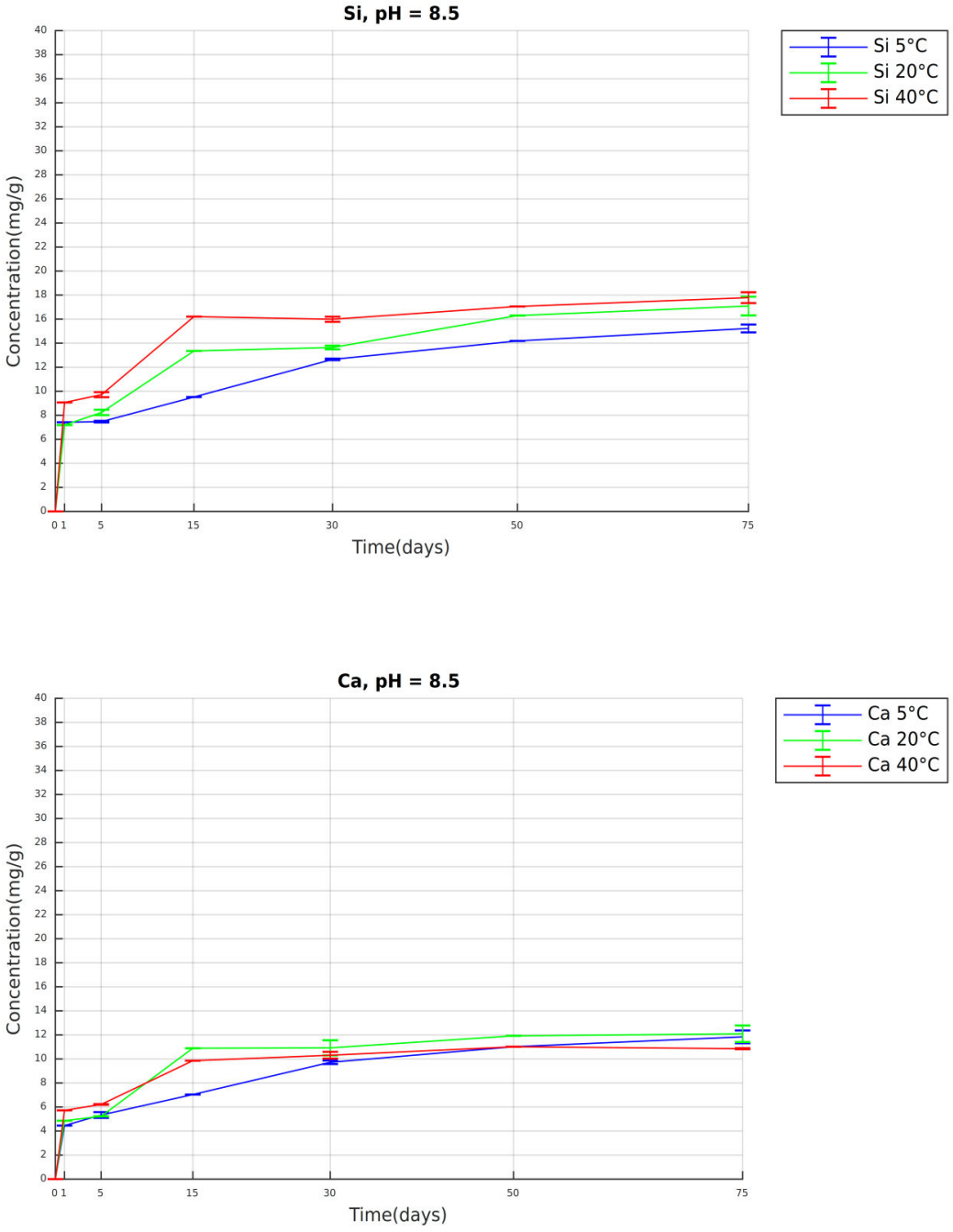

Fig. 135 Sample *Triticum durum,* Cyprus: concentration (mg/g) of Si (above) and Ca (below) over the course of 75 days at pH 8.5 and temperature 5 ˚C, 20˚C, 40 ˚C

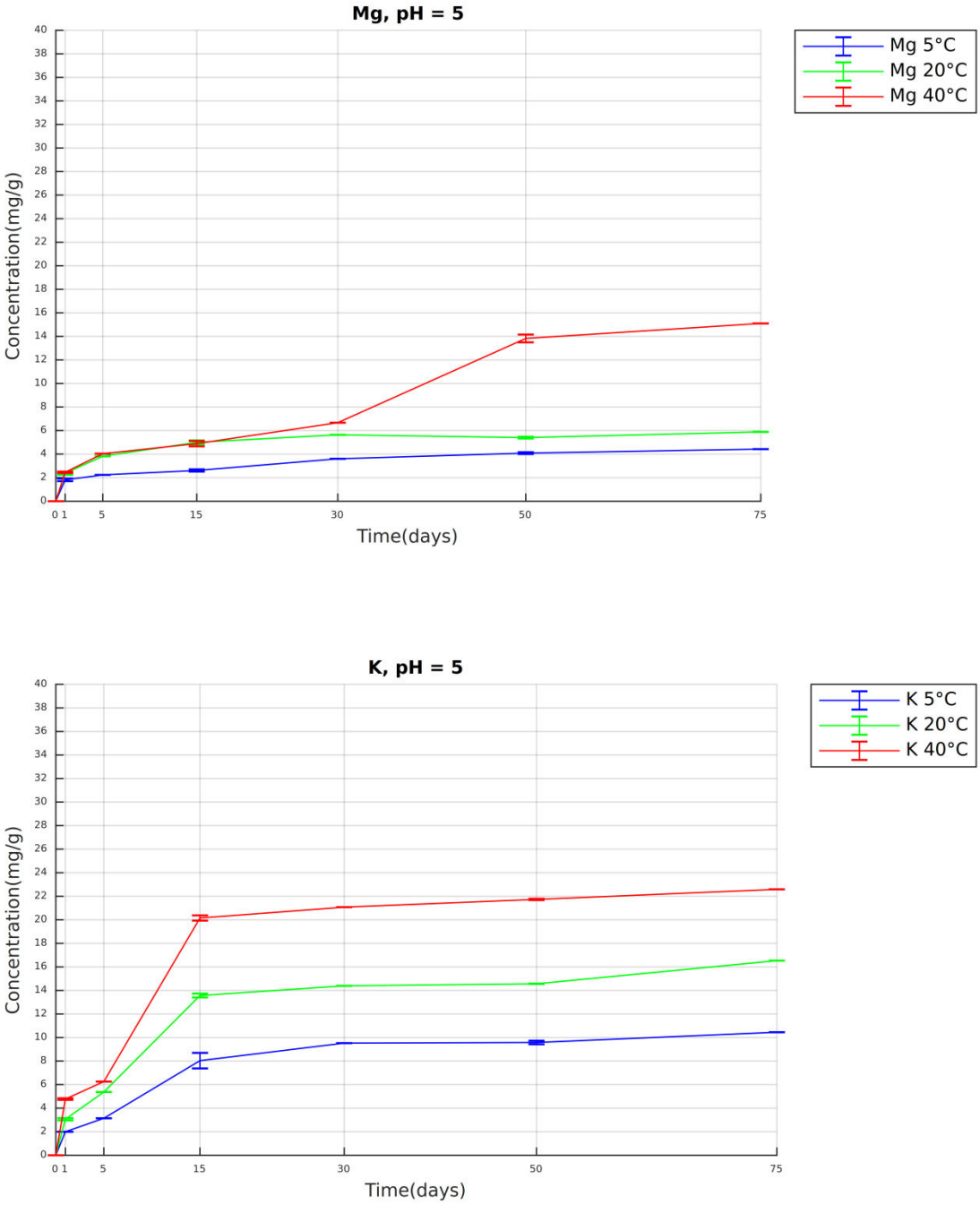

Fig. 136 Sample *Triticum durum,* Crete: concentration (mg/g) of Mg (above) and K (below) over the course of 75 days at pH 5 and temperature 5 ˚C, 20˚C, 40 ˚C

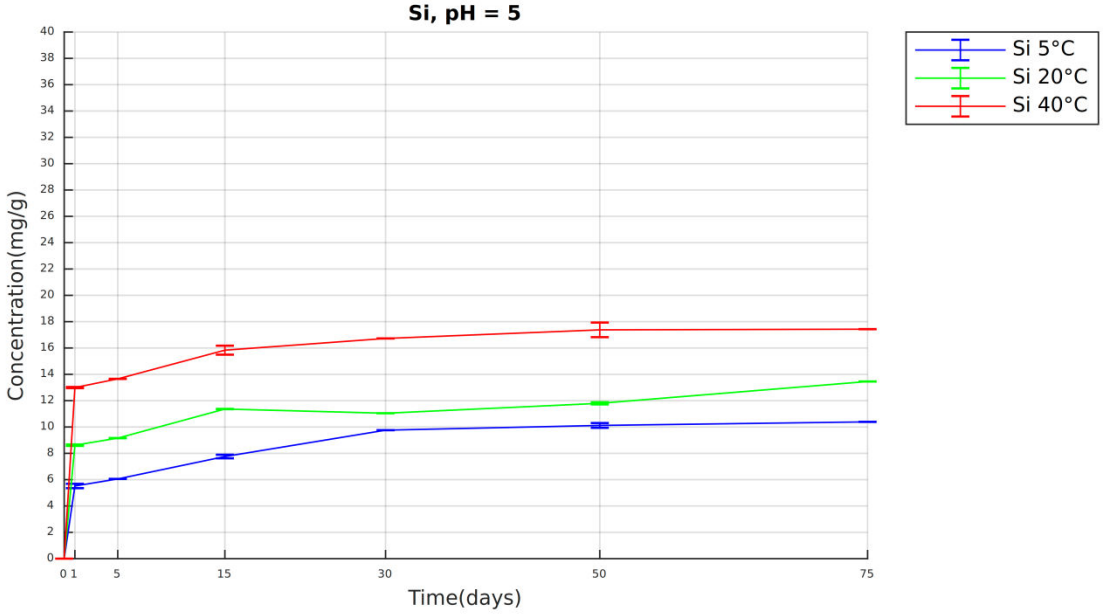

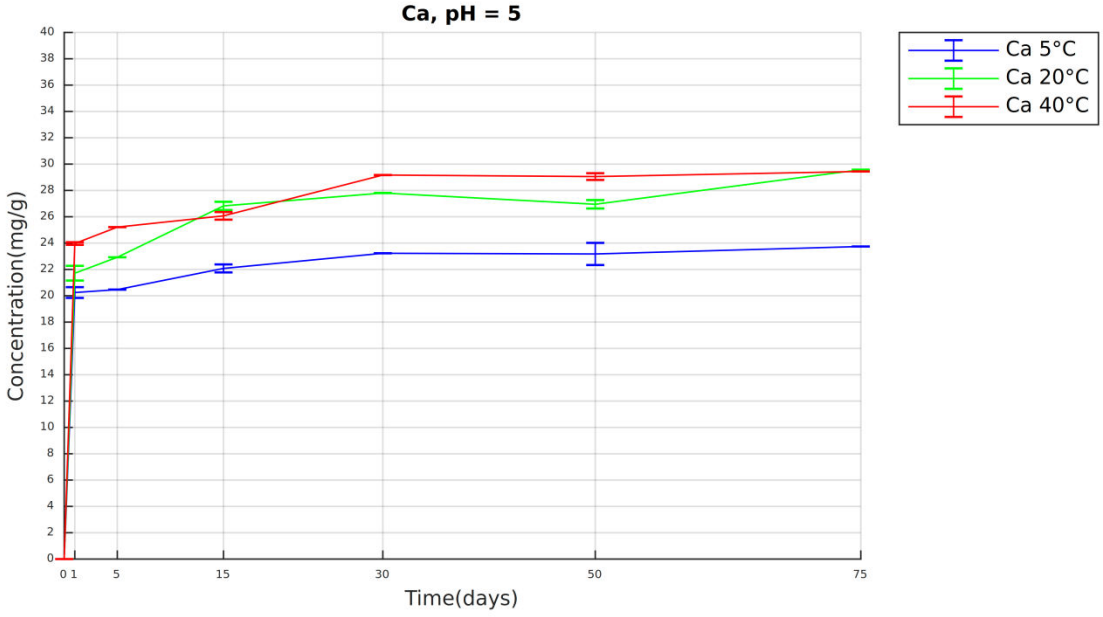

Fig. 137 Sample *Triticum durum,* Crete: concentration (mg/g) of Si (above) and Ca (below) over the course of 75 days at pH 5 and temperature 5 ˚C, 20˚C, 40 ˚C

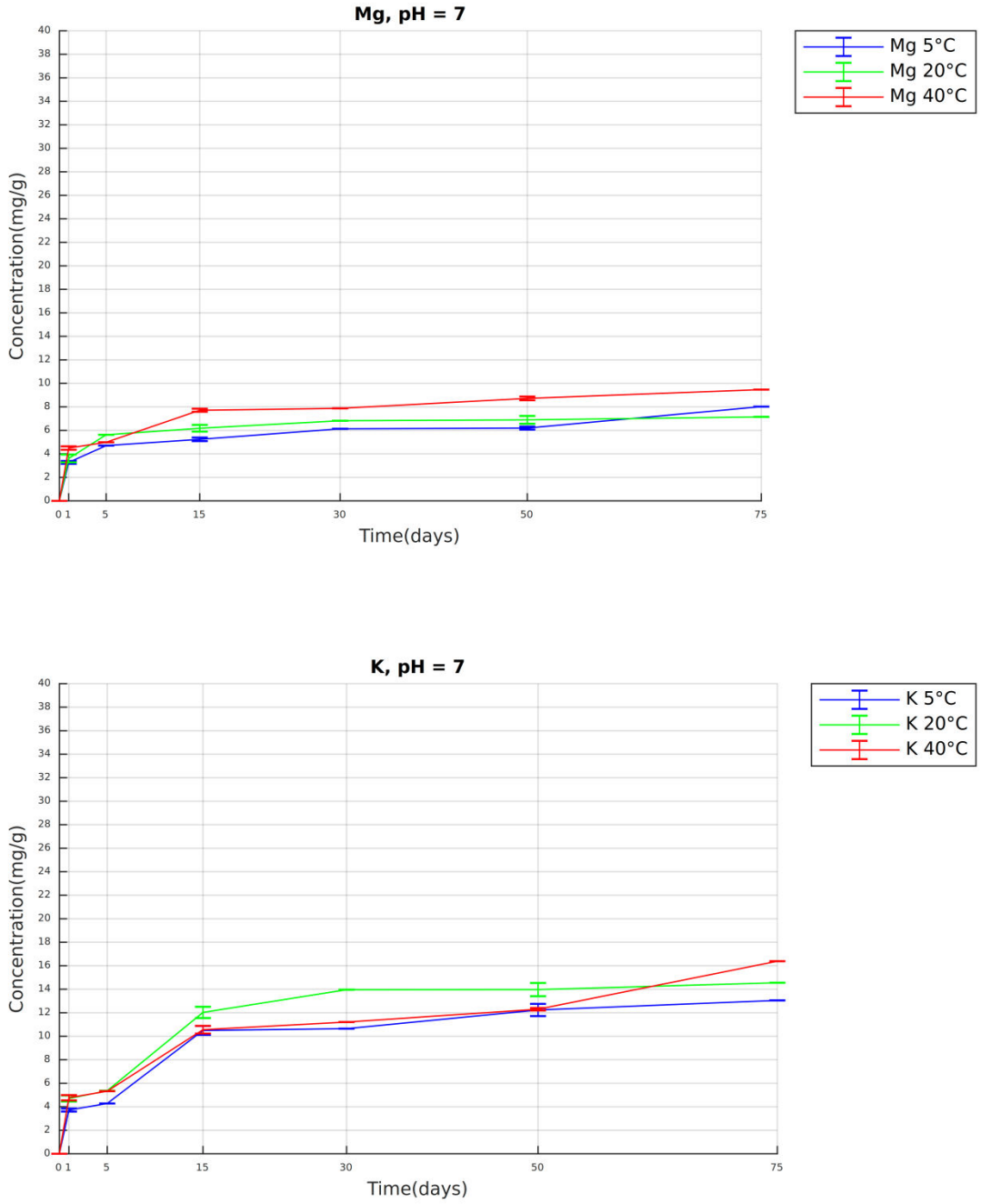

Fig. 138 Sample *Triticum durum,* Crete: concentration (mg/g) of Mg (above) and K (below) over the course of 75 days at pH 7 and temperature 5 ˚C, 20˚C, 40 ˚C

CRETE

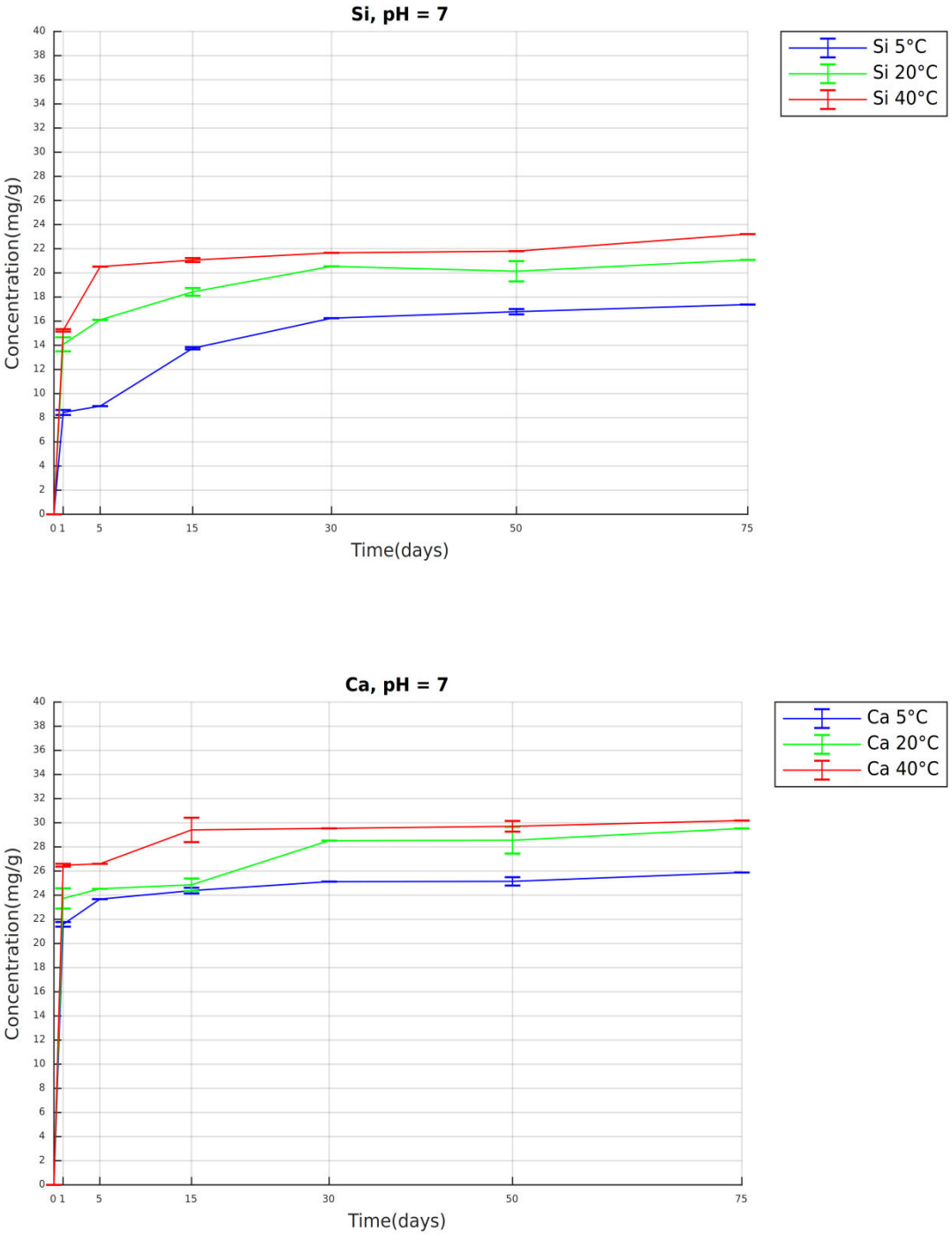

Fig. 139 Sample *Triticum durum,* Crete: concentration (mg/g) of Si (above) and Ca (below) over the course of 75 days at pH 7 and temperature 5 ˚C, 20˚C, 40 ˚C

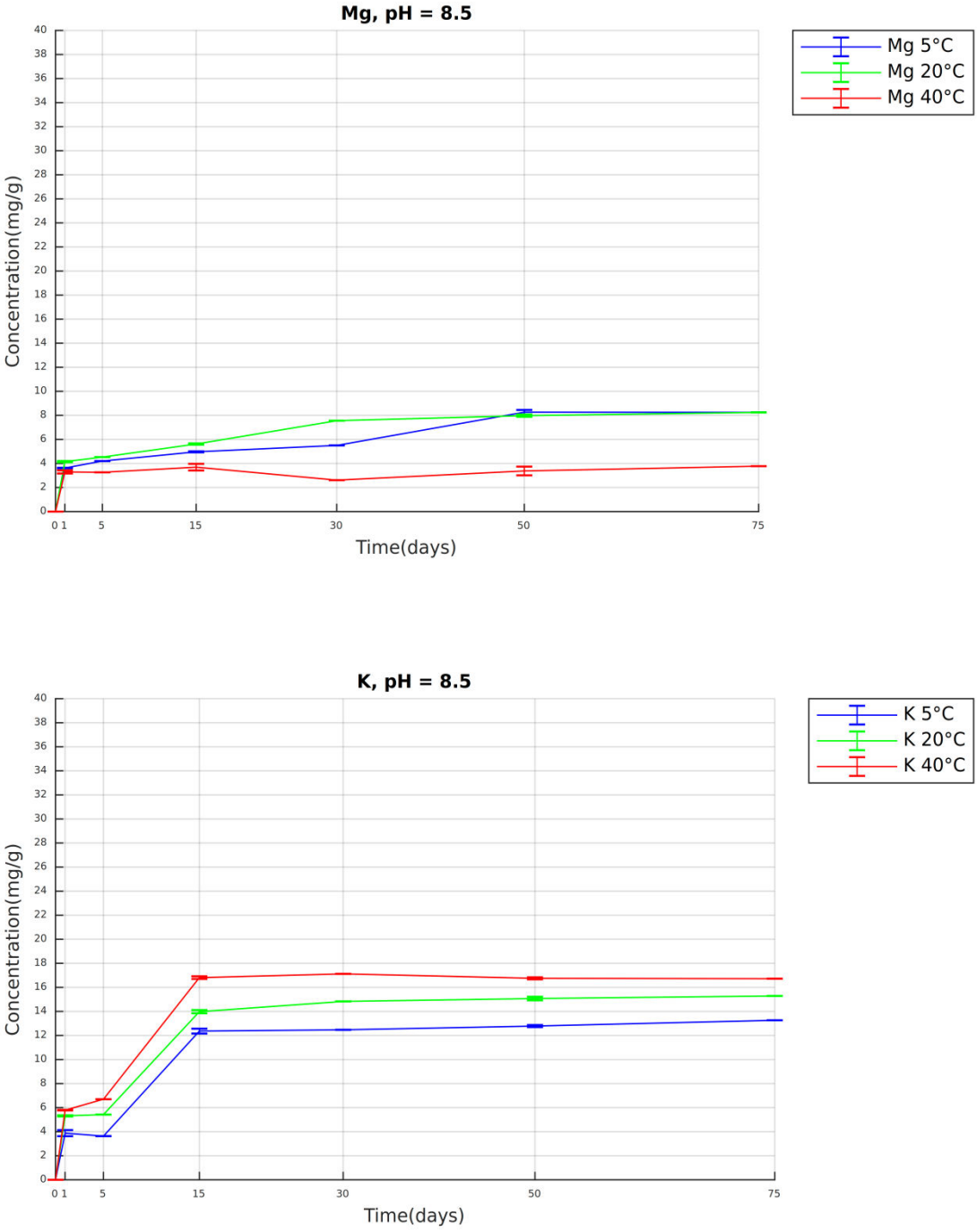

Fig. 140 Sample *Triticum durum,* Crete: concentration (mg/g) of Mg (above) and K (below) over the course of 75 days at pH 8.5 and temperature 5 ˚C, 20˚C, 40 ˚C

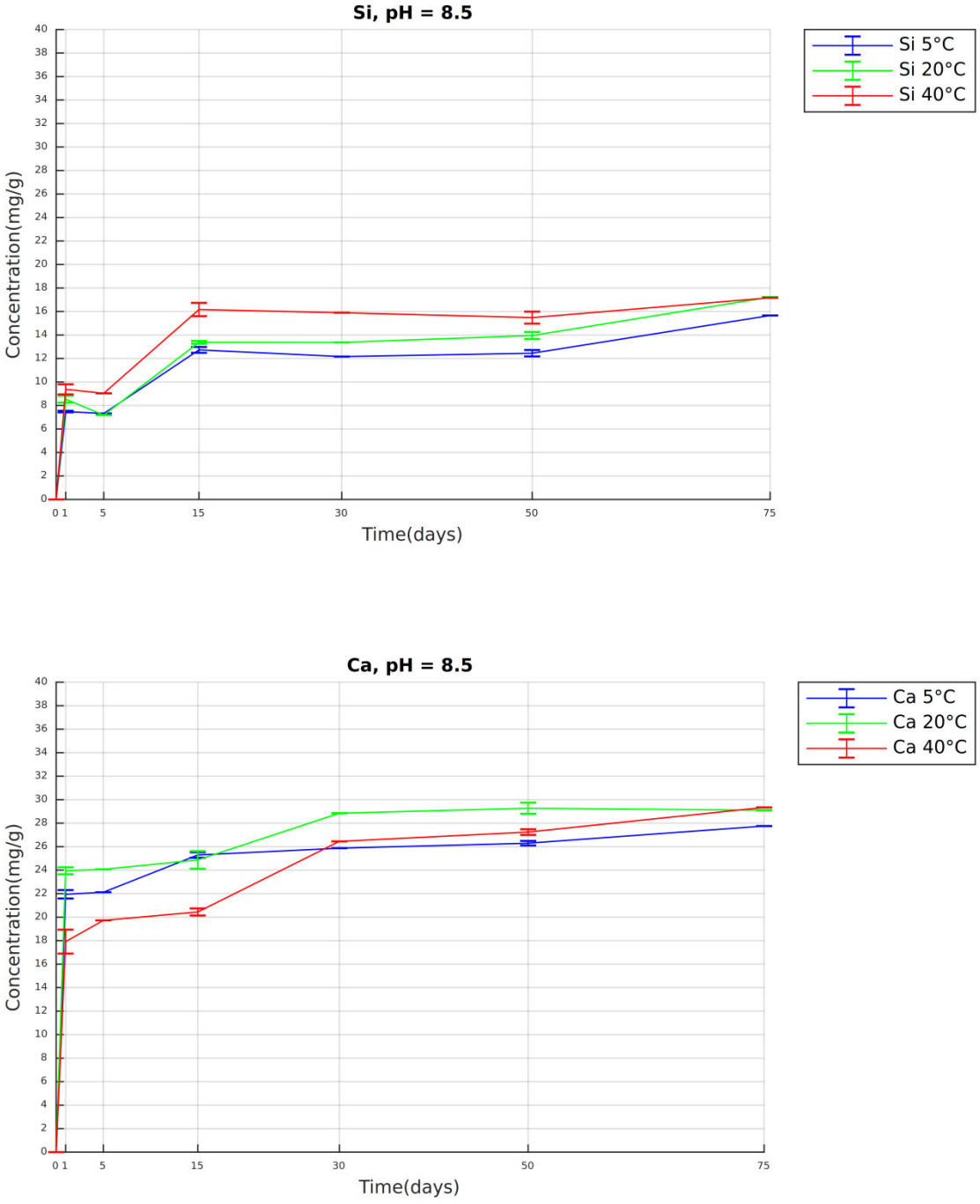

Fig. 141 Sample *Triticum durum,* Crete: concentration (mg/g) of Si (above) and Ca (below) over the course of 75 days at pH 8.5 and temperature 5 ˚C, 20˚C, 40 ˚C

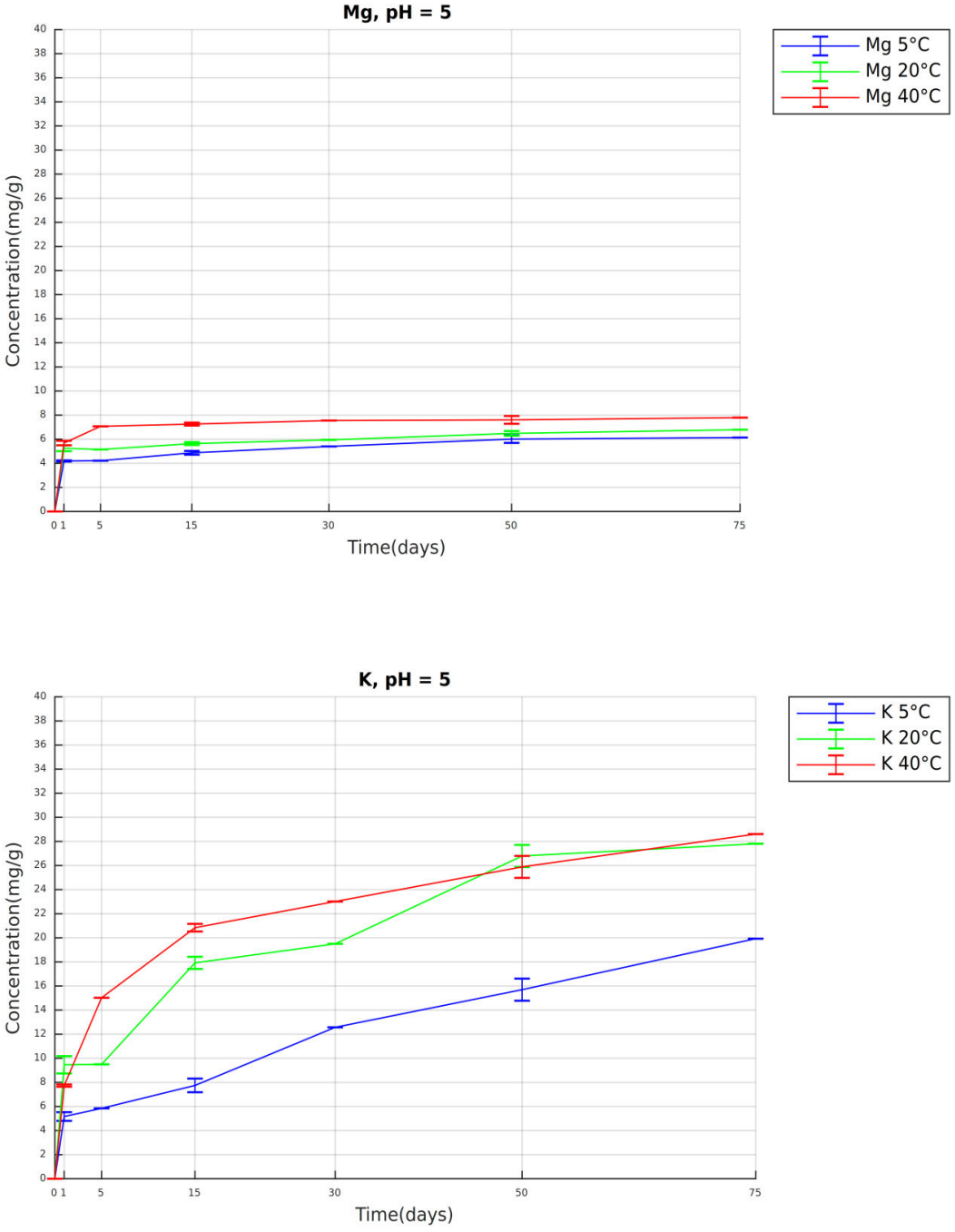

Fig. 142 Sample *Triticum monococcum,* Volos: concentration (mg/g) of Mg (above) and K (below) over the course of 75 days at pH 5 and temperature 5 ˚C, 20˚C, 40 ˚C

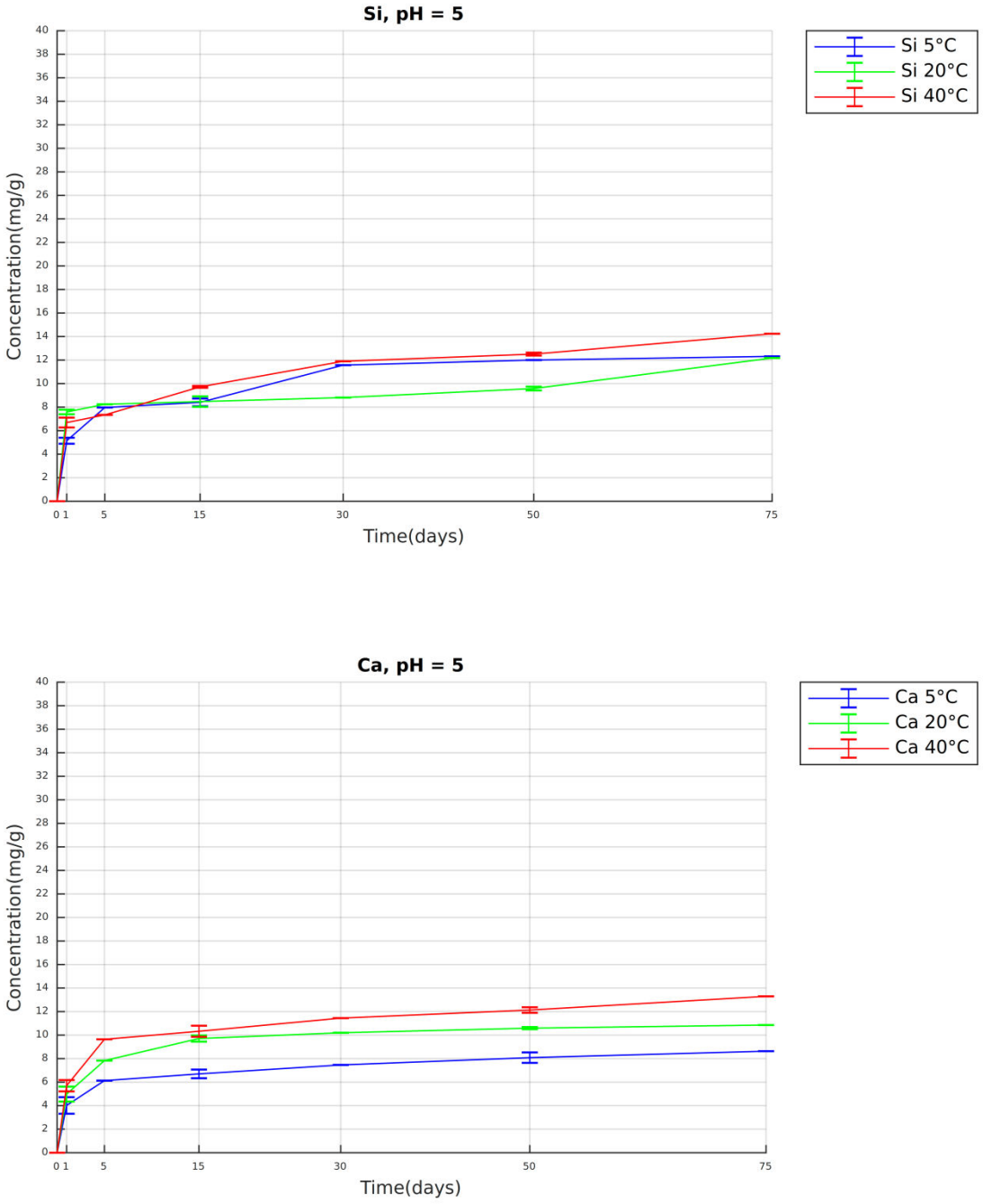

Fig. 143 Sample *Triticum monococcum,* Volos: concentration (mg/g) of Si (above) and Ca (below) over the course of 75 days at pH 5 and temperature 5 ˚C, 20˚C, 40 ˚C

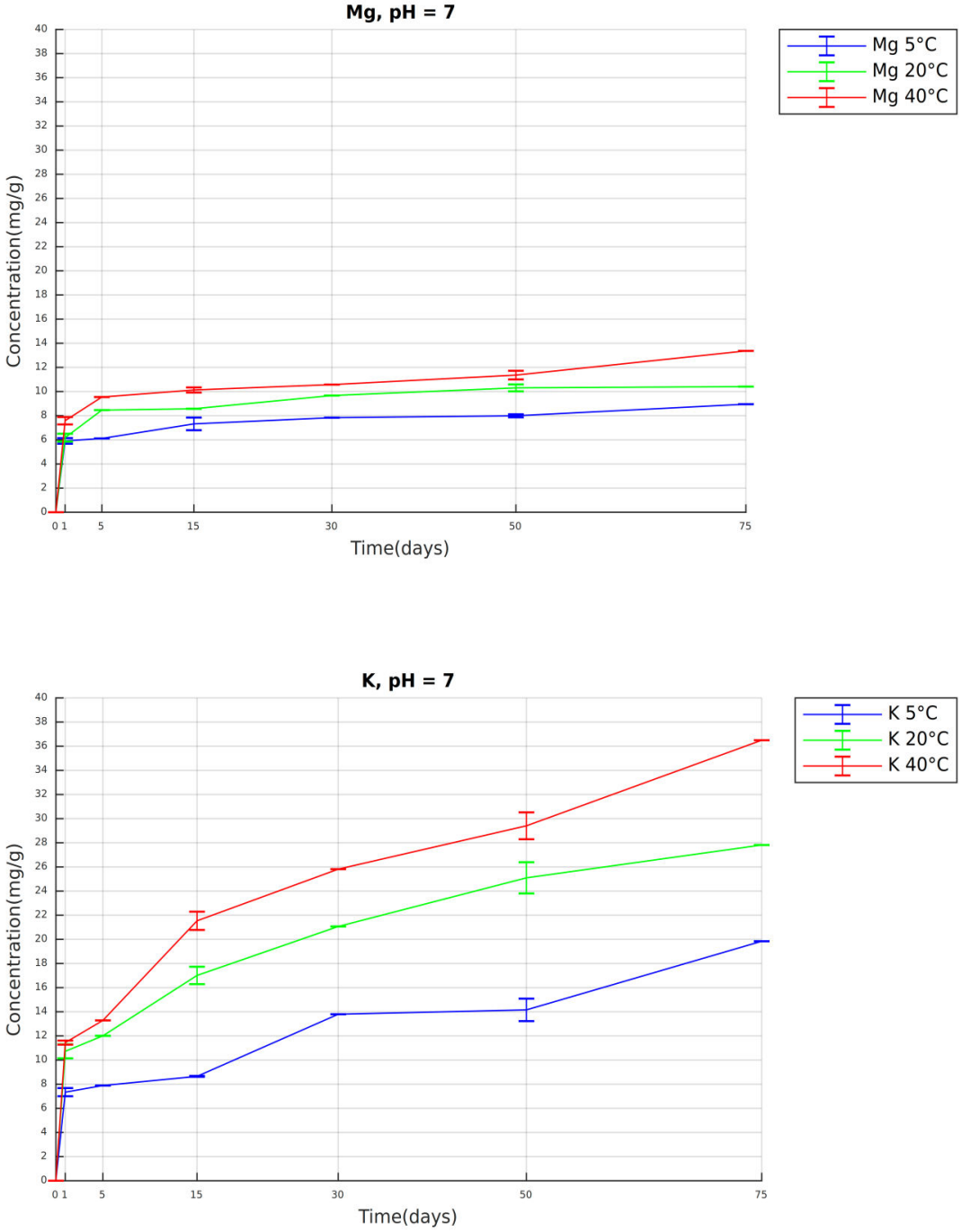

Fig. 144 Sample *Triticum monococcum,* Volos: concentration (mg/g) of Mg (above) and K (below) over the course of 75 days at pH 7 and temperature 5 ˚C, 20˚C, 40 ˚C

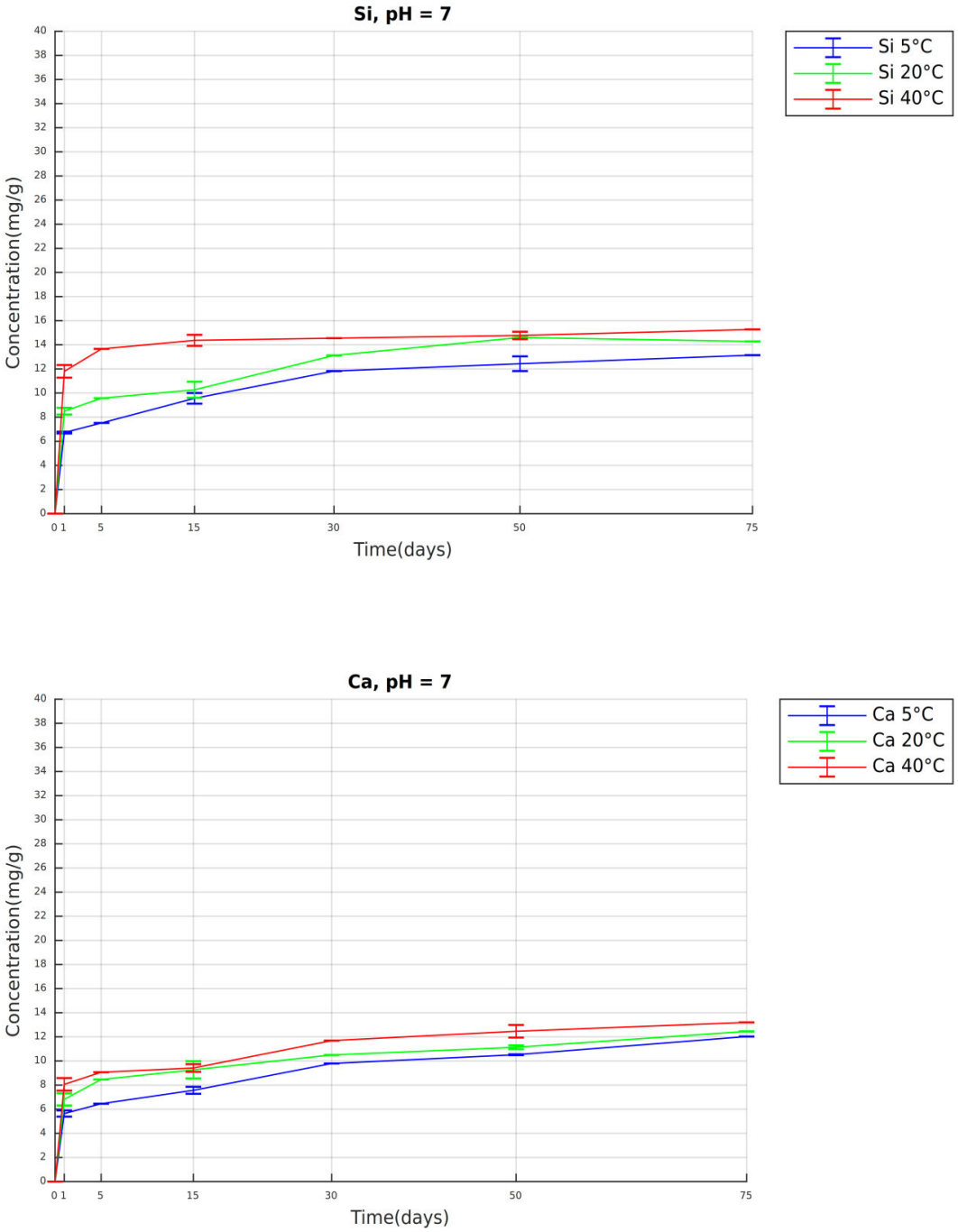

Fig. 145 Sample *Triticum monococcum,* Volos: concentration (mg/g) of Si (above) and Ca (below) over the course of 75 days at pH 7 and temperature 5 ˚C, 20˚C, 40 ˚C

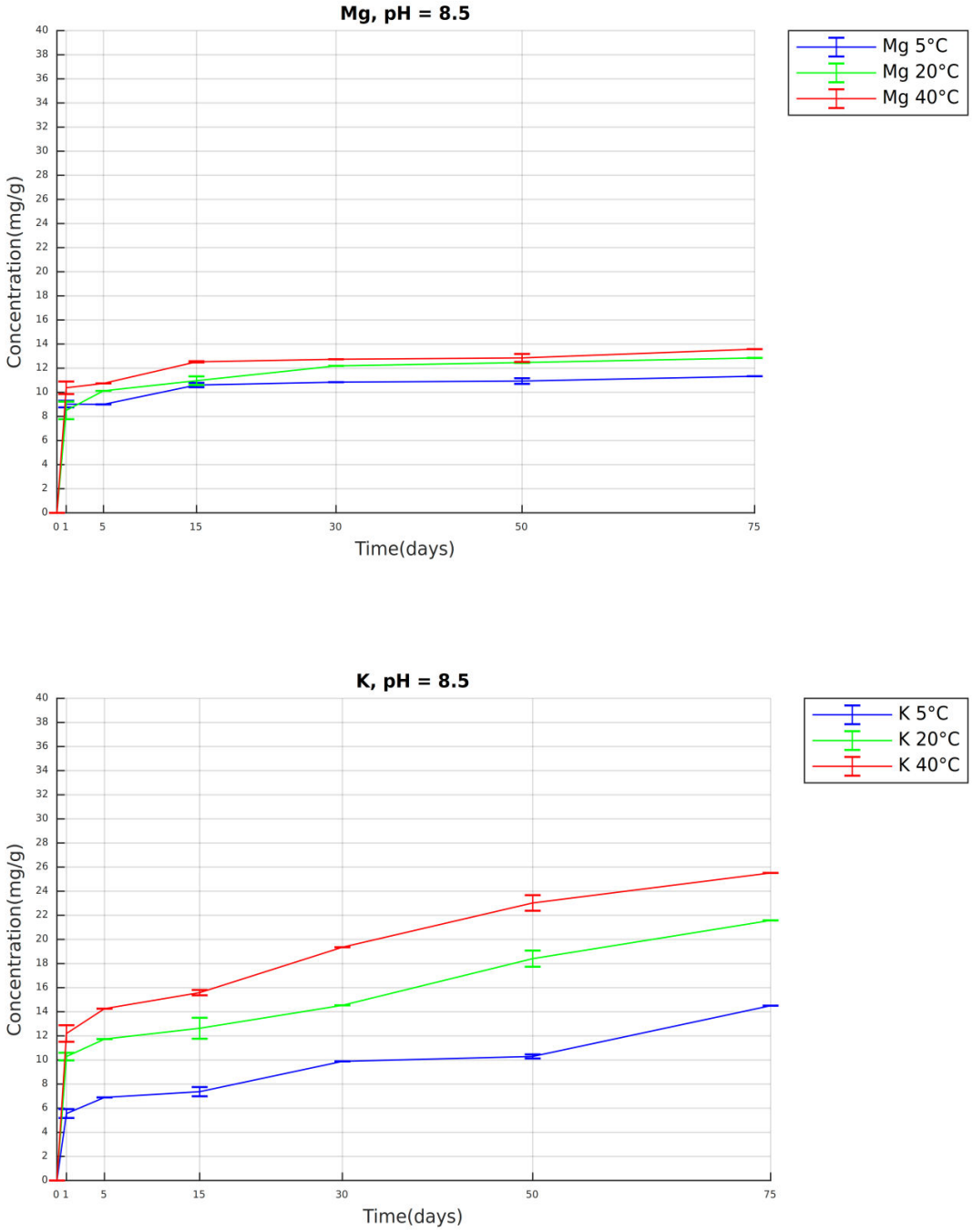

Fig. 146 Sample *Triticum monococcum,* Volos: concentration (mg/g) of Mg (above) and K (below) over the course of 75 days at pH 8.5 and temperature 5 ˚C, 20˚C, 40 ˚C

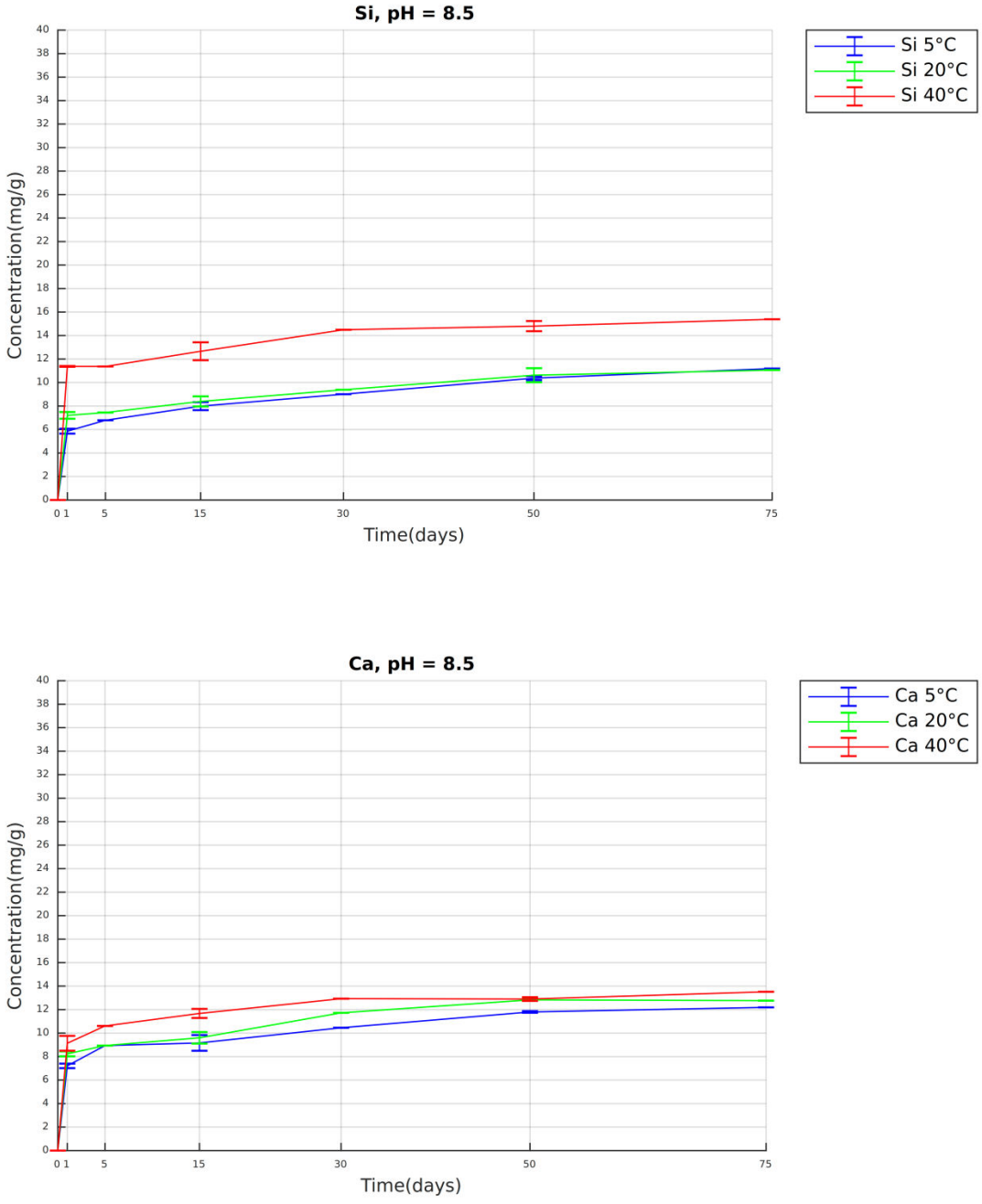

Fig. 147 Sample *Triticum monococcum,* Volos: concentration (mg/g) of Si (above) and Ca (below) over the course of 75 days at pH 8.5 and temperature 5 ˚C, 20˚C, 40 ˚C

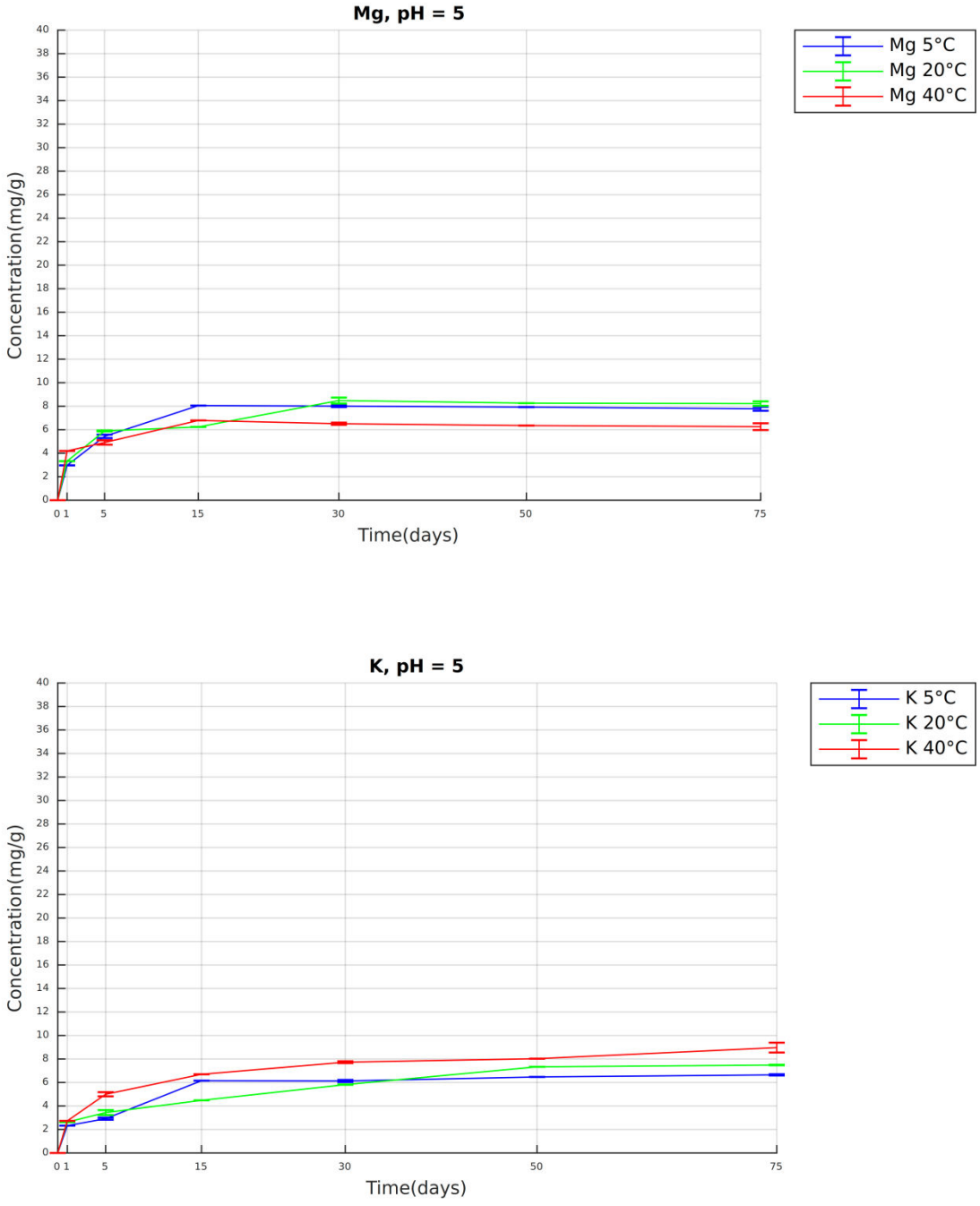

Fig. 148 Sample *Triticum monococcum,* Pella I: concentration (mg/g) of Mg (above) and K (below) over the course of 75 days at pH 5 and temperature 5 ˚C, 20˚C, 40 ˚C

PELLA I

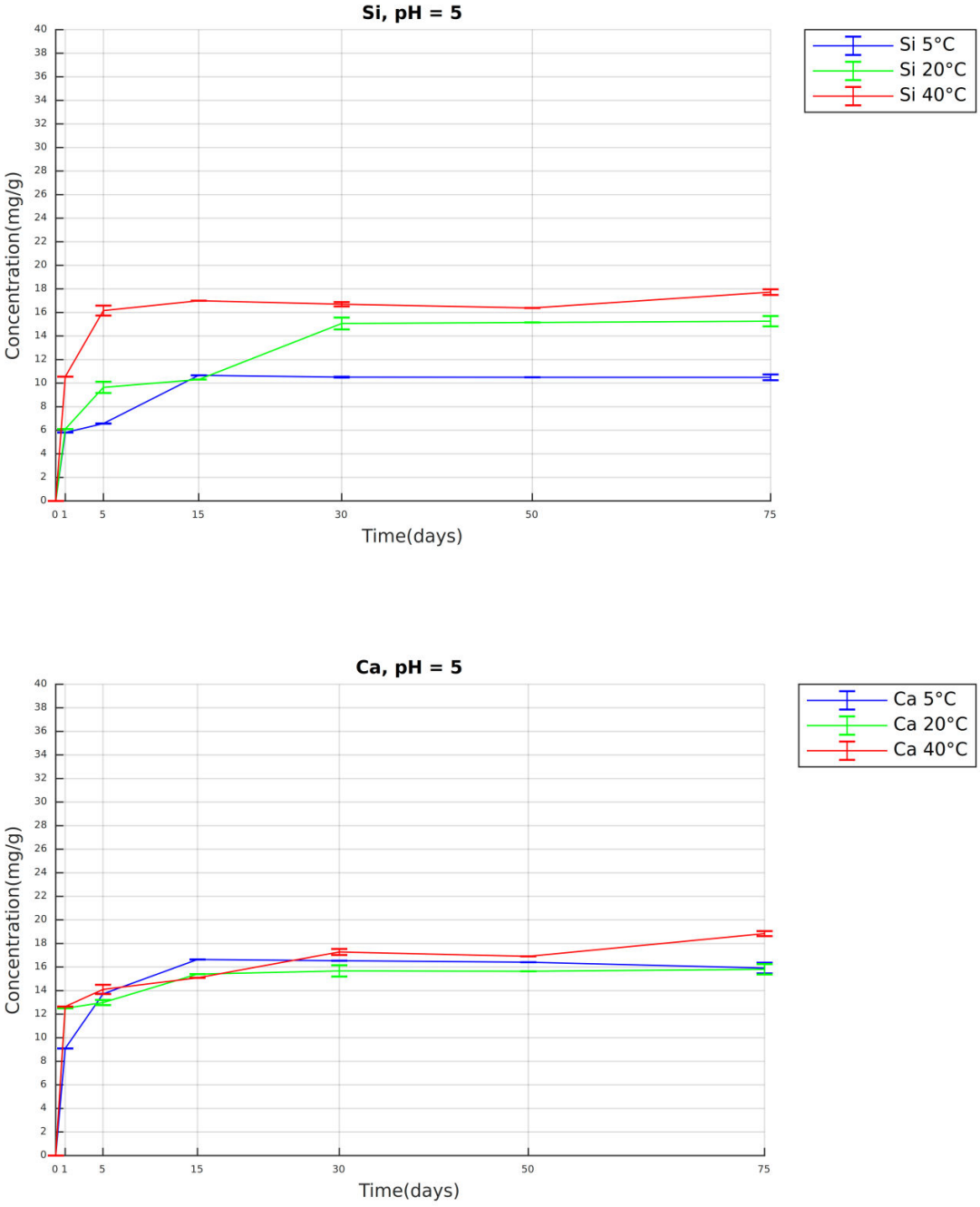

Fig. 149 Sample *Triticum monococcum,* Pella I: concentration (mg/g) of Si (above) and Ca (below) over the course of 75 days at pH 5 and temperature 5 ˚C, 20˚C, 40 ˚C

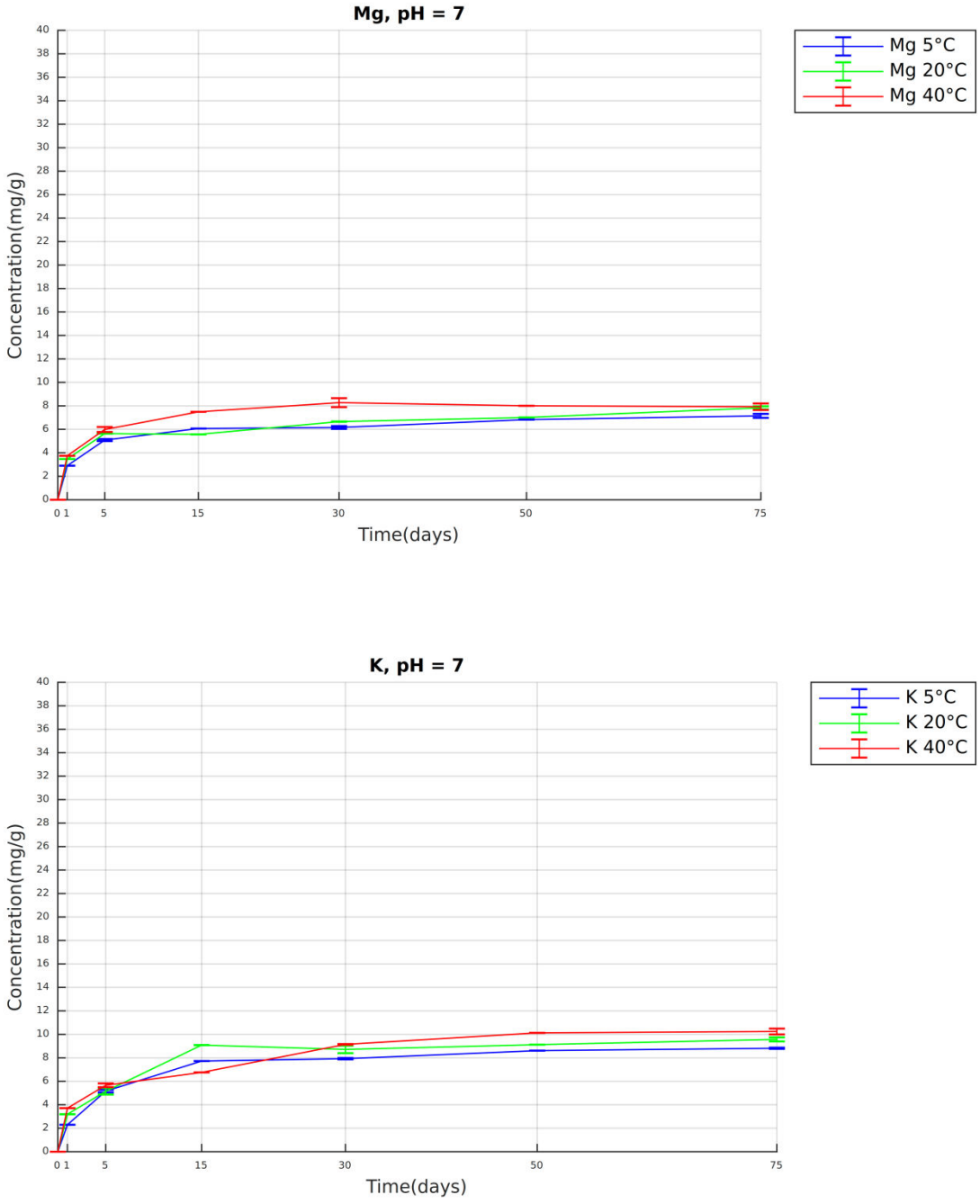

Fig. 150 Sample *Triticum monococcum,* Pella I: concentration (mg/g) of Mg (above) and K (below) over the course of 75 days at pH 7 and temperature 5 ˚C, 20˚C, 40 ˚C

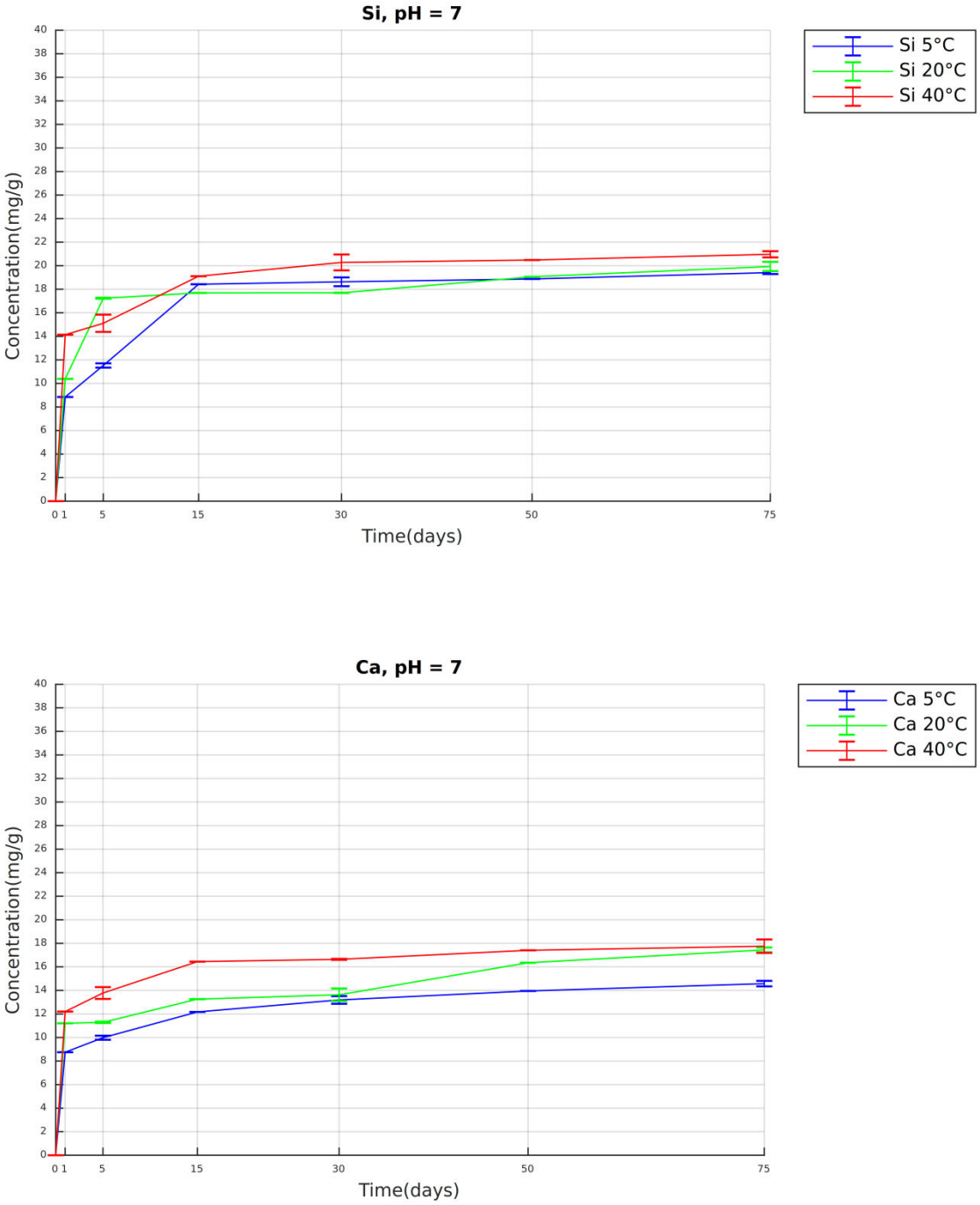

Fig. 151 Sample *Triticum monococcum,* Pella I: concentration (mg/g) of Si (above) and Ca (below) over the course of 75 days at pH 7 and temperature 5 ˚C, 20˚C, 40 ˚C

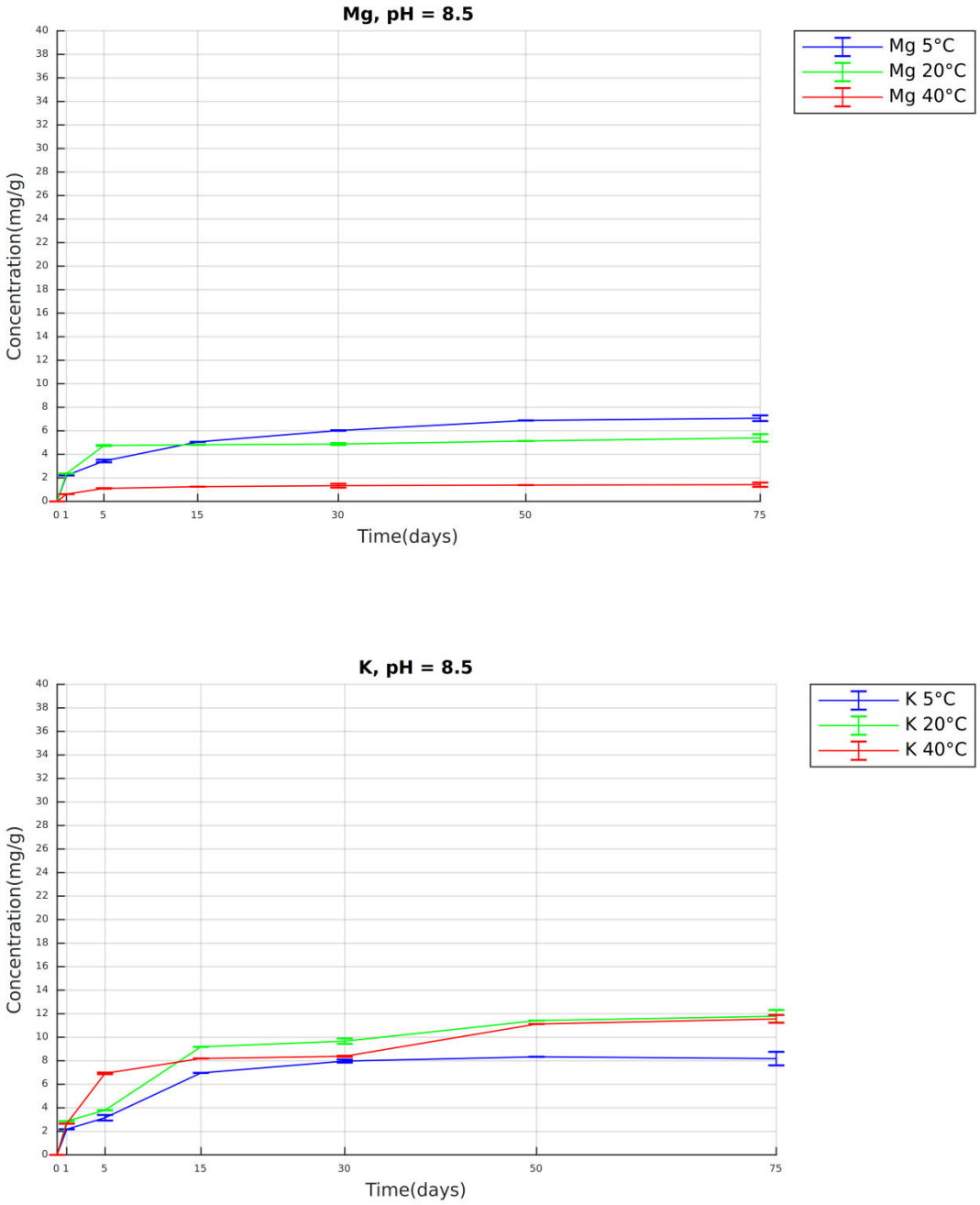

Fig. 152 Sample *Triticum monococcum,* Pella I: concentration (mg/g) of Mg (above) and K (below) over the course of 75 days at pH 8.5 and temperature 5 ˚C, 20˚C, 40 ˚C

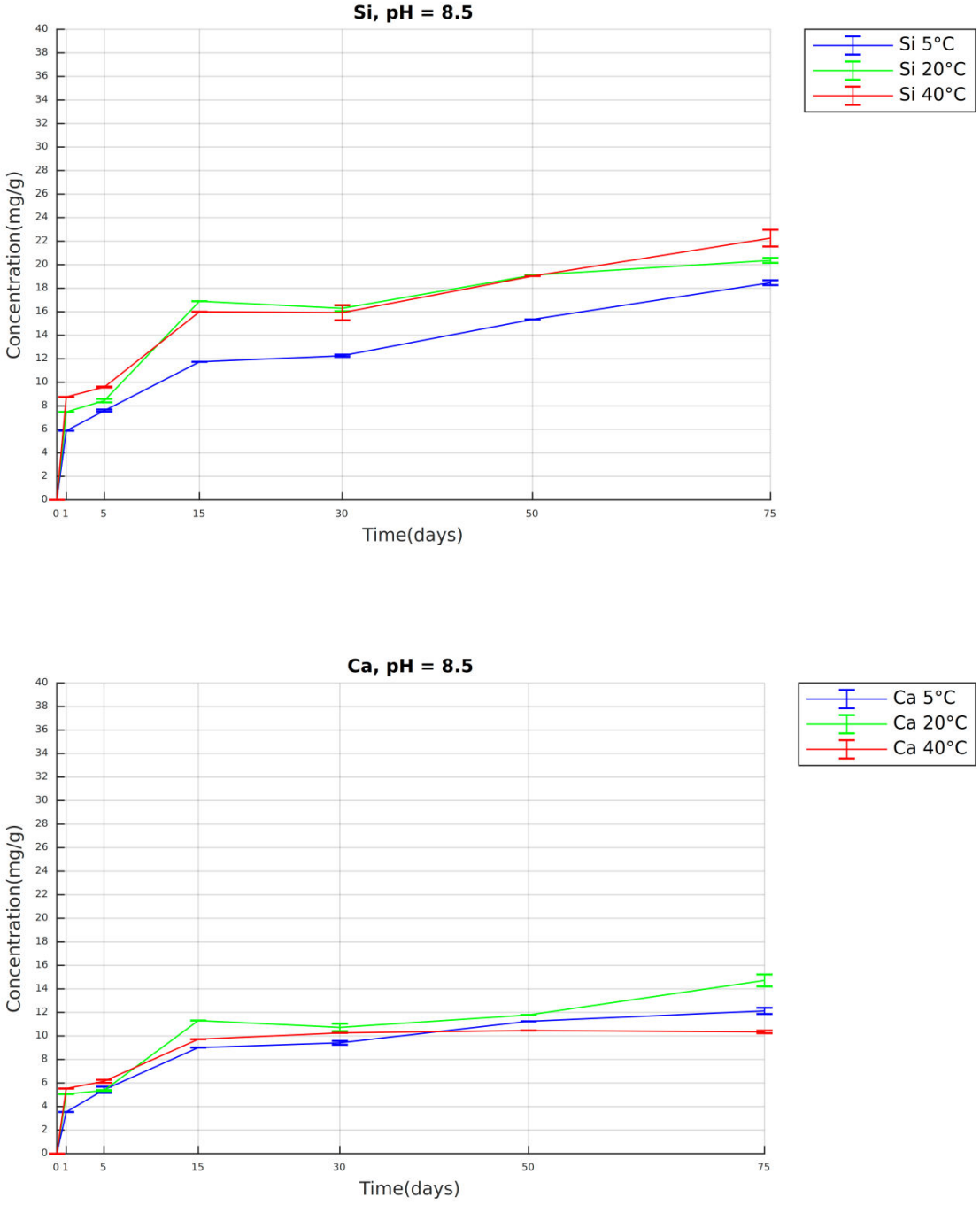

Fig. 153 Sample *Triticum monococcum,* Pella I: concentration (mg/g) of Si (above) and Ca (below) over the course of 75 days at pH 8.5 and temperature 5 ˚C, 20˚C, 40 ˚C

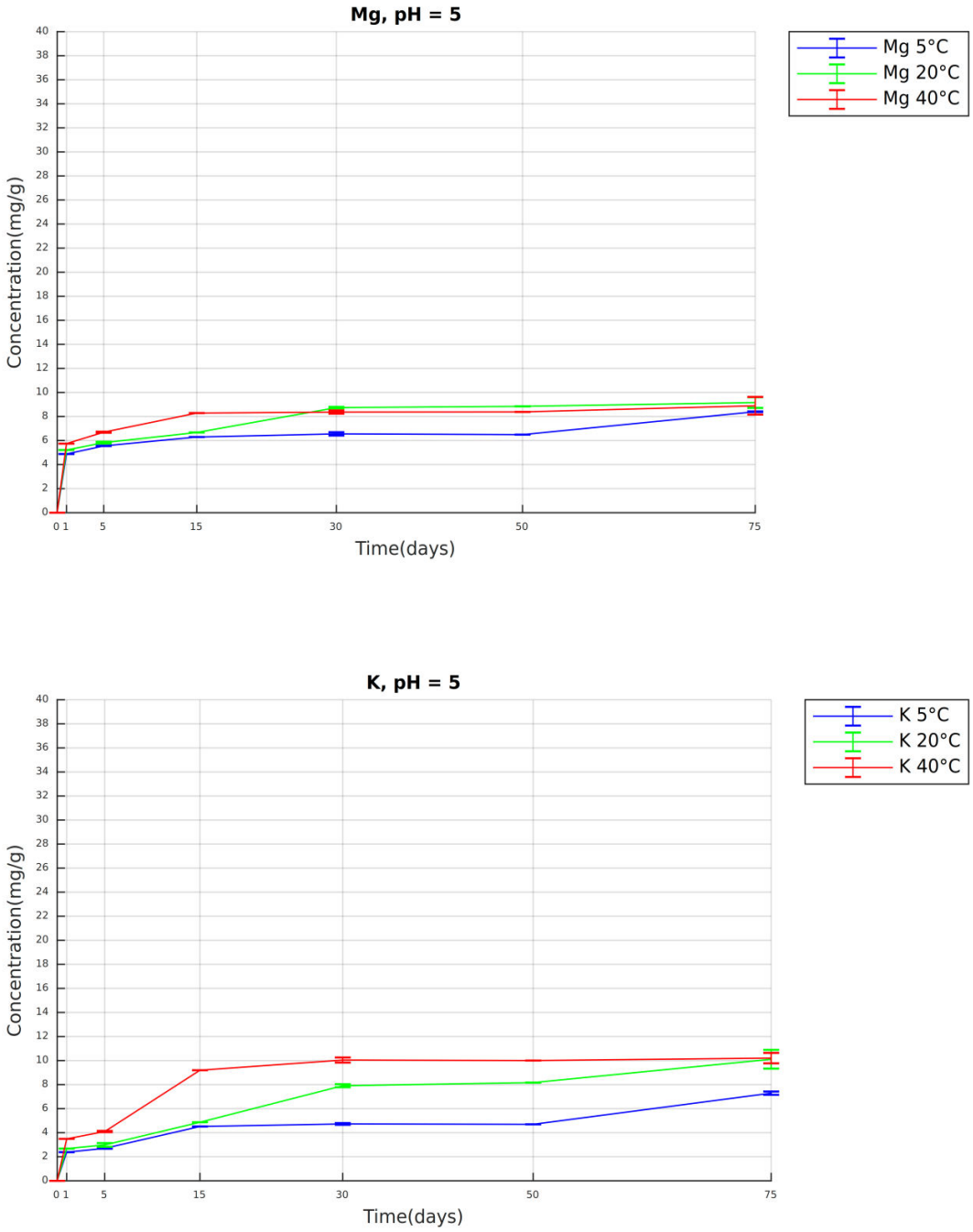

Fig. 154 Sample *Triticum durum,* Pella II: concentration (mg/g) of Mg (above) and K (below) over the course of 75 days at pH 5 and temperature 5 ˚C, 20˚C, 40 ˚C

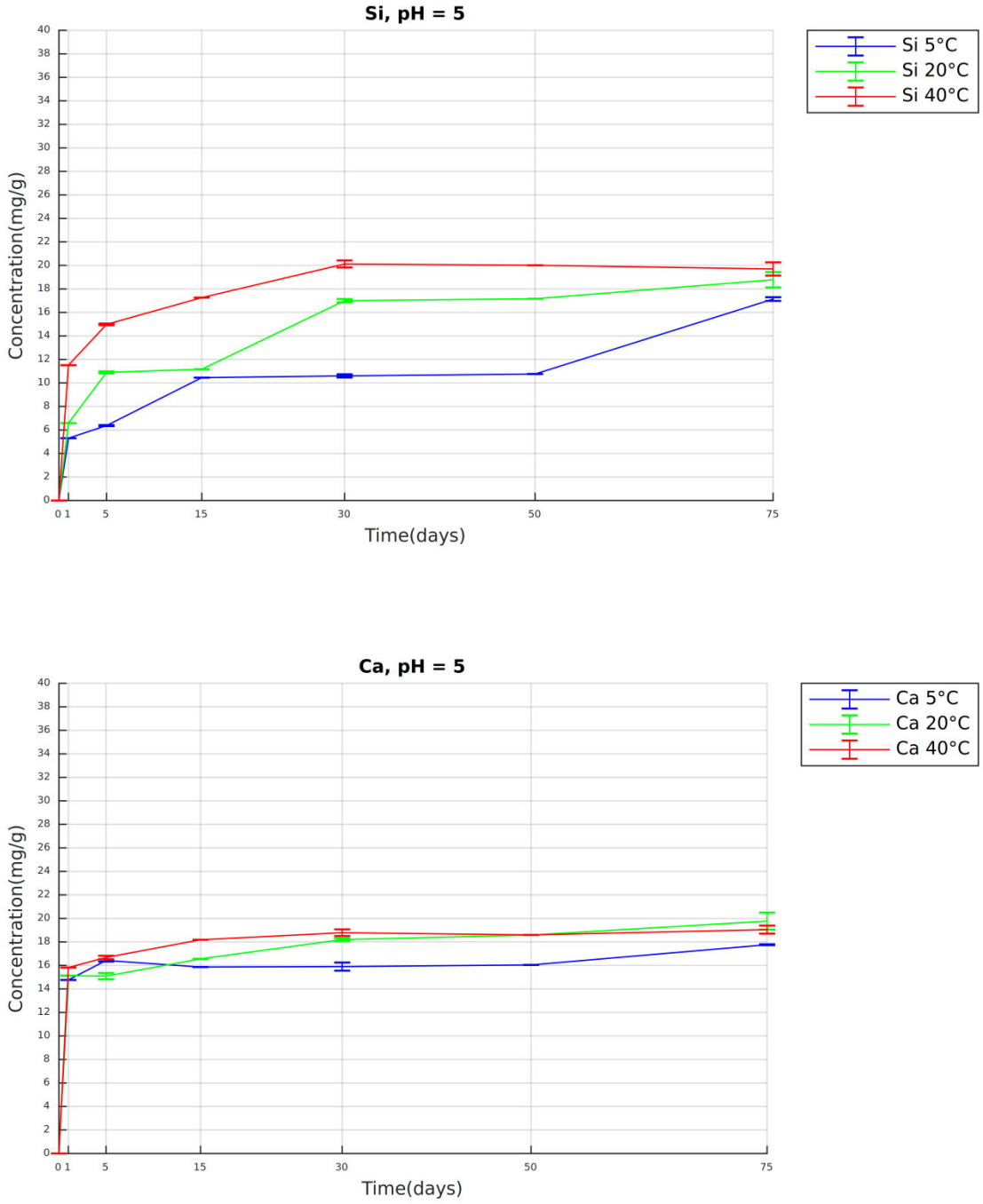

Fig. 155 Sample *Triticum durum,* Pella II: concentration (mg/g) of Si (above) and Ca (below) over the course of 75 days at pH 5 and temperature 5 ˚C, 20˚C, 40 ˚C

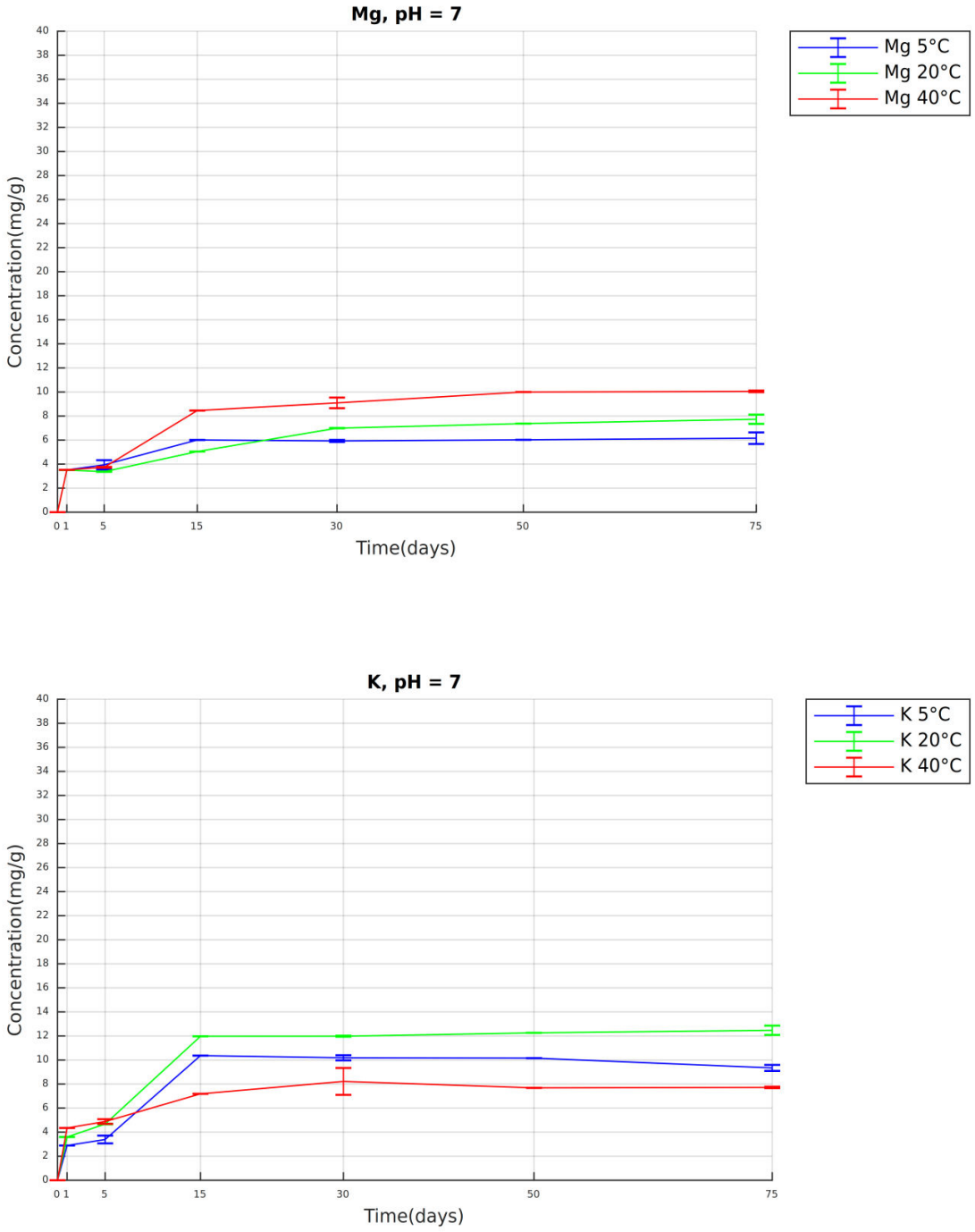

Fig. 156 Sample *Triticum durum,* Pella II: concentration (mg/g) of Mg (above) and K (below) over the course of 75 days at pH 7 and temperature 5 ˚C, 20˚C, 40 ˚C

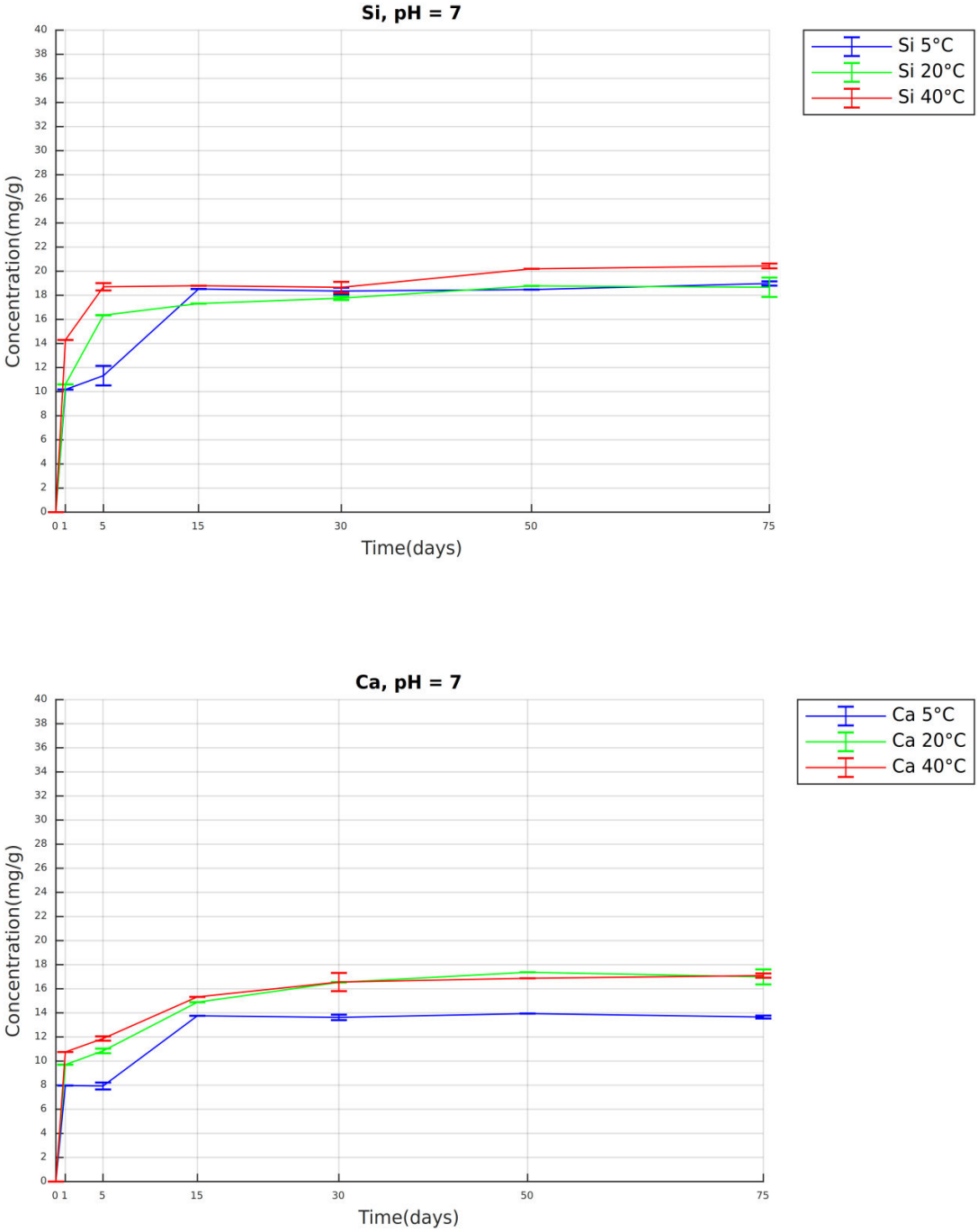

Fig. 157 Sample *Triticum durum,* Pella II: concentration (mg/g) of Si (above) and Ca (below) over the course of 75 days at pH 7 and temperature 5 ˚C, 20˚C, 40 ˚C

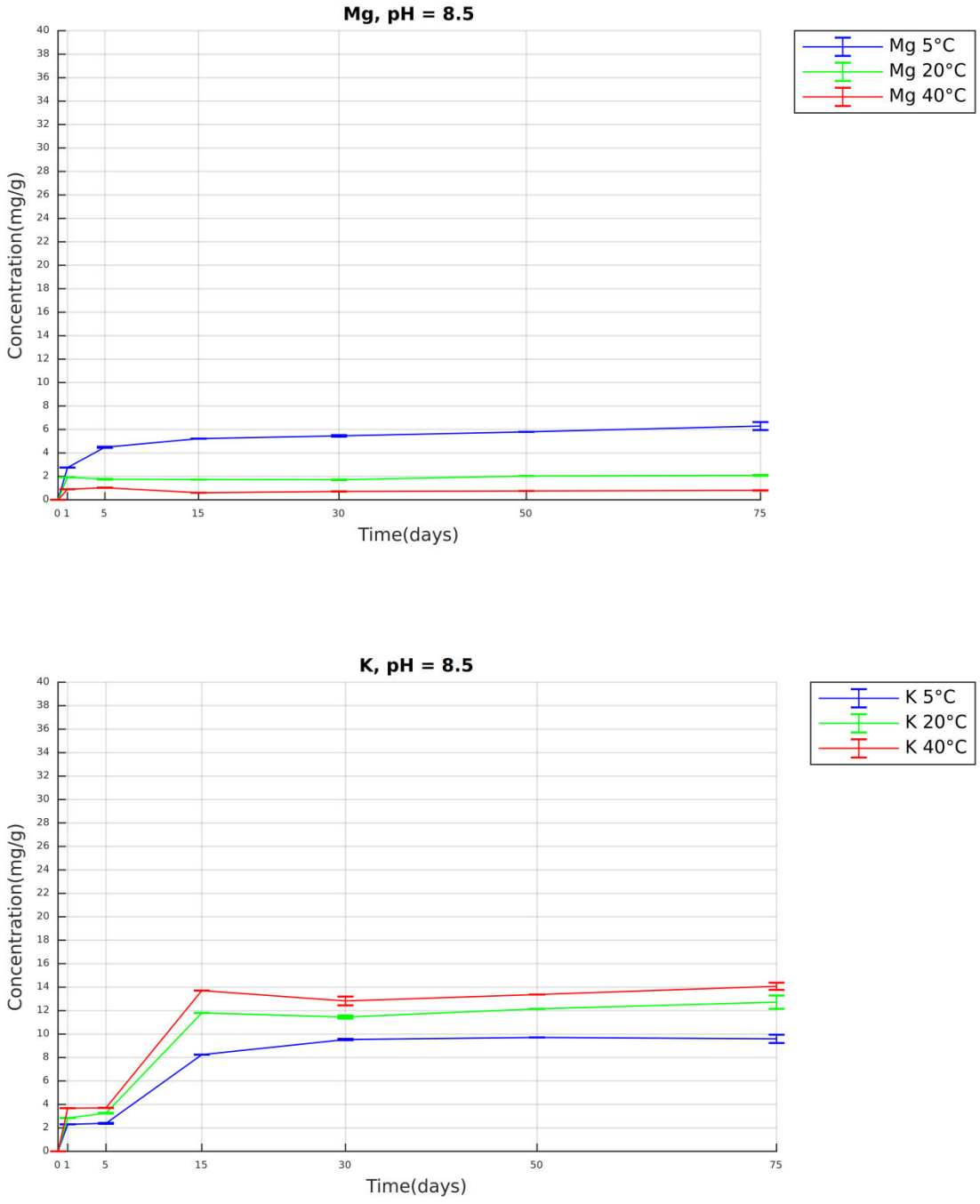

Fig. 158 Sample *Triticum durum,* Pella II: concentration (mg/g) of Mg (above) and K (below) over the course of 75 days at pH 8.5 and temperature 5 ˚C, 20˚C, 40 ˚C

PELLA II

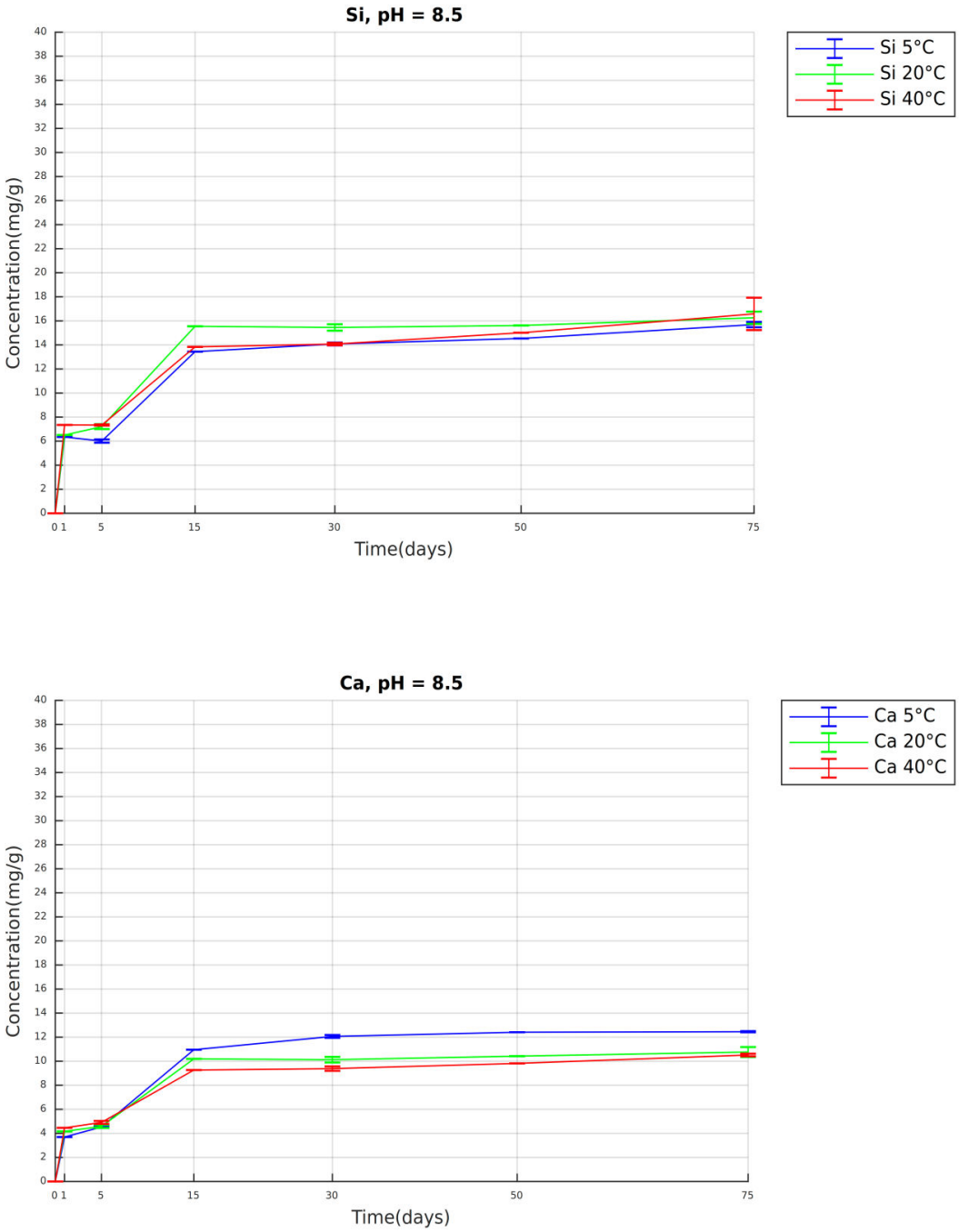

Fig. 159 Sample *Triticum durum,* Pella II: concentration (mg/g) of Si (above) and Ca (below) over the course of 75 days at pH 8.5 and temperature 5 ˚C, 20˚C, 40 ˚C

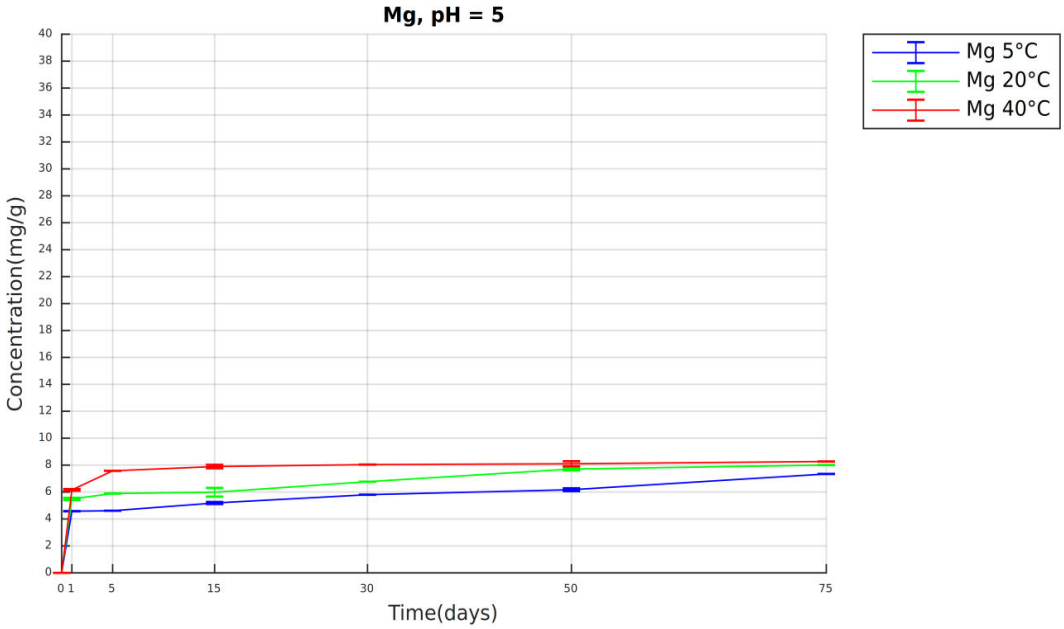

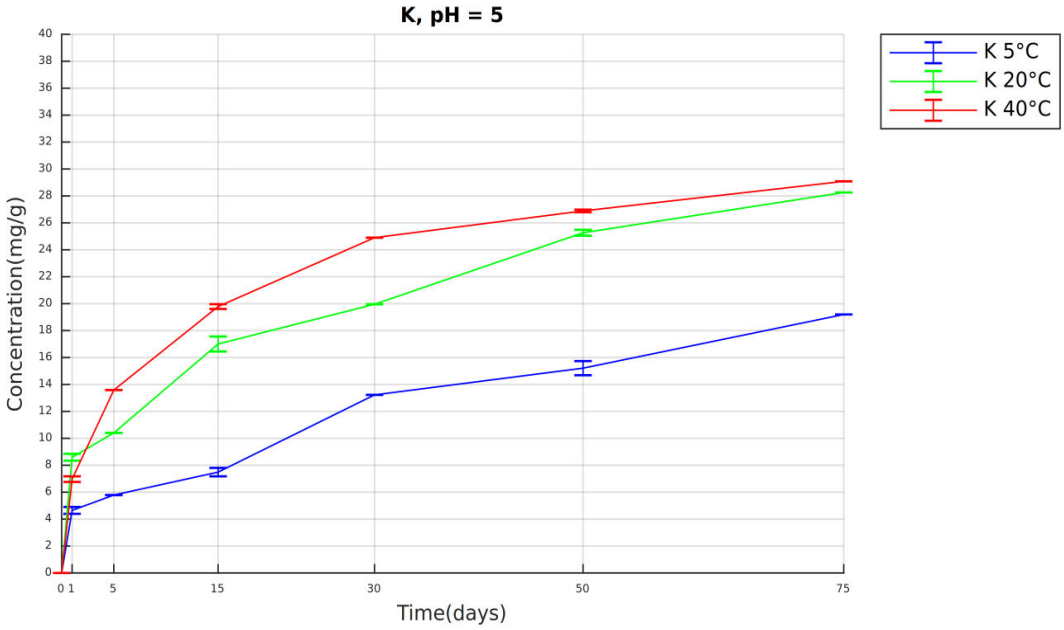

Fig. 160 Sample *Triticum durum,* Corfu: concentration (mg/g) of Mg (above) and K (below) over the course of 75 days at pH 5 and temperature 5 ˚C, 20˚C, 40 ˚C

CORFU

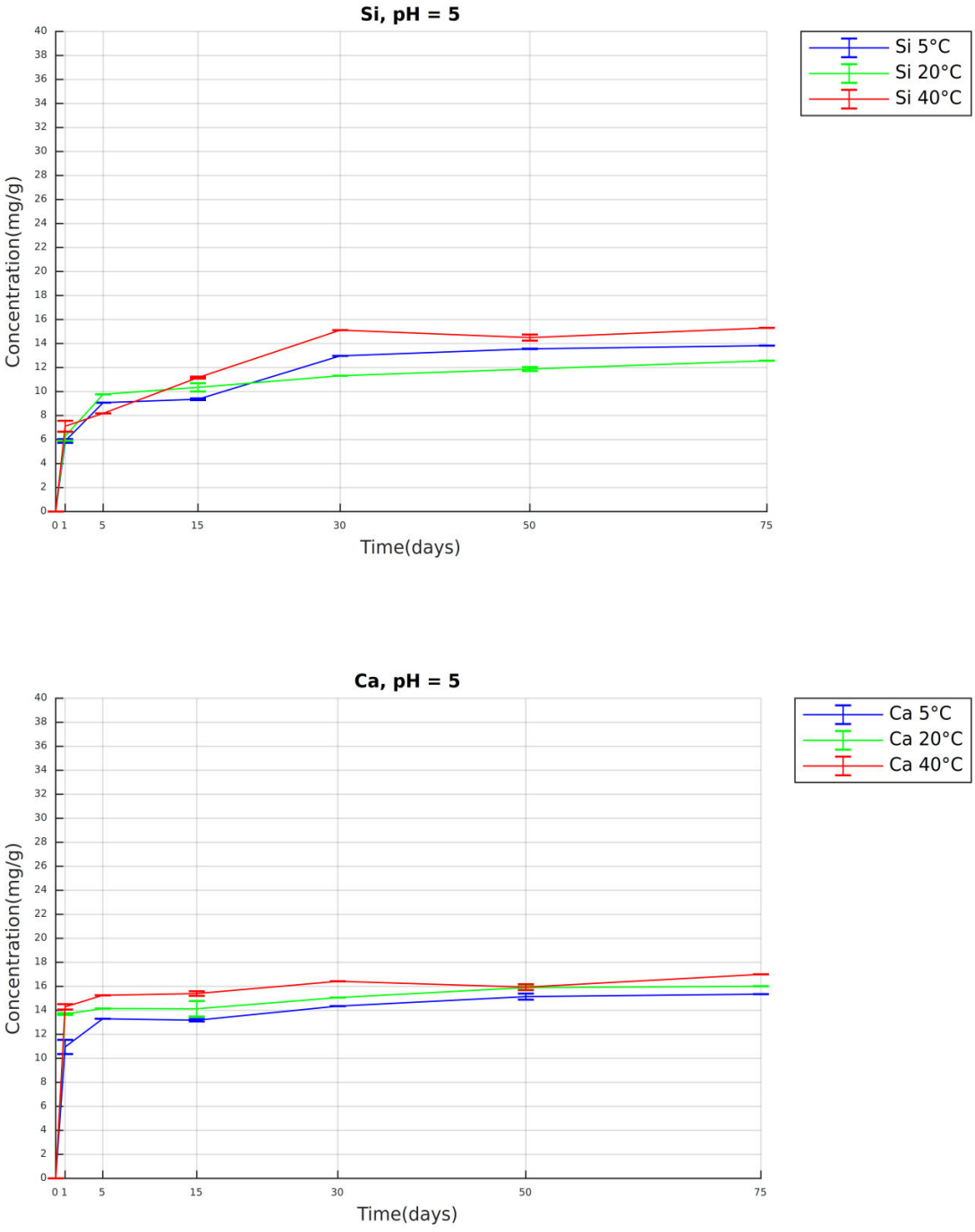

Fig. 161 Sample *Triticum durum,* Corfu: concentration (mg/g) of Si (above) and Ca (below) over the course of 75 days at pH 5 and temperature 5 ˚C, 20˚C, 40 ˚C

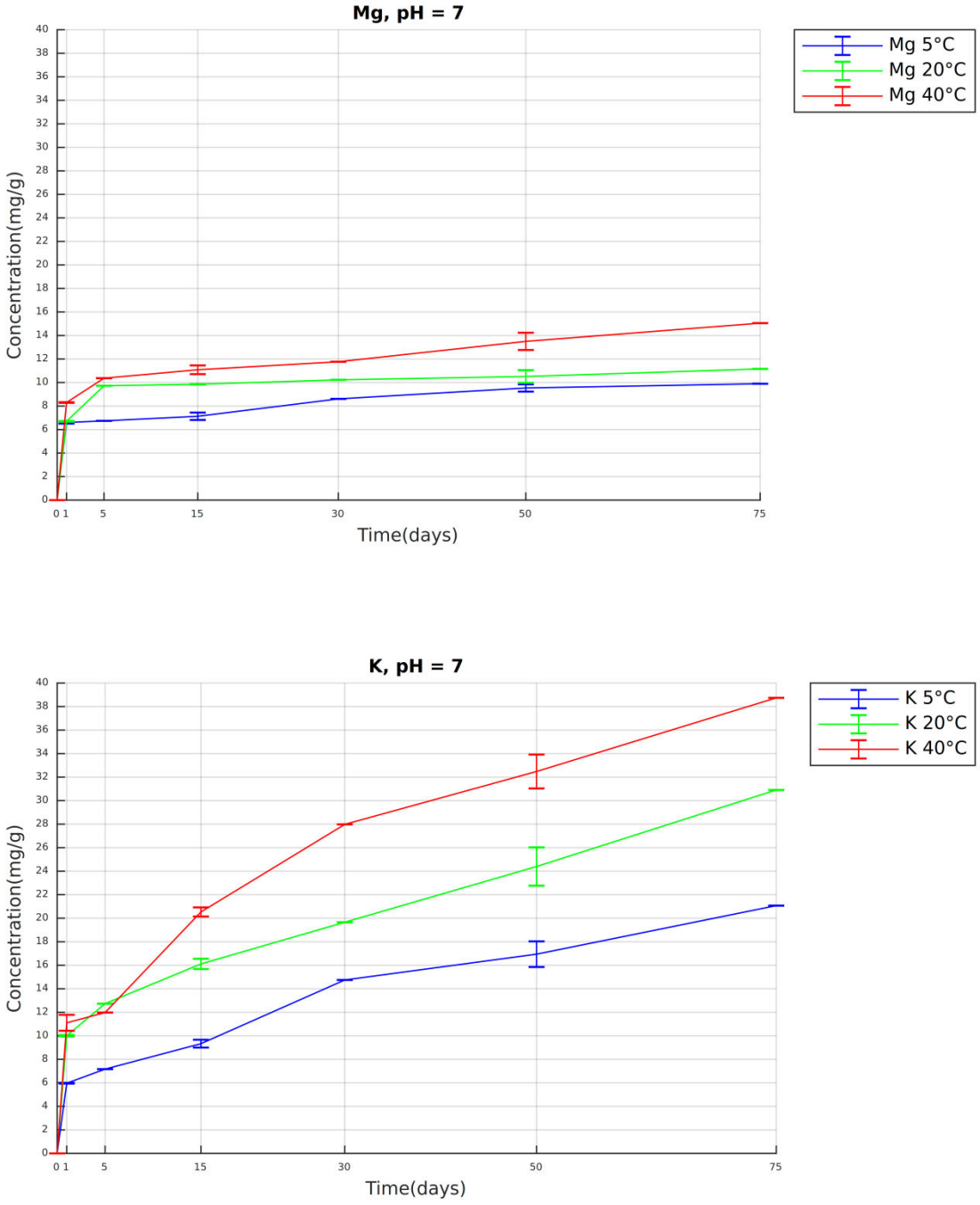

Fig. 162 Sample *Triticum durum,* Corfu: concentration (mg/g) of Mg (above) and K (below) over the course of 75 days at pH 7 and temperature 5 ˚C, 20˚C, 40 ˚C

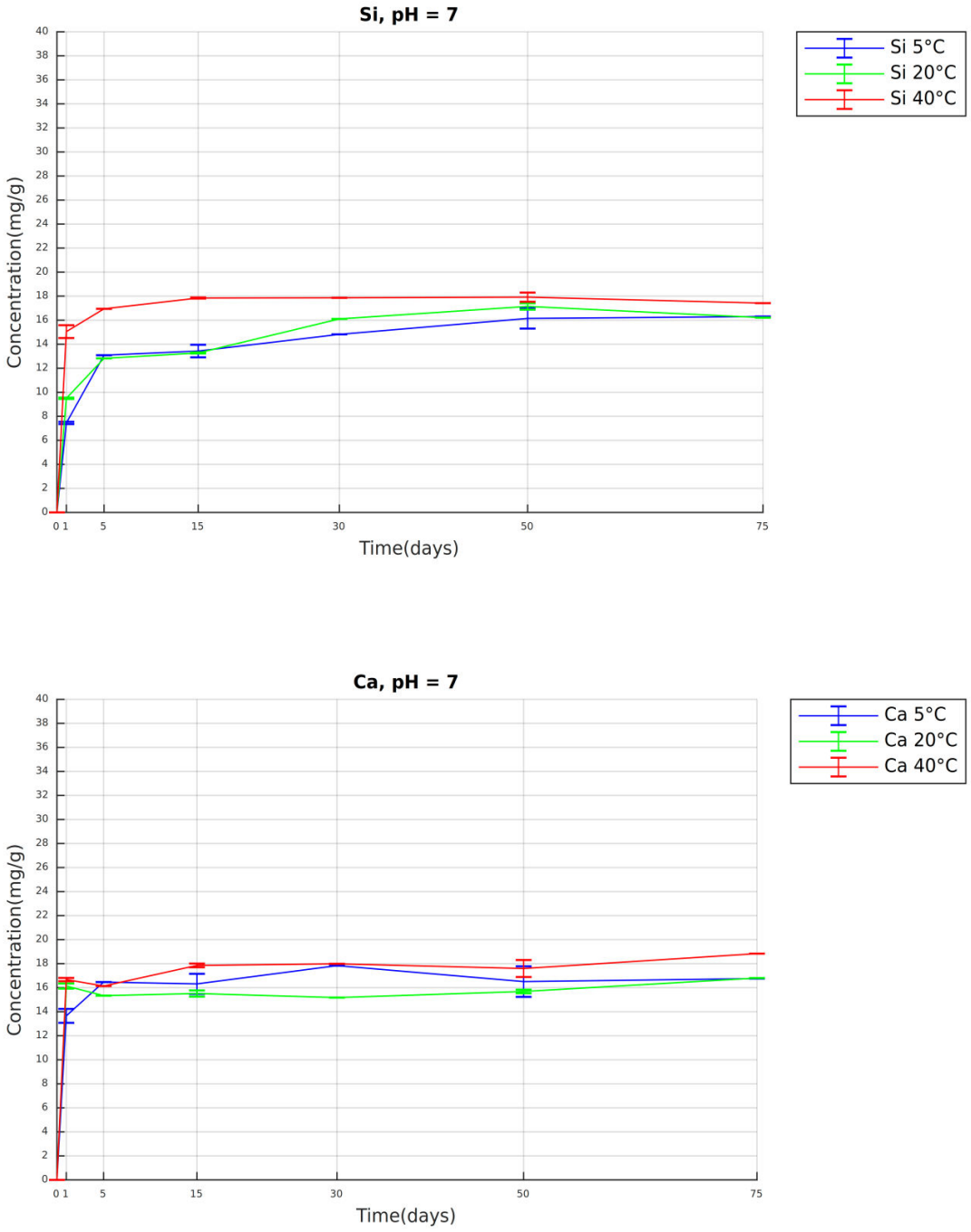

Fig. 163 Sample *Triticum durum,* Corfu: concentration (mg/g) of Si (above) and Ca (below) over the course of 75 days at pH 7 and temperature 5 ˚C, 20˚C, 40 ˚C

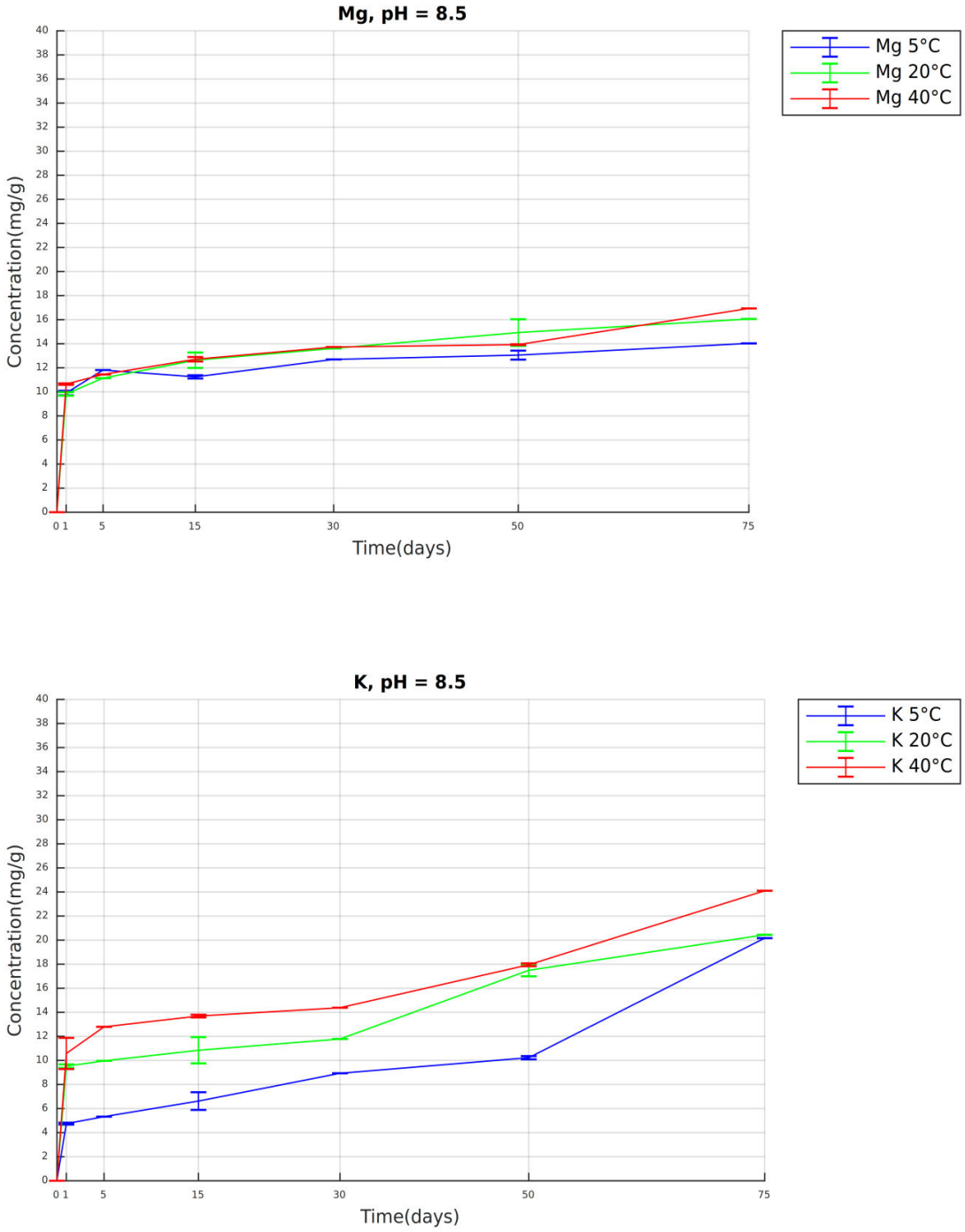

Fig. 164 Sample *Triticum durum,* Corfu: concentration (mg/g) of Mg (above) and K (below) over the course of 75 days at pH 8.5 and temperature 5 ˚C, 20˚C, 40 ˚C

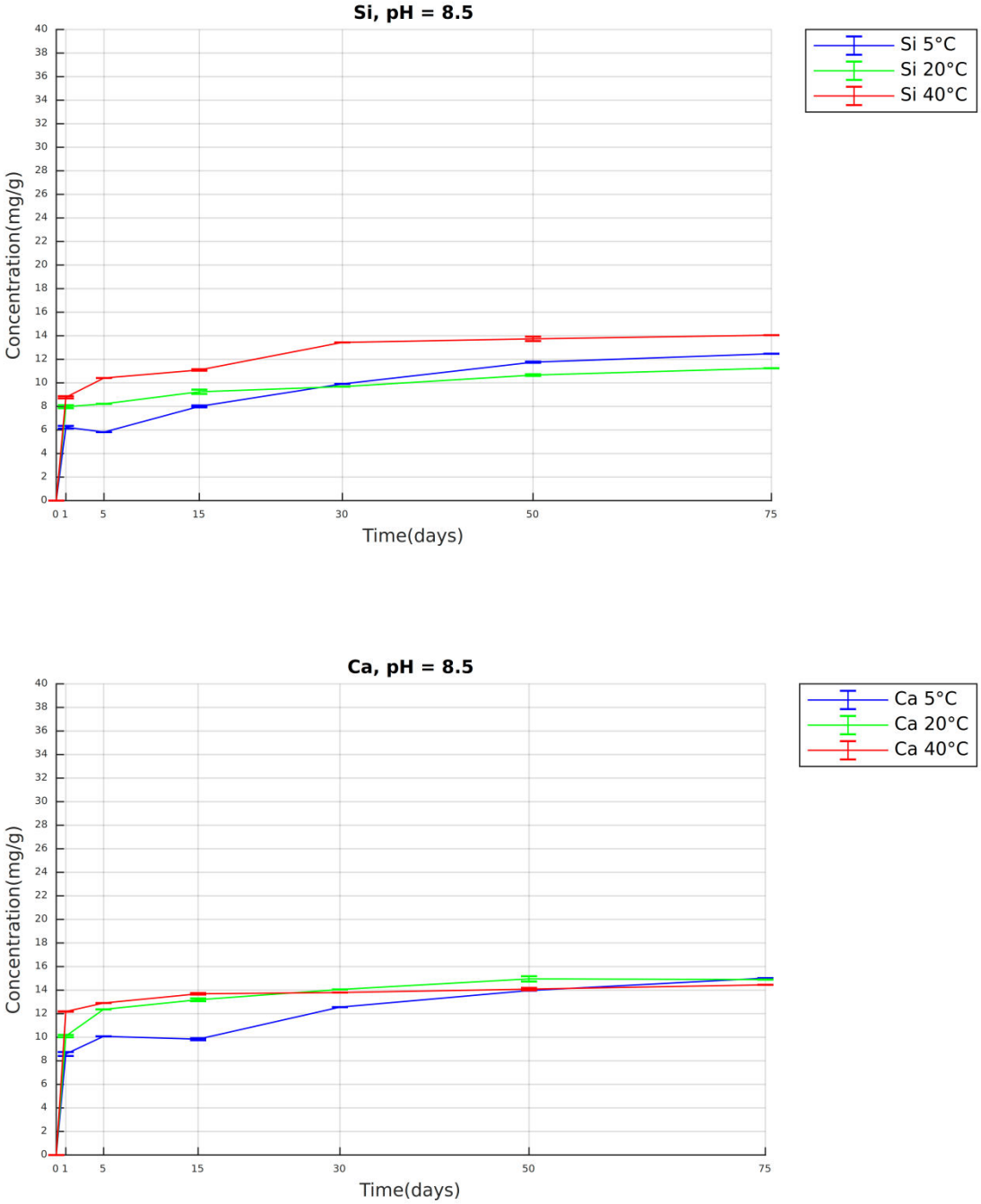

Fig. 165 Sample *Triticum durum,* Corfu: concentration (mg/g) of Si (above) and Ca (below) over the course of 75 days at pH 8.5 and temperature 5 ˚C, 20˚C, 40 ˚C

Appendix – part 4

(Concentrations of Sr and Ba over time)

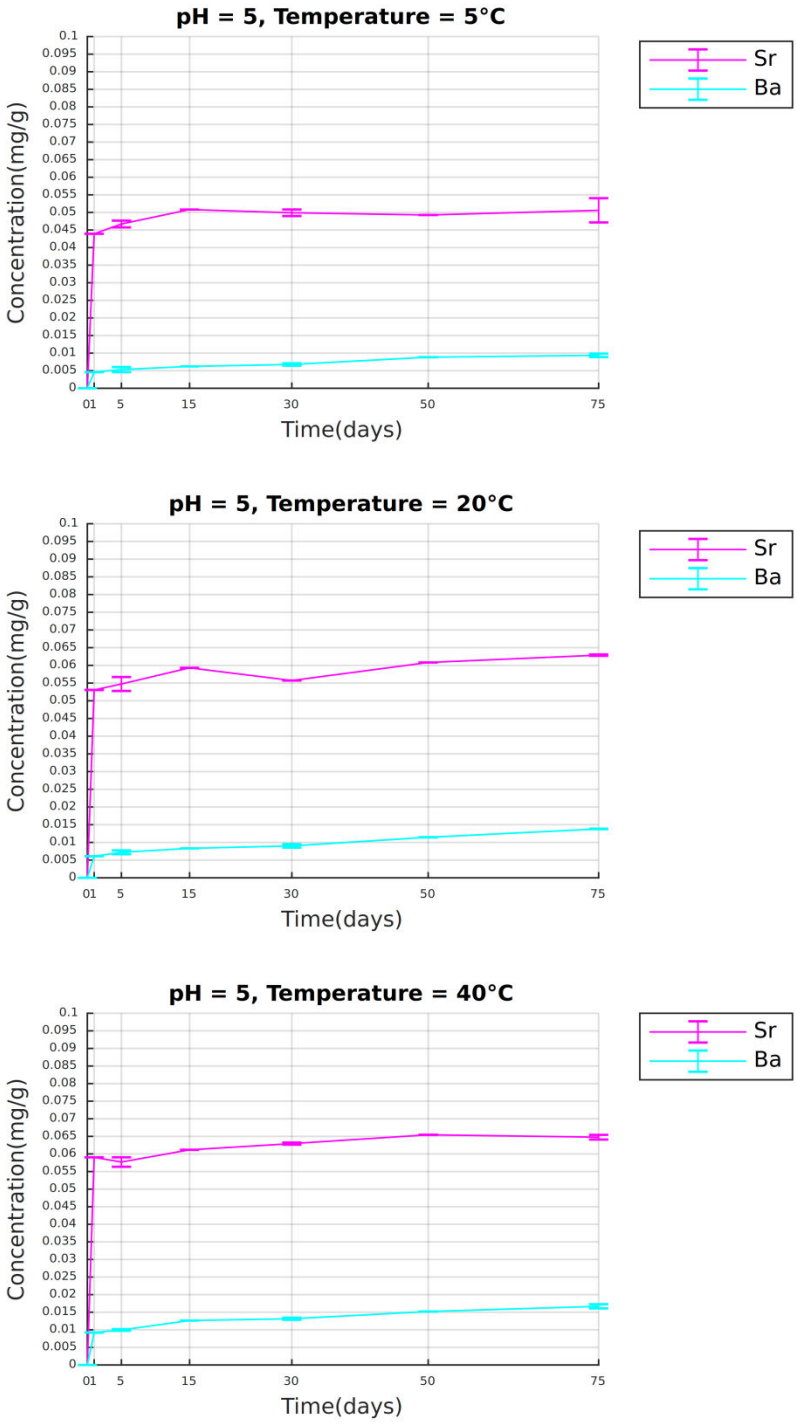

Fig. 166 Sample *Triticum durum*, Cyprus: concentration (mg/g) of Sr and Ba over the course of 75 days at pH 5 and temperature 5 ˚C, 20˚C, 40 ˚C

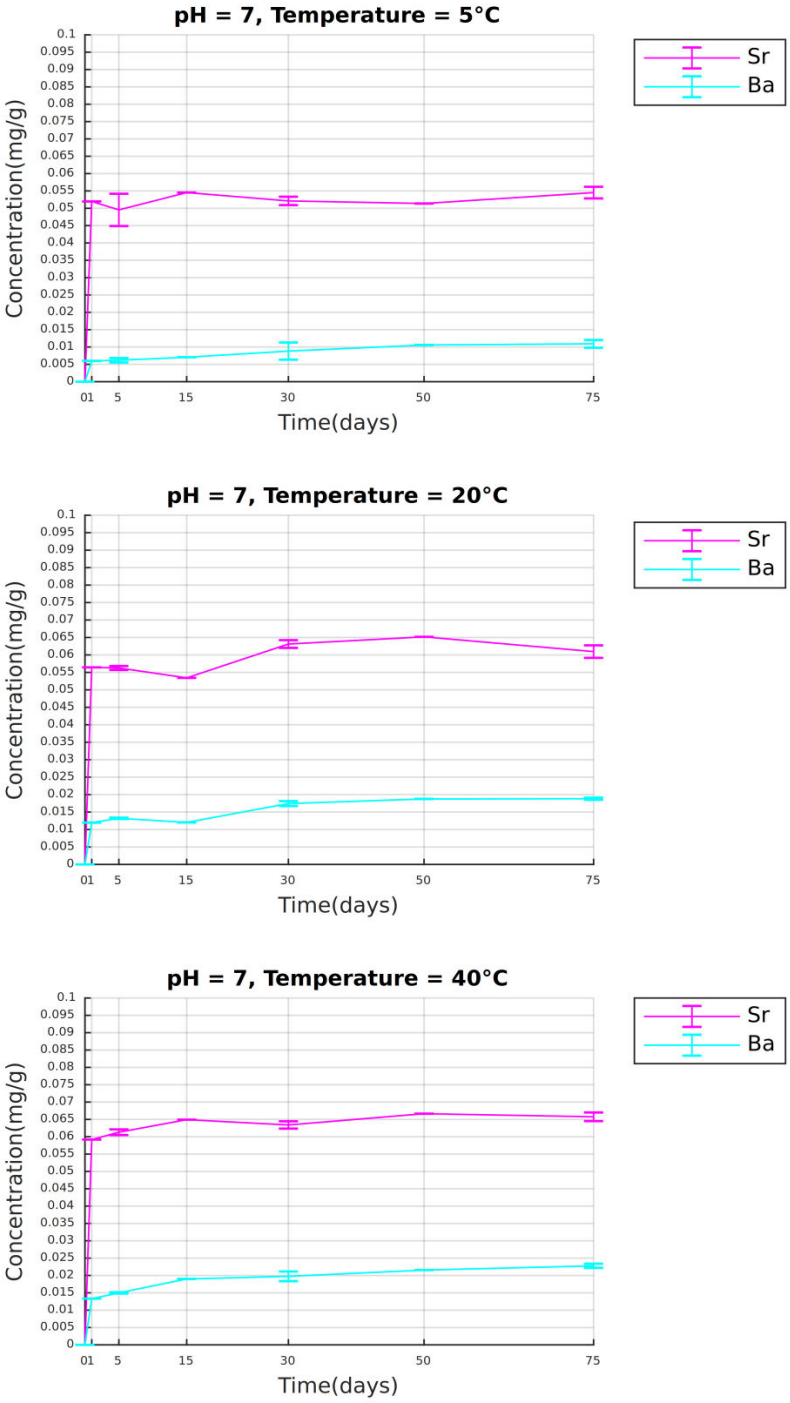

Fig. 167 Sample *Triticum durum*, Cyprus: concentration (mg/g) of Sr and Ba over the course of 75 days at pH 7 and temperature 5 ˚C, 20˚C, 40 ˚C

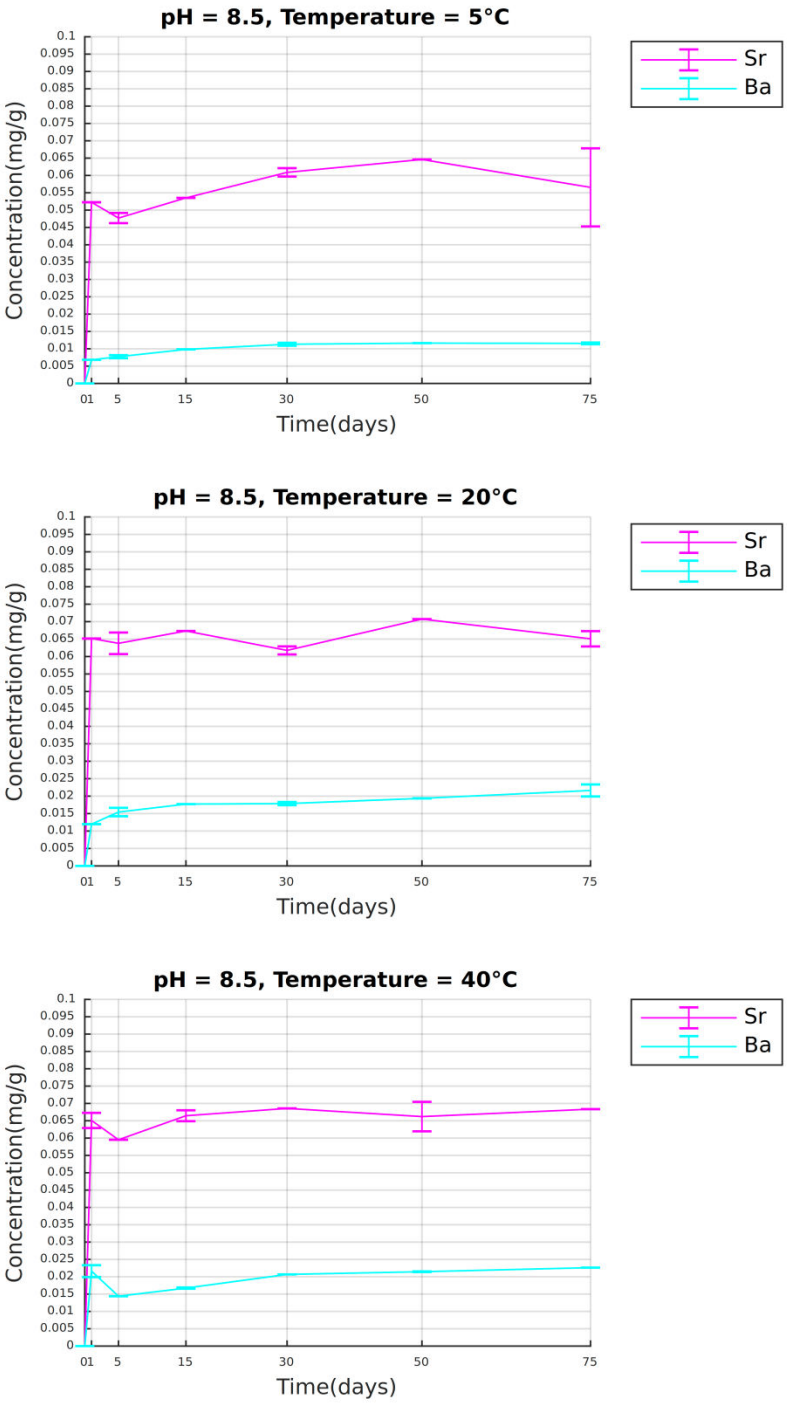

Fig. 168 Sample *Triticum durum*, Cyprus: concentration (mg/g) of Sr and Ba over the course of 75 days at pH 8.5 and temperature 5 ˚C, 20˚C, 40 ˚C

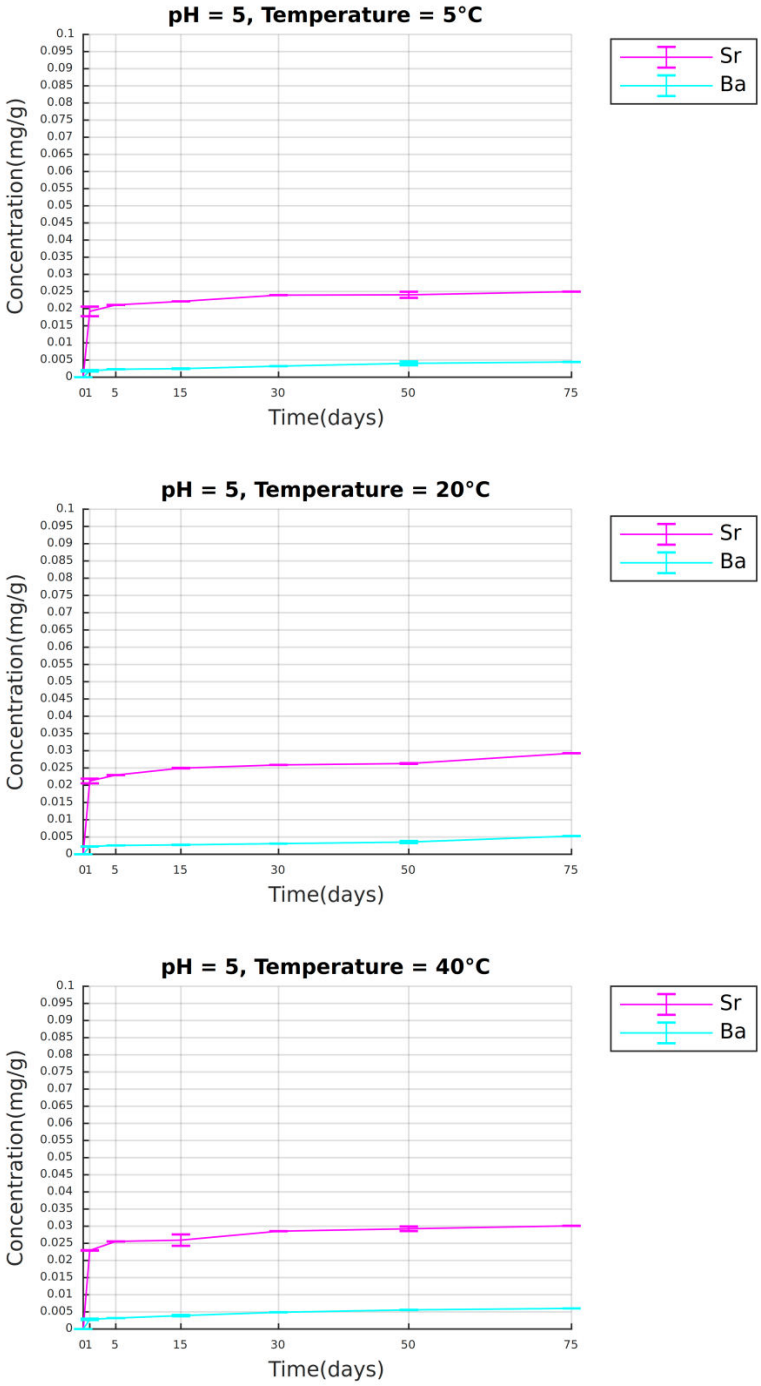

Fig. 169 Sample *Triticum durum*, Crete: concentration (mg/g) of Sr and Ba over the course of 75 days at pH 5 and temperature 5 ˚C, 20˚C, 40 ˚C

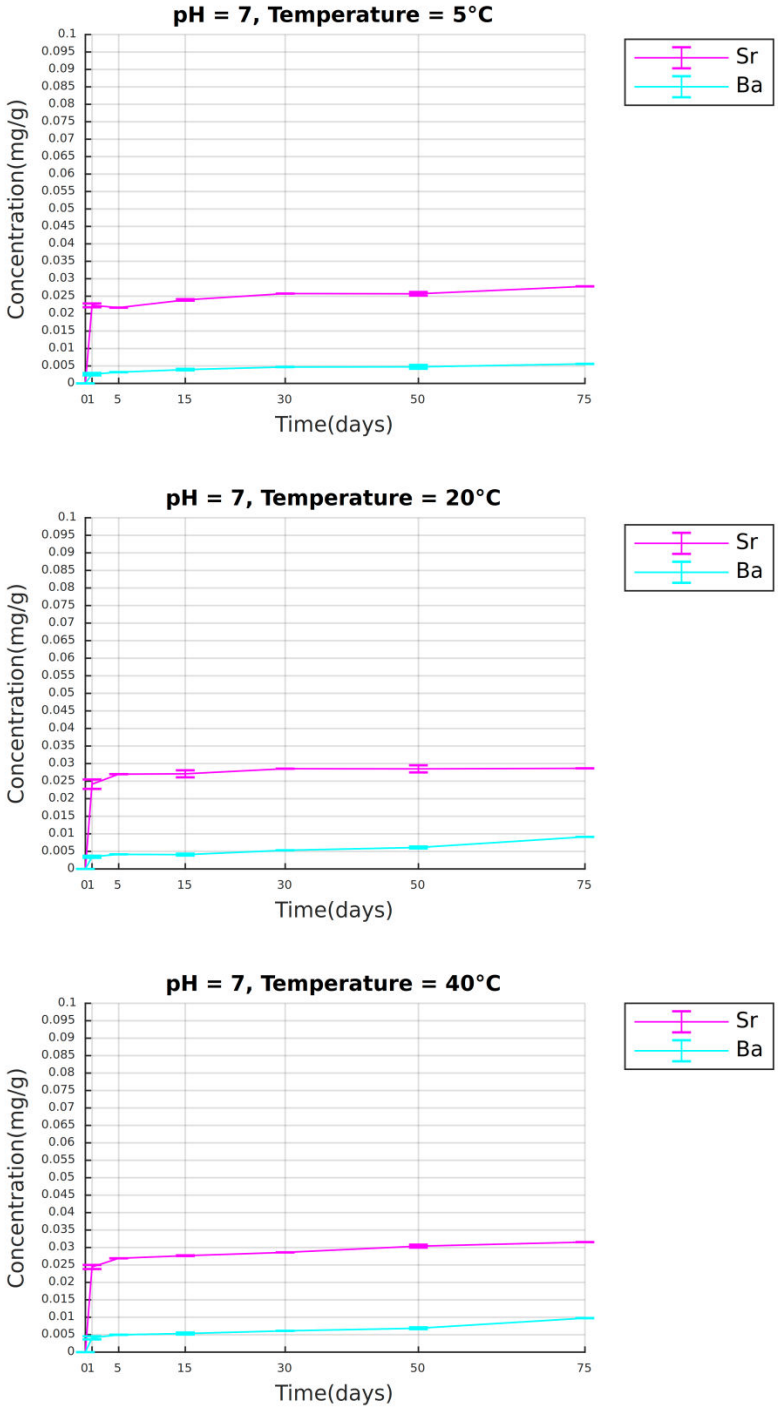

Fig. 170 Sample *Triticum durum*, Crete: concentration (mg/g) of Sr and Ba over the course of 75 days at pH 7 and temperature 5 ˚C, 20˚C, 40 ˚C

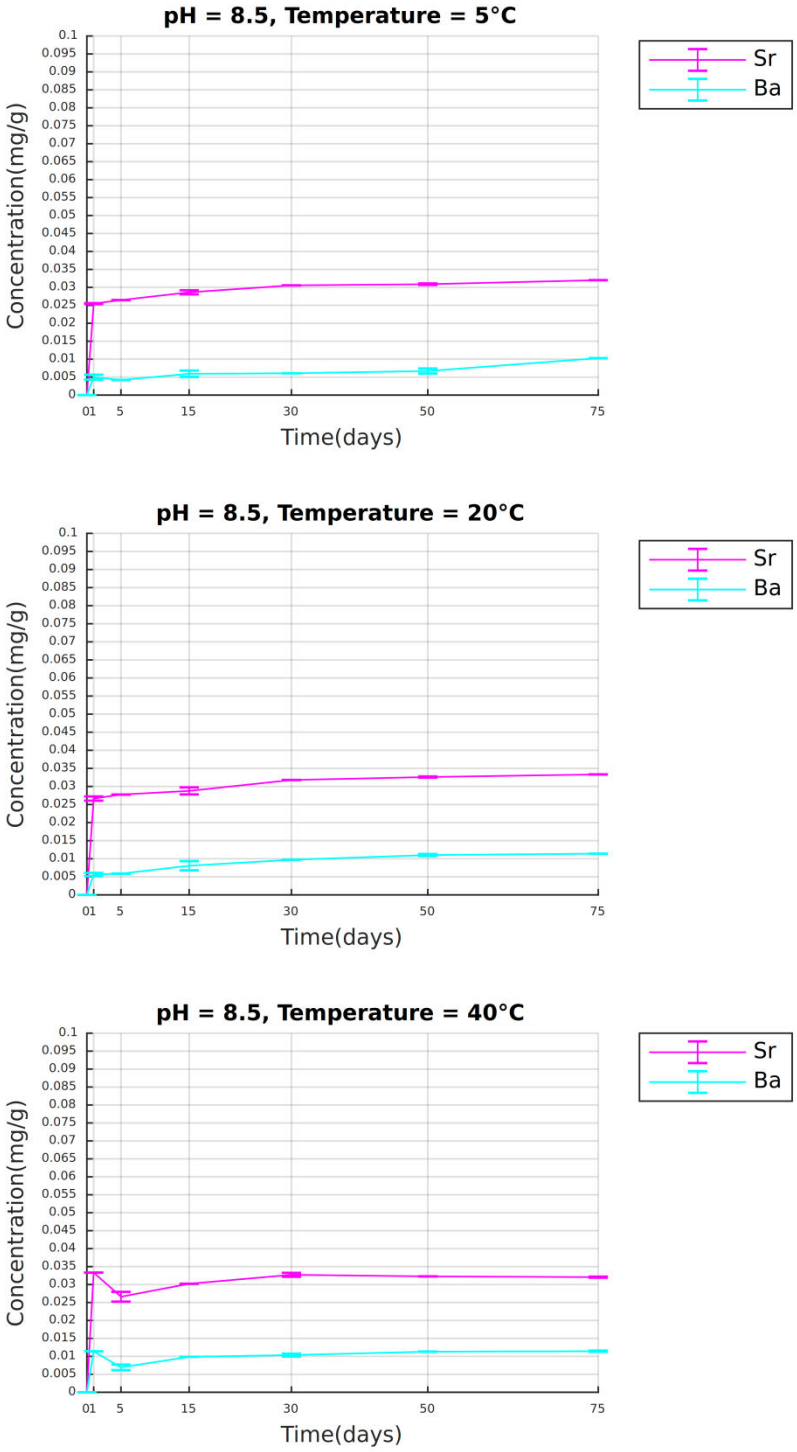

Fig. 171 Sample *Triticum durum*, Crete: concentration (mg/g) of Sr and Ba over the course of 75 days at pH 8.5 and temperature 5 ˚C, 20˚C, 40 ˚C

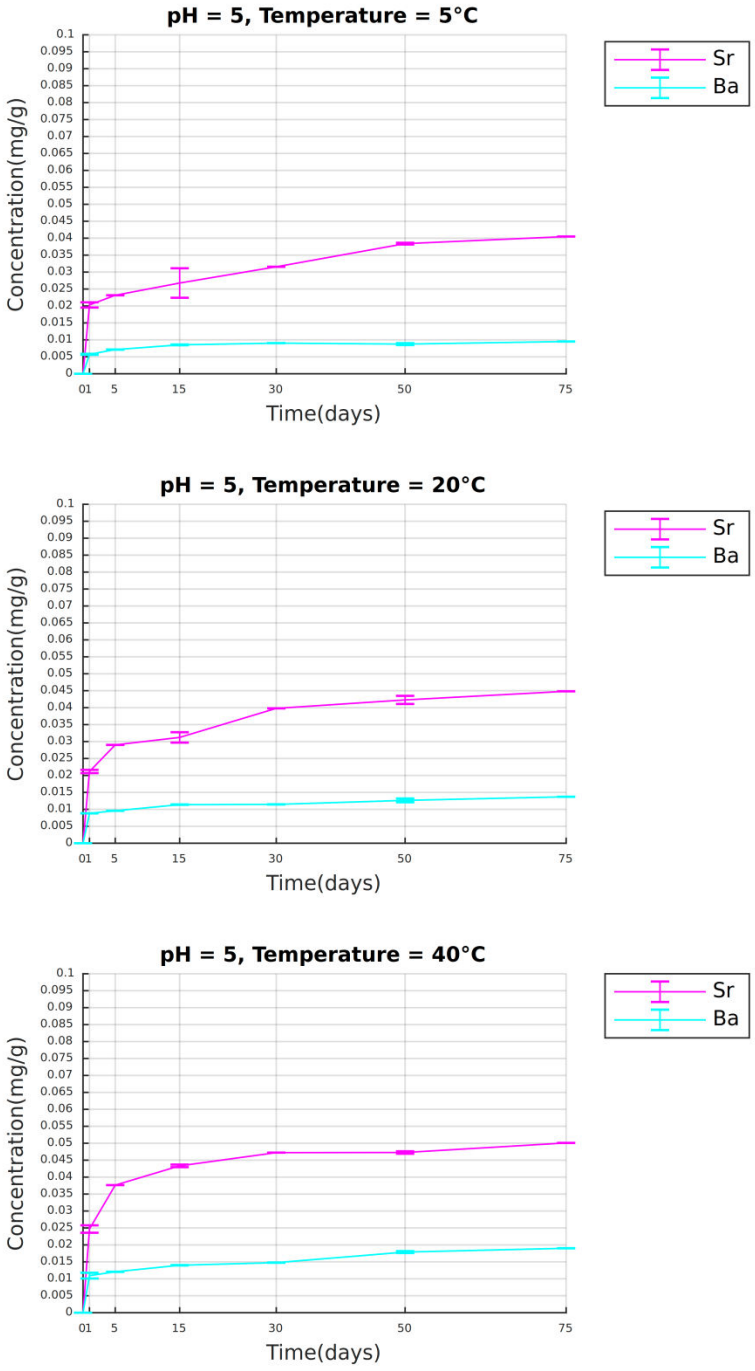

Fig. 172 Sample *Triticum monococcum,* Volos: concentration (mg/g) of Sr and Ba over the course of 75 days at pH 5 and temperature 5 ˚C, 20˚C, 40 ˚C

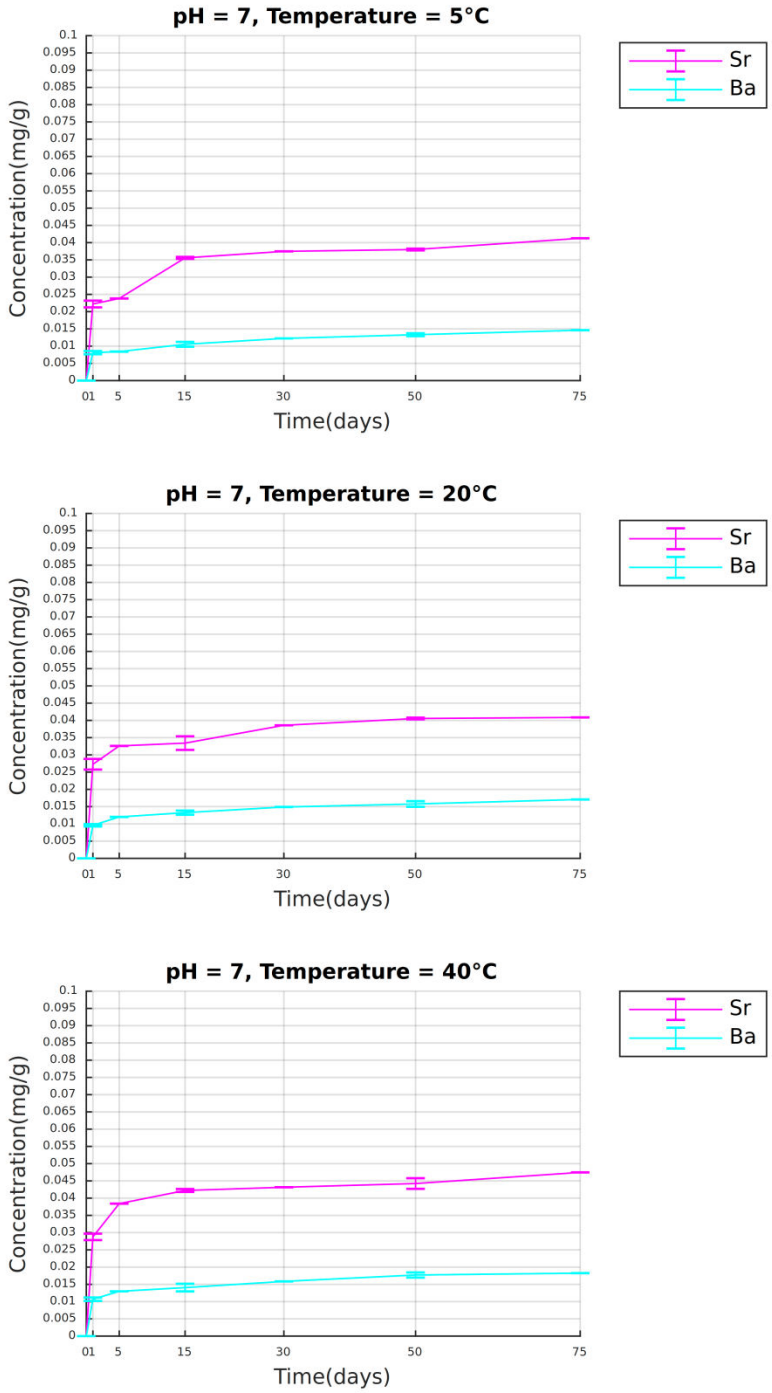

Fig. 173 Sample *Triticum monococcum,* Volos: concentration (mg/g) of Sr and Ba over the course of 75 days at pH 7 and temperature 5 ˚C, 20˚C, 40 ˚C

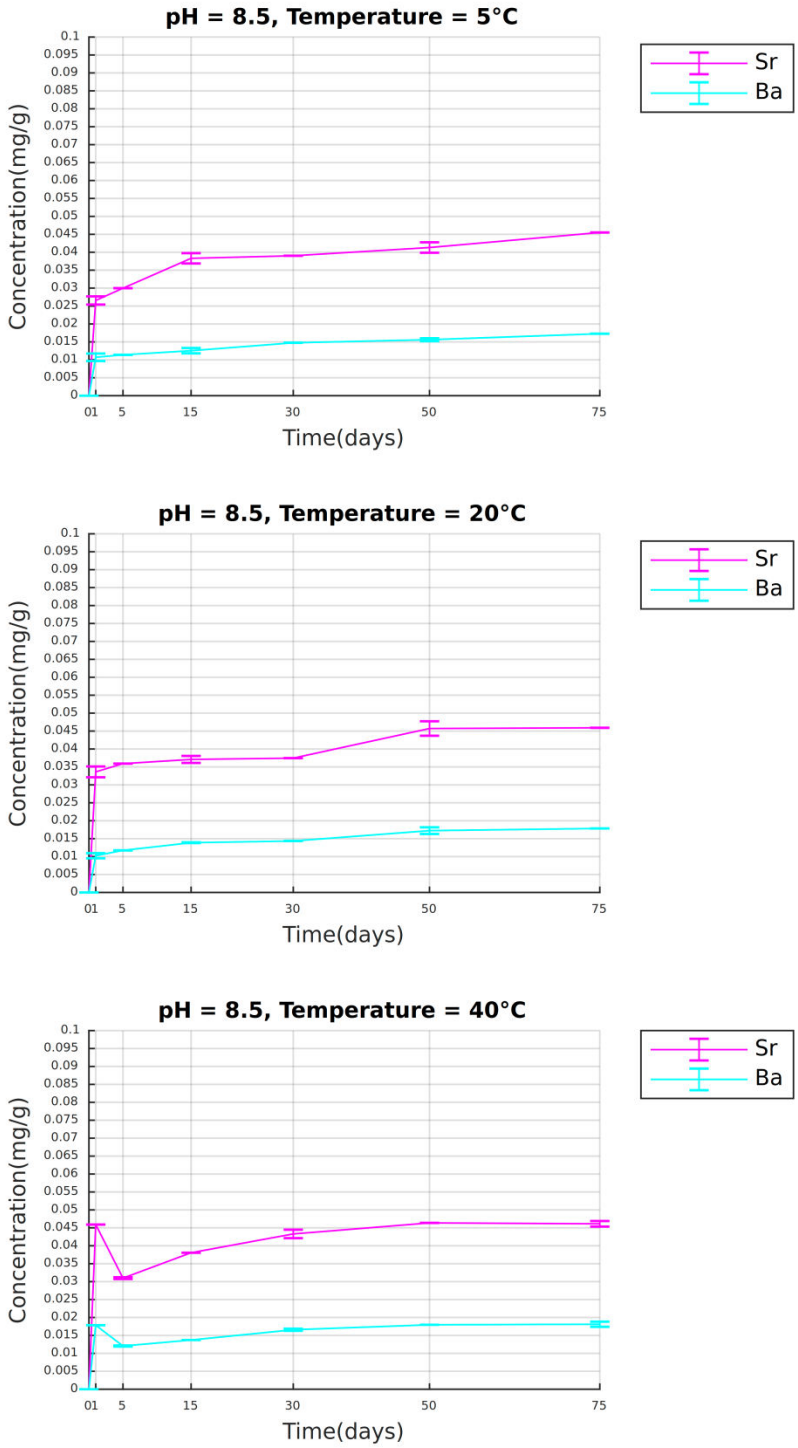

Fig. 174 Sample *Triticum monococcum,* Volos: concentration (mg/g) of Sr and Ba over the course of 75 days at pH 8.5 and temperature 5 ˚C, 20˚C, 40 ˚C

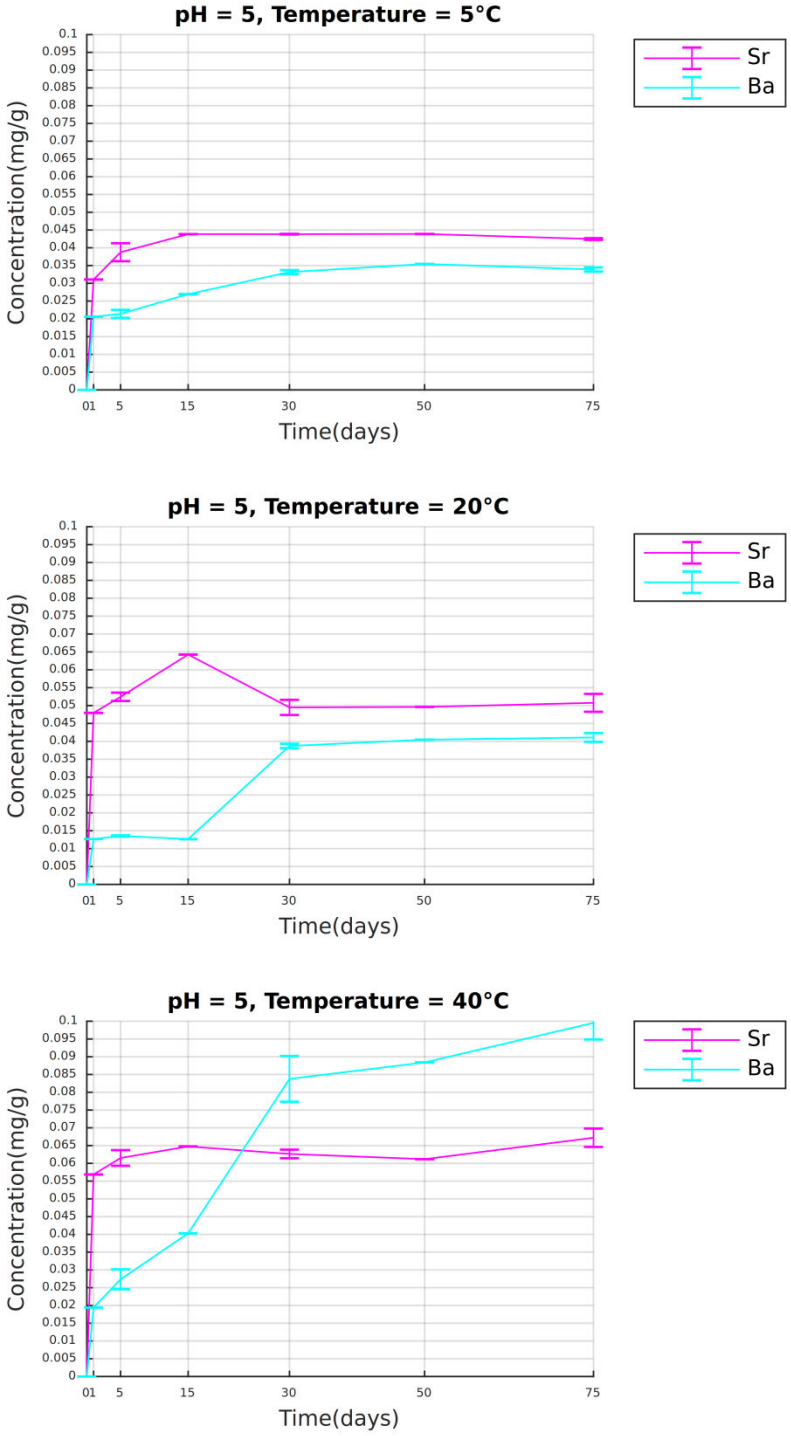

Fig. 175 Sample *Triticum monococcum,* Pella I: concentration (mg/g) of Sr and Ba over the course of 75 days at pH 5 and temperature 5 ˚C, 20˚C, 40 ˚C

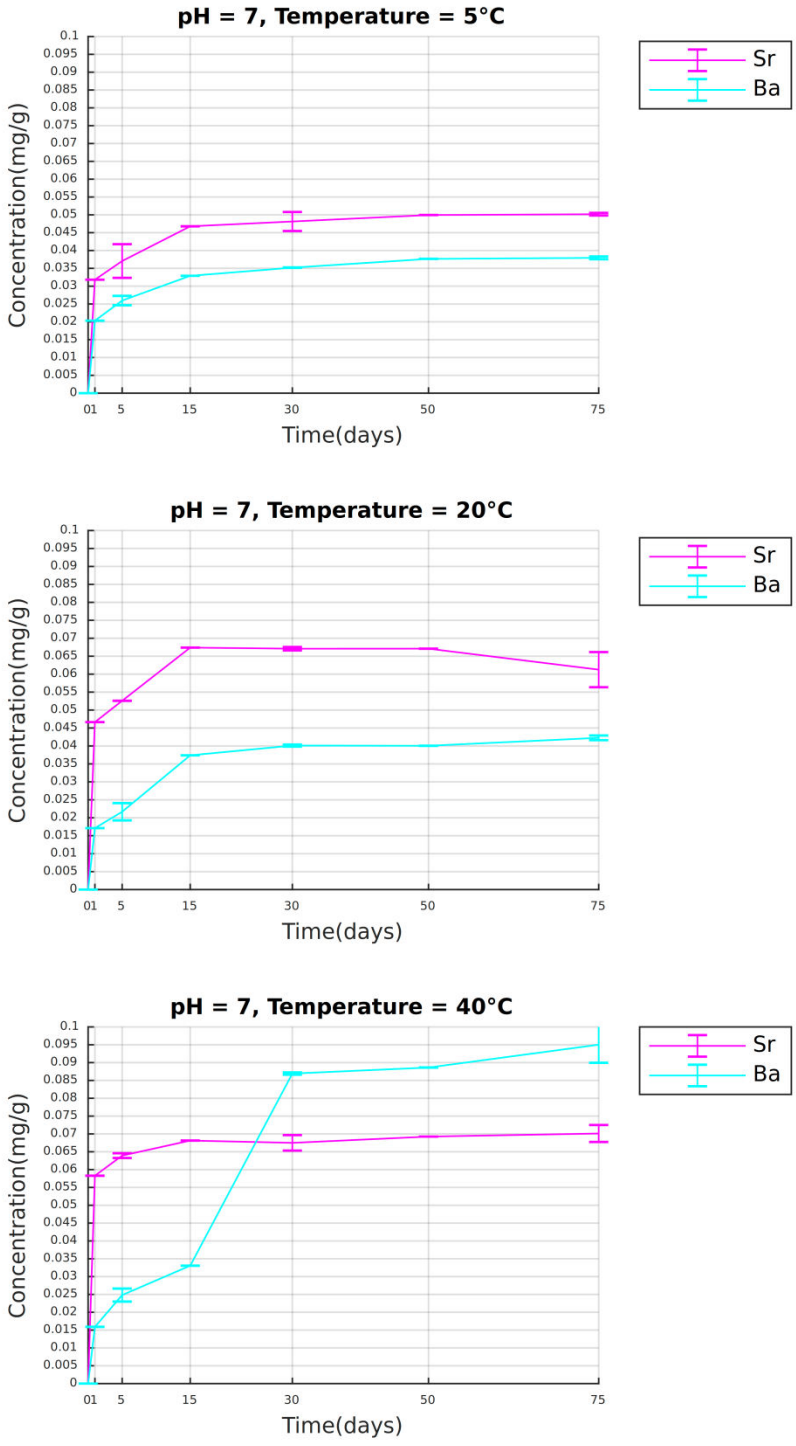

Fig. 176 Sample *Triticum monococcum,* Pella I: concentration (mg/g) of Sr and Ba over the course of 75 days at pH 7 and temperature 5 ˚C, 20˚C, 40 ˚C

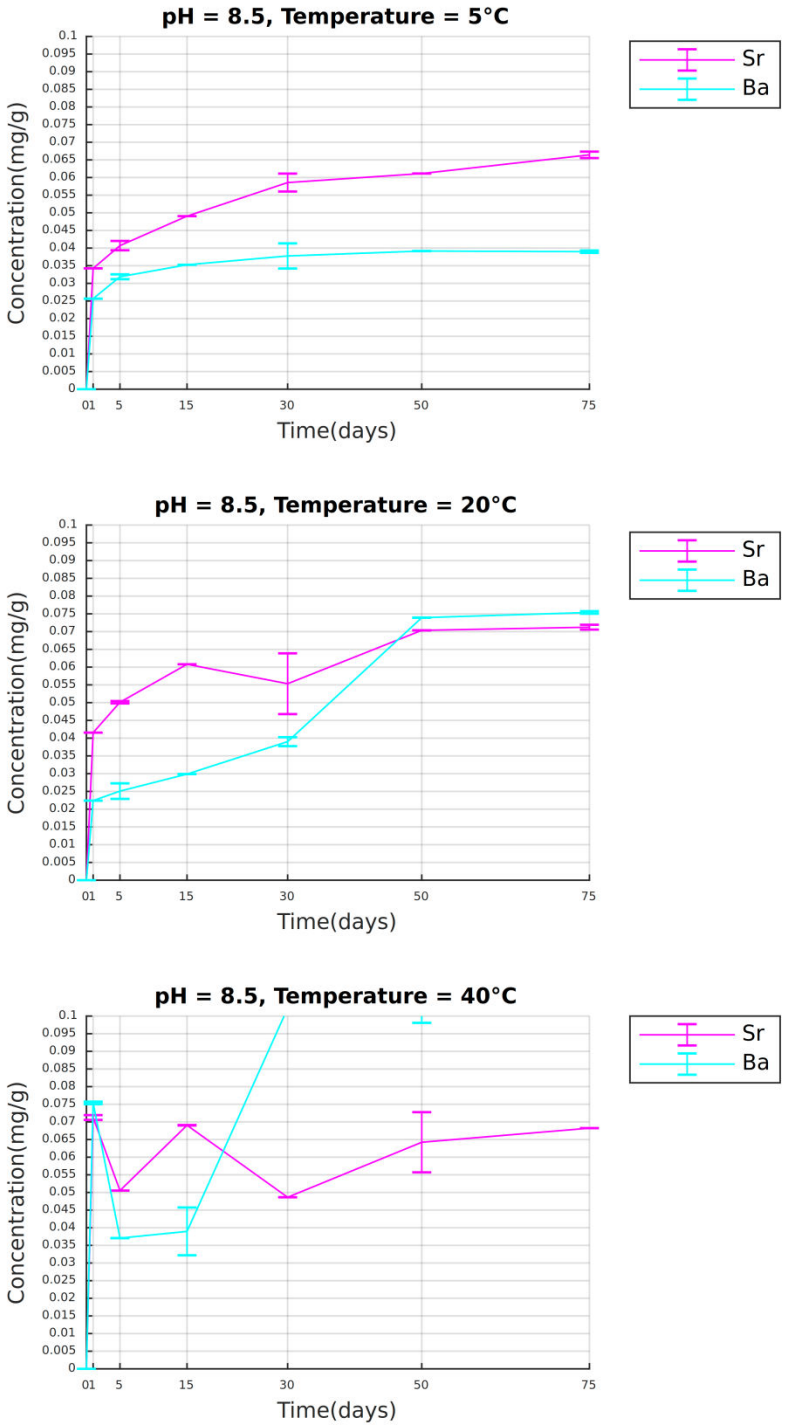

Fig. 177 Sample *Triticum monococcum,* Pella I: concentration (mg/g) of Sr and Ba over the course of 75 days at pH 8.5 and temperature 5 ˚C, 20˚C, 40 ˚C

PELLA II

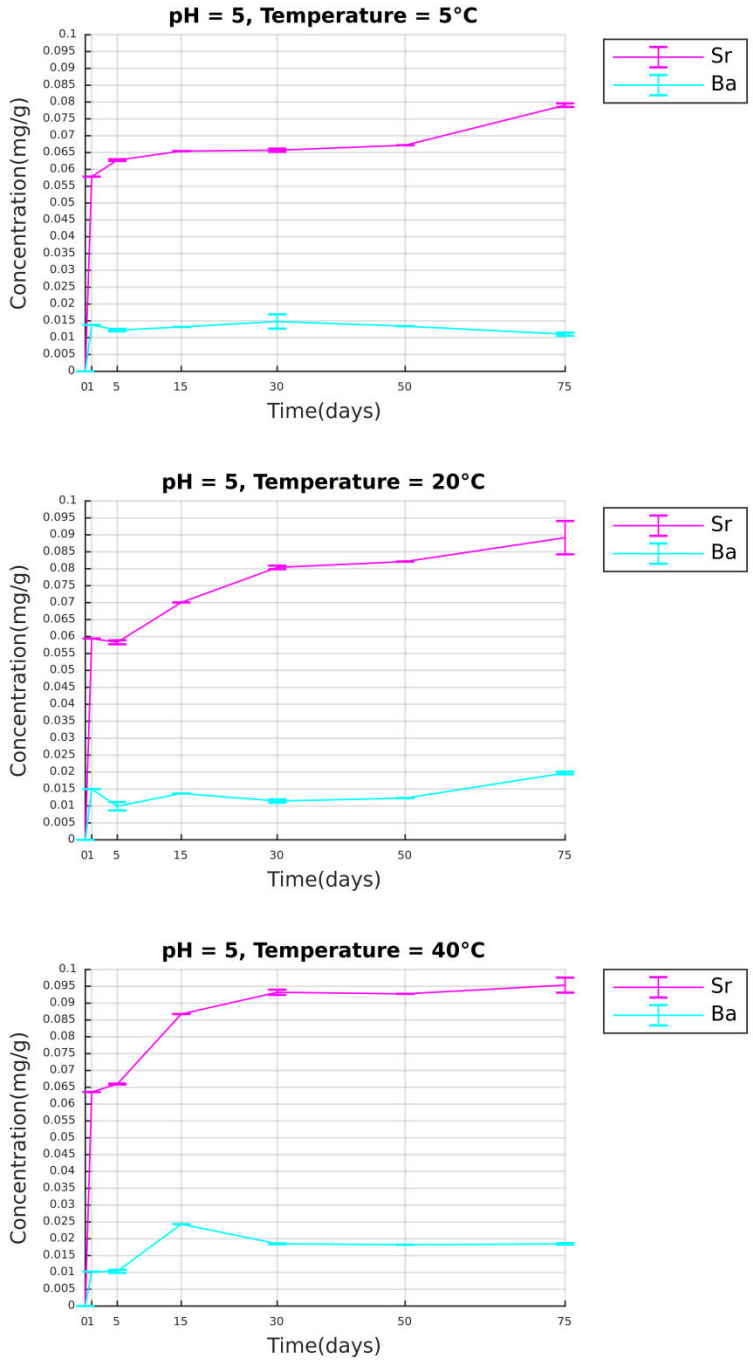

Fig. 178 Sample *Triticum durum,* Pella II: concentration (mg/g) of Sr and Ba over the course of 75 days at pH 5 and temperature 5 ˚C, 20˚C, 40 ˚C

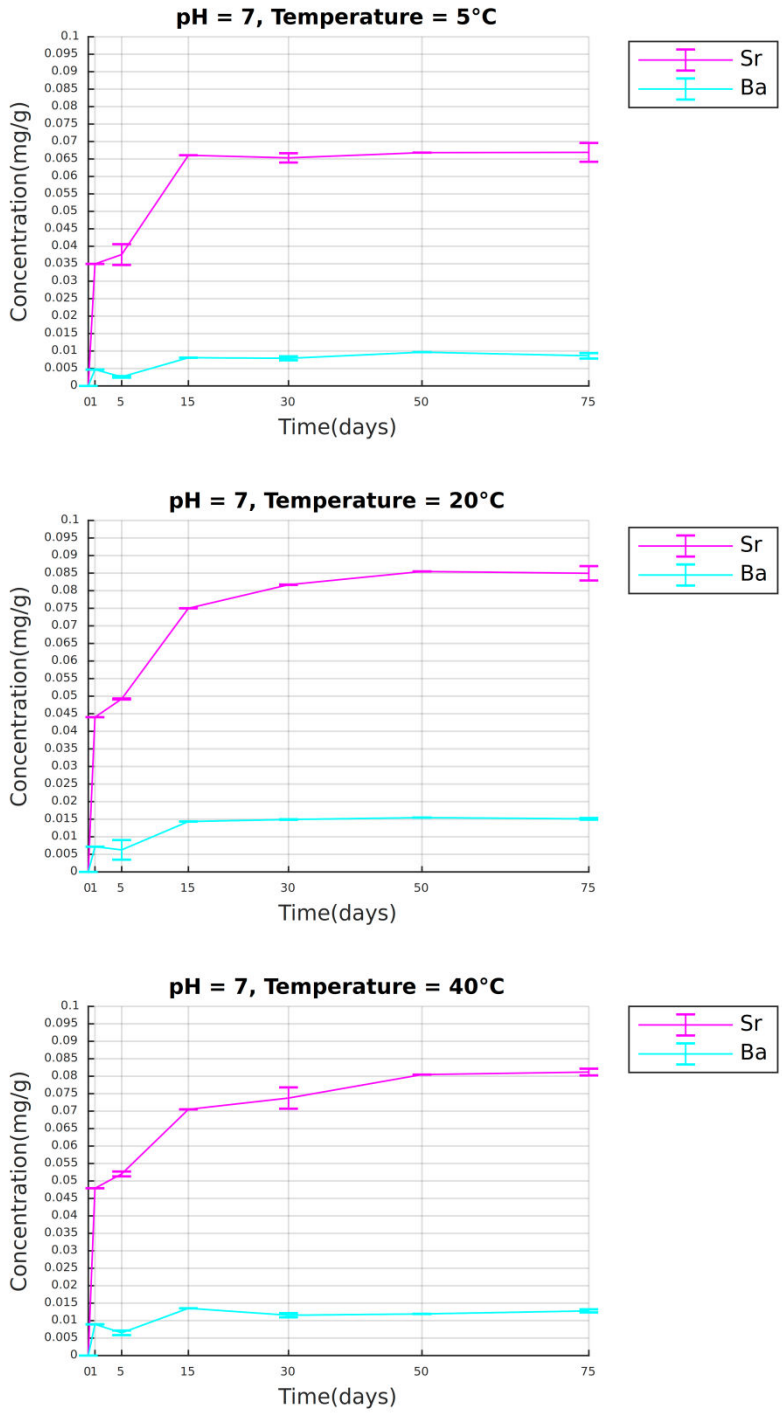

Fig. 179 Sample *Triticum durum,* Pella II: concentration (mg/g) of Sr and Ba over the course of 75 days at pH 7 and temperature 5 ˚C, 20˚C, 40 ˚C

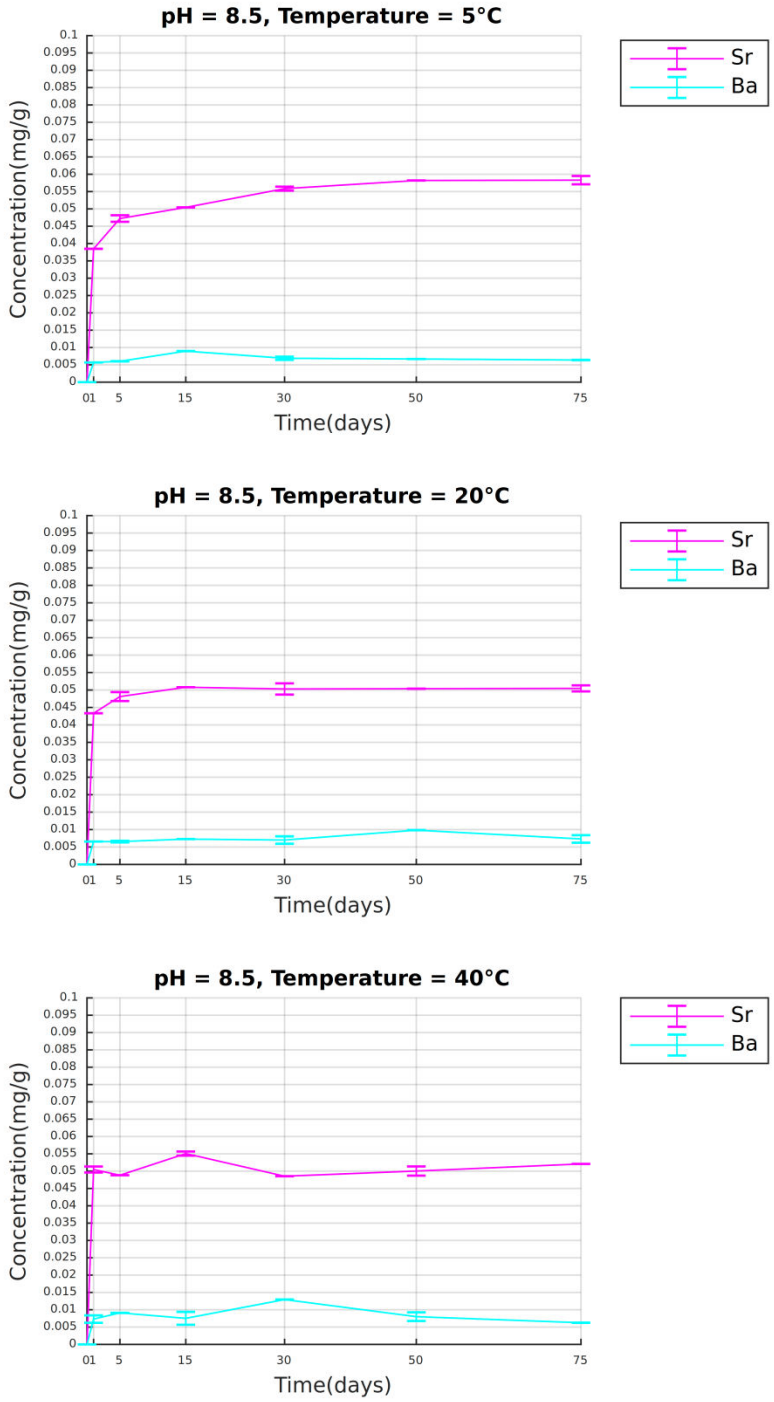

Fig. 180 Sample *Triticum durum,* Pella II: concentration (mg/g) of Sr and Ba over the course of 75 days at pH 8.5 and temperature 5 ˚C, 20˚C, 40 ˚C

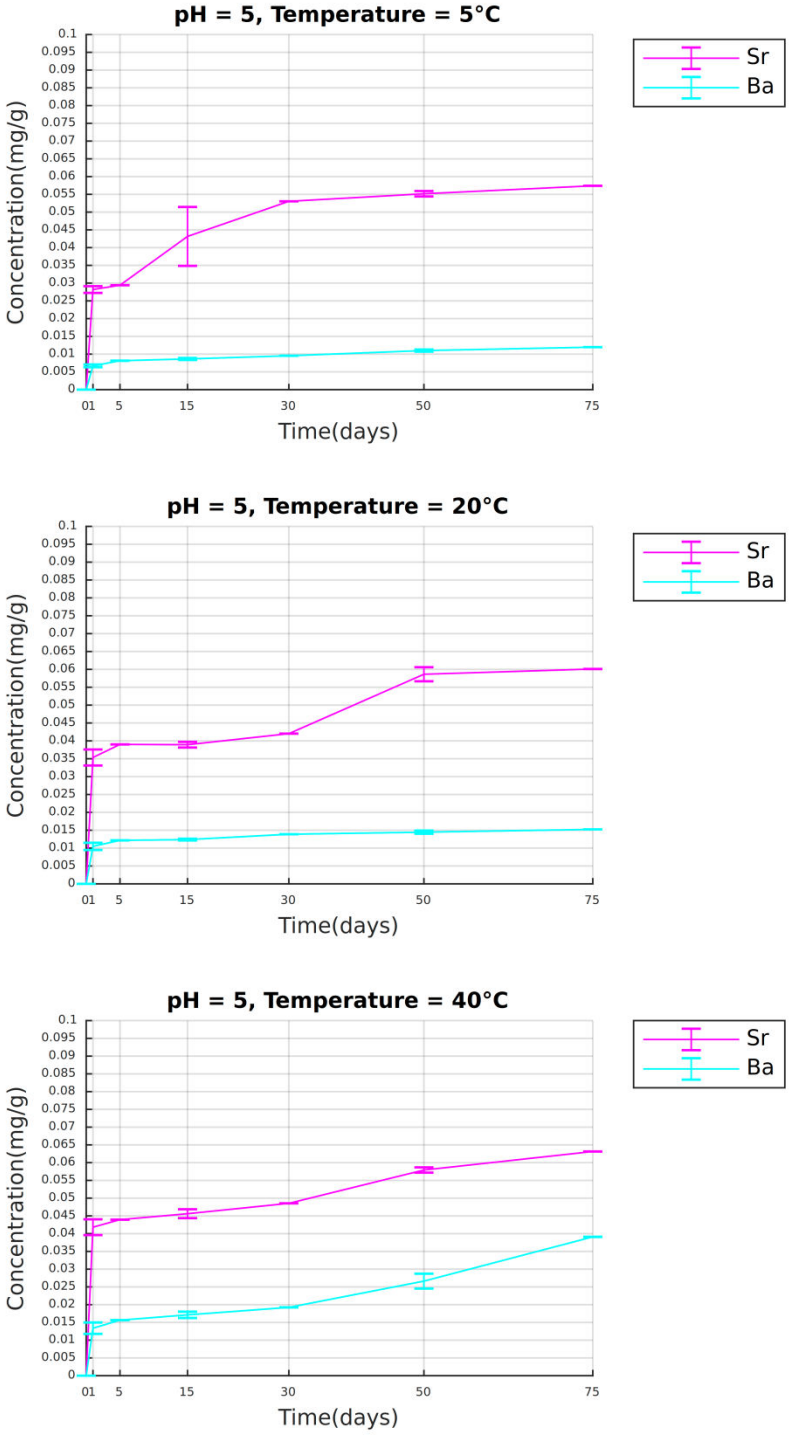

Fig. 181 Sample *Triticum durum,* Corfu: concentration (mg/g) of Sr and Ba over the course of 75 days at pH 5 and temperature 5 ˚C, 20˚C, 40 ˚C

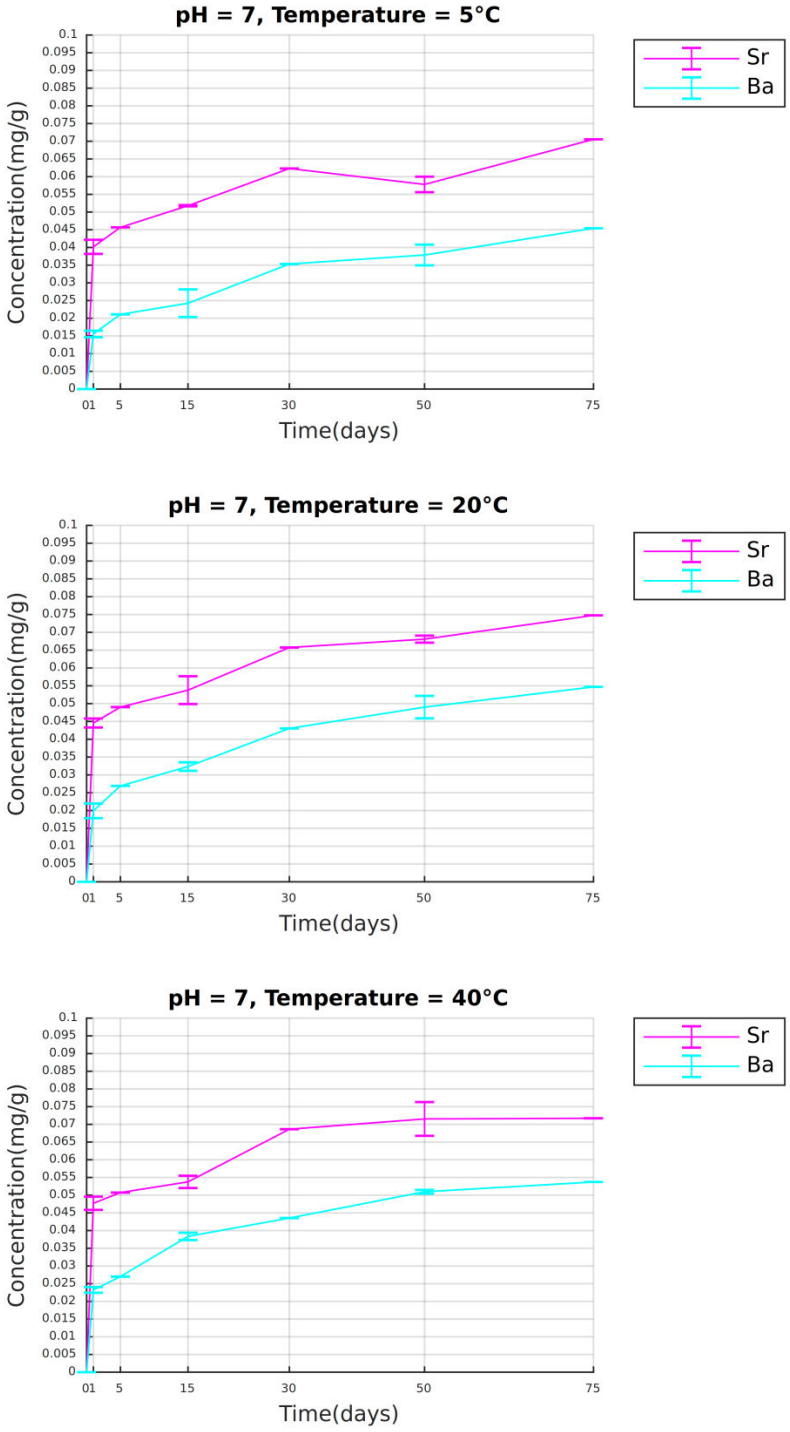

Fig. 182 Sample *Triticum durum,* Corfu: concentration (mg/g) of Sr and Ba over the course of 75 days at pH 7 and temperature 5 ˚C, 20˚C, 40 ˚C

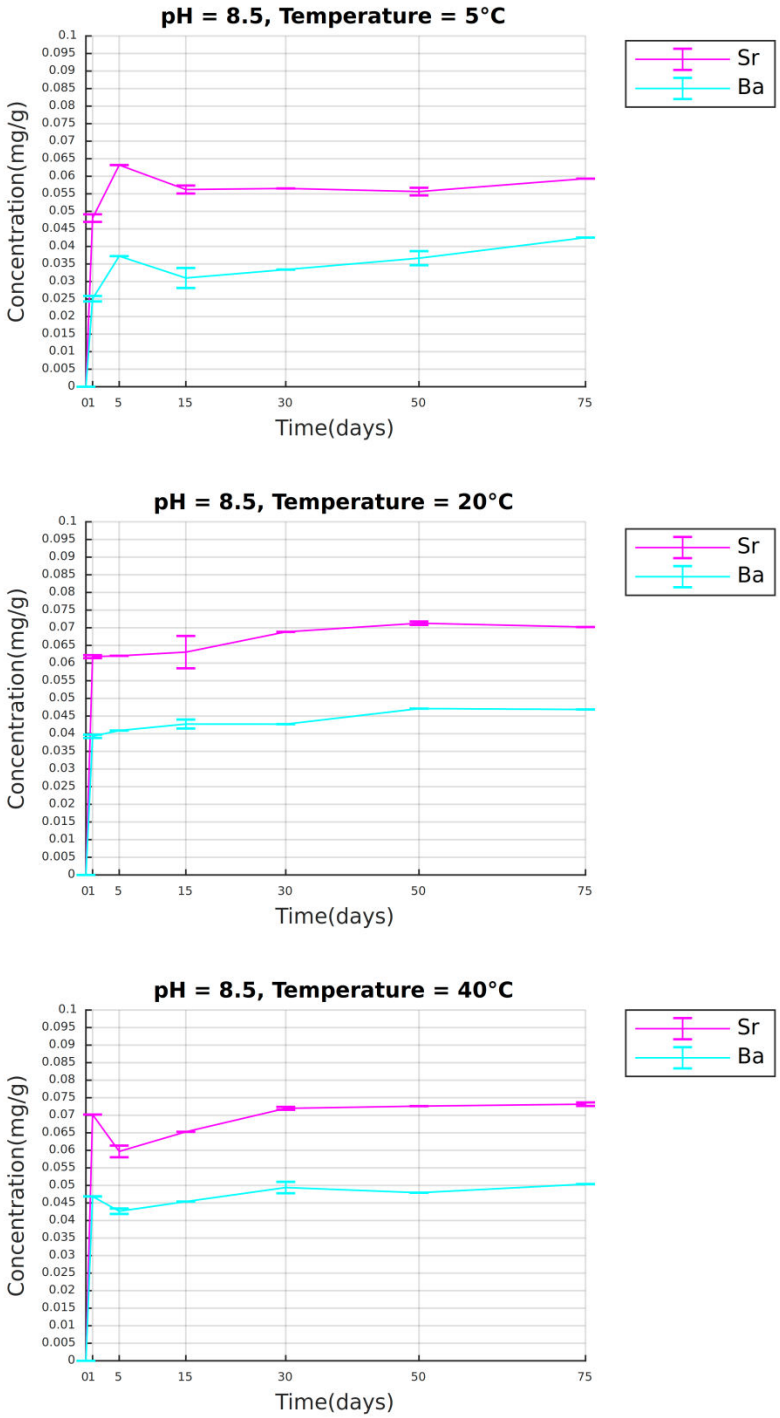

Fig. 183 Sample *Triticum durum,* Corfu: concentration (mg/g) of Sr and Ba over the course of 75 days at pH 8.5 and temperature 5 ˚C, 20˚C, 40 ˚C

Appendix – part 5

(Silicon reaction rates)

(a)

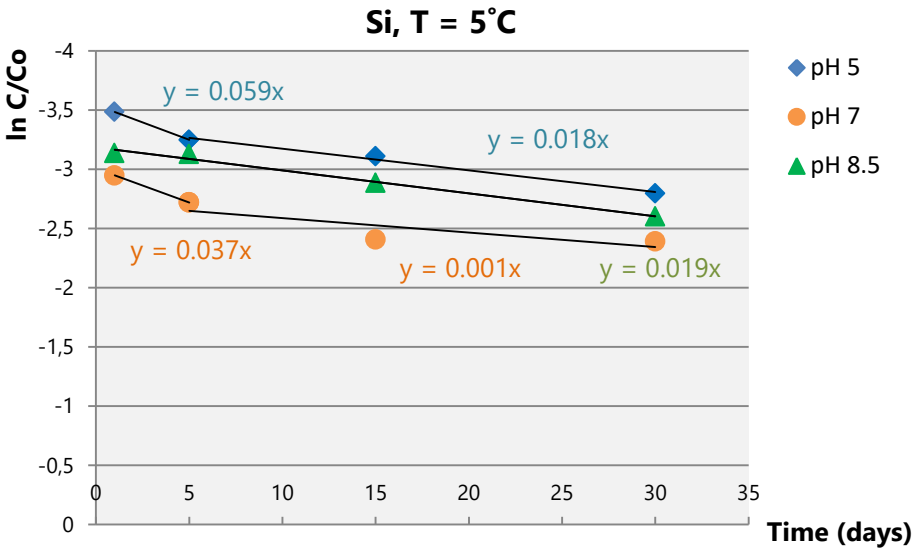
Si, T = 5˚C
ln C/Co
-4
-3,5
-3
-2,5
-2
-1,5
-1
-0,5
0
0
5
10
15
20
25
30
35
Time (days)
y = 0.059x
y = 0.018x
y = 0.037x
y = 0.001x
y = 0.019x
pH 5
pH 7
pH 8.5

(b)

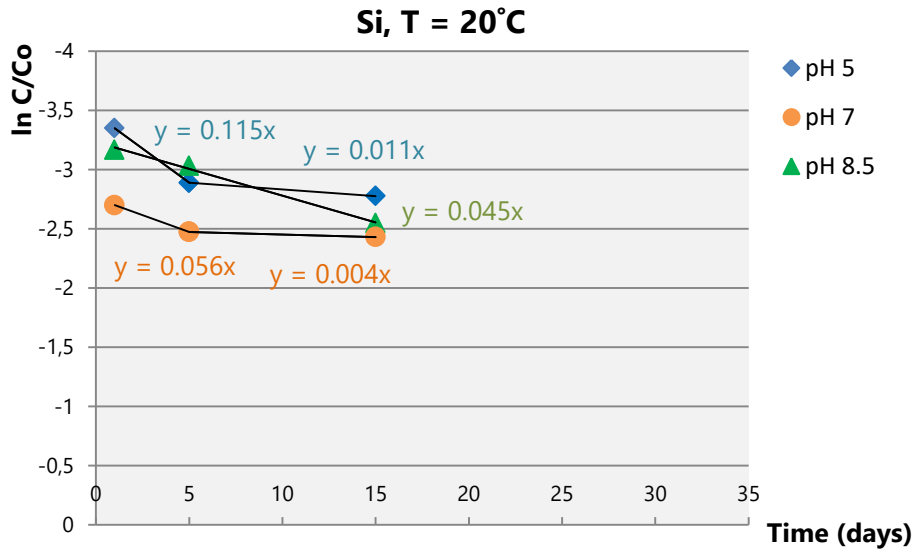
Si, T = 20˚C
ln C/Co
-4
-3,5
-3
-2,5
-2
-1,5
-1
-0,5
0
0
5
10
15
20
25
30
35
Time (days)
y = 0.115x
y = 0.011x
y = 0.045x
y = 0.056x
y = 0.004x
pH 5
pH 7
pH 8.5

(c)

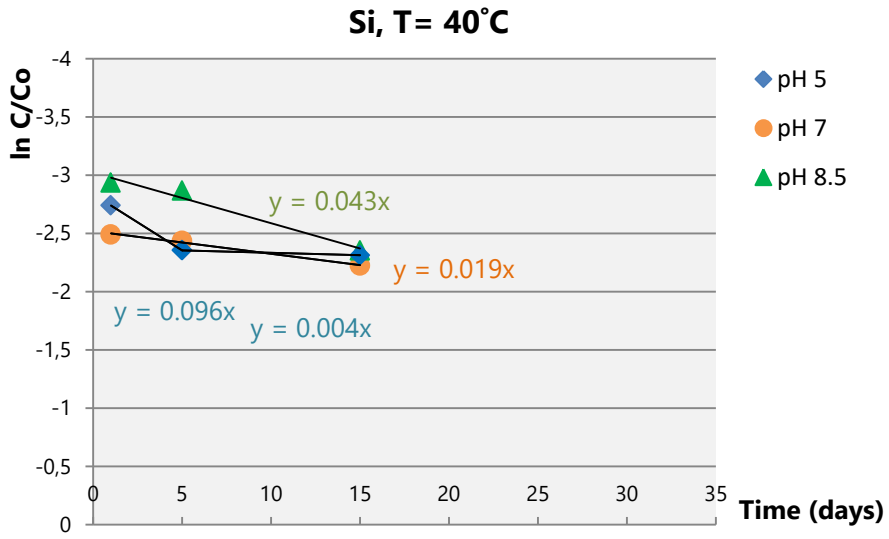

Fig. 184 The ln C/C_o versus time (days) curves for leaching of Si at pH 5, 7, 8.5 and temperature: **(a)** 5, **(b)** 20; and **(c)** 40 °C for the sample *Triticum durum* from Cyprus

(a)

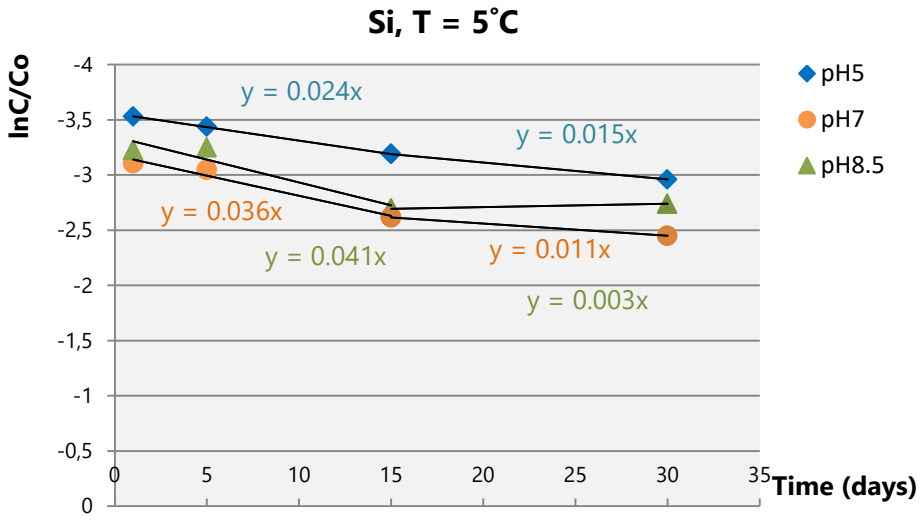
Si, T = 5˚C
lnC/Co
-4
-3,5
-3
-2,5
-2
-1,5
-1
-0,5
0
0
5
10
15
20
25
30
35
Time (days)
y = 0.024x
y = 0.015x
y = 0.036x
y = 0.041x
y = 0.011x
y = 0.003x
pH5
pH7
pH8.5

(b)

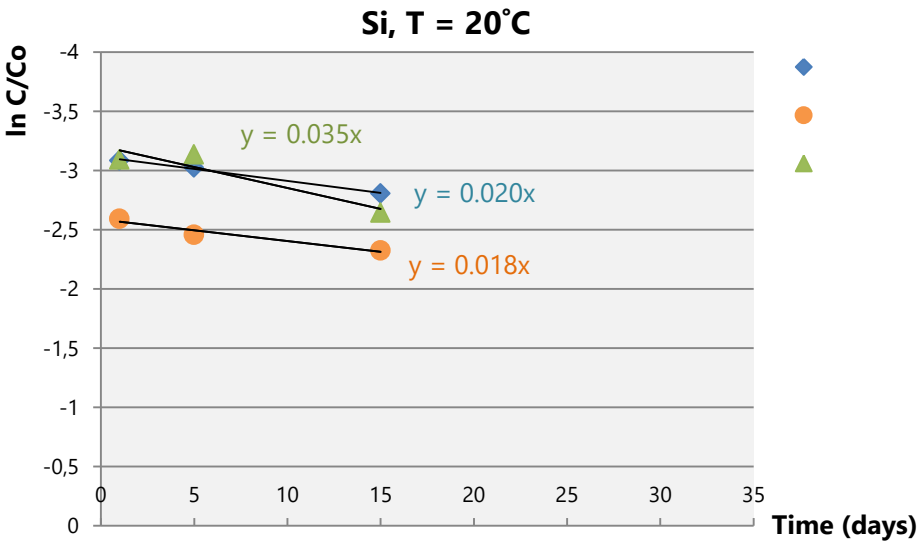
Si, T = 20˚C
ln C/Co
-4
-3,5
-3
-2,5
-2
-1,5
-1
-0,5
0
0
5
10
15
20
25
30
35
Time (days)
y = 0.035x
y = 0.020x
y = 0.018x

(c)

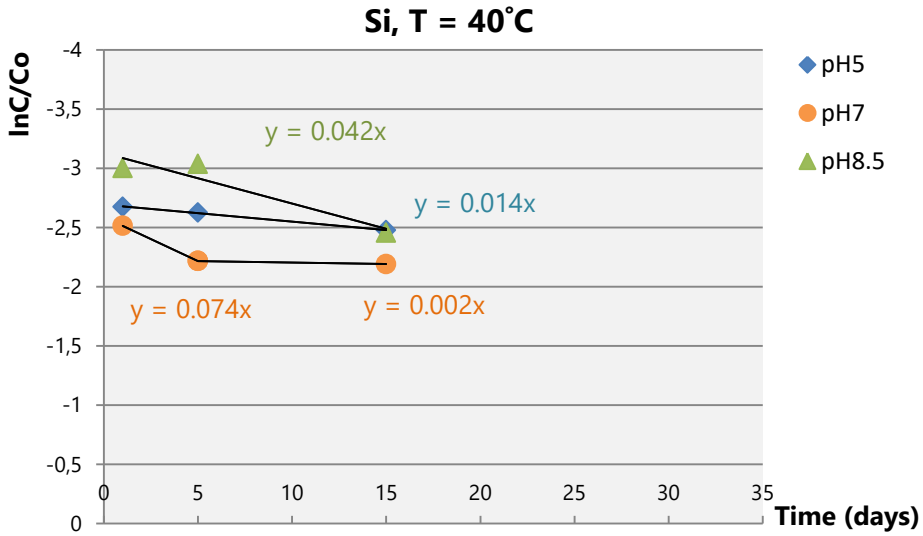

Fig. 185 The ln C/C_o versus time (days) curves for leaching of Si at pH 5, 7, 8.5 and temperature: **(a)** 5, **(b)** 20; and **(c)** 40 °C for the sample *Triticum durum* from Crete

(a)

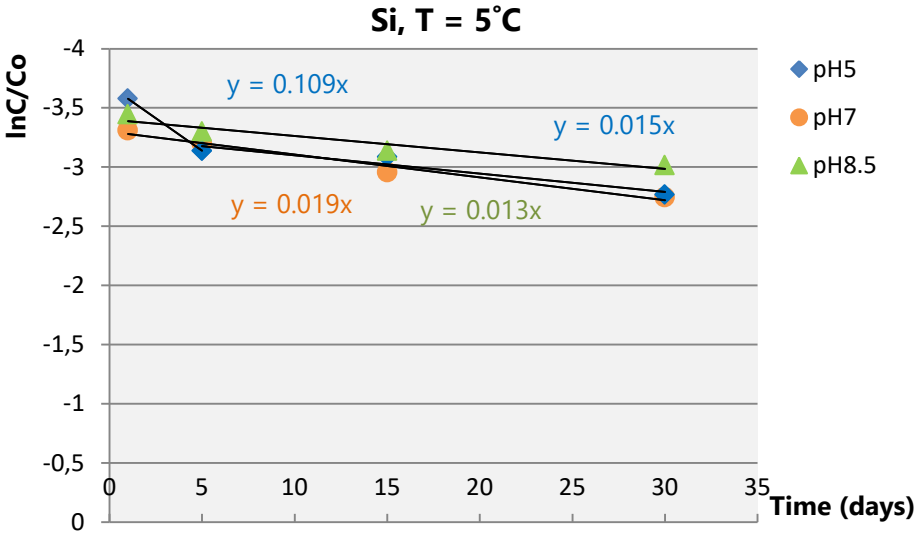
Si, T = 5˚C
lnC/Co
-4
-3,5
-3
-2,5
-2
-1,5
-1
-0,5
0
0
5
10
15
20
25
30
35
Time (days)
y = 0.109x
y = 0.015x
y = 0.019x
y = 0.013x
pH5
pH7
pH8.5

(b)

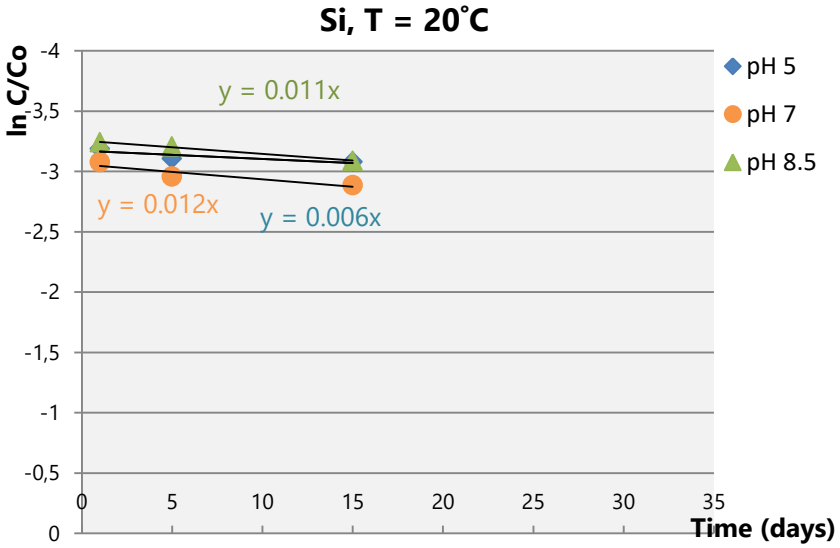
Si, T = 20˚C
ln C/Co
-4
-3,5
-3
-2,5
-2
-1,5
-1
-0,5
0
0
5
10
15
20
25
30
35
Time (days)
y = 0.011x
y = 0.012x
y = 0.006x
pH 5
pH 7
pH 8.5

(c)

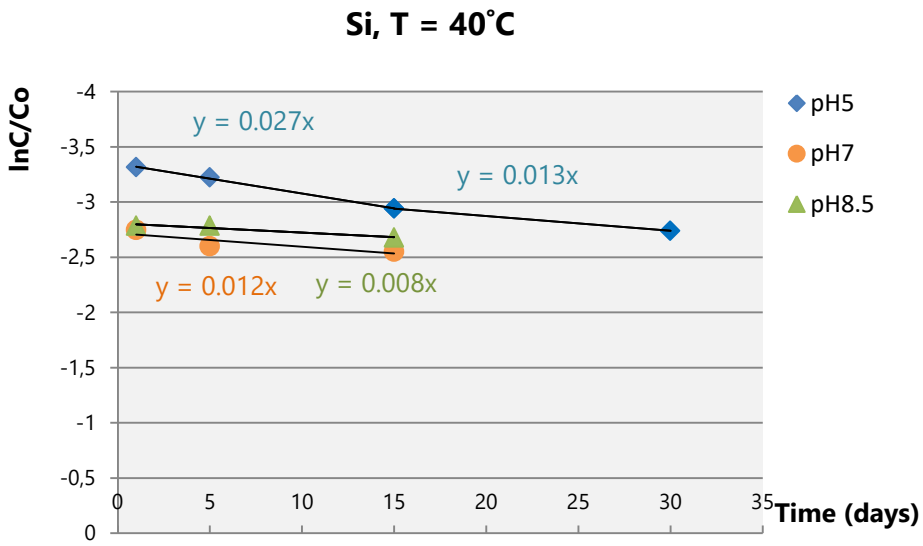

Fig. 186 The ln C/C_o versus time (days) curves for leaching of Si at pH 5, 7, 8.5 and temperature: **(a)** 5, **(b)** 20; and **(c)** 40 °C for the sample *Triticum monococcum* from Volos

(a)

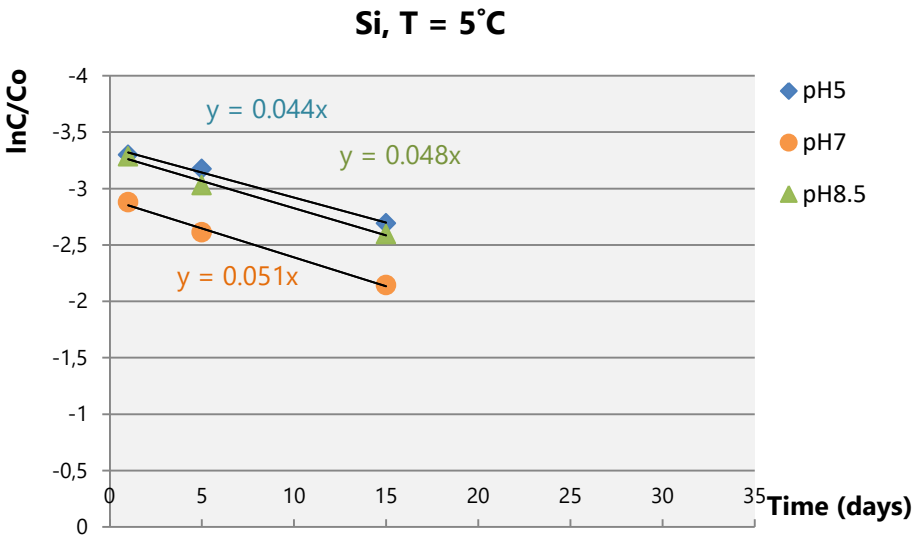
Si, T = 5˚C
lnC/Co
-4
-3,5
-3
-2,5
-2
-1,5
-1
-0,5
0
0
5
10
15
20
25
30
35
Time (days)
y = 0.044x
y = 0.048x
y = 0.051x
pH5
pH7
pH8.5

(b)

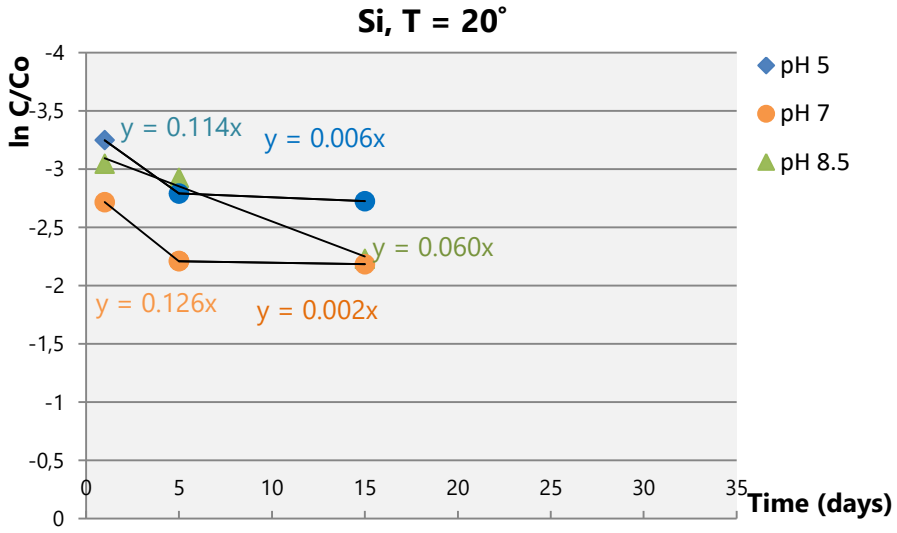
Si, T = 20˚
ln C/Co
-4
-3,5
-3
-2,5
-2
-1,5
-1
-0,5
0
0
5
10
15
20
25
30
35
Time (days)
y = 0.114x
y = 0.006x
y = 0.060x
y = 0.126x
y = 0.002x
pH 5
pH 7
pH 8.5

(c)

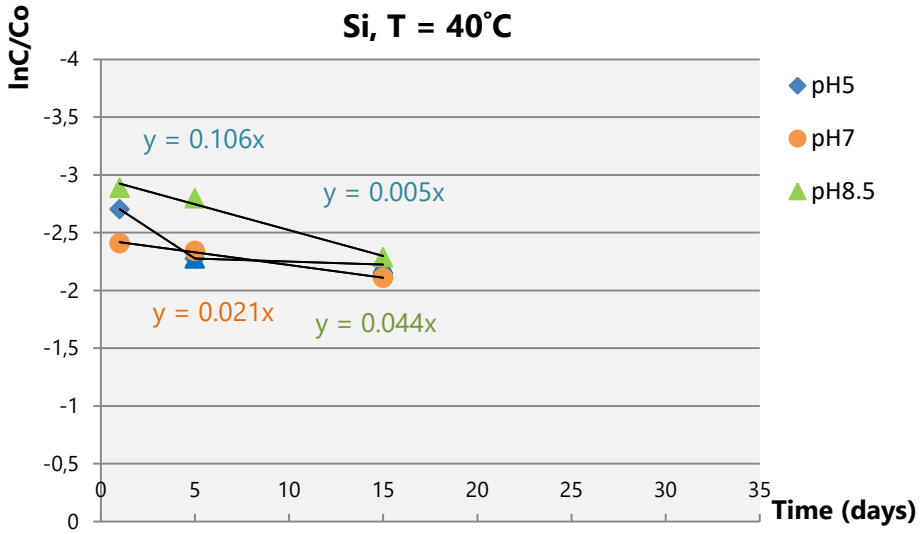

Fig. 187 The ln C/C_o versus time (days) curves for leaching of Si at pH 5, 7, 8.5 and temperature: **(a)** 5, **(b)** 20; and **(c)** 40 °C for the sample *Triticum monococcum* from Pella

(a)

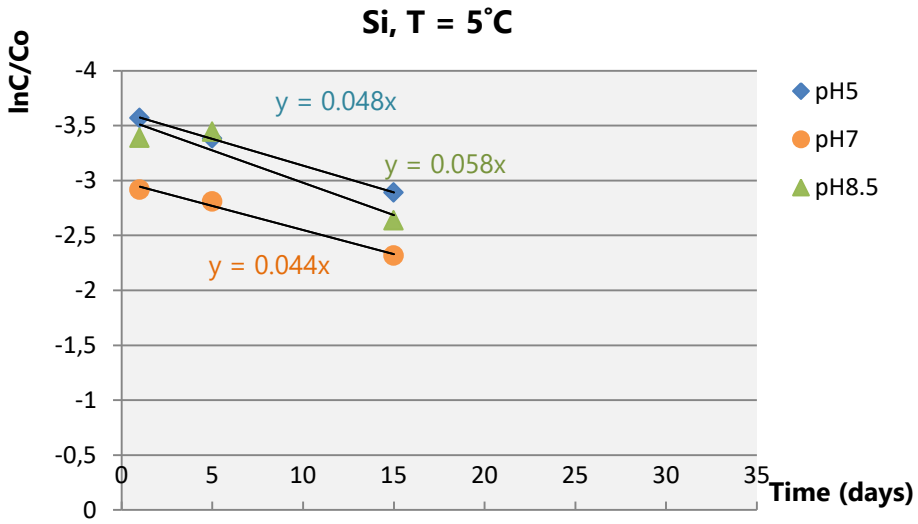
Si, T = 5˚C
lnC/Co
-4
-3,5
-3
-2,5
-2
-1,5
-1
-0,5
0
0
5
10
15
20
25
30
35
Time (days)
y = 0.048x
y = 0.058x
y = 0.044x
pH5
pH7
pH8.5

(b)

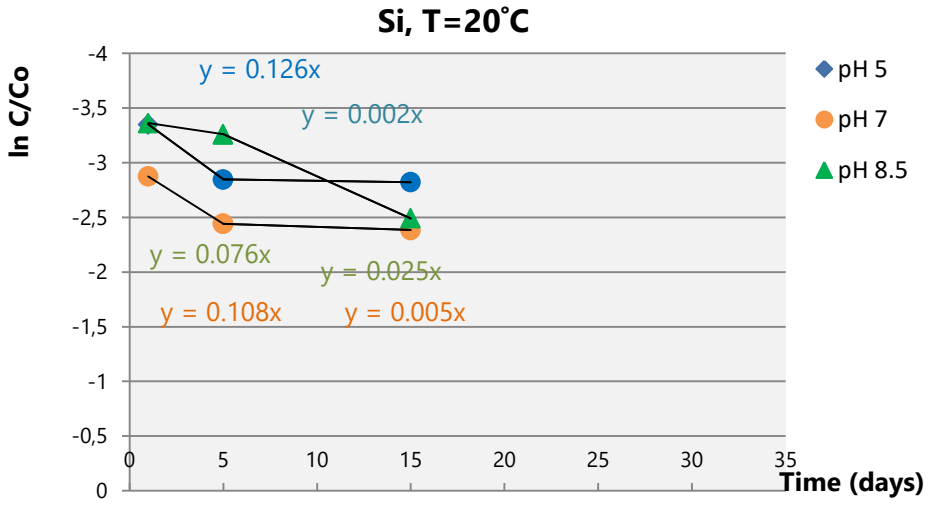
Si, T=20˚C
ln C/Co
-4
-3,5
-3
-2,5
-2
-1,5
-1
-0,5
0
0
5
10
15
20
25
30
35
Time (days)
y = 0.126x
y = 0.002x
y = 0.076x
y = 0.025x
y = 0.108x
y = 0.005x
pH 5
pH 7
pH 8.5

(c)

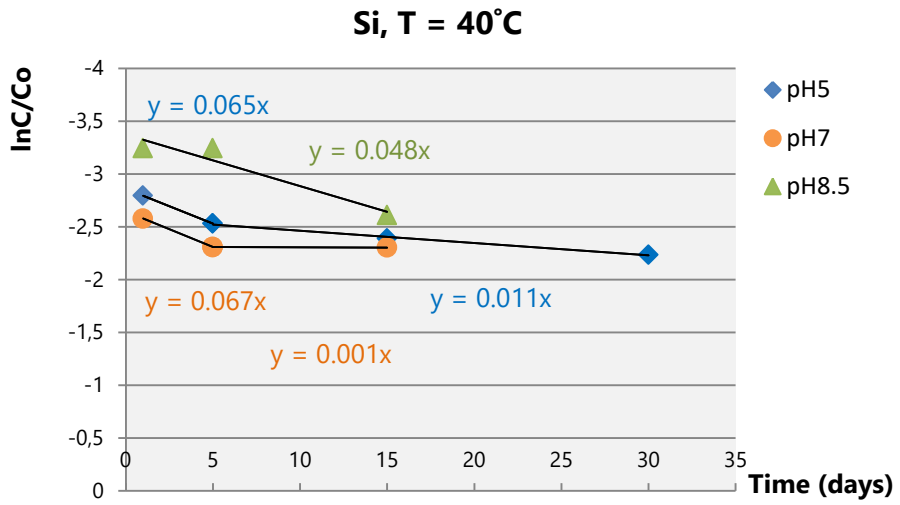

Fig. 188 The ln C/C_o versus time (days) curves for leaching of Si at pH 5, 7, 8.5 and temperature: **(a)** 5, **(b)** 20; and **(c)** 40 °C for the sample *Triticum durum* from Pella

(a)

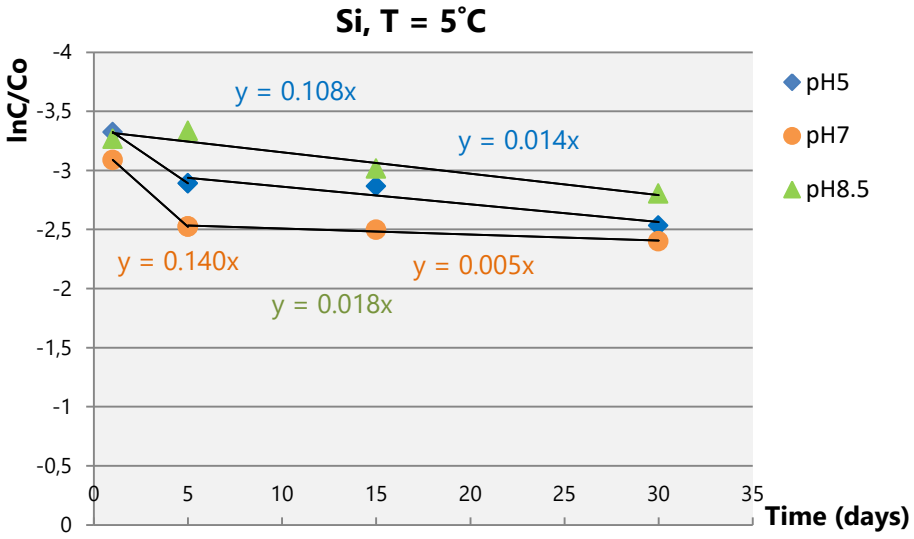
Si, T = 5˚C
lnC/Co
-4
-3,5
-3
-2,5
-2
-1,5
-1
-0,5
0
0
5
10
15
20
25
30
35
Time (days)
y = 0.108x
y = 0.014x
y = 0.140x
y = 0.005x
y = 0.018x
pH5
pH7
pH8.5

(b)

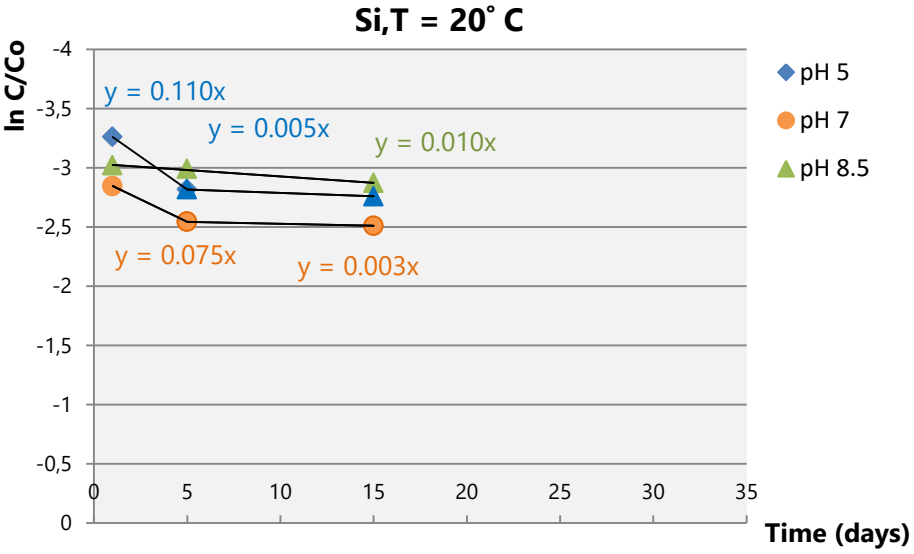
Si,T = 20˚ C
ln C/Co
-4
-3,5
-3
-2,5
-2
-1,5
-1
-0,5
0
0
5
10
15
20
25
30
35
Time (days)
y = 0.110x
y = 0.005x
y = 0.010x
y = 0.075x
y = 0.003x
pH 5
pH 7
pH 8.5

(c)

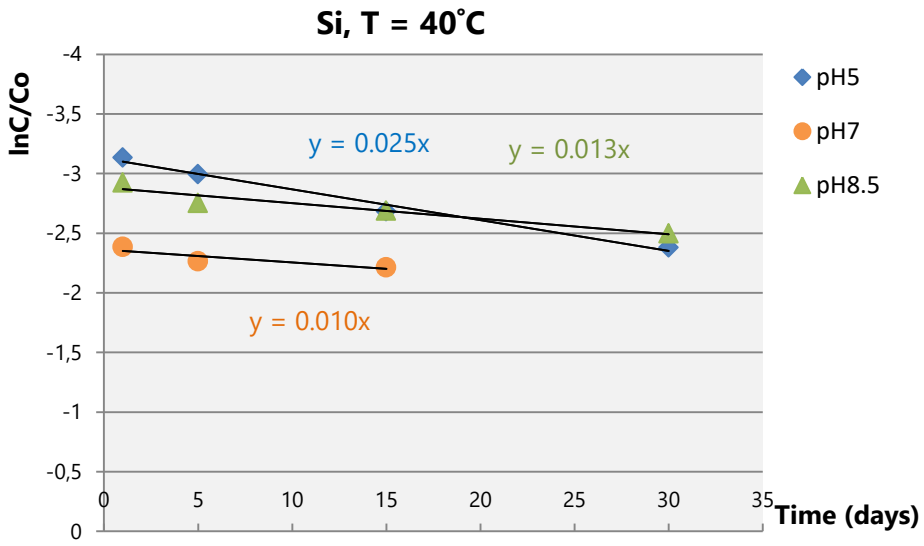

Fig. 189 The ln C/C_o versus time (days) curves for leaching of Si at pH 5, 7, 8.5 and temperature: **(a)** 5, **(b)** 20; and **(c)** 40 °C for the sample *Triticum durum* from Corfu

Appendix – part 6

3D diagrams

(pH, temperature and Si concentrations over time)

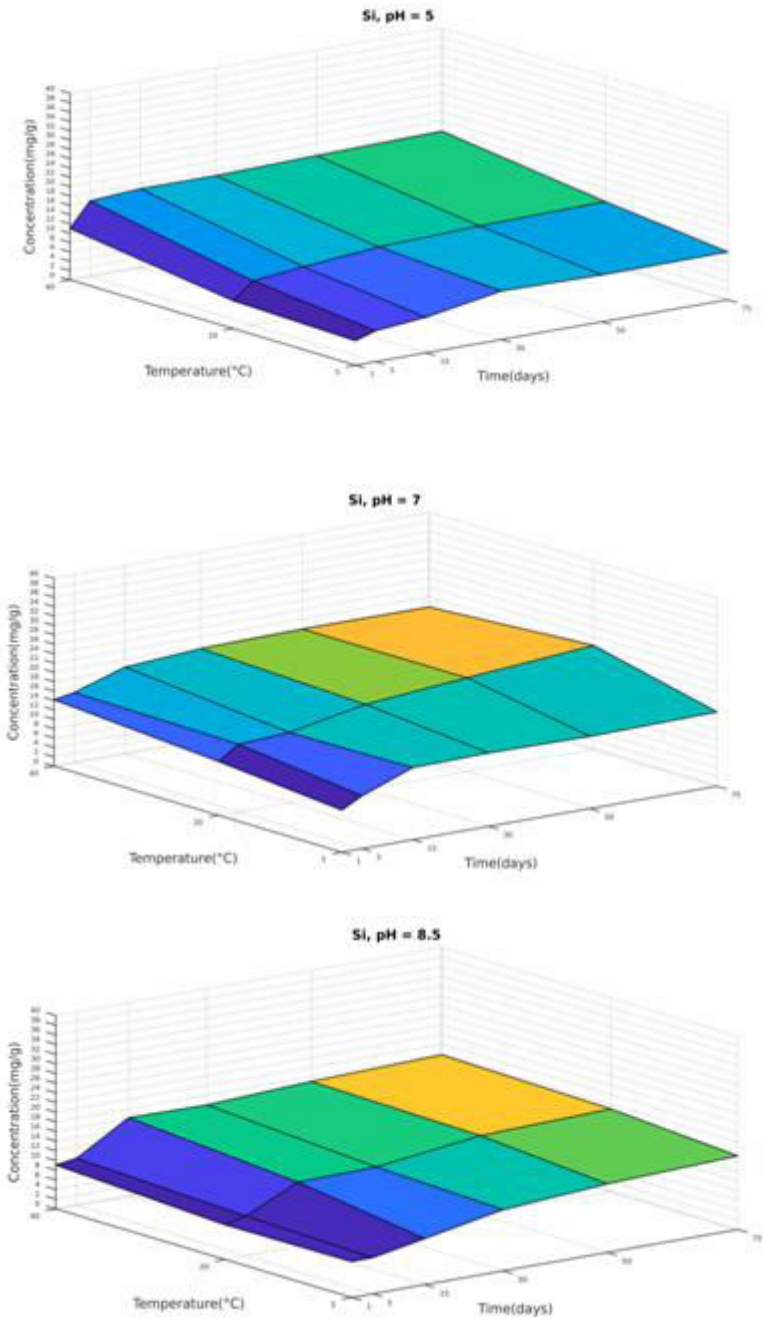

Fig. 190 Sample *Triticum durum,* Cyprus: silicon concentration (mg/g) at **pH 5, 7, 8.5** and temperature 5, 20, 40˚C

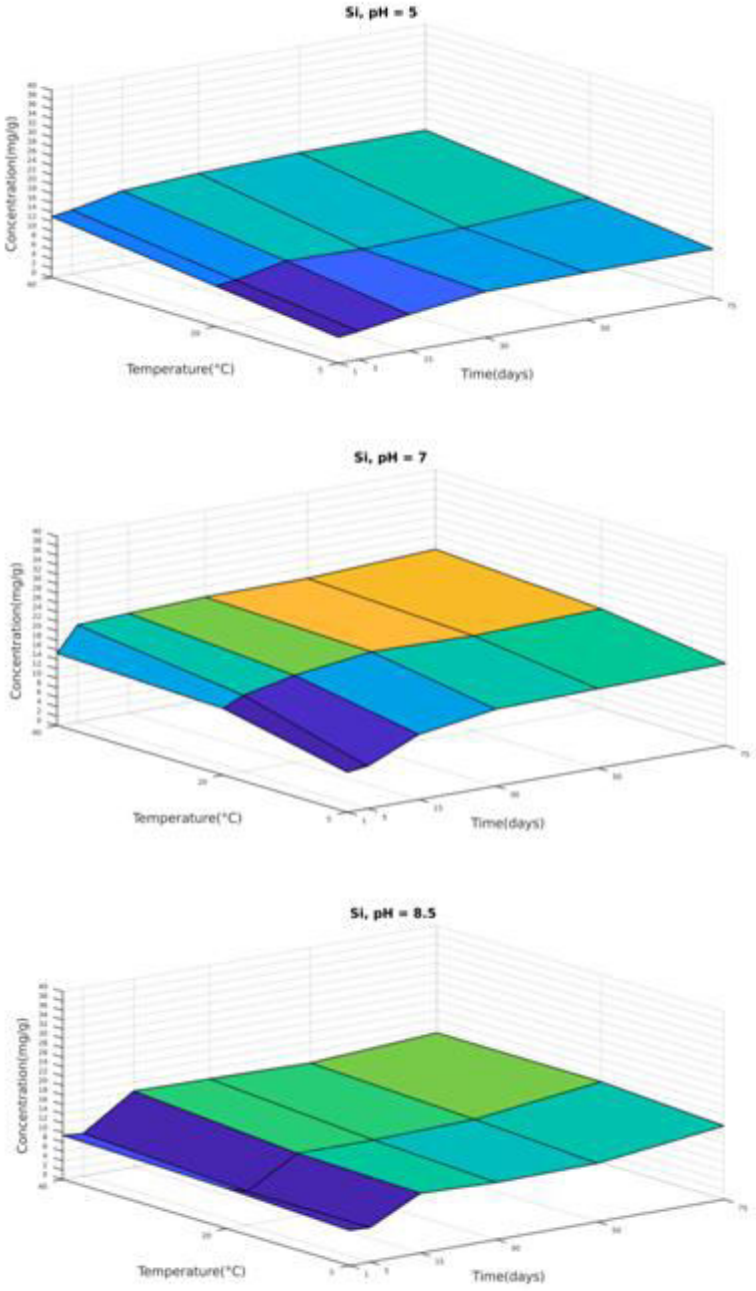

Fig. 191 Sample *Triticum durum,* Crete: silicon concentration (mg/g) at **pH 5, 7, 8.5** and temperature 5, 20, 40˚C

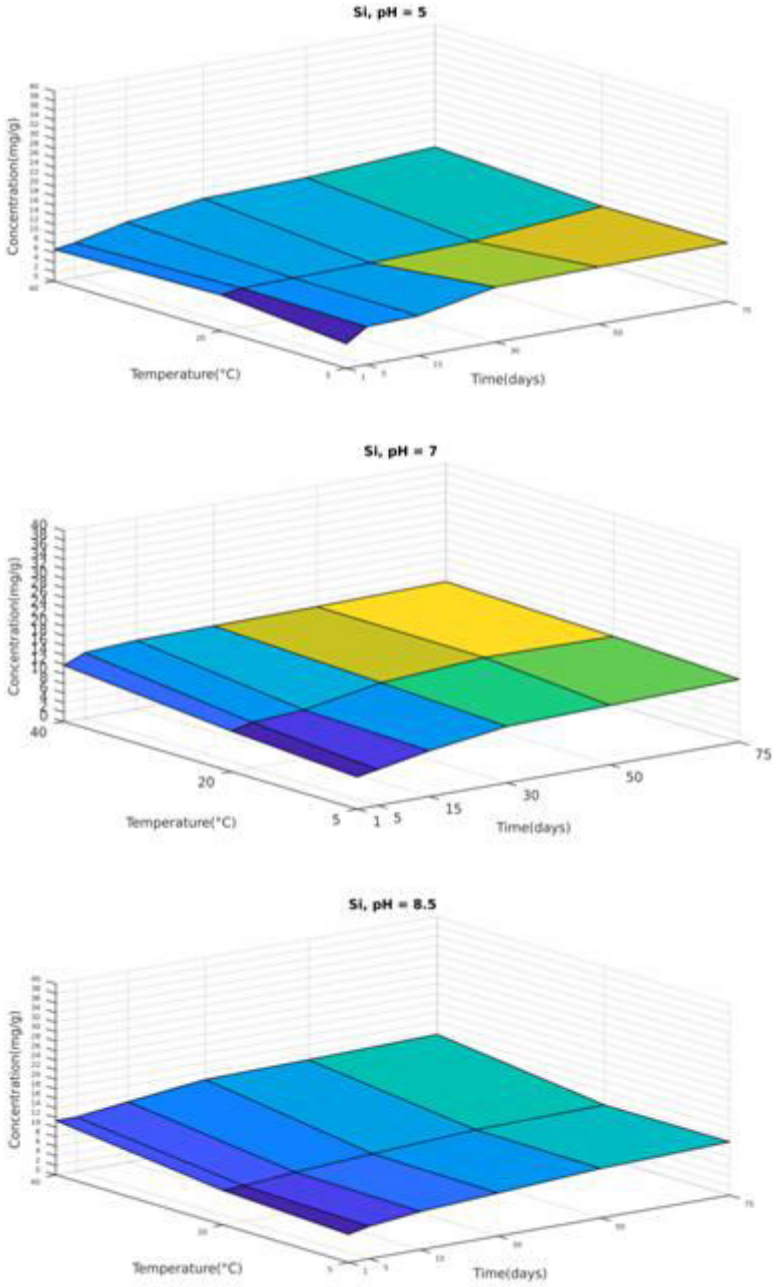

Fig. 192 Sample *Triticum monococcum,* Volos: silicon concentration (mg/g) at **pH 5, 7, 8.5** and temperature 5, 20, 40˚C

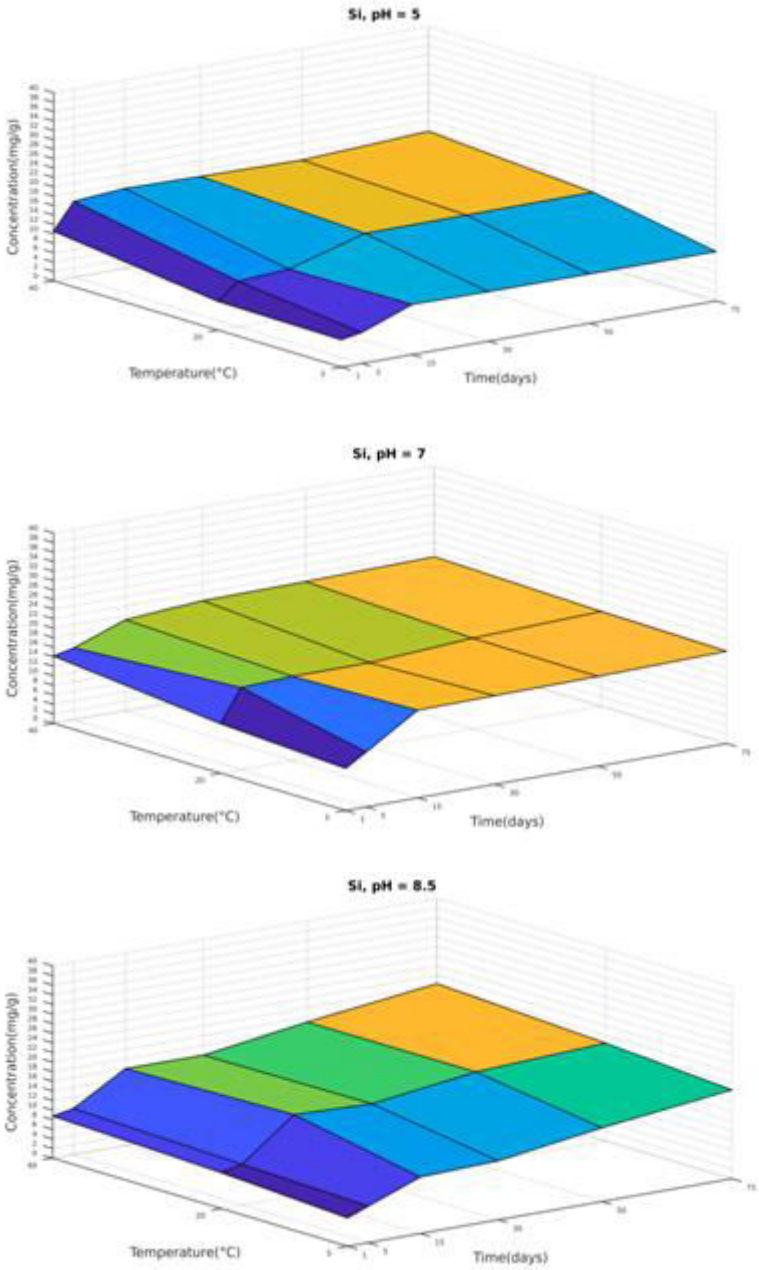

Fig. 193 Sample *Triticum monococcum,* Pella I: silicon concentration (mg/g) at **pH 5, 7, 8.5** and temperature 5, 20, 40˚C

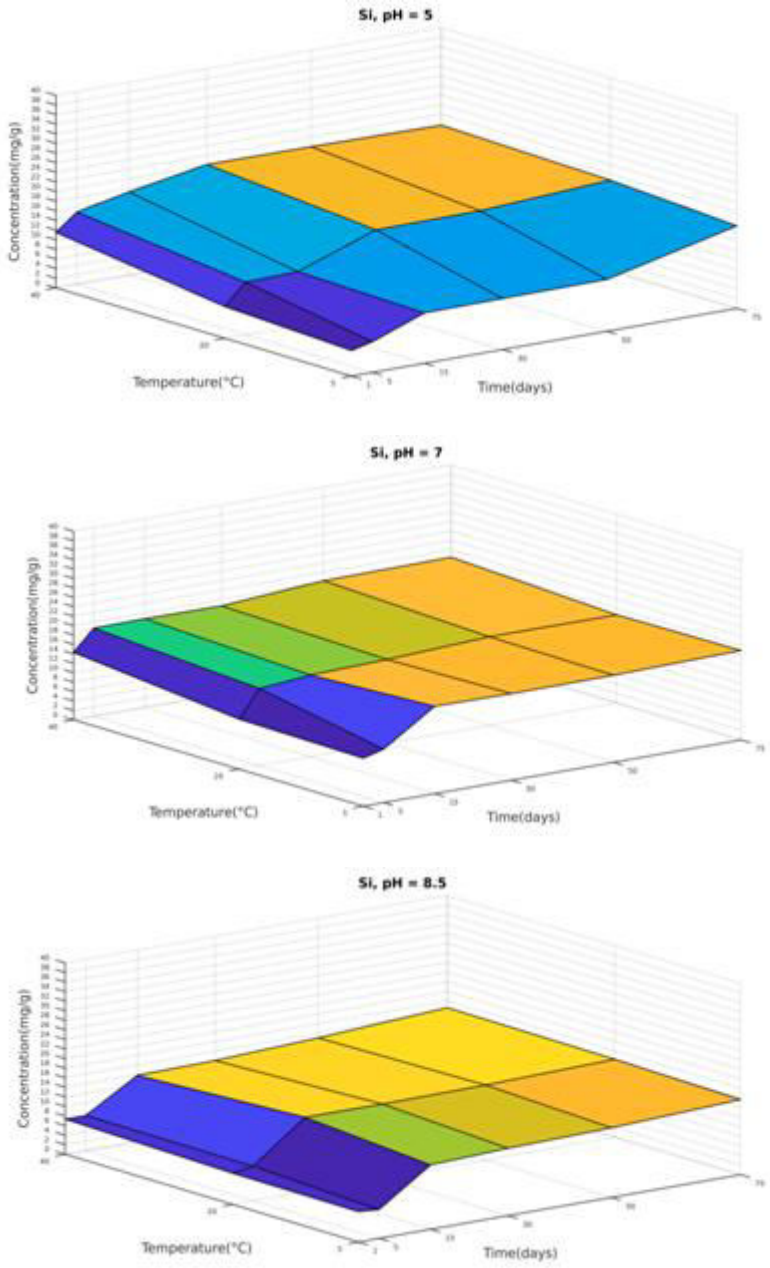

Fig. 194 Sample *Triticum durum,* Pella II: silicon concentration (mg/g) at **pH 5, 7, 8.5** and temperature 5, 20, 40˚C

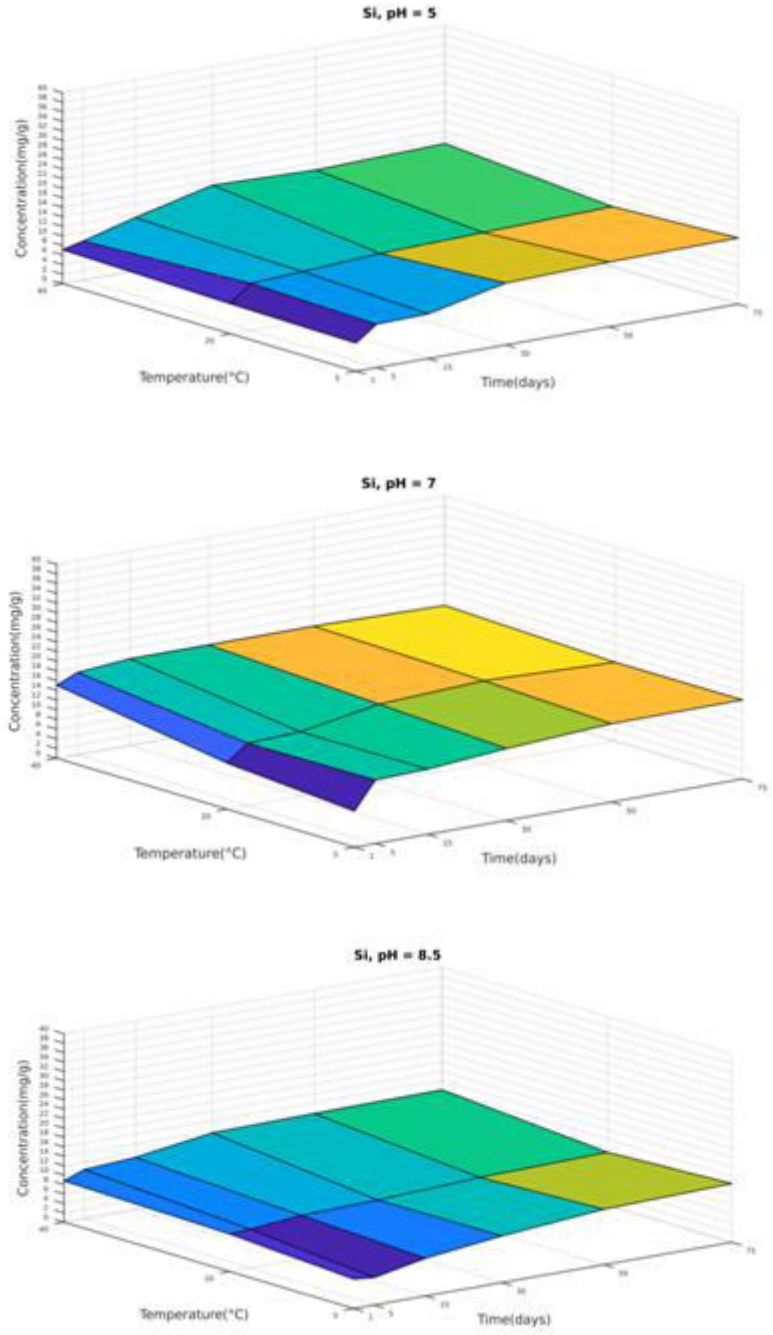

Fig. 195 Sample *Triticum durum,* Corfu: silicon concentration (mg/g) at **pH 5, 7, 8.5** and temperature 5, 20, 40˚C

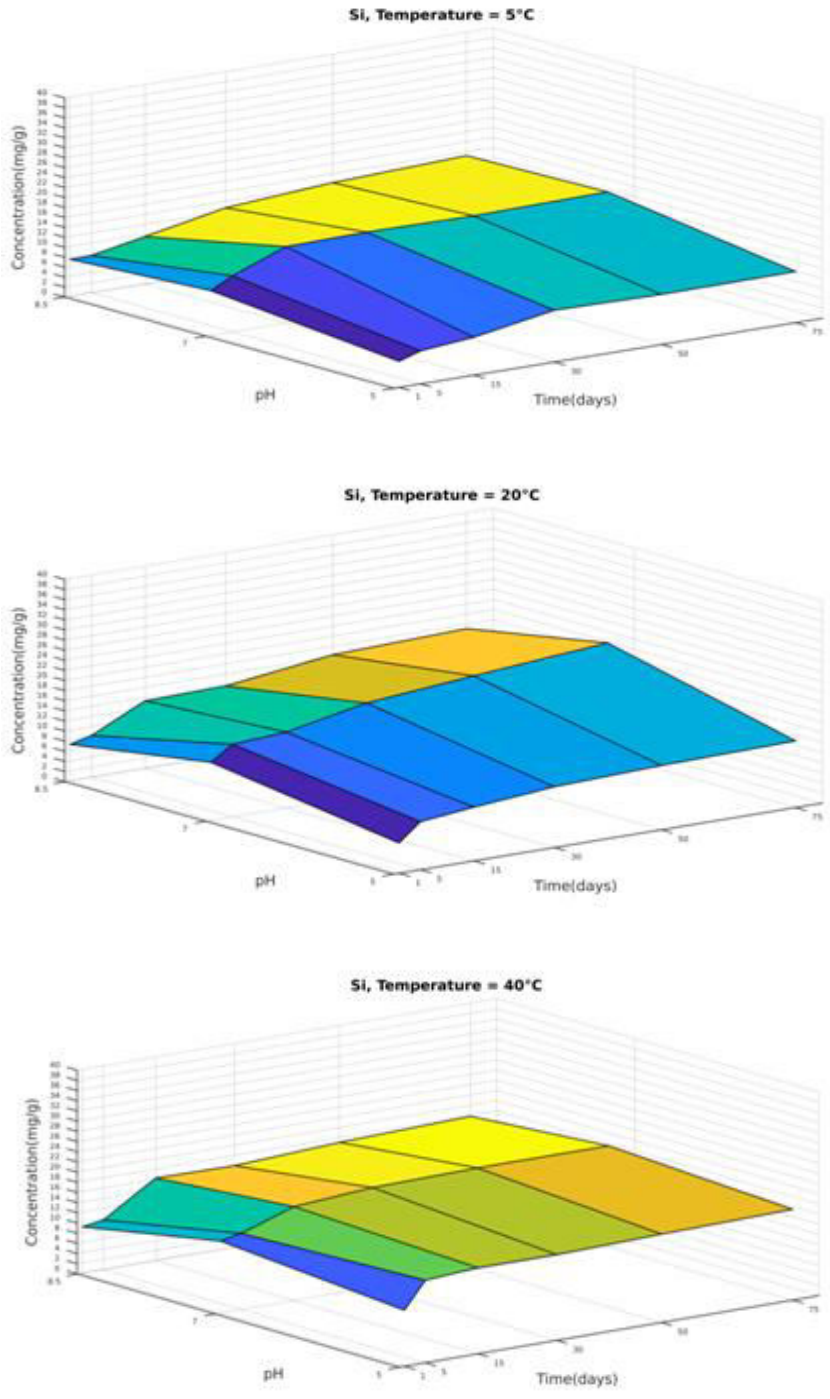

Fig. 196 Sample *Triticum durum,* Cyprus: silicon concentration (mg/g) at pH 5, 7, 8.5 and **temperature 5, 20, 40˚C**

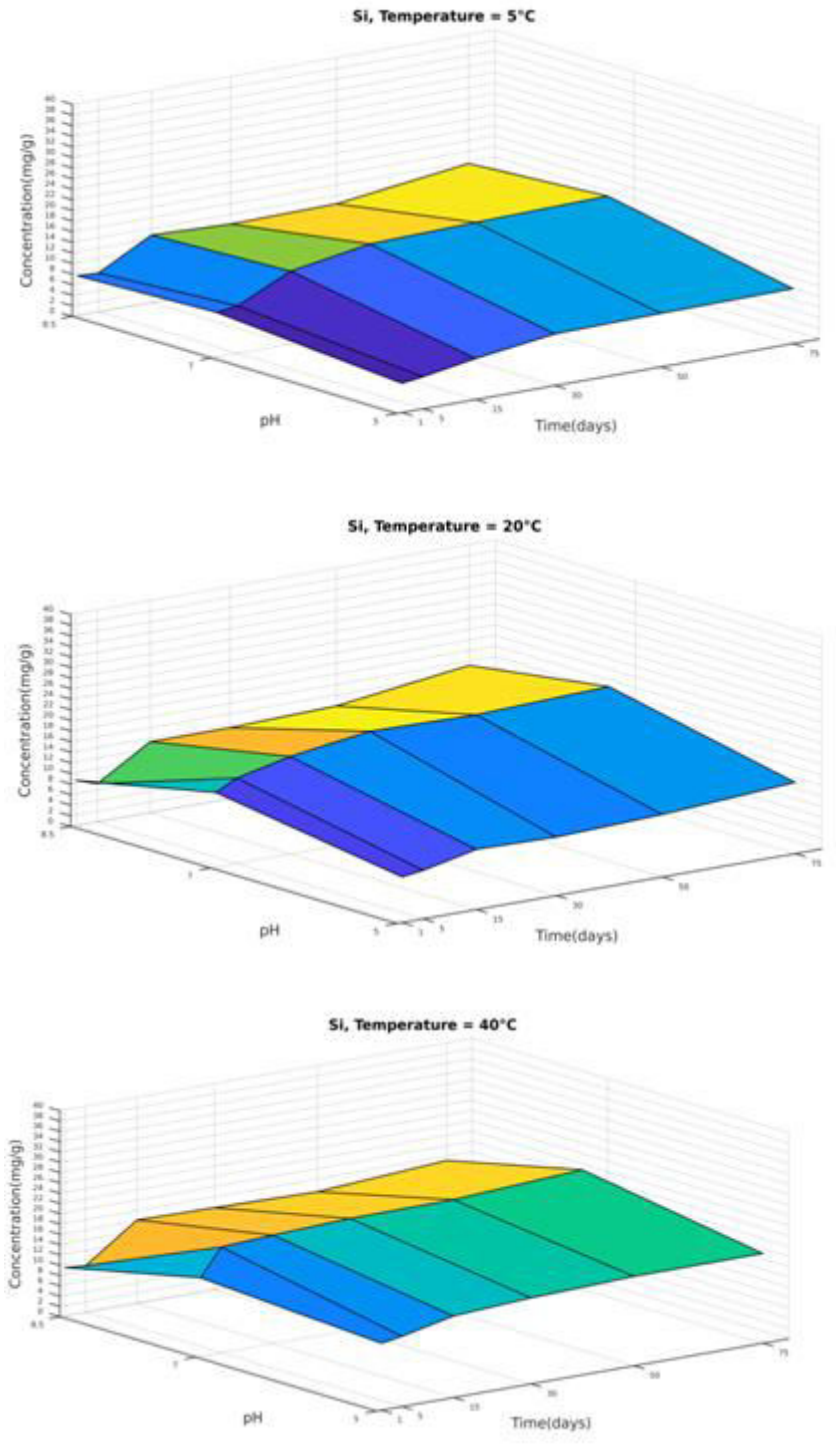

Fig. 197 Sample *Triticum durum*, Crete: silicon concentration (mg/g) at pH 5, 7, 8.5 and **temperature 5, 20, 40˚C**

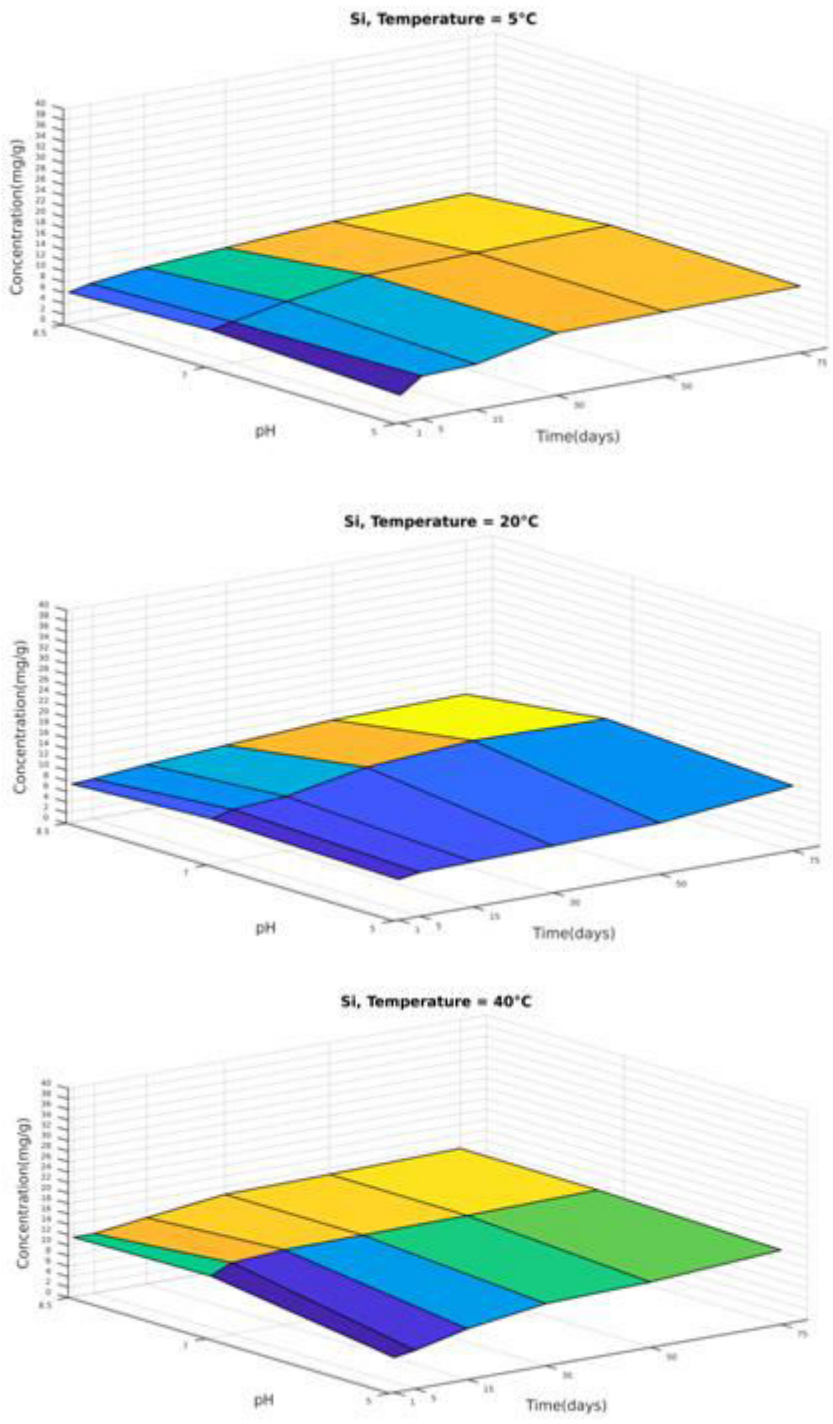

Fig. 198 Sample *Triticum monococcum,* Volos: silicon concentration (mg/g) at pH 5, 7, 8.5 and **temperature 5, 20, 40˚C**

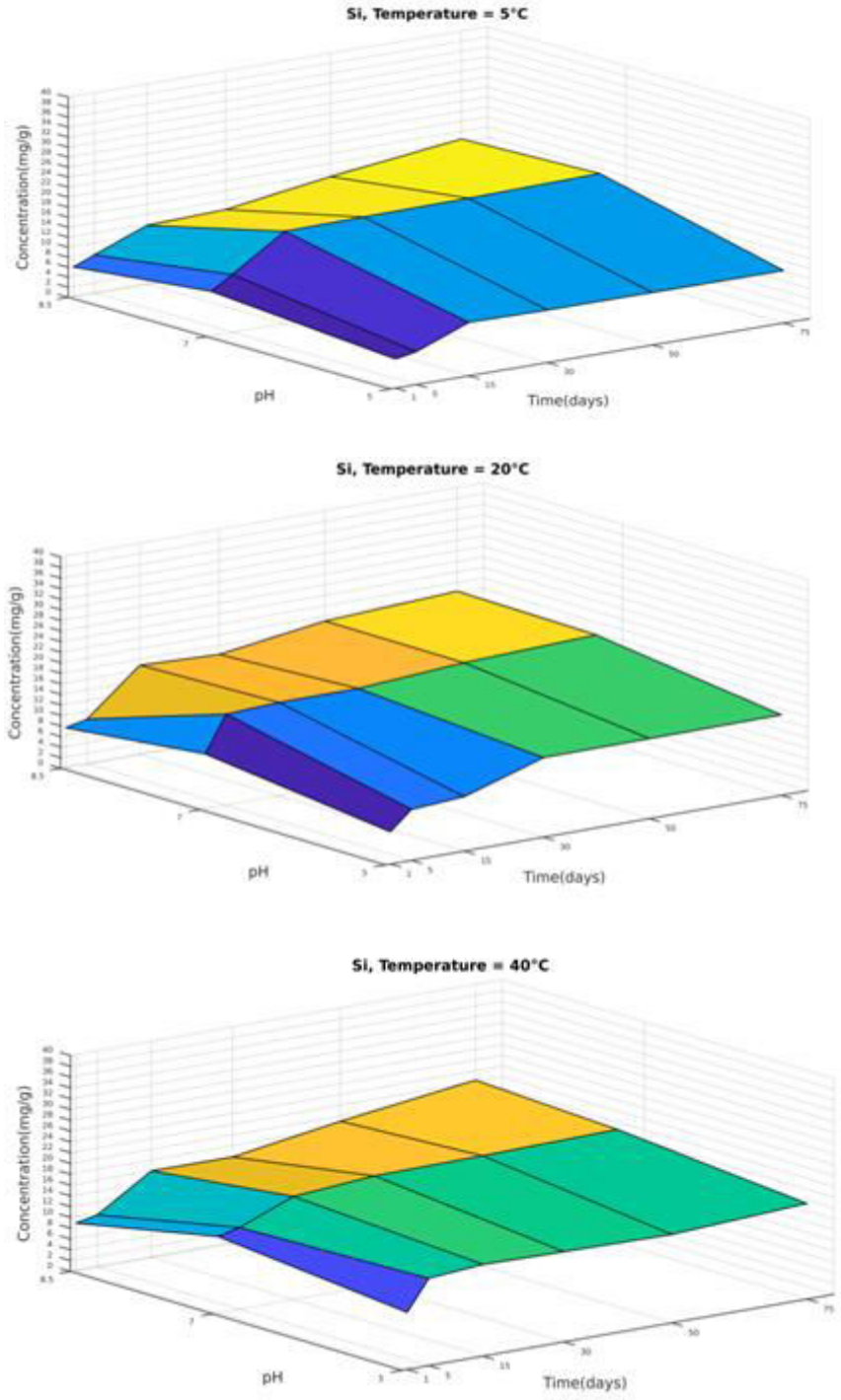

Fig. 199 Sample *Triticum monococcum,* Pella I: silicon concentration (mg/g) at pH 5, 7, 8.5 and **temperature 5, 20, 40˚C**

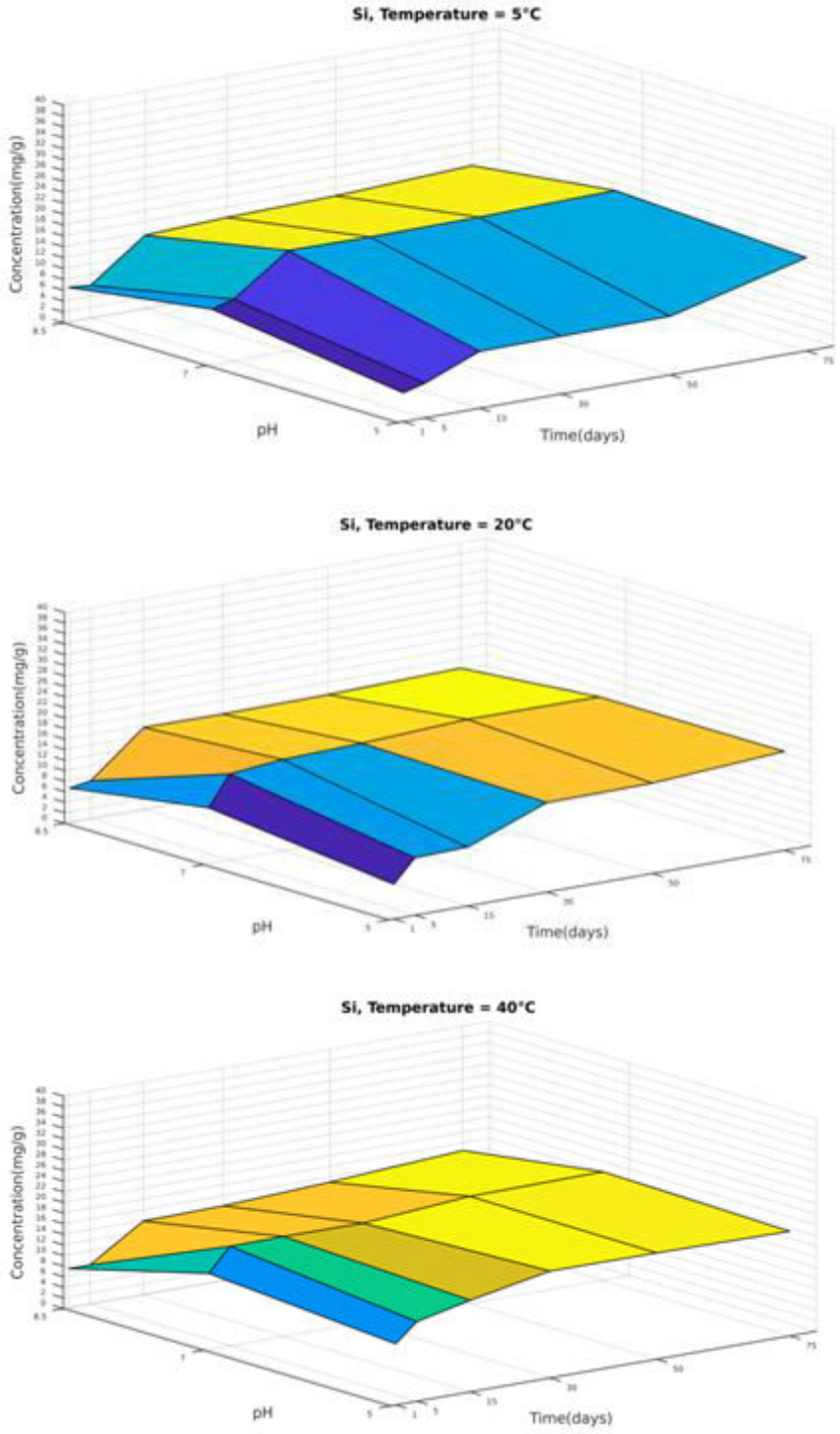

Fig. 200 Sample *Triticum durum,* Pella II: silicon concentration (mg/g) at pH 5, 7, 8.5 and **temperature 5, 20, 40˚C**

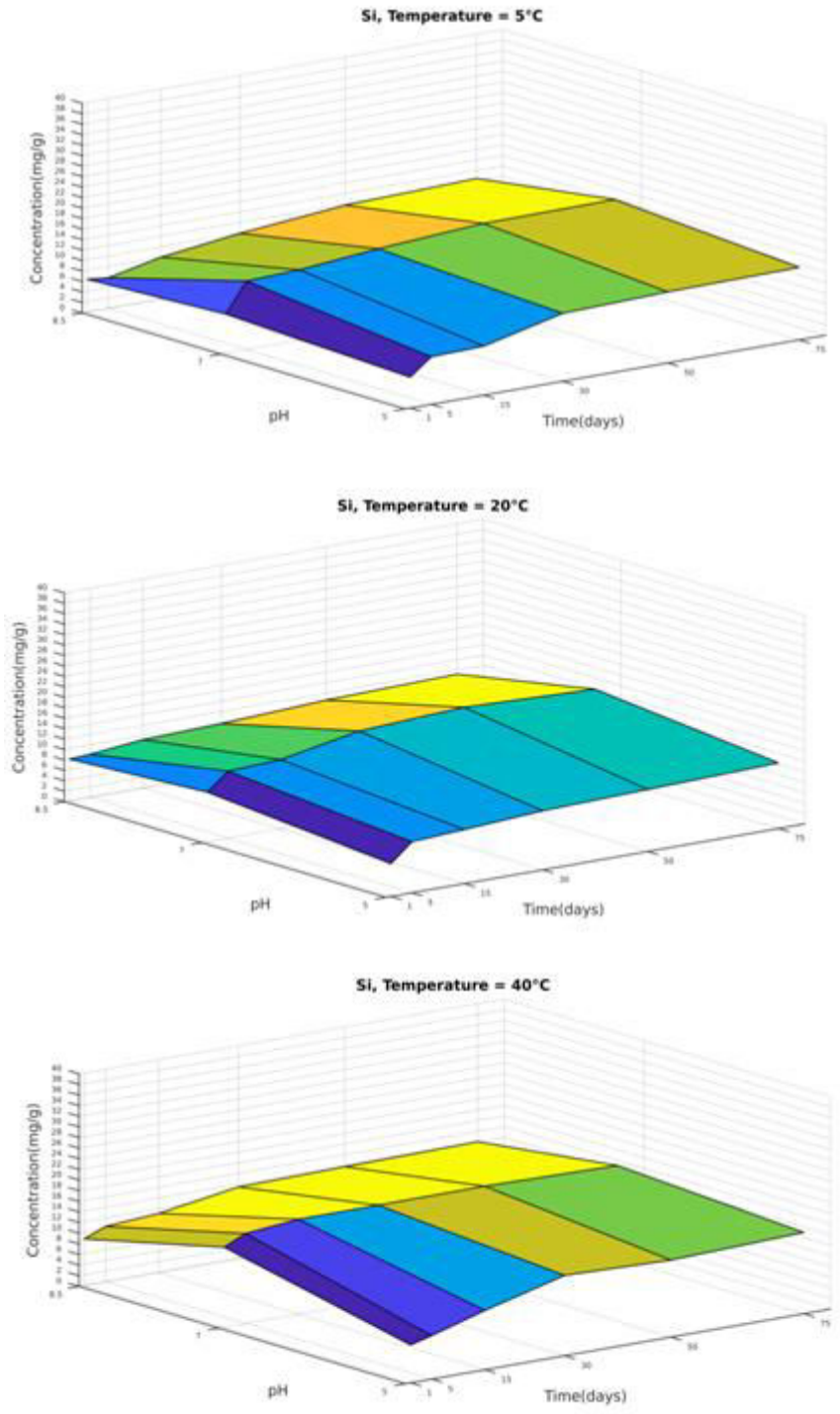

Fig. 201 Sample *Triticum durum,* Corfu: silicon concentration (mg/g) at pH 5, 7, 8.5 and **temperature 5, 20, 40˚C**

LIST OF FIGURES

Fig. 8 Wheat phytoliths: muticellular structures **(a)** before dissolution; **(b)** after dissolution. The chemical/mechanical alterations of the phytoliths after the dissolution experiments are evident (photomicrographs: Andriopoulou)

Fig. 9 The relative difference between average percentages of phytolith morphotypes (all samples), before and after the dissolution experiments (pH=7, T=20˚C)

Fig. 10 The relative difference between average percentages of phytolith morphotypes (all samples), before and after the dissolution experiments (pH=7, T=40˚C)

Fig. 11 The relative difference between average percentages of phytolith morphotypes (all samples), before and after the dissolution experiments (pH=8.5, T=20˚C)

Fig. 12 The relative difference between average percentages of phytolith morphotypes (all samples), before and after the dissolution experiments (pH=8.5, T=40˚C)

Fig. 13 Photomicrographs: **(a)** transparent wheat phytolith extracted from archaeological sediment; and **(b)** opaque phytolith extracted from ''modern'' soil. Opaqueness results from organic matter occluded within the phytolith. Organic matter degrades very fast in terms of the archaeological timescale (photomicrographs: Andriopoulou)

Fig. 14 Concentrations of phytoliths in the studied soils

Fig. 15 Hulled wheat (wheat with persistently enclosing hulls like *Triticum monoccocum*) processing stages: **(1)** threshing, **(2)** raking, **(3)** first winnowing - light weed seeds and some awns are removed, **(4)** coarse sieving - weed seed heads, unbroken ears, straw fragments are removed and unbroken ears are rethreshed, **(5)** first fine sieving - small weed seeds and awns are removed, **(6)** pounding, **(7)** second winnowing - paleas, lemmas and some awns are removed, **(8)** sieving with medium-coarse sieve - spikelet forks and unbroken spikelets - repounded, **(9)** second fine sieving - glume bases, awns, remaining small weed seeds, tail grain and awns removed; and **(10)** hand sorting - removal of grain-sized weeds by hand (source: Stevens 2003, in Zapata *et al.* 2004)

Fig. 16 Main processes affecting organic residues in archaeological ceramics [source: adapted from Historic England (2017) after Stacey (2009), in Roffet-Salque *et al.* (2017)]

Fig. 17 Photomicrographs: **(a)** unidentified morphotype with surface alterations, probably due to melting. The phytolith is extracted from *TB2008* sample; and **(b)** transparent decorated phytolith in the centre of the photomicrograph. The phytolith is extracted from *TB2013* sample and probably comes from wheat (*Triticum* spp.) or barley (*Hordeum* spp.)inflorescence (photomicrographs: Andriopoulou)

Fig. 18 XRD traces for *Triticum durum* and *Triticum monococcum* stem-leaves from Pella using dry and wet method: **(a)** *Triticum monococcum* stem-leaves (wet method), **(b)** *Triticum durum* stem-leaves (wet method), **(c)** *Triticum monococcum* stem-leaves (dry method); and **(d)** *Triticum durum* stem-leaves (dry method). The hump in the range 10-30 °2θ is related with the presence of amorphous matter (i.e. phytoliths). The following mineral phases are present in these samples: Arcanite (Arc), Barbosalite (Brb), Bassanite (Bss), Baylissite (Bls), Calcite (Cal), Chlorocalcite (Chlc), Illite/Muscovite (Ill / Ms) Monohydrocalcite (Mnhc), Mundrabillaite (Md), Strontianite (Str), and probably Struvite (St)

Fig. 19 XRD traces for *Triticum durum* and *Triticum monococcum* inflorescence from Pella using dry and wet method: **(a)** *Triticum monococcum* inflorescence (wet method), **(b)** *Triticum durum* inflorescence (wet method), **(c)** *Triticum monococcum* inflorescence (dry method); and **(d)** *Triticum durum* inflorescence (dry method). The hump in the range 10-30 °2θ is related with the presence of amorphous matter (i.e. phytoliths). The following mineral phases are present in these samples: Anhydrite (Anh), Aphthitalite (Aph), Arcanite (Arc), Barbosalite (Brb), Bassanite (Bss), Baylissite (Bls), Brucite (Brc), Calcite (Cal), Chlorocalcite (Chlc), Monohydrocalcite (Mnhc), Mundrabillaite (Md), Strontianite (Str), and probably Ammonium carbonate hydrate (Ammc) and Struvite (St)

Fig. 20 XRD traces for *Triticum monococcum* inflorescence from: **(a)** Pella I; and **(b)** Volos using dry method. The hump in the range 10-30 °2θ is related with the presence of amorphous matter (i.e. phytoliths). The following mineral phases are present in these samples: Arcanite (Arc), Aphthitalite (Aph), Barbosalite (Brb), Bassanite (Bss), Brucite (Brc), Chlorocalcite (Chlc), Celestite (Cls), Monohydrocalcite (Mnhc), Mundrabillaite (Md), Strontianite (Str), and probably Struvite (St)

Fig. 21 XRD traces for *Triticum durum* inflorescence from: **(a)** Corfu, **(b)** Pella II, **(c)** Crete; and **(d)** Cyprus using dry method. The hump in the range 10-30 °2θ is related with the presence of amorphous matter (i.e. phytoliths). The following mineral phases are present in these samples: Anhydrite (Anh), Arcanite (Arc), Aphthitalite (Aph), Barbosalite (Brb), Bassanite (Bss), Baylissite (Bls), Brucite (Brc), Chlorocalcite (Chlc), Monetite (DCPA), Monohydrocalcite (Mnhc), Mundrabillaite (Md), Schertelite (Scher), Strontianite (Str), and probably Ammonium carbonate hydrate (Ammc) and Struvite (St)

Fig. 22 XRD traces for *Triticum monococcum* inflorescence from **(a)** Pella I; and **(b)** Volos using dry method. The hump in the range 10-30 °2θ is related with the presence of amorphous matter (i.e. phytoliths). The following mineral phases are present in these samples: Anhydrite (Anh), Arcanite (Arc), Aphthitalite (Aph), Barbosalite (Brb), Bassanite (Bss), Brucite (Br), Chlorocalcite (Chlc), Monohydrocalcite (Mnhc) and Mundrabillaite (Md)

Fig. 23 XRD traces for soils: **(a)** Cyprus: Albite (Ab), Ankerite (Ank), Calcite (Cal), Kaolinite (Kln), Illite/Muscovite (Ill / Ms), Serpentine (Srp), Smectite (Sme) and Quartz (Qtz), **(b)** Crete: Albite (Ab), Anatase (Ant), Calcite (Cal), Chlorite (Chl), K-feldspar (orthoclase) (Kfs), Illite/Muscovite (Ill / Ms), Paragonite (Pg), Serpentine (Srp), Smectite (Sme), Talc (Tlc), and Quartz (Qtz), **(c)** Volos: Albite (Ab),

Anatase (Ant), Calcite (Cal), Chlorite (Chl), Hornblende (Hbl), Kaolinite (Kln), K-feldspar (orthoclase) (Kfs), Illite/Muscovite (Ill / Ms), Serpentine (Srp), Talc (Tlc) and Quartz (Qtz), **(d)** Pella I: Albite (Ab), Anatase (Ant), Calcite (Cal), Dolomite (Dol), Hornblende (Hbl), K-feldspar (orthoclase) (Kfs), Illite/Muscovite, (Ill / Ms), Smectite (Sme), Talc (Tlc) and Quartz (Qtz), **(e)** Pella II: Albite (Ab), Anatase (Ant), Calcite (Cal), Dolomite (Dol), Hornblende (Hbl), K-feldspar (orthoclase) (Kfs), Illite/Muscovite (Ill / Ms), Smectite (Sme), Talc (Tlc) and Quartz (Qtz); and **(f)** Corfu: Albite (Ab), Anatase (Ant), Calcite (Cal), Kaolinite (Kln), K-feldspar (orthoclase) (Kfs), Illite/Muscovite (Ill / Ms), Smectite (Sme) and Quartz (Qtz)

Fig. 24 XRD traces for archaeological sediments: **(a)** *KN5*: Albite (Ab), Calcite (Cal), Illite/Muscovite (Ill / Ms), Quartz (Qtz), **(b)** *KN10:* Albite (Ab), Calcite (Cal), Illite/Muscovite (Ill / Ms), Quartz (Qtz), Smectite (Sme), **(c)** *ΚΑΣ25*: Albite (Ab), Anatase (Ant), Calcite (Cal), Chlorite (Chl), Dolomite (Dol), Gypsum (Gyp), Halite (Hl), Hematite (Hem), Hornblende (Hbl), Illite/Muscovite (Ill / Ms), Quartz (Qtz), Smectite (Sme), **(d)** *ΚΑΣ27:* Albite (Ab), Anatase (Ant), Calcite (Cal), Chlorite (Chl), Dolomite (Dol), Gypsum (Gyp), Halite (Hl), Hematite (Hem), Hornblende (Hbl), Quartz (Qtz), **(e)** *TB2008*: Albite (Ab), Anatase (Ant), Calcite (Cal), Chlorite (Chl), Hornblende (Hbl), K-feldspar (Kfs), Pyrite (Py), Quartz (Qtz), Talc (Tlc); and **(f)** *TB2013*: Albite (Ab), Anatase (Ant), Calcite (Cal), Chlorite (Chl), Illite/Muscovite (Ill / Ms), K-feldspar (Kfs), Quartz (Qtz)

Fig. 25 FTIR spectra for *Triticum durum* or *Triticum monococcum* stem-leaves using dry method: **(a)** *Triticum durum* Cyprus, **(b)** *Triticum durum* Crete, **(c)** *Triticum monococcum* Volos; and **(d)** *Triticum durum* Corfu. Main bands at: ~465 cm^{-1}, 798 cm^{-1} and 1092 cm^{-1} (SiO_2 species), ~900-1000 cm^{-1} (Si-OH bending), ~1000-1200 cm^{-1} (Si-O stretching overlap with the SO_4 and PO_4 stretching) ~1630 cm^{-1} and ~3415 cm^{-1} (adsorbed water), (~3200-3600 cm^{-1}) (adsorbed water and hydrous sulphates and phosphates), ~2,800-3600 cm^{-1} (hydroxyl molecules)

Fig. 26 FTIR spectra for *Triticum durum* or *Triticum monococcum* inflorescence using dry method: **(a)** *Triticum durum* Cyprus, **(b)** *Triticum durum* Crete, **(c)** *Triticum monococcum* Volos; and **(d)** *Triticum durum* Corfu. Main bands at: ~465 cm^{-1}, ~798 cm^{-1} and ~1092 cm^{-1} (SiO_2 species), ~900-1000 cm^{-1} (Si-OH bending), ~1000-1200 cm^{-1} (Si-O stretching overlap with the SO_4 and PO_4 stretching) ~1630 cm^{-1} and ~3415 cm^{-1} (adsorbed water), (~3200-3600 cm^{-1}) (adsorbed water and hydrous sulphates and phosphates), ~2,800-3600 cm^{-1} (hydroxyl molecules)

Fig. 27 FTIR spectra for *Triticum durum* and *Triticum monococcum* stem-leaves from Pella using dry and wet method: **(a)** *Triticum durum* stem-leaves (dry method), **(b)** *Triticum monococcum* stem-leaves (dry method), **(c)** *Triticum durum* stem-leaves (wet method); and **(d)** *Triticum monococcum* stem-leaves (wet method). Main bands at: ~465 cm^{-1}, ~798 cm^{-1} and ~1092 cm^{-1} (SiO_2 species), ~900-1000 cm^{-1} (Si-OH bending), ~1000-1200 cm^{-1} (Si-O stretching overlap with the SO_4 and PO_4 stretching) ~1630 cm^{-1} and ~3415 cm^{-1} (adsorbed water), (~3200-3600 cm^{-1}) (adsorbed water and hydrous sulphates and phosphates), ~2,800-3600 cm^{-1} (hydroxyl molecules), ~1430 cm^{-1} (carbonate asymmetric stretching band), ~713 cm^{-1} and ~874 cm^{-1} (plane bending vibrations of the CO_3^{2-} ion in carbonate minerals), ~1330-1700 cm^{-1} (organic matter)

Fig. 28 FTIR spectra for *Triticum durum* and *Triticum monococcum* inflorescence from Pella using dry and wet method: **(a)** *Triticum durum* inflorescence (dry method), **(b)** *Triticum monococcum* inflorescence (dry method), **(c)** *Triticum durum* inflorescence (wet method); and **(d)** *Triticum monococcum* inflorescence (wet method). Main bands at: ~465 cm^{-1}, ~798 cm^{-1} and ~1092 cm^{-1} (SiO_2 species), ~900-1000 cm^{-1} (Si-OH bending), ~1000-1200 cm^{-1} (Si-O stretching overlap with the SO_4 and PO_4 stretching) ~1630 cm^{-1} and ~3415 cm^{-1} (adsorbed water), (~3200-3600 cm^{-1}) (adsorbed water and hydrous sulphates and phosphates), ~2,800-3600 cm^{-1} (hydroxyl molecules), ~1430 cm^{-1} (carbonate asymmetric stretching band), ~713 cm^{-1} and ~874 cm^{-1} (plane bending vibrations of the CO_3^{2-} ion in carbonate minerals),~1330-1700 cm^{-1} (organic matter)

Fig. 29 SEM photomicrographs of the phytoliths: **(a, b)** phytolith assemblage with evident mechanical and chemical alterations after dissolution (75 days). Phytoliths were extracted from *Triticum durum* Corfu using the dry method (photomicrographs: Andriopoulou)

Fig. 30 SEM photomicrographs of the phytoliths: **(a)** phytolith assemblage from *Triticum durum* from Pella using the wet method. The parallelepipedal elongate cell presented in the center has rugulate and pitted surface; and **(b)** dentritic and echinate long cells in anatomical connection from *Triticum durum* inflorescence from Pella using the dry method. Heating depending the conditions may enhance the cohesion of phytoliths (photomicrographs: Andriopoulou)

Fig. 31 Photomicrographs of phytoliths from the optical microscope: **(a)** parallelepipedal elongate cell from *Triticum durum* using the wet ashing method. The phytolith presented in the centre is opaque and overshadowed with organic matter; and **(b)** dentritic and echinate long cells in anatomical connection from *Triticum durum* inflorescence using the dry ashing method. The phytoliths are more clear and transparent to light (photomicrographs: Andriopoulou)

Fig. 32 Characteristic EDS spectra of phytolith from: **(a)** *Triticum monococcum* leaf (cell wall) from Pella using dry method. Oxygen (O), silicon (Si), carbon (C), magnesium (Mg), phosphorus (P), sulphur (S), potassium (K), and calcium (Ca) are present, **(b)** *Triticum monococcum* leaf (cell wall) from Pella using wet method. Presence of oxygen (O), silicon (Si), carbon (C), magnesium (Mg), potassium (K), and calcium (Ca), **(c)** *Triticum monococcum* leaf (cell centre) from Pella using dry method. Presence of oxygen (O), silicon (Si), magnesium (Mg), aluminium (Al), phosphorus (P), potassium (K), calcium (Ca), and iron (Fe); and **(d)** *Triticum monococcum* leaf (cell centre) from Pella using wet method. Presence of oxygen (O), silicon (Si), magnesium (Mg), phosphorus (P), potassium (K), and calcium (Ca)

Fig. 33 SEM photomicrograph that presents a phytolith assemblage (*Triticum durum*, Crete, dry method) and its EDS spectrum. Among other chemical elements, strontium (Sr) was observed in phytoliths from either inflorescence or stem/leaves (photomicrograph: Andriopoulou)

Fig. 34 EDS spectrum of phytoliths from *Triticum durum* inflorescence from Cyprus using dry method and SEM photomicrograph that presents elongates epidermal appendages (hairs) in the cell wall. Copper (Cu) was detected in the narrow end (orange arrow) of the SiO_2-rich hairs (photomicrograph: Andriopoulou)

Fig. 35 The following groups of soils with similar chemical characteristics are observed: a. Crete, Pella I and Pella II, b. Volos and Corfu and c. Cyprus. **(a)** correlation of the concentration of Si in plant inflorescence (green dots: PLANT I) or in plant stem-leaves (yellow dots: PLANT S-L) and the concentration of Si in the soils, where the plants were grown (CY: Cyprus, CR: Crete, VO: Volos, P_1: Pella I, P_2: Pella II, CO: Corfu); and **(b)** correlation of the concentration of Si in entire plants (excluding roots) (brown dots) and the concentration of Si in the soils, where the plants were grown (CY: Cyprus, CR: Crete, VO: Volos, P_1: Pella I, P_2: Pella II, CO: Corfu)

Fig. 36 (a) Principal arrangement of SiO_2-rich phytolith structures (green colour), **(b)** SiO_2-rich phytolith structures fulfilled by occluded particles such as potassium (purple colour), **(c)** and **(d)** plant cell during desilification process (source: Nguyen 2015)

Fig. 37 The elemental concentration of phytoliths extracted from inflorescence (green columns), stem-leaves (yellow columns) and soil (brown line) from *Triticum durum* (D) Cyprus sample

Fig. 38 The elemental concentration of phytoliths extracted from inflorescence (green columns), stem-leaves (yellow columns) and soil (brown line) from *Triticum durum* (D) Crete sample

Fig. 39 The elemental concentration of phytoliths extracted from inflorescence (green columns), stem-leaves (yellow columns) and soil (brown line) from *Triticum monococcum* (M) Volos sample

Fig. 40 The elemental concentration of phytoliths extracted from inflorescence (green columns), stem-leaves (yellow columns) and soil (brown line) from *Triticum durum* (D) Corfu sample

Fig. 41 The elemental concentration of phytoliths extracted from inflorescence (green columns), stem-leaves (yellow columns) and soil (brown line) from *Triticum monococcum* (M) Pella sample

Fig. 42 The elemental concentration of phytoliths extracted from inflorescence (green columns), stem-leaves (yellow columns) and soil (brown line) from *Triticum durum* (D) Pella sample

Fig. 43 Wheat grains: **(a)** naked; and **(b)** hulled (source: Alonso 2019)

Fig. 44 DTG-TG curves for stem-leaves (dry method): **(a)** Cyprus, **(b)** Crete, **(c)** Volos, **(d)** Pella I, **(e)** Pella II, **(f)** Corfu

Fig. 45 DTG-TG curves for inflorescences (dry method): **(a)** Cyprus, **(b)** Crete, **(c)** Volos, **(d)** Pella I, **(e)** Pella II, **(f)** Corfu

Fig. 46 DTG-TG curves for stem-leaves and inflorescence from Pella using dry method: **(a)** *Triticum monococcum* inflorescence, **(b)** *Triticum durum* inflorescence, **(c)** *Triticum monococcum* stem-leaves; and **(d)** *Triticum durum* stem-leaves

Fig. 47 DTG-TG curves for stem-leaves and inflorescence from Pella using wet method: **(a)** *Triticum monococcum* inflorescence, **(b)** *Triticum durum* inflorescence, **(c)** *Triticum monococcum* stem-leaves; and **(d)** *Triticum durum* stem-leaves

Fig. 48 Concentration (mg/g) of Mg, Si, K, Ca over the course of 75 days at pH 5 and temperature 5˚C, 20˚C, 40 ˚C (*Triticum durum,* Cyprus)

Fig. 49 Silicon concentration (mg/g) at **pH 5, 7, 8.5** and temperature 5, 20, 40˚C (*Triticum durum,* Cyprus)

Fig. 50 Silicon concentration (mg/g) at pH 5, 7, 8.5 and **temperature 5, 20, 40˚C** (*Triticum durum,* Cyprus)

Fig. 51 Generalised concept of the dissolution: **(a)** the dissolution process according to the reaction-diffusion theory, where Cs is the solute concentration on the surface; Ci is the solute concentration on the interface; and Cb is the solute concentration in bulk; and **(b)** surface of a crystal according to surface layer dissolution model. Types of crystal imperfections/dislocations (e.g. steps, kinks, terraces, ledges, vacancies) are shown (sources: Dorozhkin 2012; Ehrlich *et al.* 2009)

Fig. 52 Concentration (mg/g) of Si (above) and Ca (below) over the course of 75 days at pH 5 and temperature 5 ˚C, 20˚C, 40 ˚C (*Triticum durum*, Cyprus)

Fig. 53 (a) Silicon reaction rates *k1* (d^{-1}) of dissolved phytoliths from *Triticum monococcum* and *Triticum durum* (under pH 5, pH 7, pH 8.5, and temperature=20˚C) and precipitation of area of study (Crete, Volos, Pella)

Fig. 53 (b) Silicon reaction rates *k1* (d^{-1}) of dissolved phytoliths from *Triticum monococcum* and *Triticum durum* (under pH 5, pH 7, pH 8.5, and temperature=20˚C) and temperature of area of study (Crete, Volos, Pella)

Fig. 54 The ln C/C_o versus time (days) curves for leaching of Si at pH 5, 7, 8.5 values and temperature 20 °C for the samples: **(a)** *Triticum durum* from Crete (P = 410 mm, T = 19.91 ˚C); and **(b)** *Triticum durum* from Pella II (P = 763.7 mm, T = 14.22 ˚C)

Fig. 67 The relative difference between the presence of phytolith morphotypes (Cyprus, *Triticum durum*) before and after the dissolution experiments (pH=8.5, T=40˚C)

Fig. 68 The absolute value for the presence of phytolith morphotypes (Cyprus, *Triticum durum*). Blue line represents data before dissolution and orange line after dissolution (pH=7 and T=20˚C)

Fig. 69 The absolute value for the presence of phytolith morphotypes (Cyprus, *Triticum durum*). Blue line represents data before dissolution and orange line after dissolution (pH=7 and T=40˚C)

Fig. 70 The absolute value for the presence of phytolith morphotypes (Cyprus, *Triticum durum*). Blue line represents data before dissolution and orange line after dissolution (pH=8.5 and T=20˚C)

Fig. 71 The absolute value for the presence of phytolith morphotypes (Cyprus, *Triticum durum*). Blue line represents data before dissolution and orange line after dissolution (pH=8.5 and T=40˚C)

Fig. 72 The relative difference between the presence of phytolith morphotypes (Crete, *Triticum durum*) before and after the dissolution experiments (pH=7, T=20˚C)

Fig. 73 The relative difference between the presence of phytolith morphotypes (Crete, *Triticum durum*) before and after the dissolution experiments (pH=7, T=40˚C)

Fig. 74 The relative difference between the presence of phytolith morphotypes (Crete, *Triticum durum*) before and after the dissolution experiments (pH=8.5, T=20˚C)

Fig. 75 The relative difference between the presence of phytolith morphotypes (Crete, *Triticum durum*) before and after the dissolution experiments (pH=8.5, T=40˚C)

Fig. 76 The absolute value for the presence of phytolith morphotypes (Crete, *Triticum durum*). Blue line represents data before dissolution and orange line after dissolution (pH=7 and T=20˚C)

Fig. 77 The absolute value for the presence of phytolith morphotypes (Crete, *Triticum durum*). Blue line represents data before dissolution and orange line after dissolution (pH=7 and T=40˚C)

Fig. 78 The absolute value for the presence of phytolith morphotypes (Crete, *Triticum durum*). Blue line represents data before dissolution and orange line after dissolution (pH=8.5 and T=20˚C)

Fig. 79 The absolute value for the presence of phytolith morphotypes (Crete, *Triticum durum*). Blue line represents data before dissolution and orange line after dissolution (pH=8.5 and T=40˚C)

Fig. 80 The relative difference between the presence of phytolith morphotypes (Volos, *Triticum monococcum*) before and after the dissolution (pH=7, T=20˚C)

Fig. 81 The relative difference between the presence of phytolith morphotypes (Volos, *Triticum monococcum*) before and after the dissolution (pH=7 and T=40˚C)

Fig. 82 The relative difference between the presence of phytolith morphotypes (Volos, *Triticum monococcum*) before and after the dissolution (pH=8.5, T=20˚C)

Fig. 83 The relative difference between the presence of phytolith morphotypes (Volos, *Triticum monococcum*) before and after the dissolution (pH=8.5 and T=40˚C)

Fig. 84 The absolute value for the presence of phytolith morphotypes (Volos, *Triticum durum*). Blue line represents data before dissolution and orange line after dissolution (pH=7 and T=20˚C)

Fig. 85 The absolute value for the presence of phytolith morphotypes (Volos, *Triticum durum*). Blue line represents data before dissolution and orange line after dissolution (pH=7 and T=40˚C)

Fig. 86 The absolute value for the presence of phytolith morphotypes (Volos, *Triticum durum*). Blue line represents data before dissolution and orange line after dissolution (pH=8.5 and T=20˚C)

Fig. 87 The absolute value for the presence of phytolith morphotypes (Volos, *Triticum durum*). Blue line represents data before dissolution and orange line after dissolution (pH=8.5 and T=40˚C)

Fig. 88 The relative difference between the presence of phytolith morphotypes (Pella I, *Triticum monococcum*) before and after the dissolution (pH=7 and T=20˚C)

Fig. 89 The relative difference between the presence of phytolith morphotypes (Pella I, *Triticum monococcum*) before and after the dissolution (pH=7 and T=40˚C)

Fig. 90 The relative difference between the presence of phytolith morphotypes (Pella I, *Triticum monococcum*) before and after the dissolution (pH=8.5 and T=20˚C)

Fig. 91 The relative difference between the presence of phytolith morphotypes (Pella I, *Triticum monococcum*) before and after the dissolution (pH=8.5 and T=40˚C)

Fig. 92 The absolute value for the presence of phytolith morphotypes (Pella I, *Triticum monococcum*). Blue line represents data before dissolution and orange line after dissolution (pH=7 and T=20˚C)

Fig. 93 The absolute value for the presence of phytolith morphotypes (Pella I, *Triticum monococcum*). Blue line represents data before dissolution and orange line after dissolution (pH=7 and T=40˚C)

Fig. 94 The absolute value for the presence of phytolith morphotypes (Pella I, *Triticum monococcum*). Blue line represents data before dissolution and orange line after dissolution (pH=8.5 and T=20˚C)

Fig. 95 The absolute value for the presence of phytolith morphotypes (Pella I, *Triticum monococcum*). Blue line represents data before dissolution and orange line after dissolution (pH=8.5 and T=40˚C)

Fig. 96 The relative difference between the presence of phytolith morphotypes (Pella II, *Triticum durum*) before and after the dissolution (pH=7 and T=20˚C)

Fig. 97 The relative difference between the presence of phytolith morphotypes (Pella II, *Triticum durum*) before and after the dissolution (pH=7 and T=40˚C)

Fig. 98 The relative difference between the presence of phytolith morphotypes (Pella II, *Triticum durum*) before and after the dissolution (pH=8.5 and T=20˚C)

Fig. 99 The relative difference between the presence of phytolith morphotypes (Pella II, *Triticum durum*) before and after the dissolution (pH=8.5 and T=40˚C)

Fig. 100 The absolute value for the presence of phytolith morphotypes (Pella II, *Triticum durum*). Blue line represents data before dissolution and orange line after dissolution (pH=7 and T=20˚C)

Fig. 101 The absolute value for the presence of phytolith morphotypes (Pella II, *Triticum durum).* Blue line represents data before dissolution and orange line after dissolution (pH=7 and T=40˚C)

Fig. 102 The absolute value for the presence of phytolith morphotypes (Pella II, *Triticum durum*). Blue line represents data before dissolution and orange line after dissolution (pH=8.5 and T=20˚C)

Fig. 103 The absolute value for the presence of phytolith morphotypes (Pella II, *Triticum durum*). Blue line represents data before dissolution and orange line after dissolution (pH=8.5 and T=40˚C)

Fig. 104 The relative difference between the presence of phytolith morphotypes (Corfu, *Triticum durum*) before and after the dissolution (pH=7 and T=20˚C)

Fig. 105 The relative difference between the presence of phytolith morphotypes (Corfu, *Triticum durum*) before and after the dissolution (pH=7 and T=40˚C)

Fig. 106 The relative difference between the presence of phytolith morphotypes (Corfu, *Triticum durum*) before and after the dissolution (pH=8.5 and T=20˚C)

Fig. 107 The relative difference between the presence of phytolith morphotypes (Corfu, *Triticum durum*) before and after the dissolution (pH=8.5 and T=40˚C)

Fig. 108 The absolute value for the presence of phytolith morphotypes (Corfu, *Triticum durum*). Blue line represents data before dissolution and orange line after dissolution (pH=7 and T=20˚C)

Fig. 109 The absolute value for the presence of phytolith morphotypes (Corfu, *Triticum durum*). Blue line represents data before dissolution and orange line after dissolution (pH=7 and T=40˚C)

Fig.110 The absolute value for the presence of phytolith morphotypes (Corfu, *Triticum durum*). Blue line represents data before dissolution and orange line after dissolution (pH=8.5 and T=20˚C)

Fig. 111 The absolute value for the presence of phytolith morphotypes (Corfu, *Triticum durum*). Blue line represents data before dissolution and orange line after dissolution (pH=8.5 and T=40˚C)

Fig. 112 Sample *Triticum durum*, Cyprus: concentration (mg/g) of Mg, Si, K, Ca over the course of 75 days at pH 5 and temperature 5 ˚C, 20˚C, 40 ˚C

Fig. 113 Sample *Triticum durum*, Cyprus: concentration (mg/g) of Mg, Si, K, Ca over the course of 75 days at pH 7 and temperature 5 ˚C, 20˚C, 40 ˚C

Fig. 114 Sample *Triticum durum*, Cyprus: concentration (mg/g) of Mg, Si, K, Ca over the course of 75 days at pH 8.5 and temperature 5 ˚C, 20˚C, 40 ˚C

Fig. 115 Sample *Triticum durum*, Crete: concentration (mg/g) of Mg, Si, K, Ca over the course of 75 days at pH 5 and temperature 5 ˚C, 20˚C, 40 ˚C

Fig. 116 Sample *Triticum durum*, Crete: concentration (mg/g) of Mg, Si, K, Ca over the course of 75 days at pH 7 and temperature 5 ˚C, 20˚C, 40 ˚C

Fig. 117 Sample *Triticum durum*, Crete: concentration (mg/g) of Mg, Si, K, Ca over the course of 75 days at pH 8.5 and temperature 5 ˚C, 20˚C, 40 ˚C

Fig. 118 Sample *Triticum monococcum*, Volos: concentration (mg/g) of Mg, Si, K, Ca over the course of 75 days at pH 5 and temperature 5 ˚C, 20˚C, 40 ˚C

Fig. 119 Sample *Triticum monococcum*, Volos: concentration (mg/g) of Mg, Si, K, Ca over the course of 75 days at pH 7 and temperature 5 ˚C, 20˚C, 40 ˚C

Fig. 120 Sample *Triticum monococcum*, Volos: concentration (mg/g) of Mg, Si, K, Ca over the course of 75 days at pH 8.5 and temperature 5 ˚C, 20˚C, 40 ˚C

Fig. 121 Sample *Triticum monococcum,* Pella I: concentration (mg/g) of Mg, Si, K, Ca over the course of 75 days at pH 5 and temperature 5 ˚C, 20˚C, 40 ˚C

Fig. 122 Sample *Triticum monococcum,* Pella I: concentration (mg/g) of Mg, Si, K, Ca over the course of 75 days at pH 7 and temperature 5 ˚C, 20˚C, 40 ˚C

Fig. 123 Sample *Triticum monococcum,* Pella I: concentration (mg/g) of Mg, Si, K, Ca over the course of 75 days at pH 8.5 and temperature 5 ˚C, 20˚C, 40 ˚C

Fig. 124 Sample *Triticum monococcum,* Pella II: concentration (mg/g) of Mg, Si, K, Ca over the course of 75 days at pH 5 and temperature 5 ˚C, 20˚C, 40 ˚C

Fig. 125 Sample *Triticum durum,* Pella II: concentration (mg/g) of Mg, Si, K, Ca over the course of 75 days at pH 7 and at temperature 5 ˚C, 20˚C, 40 ˚C

Fig. 126 Sample *Triticum durum,* Pella II: concentration (mg/g) of Mg, Si, K, Ca over the course of 75 days at pH 8.5 and temperature 5 ˚C, 20˚C, 40 ˚C

Fig. 127 Sample *Triticum durum,* Corfu: concentration (mg/g) of Mg, Si, K, Ca over the course of 75 days at pH 5 and temperature 5 ˚C, 20˚C, 40 ˚C

Fig. 128 Sample *Triticum durum,* Corfu: concentration (mg/g) of Mg, Si, K, Ca over the course of 75 days at pH 7 and temperature 5 ˚C, 20˚C, 40 ˚C

Fig. 129 Sample *Triticum durum,* Corfu: concentration (mg/g) of Mg, Si, K, Ca over the course of 75 days at pH 8.5 and temperature 5 ˚C, 20˚C, 40 ˚C

Fig. 130 Sample *Triticum durum,* Cyprus: concentration (mg/g) of Mg (above) and K (below) over the course of 75 days at pH 5 and temperature 5 ˚C, 20˚C, 40 ˚C

Fig. 131 Sample *Triticum durum,* Cyprus: concentration (mg/g) of Si (above) and Ca (below) over the course of 75 days at pH 5 and temperature 5 ˚C, 20˚C, 40 ˚C

Fig. 132 Sample *Triticum durum,* Cyprus: concentration (mg/g) of Mg (above) and K (below) over the course of 75 days at pH 7 and temperature 5 ˚C, 20˚C, 40 ˚C

Fig. 133 Sample *Triticum durum,* Cyprus: concentration (mg/g) of Si (above) and Ca (below) over the course of 75 days at pH 7 and temperature 5 ˚C, 20˚C, 40 ˚C

Fig. 134 Sample *Triticum durum,* Cyprus: concentration (mg/g) of Mg (above) and K (below) over the course of 75 days at pH 8.5 and temperature 5 ˚C, 20˚C, 40 ˚C

Fig. 135 Sample *Triticum durum,* Cyprus: concentration (mg/g) of Si (above) and Ca (below) over the course of 75 days at pH 8.5 and temperature 5 ˚C, 20˚C, 40 ˚C

Fig. 136 Sample *Triticum durum,* Crete: concentration (mg/g) of Mg (above) and K (below) over the course of 75 days at pH 5 and temperature 5 ˚C, 20˚C, 40 ˚C

Fig. 137 Sample *Triticum durum,* Crete: concentration (mg/g) of Si (above) and Ca (below) over the course of 75 days at pH 5 and temperature 5 ˚C, 20˚C, 40 ˚C

Fig. 138 Sample *Triticum durum,* Crete: concentration (mg/g) of Mg (above) and K (below) over the course of 75 days at pH 7 and temperature 5 ˚C, 20˚C, 40 ˚C

Fig. 139 Sample *Triticum durum,* Crete: concentration (mg/g) of Si (above) and Ca (below) over the course of 75 days at pH 7 and temperature 5 ˚C, 20˚C, 40 ˚C

Fig. 140 Sample *Triticum durum,* Crete: concentration (mg/g) of Mg (above) and K (below) over the course of 75 days at pH 8.5 and temperature 5 ˚C, 20˚C, 40 ˚C

Fig. 141 Sample *Triticum durum,* Crete: concentration (mg/g) of Si (above) and Ca (below) over the course of 75 days at pH 8.5 and temperature 5 ˚C, 20˚C, 40 ˚C

Fig. 142 Sample *Triticum monococcum,* Volos: concentration (mg/g) of Mg (above) and K (below) over the course of 75 days at pH 5 and temperature 5 ˚C, 20˚C, 40 ˚C

Fig. 143 Sample *Triticum monococcum,* Volos: concentration (mg/g) of Si (above) and Ca (below) over the course of 75 days at pH 5 and temperature 5 ˚C, 20˚C, 40 ˚C

Fig. 144 Sample *Triticum monococcum,* Volos: concentration (mg/g) of Mg (above) and K (below) over the course of 75 days at pH 7 and temperature 5 ˚C, 20˚C, 40 ˚C

Fig. 145 Sample *Triticum monococcum,* Volos: concentration (mg/g) of Si (above) and Ca (below) over the course of 75 days at pH 7 and temperature 5 ˚C, 20˚C, 40 ˚C

Fig. 146 Sample *Triticum monococcum,* Volos: concentration (mg/g) of Mg (above) and K (below) over the course of 75 days at pH 8.5 and temperature 5 ˚C, 20˚C, 40 ˚C

Fig. 147 Sample *Triticum monococcum,* Volos: concentration (mg/g) of Si (above) and Ca (below) over the course of 75 days at pH 8.5 and temperature 5 ˚C, 20˚C, 40 ˚C

Fig. 148 Sample *Triticum monococcum,* Pella I: concentration (mg/g) of Mg (above) and K (below) over the course of 75 days at pH 5 and temperature 5 ˚C, 20˚C, 40 ˚C

Fig. 149 Sample *Triticum monococcum,* Pella I: concentration (mg/g) of Si (above) and Ca (below) over the course of 75 days at pH 5 and temperature 5 ˚C, 20˚C, 40 ˚C

Fig. 150 Sample *Triticum monococcum,* Pella I: concentration (mg/g) of Mg (above) and K (below) over the course of 75 days at pH 7 and temperature 5 ˚C, 20˚C, 40 ˚C

Fig. 151 Sample *Triticum monococcum,* Pella I: concentration (mg/g) of Si (above) and Ca (below) over the course of 75 days at pH 7 and temperature 5 ˚C, 20˚C, 40 ˚C

Fig. 152 Sample *Triticum monococcum,* Pella I: concentration (mg/g) of Mg (above) and K (below) over the course of 75 days at pH 8.5 and temperature 5 ˚C, 20˚C, 40 ˚C

Fig. 153 Sample *Triticum monococcum,* Pella I: concentration (mg/g) of Si (above) and Ca (below) over the course of 75 days at pH 8.5 and temperature 5 ˚C, 20˚C, 40 ˚C

Fig. 154 Sample *Triticum durum,* Pella II: concentration (mg/g) of Mg (above) and K (below) over the course of 75 days at pH 5 and temperature 5 ˚C, 20˚C, 40 ˚C

Fig. 155 Sample *Triticum durum,* Pella II: concentration (mg/g) of Si (above) and Ca (below) over the course of 75 days at pH 5 and temperature 5 ˚C, 20˚C, 40 ˚C

Fig. 156 Sample *Triticum durum,* Pella II: concentration (mg/g) of Mg (above) and K (below) over the course of 75 days at pH 7 and temperature 5 ˚C, 20˚C, 40 ˚C

Fig. 157 Sample *Triticum durum,* Pella II: concentration (mg/g) of Si (above) and Ca (below) over the course of 75 days at pH 7 and temperature 5 ˚C, 20˚C, 40 ˚C

Fig. 158 Sample *Triticum durum,* Pella II: concentration (mg/g) of Mg (above) and K (below) over the course of 75 days at pH 8.5 and temperature 5 ˚C, 20˚C, 40 ˚C

Fig. 159 Sample *Triticum durum,* Pella II: concentration (mg/g) of Si (above) and Ca (below) over the course of 75 days at pH 8.5 and temperature 5 ˚C, 20˚C, 40 ˚C

Fig. 160 Sample *Triticum durum,* Corfu: concentration (mg/g) of Mg (above) and K (below) over the course of 75 days at pH 5 and temperature 5 ˚C, 20˚C, 40 ˚C

Fig. 161 Sample *Triticum durum,* Corfu: concentration (mg/g) of Si (above) and Ca (below) over the course of 75 days at pH 5 and temperature 5 ˚C, 20˚C, 40 ˚C

Fig. 162 Sample *Triticum durum,* Corfu: concentration (mg/g) of Mg (above) and K (below) over the course of 75 days at pH 7 and temperature 5 ˚C, 20˚C, 40 ˚C

Fig. 163 Sample *Triticum durum,* Corfu: concentration (mg/g) of Si (above) and Ca (below) over the course of 75 days at pH 7 and temperature 5 ˚C, 20˚C, 40 ˚C

Fig. 164 Sample *Triticum durum,* Corfu: concentration (mg/g) of Mg (above) and K (below) over the course of 75 days at pH 8.5 and temperature 5 ˚C, 20˚C, 40 ˚C

Fig. 165 Sample *Triticum durum,* Corfu: concentration (mg/g) of Si (above) and Ca (below) over the course of 75 days at pH 8.5 and temperature 5 ˚C, 20˚C, 40 ˚C

Fig. 166 Sample *Triticum durum*, Cyprus: concentration (mg/g) of Sr and Ba over the course of 75 days at pH 5 and temperature 5 ˚C, 20˚C, 40 ˚C

Fig. 167 Sample *Triticum durum*, Cyprus: concentration (mg/g) of Sr and Ba over the course of 75 days at pH 7 and temperature 5 ˚C, 20˚C, 40 ˚C

Fig. 168 Sample *Triticum durum*, Cyprus: concentration (mg/g) of Sr and Ba over the course of 75 days at pH 8.5 and temperature 5 ˚C, 20˚C, 40 ˚C

Fig. 169 Sample *Triticum durum*, Crete: concentration (mg/g) of Sr and Ba over the course of 75 days at pH 5 and temperature 5 ˚C, 20˚C, 40 ˚C

Fig. 170 Sample *Triticum durum*, Crete: concentration (mg/g) of Sr and Ba over the course of 75 days at pH 7 and temperature 5 ˚C, 20˚C, 40 ˚C

Fig. 171 Sample *Triticum durum*, Crete: concentration (mg/g) of Sr and Ba over the course of 75 days at pH 8.5 and temperature 5 ˚C, 20˚C, 40 ˚C

Fig. 172 Sample *Triticum monococcum,* Volos: concentration (mg/g) of Sr and Ba over the course of 75 days at pH 5 and temperature 5 ˚C, 20˚C, 40 ˚C

Fig. 173 Sample *Triticum monococcum,* Volos: concentration (mg/g) of Sr and Ba over the course of 75 days at pH 7 and temperature 5 ˚C, 20˚C, 40 ˚C

Fig. 174 Sample *Triticum monococcum,* Volos: concentration (mg/g) of Sr and Ba over the course of 75 days at pH 8.5 and temperature 5 ˚C, 20˚C, 40 ˚C

Fig. 175 Sample *Triticum monococcum,* Pella I: concentration (mg/g) of Sr and Ba over the course of 75 days at pH 5 and temperature 5 ˚C, 20˚C, 40 ˚C

Fig. 176 Sample *Triticum monococcum,* Pella I: concentration (mg/g) of Sr and Ba over the course of 75 days at pH 7 and temperature 5 ˚C, 20˚C, 40 ˚C

Fig. 177 Sample *Triticum monococcum,* Pella I: concentration (mg/g) of Sr and Ba over the course of 75 days at pH 8.5 and temperature 5 ˚C, 20˚C, 40 ˚C

Fig. 178 Sample *Triticum durum,* Pella II: concentration (mg/g) of Sr and Ba over the course of 75 days at pH 5 and temperature 5 ˚C, 20˚C, 40 ˚C

Fig. 179 Sample *Triticum durum,* Pella II: concentration (mg/g) of Sr and Ba over the course of 75 days at pH 7 and temperature 5 ˚C, 20˚C, 40 ˚C

Fig. 180 Sample *Triticum durum,* Pella II: concentration (mg/g) of Sr and Ba over the course of 75 days at pH 8.5 and temperature 5 ˚C, 20˚C, 40 ˚C

Fig. 181 Sample *Triticum durum,* Corfu: concentration (mg/g) of Sr and Ba over the course of 75 days at pH 5 and temperature 5 ˚C, 20˚C, 40 ˚C

Fig. 182 Sample *Triticum durum,* Corfu: concentration (mg/g) of Sr and Ba over the course of 75 days at pH 7 and temperature 5 ˚C, 20˚C, 40 ˚C

Fig. 183 Sample *Triticum durum,* Corfu: concentration (mg/g) of Sr and Ba over the course of 75 days at pH 8.5 and temperature 5 ˚C, 20˚C, 40 ˚C

Fig. 184 The ln C/C_o versus time (days) curves for leaching of Si at pH 5, 7, 8.5 and temperature: **(a)** 5, **(b)** 20, and **(c)** 40 °C for the sample *Triticum durum* from Cyprus

Fig. 185 The ln C/C_o versus time (days) curves for leaching of Si at pH 5, 7, 8.5 and temperature: **(a)** 5, **(b)** 20; and **(c)** 40 °C for the sample *Triticum durum* from Crete

Fig. 186 The ln C/C_o versus time (days) curves for leaching of Si at pH 5, 7, 8.5 and temperature: **(a)** 5, **(b)** 20; and **(c)** 40 °C for the sample *Triticum monococcum* from Volos

Fig. 187 The ln C/C_o versus time (days) curves for leaching of Si at pH 5, 7, 8.5 and temperature: **(a)** 5, **(b)** 20; and **(c)** 40 °C for the sample *Triticum monococcum* from Pella

Fig. 188 The ln C/C_o versus time (days) curves for leaching of Si at pH 5, 7, 8.5 and temperature: **(a)** 5, **(b)** 20; and **(c)** 40 °C for the sample *Triticum durum* from Pella

Fig. 189 The ln C/C_o versus time (days) curves for leaching of Si at pH 5, 7, 8.5 and temperature: **(a)** 5, **(b)** 20; and **(c)** 40 °C for the sample *Triticum durum* from Corfu

Fig. 190 Sample *Triticum durum,* Cyprus: silicon concentration (mg/g) at **pH 5, 7, 8.5** and temperature 5, 20, 40˚C

Fig. 191 Sample *Triticum durum,* Crete: silicon concentration (mg/g) at **pH 5, 7, 8.5** and temperature 5, 20, 40˚C

Fig. 192 Sample *Triticum monococcum,* Volos: silicon concentration (mg/g) at **pH 5, 7, 8.5** and temperature 5, 20, 40˚C

Fig. 193 Sample *Triticum monococcum,* Pella I: silicon concentration (mg/g) at **pH 5, 7, 8.5** and temperature 5, 20, 40˚C

Fig. 194 Sample *Triticum durum,* Pella II: silicon concentration (mg/g) at **pH 5, 7, 8.5** and temperature 5, 20, 40˚C

Fig. 195 Sample *Triticum durum,* Corfu: silicon concentration (mg/g) at **pH 5, 7, 8.5** and temperature 5, 20, 40˚C

Fig. 196 Sample *Triticum durum,* Cyprus: silicon concentration (mg/g) at pH 5, 7, 8.5 and **temperature 5, 20, 40˚C**

Fig. 197 Sample *Triticum durum*, Crete: silicon concentration (mg/g) at pH 5, 7, 8.5 and **temperature 5, 20, 40˚C**

Fig. 198 Sample *Triticum monococcum,* Volos: silicon concentration (mg/g) at pH 5, 7, 8.5 and **temperature 5, 20, 40˚C**

Fig. 199 Sample *Triticum monococcum,* Pella I: silicon concentration (mg/g) at pH 5, 7, 8.5 and **temperature 5, 20, 40˚C**

Fig. 200 Sample *Triticum durum,* Pella II: silicon concentration (mg/g) at pH 5, 7, 8.5 and **temperature 5, 20, 40˚C**

Fig. 201 Sample *Triticum durum,* Corfu: silicon concentration (mg/g) at pH 5, 7, 8.5 and **temperature 5, 20, 40˚C**

LIST OF TABLES

Table 14 Chemical composition of phytoliths [inflorescences (I), stems-leaves (S-L)] using dry and wet extraction method for *Triticum monococcum* (M) or *Triticum durum* (D) for plant sample from Pella I and Pella II

Table 15 Chemical composition of phytoliths extracted from the entire plant, excluding the roots, using dry extraction method for *Triticum monococcum* (M) or *Triticum durum* (D) for plant samples from Cyprus, Crete, Volos, Pella I, Pella II and Corfu

Table 16 Chemical composition of the soils, where the plants were grown

Table 17 Chemical composition of the archaeological sediments

Table 18 Silicon reaction rates (d^{-1}) obtained from one stage (*k*) and silicon reaction rates (d^{-1}) obtained from two stages (*k*1 and *k*2) of dissolved phytoliths (*Triticum durum* Cyprus, *Triticum durum* Crete, *Triticum monococcum* Volos, *Triticum monococcum* Pella I, *Triticum durum* Pella II, *Triticum durum* Corfu samples) at pH 5, 7, 8.5 and temperature 5 ˚C, 20˚C, 40 ˚C

Table 19 Silicon reaction rates (d^{-1}) obtained from one stage (*k*) and silicon reaction rates (d^{-1}) obtained from two stages (*k*1 and *k*2) of dissolved phytoliths (Cyprus, Crete, Volos, Pella I, Pella II, Corfu samples) in relation with the total annual precipitation (mm) for the year 2014. The experiments at 20 ˚C that were carried out under continuous agitation in a shaking table are presented in colour blue

Table 20 Silicon reaction rates (d^{-1}) obtained from one stage (*k*) and silicon reaction rates (d^{-1}) obtained from two stages (*k*1 and *k*2) of dissolved phytoliths (Cyprus, Crete, Volos, Pella I, Pella II, Corfu samples) in relation with the average annual temperature (^{o}C) for the year 2014. The experiments at 20 ˚C that were carried out under continuous agitation in a shaking table are presented in colour blue

Table 21 (pages (234-236) Cyprus sample (*Triticum durum*)

Table 22 (pages 237-239) Cretan sample (*Triticum durum*)

Table 23 (pages 240-242) Volos sample (*Triticum monococcum*)

Table 24 (pages 243-245) Pella I sample (*Triticum monococcum*)

Table 25 (pages 246-248) Pella II sample (*Triticum durum*)

Table 26 (pages 249-251) Corfu sample (*Triticum durum*)

* Tables 21-26 show the concentration (mg/g) of the studied elements (Mg, Al, Si, K, Ca, Fe, Sr, Ba) from phytoliths over the course of 75 days. The standard deviation for the repetition of two measurements of the concentration is given. Dissolution was carried out in batch experiments at pH (5, 7, 8.5) and temperature (5, 20, 40 ˚C); by adding 0.15 g of phytoliths that were extracted from entire wheat (excluding roots) in 45 mL of H_2O. Code 1-5-5-1 is for sample 1, pH 5, temperature 5, day 1 etc.

REFERENCES

A

Acuña-Mesen R and García-Díaz E (1998) New *Cuvieronius hyodon* (Proboscidea: Gomphotheriidae) from the Pleistocene of Costa Rica. *Revista Biol Trop 46*:1167-1172

Adler HH and Kerr PF (1962) Infrared study of aragonite and calcite. *Am Mineral 47*:700-717

Adler HH and Kerr PF (1965) Variations in infrared spectra, molecular symmetry and site symmetry of sulfate minerals. *Am Mineral 50*:132-147

Adrymi-Sismani V (2007) Iolkos: myth, archaeology and history. In: Gordeziani (ed), *The Argonautica and World Culture*. Phasis, Greek and Roman studies 10, Tbilisi, pp 20-32

Albert RM, Bamford MK, Cabanes D (2006) Taphonomy of phytoliths and macroplants in different soils from Olduvai Gorge (Tanzania) and the application to Plio-Pleistocene palaeoanthropological samples. *Quatern Int 148*:78-94

Albert RM, Bamford MK, Cabanes D (2009) Palaeoecological significance of palms at Olduvai Gorge, Tanzania, based on phytolith remains. *Quat Int 193*:41-48

Albert RM and Cabanes D (2008) Fire in prehistory: an experimental approach to combustion processes and phytolith remains. *Isr J Earth Sci 56*:175-189

Albert RM, Shahack-Gross R, Cabanes D, Gilboa A, Lev-Yadun S, Portillo M, Sharon I, Boaretto E, Weiner S (2008) Phytolith-rich layers from the Late Bronze and Iron Ages at Tel Dor (Israel): mode of formation and archaeological significance. *J Archaeol Sci 35*:57-75

Albert RM and Weiner S (2001) Study of phytoliths in prehistoric ash layers using a quantitative approach. In: Meunier JD and Coline F (eds), *Phytoliths: Applications in Earth Sciences and Human History*. Lisse: A.A. Balkeme Publishers, pp 251-266

Albert RM, Weiner S, Bar-Yosef O, Meignen L (2000) Phytoliths in the middle palaeolithic deposits of Kebara Cave, Mt Carmel, Israel: study of the plant materials used for fuel and other purposes. *J Archaeol Sci 27*:931-47

Alexandre A, Basile-Doelsch I, Delhaye T, Borshneck D, Mazur1 JC, Reyerson P, Santos GM (2015) New highlights on phytolith structure and occluded carbon location: 3-D X-ray microscopy and NanoSIMS results. *Biogeosciences Discuss 11*:14699-14727

Alexandre A, Meunier JD, Colin F, Koud JM (1997a) Plant impact on the biogeochemical cycle of silicon and related weathering processes. *Geochim Cosmochim Acta 61*:677-682

Alexandre A, Meunier JD, Lézine AM, Vincens A, Schwartz D (1997b) Phytoliths: indicators of grassland dynamics during the late Holocene in intertropical Africa. *Palaeogeogr Palaeocl 136*:213-229

Alfredsson H, Clymans W, Stadmark J, Conley DJ, Rousk J (2016) Bacterial and fungal colonization and decomposition of submerged plant litter: consequences for biogenic silica dissolution. *FEMS Microbiol Ecol 92*:1-12

Allué E (2009) Estudi antracològic del jaciment de Forat de Conqueta (Santa Linya, Lleida), [Study of the charcoal remains at the site of Forat de Conqueta (Santa Linya, Lleida)]. *Treballs D'arqueologia 17*:27-35 (in Catalan)

Allué E, Picornell-Gelabert L, Daura J, Sanz M (2017) Reconstruction of the palaeoenvironment and anthropogenic activity from the Upper Pleistocene/Holocene anthracological records of the NE Iberian Peninsula (Barcelona, Spain). *Quat Int 457*:172-189

Alonso N (2019) A first approach to women, tools and operational sequences in traditional manual cereal grinding. *Archaeol Anthropol Sci 11*:4307-4324

Anala R and Nambisan P (2015) Study of morphology and chemical composition of phytoliths on the surface of paddy straw. *Paddy Water Environ 13*:521-527

Anderson OR (1983) *Radiolaria*. Springer-Verlag, New York, US

Andreou S, Kostakis K, Chourmouziadis G (1990) Ανασκαφή στην Τούμπα Θεσσαλονίκη; 1989, [Excavation at Toumba of Thessaloniki]. *Εγνατία 2*:381-404 (in Greek)

Andreou S and Kostakis K (1996) Προϊστορική Τούμπα της Θεσσαλονίκης. Παλιά και νέα ερωτήματα, [Prehistoric Toumba of Thessaloniki. Old and new questions]. *ΑΕΜΘ* 10: 369-388 (in Greek)

Andriopoulou NC (2014) *Phytolith analysis of cereals, modern soils and experimental crop processing activities: application to archaeology*. Unpublished master's thesis, University of Ferrara, IT

Andriopoulou NC and Christidis GE (2020) Multi-analytical characterisation of wheat biominerals: impact of methods of extraction on the mineralogy and chemistry of phytoliths. *Archaeol Anthropol Sci 12:*186

Andriopoulou NC, Michailidis D, Christidis GE, Partsinevelos P (2019) 3D representation of biominerals integrating microscopy and photogrammetry: implications in geoarchaeology. Geophysical Research Abstracts Vol. 21, EGU2019-10780-1, *European Geoscience Union General Assembly*, Vienna, Austria

Andriopoulou NC and Partsinevelos P (2019) Digital surface reconstruction of biominerals under a quantitative perspective: implications in the taxonomy and preservation of archaeomalacological material. Conference: On shifting grounds - the study of archaeological practices in a changing world, Rethymnon, Crete, Greece

Aizenberg J, Albeck S, Weiner S, Addadi L (1994) Crystal-protein interactions studied by overgrowth of calcite on biogenic skeletal elements. *J Cryst Growth 142*:156-164

Aoki Y, Hoshino M, Matsubara T (2007) Silica and testate amoebae in a soil under pine-oak forest. *Geoderma 142*:29-35

Aposkitou M (1979) Μίνως Καλοκαιρινός. Εκατό χρόνια από την πρώτη ανασκαφή της Κνωσού, [Minos Kalokerinos. One hundred years from the first excavation of Knossos]. *Κρητολογία 8*:81-94 (in Greek)

Arnott HJ (1982) Three systems of biomineralization in plants with comments on the associated organic matrix. In: Nancollas GH (ed), *Biological Mineralization and Demineralization*. Springer-Verlag, Berlin, Heidelberg, New York, pp 199-218

Asderaki-Tzoumerkioti E, Rehren Th, Skafida E, Vaxevanopoulos M, Connolly PJ (2018) Kastro Palea settlement, Volos, Greece: a diachronical technological approach to bronze metalwork. *STAR: Science and Technology of Archaeological Research 3*:179-193

Awadh SM and Yaseen ZM (2019) Investigation of silica polymorphs stratified in siliceous geode using FTIR and XRD methods. *Mater Chem Phys 228*:45-50

B

Ball TB and Brotherson JD (1992) The effect of varying environmental conditons on phytolith morphometries in two species of grass (*Bouteloua curtipendula* and *Panicum virgatum*). *Scanning Microsc Int 6*:1163-1181

Ball TB, Chandler-Ezell K, Dickau R, Duncan N, Hart TC, Iriarte J, Lentfer C, Logan A, Lu H, Madella M, Pearsall DM, Piperno DR, Rosen AM, Vrydaghs L, Weisskopf A, Zhang J (2016) Phytoliths as a tool for investigations of agricultural origins and dispersals around the world. *J Archaeol Sci 68*:32-45

Ball TB, Gardner JS, Anderson N (1999) Identifying inflorescence phytoliths from selected species of wheat (*Triticum monococcum, T. dicoccon, T. dicoccoides* and *T. aestivum*)

and barley (*Hordeum vulgare* and *H. spontaneum*) (Gramineae). *Am J Bot 86*:1615-1623

Bamford MK, Albert RM, Cabanes D (2006) Plio-Pleistocene macroplant fossil remains and phytoliths from Lowermost Bed II in the Eastern palaeolake margin of Olduvai Gorge, Tanzania. *Quat Int 148*:95-112

Bange GGJ (1953) On the quantitative explanation of stomatal transpiration. *Acta Bot Neerl 2*:255-97

Barboni D, Bonnefille R, Alexandre A, Meunier JD (1999) Phytoliths as paleoenvironmental indicators, West Side Middle Awash Valley, Ethiopia. *Palaeogeogr Palaeocl 152*:87-100

Barnes IL, Moore LJ, Machlan LA, Murphy TJ, Shields WR (1975) Absolute isotopic abundance ratios and atomic weight of a reference sample of silicon. *J Res Natl Bur Stand 79*:727-735

Bartoli F and Wilding L (1980) Dissolution of biogenic opal as a function of its physical and chemical properties. *Soil Sci Soc Am J 44*:873-878

Batten G, Wardlaw I, Aston M (1986) Growth and the distribution of phosphorus in wheat developed under various phosphorus and temperature regimes. *Aust J Agr Res 37*:459-469

Batziou-Efstathiou A (2003) Η Υστεροελλαδική ΙΙΙΓ στο Κάστρο του Βόλου, [The Late Helladic IIIC in the Castle of Volos]. *ΠΜΚ* 2:253-262 (in Greek)

Bauer P, Elbaum R, Weiss IM (2011) Calcium and silicon mineralization in land plants: transport, structure and function. *Plant Sci 180*:746-756

Baumann H (1960) Behavior of silicic acid in human blood and urine. *Hoppe-Seyler's Z Physiol Chem 320*:11-20

Bélanger RR, Benhamou N, Menzies JG (2003) Cytological evidence of an active role of silicon in wheat resistance to powdery mildew (*Blumeria graminis* f. sp. tritici). *Phytopathology 93*:402-412

Bennet J (2013) Minoan Crete: a world of objects, a world of places. In: Galanakis Y (ed). *The Aegean World. A Companion Guide to the Cycladic, Minoan and Mycenaean Collections in the Ashmolean Museum*. University of Oxford (Oxford/Athens: Ashmolean Museum/Kapon Editions), pp 102-117

Bergson H (1911) *Creative Evolution.* Translated by Mitchell A, Henry Holt and Company

Berlin AM, Ball TB, Thompson R, Kittleson D, Herbert SC (2003) Ptolemaic agriculture, "Syrian wheat" and *Triticum aestivum*. *J Archaeol Sci 30*:115-121

Berner RA (2003) The long-term carbon cycle, fossil fuels and atmospheric composition. *Nature 426*:323-326

Berthoud AJ (1912) Theorie de la formation des faces d'un crystal, [Formation theory of crystal phases]. *J Chim Phys 10*:624-635 (in French)

Bybordy A (2014) Interactive effects of silicon and potassium nitrate in improving salt tolerance of wheat. *Int J Agric 13*:1889-1899

Blackman E (1969) Observations on the development of the silica cells of the leaf sheath of wheat *(Triticum aestivum)*. *Canad J Bot 47*:827-838

Boursier P, Lynch J, Lauchli A, Epstein E (1987) Chloride partitioning in leaves of salt-stressed sorghum, maize, wheat and barley. *Aust J Plant Physiol 14*:463-73

Bowdery D (1989) Phytolith analysis: introduction and applications. In: Beck W, Clarke A, Head L (eds), *Plants in Australian Archaeology*. Tempus 1. Anthropology Museum, St. Lucia: University of Queensland, pp 161-196

Braadbaart F, Sarpaki A, Veldc H, van Osd B (2019) Charred organic material, heated by anthropogenic fires and hot volcanic products from the Minoan eruption, excavated from the Bronze Age site of Akrotiri on the Cycladic island of Thera (Greece). *IANSA* X:129-141

Brewer CA (2016) *Designing better maps: a guide for GIS users*. 2nd edn, Esri Press

Brochier JE and Thinon M (2003) Calcite crystals, starch grains aggregates or…POCC? Comment on calcite crystals inside archaeological plant tissues. *J Archaeol Sci 30*:1211-1214

Browne CA (1944) A sourcebook of Agricultural Chemistry. *Chronica Botanica 8*:1-290

Buján E (2013) Elemental composition of phytoliths in modern plants (Ericaceae). *Quat Int 287*:114-120

Burjachs F (1994) Palynology of the upper Pleistocene and Holocene of the North-East Iberian Peninsula: Pla de l'Estany, Catalonia. *Hist Biol 9*:17-33

C

Cabanes D, Burjachs F, Expósito I, Rodríguez A, Allué E, Euba I, Vergès JM (2009) Formation processes through archaeobotanical remains: the case of the Bronze Age levels in El Mirador Cave, Sierra de Atapuerca, Spain. *Quat Int 193*:160-173

Cabanes D, Gadot Y, Cabanes M, Finkelstein I, Weiner S, Shahack-Gross R (2012) Human impact around settlement sites: a phytolith and mineralogical study for assessing site boundaries, phytolith preservation, and implications for spatial reconstructions using plant remains. *J Archaeol Sci 3*:2697-2705

Cabanes D and Shahack-Gross R (2015) Understanding fossil phytolith preservation: the role of partial dissolution in paleoecology and archaeology. *PLos One 10*:e0125532

Cabanes D, Weiner S, Shahack-Gross R (2011) Stability of phytoliths in the archaeological record: a dissolution study of modern and fossil phytoliths. *J Archaeol Sci 38*:2480-2490

Calegari MR, Madella M, Buso AA, Osterrieth M, Lorente FL, Pessenda LCR (2015) Holocene vegetation and climate inferences from phytoliths and pollen from Lagoa do Macuco, North Coast of Espírito Santo State, Brazil. *Quat Environ Geosci 6*:41-50

Campbell M (2017) *Meaning, origin and history of the name opal*. Behind the name

Canti MG (2003) Aspects of the chemical and microscopic characteristics of plant ashes found in archaeological soils. *Catena 54*:339-361

Carnelli AL, Madella M, Theurillat JP, Ammann B (2002) Aluminum in the opal silica reticule of phytoliths: a new tool in palaeoecological studies. *Am J Bot 89*:346-351

Casey WH, Kinrade SD, Knight CTG, Rains DW, Epstein E (2004) Aqueous silicate complexes in wheat, *Triticum aestivum* L. *Plant Cell Environ* 27:51-54

Castelden R (2001) *Minoans, life in Bronze Age Crete*. Taylor and Francis e-Library

Chain F, Côté-Beaulieu C, Belzile F, Menzies JG, Bélanger RR (2009) A comprehensive transcriptomic analysis of the effect of silicon on wheat plants under control and pathogen stress conditions. *Mol Plant Microbe Interact 22*:1323-1330

Chandrasekhar S, Pramada EM, Raghavan E, Satyanarayana KG, Gupta TN (2002) Microsilica from rice husk as a possible substitute for condensed silica fume for high performance concrete. *J Mater Sci Lett 21*:1245-1247

Chapuis JL (1980) Methodes d'etude du regime alimentaire du lapin de Garenne, *Oryctolagus cuniculus* (L.) par l'analyse micrographique des feces, [Methods for studying the diet of the Garenne rabbit, *Oryctolagus cuniculus* (L.) by micrographic analysis of feces]. *Terre et Vie 34*:159-198 (in French)

Cheng F, Cao Q, Guan Y, Cheng H, Wang X, Miller JD (2013) FTIR analysis of water structure and its influence on the flotation of arcanite (K_2SO_4) and epsomite ($MgSO_4{\cdot}7H_2O$). *Int J Miner Process 122*:36-42

Chester R and Elderfield H (1968) The infrared determination of opal in siliceous deep-sea sediments. *Geochim Cosmochim Acta 32*:1128-1140

Chevalier L, Desbuquois C, Le Lannic J, Charrier M (2001) Poaceae in the natural diet of the snail *Helix aspersa* Müller (Gastropoda, Pulmonata). *Compt Rend Hebd Acad Sci III 324*:979-987

Christakis KS (2018) The pithoi of King Minos. Potters and potting groups in Late Minoan Knossos. In: Baldacci G and Caloi I (eds), *Rhadamanthys. Studies in Minoan Archaeology in honour of Filippo Carinci on the occasion of his 70th birthday* (BAR IS 2884), Oxford, pp 189-195

Chukanov NV and Chervonnyi AD (2014) *Infrared spectroscopy of minerals and related compounds*. Springer: Dordrecht, Heidelberg, New York, London

Cionchon RL, Piperno DR, Thompson RG (1990) Opal phytoliths found on the teeth of the extinct ape *Gigantopithecus blacki*: implications for paleodietary studies. *Proc Natl Acad Sci US 87*:8120-8124

Clarke J (2003) The occurrence and significance of biogenic opal in the regolith. *Earth-sci Rev 60*:175-194

Cocker KM, Evans DA, Hodson MJ (1998) The amelioration of aluminium toxicity by silicon in wheat (*Triticum aestivum* L.): malate exudation as evidence for an in planta mechanism. *Planta 204*:318-323

Colledge S and Conolly J (2007) A review and synthesis of the evidence for the origins of farming on Cyprus and Crete. In: Colledge S and Conolly, J (eds), *The origins and spread of domestic plants in Southwest Asia and Europe*. California: UCL Institute of Archaeology/Left Coast Press, pp 53-74

Collin RL and Chisholm NWT (1991) Geomorphological Photogrammetry. *Photogramm Rec 13*:845-854

Compton RG, Harding MS, Pluck MR, Atherton JH, Brennan CM (1993) Mechanism of solid/liquid interfacial reactions. The dissolution of benzoic acid in aqueous solution. *J Phys Chem 97*:10416-10420

Conley DJ (2002) Terrestrial ecosystems and the global biogeochemical silica cycle. *Global Biogeochem Cycles 16*:68-1-68-8

Corbineau R, Reyerson PE, Alexandre A, Santos GM (2013) Towards producing pure phytolith concentrates from plants that are suitable for carbon isotopic analysis. *Rev Palaeobot Palyno 197*:179-185

Cornell RM and Schwertmann U (2001) *The iron oxides: structure, properties*. Weinheim: Wiley

Coté GC (2009) Diversity and distribution of idioblasts producing calcium oxalate crystals in *Dieffenbachia seguine* (Araceae). *Am J Bot 96*:1245-1254

da Costa FGCM, Souza PCT, Klein DE, Bove CP (2016) Application of acetolysis in phytoliths extraction. *Rev Palaeobot Palyno 228*:93-97

dal Corso M, Out WA, Ohlrau R, Hofmann R, Dreibrodt S, Videiko M, Müller J, Kirleis W (2018) Where are the cereals? Contribution of phytolith analysis to the study of subsistence economy at the Trypillia site Maidanetske (ca. 3900-3650 BCE), central Ukraine. *J Arid Environ 157*:137-148

Cummings LS and Magennis A (1997) A phytolith and starch record of food and grit in Mayan human tooth tartar. In: Pinilla A, Juan-Tresserras J, Machado MJ (eds), *Estado actual de los estudios de fitolitos en suelos y plantas*. Monografias del Centro de Ciencias Medioambientales, 4. Consejo Superior de Investigaciones Cientificas and Centro de Ciencias Medioambientales, Madrid, pp 211-218

Currie HA and Perry CC (2007) Silica in plants: biological, biochemical and chemical studies. *Ann Bot 100*:1383-1389

D

Davy H (1814) *Elements of agricultural chemistry*. (In a course of lectures for the Board of Agriculture), 2nd edn, Barnard JG, London

Deflandre G (1963) Les phytolithaires (Ehrenberg): Nature et signification micropaleontologique, pedologique et geologique, [Plant stones (Ehrenberg): Nature and micropaleontological, pedological and geological significance]. *Protoplasma 57*:234-259 (in French)

Deilaki E, (1973-1974) Ανασκαφικές Έρευνες. Περιοχή Ιωλκού (Παλιά Βόλου), Οδός Αγίων Θεοδώρων, [Excavations. Iolkos area (Palea Volos), Agioi Theodoron Street]. ΑΔ 29, Χρονικά: 546-547 (in Greek)

Delplace G, Schreck E, Pokrovsky OS, Zouiten C, Blondet I, Darrozes J, Viers J (2020) Accumulation of heavy metals in phytoliths from reeds growing on mining environments in Southern Europe, *Sci Total Environ 712:*135595

Denis GA (2017) Phytolith transport in texturally differentiated soils. *Annu Res Rev in Biol 18:1-10*

Derry LA, Kurtz AC, Ziegler K, Chadwick OA (2005) Biological control of terrestrial silica cycling and export fluxes to watersheds. *Nature 433*:728-731

Dick WA and Gregorich EG 2004. Developing and maintaining soil organic matter levels. In: Schjønning P, Elmholt S, Christensen BT (ed), *Managing soil quality challenges in modern agriculture*. CAB International, Wallingford, pp 103-120

Dietrich D, Hinke S, Baumann W, Fehlhaber R, Bäucker E, Rühle G, Wienhaus O, Marx G (2003) Silica accumulation in *Triticum aestivum* L. and *Dactylis glomerata* L. *Anal Bioanal Chem 376*:399-404

Dixit S and Van Cappellen P (2002) Surface chemistry and reactivity of biogenic silica. *Geochim Cosmochim Acta 66*:2559-2568

Dominguez-Rodrigo M, Serrallonga J, Juan-Tresserras J, Alcala L, Luque L (2001) Woodworking activities by early humans: a plant residue analysis on Acheulian stone tools from Peninj (Tanzania). *J Hum Evol 40*:289-299

Dorofeev VF, Filatenko AA, Migushova EF, Udachin RA, Jakubziner MM (1979) Pshenitsa, [Wheat]. In: Dorofeev VF and Korovina ON (eds), Kulturnaia Flora SSSR, [*Flora of cultivated plants of the USSR*]. Kolos, Leningrad (in Russian)

Dorozhkin S (2012) Dissolution mechanism of calcium apatites in acids: a review of literature. *World J Methodol 2*:1-17

Dove PM and Crerar DA (1990) Kinetics of quartz dissolution in electrolyte solutions using a hydrothermal mixed flow reactor. *Geochim Cosmochim Acta 54*:955-969

Dove PM and Elston SF (1992) Dissolution kinetics of quartz in sodium chloride solutions: analysis of existing data and a rate model for 25˚C. *Geochim Cosmochim Acta 56*:4147-4156

Drever JI (1994) The effect of land plants on weathering rates of silicate minerals. *Geochim Cosmochim Acta 58*:2325-2332

Duffin C (2006) Silicate minerals: an overview. *British Micromount Society 210*:1-39

Durgesh KT, Vijay PS, Sheo MP, Devendra KC, Nawal KD, Awadhesh KR (2015) Silicon-mediated alleviation of Cr(VI) toxicity in wheat seedlings as evidenced by chlorophyll florescence, laser induced breakdown spectroscopy and anatomical changes. *Ecotox Environ Safe 113*:133-144

Dvorak (2001) *Triticum species (wheat)*. Encyclopedia of Genetics, pp 2060-2068

E

Efstratiou N, Karetsou A, Banou E, Margomenou D (2004) The Neolithic settlement of Knossos: new light on an old picture. In: Cadogan G, Hatzaki E, Vasilakis A (eds), *Knossos: palace, city, state*. Proceedings of the conference in Herakleion, organised by the British School of Athens and the 23rd Ephoreia of Prehistoric and Classical Antiquities, November 2000, for the centenary of Sir Arthur Evans's excavations at Knossos*, BSA Studies* 12, London, pp 39-51

Ehrenberg CG (1841) *Nachtrag zu dem Vortrage iiber Verbreitung und Einfluss des mikroskopischen Lebens in Sud- und Nordamerika,* [Appendix to the lecture on the distribution and influence of microscopic life in South and North America]. Monatsber Preuss Akad Wiss Berlin, pp 139-144 (in German)

Ehrlich H, Demadis KD, Pokrovsky OS, Koutsoukos PG (2010) Modern views on desilicification: biosilica and abiotic silica dissolution in natural and artificial environments. *Chem Rev 110*:4656-4689

Ehrlich H, Koutsoukos PG, Demadis KD, Pokrovsky OS (2009) Principles of demineralization: modern strategies for the isolation of organic frameworks. Part II. Decalcification. *Micron 40*:169-193

Elbaum R, Weiner S, Albert R, Elbaum M (2003) Detection of burning of plant materials in the archaeological record by changes in the refractive indices of siliceous phytoliths. *J Archaeol Sci 30*:217-226

Elbaum R, Melamed-Bessudo C, Tuross N, Levy AA, Weiner S (2007) New methods to isolate organic materials from silicified phytoliths reveal fragmented glycoproteins but no DNA. *Quat Int 193:11-19*

Eneji AE, Inanaga S, Muranaka S, Li J, Hattori T, An P, Tsuji W (2008) Growth and nutrient use in four grasses under drought stress as mediated by silicon fertilisers. *J Plant Nutr 31*:355-36

Epstein E (1994) The anomaly of silicon in plant biology. *Proc Natl Acad Sci 91*:11-17

Epstein E (1999) Silicon. Annu. Rev. *Plant Physiol Plant Mol Biol 50*:641-664

Epstein E and Bloom A (2005) *Mineral nutrition of plants: principles and perspectives*. 2nd edn, Sinauer Associates, Sunderland

Ertug-Yaras F (2002) Pounders and grinders in a modern central Anatolian village. In: Procopiou H and Treuil R (eds), Moudre et Broyer. *L'interprétation fonctionnelle de l'outillage de mouture et de broyage dans la Préhistoire et l'Antiquité*. I. Méthodes, pp 211-227

Esau K (1965) *Plant Anatomy*. 2nd edn, John Wiley, New York, US

Esteban I, Marean C, Fisher E, Karkanas P, Cabanes D, Albert RM (2018) Phytoliths as an indicator of early modern humans plant gathering strategies, fire fuel and site occupation intensity during the Middle Stone Age at Pinnacle Point 5-6 (South Coast, South Africa). *PLos One 13*:e0198558

Etiegni L and Campbell AG (1991) Physical and chemical characteristics of wood ash. *Bioresour Technol 37*:173-178

Evans AJ (1901) Knossos. Summary report of the excavations in 1900: I. The Palace. *Annual of the BSA 6*:3-70

Evans AJ (1903) The Palace of Knossos. Provisional report for the year 1903, *BSA 9*:1-153

Evans J, Cann JR, Renfrew AC, Cornwall IW, Western AC (1964) Excavations in the Neolithic settlement of Knossos, 1957-1960. Part I. *The Annual of the BSA 59*:132-240

Evett RR and Cuthrell RQ (2016) A conceptual framework for a computer-assisted, morphometric-based phytolith analysis and classification system. *J Archaeol Sci 68*:70-78

Excley and Birchall (1992) Hydroxyaluminosilicate formation in solutions of low total aluminum concentration. *Polyhedron 11*:1901

F

Falconer SE and Fall PL (2013) Household and community behavior at Bronze Age Politiko-Troullia, Cyprus. *J Field Archaeol 38*:101-119

Farmer VC (2005) Forest vegetation does recycle substantial amounts of silicon from and back to the soil solution with phytoliths as an intermediate phase, contrary to recent reports. *Eur J Soil Sci 56*:271-272

Figueroa PM, Flores L, Sanchez J, Cesaretti NN (2008) Biosilicification (chalcedony) in human cerebral cortex, hippocampus and cerebellum from aged patients. *Micron 39*: 859-867

Fishkis O, Ingwersen J, Lamers M, Denysenko D, Streck T (2010) Phytolith transport in soil: a field study using fluorescent labeling. *Geoderma 157*:27-36

Flörke OW, Köhler-Herbertz B, Langer K, Tönges I (1982) Water in microcrystalline quartz of volcanic origin: agates. *Contrib Mineral Petrol 80*:324-333

Folk R and Hoops G (1982) An early Iron-age layer of glass made from plants at Tel Yinàm, Israel. *J Field Archaeol 9*:455-466

Fonash SJ and Marcel VdV (2018) *Engineering, Medicine and Science at the Nano-Scale*. John Wiley and Sons, Inc

Ford RI (1979) Paleoethnobotany in American Archaeology. In: Schiffer MB (ed), *Advances in Archaeological Method and Theory*. Academic Press, New York, US, pp 285-336

Forman SA and Sauer F (1962) Some changes in the urine of the sheep fed on hay rich in silica. *Can J Animal Sci 42*:9-17

Franceschi VR and Schueren AM (1986) Incorporation of strontium into plant calcium oxalate crystals. *Protoplasma130*:199-205

Fraysse F, Cantais F, Pokrovsky O, Schott J, Meunier J (2006a) Aqueous reactivity of phytoliths and plant litter: physico-chemical constraints on terrestrial biogeochemical cycle of silicon. *J Geochem Explor 88*:202-205

Fraysse F, Pokrovsky OS, Meunier JD (2010) Experimental study of terrestrial plant litter interaction with aqueous solutions. *Geochim Cosmochim Acta 74*:70-84

Fraysse F, Pokrovsky O, Schott J, Meunier J (2006b) Surface properties, solubility and dissolution kinetics of bamboo phytoliths. *Geochim Cosmochim Acta 70*:1939-1951

Fraysse F, Pokrovsky O, Schott J, Meunier J (2009) Surface chemistry and reactivity of plant phytoliths in aqueous solutions. *Chem Geol 258*:197-206

Fredlund GG and Tieszen LT (1994) Modern phytolith assemblages from the North American Great Plains. *J Biogeogr 21*:321-335

Friedrich G, Herzig P, Keyssner S, Maliotis G (1984) The distribution of Hg, Ba, Ca and Zn in the vicinity of cupriferous sulfide deposits, Troodos complex, Cyprus. *J Geochem Explor 21*:167-174

Friesem DE (2016) Geo-ethnoarchaeology in action. *J Archaeol Sci 70*:145-157

Friesem DE, Zaidner Y, Shahack-Gross R (2014) Formation processes and combustion features at the lower layers of the Middle Palaeolithic open-air site of Nesher Ramla. *Israel Quat Int 331*:128-138

Frost RL and Weier ML (2004) Thermal treatment of whewellite - a thermal analysis and Raman spectroscopic study. *Thermochim Acta 409*:79-85

Fuller DQ, Willcox G, Allaby RG (2012) Early agricultural pathways: moving outside the ''core area" hypothesis in Southwest Asia. *J Exp Bot 63*:617-633

Fuller DQ and Gonzalez Carretero L (2018) The archaeology of Neolithic cooking traditions: archaeobotanical approaches to baking, boiling and fermenting. *Archaeol Int 21*:109-121

Fuller DQ and Lucas L (2014) *Wheats: origins and development*. Encyclopedia of Global Archaeology, pp 7812-7817

G

Gal A, Brumfeld V, Weiner S, Addadi L, Oron D (2012) Certain biominerals in leaves function as light scatterers. *Adv Opt Mater 24*:77-83

Gale NH (1991) Copper oxide ingots: their origin and their place in the Bronze Age metals trade in the Mediterranean. In: Gale NH (ed), *Bronze Age Trade in the Mediterranean*. Studies in Mediterranean Archaeology 90, Aströms, Jönsered, pp 197-239

Gale NH and Stos-Gale ZA (1982) Bronze Age copper sources in the Mediterranean: a new approach. *Science 216*:11-19

Galloway JN (1996) Anthropogenic mobilization of sulfur and nitrogen: immediate and delayed consequences. *Annu Rev Energy Environ 21*:261-292

García-Granero JJ, Lancelotti C, Madella M (2017) A methodological approach to the study of microbotanical remains from grinding stones: a case study in Northern Gujarat (India). *Veget Hist Archaeobot 26*:43-57

Garnett TP and Graham RD (2005) Distribution and remobilization of iron and copper in wheat. *Ann Bot 95*:817-826

Garvie L (2003) Decay-induced biomineralization of the saguaro cactus (*Carnegiea gigantea*). *Am Mineral 88*:1879-1888

Gass IG (1980) The Troodos massif: its role in the unravelling of the ophiolite problem and its significance in the understanding of constructive plate margin processes. In: Panayiotou A (ed), *Ophiolites*. Int Ophiolite Symp, Cyprus 1979, pp 23-35

Geis JM (1973) Biogenic silica in selected species of deciduous angiosperms. *Soil Sci 116*:113-130

Gendron-Badou A, Coradin T, Maquet J, Fröhlich F, Livage J (2003) Spectroscopic characterization of biogenic silica. *J Non-cryst Solids 316*:331-337

Georgiadis A, Marhanb S, Lattachera A, Mädera P, Rennerta T (2019) Do earthworms affect the fractionation of silicon in soil? *Pedobiologia - J Soil Ecol 75*:1-7

Gérard F, Mayer KU, Hodson MJ, Ranger J (2008) Modelling the biogeochemical cycle of silicon in soils: application to a temperate forest ecosystem. *Geochim Cosmochim Acta 72*:741-758

Ghaly A and Ergudenler A (1991) Thermal degradation of cereal straws in air and nitrogen. *Appl Biochem Biotech 28*:111-126

Gibbs JW (1874-1878) V. *The equilibrium of heterogeneous substance*. Transactions of the Connecticut Academy of Arts and Sciences III, New Haven, pp 108-525

Godderis Y, François LM, Probst A, Schott J, Moncoulon D, Labat D, Viville D (2006) Modelling weathering processes at the catchment scale: the WITCH numerical model. *Geochim Cosmochim Acta 70*:1128-1147

Goldberg P and Macphail RI (2006) *Practical and Theoretical Geoarchaeology*. Blackwell, Malden, MA

Goncharov NP, Golovnina KA, Kondratenko EY (2009) Taxonomy and molecular phylogeny of natural and artificial wheat species. *Breeding Sci 59*:492-498

Gong HJ, Chen KM, Chen GC, Wang SM, Zhang CL (2003) Effects of silicon on growth of wheat under drought. *J Plant Nutr 26*:1055-1063

Gong H, Zhu X, Chen K, Wang S, Zhang C (2005) Silicon alleviates oxidative damage of wheat plants in pots under drought. *Plant Sci 169*:313-321

Graetsch H, Flörke OW, Miehe G (1985) The nature of water in chalcedony and opal-C from Brazilian agate geodes. *Phys Chem Minerals 12*:300-306

Greenwood JE, Truesdale VW, Rendell AR (2001) Biogenic silica dissolution in seawater - in vitro chemical kinetics. *Prog Oceanog 48*:1-23

Grégoire C, Rémus-Borel W, Vivancos J, Labbé C, Belzile F, Bélanger RR (2012) Discovery of a multigene family of aquaporin silicon transporters in the primitive plant *Equisetum arvense*. *Plant J 72*:320-330

Gregory P, Crawford D, McGowan M (1979) Nutrient relations of winter wheat: 1. Accumulation and distribution of Na, K, Ca, Mg, P, S and N. *J Agr Sci 93*:485-494

Gu Y, Zhao Z, Pearsall DM (2013) Phytolith morphology research on wild and domesticated rice species in East Asia. *Quat Intl 287*:141-148

Gügel IL, Grupe G, Kunzelmann KH (2001) Simulation of dental microwear: characteristic traces by opal phytoliths give clues to ancient human dietary behavior. *Amer J Phys Anthropol 114*:124-138

Guntzer F, Keller C, Meunier JD (2012) Benefits of plant silicon for crops: a review. *Agron Sustain Dev 32*:201-213

H

Haeckel E (1904) *Kunstformen der Natur [Art Forms in Nature]*. Dogma (in German)

Halstead P (1994) The North-South divide: regional paths to complexity in prehistoric Greece. In: Mathers C and Stoddart S (eds), *Development and Decline in the Mediterranean Bronze Age*. JR Collins Pubs, Sheffield Archaeological Monographs 8, pp 195-219

Hansen J (1994) Khirokitia plant remains preliminary report. In: Le Brun A (ed), *Fouilles recentes a Khirokitia (Chypre)* 1988-1991. Paris: Editions Recherche sur les Civilisations, pp 393-409

Harrison CC (1996) Evidence for intramineral macromolecules containing protein from plant silicas. *Phytochemistry 41*:37-42

Hart DM (2001) Elements occluded within phytoliths. In: Meunier JD and Colin F (eds), *Phytoliths - Applications in Earth Sciences and Human History*. 1st edn, Lisse France: AA Balkema Publishers, pp 313-316

Hart DM (2003) The influence of soil fauna on phytolith distribution in an Australian soil. Papers from a conference held at the ANU, August 2001, Canberra, Australia. In: Hart DM and Wallis LA (eds), *Phytolith and starch research in the Australian-Pacific-Asian regions: the state of the art*. Terra Australis 19, Pandanus Books, pp 83-91

Hart DM and Humphreys GS (1997) The mobility of phytoliths in soils: pedological considerations. 1st European meeting on phytolith research. In: Pinilla A, Juan-Tresserras J, Machado MJ (eds), *State-of-the-art of Phytoliths in Soils and Plants*. The Centro de Clencias Medioambientales Monograph, Madrid, pp 93-100

Hart TC (2016) Issues and directions in phytolith analysis. *J Archaeol Sci 68*:24-31

Hart JP and Matson RG (2009) The use of multiple discriminant analysis in classifying prehistoric phytolith assemblages recovered from cooking residues. *J Archaeol Sci 36*:74-83

Harvey EL and Fuller DQ (2005) Investigating crop processing using phytolith analysis: the example of rice and millets. *J Archaeol Sci 32*:739-752

Hauser EA (1955) The colloid science of silica and silicones. *Clays clay Miner 4*:45-53

Hayden B, Nixon-Darcus L, Ansell L (2016) Our daily bread? The origins of grinding grains and breadmaking. In: Steel L and Zinn K (eds), *Materiality of food 'stuffs': transformations, symbolic consumption and embodiments*. Routledge, New York, US, pp 57-58

He H, Bleby TM, Veneklaas EJ, Lambers H, Kuo J (2012a) Morphologies and elemental compositions of calcium crystals in phyllodes and branchlets of *Acacia robeorum* (Leguminosae: Mimosoideae). *Ann Bot 109*:887-896

He H, Bleby TM, Veneklaas EJ, Lambers H, Kuo J (2012b) Precipitation of calcium, magnesium, strontium and barium in tissues of four Acacia species (Leguminosae: Mimosoideae). *PLoS One 7*:e41563

He H, Veneklaas EJ, Kuo J, Lambers H (2014) Physiological and ecological significance of biomineralization in plants. *Trends in Plant Sci 19*:166-174

Heaney PJ (1993) A proposed mechanism for the growth of chalcedony. *Contrib Mineral Petr 115*:66-74

Helbaek H (1968) *Knossos wheat*. Unpublished manuscript [from Sapaki 2009]

Henriet C, Bodarwe L, Dorel M, Draye X, Delvaux B (2008) Leaf silicon content in banana (*Musa* spp.) reveals the weathering stage of volcanic ash soils in Guadeloupe. *Plant Soil 313*:71-82

Hildebrand M and Wetherbee R (2003) Components and control of silicification in diatoms. *Prog Mol Subcell Biol 33*:11-57

Historic England (2017) *Organic residue analysis and archaeology: supporting information*. Historic England, Swindon

Hixson AW and Crowell JH (1931) Dependence of reaction velocity upon surface and agitation. *Ind Eng Chem 23*:923-931

Ho MW (2013) Circular thermodynamics of organisms and sustainable systems. *Systems 1*:30-49

Hochella MF and Banfield J (1995) Chemical weathering of silicates in nature: A microscopic perspective with theoretical considerations. In: White A and Brantley S (eds), *Chemical weathering rates of silicate minerals. Revi Mineral 31*:353-406

Hocking PJ (1994) Dry-matter production, mineral nutrient concentrations and nutrient distribution and redistribution in irrigated spring wheat. *J Plant Nutr 17*:1289-1308

Hodson MJ (2016) The development of phytoliths in plants and its influence on their chemistry and isotopic composition. Implications for palaeoecology and archaeology. *J Archaeol Sci 68*:62-69

Hodson MJ and Evans D (1995) Aluminium/silicon interactions in higher plants. *J Exp Bot 46*:161-171

Hodson MJ, Parker AG, Leng MJ, Sloane HJ (2008) Silicon, oxygen and carbon isotope composition of wheat (*Triticum aestivum* L.) phytoliths: implications for palaeoecology and archaeology. *J Quaternary Sci 23*:331-339

Hodson MJ and Sangster AG (1993) The interaction between silicon and aluminium in *Sorghum bicolor* (L.) Moench: growth analysis and X-ray microanalysis. *Ann Bot 72*:389-400

Hodson MJ and Sangster AG (2002) X-ray microanalytical studies of mineral localization in the needles of white pine (*Pinus strobus* L.). *Ann Bot 89*:367-374

Hodson MJ, White PJ, Mead A, Broadley MR (2005) Phylogenetic variation in the silicon composition of plants. *Ann Bot 96*:1027-1046

Hodder I (2012) *Entangled. An archaeology of the relationships between humans and things*. Oxford, Wiley-Blackwell

Hopf M (1983) The plants found at Jericho. In: Kenyon KM, Holland TA (eds), *Excavations in Jericho.* Br School Archeol Jerusalem, London, pp 580-621

Horner HT, Wagner Jr, Wagner BL (1980) The association of druse crystals with the developing stomium of *Capsicum annuum* (Solanaceae) anthers. *Am J Bot 67*:1347-1360

Hossain MT, Mori R, Soga K, Wakabayashi K, Kamisaka S, Fujii S, Yamamoto R, Hoson T (2002) Growth promotion and an increase in cell wall extensibility by silicon in rice and some other Poaceae seedlings. *J Plant Res 115*:23-27

Hussain I, Ashraf M, Rasheed R, Asghar A, Sajid M, Iqbal M (2015) Exogenous application of silicon at the boot stage decreases accumulation of cadmium in wheat (*Triticum aestivum* L.) grains. *Braz J Bot 38*:223-234

I

ICPN Working Group: Madella M, Alexandre A, Ball T (2005) International Code for Phytolith Nomenclature 1.0. *Ann Bot 96*:253-260

Iler RK (1979) *The chemistry of silica. Solubility, polymerization, colloid and surface properties*. Biochemistry, John Wiley and Sons, New York, Chichester, Brisbane, Toronto

Ingold T (2000) *The perception of the environment: essays on livelihood, dwelling and skill*. Routledge

International Committee for Phytolith Taxonomy (ICPT): Neumann K, Strömberg CAE, Ball T, Albert RM, Vrydaghs L, Cummings LS (2019) International Code for Phytolith Nomenclature (ICPN) 2.0. *Ann Bot 124*:189-199

Irving JT (1981) Epitaxy down the ages. In: Veis A (ed), *The chemistry and biology of mineralized connective tissues*. Elsevier, New York, Amsterdam, pp 253-255

J

Jakes KA and Mitchell JC (1996) Cold plasma ashing preparation of plant phytoliths and their examination with Scanning Electron Microscopy and Energy Dispersive Analysis of X-rays. *J Archaeol Sci 23*:149-156

Jarvis SC (1987) The uptake and transport of silicon by perennial ryegrass and wheat. *Plant Soil 97*:429-437

Javed SH, Naveed S, Ramzan N (2010) Characterization of amorphous silica obtained from KMnO/sub 4/ treated rice husk. *J Chem Soc Pakistan 32*:78-82

Jenkins E (2009) Phytolith taphonomy: a comparison of dry ashing and acid extraction on the breakdown of conjoined phytoliths formed in *Triticum durum*. *J Archaeol Sci 36*:2402-2407

Jenkins E, Jamjoum K, Al-Nuimat S (2011) Irrigation and phytolith formation: an experimental study. In: Mithen SJ and Black E (eds), *Water, life and civilisation: climate, environment and society in the Jordan Valley*. Cambridge University Press/UNESCO, Cambridge/New York, pp 347-372

Jenkins E, Jamjoum K, Nuimat S, Stafford R, Nortcliff S, Mithen S (2016) Identifying ancient water availability through phytolith analysis: an experimental approach. *J Archaeol Sci 73*:82-93

Jones G (1982) Cereal and pulse remains from Protogeometric and Geometric Iolkos, Thessaly, *Anthropologika 3*:75-78

Jones G (1984) The LMII plant remains. In: Popham MR (ed), *The Minoan Unexplored Mansion at Knossos*. *BSA 17*:303-306

Jones G, Wardle K, Halstead P, Wardle D (1986) Crop storage at Assiros. *Sci Am 254*:96-103

Jones JB and Segnit ER (1971) The nature of opal. I. Nomenclature and constituent phases. *J Geol Soc Australia 18*:57-68

Jones LHP and Milne AA (1963) Studies of silica in the oat plant. *Plant Soil 18*:207-220

Jones MK, Allaby RG, Brown TA (1998) Wheat domestication. *Science 279*:302-303

Jones RL and Beavers AH (1963) Some mineralogical and chemical properties of plant opal. *Soil Sci 96*:375-379

Jouquet P, Jamoteau F, Majumdard S, Podwojewskia P, Nagabovanallid P, Canere L, Barbonic D, Meunier JD (2020) The distribution of silicon in soil is influenced by termite bioturbation in South Indian forest soils. *Geoderma 37*:114362

Jugdaohsingh R (2007) Silicon and bone health. *J Nutr Health Aging 11*:99-110

Jugdaohsingh R, Tucker KL, Qiao N, Cupples LA, Kiel DP, Powell JJ (2004) Dietary silicon intake is positively associated with bone mineral density in men and premenopausal women of the Framingham Off-spring Cohort. *J Bone Mineral Res 13*:297-307

Junius MM (1985) *The practical handbook of plant alchemy: an herbalist's guide to reparing medicinal essences, tinctures and elixirs.* Translated by Muller L, Healing Arts Press

K

Kaltsikes PJ and Larter EN (1970) The interaction of genotype and environment in durum wheat. *Euphytiea 19*:236-242

Kamatani A (1982) Dissolution rates of silica from diatoms decomposing at various temperatures. *Mar Biol 68*:91-96

Kamatani A, Riley JP, Skirrow G (1980) The dissolution of opaline silica of diatom tests in sea water. *J Oceanogr Soc Jap 36*:201-208

Kameník J, Mizera J, Řanda Z (2013) Chemical composition of plant silica phytoliths. *Environ Chem Lett 11*:189-195

Karamanos AI (2008) Τα σιτηρά των εύκρατων κλιμάτων, [The cereals of temperate climates]. Εκδόσεις Παπαζήσης (in Greek)

Karetsou A (2004) Knossos after Evans: past interventions, present state and future solutions. In: Cadogan G, Hatzaki E, Vasilakis A (eds), *Knossos: palace, city, state. Proceedings of the Conference in Herakleion,* Organised by the British School of Athens and the 23rd Ephoreia of Prehistoric and Classical Antiquities, November 2000, for the centenary of Sir Arthur Evans's excavations at Knossos, BSA Studies 12, London, pp 547-555

Karkanas P (2006) Late Neolithic household activities in marginal areas: the micromorphological evidence from the Kouveleiki caves, Peloponnese, Greece. *J Archaeol Sci 33:*1628-1641

Karkanas P (2010a) Preservation of anthropogenic materials under different geochemical processes: a mineralogical approach. *Quat Int 214*:63-69

Karkanas P (2010b) *Εισαγωγή στη Γεωαρχαιολογία, [Introduction to Geoarchaeology]*. Νεφέλη (in Greek)

Karkanas P, Bar-Yosef O, Goldberg P (2000) Diagenesis in prehistoric caves: the use of minerals that form *in situ* to assess the completeness of the archaeological record. *J Archaeol Sci 27*:915-929

Karkanas P, Rigaud JP, Simek JF, Albert RM, Weiner S (2002) Ash, bones and guano: a study of the minerals and phytoliths in the sediments of Grotte XVI, Dordogne, France. *J Archaeol Sci 29*:721-732

Karlen D and Whitney D (1980) Dry matter accumulation, mineral concentrations, and nutrient distribution in winter wheat. *Agron J 72*:281-288

Katz O, Cabanes D, Weiner S, Maeir AM, Boaretto E, Shahack-Gross R (2010) Rapid phytolith extraction for analysis of phytolith concentrations and assemblages during an excavation: An application at Tell es-Safi/Gath, Israel. *J Archaeol Sci 37*:1557-1563

Katz O, Lev-Yadun S, Bar (Kutiel) P (2013) Plasticity and variability in the patterns of phytolith formation in Asteraceae species along a large rainfall gradient in Israel. *Flora 208*:438-444

Kelly EF (1990*) Method for extracting opal phytoliths from soil and plant material*. Internal report. Colorado State University, US

Kiriatzi E (2000) Κεραμική τεχνολογία και παραγωγή. Η κεραμική της Ύστερης Εποχής του Χαλκού από την Τούμπα Θεσσαλονίκης, [Ceramic technology and production. Late Bronze Age pottery from Toumba Thessaloniki]. Διδακτορική Διατριβή, Αριστοτέλειο Πανεπιστήμιο Θεσσαλονίκης, [Doctoral thesis, Aristotle University of Thessaloniki, GR] (in Greek)

Kochian LV (1995) Cellular mechanisms of aluminum toxicity and resistance in plants. *Annu. Rev. Plant Physiol Plant Mol* Biol *46*:237-260

Köhler-Schneider M (2003) Contents of a storage pit from the late Bronge Age Stillfried, Austria: another record for the ''new'' glume wheat. *Veg Hist Archaeobot 12:*105-111

Kopaka K (2015) Minos Kalokairinos and his early excavation at Knossos. An overview, a portrait, and a return to the Kephalapithoi. In: Macdonald CF, Hatzaki E, Andreou S

(eds), *The great islands*. Studies of Crete and Cyprus presented to G Cadogan, Athens, pp 143-51

Körte A (1899) Kleinasiatische Studien IV: ein Altphrygischer Tumulus bei Bos-Oejuek (Lamunia), [Minor Asian studies IV: an ancient Phrygian tumulus at Bos-Oejuek (Lamunia)]. *AM24* (in German)

Kossel W (1927) Zur Theorie des Kristallwachstums, [The theory of crystal growth]. Gesellschaft Wissenschaften zu Gottingen, *Math-Phys Klasse*:135-143 (in German)

Kostakis K and Andreou S (1987) Προκαταρκτικές παρατηρήσεις για την οργάνωση του χώρου στην προϊστορική Τούμπα Θεσσαλονίκης, [Preliminary observations for space organization at prehistoric Toumba Thessaloniki]. *ΑΕΜΘ 1*:223-232 (in Greek)

Kostov I (2008) *Orphic Lithica* as a source of late antiquity mineralogical knowledge. Annual of the University of Mining and Geology "Rilski ST I", *Geol and Geophys 51*:109-115

Krejci MR, Wasserman B, Finney L, McNulty I, Legnini D, Vogt S, Joester D (2011) Selectivity in biomineralization of barium and strontium. *J Struct Biol 176*:192-202

Kroll H (1981) Thessalische Kulturpflanzen, [Thessalian crops]. *Archeo-Physika 8*:173-189 (in German)

Kroll H (2003) Rural plenty: the result of hard work-rich middle Bronze Age plant remains from Agios Mamas, Chalkidiki. In: Wagner GA, Pernicka E, Uerpmann HP (eds), *Troia and the Troad*. Natural Science in Archaeology, Springer, Heidelberg, Berlin, pp 293-301

Kuo-Huang LL, Ku MSB, Franceschi VR (2007) Correlations between calcium oxalate crystals and photosynthetic activities in palisade cells of shadeadapted *Peperomia glabella*. *Bot Stud 48*:155-164

Kutman UB, Kutman BJ, Ceylan Y, Ova EA, Cakmak I (2012) Contributions of root uptake and remobilization to grain zinc accumulation in wheat depending on post-anthesis zinc availability and nitrogen nutrition. *Plant Soil 361*:177-187

Kutman UB, Yildiz B, Cakmak I (2011) Improved nitrogen status enhances zinc and iron concentrations both in the whole grain and the endosperm fraction of wheat. *J Cereal Sci 53*:118-125

Kutuzova RS (1968) Silica transformation during the mineralization of plant residues. *Sov Soil Sci 7*:970-978

L

Lalueza Fox C, Perez-Perez A, Juan J (1994) Dietary information through the examination of plant phytoliths on the enamel surface of human dentition. *J Archaeol Sci 21*:29-34

Lane SN, Richards KS, Chandler JH (1993) Developments in photogrammetry: the geomorphological potential. *Prog Phys Geog 17*:306-328

Langer K and Flörke OW (1974) Near infrared absorption spectra (4000-9000 cm^{-1}) of opals and the role of "water" in these $SiO_2 \cdot nH_2O$ minerals. *Fortschr Miner 52*:17-51

Lanning F (1961) Calcite in *Lesquerella ovalifolia* trichomes. *Science 133*:380-380

Lawson DS, Hurd DC, Pankratz HS (1978) Silica dissolution rates of decomposing phytoplankton assemblages at various temperature. *Am J Sci 278*:1373-1393

Lersten NR and Horner HT (2011) Unique calcium oxalate "duplex" and "concretion" idioblasts in leaves of tribe Naucleeae (Rubiaceae). *Am J Bot 98*:1-11

Li T (2018) Identifying sources of fibre in Chinese handmade papers by phytoliths: a methodological exploration. *STAR 4:*1-11

Liang Y, Hua H, Zhu YG, Zhang J, Chang C, Römheld V (2006) Importance of plant species and external silicon concentration to active silicon uptake and transport. *New Phytol 172*:63-72

Liang Y, Sun W, Zhu YG, Christie P (2007) Mechanisms of silicon-mediated alleviation of abiotic stresses in higher plants: a review. *Environ Poll 147*:422-428

Liang YC, Zhu J, Li ZJ, Chu G, Ding Y, Zhang J, Sun W (2008) Role of silicon in enhancing resistance to freezing stress in two contrasting winter wheat cultivars. *Environ Exper Bot 64*:286-294

Lins U, Barros CF, da Cunha M, Miguens FC (2002) Structure, morphology, and composition of silicon biocomposites in the palm tree *Syagrus coronata* (Mart.) Becc. *Protoplasma 220*:89-96

Liodakis S, Katsigiannis G, Kakali G (2005) Ash properties of some dominant Greek forest species. *Thermochim Acta 437*:158-167

Lippmann F (1973) *Sedimentary Carbonate Minerals.* Springer, Berlin

Liu L, Li Y, Hou J (2020) Making beer with malted cereals and qu starter in the Neolithic Yangshao culture, China. *J Archaeol Sci Rep 29*:102134

Livarda A (2008) The archaeobotanical remains. In: Hatzaki E, Prent M, Coldstream JN, Evely D, Livarda A (eds), *Knossos, the Little Palace North project, part I: the Early Greek periods. BSA 103*:259-71

Loucaides S, Behrends T, Van Cappellen P (2010) Reactivity of biogenic silica: surface versus bulk charge density. *Geochim Cosmochim Acta 74*:517-530

Loucaides S, Van Cappellen P, Behrends T (2008) Dissolution of biogenic silica from land to ocean: role of salinity and pH. *Limnol Oceanogr 53*:1614-1621

Lowe JJ and Walker MJ (1997) *Reconstructing Quaternary Environments*. 2nd edn, John Wiley and Sons, Inc, New York, US

Lowenstam HA (1981) Minerals formed by organisms. *Science 211*:1126-1131

Lowenstam HA and Weiner S (1989) *On Biomineralization*. Oxford University Press, New York, US

Lu H, Liu Z, Wu N, Berné S, Saito Y, Liu B, Wang L (2002) Rice domestication and climatic change: phytolith evidence from Eats China, Boreas 31:378-385

Lucas Y, Luizão FJ, Chauvel A, Rouiller J, Nahon D (1993) The relation between biological activity of the rain forest and mineral composition of soils. *Science 260*:521-523

M

Ma JF (2004) Role of silicon in enhancing the resistance of plants to biotic and abiotic stresses. *Soil Sci Plant Nutr 50*:11-18

Ma JF and Takahashi E (2002) *Soil, fertilizer and plant silicon, research in Japan*. Elsevier, Amsterdam, The Netherlands

Ma JF and Yamaji N (2006) Silicon uptake and accumulation in higher plants. *Trends Plant Sci 11*:392-397

Ma JF and Yamaji N (2008) Functions and transport of silicon in plants. *Cell Mol Life Sci 65*:3049-3057

Mackenzie D (1903) The Pottery of Knossos. *JHS 23*:157-205

Mackenzie FT and Garrels RM (1966) Chemical mass balance between rivers and oceans. *Am J Science 264*:507-525

Madella M (2013*)* Plant economy and the use of space: evidence from the opal phytoliths. In: Efstratiou N, Karetsou A, Ntinou M (eds), *The Neolithic settlement of Knossos in Crete. New evidence for the early occupation of Crete and the Aegean islands*. INSTAP Academic Press, Philadelphia, Pennsylvania, pp 119-132

Madella M, Jones MK, Echlin P, Powers-Jones A, Moore M (2009) Plant water availability and analytical microscopy of phytoliths: implications for ancient irrigation in arid zones. *Quat Int 193*:32-40

Madella M, Jones MK, Goldberg P, Goren Y, Hovers E (2002) The exploitation of plant resources by Neandertals in Amud Cave, Israel: the evidence from phytolith studies. *J Archaeol Sci 29*:703-719

Madella M and Lancelotti C (2012) Taphonomy and phytoliths: a user manual. *Quat Int 275*:76-83

Maillard A, Diquélou S, Billard V, Laîné P, Garnica M, Prudent M, Garcia-Mina JM, Yvinm JC, Ourry A (2015) Leaf mineral nutrient remobilization during leaf senescence and modulation by nutrient deficiency. *Front Plant Sci 6*:1-15

Maldonado M, Navarro L, Grasa A, Gonzalez A, Vaquerizo I (2011) Silicon uptake by sponges: a twist to understanding nutrient cycling on continental margins. *Sci Rep 1*:1-8

Mali M and Aery N (2008) Influence of silicon on growth, relative water contents and uptake of silicon, calcium and potassium in wheat grown in nutrient solution. *J Plant Nutr 31*:1867-1876

Manetas Y (2018) *Περί φυτών αφηγήματα: Μικρές ιστορίες για φυτά που άλλαξαν τον κόσμο, [Plant narratives: Small stories about plants that changed the world]*. Πανεπιστημιακές εκδόσεις Κρήτης, 4η έκδ, σ. 21 (in Greek)

Mann S (2001) *Biomineralization: principles and concepts in bioinorganic materials chemistry*. Oxford University Press, New York, US

Marafon AC and Endres L (2013) Silicon: fertilization and nutrition in higher plants. *Amer-Eurasian J Agri Environ Sci 56*:380-388

Marshall CE (1949) *The colloid chemistry of the silicate minerals*. Academic Press, Inc, New York, US

Marschner H (1995) *Mineral nutrition of higher plants*. 2nd edn, Academic press, London, UK

Marumo Y and Yanai H (1986) Morphological analysis of opal phytoliths for soil discrimination in forensic science investigation. *J Forensic Sci 31*:1039-1049

Masoni A, Ercoli L, Mariotti M, Arduini I (2007) Post-anthesis accumulation and remobilization of dry matter, nitrogen and phosphorus in durum wheat as affected by soil type. *Eur J Agron 26*:179-186

Massey FP, Ennos AR, Hartley SE (2006) Silica in grasses as a defence against insect herbivores: contrasting effects on folivores and a phloem feeder. *J Anim Ecol 75*:595-603

Matichenkov VV and Bocharnikova EA (2001) The relationship between silicon and soil physical and chemical properties. In: Datnoff LE, Snyder GH, Korndorfer GH (eds), *Silicon in Agriculture*. Studies in Plant Science 8, Elsevier, Amsterdam, pp 209-219

Matsuoka Y (2011) Evolution of polyploid *Triticum* wheats under cultivation: the role of domestication, natural hybridization and allopolyploid speciation in their diversification. *Plant cell physiol 52*:750-764

Matthews W (2010) Geoarchaeology and taphonomy of plant remains and microarchaeological residues in early urban environments in the Ancient Near East. *Quat Int 214*:98-113

Mazen AMA, Zhang D, Franceschi VR (2004) Calcium oxalate formation in *Lemna minor*: physiological and ultrastructural aspects of high capacity calcium sequestration. *New Phytol 161*:435-448

McAinsh MR and Pittman JK (2008) Shaping the calcium signature. *New Phytol 181*:275-294

McClare CWF (1971) Chemical machines, Maxwell's demon and living organisms. *J Theor Biol 30*:1-34

McInerney FA, Strömberg CAE, James WC (2011) The Neogene transition from C3 to C4 grasslands in North America: stable carbon isotope ratios of fossil phytoliths. *Paleobiology 37*:23-49

McNaughton SJ and Tarrants JL (1983) Grass leaf silicification: natural selection for an inducible defense against herbivores. *Proc Natl Acad Sci US 80*:790-791

Meena V, Dotaniya M, Coumar V, Rajendiran S, Kundu S, Rao AS (2014) A case for silicon fertilization to improve crop yields in tropical soils. *Proc Natl Acad Sci India 84*:505-518

Megaloudi F (2006) *Plants and Diet in Greece from Neolithic to Classic Periods: The Archaeobotanical Remains*, British Archaeological Reports International Series 1516, Oxford

Megas G (2001) *Ελληνικές γιορτές και έθιμα της λαϊκής λατρείας,* [*Greek feasts and customs of folk worship*]. Βιβλιοπωλείον της Εστίας, σ. 34 (in Greek)

Mehra PN and Sharma OP (1965) Epidermal silica cells in the Cyperaceae. *Bot Gaz 126*:53-58

Metcalfe CR and Chalk L (1983) *Anatomy of the dicotyledons.* Clarendon, Oxford, UK

Meunier JD, Colin F, Alaecon C (1999) Biogenic silica storage in soils. *Geology 27*:835-838

Meunier JD and Collin F (2001) *Phytoliths - Applications in Earth Sciences and Human history*. 1st edn, Lisse France: AA Balkema Publishers

Middleton WD and Price DT (1996) Identification of activity areas by multi-element characterization of sediments from modern and archaeological house floors using inductively coupled plasma-atomic emission spectroscopy. *J Archaeol Sci 23*:673-687

Miligou-Markantoni M (2006) *Δένδρα, φυτά, άνθη στο λαϊκό πολιτισμό των νεώτερων Ελλήνων, [Trees, plants and flowers of folk culture of modern Greeks]*. Ιδιωτική Έκδοση, σ. 663 (in Greek)

Miller NF (1984) The use of dung as fuel: an ethnographic example and an archaeological application. *Paléorient 10*:71-79

Milton C and Davidson N (1946) Notes on straw-silica glass from California. *Am Mineral 31*:495-498

Misra MK, Ragland KW, Baker AJ (1993) Wood ash composition as a function of furnace temperature. *Biomass Bioenerg 4*:103-116

Mitani N and Ma JF (2005) Uptake system of silicon in different plant species. *J Exp Bot 56*:1255-1261

Moenke HHW (1974) Vibrational spectra and the crystalchemical classification of minerals. In: Farmer VC (ed), *The Infrared spectra of minerals.* Mineralogical Society Monograph 4. Adlard and Son, Dorking, Surrey, pp 111-118

Monje PV and Baran EJ (2000) First evidences of the bioaccumulation of α-quartz in cactaceae. *J Plant Physio 157*:457-460

Moores E and Vine FJ (1971) The Troodos Massif, Cyprus, and other ophiolites as ocean crust: evaluation and implications. In: Allerton S and Vine FJ (eds), *Spreading evolution of the Troodos ophiolite, Cyprus. Geology 19*:637-640

Morikawa CK and Saigusa M (2004) Mineral composition and accumulation of silicon in tissues of blueberry (*Vaccinum corymbosus* cv. Bluecrop) cuttings. *Plant Soil 258*:1-8

Morrison LA (1998) Lectotypification of *Triticum turgidum* and *Triticum spelta* (*Poaceae*). *Taxon 47*:705-710

Morowitz HJ (1968) *Energy flow in biology: biological organization as a problem in thermal physics*. Academic, New York, US

Moschen R, Lücke A, Schleser G (2005) Sensitivity of biogenic silica oxygen isotopes to changes in surface water temperature and palaeoclimatology. *Geophys Res Lett 32*:7708

de Moulins D (2000) Abu Hureyra 2: plant remains from the Neolithic. In: Moore AMT, Hillman GC, Legge AJ (eds), *Village on the Euphrates: from foraging to farming at Abu Hureyra*. Oxford University Press, New York, US, pp 399-422

Murat M and Foucault M (1977) Sulphates de calcium et matériaux dérivés, [Calcium sulphates and derived materials]. Colloques internationaux de la RILEM, Saint Rémy les Chevreuse, France, 546 (in French)

Mulholland SC and Rapp G (1992) *Phytolith Systematics. Advances in Archaeological and Museum Science 1*. Springer, Boston

Murphy DJ (2007) *People, Plants, and Genes. The story of crops and humanity*. Oxford University Press, New York, US

Myreni SCB (2000) X-ray and vibrational spectroscopy of sulfate in earth material. In: Alpers, CN, Jambor JL, Nordstrom DK (eds), *Sulfate minerals, crystallography geochemistry and environmental significance. Rev Mineral Geochem 40*:113-172

N

Neethirajan S, Gordon R, Wang L (2009) Potential of silica bodies (phytoliths) for nanotechnology. *Trends Biotechnol 8*:461-467

Nelson DG, Featherstone JD, Duncan JF, Cutress TW (1983) Effect of carbonate and fluoride on the dissolution behaviour of synthetic apatites. *Caries Res 17*:200-211

Nelson DM, Treguer P, Brzezinski MA, Leynaert A, Queguiner B (1995) Production and dissolution of biogenic silica in the ocean: revised global estimates, comparison with regional data and relationship to biogenic sedimentation. *Glob Biogeochem Cycles 9*:359-372

Nesbitt M and Samuel D (1996) From staple crop to extinction? The archaeology and history of the hulled wheat. In: Padulosi S, Hammer K, Heller J (eds), *Hulled wheats, promoting the conservation and used of underutilized and neglected crops*. IPGRI, Rome, pp 40-99

Nguyen NM, Dultz S, Guggenberger G (2014) Effects of pretreatment and solution chemistry on solubility of rice-straw phytoliths. *J Plant Nutr Soil Sc 177*:349-359

Nguyen NM, Dultz S, Picardal F, Bui ATK, Van Pham Q, Schieber J (2015) Release of potassium accompanying the dissolution of rice straw phytolith. *Chemosphere 119*:371-376

Nitsch E, Andreou S, Creuzieux A, Gardeisen A, Halstead P, Isaakidou V, Karathanou A, Kotsachristou D, Nikolaidou D, Papanthimou A, Petridou C, Triantaphyllou S, Valamoti SM, Vasileiadou A, Bogaard A (2017) A bottom-up view of food surplus: using stable carbon and nitrogen isotope analysis to investigate agricultural strategies and diet at Bronze Age Archontiko and Thessaloniki Toumba, northern Greece, *World Archaeol 49*:105-137

Nitta I, Kida A, Fujibayashi Y, Katayama H, Sugimura Y (2006) Calcium carbonate deposition in a cell wall sac formed in mulberry idioblasts. *Protoplasma 228*:201-208

Noyes AA and Whitney WR (1897) The rate of solution of solids in their own solutions. *J Am Chem Soc 19*:930-993

O

Ollendorf AL (1992) Toward a classification scheme of Sedge (Cyperaceae) phytoliths. In: Rapp GJ and Mulholland SC (eds), *Phytolith systematics. Emerging issues*. Plenum Press, New York, US, pp 91-111

O'Neill C, Jordan E, Bhatt T, Newman R (1986) Silica and oesophageal cancer. *CIBA Found Symp 121*:214-230

Osterrieth M, Madella M, Zurro D, Alvarez MF (2009) Taphonomical aspects of silica phytoliths in the loess sediments of the Argentinean Pampas. *Quat Int 193*:707-779

Out WA (2009) Firewood collection strategies at Dutch wetland sites in the process of Neolithisation. *The Holocene 20*:191-204

Out WA, Pertusa Grau JF, Madella M (2014) A new method for morphometric analysis of opal phytoliths from plants. *Microsc Microanal 20*:1867-1887

P

Palmer LR (1961) *Mycenaeans and Minoans*. London: Faber and Faber

Parr JF (2006) Effect of fire on phytolith coloration. *Geoarchaeology 21*:171-185

Parr JF, Lentfer CJ, Boyd WE (2001) A comparative analysis of wet and dry ashing techniques for the extraction of phytoliths from plant material. *J Archaeol Sci 28*:875-886

Parr JF and Sullivan LA (2005) Soil carbon sequestration in phytoliths. *Soil Biol Biochem 37*:117-124

Pasquale T and Throne J (2012) *Insect and mite pests of Durum wheat* (Chapter 5: Durum wheat). 2nd edn, Chemistry and Technology, American Associate of Cereal Chemists International, pp 73-83

Pearsall DM (2015) *Paleoethnobotany*. 3rd edn, Walnut Creek: Left Coast Press, New York, US

Peña-Chocarro L, Zapata L, González JE, Ibáñez JJ (2009) Einkorn (*Triticum monococcum L*) cultivation in mountain communities of the western Rif (Morocco): an ethnoarchaeological project. In: Fairnbairn AS and Weiss E (eds), *From foragers to farmers*. Gordon Hillman Festschrift, pp 103-111

Percival J (1921) *The wheat plant; (a monograph)*. Duckworth London

Pérez Cuadra V and Hermann P (2013) Characterization and macropattern of calcium oxalate phytoliths in Argentinean endemic species of Chenopodioideae (Amaranthaceae). *Quat Int 287*:83-88

Perry CC (2003) Silicification: the processes by which organisms capture and mineralize silica. *Rev Minera Geochem 54*:291-327

Perry CC and Lu Y (1992) Preparation of silicas from silicon complexes: role of cellulose in polymerisation and aggregation control. *J Chem Soc Faraday Trans 88*:2915-2921

Petö A, Kenéz A, Cabainné Prunner A, Lisztes-Szabó Z (2015) Activity area analysis of a Roman period semi-subterranean building by means of integrated archaeobotanical and geoarchaeological data. *Veg Hist Archaeobot 24:*101-120

Petö A and Vrydaghs L (2016) Phytolith analysis of ceramic thin-sections. First taphonomical insights from experiments with vegetal tempering. In: Sibbesson E, Jervis B, Coxon S (eds), *Insight from innovation. New light on archaeological ceramics*. Papers presented in honour of Prof. D Peacock's, contributions to archaeological ceramic studies, The Highfield Press, Southampton Monographs in Archaeology New Series, pp 57-73

Pierantoni M, Tenne R, Brumfeld V, Kiss V, Oron D, Addadi L, Weiner S (2017) Plants and light manipulation: the integrated mineral system in okra leaves. *Adv Sci News* 4:1600416

Pierantoni M, Tenne R, Rephael B, Brumfeld V, van Casteren A, Kupczik K, Oron D, Addadi L, Weiner S (2018) Mineral deposits in *Ficus* leaves: morphologies and locations in relation to function. *Plant Physiol 176*:1751-1763

Piper CS (1939) The use of perchloric acid in the digestion of plant materials. Australian *Chem Inst J and Proe 6*:421-427

Piperno DR (1988) *Phytolith analysis. An archaeological and geological perspective*. Academic Press, San Diego

Piperno DR (2006) *Phytoliths. A comprehensive guide for archaeologists and paleoecologists*. Lanham: AltaMira Press

Pironon J, Meunier JD, Alexandre A, Mathieu R, Mansuy L, Grosjean A, Jarde E (2001) Individual characterisation of phytoliths: experimental approach and consequences on palaeoenvironmental understanding. In: Meunier JD and Colin F (eds), *Phytoliths - Applications in Earth Science and Human History*. 1st edn, Lisse France: AA Balkema Publishers, pp 329-341

Pondaven P, Ragueneau O, Tréguer P, Hauvespre A, Dezileau L, Reyss JL (2000) Resolving the 'opal paradox' in the Southern Ocean. *Nature 405*:168-172

Ponzi R and Pizzolongo P (2003) Morphology and distribution of epidermal phytoliths in *Triticum aestivum* L. *Plant Biosyst 137*:3-10

Portillo M and Albert RM (2011) Husbandry practices and livestock dung at the Numidian site of Althiburos (el Médéina, Kef Governorate, Northern Tunisia): the phytolith and spherulite evidence. *J Archaeol Sci 38*:3224-3233

Prajapati K, Rajendiran S, Vassanda Coumar M, Dotaniya M, Meena V, Srivastava A, Khamparia NK, Rawat AK, Kundu S (2014) Bio-Sequestration of carbon in rice phytoliths. *Natl Acad Sci Lett 38*:129-133

Prasad V, Strömberg CAE, Alimohammadian H, Sahni A (2005) Dinosaur coprolites and the early evolution of grasses and grazers. *Science 310*:1177-1180

Prat H (1931) L' épiderme des Graminées: étude anatomique et systématique, [The epidermis of Gramineae: anatomical and systematic study]. Dissertation, University of Paris, FR (in French)

Preisig HR (1994) Siliceous structures and silicification in flagellated protists. *Protoplasma 181*:29-42

Prentice AJ and Webb EA (2016) The effect of progressive dissolution on the oxygen and silicon isotope composition of opal-A phytoliths: implications for palaeoenvironmental reconstruction. *Palaeogeogr Palaeoclimatol Palaeoecol 453*:42-51

Pritchard S, Prior S, Rogers H, Peterson C (2000) Calcium sulfate deposits associated with needle substomatal cavities of container-grown longleaf pine (*Pinus palustris*) seedlings. *Int J Plant Sci 161*:917-923

Prychid CJ, Rudall PJ, Gregory M (2003) Systematic and biology of silica bodies in monocotyledons. *Bot Rev 69*:377-440

Puppe D, Ehrmann O, Kaczorek D, Wanner M, Sommer M (2015) The protozoic Si pool in temperate forest ecosystems - quantification, abiotic controls and interactions with earthworms. *Geoderma 243-244*:196-204

Puppe D, Höhn A, Kaczorek D, Wanner M, Wehrhan M, Sommer M (2017) How big is the influence of biogenic silicon pools on short-term changes in water-soluble silicon in soils? Implications from a study of a 10-year-old soil-plant system. *Biogeosciences 14*:5239-5252

Puppe D and Leue M (2018) Physicochemical surface properties of different biogenic silicon structures: results from spectroscopic and microscopic analyses of protistic and phytogenic silica. *Geoderma 330*:212-220

Pyatt FB (1999) Comparison of foliar and stem bioaccumulation of heavy metals by Corsican pines in the mount Olympus area of Cyprus. *Ecotoxicol Environ Saf 42*:57-61

R

Radomski K and Neumann K (2011) Grasses and grinding stones: inflorescence phytoliths from modern West African Poaceae and archaeological stone artifacts. In: Fahmy A, Kahlheber S, D'Andrea AC (eds), *Windows on the African Past: Current Approaches to African Archaeobotany*. Africa Magna Verlag, Frankfurt, pp 153-166

Rains DW, Epstein E, Zasoski RJ, Aslam M (2006) Active silicon uptake by wheat. *Plant Soil 280*:223-228

Rashid I, Mir SH, Zurro D, Dar RA, Reshi ZA (2019) Phytoliths as proxies of the past. *Earth-Sci Rev 194*:234-250

Raven JA (1983) The transport and function of silicon in plants. *Biol Rev 58*:179-207

Raven JA and Giordano M (2009) Biomineralization by photosynthetic organisms: Evidence of coevolution of the organisms and their environment? *Geobiology 7*:140-154

Rehren T, Asderaki E, Skafida E, Karnava A (2015) Bronze Age crucibles from the Kastro-Palaia settlement, Volos, Greece - a contradiction of form and function? *Historical Metallurgy 47*:111-124

Reinhard KJ and Danielson DR (2005) Pervasiveness of phytoliths in prehistoric Southwestern diet and implications for regional and temporal trends for dental microwear. *J Archaeol Sci 32*:981-988

Reitz EJ and Wing ES (2008) *Zooarchaeology*. 2nd edn, Cambridge University Press

Renfrew JM (2003) Grains, seeds, and fruits from prehistoric Sitagroi. In: Elster ES, Renfrew C (eds), *Prehistoric Sitagroi: Excavations in Northeast Greece*, 1968-1970. The Final Report 2, Monumenta Archaeologica 20, Cotsen Institute of Archaeology, Los Angeles, pp 1-29

Renfrew C and Bahn P (2019) *Archaeology*. 8th edn. London: Thames and Hudson

Rey L (1921) *Observations sur les premiers habitats de la Macédoine. Recueillies par le service archéologique de l'armée d' Orient 1916-1919 (Region de Salonique*), *[Observations on the earliest habitats of Macedonia. Collected by the archaeological service of the eastern army 1916-1919 (Salonika region)],* de Boccard E (ed) (in French)

Rimstidt JD and Barnes HL (1980) The kinetics of silica-water reactions. *Geochim Cosmochim Acta 44*:1683-1699

Rizwan M, Meunier JD, Miche H, Keller C (2012) Effect of silicon on reducing cadmium toxicity in durum wheat (*Triticum turgidum* L. cv. Claudio W.) grown in a soil with aged contamination. *J Hazard Mater 209-210*:326-334

Rodríguez-Cintas A and Cabanes D (2017) Phytolith and FTIR studies applied to combustion structures: The case of the Middle Paleolithic site of El Salt (Alcoy, Alicante). *Quat Int 431*:16-26

Rodríguez N, Menéndez N, Tornero J, Amils R, de la Fuente V (2005) Internal iron biomineralization in *Imperata cylindrica*, a perennial grass: chemical composition, speciation and plant localization. *New Phytol 165*:781-789

Roffet-Salque M, Dunne J, Altoft DT, Casanova E, Cramp LJE, Smyth J, Whelton HL, Evershed RP (2017) From the inside out: upscaling organic residue analyses of archaeological ceramic. *J Archaeol Sci Rep 16*:627-640

Rosen AM (1986) *Cities of clay - The Geoarchaeology of tells*. University of Chicago Press, Chicago

Rosen AM (1999) Phytoliths as indicators of prehistoric irrigation farming. In: Anderson P (ed), *Prehistory of Agriculture: new experimental and ethnographic approaches*. UCLA, Institute of Archaeology, Los Angeles, pp 193-198

Rosen AM (2005) Phytolith indicators of plant and land use at Çatalhöyük. In: Hodder I (ed), *Inhabiting Çatalhöyük: reports from the 1995-1999 seasons*. McDonald Institute Monographs/BIAA Monograph 39. McDonald Institute for Archaeological Research and British Institute at Ankara, Cambridge and London, pp 203-212

Rosen AM and Weiner S (1994) Identifying ancient irrigation: a new method using opaline phytoliths from emmer wheat. *J Archaeol Sci 21*:125-132

Ross SD (1974a) Phosphates and other oxy-anions of group V. In: Farmer VC (ed), *The Infrared spectra of minerals*. Mineralogical Society, London, pp 383-422

Ross SD (1974b) Sulphates and other oxy-anions of group VI. In: Farmer VC (ed), *The Infrared spectra of minerals*. Mineralogical Society, London, pp 422-444

Rovner I (1971) Potential of opal phytoliths for use in paleoecological reconstruction. *Quat Res 1*:343-359

Rovner I (1972) Note on a safer procedure for opal phytolith extraction. *Quat Res 2*:591-592

Rowlett RM (2000) Fire control by *Homo erectus* in East Africa and Asia. *Acta Anthropol Sin 19*:198-208

Rubel W (2011) *Bread. A global history*. London: Reaktion Books

Rudall PJ, Prychid CJ, Gregory T (2014) Epidermal patterning and silica phytoliths in grasses: an evolutionary history. *Botanical Rev 80*:59-71

Runge F and Runge J (1997) Opal phytoliths in East African plants and soils. In: Pinilla A, Juan-Tresserras J, Machado MJ (eds), *Estado actual de los estudios de fitolitos en suelos y plantas*. Monografias del Centro de Ciencias Medioambientales, 4. Consejo Superior de Investigaciones Cientificas and Centro de Ciencias Medioambientales, Madrid, pp 71-81

S

Sachs J (1862) Ergebnisse einiger neuerer Untersuchungen über die in Pflanzen enthaltene Kieselsäure, [Results of some new studies on the silicic acid contained in plants]. *Flora 4*:49-55 (in German)

Sala B and Masini F (2007) Late Pliocene and Pleistocene small mammal chronology in the Italian peninsula. *Quat Int* 160:4-16

Sánchez Goñi MF, Desprat S, Daniau AL, Bassinot FC, Polanco-Martínez JM, Harrison SP, Allen JRM, Anderson RS, Behling H, Bonnefille R, Burjachs F, Carrión JS, Cheddadi R, Clark JS, Combourieu-Nebout N, Mustaphi CJC, Debusk GH, Dupont LM, Finch JM, Fletcher WJ, Giardini M, González C, Gosling WD, Grigg LD, Grimm EC, Hayashi R, Helmens K, Heusser LE, Hill T, Hope G, Huntley B, Igarashi Y, Irino T, Jacobs B, Jiménez-Moreno G, Kawai S, Kershaw AP, Kumon F, Lawson IT, Ledru MP, Lézine AM, Liew PM, Magri D, Marchant R, Margari V, Mayle FE, McKenzie GM, Moss P, Müller S, Müller UC, Naughton F, Newnham RM, Oba T, Pérez-Obiol R, Pini R, Ravazzi C, Roucoux KH, Rucina SM, Scott L, Takahara H, Tzedakis PC, Urrego DH, van Geel B, Valencia BG, Vandergoes, MJ, Vincens A, Whitlock CL, Willard DA, Yamamoto M (2017) The ACER pollen and charcoal database: a global resource to document vegetation and fire response to abrupt climate changes during the last glacial period. *Earth Syst Sci Data 9*:679-695

Sangster AG and Hodson MJ (1992) Silica deposition in subterranean organs. In: Mulholland SC and Rapp G (eds), *Phytolith systematics. Advances in archaeological and museum science 1*. Springer, Boston

Sangster AG, Hodson MJ, Ling LEC (2009) Biomineralisation/environment interactions in conifers: illustrated by hemlock, *Tsuga canadensis* (L.) Carr. *Quat Int 193*:3-10

Sangster AG, Hodson MJ, Tubb HJ (2001) Silicon deposition in higher plants. In: Datnoff LE, Snyder GH, Korndorfer GH (eds), *Silicon in agriculture. Studies in plant science 8*. Elsevier, Amsterdam, pp 85-113

Santosh K, Milan S, Rivka E (2017) Silicification in grasses: variation between different cell types. Mini review article, *Front Plant Sci 8*:1-8

Sarpaki A (1995) Toumba Balomenou, Chaeronia: plant remains from the Early and Middle Neolithic levels. In: Kroll H, Pasternak R (eds), *Res archaeobotanicae*. 9th Symposium IWGP, Kiel: Oetker-Voges Verlag, pp 281-300

Sarpaki A (2009) Knossos, Crete: invaders, "sea-goers", or previously "invisible", the Neolithic plant economy appears fully-fledged in 9000 BP. In: Fairburn A and Weiss E (eds), *From Foragers to Farmers*. Oxford, pp 220-234

Sarpaki A (2012) The taming of an island environment: Crete from dawn to noon (Neolithic to the end of the Bronze Age). In: Cadogan G, Iacovou M, Kopaka K, Whitley J (eds), *Parallel Lives: ancient island societies in Crete and Cyprus*. London, pp 35-45

Sarret G, Isaure M, Marcus M, Harada E, Choi Y, Pairis S, Fakra S, Manceau A (2007) Chemical forms of calcium in Ca, Zn- and Ca, Cd-containing grains excreted by tobacco trichomes. *Can J Chem 85*:738-746

Saqib M, Zörb C, Schubert S (2008) Silicon-mediated improvement in the salt resistanceof wheat (*Triticum aestivum*) results from increased sodium exclusion and resistance to oxidative stress. *Funct Plant Biol 35*:633-639

de Saussure NT (1804) *Recherches chimiques sur la végétation*, [*Chemical research of vegetation*]. Nyon, Paris (in French)

Sawkins FJ (1990) *Metal deposits in relation to plate tectonics*. 2nd edn, Springer-Verlag, Berlin

Schiffer MB (1987) *Formation processes of the archaeological record*. University of New Mexico Press, Albuquerque

Schiegl S, Goldberg P, Bar-Yosef O, Weiner S (1996) Ash deposits in Hayonim and Kebara caves, Israel: macroscopic, microscopic and mineralogical observations, and their archaeological implications. *J Archaeol Sci 23*:763-781

Schrödinger E (1944) *What is life? The physical aspect of the living cell*. Cambridge University Press, p 194

Scott L (2002) Grassland development under glacial and interglacial conditions in Southern Africa: review of pollen, phytolith and isotope evidence. *Palaeogeogr Palaeoclimatol Palaeoecol 177*:47-57

Setoguchi H, Okazaki M, Suga S (1989) Calcification in higher plants with special reference to cystoliths. In: Crick RE (ed), *Origin, evolution, and modern aspects of biomineralization in plants and animals*. Springer, Boston, pp 409-418

Shahack-Gross R, Albert RM, Gilboa A, Nagar-Hilman O, Sharon I, Weiner S (2005) Geoarchaeology in an urban context: the uses of space in a Phoenician monumental building at Tel Dor (Israel). *J Archaeol Sci* 32:1417-1431

Shahack-Gross R, Boaretto E, Cabanes D, Katz O, Finkelstein I (2014) Subsistence economy in the Negev Highlands: the Iron Age and the Byzantine/Early Islamic period. *Levant 46*:98-117

Shahack-Gross R and Finkelstein I (2008) Subsistence practices in an arid environment: a geoarchaeological investigation in an Iron Age site, the Negev Highlands, Israel. *J Archaeol Sci 35*:965-982

Shillito LM, Almond MJ, Nicholson J, Pantos M, Matthews W (2009) Rapid characterisation of archaeological midden components using FT-IR spectroscopy, SEM-EDX and micro-XRD. *Spectrochim Acta 73*:133-139

Shillito LM, Matthews W, Almond MJ (2008) Investigating midden formation processes and cultural activities at Neolithic Çatalhöyük, Turkey. *Antiquity 82*:317

Siart C, Forbriger M, Bubenzer O (2018) *Digital Geoarchaeology: new techniques for interdisciplinary human-environmental research*. Springer International Publishing

Sinclair TR, Pinter PJ, Kimball BA, Adamsen FJ, LaMorte RL, Wall GW, Hunsaker DJ, Adam N, Brooks TJ, Garcia RL, Thompson T, Leavitt S, Matthias A. 2000. Leaf nitrogen concentration of wheat subjected to elevated [CO_2] and either water or N deficits. *Agric Ecosyst Environ 79*:53-60

Skafida E (2012) Κάστρο Παλαιών Βόλου κατά τη Ρωμαϊκή περίοδο, [Kastro Palea of Volos During the Roman Period]. *AETHSE 3*:365-372 (in Greek)

Skafida E, Karnava A, Olivier JP (2012) Two new Linear B tablets from the site of Kastro-Palaia in Volos. In: Carlier P, de Lamberterie Ch, Egetmeyer M, Guilleux N, Rougemont Fr, Zurbach J (eds), *Études mycéniennes 2010. Actes du XIIIe colloque international sur les textes égéens*. Sèvres, Paris, pp 55-73

Skafida E, Karnava A, Olivier JP, Rehren Th, Asderaki-Tzoumerkioti E, Vaxevanopoulos M, Maniatis I, Tsartsidou G, Georgiou I, Tsigara M (2015) Ο οικισμός της Ύστερης Εποχής Χαλκού στο Κάστρο-Παλαιά του Βόλου: από τις ανασκαφές του Δ.Ρ. Θεοχάρη στα νέα αποτελέσματα της πρόσφατης διεπιστημονικής έρευνας, [The Late Bronze Age site at Kastro Palaia of Volos: from the excavations of Theocharis DR to the new results of the recent interdisciplinary investigation]. *AETHSE 4*:145-157 (in Greek)

Smil V (2000) Phosphorus in the environment: natural flows and human interferences. *Annu Rev Energ Environ 25*:53-88

Smith A, Proctor L, Hart TC, Stein GL (2019) The burning issue of dung in archaeobotanical samples: a case-study integrating macro-botanical remains, dung spherulites, and phytoliths to assess sample origin and fuel use at Tell Zeidan, Syria. *Veg Hist and Archaeobot 28*:229-246

Snyder GH, Matichenkov VV, Datnoff LE (2006) Silicon. In: Barker AV and Pilbeam DJ (eds), *Handbook of Plant Nutrition*. Taylor and Francis, Belle Glade, US, pp 551-562

Sommer M, Kaczorek D, Kuzyakov Y, Breuer J (2006) Silicon pools and fluxes in soils and landscapes-a review. *J Plant Nutr Soil Sci 169*:310-329

Song Z, Wang H, Strong PJ, Li Z, Jiang P (2012) Plant impact on the coupled terrestrial biogeochemical cycles of silicon and carbon: implications for biogeochemical carbon sequestration. *Earth-Sci Rev115*:319-331

Soreng RJ, Peterson PM, Romaschenko K, Davidse G, Zuloaga FO, Judziewicz EJ, Filgueiras TS, Davis JI, Morrone O (2015) A worldwide phylogenetic classification of the Poaceae (Gramineae). *J Syst Evol 53*:117-137

Sørensen I, Pettolino FA, Wilson SM, Doblin B, Johansen AB, Willats WG (2008) Mixed linkage (1→3), (1→4)-β-D-glucan is not unique to the Poales and is an abundant component of *Equisetum arvense* cell walls. *Plant J 54*:510-521

Sosman RB (1965) *The phases of silica.* Rutgers University Press, New Brunswick, US

Soueref (1996) Τούμπα Θεσσαλονίκης 1985-1996: Το ανασκαφικό έργο στην τράπεζα και το νεκροταφείο, [Toumba of Thessaloniki 1985-1996: excavations in the trapeza and the cemetery], *ΑΕΜΘ* 10: 389-406 (in Greek)

de Souza PV, Machado BR, da Silva DC, Menejes IPP, Araujo MS, de Jesus FG (2014) Effect of resistance and trichome inducers on attraction of *Euschistus heros* (Hemiptera: Pentatomidae) to soybeans. *Afr J Agric Res 9*:889-894

Sowers AE and Thurston EL (1979) Ultrastructural evidence for uptake of silicon-containing silicic acid analogs by *Urtica pilulifera* and incorporation into cell wall silica. *Protoplasma 101*:11-22

Stacey R (2009) *Organic residues: origins, analysis and scope*. An overview for the archaeological ceramicist the old potter's Almanack 14, pp 1-8

Stamatopoulou M (2011) Thessaly (Archaic to Roman). *Archaeol Rep 57*:73-84

Stevens CJ (2003) An investigation of agricultural consumption and production models for Prehistoric and Roman Britain. *Environ Archaeol 8*:61-76

Stöber W (1956) Chemische Adsorption von Methylchlorsilanen an kristallinem und amorphem Siliziumdioxyd, [Chemical adsorption of methylchlorosilanes on crystalline and amorphous silicon dioxide]. *Kolloid-Zeiitschrift 149*:39-46 (in German)

Strömberg CAE (2009) Methodological concerns for analysis of phytolith assemblages: does count size matter? *Quat Int 193*:124-140

Strömberg CAE, Di Stilio VS, Song Z (2016) Functions of phytoliths in vascular plants: an evolutionary perspective. *Funct Ecol 30*:1286-1297

Strömberg CAE, Dunn RE, Crifò C, Harris EB (2018) Phytoliths in paleoecology: analytical considerations, current use and future directions. In: Croft DA, Su D, Simpson SW (eds), *Methods in Paleoecology: reconstructing Cenozoic terrestrial environments and ecological communities*. Vertebr Paleobiology Paleoanthropology, pp 235-286

Struve GA (1835) *De silicia in plantis nonnullis,* [*The silica in some plants*]. Berolini, Typis Nietackianis (in Latin)

Struyf E, Damme SV, Gribsholt B, Bal K, Beauchard O, Middeburg J, Meire P (2007) *Phragmites australis* and silica cycling in tidal wetlands. *Aquat Bot 87*:134-40

Struyf E, Smis A, Damme SV, Meire P, Conley DJ (2009) The global biogeochemical silicon cycle. *Silicon 1*:207-213

Stumm W (1992) *Chemistry of the solid-water interface*. John Wiley and Sons, New York, US

Sun X, Wu Y, Wang C, Hill D (2012) Comparing dry ashing and wet oxidation methods. The case of the rice husk (*Oryza sativa* L.). *Microsc Res Techniq 75*:1272-1276

Suwanprateeb J and Hatthapanit K (2002) Rice-husk-ash-based silica as a filler for embedding composites in electronic devices. *J Appl Polymer Sci 86*:3013-3020

Sverdrup H and Warfvinge P (1993) Calculating field weathering rates using a mechanistic geochemical model PROFILE. *Appl Geochem 8*:273-283

T

Taylor MG, Simkiss K, Greaves GN, Okazaki M, Mann S (1993) An X-ray absorption spectroscopy study of the structure and transformation of amorphous calcium carbonate from plant cystoliths. *Proc R Soc Lond 252*:5-80

Theunissen J (1994) Intercropping in field vegetable crops: pest management by agrosystem diversification (an overview). *Pestic Sci 42*:65-68

Theocharis DR (1957) 7. Ανασκαφές στην Ιωλκό, [7. Excavations in Iolkos]. *ΠΑΕ*:*54-69* (in Greek)

Theocharis DR (1961) 11. Ανασκαφές στην Ιωλκό, [11. Excavations in Iolkos]. *ΠΑΕ*:119-130 (in Greek)

Thomson D'AW (1917) *On growth and form*. University Press, Cambridge

Thompson R, Kluth R, Kluth D (1995) Brainerd ware pottery function explored through opal phytolith analysis of food residues (abstracts of presentations at the 18th annual conference of the Society of Ethnobiology Arizona State Museum, The University of Arizona), *J Ethnobiol 15*:287-310

Tran TTT, Nguyen TT, Nguyen VT, Huong THH, Huynha, Nguyena TTH, Nguyen MN (2019) Copper encapsulated in grass-derived phytoliths: characterization, dissolution properties and the relation of content to soil properties. *J Environmental Manage 249*:109423

Traoré DD, Gu Y, Liu H, Shemsanga C, Ge J (2015) Vegetation types and climate conditions reflected by the modern phytolith assemblages in the subalpine Dalaoling Forest Reserve, central China. *Front Earth Sci 9*:268-275

Tréguer PJ, Nelson DM, Van Bennekom AJ, DeMaster DJ, Leynaert A, Quéguiner B (1995) The silica balance in the world ocean: a reestimate. *Science 268*:375-379

Trembath-Reichert E, Wilson JP, McGlynn SE, Fischer WW (2015) Four hundred million years of silica biomineralization in land plants. *PNAS 112*:5449-5454

Trinh TK, Nguyen TTH, Nguyen TN, Wu TY, Meharg AA, Nguyen MN (2017) Characterization and dissolution properties of phytolith occluded phosphorus in rice straw. *Soil Till Res 171*:19-24

Tripathi DK, Singh VP, Prasad SM, Chauhan DM, Dubey NK, Rai AK (2015) Silicon-mediated alleviation of Cr(VI) toxicity in wheat seedlings as evidenced by chlorophyll florescence, laser induced breakdown spectroscopy and anatomical changes. *Ecotoxicol Environ Saf 113*:133-144

Tsartsidou G, Lev-Yadun S, Albert RM, Miller-Rosen A, Efstratiou N, Weiner S (2007) The phytolith archaeological record: strengths and weaknesses evaluated based on a quantitative modern reference collection from Greece. *J Archaeol Sci 34*:1262-1275

Tsartsidou G, Lev-Yadun S, Efstratiou N, Weiner S (2008) Ethnoarchaeological study of phytolith assemblages from an agro-pastoral village in Northern Greece (Sarakini): development and application of a phytolith difference index. *J Archaeol Sci 35*:600-613

Tsartsidou G, Lev-Yadun S, Efstratiou N, Weiner S (2009) Use of space in a Neolithic village in Greece (Makri): phytolith analysis and comparison of phytolith assemblages from an ethnographic setting in the same area. *J Archaeol Sci 36*:2342-2352

Tsountas C (1900) Εργασίαι εν Βόλω, [Works in Volos]. *ΠΑΕ*:72-73 (in Greek)

Tubb HJ, Hodson MJ, Hodson GC (1993) The inflorescence papillae of the Triticeae: a new tool for taxonomic and archaeological research. *Ann Bot 72*:537-545

Tuna AL, Kaya C, Higgs D, Murillo-Amador B, Aydemir S, Girgin AR (2008) Silicon improves salinity tolerance in wheat plants. *Environ Exp Bot 62*:10-16

Twiss PC (1986) Morphology of opal phytoliths in C3 and C4 grasses. *Phytolith Newslett* 3:4-11

Twiss PC, Suess E, Smith RM (1969) Morphological classification of grass phytoliths. *Soil Sci Soc Am Proc 33*:109-115

U

Umemoto K, Itntoh M, Hozumi K (1973) Identification of the plant source of the Chinese crude drug "Dan-zhu-ye" using the low-temperature plasma ashing technique. *Mikrochim Acta 2*:301-313

Unzué-Belmonte D, Struyf E, Clymans W, Tischer A, Potthast K, Bremer M, Meire P, Schaller J (2016) Fire enhances solubility of biogenic silica. *Sci Total Environ 572*:1289-1296

V

Valamoti SM (2003) Neolithic and early Bronze Age "food" from Northern Greece: the archaeobotanical evidence. In: Parker-Pearson M (ed), *Food, culture and identity in the Neolithic and Early Bronze Age*. BAR, Oxford, pp 97-11

Valamoti SM (2009) Η αρχαιοβοτανική έρευνα της διατροφής στην προϊστορική Ελλάδα, [The archaeobotanical research of nutrition in prehistoric Greece]. University Studio Press (in Greek)

Valamoti SM (2011) Ground cereal food preparations from Greece: the prehistory and modern survival of traditional Mediterranean ''fast foods''. *Archaeol Anthropol Sci 3*:19-39

Vamvuka D and Kakaras E (2011) Ash properties and environmental impact of various biomass and coal fuels and their blends. *Fuel Process Technol 92*:570-581

Van Cappellen P and Qiu L (1997a) Biogenic silica dissolution in sediments of the Southern Ocean. I. Solubility. *Deep-Sea Res II 44*:1109-1128

Van Cappelen P and Qiu L (1997b) Biogenic silica dissolution in sediments of the Southern Ocean. II. Kinetics. *Deep-Sea Res II 44*:1129-1149

Van Cappellen P, Dixit S, Gallinari M (2002) Biogenic silica dissolution and the marine Si cycle: kinetics, surface chemistry and preservation. *Oceanis 28*:417-454

Van der Vorm PDJ (1980) Uptake of Si by five plant species, as influenced by variation in Si-supply. *Plant Soil 56*:153-156

Van Zeist W (1981) Plant remains from Cape Andreas-Kastros (Cyprus). In: Le Brun A (ed), *Un site néolithique precéramiqueen Chypre: cap Andreas-Kastros*. Editions ADPF, Paris, pp 95-99

W

Wainwright SA, Biggs WD, Currey JD, Gosline JM (1976) *Mechanical design in organisms*. Wiley, New York, US

Wang X, Jiang H, Shang X, Wang T, Wu Y, Zhang P, Wang W, Wang C (2014) Comparison of dry ashing and wet oxidation methods for recovering articulated husk phytoliths of foxtail millet and common millet from archaeological soil. *J Archaeol Sci 45*:234-239

Wardlaw IF and Willenbrink J (2000) Mobilization of fructan reserves and changes in enzyme activities in wheat stems correlate with water stress during kernel filling. *New Phytol 148*:413-422

Warren P (2000) Sir Arthur Evans and his achievement. *Bulletin of the Institute of Classical Studies 44*:199-211

Watling KM, Parr JF, Rintoul L, Brown CL, Sullivan LA (2011) Raman, infrared and XPS study of bamboo phytoliths after chemical digestion. *Spectrochim Acta 80*:106-111

Webb MA (1999) Cell-mediated crystallization of calcium oxalate in plants. *Plant Cell 11*:751-761

Wendrich W and Ryan P (2010) Phytoliths and basketry materials at Çatalhöyük (Turkey): timelines of growth, harvest and objects life histories. *Paléorient 38*:55-63

Weiner S (2010) *Microarchaeology*. Cambridge University Press, New York, US

Weiner S (1984) Organization of organic matrix components in mineralized tissues. *Amer Zool 24*:945-951

Weisskopf AR (2010) *Vegetation, agriculture and social change in Late Neolithic China: a phytolith study,* Doctoral thesis, University College London, UK

Weisskopf A, Qin L, Ding J, Ding P, Sun G, Fuller D (2015) Phytoliths and rice: from wet to dry and back again in the Neolithic Lower Yangtze. *Antiquity 89*:1051-1063

Westoby MJ, Brasington J, Glasser NF, Hambrey MJ, Reynolds JM (2012) Structure-from-motion photogrammetry: a low-cost, effective tool for geoscience applications. *Geomorphology 179*:300-314

White WB (1971) Infrared characterization of water and hydroxyl ion in the basic magnesium carbonate minerals. *Am Mineral 56*:46-53

Wilding LP and Drees LR (1974) Contributions of forest opal and associated crystalline phases to fine silt and clay fractions of soils. *Clays Clay Miner 22*:295-306

Wilding L, Smeek ENE, Drees LR (1977) Silica in soils: quartz, cristobalite, tridymite and opal. In: Dixon JB, Weed SB, Dinauer RC (eds), *Minerals in soil environments. Soil Sci Soc Am*, Madison, Wise, pp 471-552

Winklera DE, Schulz-Kornasb E, Kaiserc TM, De Cuyperd A, Clausse M, Tütkena T (2019) Forage silica and water content control dental surface texture in guinea pigs and provide implications for dietary reconstruction. *Proc Natl Acad Sci US 116*:1325-1330

Wirth GS and Gieskes JM (1979) The initial kinetics of the dissolution of vitreous silica in aqueous media. *J Coll Int Sci 68*:492-500

Wolf PR, DeWitt BA, Wilkinson BE (2014) *Elements of Photogrammetry with application in GIS*. 4th edn, McGraw-Hill Education

Wollast R and Mackenzie FT (1983) The global cycle of silica. In: Aston SR (ed), *Silicon geochemistry and biochemistry*. Academic Press, San Diego, pp 39-76

Wroth K, Cabanes D, Marston JM, Aldeias V, Sandgathe D, Turq A, Goldberg P, Dibble HL (2019) Neanderthal plant use and pyrotechnology: phytolith analysis from Roc de Marsal, France. *Archaeol Anthropol Sci 11*:4325-4346

Wu Y, Yang Y, Wang H, Wang C (2014) The effects of chemical composition and distribution on the preservation of phytolith morphology. *Appl Phys A 114*:503-507

Wu Y, Wang C, Hill DV (2012) The transformation of phytolith morphology as the result of their exposure to high temperature. *Microsc Res Techniq 75*:852-855

Wüst RAJ and Bustin RM (2003) Opaline and Al-Si phytoliths from a tropical mire system of West Malaysia: abundance, habit, elemental composition, preservation and significance. *Chem Geol 200*:267-292

Y

Yao YF, Li X, Jiang HE, Ferguson DK, Hueber F, Ghosh R, Bera S, Li CS (2012) Pollen and phytoliths from fired ancient potsherds as potential indicators for deciphering past vegetation and climate in Turpan, Xinjiang, NW China. *PLoS One 7*:e39780

Yeo AR, Flowers SA, Rao G, Welfare K, Senanayake N, Flowers TJ (1999) Silicon reduces sodium uptake in rice (*Oryza sativa* L.) in saline conditions and this is accounted for by a reduction in the transpirational bypass flow. *Plant Cell Environ 22*:559-565

Z

Zapata L, Peña-Chocarro L, Perez-Jorda G, Stika HP (2004) Difusión de la argricultura en la Peninsula Iberica. [Agicultural diffusion in the Iberian peninsula]. In: Arias P, Ontañon R, Garcia-Monco C (eds), *Actas del III Congreso del Neolitico de la Peninsula Iberica*.

Santander: Servicio de publicaciones de la Univeridad de Cantabria, pp 103-113 (in Spanish)

Zhang J, Houyuan L, Guoping S, Flad R, Wu N, Huan X, He K, Wang Y (2016) Phytoliths reveal the earliest fine reedy textile in China at the Tianluoshan site. *Scientific Reports 6*:18664

Zhang X, Wang XQ, Wand DF (2017) Immobilization of heavy metals in sewage sludge during land application process in China: a review. *Sustainability 9*:1-19

Zhao Z, Pearsall DM, Benfer RA, Piperno DR (1998) Distinguishing rice (*Oryza sativa* Poaceae) from wild *Oryza* species through phytolith analysis. II: finalized method. *Econ Bot 52*:134-145

Zhuravlev LT (2000) The surface chemistry of amorphous silica. Zhuravlev model. *Colloids Surf A Physicochem Eng Asp 173*:*1-38*

Zohary D, Hopf M, Weiss E (2012) *Domestication of plants in the Old World*. 4th edn, Oxford University Press